CONTROL AND SIMULATION OF AN ACTIVE SUSPENSION SYSTEM

GAO JIANMIN, BSc and MSc

A thesis submitted in partial fulfilment of the requirements of the University of Wolverhampton for the degree of Doctor of Philosophy

March 1997

This work or any part thereof has not previously been presented in any form to the University or to any other whether for the purposes of assessment, publication or bibliographies cited in the work, I confirm that the intellectual content of the work is the result of my own efforts and no other person.

Signature.....Gao J.....

Date.....17/3/1997.....

ACKNOWLEDGEMENT

The author would like to express his appreciation to Dr. N. J. Leighton, Dr. C. Morgan and Dr. R. McCafferty for their distinguished guidance and supervision. He really enjoyed working with them.

The author would like to thank all relevant persons who gave him their generous help, especially those technical staffs, Mr. John Harris, Mr. John Pitt, Mr. Ernie Tranter, and Mr. Nigel Smith, etc. He also wants to acknowledge his roommates, Mr. Y. Koo, Mr. J. Rea, Mr. S. Yao, Mr. D. Turner, Mr. T. Kaipio and Dr. L. Semlov, etc. for their friendship, discussion and assistance.

The author is very grateful to the University of Wolverhampton of the United Kingdom for the financial support during his study.

Finally, the author wish to thank his family, without whose support, encouragement, patience, and sacrifice this work would have never been completed.

ABSTRACT

In this thesis, both theoretical and experimental research work has been carried out in the area of active suspensions for automotive application. A PC based digital control system and interfaces to an existing trailer with an active zero rate suspension system, sensors and electronics has been developed. The required control software has been written in C++. A nonlinear half (and quarter) car model with limited actuator bandwidth has been established for the two wheeled trailer with the active suspension. Various control strategies, namely PD, MIMO PID, LQG and Fuzzy Logic, have been implemented on the physical prototype. These controllers were simulated using the validated nonlinear model and implemented on the test rig. Experimental results have shown that the whole control system functions correctly and the methodology of these applications has been correct. The performance of these control strategies has been investigated mathematically and experimentally for the particular test rig in terms of ride comfort and handling. It has been shown that the MIMO PID performs the best. The effects of the nonlinearity and limited bandwidth of actuators were also investigated in the nonlinear model, which resulted in a novel explanation for the instability in test rig.

A PC based active tuneable vibration absorber (ATVA) has been developed and built from concept to prototype. This system includes an accelerometer on the hub, an absorber tuned by a stepping motor, a PC computer and the relevant interfaces. The corresponding control strategy and software have also been developed for the ATVA. Experiments on a developed unsprung mass test rig and simulation have been used to evaluate the performance of the ATVA. It has been shown that the whole system including hardware, software and algorithm is effective and the developed ATVA can be a candidate to damp out hub vibration.

The performance of the combination of the zero rate suspension and the ATVA has been predicted by simulating the trailer response under road profile inputs. The nonlinear half car model with MIMO PID with sky hook damping and ATVA under white noise excitation was employed for this purpose. It has been shown that the combination can provide both ride comfort and handling.

A PC based measurement system for identifying the transfer function of vehicle suspensions has also been developed from concept to the prototype. This work includes designing and building the measurement platform and interfaces to the PC computer, writing software for signal sampling and processing, and developing the test method and algorithm. Results from this system have been validated against two standard methods, a conventional hydraulic shaker and a quarter car test rig with swept sine wave excitation. The developed system has been proved to function correctly.

CONTENTS

Chapter 1

Fundamental Background and Literature Review

1.1 Introduction

Passive suspensions on ground vehicles have developed over the last 100 years to a very high level of sophistication. Contemporary suspension systems predominantly contain passive energystoring and dissipating elements, i.e. springs and dampers. These conventional vibration isolation devices have the advantage of being easy to manufacture, implement and maintain, but lack the ability to achieve a good compromise between conflicting design requirements, such as effective handling qualities and good ride comfort. Recently, however, advances in optimisation techniques for automatic control, in addition to the availability of sophisticated transducers, processors and actuators, have had encouraging implications for vehicle suspension. Active suspension seems to have evolved as a result of these advances.

The idea of using active devices to generate forces dates back at least to the 1960s. It was recognised early that vehicle suspensions involved a special case of vibration, and this interest has remained until the present because of the large potential market. For researchers who have been active in the area during the past two or three decades, the last five to ten years must have been very gratifying. This has been the period when much of the automotive industry has been working "full steam" at bringing to bear a practical active suspension system.

1.2 Active Suspension Systems

A vehicle suspension has to perform a number of tasks as follows:

- To support the vehicle weight at an appropriate mean ride height. This weight may, of course, vary considerably as vehicle loading changes.

- To isolate the body of the vehicle from road disturbances thereby improving ride comfort.
- To prevent violent vehicle body motion during steering and braking manoeuvres (roll/pitch control).
- To maintain the wheel location geometry as near optimum as possible thereby ensuring predictable vehicle handling.
- To damp out any oscillations of the body.
- To keep optimum contact between tyre and road.

Although it has been established that the ride comfort of passengers is improved by active suspension, a true implementation of the latter is hindered by its high production, implementation and maintenance cost, in addition to its complexity and, hence, lower reliability.

1.2.1 Basic description of current active suspensions[1]

Having in mind simultaneous cost and performance constraints, many suspension systems have been invented or proposed. The current range of designs falls into four broad categories; fully active, series active, parallel active and semi-active.

Fully active

In a fully active system the vehicle body is supported entirely on four actuators, typically hydraulic, which fully support the vehicle dead weight and provide isolation from road inputs as well as control of ride height, roll and pitch. Such a system is shown diagrammatically in figure 1-1 and formed the basis of the early Lotus active systems. The benefits and disadvantages can be assessed as follows:

Benefits: Rapid ride height control
Good roll/pitch control
'Sky-hook' damping (Appendix A)
Excellent decoupling of ride/handling
Can provide unsprung mass damping[2]

---

[1]This section is mainly quoted from the technical report written by Dr N. J. Leighton, 1991.

[2]Unsprung mass is the mass of the assembly of the hub and wheel which are not isolated from the road disturbances by the suspension. Sprung mass is that of the vehicle body being isolated by the suspension. Unsprung mass damping is required to keep the tyre contacting the road and hence to optimise tyre adhesion.

Drawbacks: Very high cost
Complex hydraulics & control system
No inherent 'safe mode'
Very high power consumption
Noise and harshness transmitted by actuator
Some packaging problems

Series active

In the case of series active systems the hydraulic actuator is placed in series with a spring (figure 1-2) which isolates the vehicle body from high frequency road inputs in the same way as a conventional suspension system. The hydraulic control system is thus left to remove the lower frequency components of the road input and to provide ride height, roll and pitch control. The advantages and weaknesses are summarized as follows:

Benefits: Ride height control
Reasonable roll/pitch control
Limited bandwidth 'sky-hook' damping
Good decoupling of ride/handling
Modest power consumption

Drawbacks: High cost
Complex hydraulics & control system
No unsprung mass damping
Limited 'safe mode'
Some packaging problems

Parallel active

Parallel active suspension systems utilise a passive element, typically a spring, in parallel with the hydraulic actuator unit (figure 1-3). This passive element acts to support the vehicle dead weight, thus reducing the loads on the hydraulic system and hence the power consumption. The hydraulic system is still subjected to all the frequencies present in the road input. The parallel active approach may be evaluated thus:

Benefits: Fast ride height control
Good roll/pitch control
'Sky-hook' damping
Good decoupling of ride/handling

Good 'safe mode'
Can provide unsprung mass damping

Drawbacks: Very high cost
Complex hydraulics and control system
High power consumption
Some packaging problems

Semi active

Semi-active suspensions can take many forms with the common characteristic that they nominally consume no power relying instead on modulating the behaviour of passive suspension elements. The most common semi-active systems are 'active', or 'controllable' dampers, as shown in figure 1-4. Such a system is a conventional spring damper system with the ability to control the characteristic of the damper. This can be used in two ways. The first, as a conventional suspension but with reduced damping for an improved ride when driving on relatively smooth, straight roads and with increased damping over poor surfaces and during steering or braking manoeuvres. The second, by switching the damper in and out as a function of body and hub motion can, to some extent, simulate a parallel active system. The advantages and shortcomings are evaluated as follows:

Benefits: Approximate 'sky-hook' damping
Some decoupling of ride/handling
Relatively low cost
Relatively simple
Inherent 'safe mode'
Minimal packaging problems

Drawbacks: No ride height control
No steady state roll/pitch control

1.2.2 Active zero-rate suspension (Leighton, et at 1994)

The concept of a very low spring rate suspension system has existed for some time. The system incorporates two novel principles. The first is the application of a buckling leaf spring which offers a very low effective spring rate and allows a much higher static load than a conventional spring with the same deformation. The second is the use of variable leverage which allows the possibility of changing the resultant force of the buckling spring along the line of action by varying an angle (Appendix B).

If the zero rate suspension concept is integrated into an active suspension system by applying a control system to the actuator that is used in setting the leverage of the spring and hence the force applied to the vehicle body (figure 1-5) then the resulting system does not fall into any of the above categories and must be considered independently. There are three main areas of difference as follows:

- The basic characteristic of the system allows motion between the wheel and the body without actuator movement so all high frequency road inputs can be isolated by the passive components thereby restricting the required actuator bandwidth and associated actuator velocity.
- Under static conditions the vehicle weight is supported by the passive elements with minimal load on the actuator thereby minimising actuator loads.
- Since the actuator is not the source of forces acting on the vehicle body but merely modulates the force generated in the passive components the energy input required to resist roll or pitch forces is relatively small.

In such a system, a very low mean power consumption could be realistically expected and this makes the possibility of an electrically actuated system appear conceivable. The current prototype is using five normal car batteries as its power supply. The voltage is 60V and the power consumption is below 150W per wheel. If the likely benefits and drawbacks of such a system are considered in terms of those used above the following can be perceived:

Benefits: Ride height control
Roll & pitch control
'Sky-hook' damping
Excellent decoupling of ride/handling
Low power consumption
Relatively simple actuator
Relatively low cost

Drawbacks: No unsprung mass damping
Limited 'safe mode'
Difficult packaging

1.2.3 Comparison of the active suspensions

The implication of the assessment is that the zero rate system offers substantial advantages over all current active suspensions with relatively few drawbacks. The most significant problem is that imposed by packaging, which arises from the

substantial differences in the nature of the zero rate suspension as compared to a conventional spring damper unit which would result in significant modifications being required in the vehicle structure to accommodate the different force distribution.

The comparison is summarized in table 1-1 which shows a performance ranking based on subjective ratings and weights derived by a team of suspension engineers at GKN Technology (Leighton, 1991). The feature is rated from 0 to 5, with 0 representing the least effective system and 5 the most. The total rating for each system is then calculated with and without the weighting factor.

This suggests that the semi-active (using active dampers but with no external power input) approach is the best of the current systems, closely followed by both series and parallel active. This is borne out by current market trends which show the active damper approach as the most popular current implementation. The zero rate system, however, shows a clear lead over all other considered approaches which clearly supports further investigation.

Such a novel system is currently at the Engineering Division, University of Wolverhampton (Leighton, 1994). This system forms the basis for the control investigation undertaken as a key part of this thesis.

1.2.4 Developments in industry

Active suspensions attracted considerable attention in the mid-1980s with the widely publicised demonstrations of the Lotus Espirit experimental vehicle. Lotus and technical partner TRW have continued to develop their over-15-year-old fully active hydraulic suspension which has, in many ways, become the benchmark. Ford, however, is promoting a system powered by four electric motors that mimics the Lotus hydraulic design. The company feels it could finally push active suspensions into volume production (Sawyer,1994).

In October 1988, the application of a newly developed 'Electrically Controlled Suspension' in the CARAVAN/HOMY(E24) was announced by Nissan Motor Co. Ltd. (Kadota, et al 1994). This system is based on the 'Sonar Suspension' but includes the 'Load Sensing Type' used to supplement the performance under the empty and fully load conditions. 'Sonar Suspension' has a lower setting of the shock absorber damping force, a basic factor for ride comfort, thus providing a soft ride, and it is given the function of automatic damping force change-over, which is effected when a change of vehicle attitude is detected, so as to inhibit such change,

thus giving a flat ride. 'Load Sensing Type' is a two-mode control program on ROM, the two modes being 'empty' and 'loaded'. This method of control has proved effective for the car. However, the author has not found sufficient evidence to show which category this approach (sounds like semi-active) falls in.

The first narrow-bandwidth or 'slow-acting' (series active) production units were introduced by Nissan and Toyota (Hrovat, 1993). By using a piezo-electric sensor, a control system named the 'Piezo TEMS' (Piezo Toyota Electronic Modulated Suspension) has been invented by Toyota. In this system, a road surface roughness sensor using the piezo-electric effects and a rapid-response actuator using the reverse piezo-electric effects were developed. This system gives good driveability and vehicle stability with improved ride comfort (Fukami, et al 1994).

In addition, the 'slow acting' suspension is employed by Citroen currently in their Xantia model. Jaguar Cars Ltd. and General Motors are also developing their own active suspensions with, reportedly, good performance (Sunwoo, et al 1991; and Paterson, et al 1994). Many papers on control strategies have been reported by General Motors.

Active suspensions have attracted the attention from military orgnisations. US. Army Tank-Automotive and Armaments Command are applying this technique to enhance the off-road mobility of combat vehicles (Hoogterp, 1995). The hybrid electric drive active suspension integrates a Pentastar Hybrid Electric and a Lotus Active Suspension System into a modified approach, for missions that require capabilities beyond those of a standard prototype. This vehicle combines the improved off-road mobility of a fully active suspension system with numerous additional capabilities of the hybrid electric drive system (Nestico, 1995).

Co-operation between industry and universities is also reported in this area. An approach has been investigated by Coventry University and Jaguar Cars Ltd (Webb, et al 1996). The actuator is an oleo-pneumatic approach which combines the spring and damper into a single unit. The suspension falls into the series active category. A new approach of semi-active suspension has been implemented using adaptive sky hook control in Delft University of Technology, Netherlands (Venhovens, 1994). The prototype was tested at the rear axle of a VOLVO 480. The suspension of the series car had been modified to a hydropneumatic one by VOLVO. This enabled this implementation to be made easily.

It is thus clear that many companies are competing in this field to take full advantage of future markets.

1.3 Active Vibration Absorber

To provide high performance in ride comfort and handling, an ideal suspension system should produce:

- high vehicle body damping
- low transmissibility from wheel to body
- high wheel/hub damping

as well as accurately locating the wheel/hubs and resisting roll, pitch and yaw moments.

However, these requirements cannot be simultaneously satisfied by any of the active or passive systems considered thus far. This is because the damping of the unsprung mass can only be achieved by applying forces between it and the body, either by use of a conventional damper or through a wide bandwidth (and therefore high power) active actuator. In either case this results in a high frequency transmission path to the body, and hence a non-ideal ride. Therefore, only by introducing a second actuator can the conflict between ride comfort and good handling be resolved to a high degree (Castiglioni, et al 1992). One solution to this problem is to introduce an additional mass and actuator to act as a vibration absorber (Mackovjak, et al 1995).

Since its invention almost a century ago (Frahm, 1911), the vibration absorber has been an important engineering tool for vibration suppression. This simple device, often consisting of a reaction mass and a spring element with appropriate damping, has proven very effective for reducing severe vibrations of machinery, buildings, bridges and many other mechanical systems with relatively low cost. It is, by and large, an engineering design challenge to make effective active vibration control under constraints of weight and physical dimensions.

The vibration absorber is classified into the passive type, semi-active type, full active type and hybrid type as shown in figure 1-6. The last three types are called active vibration absorbers.

The passive type is most reliable, simplest and lowest cost, but it can not adapt to changes in resonant frequency of the primary system. A mis-tuned absorber can result in larger amplitude vibrations in the primary system. The semi-active type, in

which the stiffness and damping can be tuned automatically, can compensate for this drawback of the passive type but more cost and complexity are claimed. This type is also called an active tuneable absorber. In the full active type, the actuator works as the spring and damper in which the parameters and forces can be tuned automatically. This type of absorber is most effective but claims the highest cost and most unreliability and complexity. In the hybrid type, the conventional spring and damper and the actuator are connected in parallel between the absorber mass and the primary system. This approach allows the parameters of the equivalent spring and damper to be changed automatically around those of the passive components. This type can be as effective and complicated as the full active type but with lower cost than the latter.

Active vibration absorbers for various purposes have been investigated extensively (Seto, et al 1991; Olgac, et al 1995; Patten, et al 1996; Sun, et al 1995 and Herzog, 1994). Application in the control of vehicle suspension is also attracting attention from a few researchers (Elbeheiry, et al 1995). It has been proven theoretically that this approach is an effective method to obtain both ride comfort and good handling. Some researchers have made valuable progress.

Castiglioni et al suggested (1992) that the potential improvement, inherent in active suspension systems, can be considerably increased in combination with an active vibration absorber. In that paper, a series active suspension and full active type of absorber using hydraulic actuators was investigated through a quarter car model. It was shown that the weighted car body acceleration can be reduced to 15-20% of that of a passive suspension without aggravating the dynamic tyre load. The active suspension with the active vibration absorber was tested on a hardware-in-the-loop test stand.

A very practical suggestion has been given by Mackovjak et al (1995). In this approach, a vibration absorber suspension strut includes a sealed hydraulic damper mounted in an outer tube. An absorber mass is supported on a spring inside the outer tube. The absorber mass divides an interior of the outer tube into first and second fluid chambers. A fluid conduit is provided between the chambers. A control valve controls fluid flow in the fluid conduit to provide the desired damping of wheel hop frequencies. The damper is tuned to provide the desired damping of body frequencies. The absorber can be passive, full active or semi active type. The design for this integration of active suspension and active absorber is very clever and it can save space. In the author's opinion, however, this approach has some drawbacks. Firstly, in the semi active case, the tuned component is only the damper but the

performance of an absorber is more sensitive to its frequency than its damping. Secondly, in the full active case, the damping and frequency can be tuned through hydraulic force. The natural frequency of the hub and wheel is normally higher than 10Hz, so the hydraulic actuator requires a fast actuation and, therefore, a relatively high power input.

The literature in the area has shown that the application of active vibration absorbers to vehicle wheels is worth more attention. A novel approach has been devised and developed in this doctoral project. This approach is a semi active type in which the resonant frequency of the absorber can be tuned automatically to match that of wheels. Test results have demonstrated that the approach is effective. The details will be presented in the second half of this thesis.

1.4 Modelling of Vehicles with Active Suspensions

The design of active suspensions typically relies, in the early stages, on mathematical models of a vehicle, especially in the development of control strategies. Final performance of a suspension system depends on not only hardware in the system but also on the control strategy and the effectiveness of this strategy depends on the accuracy of the models used during development. Models need to describe the significant aspects of the vehicle and suspension dynamics, but also should be as simple as possible. Invalid models will undermine the performance of the resulting controllers. Precise models normally will involve many degrees of freedom and may be highly complex, which gives rise to computation problems. The foundation of an appropriate model is therefore a significant problem in this area.

The vehicle is generally modelled as a rigid body. It has six degrees-of-freedom, consisting of longitudinal, lateral, heave, roll, pitch and yaw, which are controlled by the suspension geometry and forces and are highly coupled. Moreover, as the suspension has a mechanical structure with unsprung masses, coupling also occurs between the sprung and unsprung masses. Despite such coupling problems, a reduced-order mathematical model representing a half-car or a quarter-car model is often used for theoretical analysis and design of active suspensions.

Some of the earliest studies using simple single degree-of-freedom models (figure 1-7) pointed to the desirability of 'sky-hook' damping (Appendix A) to realise an

optimal system (Bender, 1968). Such a model is still occasionally used (Oueslati, et al 1994; Karnopp, 1990; Sunwoo, et al 1991 and Hrovat, 1991, etc.). The model requires minimal mathematical analysis but it does not consider the coupling between sprung mass and unsprung mass which is often significant.

Two degree-of-freedom quarter-car models (figure 1-8) have been widely used, possibly due to their simplicity and inclusion of the interaction of sprung and unsprung mass (Lin, et al 1993; Burton, et al 1995; Truscott, 1994; Ben Mrad, et al 1993; Levitt, et al 1991; Lieh, 1992 and Hac, et al 1992, etc.). This type of model has been extensively used to develop control methods and identify significant factors. For instance, bilinearity of a semi-active suspension (Yi, et al 1993) and nonlinear behaviour of an active suspension (Palkovics, et al 1993) were investigated; optimal control laws typically by LQ method were designed (Ray, 1992 and Hrovat, 1993, etc.); the effects of component nonlinearities on the ride performance of a hydro-pneumatic slow-active suspension system were studied theoretically (El-Demerdash, et al 1996); various control strategies such as adaptive control (Huisman, et al 1993), robust control (Ray, 1992), etc. were studied.

However, the coupling between heave and roll or between heave and pitch motions can also be significant in the behaviour of an active control system. In this case, a half-car model (figure 1-9) which can include either roll or pitch as well as heave motions is required. Such models have been applied by many investigators (Moran, et al 1992; Hrovat, 1991; Foag, 1989; Harrison, 1993; Salman, et al 1990; Hac, et al 1993 and Pilbeam, et al 1993, etc.). Based on such models, preview controllers were designed in more practical conditions (Hac, et al 1993). Controllers have been designed by means of H_∞ control theory (Moran, et al 1992), LQ optimal technique (Harrison, 1993) and neural network (Moran, et al 1993). Generally, the half car model is believed to be precise enough for active vibration isolation and attitude control of heave and roll or pitch.

Full-car models allowing simulation of all six degrees of freedom have also been used by some researchers (Lieh, 1993; Venhovens, et al 1993; Abdel Hady, et al 1989; Hedrick, et al 1990 and Cech, 1994, etc.). These require much more computation and complexity, so most of the applications were restricted to response simulation and were not generally used to develop control strategies.

Structural vibration of vehicle bodies can have an effect on the acceleration levels on the passenger seats, as a result of transmission through the floor and body panels which contributes to deterioration in subjectively perceived ride quality. One way of

reducing the structural vibration is to increase the body stiffness, which requires major design changes and usually results in increased body weight. Another option is to mitigate the problem through changes in the suspension controllers that account for body flexibility. The vehicle body therefore was modelled as a flexible structure by some researchers (Hac, et al 1994 and Lieh, 1992). It was shown from simulation that this approach introduces a balance of complexity and performance.

The models used by most researchers are linear or linearised, which is convenient for the analysis and design of the control algorithm. However, controllers designed around linear models do not always perform well in reality. The reason for this is that most practical active suspensions are nonlinear; for example, the orifice flow of hydraulic fluid and Coulomb friction forces in the actuator seals give rise to nonlinearities in an electro-hydraulic actuator (Alleyne, et al 1993); another example, semi-active actuators are typically bilinear systems (Yi, et al 1993).

Some investigators have, therefore, begun to deal with nonlinear models. Leighton et al (1994) investigated the zero rate suspension theoretically and experimentally based on a nonlinear quarter-car model. Webb, et al (1995 and 1996) presented the results of investigative study involving the performance of a non-linear vehicle suspension system configured in a low bandwidth suspension with an oleo-pneumatic actuator. Moran et al (1993) analysed the performance and dynamic behavior of artificial neural networks for forward and inverse dynamics identification and control of vehicle active suspensions with nonlinear characteristics. An observer for a bilinear semi-active suspension system was developed with completely unknown disturbances (Hac, et al 1992). Observer design for nonlinear and linear system was studied theoretically and experimentally by Hedrick et al (1994). Moved by the strong need for realistically describing the dynamic behaviour of automotive systems through adequate mathematical models, a computer-simulation-suitable nonlinear quarter car model of hydraulic active suspension system was developed (Ben Mrad, et al 1994). A nonlinear vehicle model with semi-active suspension was used and optimised by Hook-Jeeves method (Demic, 1996). Palkovices et al (1993) considered a suspension actuator as a retarded nonlinear active element which means that the feedback force is a nonlinear delayed function of the state-variables and investigated the chaotic behaviour of the suspension system based on a third degree function model.

The models mentioned above are reasonably effective for controller design for vehicle suspensions, but they are ineffective for a design engineer to understand the mechanism of suspension structures. Multi-body dynamics provides an effective

technique for this type of problem. This approach has been applied in vehicle dynamics simulation packages (Sharp, 1994 and Lee, et al 1993). The multi-body model was applied to the design of nonlinear tracking and adaptive control laws (Blankenship, et al 1993 and Cherry, et al 1995). It is expected that utilising this approach, an engineer can determine the direct effect of suspension changes on vehicle handling on a simpler and more easily understood model (Wang, et al 1993). The introduction of this approach, of course, results in more complexity. For example, nonlinearity can often be involved, which leads to problems when designing suspension controllers. Non-holonomic (Sharp, 1994) constraints (involving non-integratable relationships between velocities) can also be included in a multi-body vehicle model by assuming that the tyres roll without sliding, which can cause another big difficulty for designers. Multi-body models may be characterised as potentially containing a huge number of small terms, which contribute greatly to solution times but contribute very little to the accuracy of the solution. These mean that an expensive investigation needs to be carried out.

1.5 Control Strategies and Implementation

Various control theories or control concepts have been introduced to improve the performance of active suspensions. Extensive results have been obtained both theoretically and experimentally.

Perhaps 'sky-hook' damping is the most popular and simplest control concept in this area (this concept is explained in Appendix A). As is well known, vehicle suspensions must fulfil two different requirements: good ride quality and high running stability. In passive suspensions, with a fixed-coefficient damper, good ride quality requires 'soft' coupling between the sprung and unsprung mass, whilist high stability requires 'hard' support of the sprung mass. The conflicting problem can, to some extent, be resolved by adopting a so-called imaginary 'sky-hook' damper which involves a damping force proportional to the sprung mass absolute velocity and can be realised only in an active system. This concept has therefore attracted much interest since the early years in the field (Bender, 1968; Venhovens, 1994; Cebon, et al 1996; Williams, 1994 and Alleyne, et al 1993, etc.).

Preview is another one of the most popular control concepts (Foag, 1989; Hac, et al 1992; Huisman, et al 1993; Moran, et al 1993; Pilbeam, et al 1993; El-Demerdash, et al 1996 and Youn, et al 1993, etc.). The preview approach for full-active

suspension systems has been studied by many researchers. The results relating to slow-active systems are investigated by Pilbeam et al (1993). The approach was refined in discrete time systems by Prokopet et al (1995). This work exploits the potential for preview sensors from research associated with automotive guidance (Appleyard, et al 1995). It is shown by the publications that, in the implementation of active suspensions, the actuator's force and bandwidth bottle-neck cannot be widened by any feedback control law. The only way to achieve this is to supply the control scheme with knowledge about approaching roadway disturbances in advance. A preview control scheme can synchronise required and actual suspension force in a much more elegant and efficient way. It anticipates road disturbances instead of reacting only after the disturbance has passed the tyres. Therefore preview can not only reduce power requirements, but also improve ride comfort and road profile following simultaneously. However, preview sensors have not yet been developed to a satisfactory level and are likely to be costly.

Optimal control techniques have been used extensively to design controllers for suspension systems in the last decades. Linear-quadratic (LQ) control laws are able to produce stable control systems with adequate gain and phase margins in each feedback loop. These have been applied by many researchers (Hrovat, 1993; Lieh, 1993; Oueslati, et al 1994; Prokop, et al 1995; Lin, et al 1996; Hac, et al 1992; Harrison, 1993 and Huisman, et al 1993; etc.). Suspension models, however, inevitably contain uncertainties in parameters and actuator and sensor dynamics that can consume stability margins and degrade optimal performances. The relationship between tolerable uncertainty and stability margins was considered by many of the above researchers to be good candidates for robust control system design using LQ control laws. Ray (1992) presented stability robustness analysis and synthesis of robust stochastic-optimal control laws for a quarter car model containing uncertain parameters and uncertain sensor and actuator dynamics. Stochastic robust analysis was used in his linear quadratic Guassian (LQG) control system. The robustness of various active LQ and LQG automotive suspensions was investigated for both uncertainties (Ulsoy, et al 1994). It was observed that LQ controllers for active suspensions do not necessarily have good stability robustness properties when their weighting matrix in the performance index is not zero. The differences of performance and robustness between the LQ and LQG design depend heavily on the ride characteristics desired.

Optimal controllers minimise a defined performance index but do not have the capability to adapt to significant system parameter changes. In contrast an adaptive control scheme monitors the input disturbances, parameter variations and/or

structure variances and hence redetermines controller parameters and/or configurations via on-line adaptive algorithms. By adapting to these uncertainties, an adaptive controller aims at preventing degradation in the performance of a system. Furthermore, rapidly developing computer technology has made the implementation of adaptive control an affordable reality. Current hardware technology and knowledge of modern adaptive control theory has led to extensive investigations (Williams, 1994; Dukkipati, et al 1993; Vallurupalli, et al 1993; Kim, et al 1993 and Elbeheiry, et al 1996; etc.). Sunwoo et al (1991) presented a model reference adaptive control (MRAC) scheme for an active vehicle suspension that is capable of providing superior suspension performance and adapting to changes in vehicle suspension characteristics. For a realistic evaluation, nominal characteristics of actual commercial vehicle suspension components were used for design and simulation. A composite adaptive controller, which consists of an identifier part and a control synthesis part, was developed for active suspension (Truscott, 1994). The benefits of the composite control and adaptive vibration control was demonstrated theoretically in that paper. The trade-off between road holding and ride comfort can be relaxed by using adaptive semi-active suspension control based on the tyre load variations (Venhovens, 1994). The experiment showed that the suspension controllers can be implemented extremely quickly by using his dSPACE tools. The nonlinear 'sliding' control law was applied by Alleyne et al (1995) to an electro-hydraulic suspension system. The controller relies on an accurate model of the system. To reduce the error in the model, a standard parameter adaptation scheme, based on Lyapunov analysis, was introduced and a modified adaptive scheme was developed. Simulation and experimental results showed that the active system is better than a passive system in terms of ride quality. Furthermore, both of the adaptive schemes improve performance, with the modified scheme giving the greater improvement in performance.

A new robust optimal control design method, H_∞ control theory, is causing interest in this area (Michelberger, et al 1993 and Nagai, 1993). The main advantage of using the H_∞ approach is the preservation of controller robustness when unmodelled dynamics, nonlinear behaviour, parameter variation and sensitivity to perturbations play an important role in the system response. Likewise, this approach is useful for highly coupled multivariable systems and when the design requirements cannot be easily expressed in terms of the desired closed loop modal characteristics. It has been suggested (Nagai, 1993) that a controller designed by H_∞ control theory provides better robustness than that designed by LQG optimal theory. This H_∞ approach is based on minimisation of the H_∞ norm in which suspension

performance can be designed in the frequency domain. Therefore it is possible to consider ride quality criteria such as ISO 2631 (1974) in the controller design such as the optimal design method minimising the frequency shaping performance index. H_∞ theory has also been applied to the integrated control of vehicle steering and suspension to cope with nonlinear interaction of tire forces (Moran, et al 1992).

Other control theories are being studied in the area of active suspension. Artificial neural networks (ANN) have been applied to active suspension control design to cope with the nonlinearity, and to realise an 'intelligent' suspension by incorporating learning capability (Moran, et al 1993). According to computer simulation, active suspensions controlled by a neural network show better vibration isolation properties than those designed with LQG theory. Such a promising result has caused other scholars' interest and the paper was evaluated as 'the first work' (El-Gindy, et al 1993). To achieve the safety and ride quality improvement, Yoon et al (1996) proposed a frequency and time-mixed shape performance index with speed and road-adaptive preview logic for the design of their feed forward neuro-controller.

Another artificial intelligence control strategy employed in the area is fuzzy logic. It has been shown through simulation (Cherry, et al 1995) that the use of fuzzy logic has some advantages. First, the vague linguistic nature of the control strategy suits the subjective descriptions of vehicle ride handling behaviour used in the industry. Secondly, all rule-based controllers benefit from being independent of a representative system model. Thus the performance will be unaffected by any nonlinearities or unmodelled dynamics, although either a prototype vehicle or a realistic model will be required for evaluation and tuning. Finally, for some applications, a continuous output can be achieved via interpolation, without a significant increase in the number of rules required. The fuzzy logic tuning of controllers to changing process and environment dynamics is also a recent approach for active suspensions (Yeh, et al 1994). A model reference self-tuning fuzzy logic controller has been developed for a quarter-car model (Lin, et al 1993).

On the whole, extensive research on active suspensions has been reported. Over one hundred relevant papers in this area have been published in the last three years. However, much of this controller development has been evaluated only on models and relatively few have been implemented. Whilist the theoretical investigations have been extremely encouraging, the implementation of high performance controllers in actual systems is not widely reported which may cast doubts on the validity of the techniques.

1.6 Structure of the Doctoral Project and the Thesis

This project aims to develop a high performance control system using the novel zero-rate suspension system. The completed activities are broken into the following stages:

i) Development of a control system for the prototype based on a PC computer and appropriate interfaces to the existing power electronics and sensors.

ii) Modelling the two wheeled trailer with the zero rate suspension as a nonlinear multi input, multi output (MIMO) half car model in which the limited bandwidth is included; and validating the developed model based on the test results.

iii) Development of the required control software in C++ for various control strategies.

iv) Applying various control strategies, namely PD, MIMO PID, Fuzzy Logic and LQG, to the zero rate suspension. The application includes design, simulation and implementation of the controllers in the prototype.

v) Investigation of the performance of the various control strategies for the prototype in terms of the ride comfort and handling.

vi) Investigation of the effect of nonlinearity, actuator bandwidth and other factors on the instability of the test rig based on the nonlinear model.

vii) Developing an active tuneable vibration absorber (ATVA) and its control system from concept to the prototype. The development includes building the required test rig; designing and implementing the ATVA, the control algorithm, hardware, software and required interfaces; and evaluating the developed prototype by both simulation and experiment.

viii) Predicting the performance of the combination of the developed ATVA and the zero rate suspension controlled by the MIMO PID with sky hook damping by using simulation of the nonlinear half car model under random road excitation.

ix) Developing a PC based measurement system for identifying the transfer function of automotive suspensions from concept to the prototype. This includes designing and implementing the required mechanical configuration, electronic interfaces, required computer software and processing algorithm. The developed prototype was validated against two standard test rigs.

These activities have been completed successfully. This thesis is submitted for the degree of PhD.

The thesis has twelve chapters and the remainder of which may be summarised as follows

- The test rig for the zero rate suspension is described in Chapter 2.
- The developed measurement system for identifying the transfer function of vehicle suspension systems is presented in Chapter 3.
- The modelling process for the open loop system and the validation of that model are outlined in Chapter 4.
- The development, implementation and nonlinear behaviour of the zero rate suspension system with PD controllers is introduced in Chapter 5.
- The design, implementation and performance of the zero rate suspension system with coupled PID controller are investigated in Chapter 6.
- The comparison of various control strategies applied to the zero rate suspension system is made in Chapter 7.
- The development of active tuneable vibration absorbers (ATVA) is discussed in Chapter 8.
- The implementation and test results of the ATVA are presented in Chapter 9.
- The performance of a half car model with the zero rate suspension system and the developed ATVA is predicted through simulation in Chapter 10.
- Finally, the conclusions are summarised in Chapter 11 and future work is suggested in Chapter 12.

Feature	Weight -ing	Fully active	Series active	Parallel active	Semi active	Zero rate
Cost	5	0	2	1	5	3
Electronic complexity	1	0	0	0	5	0
Power consumption	5	0	2	1	5	4
Radical vehicle change	5	0	2	2	5	0
Packaging difficulty	3	0	1	1	5	0
Failure modes	2	0	2	3	5	3
Ride height control	4	5	3	4	0	4
Sky-hook damping	2	5	2	4	0	4
Roll/pitch control	4	5	3	4	0	4
Ride quality	5	2	4	3	0	5
Ride/handling decoupling	2	5	3	3	0	5
Degrees of control	2	5	5	5	0	5
Total unweighted	-	27	29	31	30	37
Total weighted	-	80	101	100	105	126

Table 1-1. The comparison of active suspensions. Desirable features are weighted and the effectiveness of each system in providing the feature is rated from 0 to 5, with 0 representing the least effective system and 5 the most.

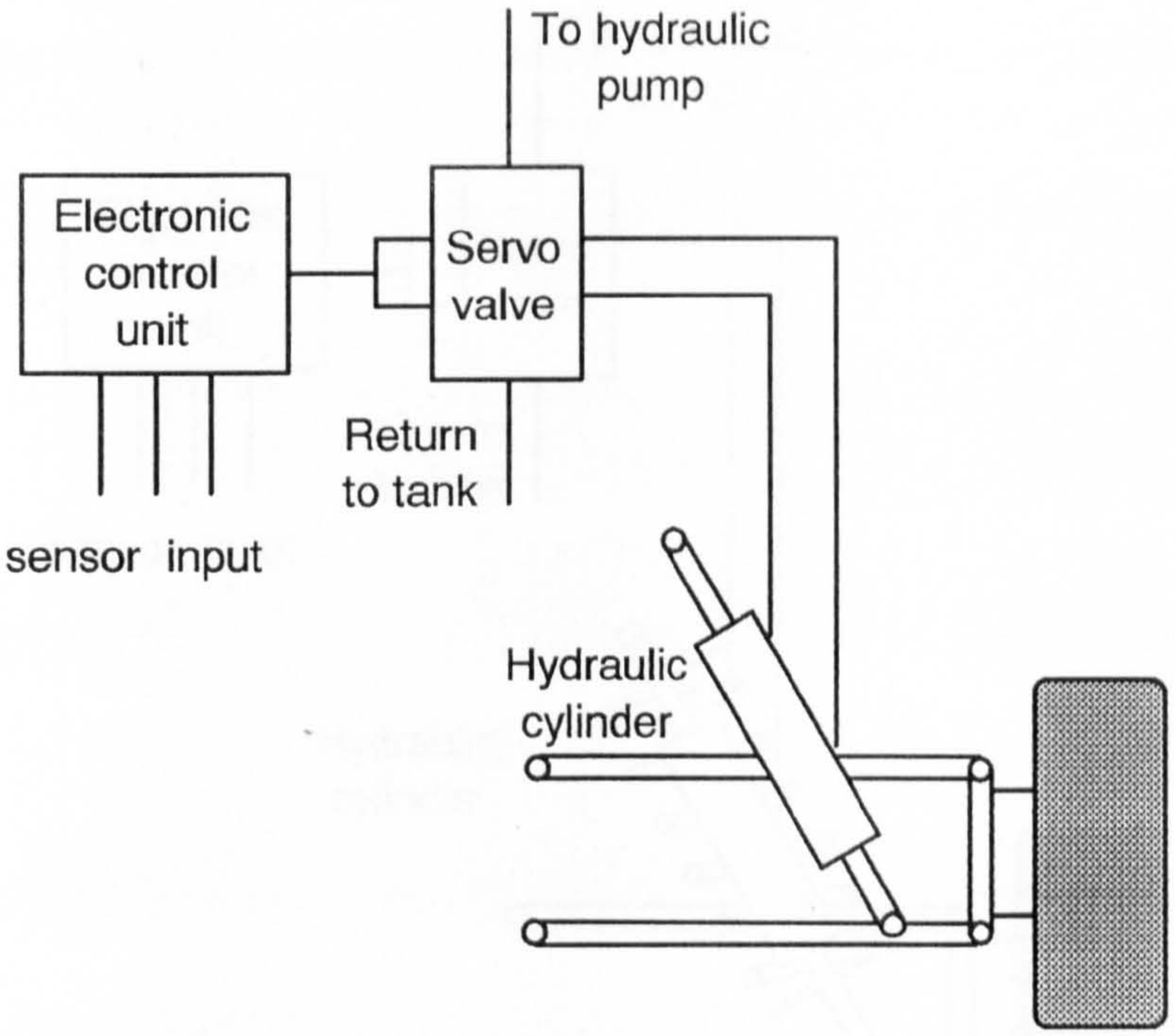

Figure 1-1 Fully active system

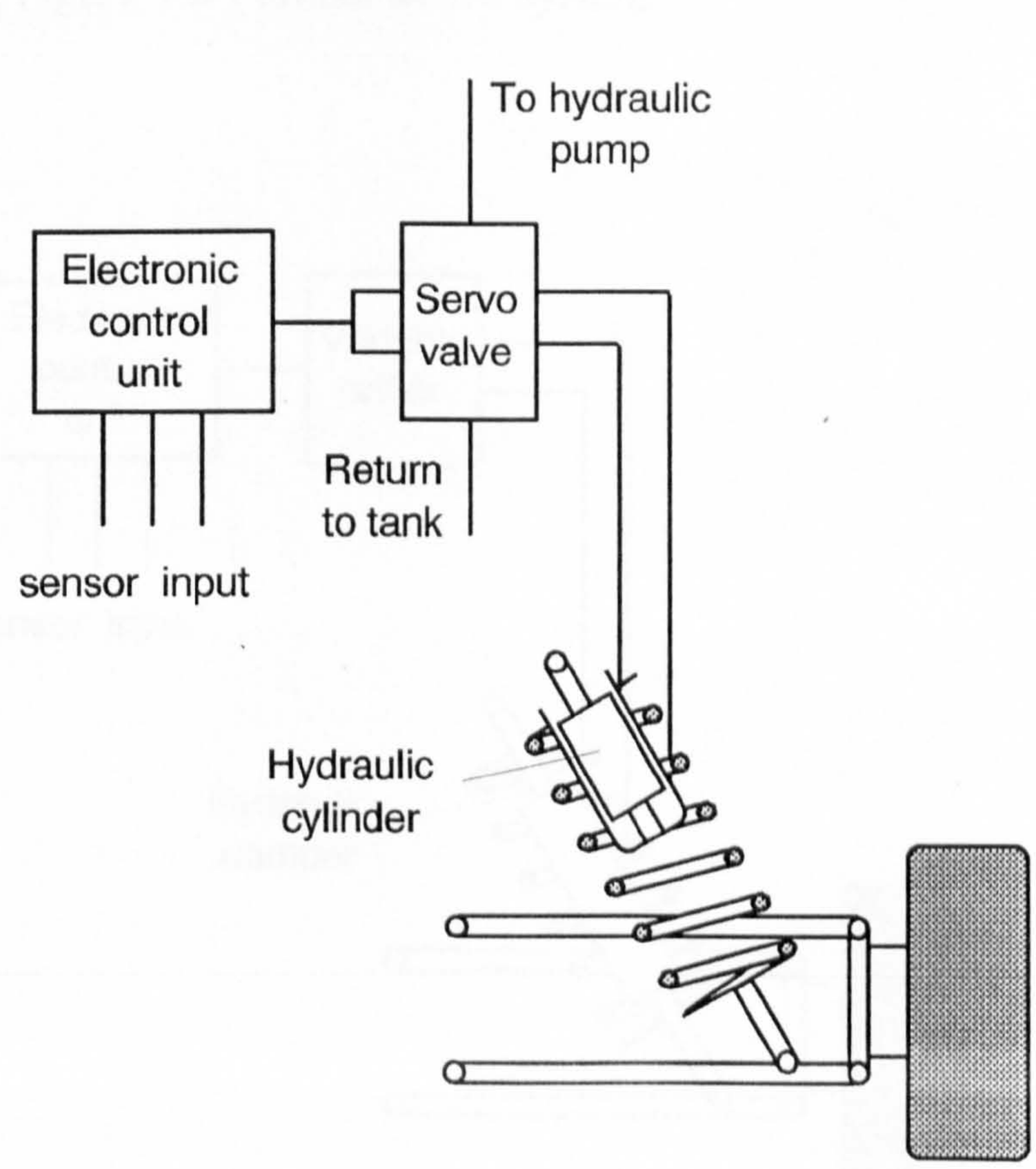

Figure 1-2 Series active system

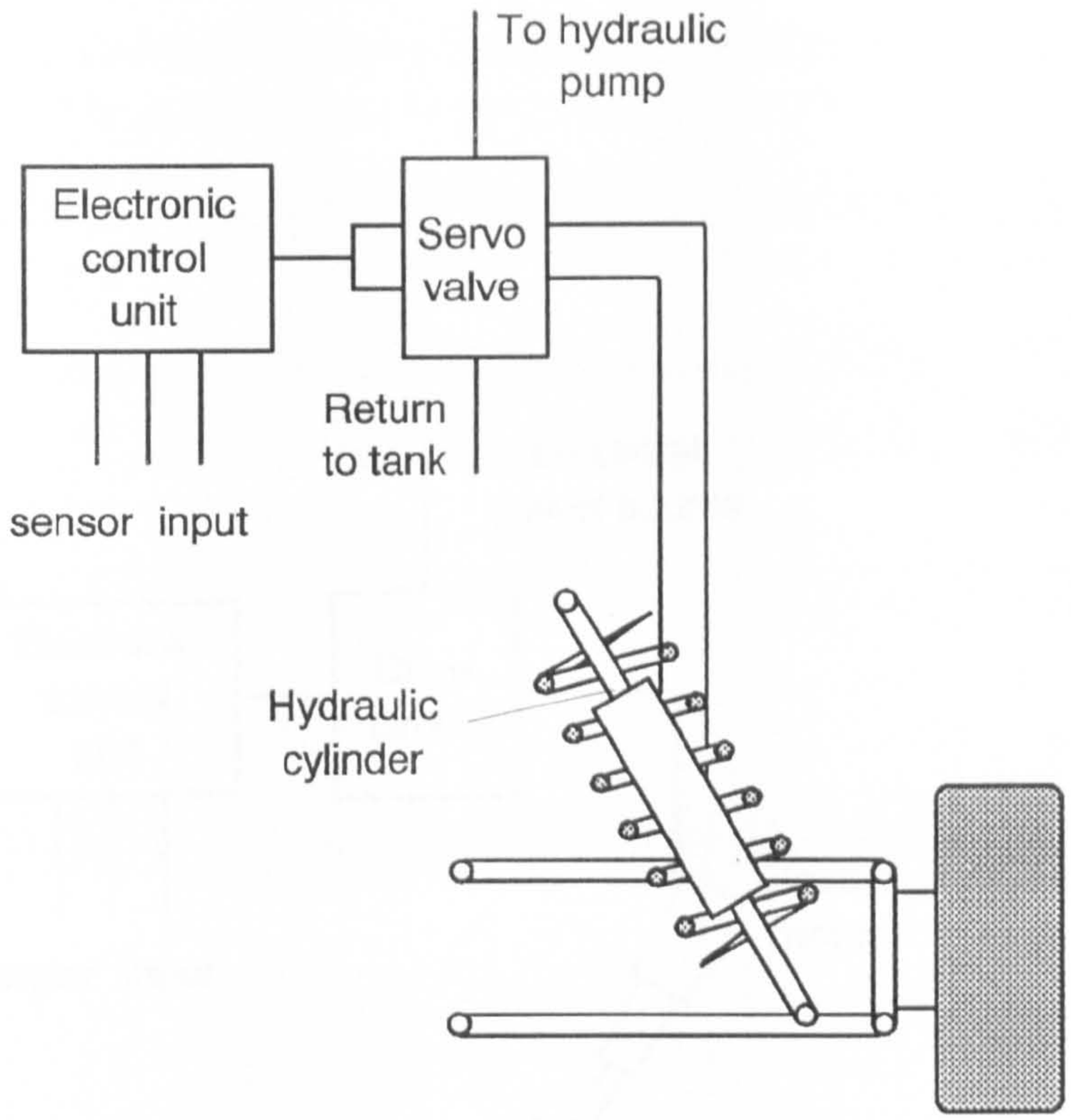

Figure 1-3 Parallel active system

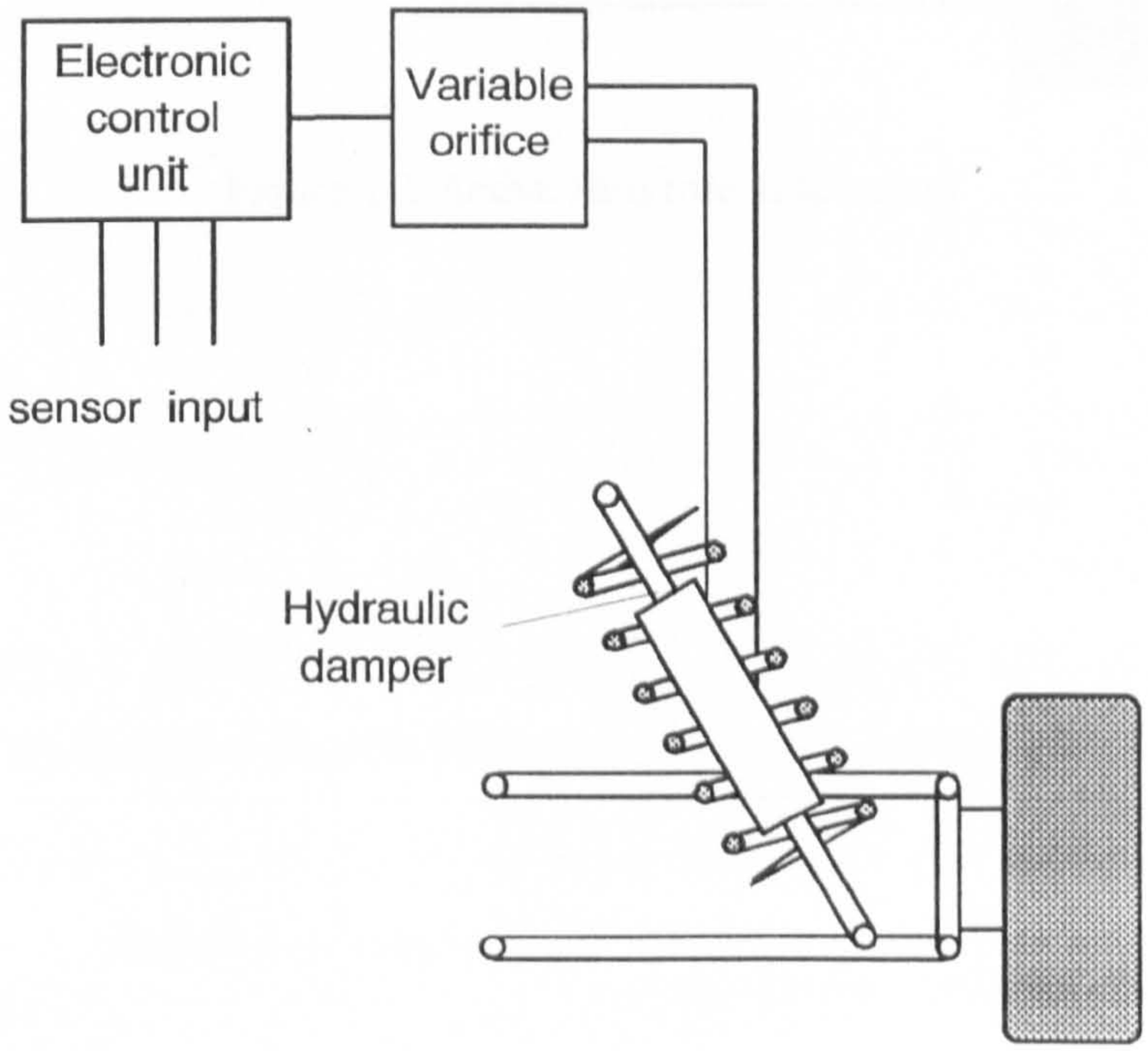

Figure 1-4 Semi active system using active damper

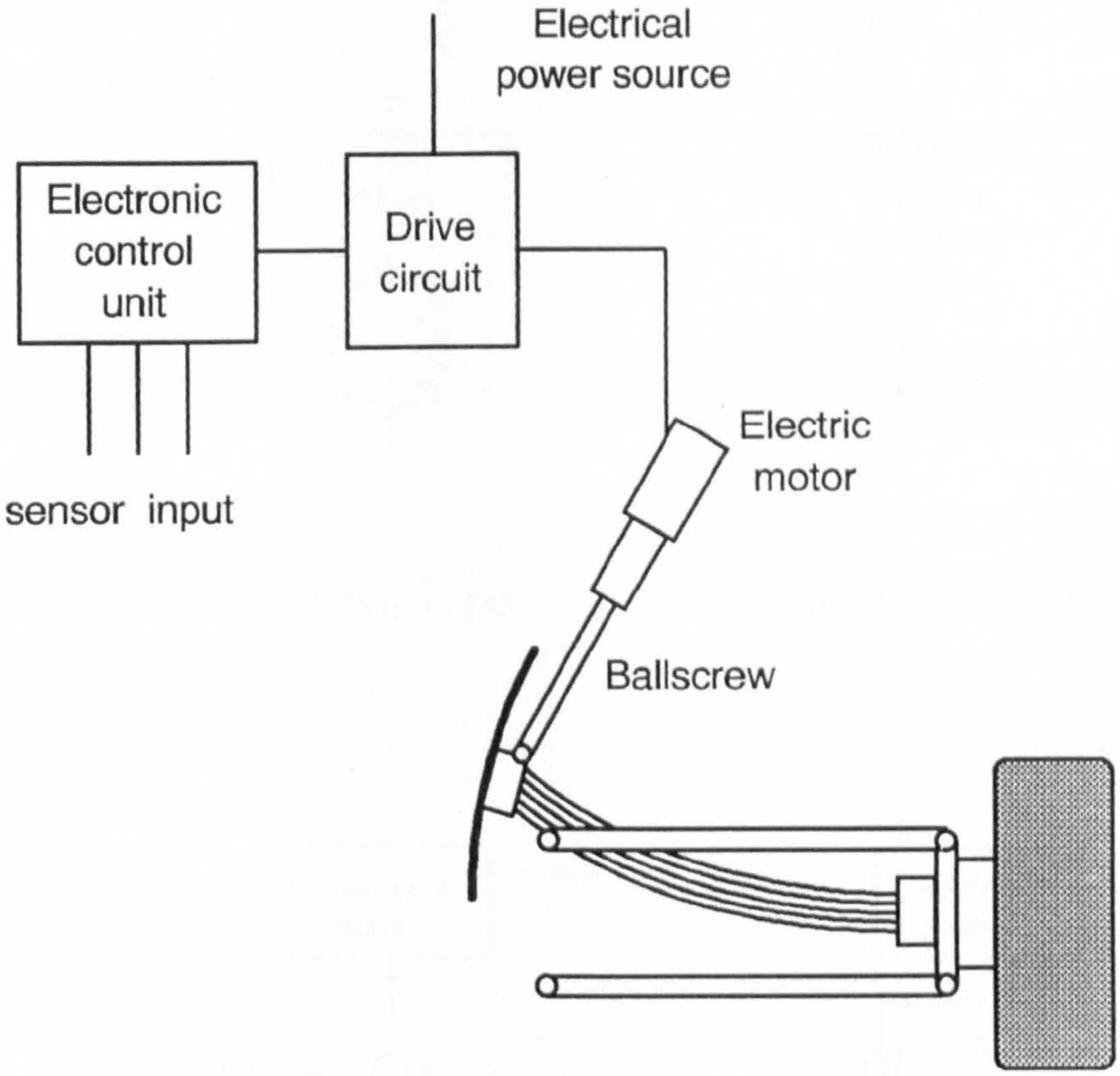

Figure 1-5 Active zero rate suspension

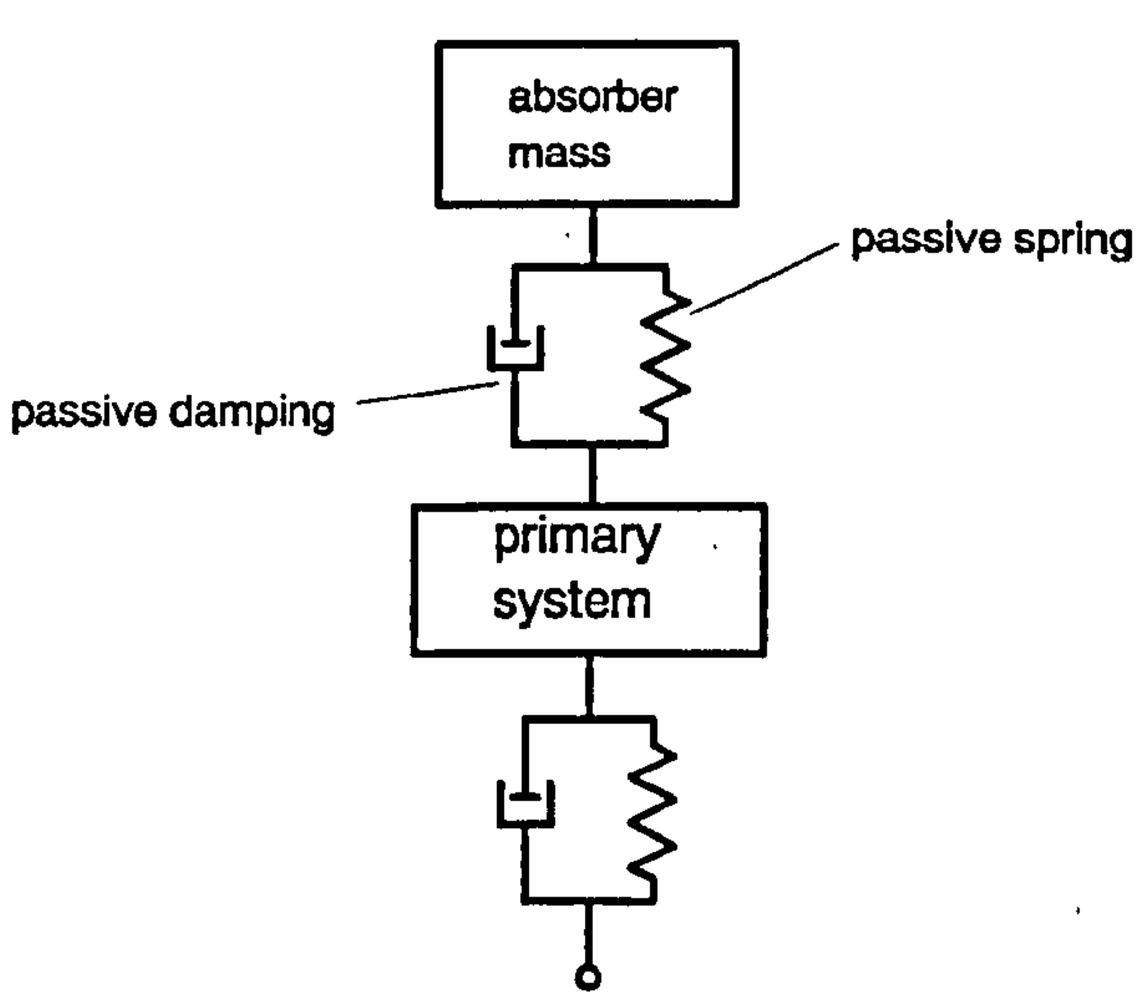

Passive Type

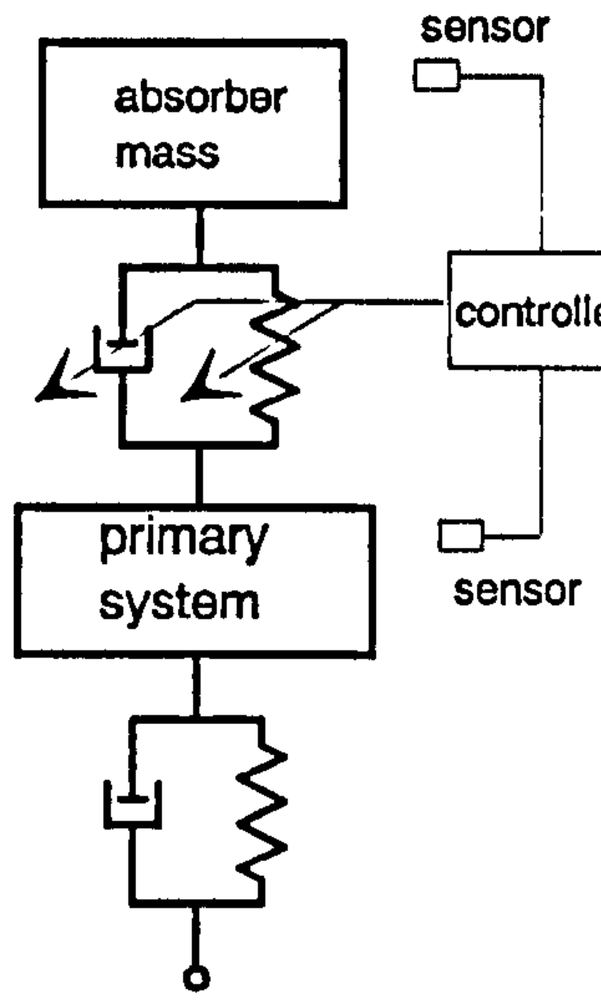

Semi Active Type

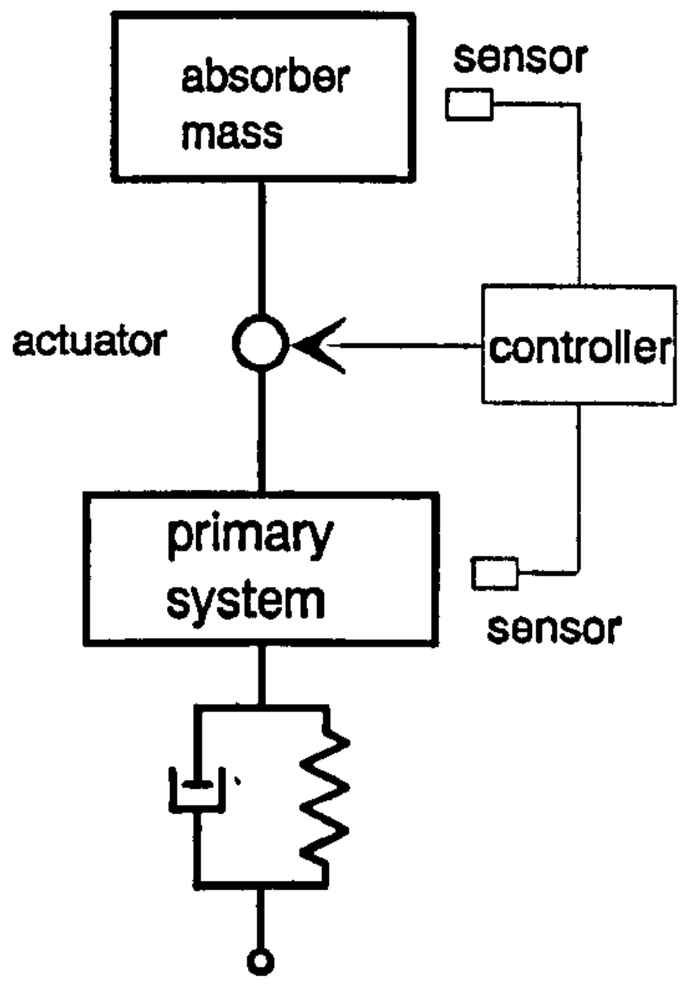

Full Active Type

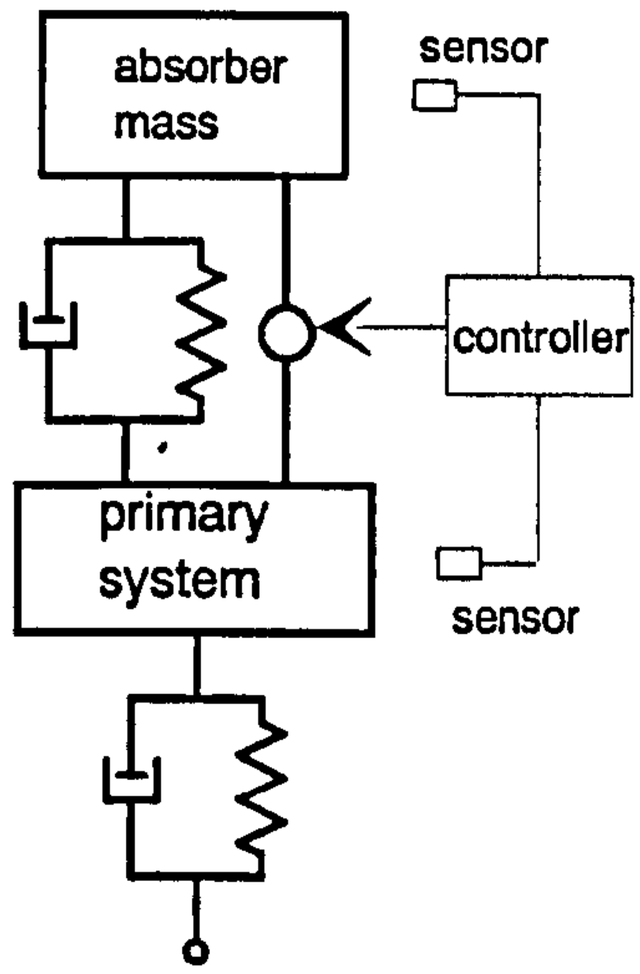

Hybrid Type

Figure 1-6 Types of passive and active absorbers

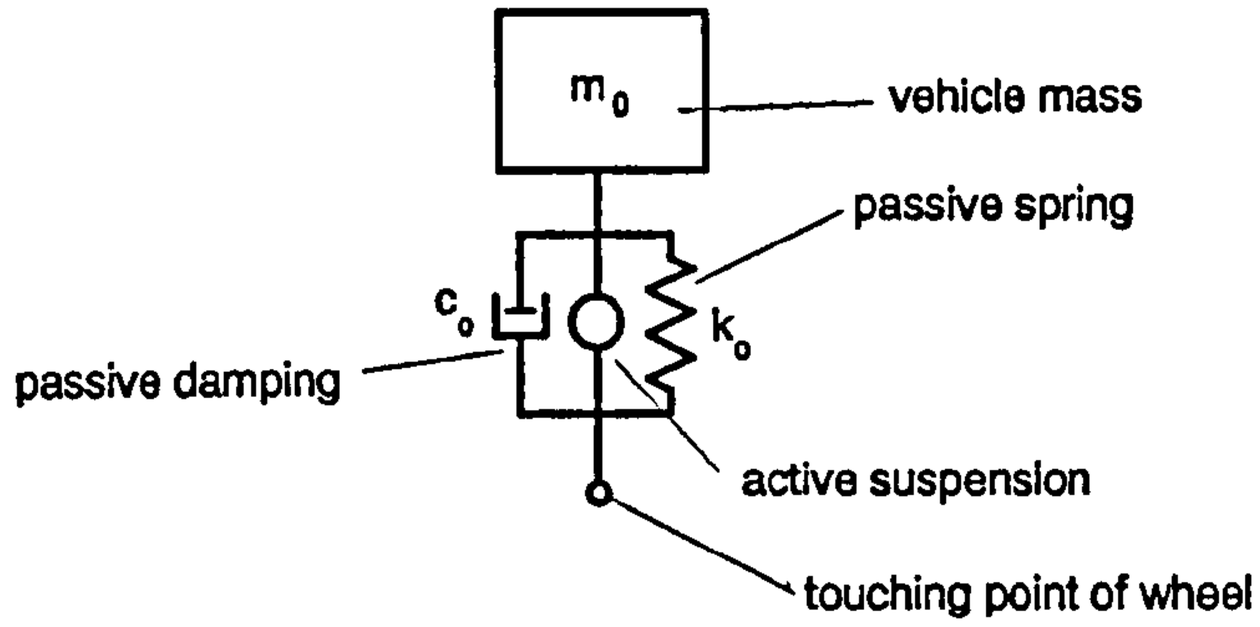

Figure 1-7 A typical one degree-of-freedom quarter car model

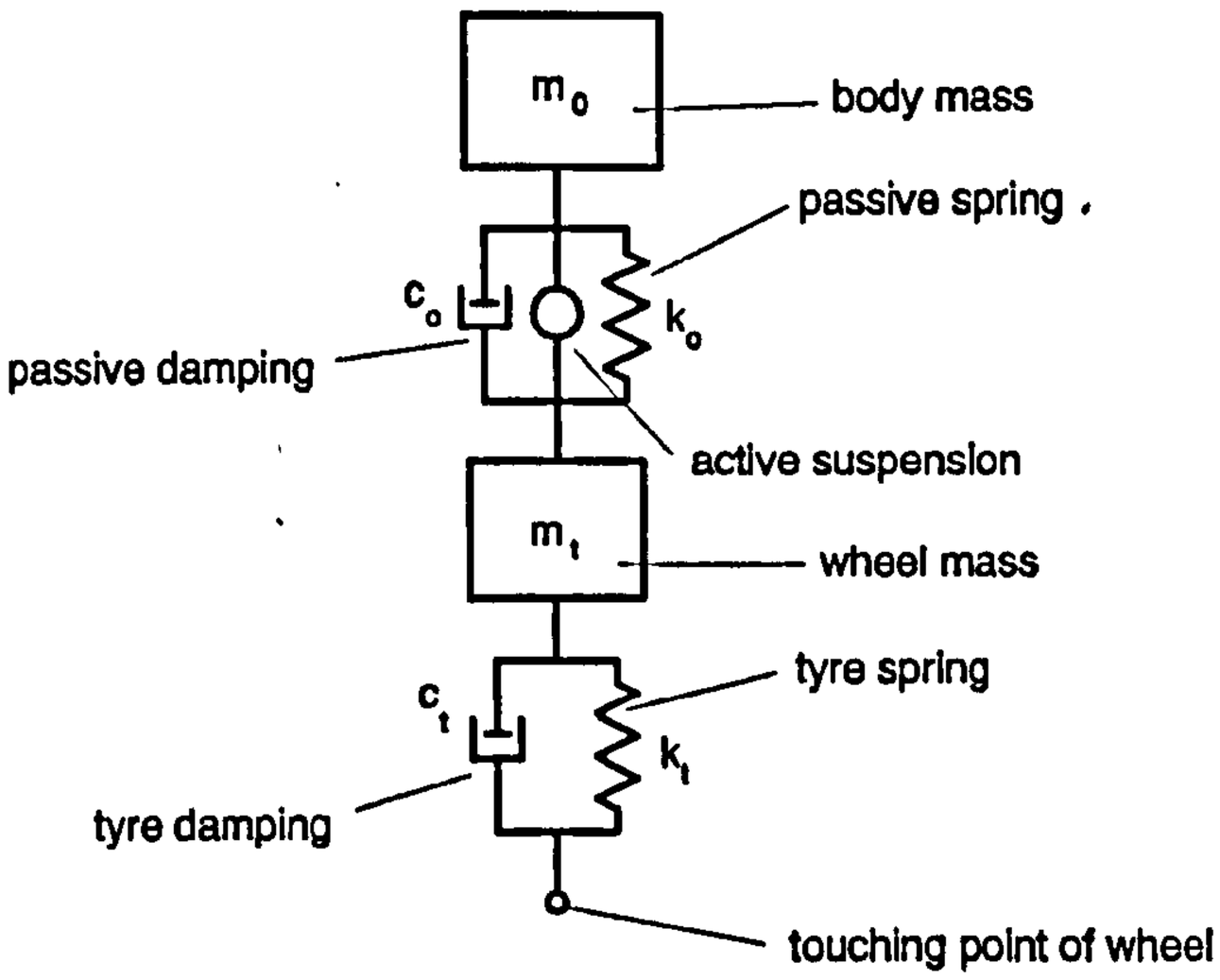

Figure 1-8 A typical two degree-of-freedom quarter car model

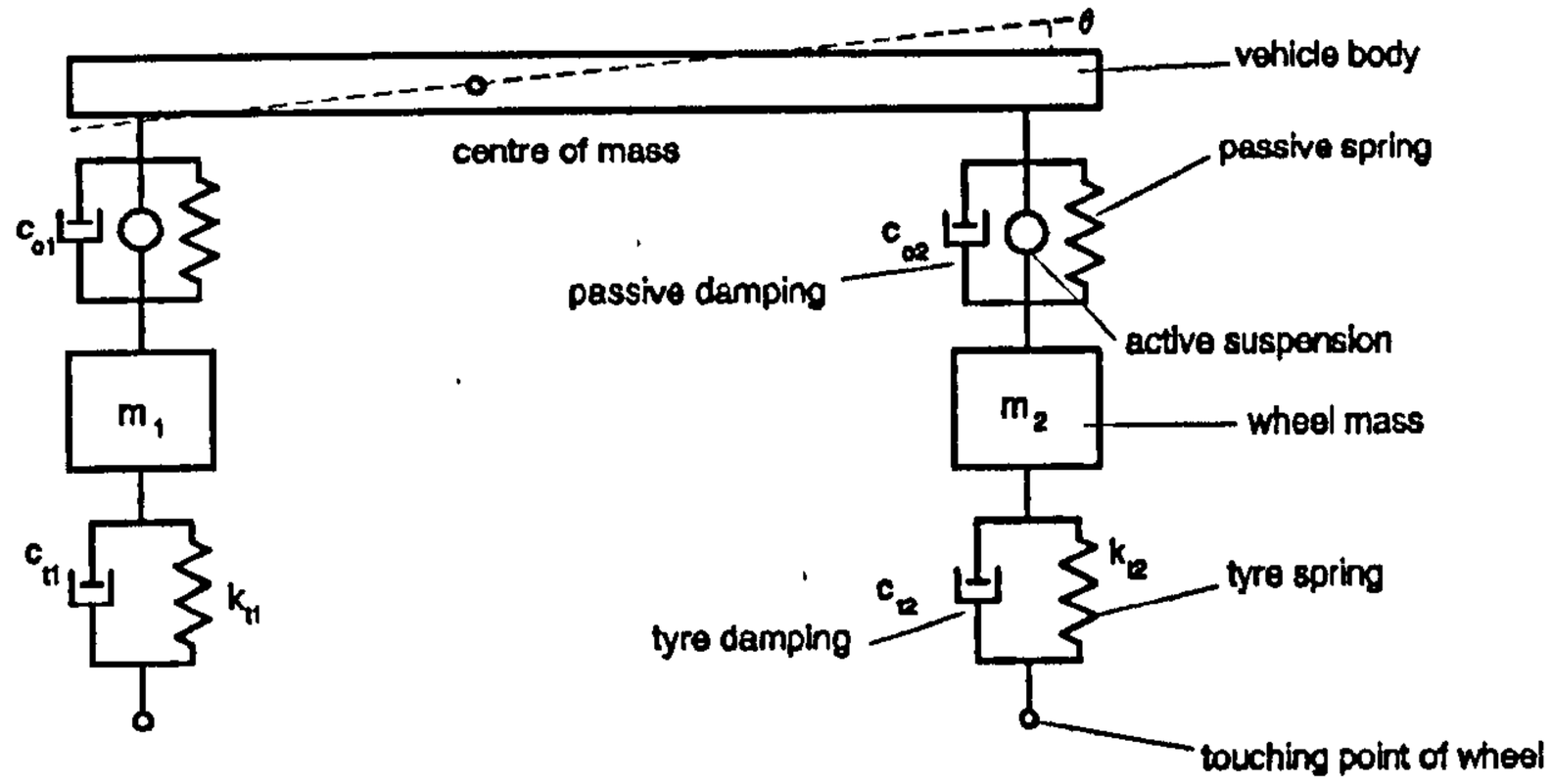

Figure 1-9 A typical four degree-of-freedom half car model

Chapter 2

Description of the Test Rig

2.1 Introduction

Three test rigs have been built in the Engineering Division, University of Wolverhampton. They are the two-wheeled trailer with zero rate suspension system, the quarter car unsprung mass test rig with active tuneable vibration absorber and the measurement system for identifying transfer functions of automotive suspensions. The first test rig will be introduced in this chapter and the others will be discussed in the relevant chapters.

The first test rig is the two-wheeled trailer in which a pair of the zero rate active suspensions and control systems are installed, as shown in the figure 2-1. It consists of the two wheeled trailer, the zero rate active suspensions, the transducers, the power amplifier, the analogue position control system and the digital control system. These parts will be introduced individually as follows.

2.2 Trailer and Zero-Rate Active Suspension

To minimize costs a two-wheeled trailer shown in figure 2-2 is used which could be towed by a conventional vehicle. The dimensions and weights of the trailer together with some aspects of the suspension geometry were designed to recreate the conditions seen by the rear suspension of a family hatchback (Ford Escort).

A set of buckled springs are installed between the hub and a track on the trailer body. The inner end of the spring is fitted to a curve track with a wheeled spring carrier pin jointed to the end of the ball screw section of the actuator, as shown in figure 2-3.

This arrangement is adjustable to allow the geometry of the spring path to be trimmed. It ensures that the correct, circular arc, path is followed by the actuator and minimises

friction in the actuation system, thereby easing the task of the actuator position control loop.

The primary components of the actuation system are a ball screw and motor. Their selection was based on the loads determined by the static model and the bandwidth predicted by the dynamic model which was discussed by Leighton (1991).

The motor is produced by Electro-craft Ltd, and is a S19-3A/T brushed ferrite cored motor/tachometer. Its continuous output is 433(watts), Max. continuous torque 1.35(Nm) and Max. no load speed 4500(rpm).

The ball screw is manufactured by S. K. F. Ltd. Its type is CCBR32 Ball screw cylinder. The pitch is 4(mm) and stroke is 125(mm).

2.3 Transducers

The suspension control system is required to take signals from the body displacement sensor and body acceleration sensor and produce an appropriate demanded actuator position signal according to the algorithm developed.

Before the PhD project was started, the installation of the transducers and the corresponding conditioning circuits had been built at GKN Technology. These are two position sensors for the actuation system, two body-to-wheel displacement sensors and two body acceleration sensors on the trailer body. The transducers can provide the information of the state of the actuators and the motion of the trailer body and wheels. The installation has been proved experimentally to be sufficient for the control of the zero rate suspensions.

The body displacement sensors are subject to frequent cyclical motion at a high frequency which eliminates the possibility of using a contacting sensor. Of the non contacting sensors two primary technologies exist; Linear Variable Displacement Transducers (LVDT) and Linear Variable Inductance Transducer (LVIT). The LVIT type of device was selected primarily because it is a potentially very low cost technology, although it is still a very new technique. The sensors were produced by Lucas Automotive Sensors.

The body acceleration sensors could be obtained from a number of sources with a variety of technologies. Again all possible approaches were considered and a micro-machined silicon selected, again from Lucas Automotive Sensors. This is again a

technology capable of producing very low cost devices and is aimed specifically at suspension control systems.

2.4 Analogue Control and Power Amplifier

The control system falls into two categories; the analogue system controlling the actuator position and the digital system controlling the suspension system, as shown in figure 2-4. Since they are basically different they will be considered separately.

The actuator control system had to take position demands in the form of a voltage from the overall suspension controller and translate these into a power drive signal to the motor to cause the actuator to move to, or maintain, this demanded position. The system was designed to give a 5Hz bandwidth and to be capable of holding position to within 0.1(mm) with a 3000(N) actuator load, as suggested by GKN Technology (Leighton, 1991) and proved to be true by the experiment in the following chapters. There are two main sections in this control system; the power drive system and the position control system.

The power drive system had to provide a motor current of up to 25(amps) at a voltage of 60(V) (supplied by a bank of lead-acid batteries) with current limiting to prevent motor overload. The drive circuit incorporates current feedback so the input to this part of the system is a current demand from the position control system. The motor drive circuit uses Pulse Width Modulation to control the voltage applied to the motor since this is the most efficient technique in terms of power utilisation.

The use of a 60(V) supply was imposed by the need to use a standard servo motor; selecting a custom wound motor would have increased cost and required higher current drive devices. Any vehicle installation would have lower voltage units capable of running from a standard vehicle battery.

The position control system uses purely analogue devices and employs a velocity feedback loop to improve dynamic response. This technique is standard for Numerically Controlled machine tool and robots where similar demands for high accuracy and rapid response exist.

The actuator position is measured by a linear potentiometer fitted alongside the ball screw and the motor velocity is measured by a tachometer mounted integral to the motor.

Once assembled the position control system and actuator was tested and found to meet the design specification. Some problems were encountered with the power output stages but modifications were introduced and the difficulties overcome.

2.5 Digital Control System

The digital control system is based on a PC computer. This Apricot computer is produced by MITSUBISHI ELECTRIC. The CPU is a 30386sx with 20(MHz) processor. The RAM is 5(MB). The hard drive has 40(MB) memory.

An analogue interface card is used to connect the computer to the analogue control circuit and the transducers. This board transfers analogue signals from the transducers into digital signals for the computer, and also transfers digital control signals produced by the computer into analogue signals for the analogue control circuits. The card, an AD1200 board, is produced by Brain Boxes and its specification is shown in table 2-1.

The connection of the whole control system is shown in the block diagram in figure 2-4. To avoid high frequency signal alias in the digital sampling, analogue filters are connected between the transducers and the A/D input.

The control software plays a key role in controlling the active suspension. The program should normally fulfil the following tasks:

- Turning on/off the control system.
- Collecting signals from sensors through A/D board.
- Processing the signals to create the appropriate control signals by proper algorithms.
- Sending the control signals to the analogue circuits through D/A board.
- Recording data for later analysis.
- Adjusting control parameters by using keyboard during control system operating.

The control software has been developed in C++. Various control strategies such as PD, MIMO PID, Fuzzy Logic and LQG have been implemented. The strategies and control performances will be investigated separately in the following chapters.

2-6 Conclusions

The prototype of the two wheeled trailer with the control system for the zero rate suspensions has been described. A PC based digital control system and interface to the existing trailer with zero rate suspensions, sensors and electronics have been developed. The experimental results have shown that this whole system functions correctly.

A to D input	8 channel differential (16 channels single) input
D to A output	2 channel output
digital input	one 8 bit TTL input
digital output	one 8 bit TTL output
frequency for A/D input	30 kHz
frequency for D/A ouput	100 kHz per channel
frequency of the TTL I/O	1 MHz

Table 2-1 The specification of the AD1200 board

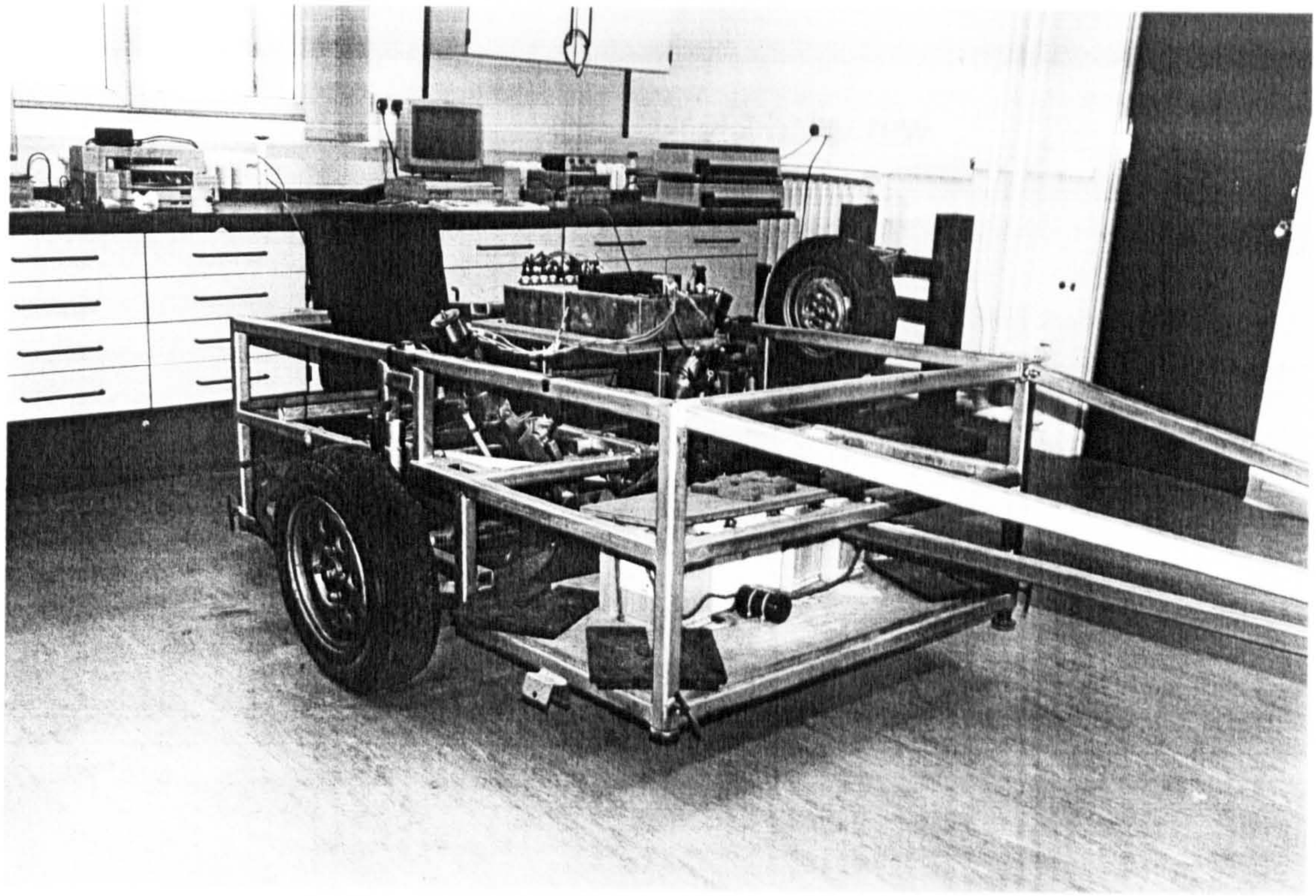

Figure 2-1 The demonstrator for zero-rate active suspension

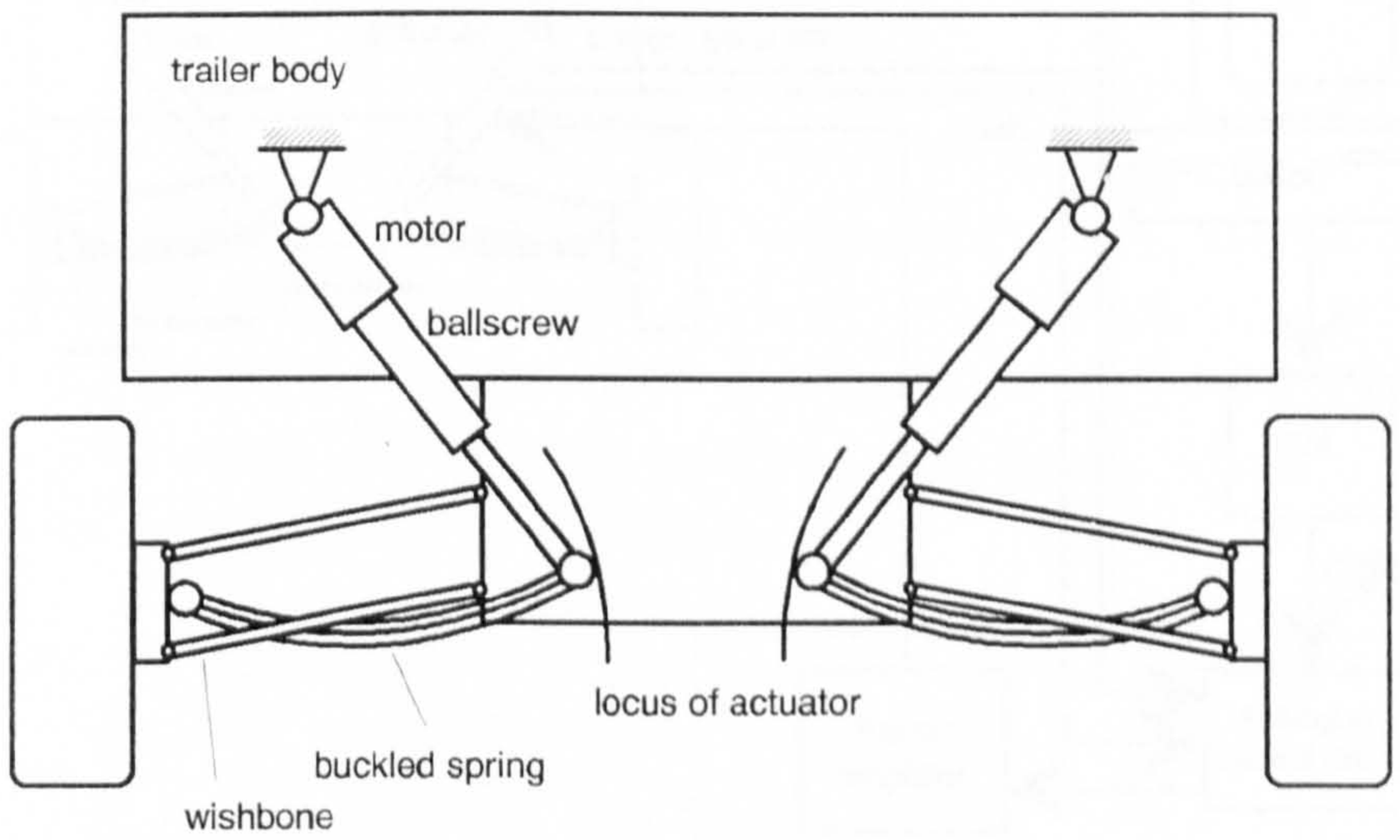

Figure 2-2 Two wheeled trailer with zero-rate active suspension

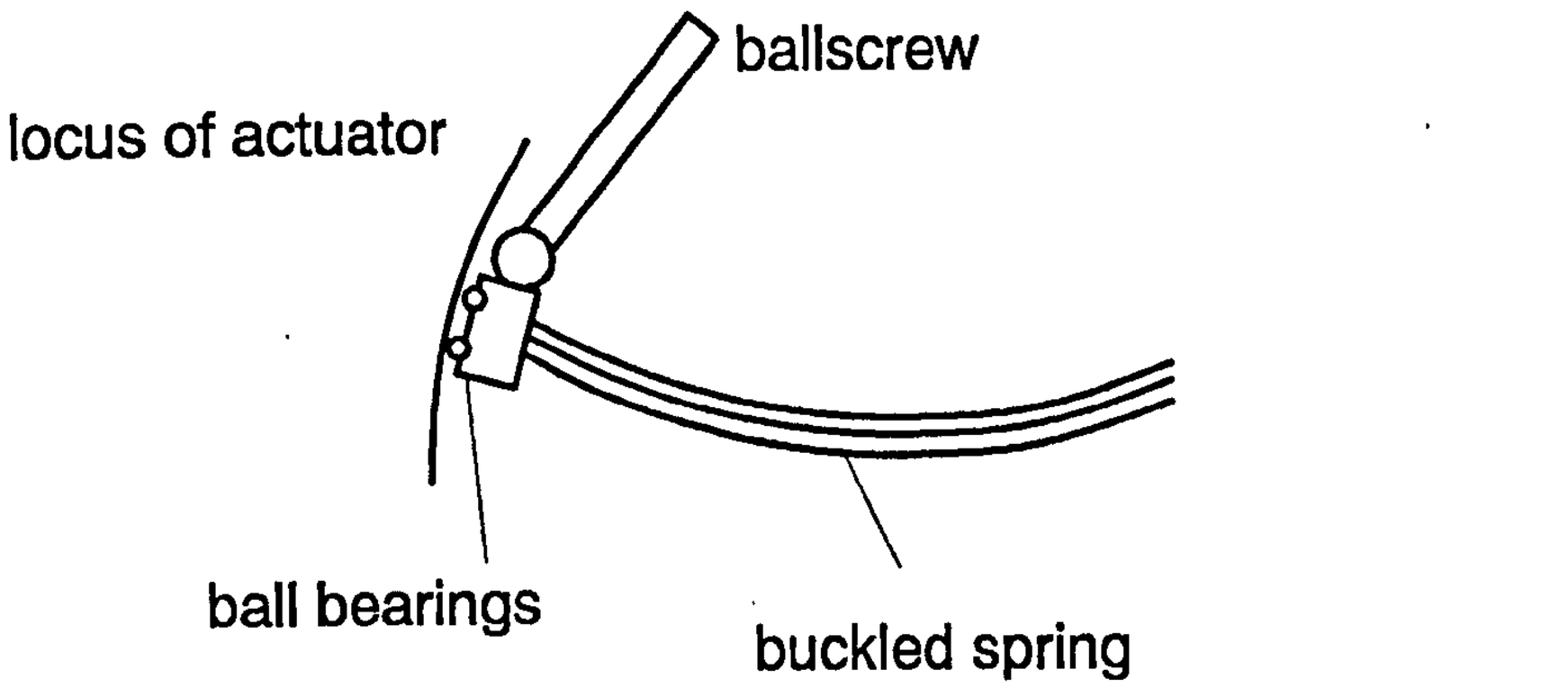

Figure 2-3 Actuator guide

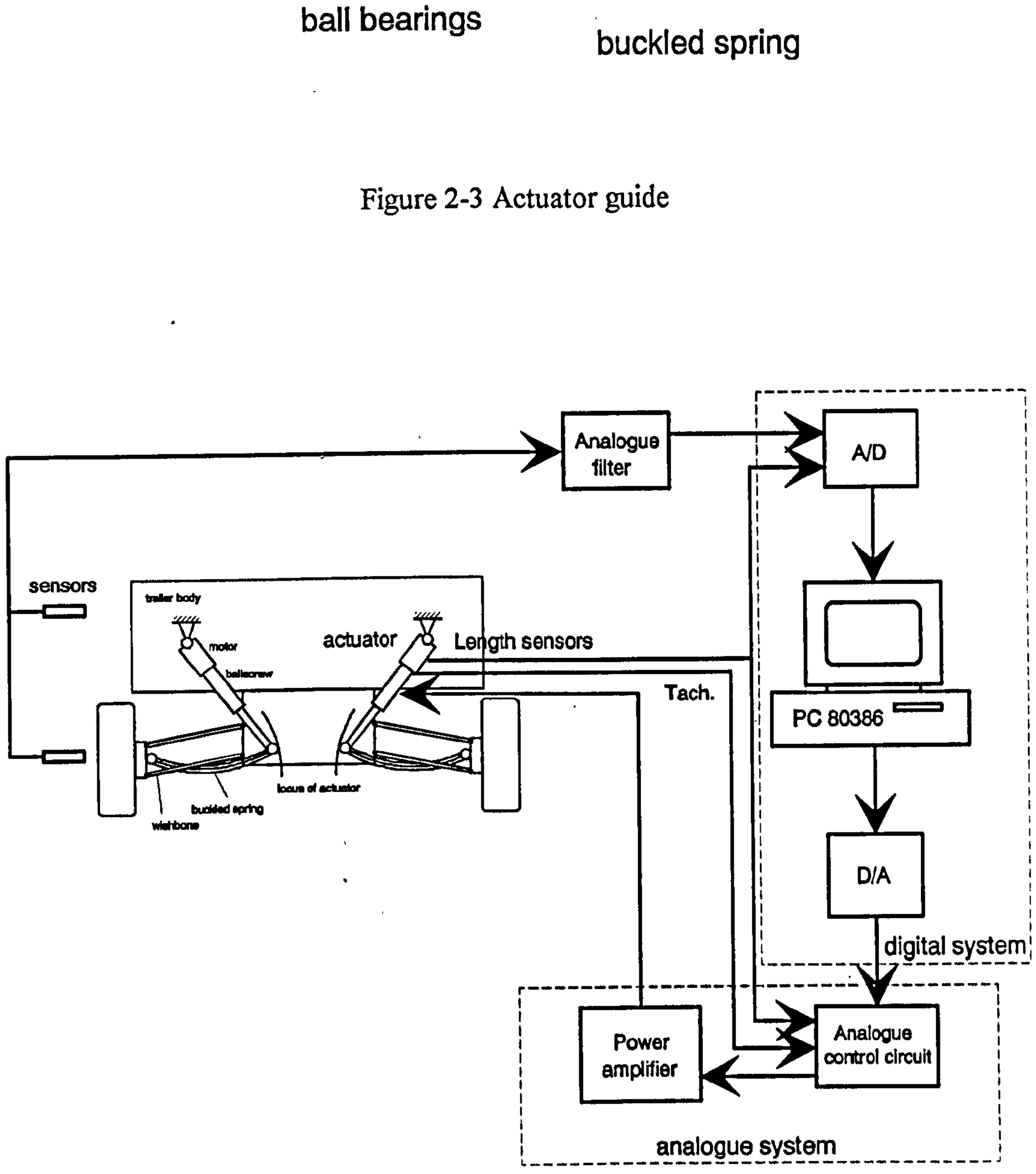

Figure 2-4 Schematically block diagram of the control system

Chapter 3

Transfer Function Measurement System

3.1 Introduction

The transfer function technique has been applied theoretically and experimentally by many investigators, for such purposes as validating models used to design controllers, identifying uncertain parameters and evaluating vibration isolation performance, etc. (Ulsoy, et al 1994; Oueslati, et al 1994; Levitt, et al 1991; Pilbeam, et al 1993 and Crolla, et al 1993; etc.).

Significant advances in the area of modal analysis technology have occurred over the past decades (Allemang, 1994). In the field of parameter estimation and system identification, a large number of methods have been developed and a huge amount of experience gained in their application (Friswell, et al 1996). Particularly techniques for identifying transfer functions of structures have been developed extensively, but few of them have been employed directly to the area of the automotive suspension systems. In the author's opinion, this is due to the large masses involved and the low frequencies present in the area of interest. The method favoured by many researchers is normally to excite the suspensions by hydraulic power systems which simulate excitations such as road profiles, sinusoidal sweep and white noise, etc. and basing the transfer function identification algorithm on the measurements obtained. The results from such methods have been reported frequently (Yi, et al 1993 and Xiong, et al 1994; etc.). This approach is costly both in terms of installation and maintenance, though satisfactory measurement can be obtained.

In this chapter, an identification technique based in the frequency domain is presented. This algorithm is applied to a two-wheeled trailer. It is shown that the results can be applied to determine both free and forced system response. A measurement system implementing the proposed technique is described and test results from a two wheel trailer are compared with those obtained using a conventional hydraulic test facility.

3.2 Theoretical Background

Suspension systems, be they active or passive, may be represented by a mathematical model which may be used to simulate and test configurations. The vehicle is generally modelled as a rigid body with six degrees-of-freedom, viz. longitudinal, lateral, heave, roll, pitch and yaw, which are controlled by the suspension geometry and forces and are highly coupled. Moreover, as the suspension has a mechanical structure with unsprung masses, coupling also occurs between the sprung and unsprung masses. Despite such coupling problems, a reduced-order mechanical model is often used for theoretical analysis and design of suspensions. Regardless of the reduction, a typical model for passive suspension systems can be expressed by the equation:

$$M\ddot{X} + C\dot{X} + KX = B_c\dot{X}_c + B_k X_c \qquad (3\text{-}1)$$

where M, C and K are the mass, damping and stiffness matrices; B_c and B_k denote the coupling between the state vector and the velocity and displacement of the road excitation, which depend on the damping and stiffness of the wheels; X is the state vector of the system which contains the displacement of each sprung and unsprung mass and X_c denotes the excitation vector which is normally produced by road profiles.

The transmission path from road excitation to the sprung body can be used to evaluate the primary ride performance of the suspension. The transfer function is an appropriate mathematical expression for such transmission. The identification of the transfer function from the excitation input, X_c, to the state vector, X, will be addressed in this chapter.

By using Laplace transformation, the transfer function from the road excitation to the state vector can be derived from equation (3-1):

$$X = (Ms^2 + Cs + K)^{-1}(B_c s + B_k)X_c = H(s)X_c \qquad (3\text{-}2)$$

If the coefficient matrices are definite, the transfer function $H(s)$ can obtained theoretically. However, the system is often not well defined and the transfer function parameter values must be determined from an estimation process based on measured results.

By applying Fourier transformation in equation (3-1), the frequency response from the road excitation to the state vector can be also derived:

$$X = (-M\omega^2 + Ci\omega + K)^{-1}(B_c i\omega + B_k)X_c = H(i\omega)X_c \qquad (3\text{-}3)$$

Actually, the transfer function *H(s)* can be obtained by replacing $i\omega$ as the complex variable s in the frequency response $H(i\omega)$. In other words, the transfer function identification can be determined through frequency response measurement, which is readily derived from time domain data by the application of FFT techniques. The method for identification of frequency response is therefore discussed next.

If the signals are obtained from forced vibrations, the identification algorithm is quite straightforward. Suppose there are n elements in the state vector X and m road inputs in the excitation vector X_c. The frequency response $H(i\omega)$ is a n by m matrix. To identify this matrix, m runs of the test with independent road input are needed. The road input in the frequency domain is denoted by $X_c^{(j)}$ $(j=1,2,...,m)$ at the jth test and the response in frequency domain to this input is denoted by $X^{(j)}$ $(j=1,2,...,m)$, i.e.

$$X^{(j)} = H(i\omega)X_c^{(j)} \qquad (3\text{-}4)$$

Obviously, the frequency response matrix $H(i\omega)$ does not change with various inputs for a linear system, so equation (3-4) can be used repeatedly. From this we can get

$$\Xi = H(i\omega)\Xi_c \qquad (3\text{-}5)$$

where $\Xi=[X^{(1)}\ X^{(2)}\ ...\ X^{(m)}]$ is a n by m response matrix, and $\Xi_c=[X_c^{(1)}\ X_c^{(2)}\ ...\ X_c^{(m)}]$ is a m by m input matrix. Ξ_c is invertible because the road input vectors $X_c^{(1)}$, $X_c^{(2)}$, ..., $X_c^{(m)}$ are linearly independent for any value of variable ω in frequency domain. The frequency response can be solved definitely from equation (3-5), i.e.

$$H(i\omega) = \Xi \cdot \Xi_c^{-1} \qquad (3\text{-}6)$$

Each value of frequency response $H(i\omega)$ at a value of ω can be obtained numerically by means of equation (3-6). Based on these identified data, a definite function matrix about $i\omega$ can be determined by fitting curves. The transfer function *H(s)* can therefore be obtained by replacing $i\omega$ by the complex variable s. Because the above derivation does not place constraints on the characteristics of the system, the transfer function can include the asymmetry of suspensions, tyre stiffness and damping for linear approach.

If the signals are obtained from free vibrations, equation (3-6) can still be used, provided an additional degree-of-freedom is introduced under each wheel with displacement measurement equipment. The dynamic equation can thus be derived as follows:

$$\begin{bmatrix} M & M_{12} \\ M_{21} & M_{22} \end{bmatrix} \begin{Bmatrix} \ddot{X} \\ \ddot{X}_w \end{Bmatrix} + \begin{bmatrix} C & C_{12} \\ C_{21} & C_{22} \end{bmatrix} \begin{Bmatrix} \dot{X} \\ \dot{X}_w \end{Bmatrix} + \begin{bmatrix} K & K_{12} \\ K_{21} & K_{22} \end{bmatrix} \begin{Bmatrix} X \\ X_w \end{Bmatrix} = 0 \qquad (3\text{-}7)$$

where M, C, K and X are the same as those in equation (3-1). X_w denotes the set of the variables for the displacement of the additional degree of freedom. The other submetrics are caused by the parameters of the added test rig and the coupling between X and X_w.

From equation (3-7), the relationship between the state vector X and the tyre contact point vector X_w can be obtained as:

$$M\ddot{X} + C\dot{X} + KX = -M_{12}\ddot{X}_w - C_{12}\dot{X}_w - K_{12}X_w \qquad (3\text{-}8)$$

where C_{12} and K_{12} are the coupling damping and stiffness matrices between X and X_w and depend only on the tyre damping and stiffness respectively. The excitation vector X_c in equation (3-1) actually denotes the displacement of the tyre contact points on all wheels, and the matrices B_c and B_k, which depend only on the tyre parameters, are the coupling between the state vector and the excitation. For the same suspension demonstrator, therefore, equation (3-8) can be written as

$$M\ddot{X} + C\dot{X} + KX = -M_{12}\ddot{X}_c + B_c\dot{X}_c + B_k X_c \qquad (3\text{-}9)$$

When $M_{12}=0$, equation (3-9) will be completely the same as equation (3-1). In other words, we can employ equation (3-6) to identify the transfer function by using the free vibration signals if we can design the additional rig to make the norm of this matrix zero or sufficient small.

Though the algorithm shown above is derived from the model for passive suspension systems, it can be applied to identify the transfer function for active suspension systems because their models can also be represented in the same form as equation (3-1).

For instance, a typical linear model for active suspension systems can be given as follows.

$$\begin{cases} M_o\ddot{X} + C_o\dot{X} + K_oX = B_c\dot{X}_c + B_kX_c + BU \\ Y = C_1X + C_2\dot{X} \end{cases} \qquad (3\text{-}10)$$

where X, X_c, B_c and B_k are the same as equation (3-1); U is the input vector for the suspension actuators; Y is the output vector which depends on the transducer installation; M_o, C_o and K_o are the mass, damping and stiffness matrices respectively;

B, C_1 and C_2 are determined by the mechanical and electronic installation for actuators and transducers.

Various control theories or concepts have been introduced to improve the performance of active suspensions. Suppose the controller for the suspension has been designed by a control strategy, i.e.

$$U = FY \tag{3-11}$$

By introducing this controller into the state equation and output equation (3-10), the equation for the closed loop can be obtained as

$$\begin{cases} M_o\ddot{X} + C_F\dot{X} + K_F X = B_c\dot{X}_c + B_k X_c \\ Y = C_1 X + C_2\dot{X} \end{cases} \tag{3-12}$$

where $C_F = C_o - BFC_2$ and $K_F = K_o - BFC_1$.

Comparing equation (3-12) with equation (3-1), their form are the same. Therefore, the identification technique for passive systems can also be used in active suspension systems.

3.3 Simulation and Validation

The identification technique shown above has been evaluated on a two-wheeled trailer with normal passive suspension. The motion of heave and roll of sprung body and the heave motion of the wheels are considered. This trailer therefore is modelled by a 4 degree-of-freedom half car model as shown in figure 3-1. Two cases will be considered in the identification: the first is that the signals are obtained from excited vibration by using hydraulic actuators on the wheels; the second is that the signals are sampled from the free vibration by adding an auxiliary degree of freedom.

3.3.1 Forced vibration

The system is described by equation (3-1) with the matrices:

$$M = \begin{bmatrix} m_0 \frac{b^2}{l^2} + \frac{I_0}{l^2} & m_0 \frac{ab}{l^2} - \frac{I_0}{l^2} & 0 & 0 \\ m_0 \frac{ab}{l^2} - \frac{I_0}{l^2} & m_0 \frac{a^2}{l^2} + \frac{I_0}{l^2} & 0 & 0 \\ 0 & 0 & m_{t1} & \\ 0 & 0 & & m_{t2} \end{bmatrix}$$

$$C = \begin{bmatrix} c_{01} & 0 & -c_{01} & 0 \\ 0 & c_{02} & 0 & -c_{02} \\ -c_{01} & 0 & c_{01} + c_{t1} & 0 \\ 0 & -c_{02} & 0 & c_{02} + c_{t2} \end{bmatrix}$$

$$K = \begin{bmatrix} k_{01} & 0 & -k_{01} & 0 \\ 0 & k_{02} & 0 & -k_{02} \\ -k_{01} & 0 & k_{01} + k_{t1} & 0 \\ 0 & -k_{02} & 0 & k_{02} + k_{t2} \end{bmatrix}$$

$$B_c = \begin{bmatrix} 0 & 0 \\ 0 & 0 \\ c_{t1} & 0 \\ 0 & c_{t2} \end{bmatrix} \quad \text{and} \quad B_k = \begin{bmatrix} 0 & 0 \\ 0 & 0 \\ k_{t1} & 0 \\ 0 & k_{t2} \end{bmatrix}$$

$$X = \{x_{01} \quad x_{02} \quad x_{t1} \quad x_{t2}\}^T$$

$$X_c = \{x_{c1} \quad x_{c2}\}^T$$

where a and b are the distances between the mass centre of the sprung body and the wheels, c_{01} and c_{02} are damping factors between the body and wheels, c_{t1} and c_{t2} denote the damping of both tyres, k_{01} and k_{02} are the stiffness of suspensions between the body and wheels, k_{t1} and k_{t2} are the stiffness of both tyres, m_0 and I_0 are the mass and initial moment of the sprung body respectively, x_{01} and x_{02} denote the displacements on both side of the sprung body, x_{t1} and x_{t2} denote the displacements of both wheels, x_{c1} and x_{c2} are the excitation on the wheels and also are the displacements of the tyre contact points on the wheels.

The trailer was tested on a conventional hydraulic test rig. A sine sweep was used to drive the actuator and the measured data were analysed by a standard instrument. The resultant frequency responses are shown by the solid lines in figures 3-2 and 3-3. In both figures, the first peak of the measured curve is at about 3Hz natural frequency which is the mode for lateral motion. The second peak is at about 6Hz natural frequency which is the mode for heave motion. The third peak at about 10Hz is

corresponding to the mode of the roll motion. The fourth small peak near 18Hz is caused by the resonance of the thin wall of the trailer. Other modes of the trailer are so high that they were over the limit of the actuator bandwidth of 25Hz.

The results identified from the simulated response are also shown as dashed lines in figures 3-2 and 3-3. The predicted transfer function was obtained from a calculated forced response rather than a direct calculation. The simulated response is calculated from the half car model in which random excitation with limited bandwidth is applied individually on each wheel. The resultant responses are employed to identify the frequency response by using equation (3-6). It can be seen that the simulated curves are quite consistent with the measured curves except at the first and the fourth peaks. The reason is that the heave and roll modes have been included in the simulation model but the lateral mode and thin-wall resonance have not. The comparison of results shows that the identification algorithm is effective and the model in use is validated.

3.3.2 Free vibration

Suppose, now, the trailer is put on two elastic bearings which allow the motion of the tyre contact point on the wheels to be measured. Such a system can be modelled as shown in figure 3-4. Its motion equation has the same form as equation (3-7) with the matrices: $M_{12} = 0$, $M_{21} = 0$, and

$$M_{22} = \begin{bmatrix} m_{p1} & 0 \\ 0 & m_{p2} \end{bmatrix}$$

$$C_{12} = C_{21}^T = \begin{bmatrix} 0 & 0 & -c_{t1} & 0 \\ 0 & 0 & 0 & -c_{t2} \end{bmatrix}^T$$

$$C_{22} = \begin{bmatrix} c_{t1} + c_{p1} & 0 \\ 0 & c_{t1} + c_{p2} \end{bmatrix}$$

$$K_{12} = K_{21}^T = \begin{bmatrix} 0 & 0 & -k_{t1} & 0 \\ 0 & 0 & 0 & -k_{t2} \end{bmatrix}^T$$

$$K_{22} = \begin{bmatrix} k_{t1} + k_{p1} & 0 \\ 0 & k_{t1} + k_{p2} \end{bmatrix}$$

where m_{p1} and m_{p2} are the masses of the elastic bearings, c_{p1} and c_{p2} are the damping factors, and k_{p1} and k_{p2} are the stiffness factors. The other matrices are the same as

those of forced vibration model. For this case, equation (3-9) becomes the same as equation (3-1), so the same identification algorithm can be used.

To verify the identification algorithm for free vibration signals, the identification process is simulated based on the half car model for free vibration. The free vibration response is calculated by integrating equation (3-7). The resultant responses are employed to identify the frequency response by using equation (3-6). The obtained results are illustrated in figures 3-5 and 3-6. These identified curves are compared with those frequency response curves which are calculated directly from the equation (3-3). The good agreement of the two types of curves in both figures shows that the identification algorithm is effective for signals obtained from free vibration of the suspension system.

To demonstrate that the identification algorithm is applicable to asymmetrical systems, the asymmetrical parameters are used in the model for figures 3-5 and 3-6. The stiffness for the left suspension is 2.7 times that for the right in the simulation. It is shown that the system with asymmetrical suspension parameters can also be identified.

3.4 Test Rig Implementation

The auxiliary test rig for this technique has been developed in the Engineering Division, University of Wolverhampton, as shown in 3-7 (a) and (b). The rig is a steel platform with sensors, which not only allows the additional degree of freedom to the vehicle but measures the displacement of the tyre contact point. The measurement system is shown in figure 3-8. The platform is installed for each wheel and the measured signal is recorded by a PC. The vibration of the vehicle can be excited by dropping each wheel.

The test data for the trailer are analysed by using the present method for free vibration. The frequency response of the identified transfer function using the developed test rig is compared with that obtained from a conventional hydraulic shaker with sine sweep excitation and a standard analyser, as shown in figure 3-9. For this response, the input signals are obtained through displacement sensors and the output signals are obtained through accelerometers, so the dimensions of this response are g/mm.

In figure 3-9, the first three modes are quite consistent. It is shown that the test rig and the identifying technique are applicable to the automotive suspension systems.

3.5 Conclusions

The simulation and experiment results have shown that the transfer function for automotive suspension systems can be identified by using free vibration signals when an appropriate auxiliary rig is built. This rig should allow the motion of the tyre contact points on wheels to be measured and should not cause mass coupling between the variables of the test rig and the suspension system. Such a passive test rig is much lower cost than a conventional hydraulic actuator system.

However, it should be clear that the passive test rig cannot replace conventional hydraulic actuator systems because the former is only proved to work in a linear model. The measurement results may be different for different deflections of the measured nonlinear system. If a nonlinear system is to be measured, this approach should be used carefully. The excitation for the free vibration should make the deflection small enough to be looked at as a linear displacement from an engineering point of view.

In the following chapters, this developed PC based test rig will be used to validate the models of the trailer, to evaluate the vibration isolation performance of the developed control strategies for the active suspension and the vibration attenuation result of the developed adaptive absorber for the unsprung mass.

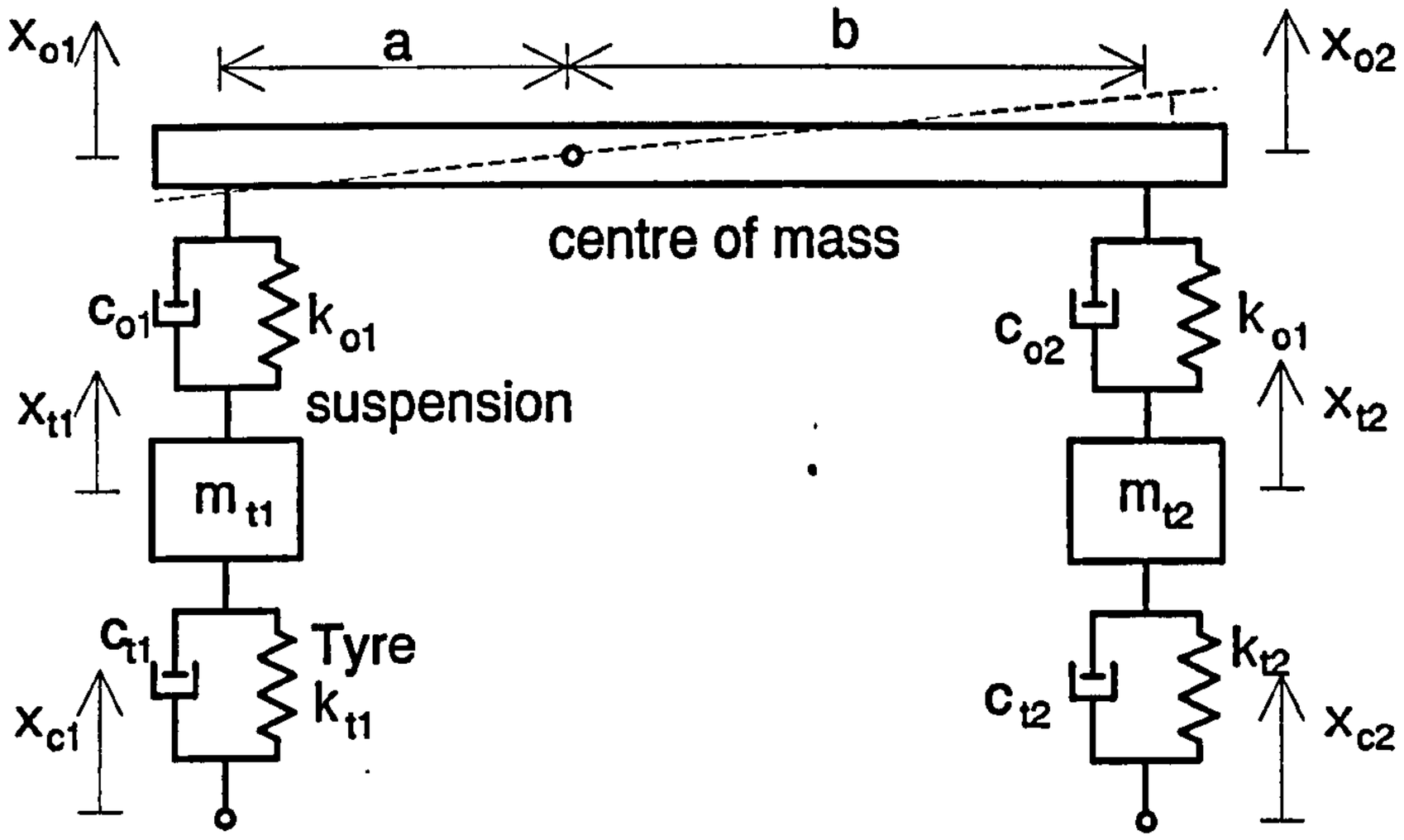

Figure 3-1 Half car model of the trailer

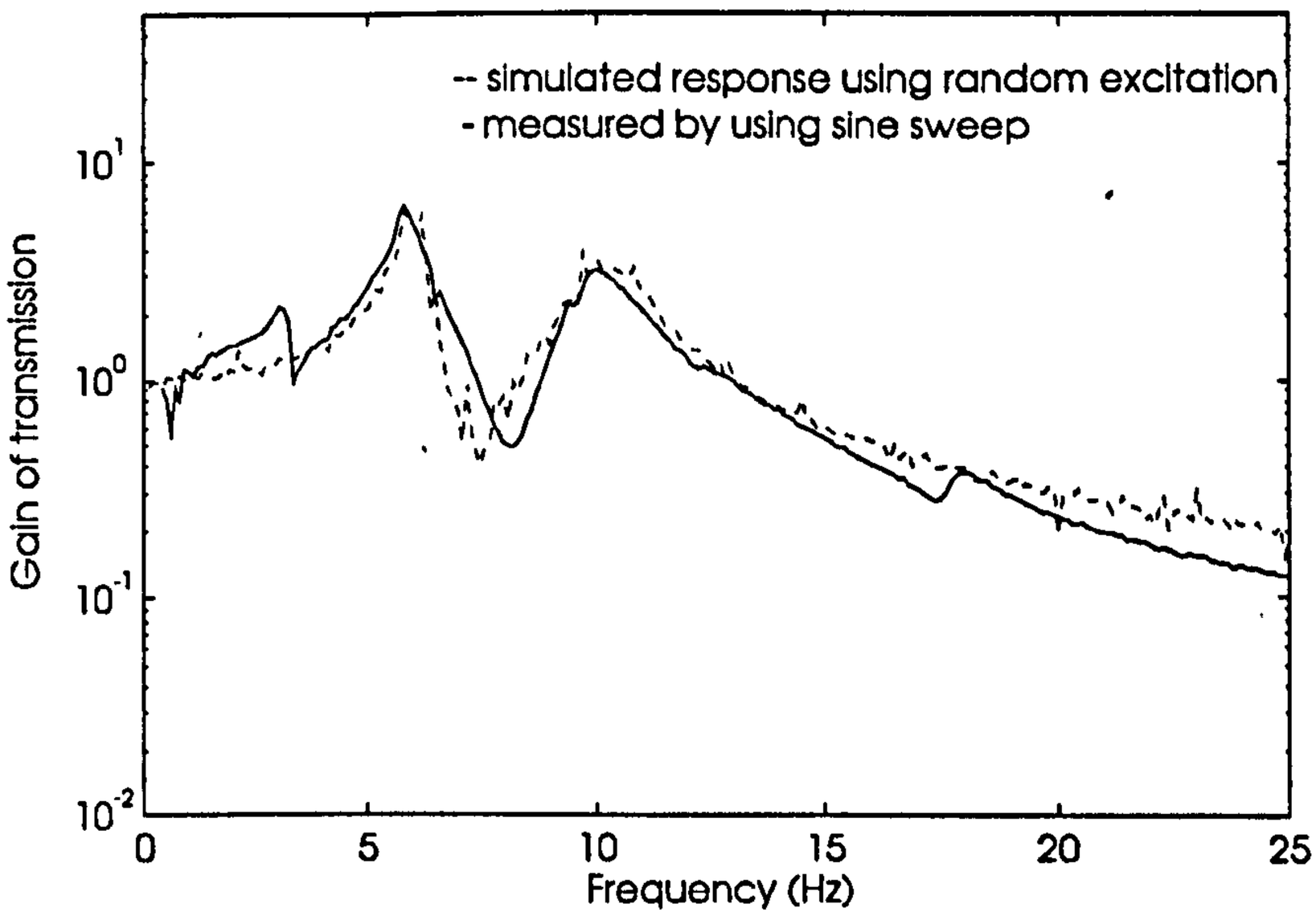

Figure 3-2 Measured and simulated frequency response for transmission from right to right

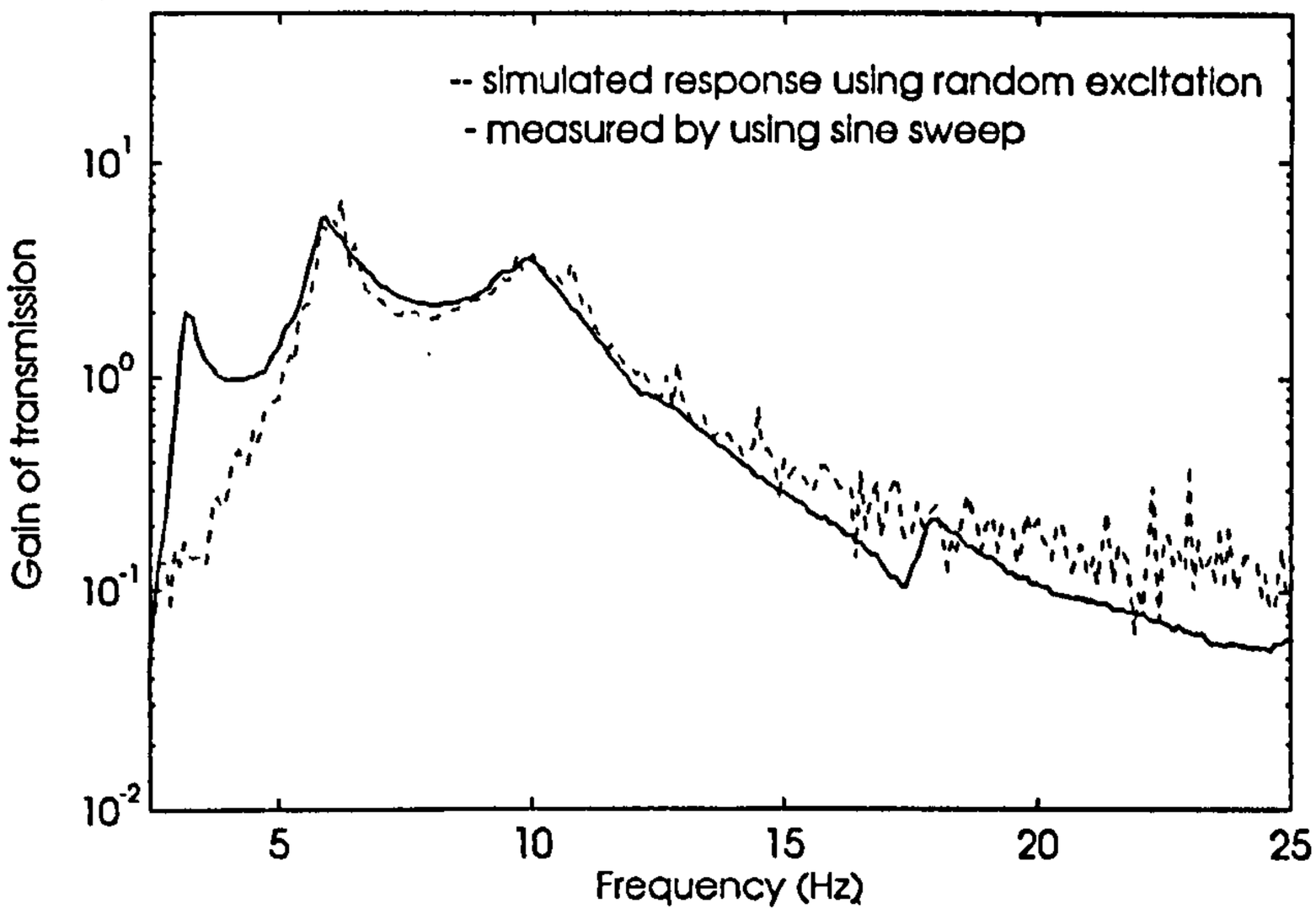

Figure 3-3 Measured and simulated frequency response for transmission from left to right

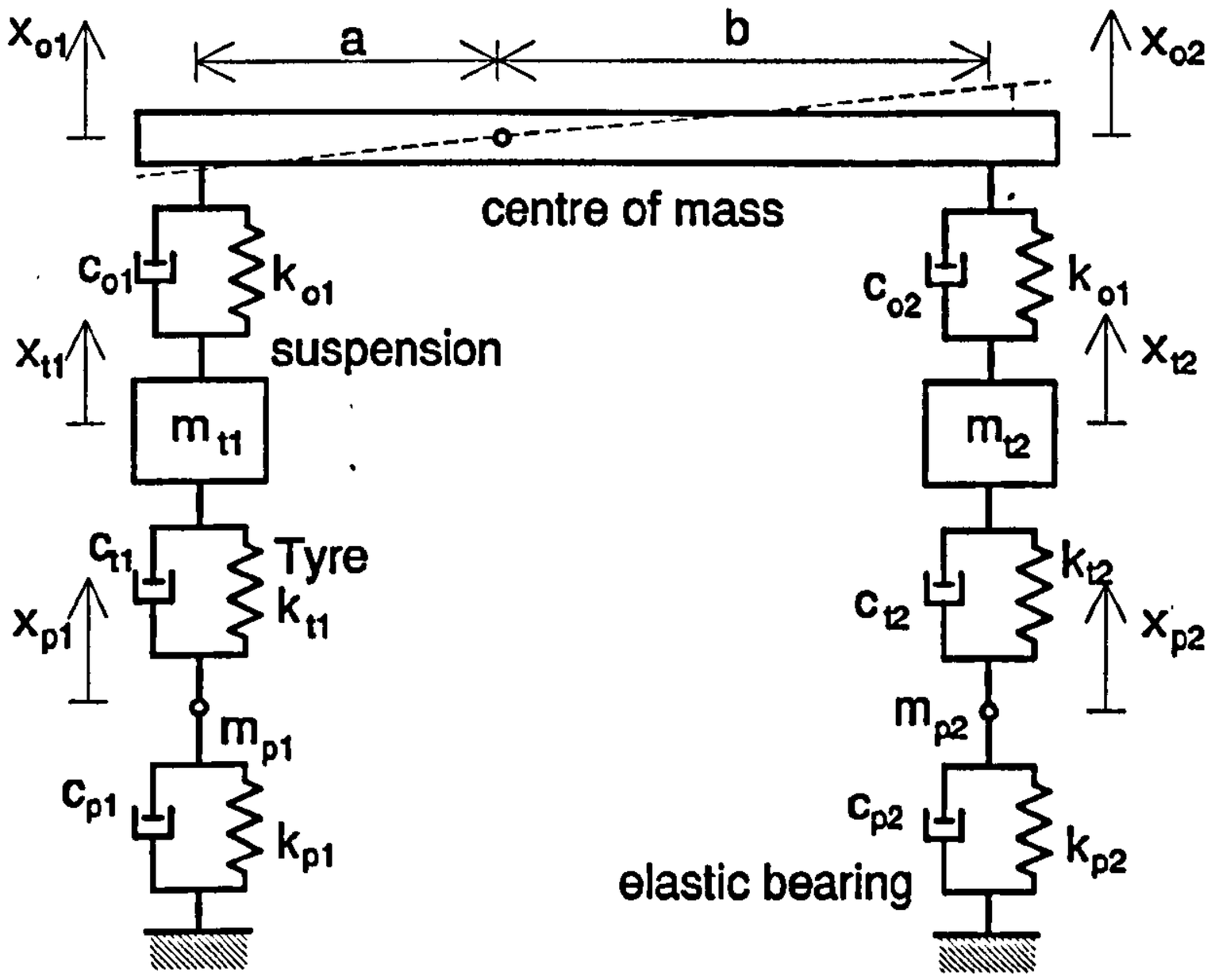

Figure 3-4 Model of the trailer and the auxiliary test rig

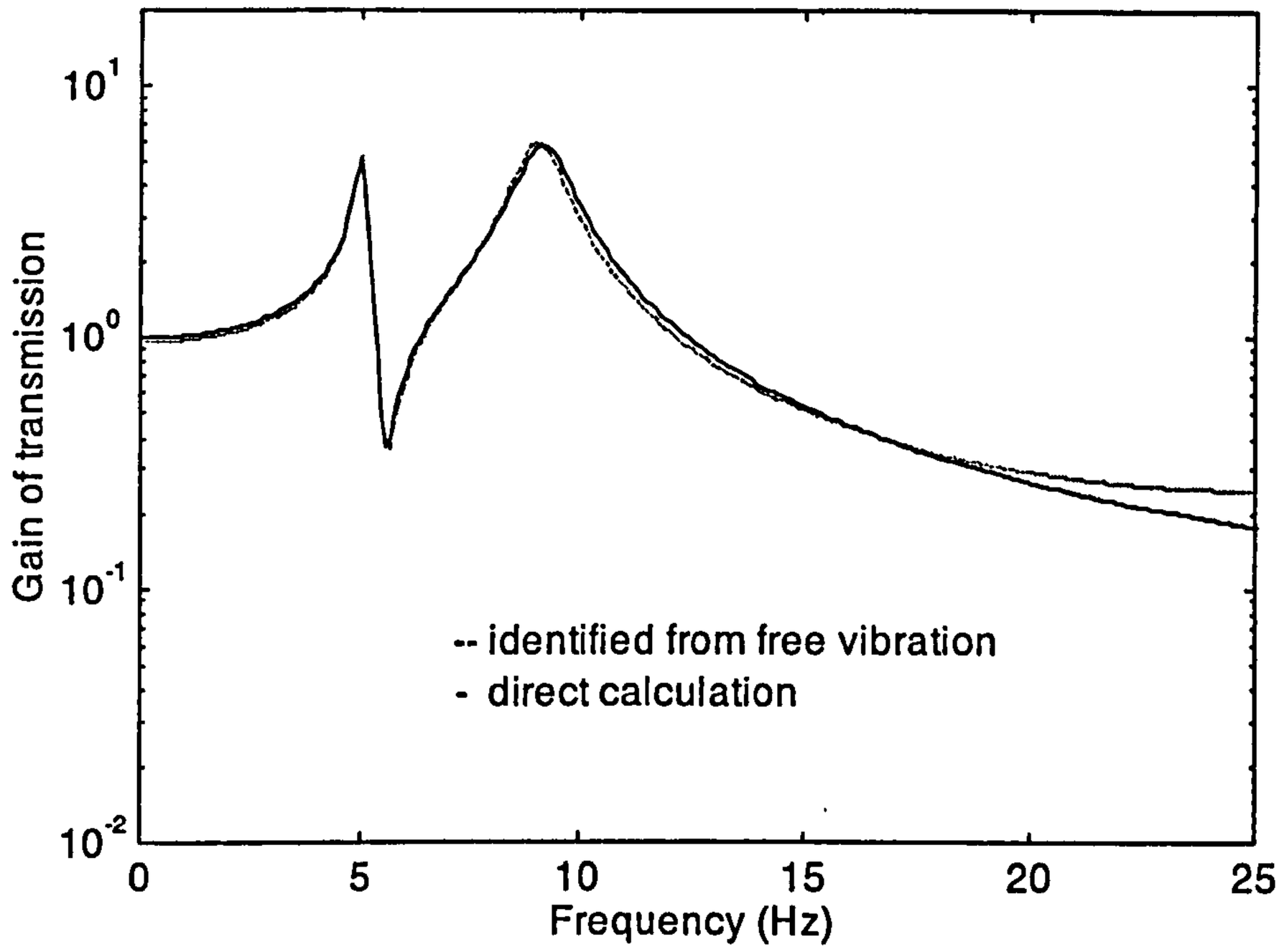

Figure 3-5 Simulated frequency response for transmission from left to left

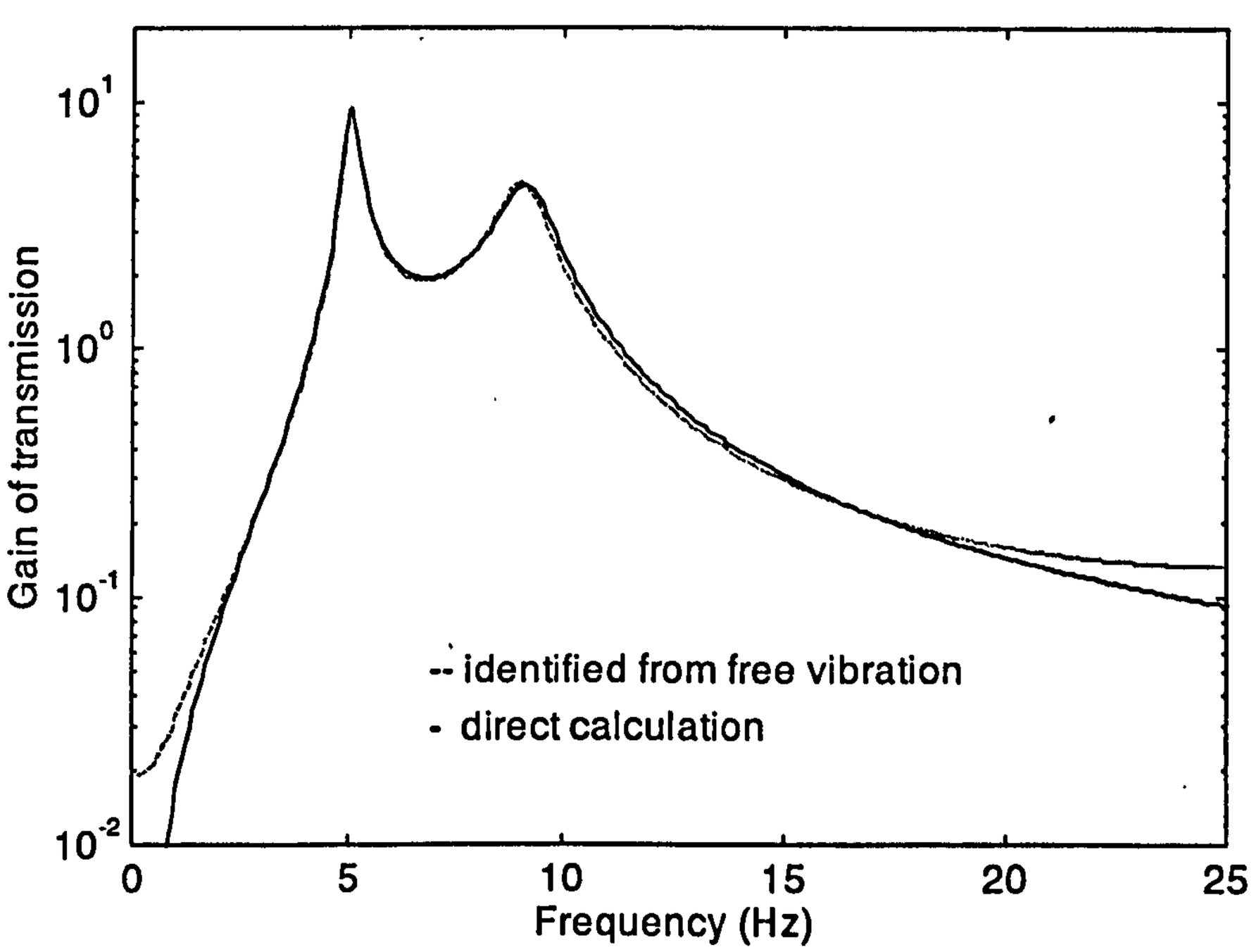

Figure 3-6 Simulated frequency response for transmission from right to left

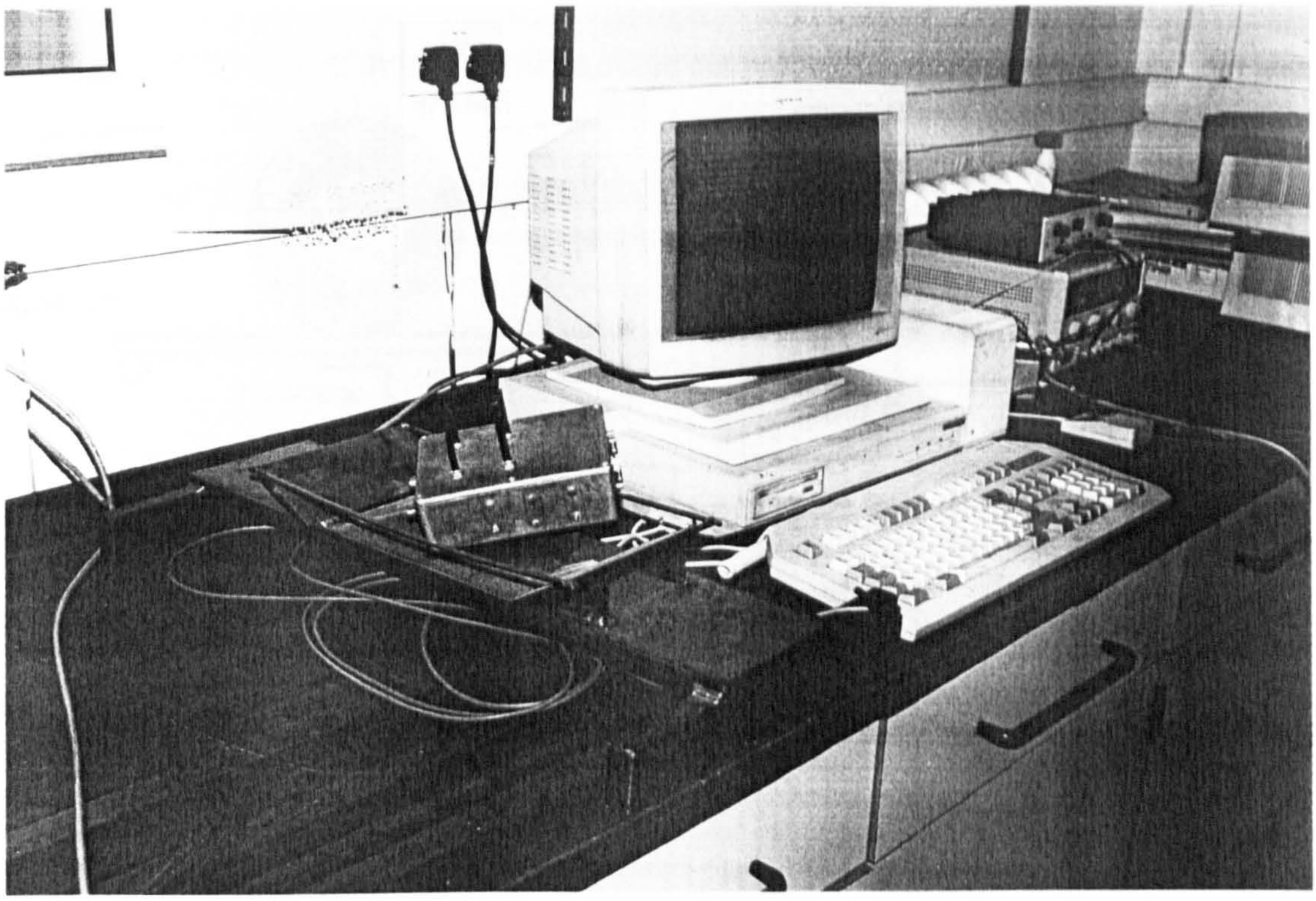

Figure 3-7 (a) The developed measurement system for identifying transfer function of automotive suspensions

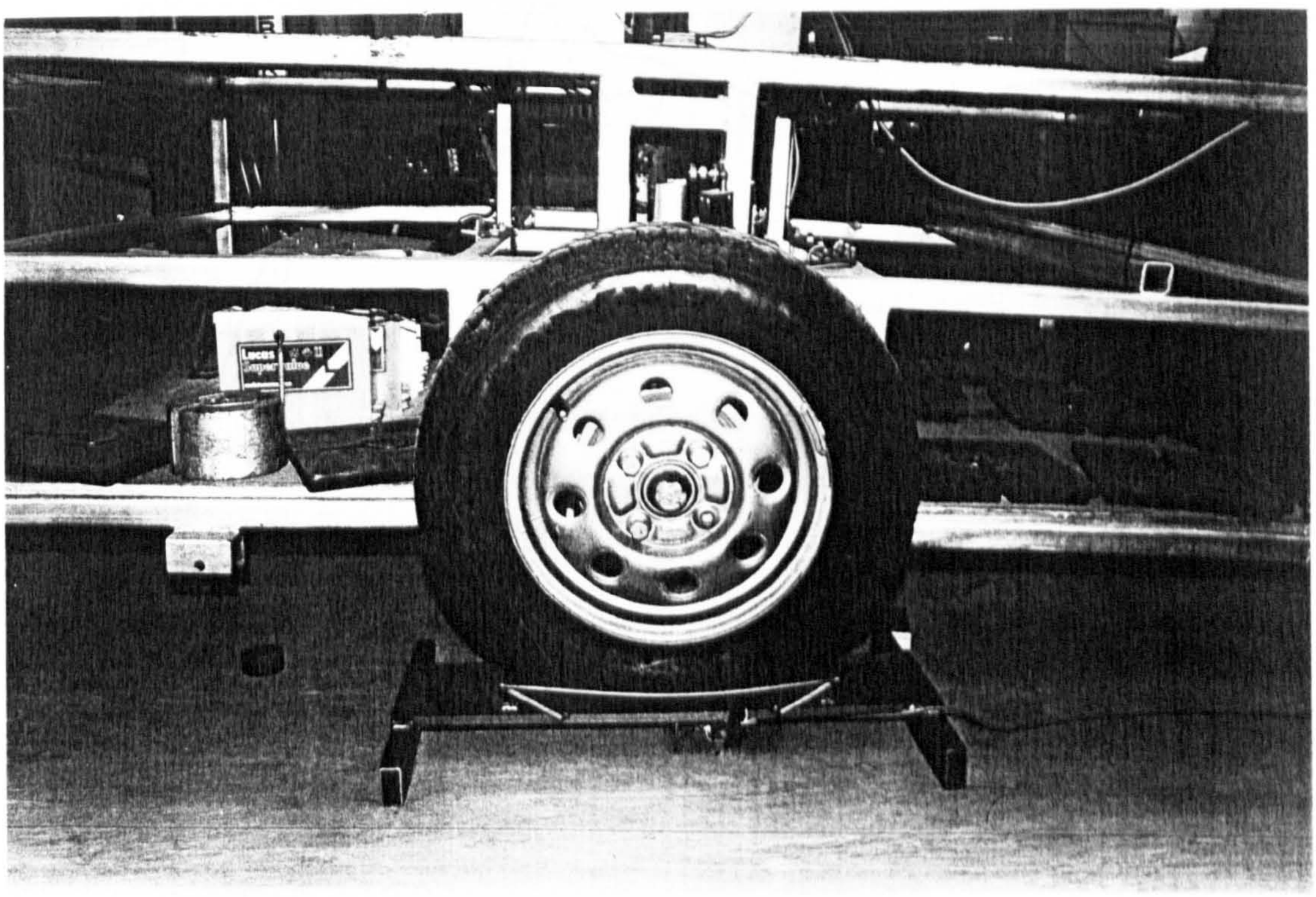

Figure 3-7 (b) The installation of the measurement system

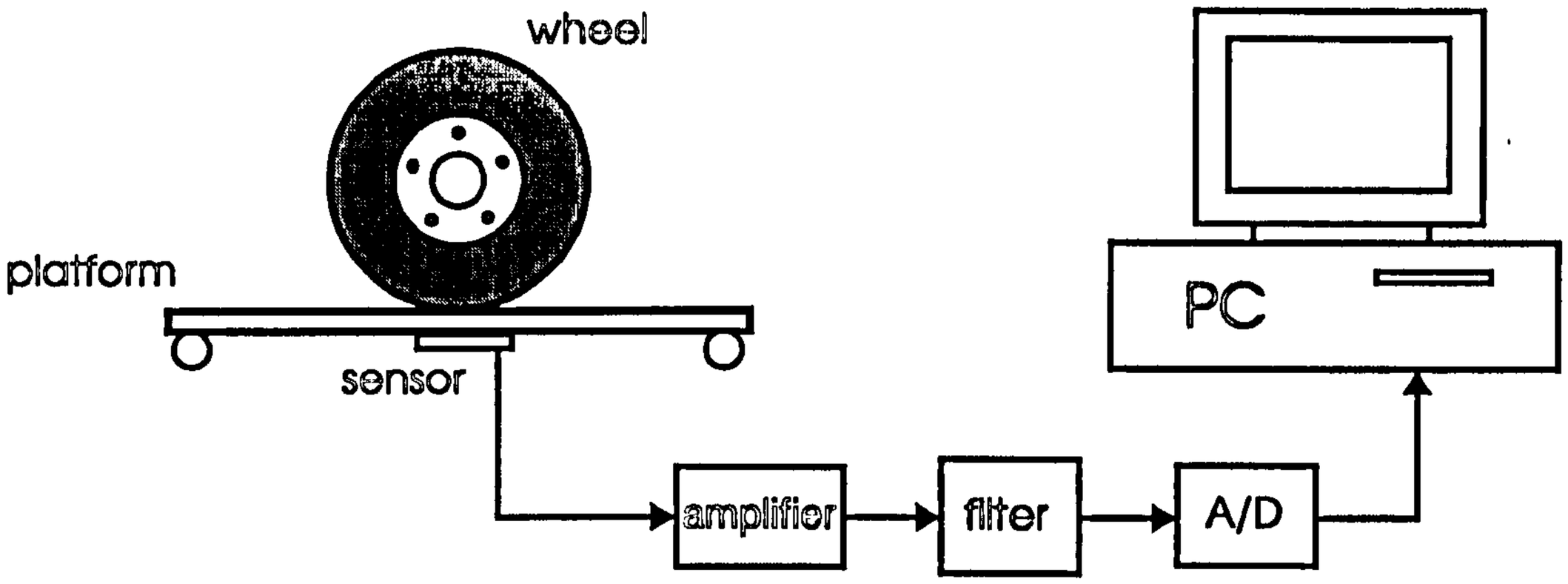

Figure 3-8 Schematic diagram for the tyre contact point measurement system

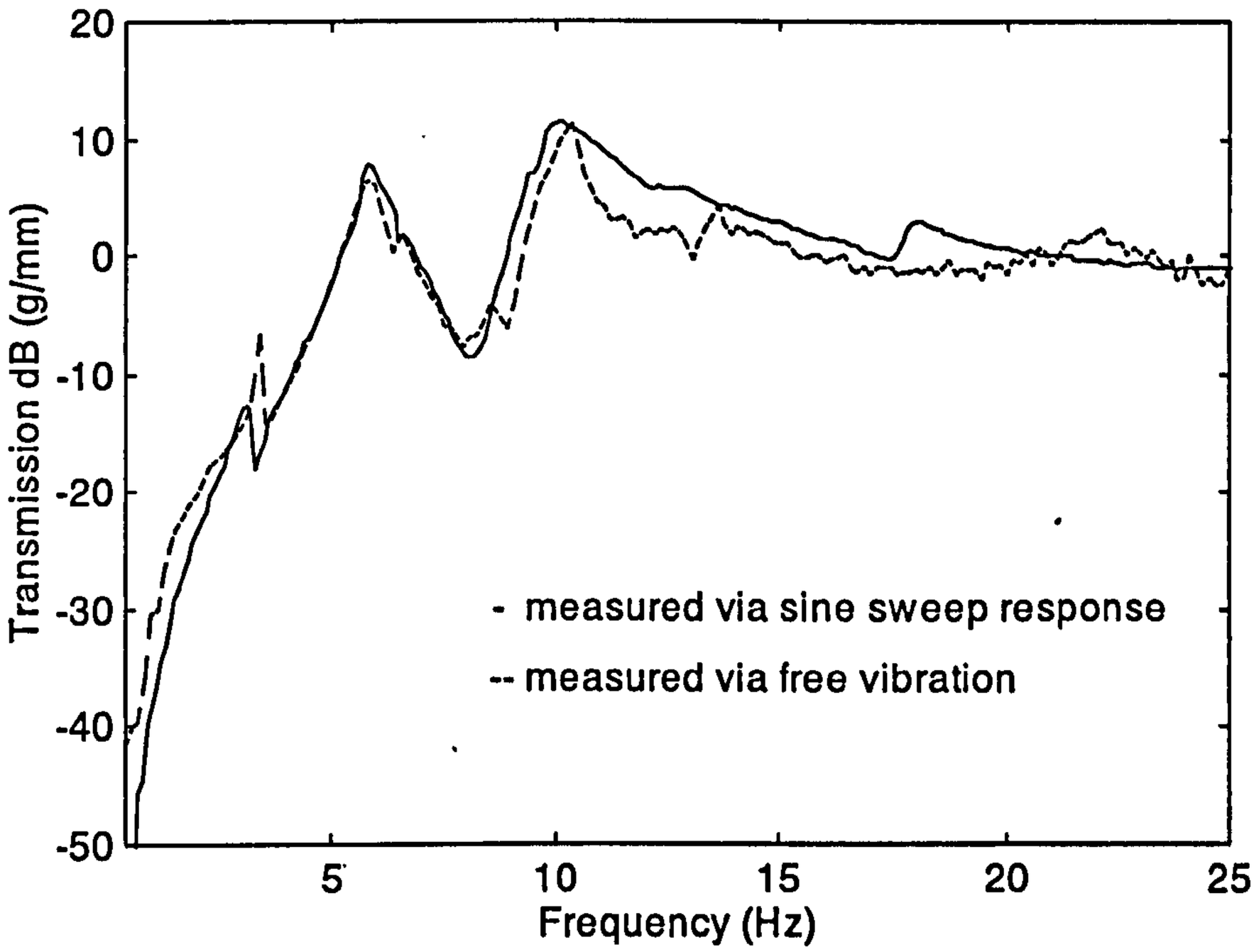

Figure 3-9 Measured frequency response by using the conventional and the suggested method

Chapter 4

Modelling and Open-Loop Performance of the Zero Rate Suspension

4.1 Introduction

It has been mentioned in chapter 1 that modelling the vehicle system is very significant for control of active suspensions. As a novel approach to active suspension, the zero rate suspension needs a profound investigation to make use of the potential of such a system and to improve control performance.

In this chapter a model of the two wheeled trailer with the zero rate suspension is developed and evaluated against test results. The open loop performance for this suspension is investigated theoretically and experimentally.

4.2 Half Car Model of the Trailer

The trailer with the active suspension system may be represented by a typical half car model with four degrees-of-freedom, by which the height and the roll of the body can be described (figure 2-2). It can be represented by an analytical model as shown in figure 4-1. In this figure, the top rigid body denotes the body of the trailer and the masses on the two sides represent the wheels. The actuator systems between the sprung body and the wheels provide forces determined by the displacement of the actuators. The dampers between the body and the wheels represent sources of conventional damping such as friction between the mechanical elements. The springs and dampers below the wheel masses represent tyre stiffness and damping.

The motion equations for this model can be derived as previously described, i.e.

$$M\ddot{X} + C_d\dot{X} + KX = B_c X_c + BU + G \qquad (4\text{-}1)$$

where

the mass matrix $M = diag\{ m_0, I, m_{t1}, m_{t2} \}$

the damping matrix $C_d = \begin{bmatrix} c_{01}+c_{02} & -c_{01}a+c_{02}b & -c_{01} & -c_{02} \\ -c_{01}a+c_{02}b & c_{01}a^2+c_{02}b^2 & c_{01}a & -c_{02}b \\ -c_{01} & c_{01}a & c_{t1}+c_{01} & 0 \\ -c_{02} & -c_{02}b & 0 & c_{t2}+c_{02} \end{bmatrix}$

the stiffness matrix $K = diag\{ 0,\ 0,\ k_{t1},\ k_{t2} \}$

the excitation matrix $B_c = \begin{bmatrix} 0 & 0 & 0 & 0 \\ 0 & 0 & 0 & 0 \\ c_{t1} & 0 & k_{t1} & 0 \\ 0 & c_{t2} & 0 & k_{t2} \end{bmatrix}$

the control matrix $B = \begin{bmatrix} 1 & 1 \\ -a & b \\ -1 & 0 \\ 0 & -1 \end{bmatrix}$

the state vector $X = \{ x_0 \quad \theta \quad x_{t1} \quad x_{t2} \}^T$

the excitation vector $X_c = \{ \dot{x}_{c1} \quad \dot{x}_{c2} \quad x_{c1} \quad x_{c2} \}^T$

the control vector $U = \{ F_{a1} \quad F_{a2} \}^T$

the static load vector $G = \{ -m_0 g \quad 0 \quad -m_{t1} g \quad -m_{t2} g \}^T$

Here:

a, b = distances between the centre of mass of the sprung body and the wheels

c_{01}, c_{02} = damping factors between the body and tyres

c_{t1}, c_{t2} = damping of each tyre

F_{a1}, F_{a2} = forces of each actuator system

I = moment of inertia about the centre of trailer body

k_{t1}, k_{t2} = stiffness of each hub assemblies

m_0 = mass of the body

m_{t1}, m_{t2} = masses of each wheel

x_0 = height of the trailer body

x_{c1}, x_{c2} = excitation of the road in the vertical direction at each wheel

x_{t1}, x_{t2} = displacement of each wheel

θ = roll angle of the trailer

From the actual installation of the sensors on the prototype, namely a vertical accelerometer on the body and a body to hub displacement transducer, The observation equation can be obtained, i.e.

$$Y = C X \qquad (4\text{-}2)$$

where the observation matrix

$$C = \begin{bmatrix} 1 & -a & 0 & 0 \\ 1 & b & 0 & 0 \\ 1 & -a & -1 & 0 \\ 1 & b & 0 & -1 \end{bmatrix}$$

the output vector $Y=\{y_{01} \quad y_{02} \quad y_{11} \quad y_{12}\}^T$

here y_{01} and y_{02} are the height of left and right side on the trailer body; and y_{11} and y_{12} are the relative height of left and right side of the trailer body to the wheels on the same side. Such a system described by equations (4-1) and (4-2) can also be shown by the block diagram of figure 4-2. According to modern control theory, the control system for the rig described by the equations (4-1) and (4-2) is completely controllable and observable. In other words, the set up of the actuators and sensors are theoretically suitable to attenuate the vibration of the trailer and control the body motion.

4.3 Model of the Actuator System

The structure of the actuator system being used is very different from current active suspensions. In order that the essentially constant force characteristic of the buckled spring element can be utilised in the suspension some means of varying the installed wheel to body force is needed. This can be achieved by a variable leverage system

whereby the mechanical advantage of the spring as seen at the wheel can be varied by altering the line of action of the spring. This can be achieved by moving one end of the spring with a ball-screw actuator, whilst reacting the spring force through a wishbone. This allows the system to be implemented in a suspension with the addition of a second wishbone or a strut arrangement as shown in figure 2-2.

The analytical model of the actuator system is shown in figure 4-3. The forces applied on the pivots at both ends of the buckled spring are analysed in this figure. There are three forces on the left pivot, i.e. F_a, the force produced by the ball-screw actuator; F_s, the force from the deformation of the buckled spring element; and F_o, the constraint force of the locus for the actuator. Again, there are also three forces on the right pivot, i.e. F_t, the vertical upwards force provided by the wheel; F_s' being equal to F_s in magnitude, the force from the deformation of the buckled spring element; and F_w, the constraint force produced by the wishbone.

Among these forces, F_t, the force of the actuator system on the wheel is of primary interest and will be derived.

The Cartesian coordinate system is referenced to the trailer body as shown in figure 4-3 and the origin is at the fulcrum of the wishbone. (x_a, y_a) is the location of the left end of the buckled spring, (x_t, y_t) is that of the right end, and (x_0, y_0) is that of the other end of the ball-screw actuator. Actually, y_t represents the displacement of the wheel relative to the trailer body.

Suppose the length of the ball-screw actuator is denoted by l, the length of the wishbone is represented by l_w, and the length of the buckled spring is marked by l_s. Let the locus of the actuator be described by the following equation.

$$f_a(x_a, y_a) = 0 \tag{4-3}$$

where (x_a, y_a) should always follow this equation. Meanwhile, the location of this point should also follow the equation

$$(x_a - x_0)^2 + (y_a - y_0)^2 = l^2 \tag{4-4}$$

Obviously, the locus of the right end of the buckled spring is a circle, i.e.

$$x_t^2 + y_t^2 = l_w^2 \tag{4-5}$$

where (x_t, y_t) should always follow this equation.

According to the force balance triangle in figure 4-3 and the sine theorem, the force F_t can be obtained as follows:

$$\frac{F_t}{\sin(\alpha - \beta)} = \frac{F_s'}{\sin(\frac{\pi}{2} - \beta)} \qquad (4\text{-}6)$$

By using equation (4-5), the angle β can be expressed by x_t *and* y_t and the equation (4-6) can then be solved as follows.

$$F_t = F_s(\frac{y_t}{x_t}\cos\alpha - \sin\alpha) \qquad (4\text{-}7)$$

where α, the angle of the force of the buckled spring can be determined by

$$tan\alpha = \frac{y_t - y_a}{x_t - x_a} \qquad (4\text{-}8)$$

here x_t, x_a and y_a can be solved as functions of l and y_t from the equations (4-3), (4-4) and (4-5).

From the Appendix B, the force of the buckled spring element, F_s can be represented as a function of the change of the distance between (x_t, y_t) and (x_a, y_a) i.e. the length of the element. The function is complex and is best solved numerically. Hence, F_s can be also derived as a function of l and y_t. The force applied by the wheel is thus a function of the length of the ball-screw actuator l and the vertical relative position of the wheel y_t, i.e.

$$F_t = f_t(l, y_t) \qquad (4\text{-}9)$$

This force is equal in magnitude to the actuator system force applied to the wheel and, as the value of F_s is required within the function, it is again a complex function that is best solved numerically.

In this model, the effect of the rates of change of these variables is not included. This implies that friction in the ball-screw locus, the connections at the ends of the buckled

springs and the pivots, etc. are not taken into account. The inclusion of these effects would dramatically complicate the model. For example, the spring element would become a combined model of a buckled spring and a beam instead of a pure buckled spring. To compensate for the effect of these omissions, an equivalent damping force was introduced, an approach favoured by most researchers.

The force of the actuator system F_t was measured, and predicted by numerical solution of equation (4-9) in which the actuator locus is given by

$$f_a(x_a,y_a)=(x_a-l_x)^2+(y_a-l_y)^2-l_w^2$$

where $l_x^2+l_y^2=l_w^2$, $l_y=-0.05$ as implemented on the test rig. The force is an approximately linear function of y_t from the results as shown in figure 4-4.

The measured stiffness of the actuator system was compared with that of the numerical results from equation (4-9), as shown in figure 4-5. The average relative error is about 5.4%, which suggests that the prediction is in good agreement with the experimental values. The measured stiffness appears to be an approximately linear relationship with the definite length of the actuator l.

In the experiment, the actuator system can raise the trailer body of 7000N weight with only 3200N/m stiffness. For conventional linear springs, the deformation of springs with the same stiffness would be over one metre under the same load. In contrast, the height of the trailer body actually is only about 10 centimetres. This is one of the distinct advantages for this actuator system.

Because of the nature of the nonlinearity, a simple relationship between the force F_t and the displacements of the actuator and wheel cannot be defined. Inspection of the function defined by (4-9) suggests that a quadratic relationship with respect to l and linear with respect to y_t would be sufficiently accurate, so higher terms in the expansion may be ignored, i.e.

$$F_t = a_0 + a_1 l + a_2 l^2 + (a_3 + a_4 l) y_t \qquad (4\text{-}10)$$

Both measured behaviours, the suspension force being a nearly linear function of the relative displacement y_t and the suspension stiffness changing approximately linearly with actuator length l, are shown by the last term in the equation (4-10). The comparison between the measurement and the prediction by equation (4-10) is shown

in Figures 4-5 and 4-6. The average relative errors are about 5.5% and 4.4% respectively. The good agreement suggests that the simplified model of the force for the actuator system is effective.

4.4 Open-loop Performance of the Active Suspension

A frequency response approach may be used to evaluate the isolation performance of the active suspension in open loop mode (i.e. with no external control loop). The frequency response functions are considered from the excitation (i.e. road profile) to the output vector (i.e. body and hub vertical motion).

From the experiment, it has been shown that the force of the actuator system is approximately a linear function of the relative displacement of the wheel. The actuator system can thus be modelled as an equivalent linear spring between the sprung body and the wheel, in which the force is a function of the length of the ball-screw actuator. The force as given by (4-10) can be split into two terms, one dependent only on the actuator length l, the other dependent on both the actuator length and the wheel to body displacement. In the open loop situation the first term $(a_0+a_1l+a_2l^2)$ may be considered fixed and it lifts the static load of the trailer whilst the second term $(a_3+a_4l)y_t$ represents an effective spring stiffness which gives rise to an oscillatory response to a body disturbance. This response can be derived from (4-1):

$$M\ddot{X} + C_d\dot{X} + K_oX = B_cX_c \qquad (4\text{-}11)$$

where

$$K_o = \begin{bmatrix} k_{a1}+k_{a2} & -k_{a1}a+k_{a2}b & -k_{a1} & -k_{a2} \\ -k_{a1}a+k_{a2}b & k_{a1}a^2+k_{a2}b^2 & k_{a1}a & -k_{a2}b \\ -k_{a1} & k_{a1}a & k_{t1}+k_{a1} & 0 \\ -k_{a2} & -k_{a2}b & 0 & k_{t2}+k_{a2} \end{bmatrix}$$

and the other matrices and vectors are the same as in equation (4-1). k_{a1} and k_{a2} are the stiffnesses of both equivalent springs which are linear functions of the length of the ball-screws. This system can also be described by figure 4-7, the block diagram.

For improved confidence in the model the free vertical vibration of the body was simulated and a test carried out on the trailer. The results with an actuator length of

0.453m are shown in figure 4-8. These suggest that the model is effective for the vibration analysis.

By using Laplace transformation, the transfer function from the road excitation to the output variables can be derived, i.e.

$$Y = C\,(M\,s^2 + C_d\,s + K_o)^{-1}\,B_c\,D(s)\begin{Bmatrix} X_{c1} \\ X_{c2} \end{Bmatrix} \qquad (3\text{-}12)$$

where

$$D(s) = \begin{bmatrix} s & 0 & 1 & 0 \\ 0 & s & 0 & 1 \end{bmatrix}^T$$

These equations were solved by implementing the model using MATLAB and hence the frequency responses for the following two cases of input and output were determined:

i) right wheel to right side of body
ii) left wheel to right side of body

These responses were simulated and measured for actuator length l=0.40m, and are shown in figures 4-9 and 4-10.

There are four poles available for the half car model, concerning the body heave, the body roll, the left wheel and the right wheel modes. Because the parameters of each wheel are normally the same, the frequencies for the left and the right wheel modes are the same. Two body modes and one of the wheel modes can therefore be seen in the frequency response when the damping is quite small. The calculated frequencies for these modes are respectively 0.65Hz, 0.90Hz and 11.5Hz. These frequencies correspond to the height, the roll and the wheel modes (the right and the left wheel modes have the same frequency). The frequencies of the two body modes are very near for this particular prototype. When the damping is significant, these two body modes merge into one peak in the frequency response. Only one body mode and one wheel mode can therefore be seen in the frequency response for this prototype.

The measured and predicted transmissions from the right tyre to the right side of the sprung body are shown in figure 4-9. The measured curve has three peaks at about 0.67Hz, 5.8Hz and 11.5Hz respectively. The peak at 0.67Hz actually represents the two sprung body modes, heave and roll, because the parasitic damping is not

insignificant. The peak at 5.8Hz denotes the lateral mode for the sprung body which is not included in the half car model and is therefore not seen in the response calculated for the model. The third peak corresponds to the wheel mode. The measured and predicted transmission from the left tyre to the right side of the sprung body are illustrated in figure 4-10. The three peaks of the measured curve are corresponding to the same modes as those in figure 4-9. It is shown in both figures that the predicted frequency response is quite consistent with the measurement for the modes included in the half car model. This means the model is valid in terms of frequency response for the available modes.

Both calculation and experiment show that the zero rate suspension system can provide heave and roll resonant frequencies of about 0.67Hz. To the author's knowledge, these are lower than those in common use in vehicle suspension systems, which gives rise to the excellent intrinsic isolation properties that were expected.

Figure 4-9 represents the transformation relationship from the road excitation at the right tyre to the right side of the body. Figure 4-10 describes the relationship from the road excitation at the left tyre to the right side of the body. At the frequencies of the first peak, the gains in both figures are similar, about 1.5-2.6. The gain at the wheel mode frequency in figure 4-9 is equivalent to that in figure 4-10, though the calculated gain for the former is larger than the latter. It is thus demonstrated that the coupling effect of the system on the gains at frequencies of the roll, the bounce and the wheel modes can not be ignored. In other words, it is wise to use a half car model for the development of vibration control for the trailer, rather than a simpler quarter car model which neglects these coupling effects.

From figures 4-9 and 4-10, it is shown that the lateral mode should not be overlooked in the analytical model because the measured gains are significant. It has been found experimentally that the lateral mode is strongly coupled with the roll mode of the sprung body. That may be one of the reasons for such a strong response at the lateral mode. The coupling is caused by the mechanism of the suspension system. This mode can probably be included in a suitable multibody model, but that will introduce considerable additional complexity and is considered very difficult. This work will be considered in the future.

4.5 Conclusions

A half car model for the prototype with active zero rate suspension has been completed, and is expressed by a 4 degree-of-freedom nonlinear differential equation and a observation equation. A nonlinearity is caused by the suspension mechanism. The validity of the set up of actuators and sensors has been confirmed theoretically by controllability and observability analysis.

It is shown experimentally and theoretically that the relationship between the force of the active suspension and the relative displacement of the sprung body is equivalent to a linear spring, and the stiffness of the suspension system is related to the length of the ball screw actuator in an approximately linear relationship. Good agreement between the measurement and the prediction confirms that the simplified nonlinear model of the suspension force is effective.

It has been shown that a low natural frequency, down to about 0.67Hz, can be achieved by this suspension which implies improved inherent vibration isolation compared to a traditional passive suspension.

The quite good agreement of calculation and experiment has validated the half car model in terms of the frequency response for its available modes. The prediction for the free vibration of the sprung body consistent with the measured result tells us that the linearized equation can be employed for small amplitude vibration analysis of the prototype.

It is found experimentally that the lateral mode at about 5.8Hz can play an important role in the response of the sprung body to the road input. This more complicated factor can be considered in a future work.

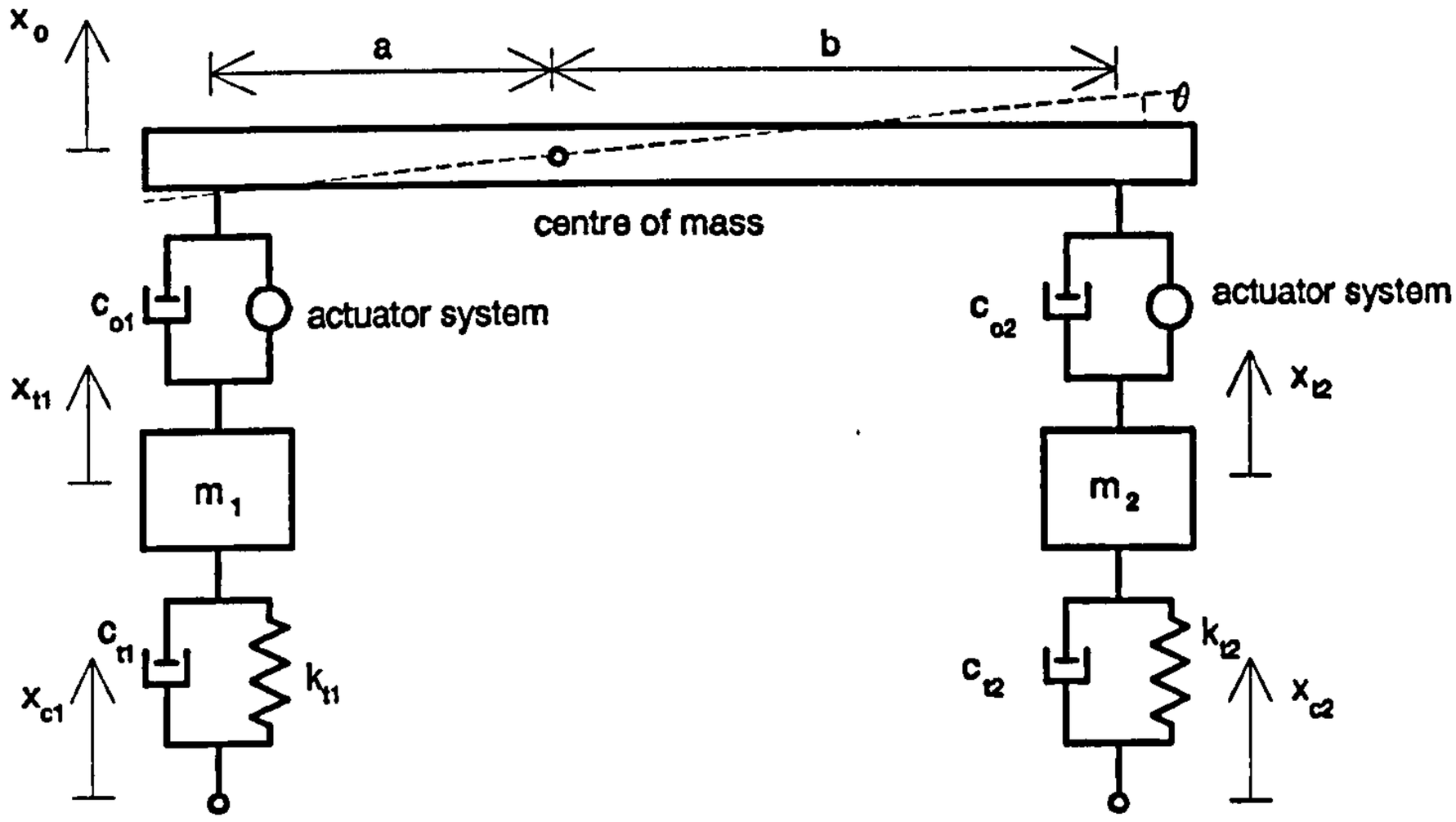

Figure 4-1 Analytical model of the trailer.

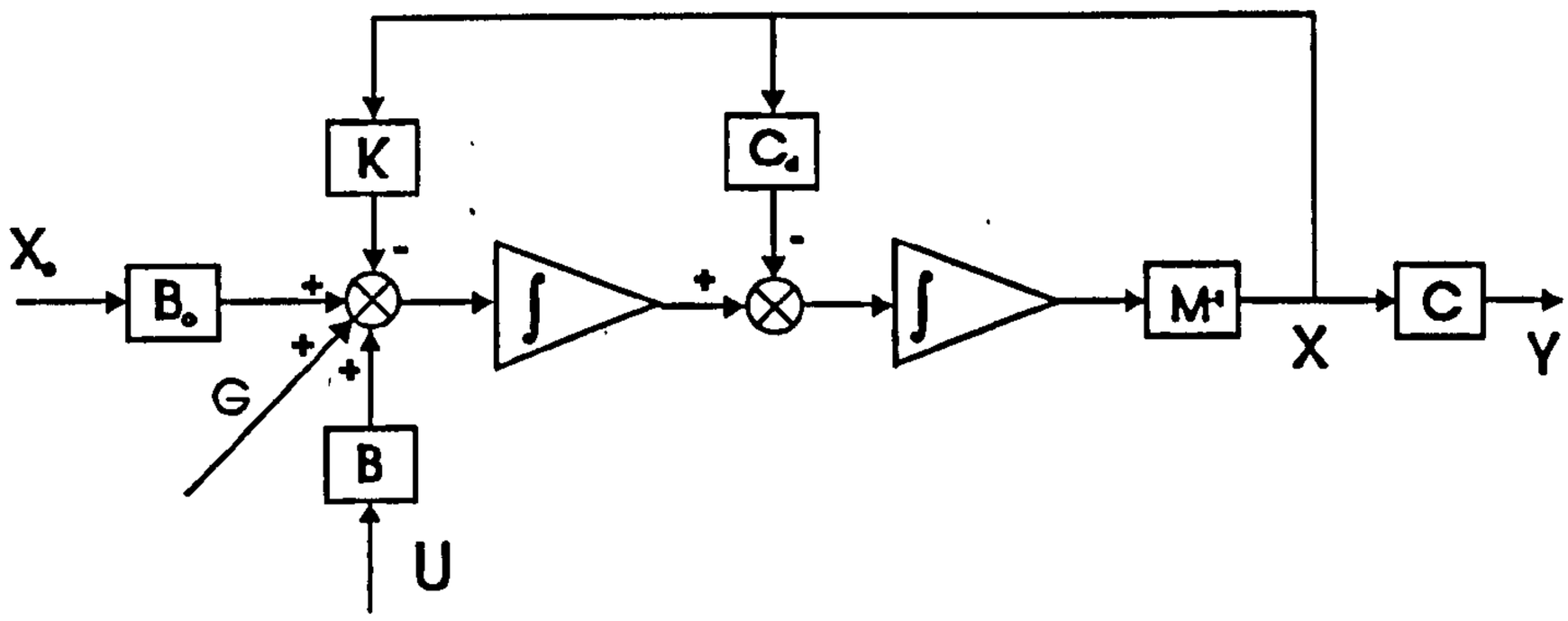

Figure 4-2 Block diagram of the system.

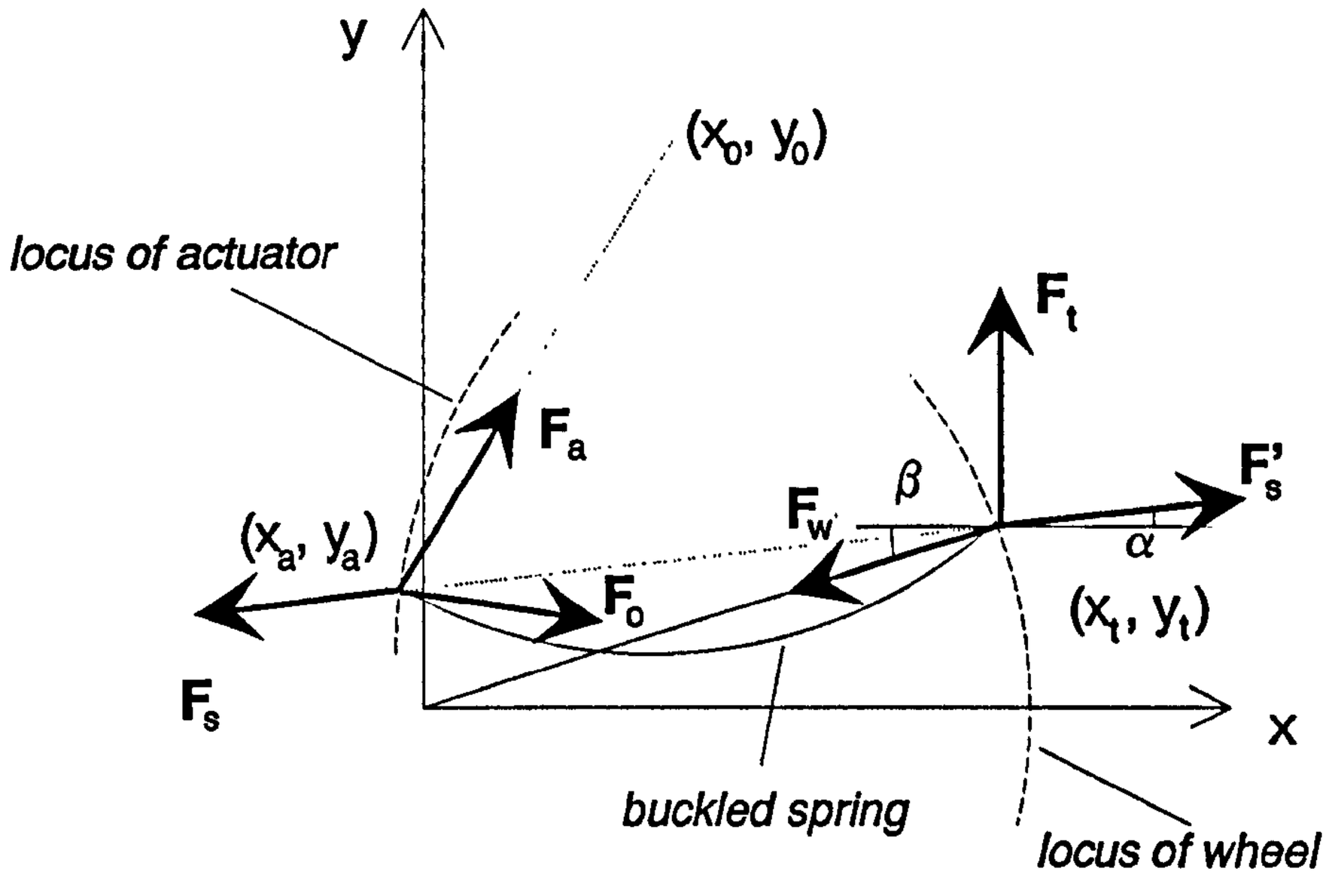

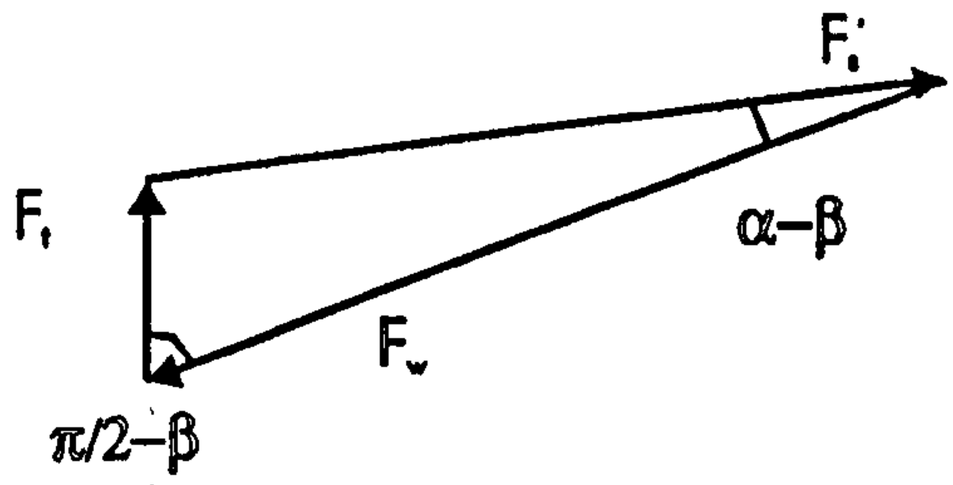

Figure 4-3 Analytical model of the actuator system.

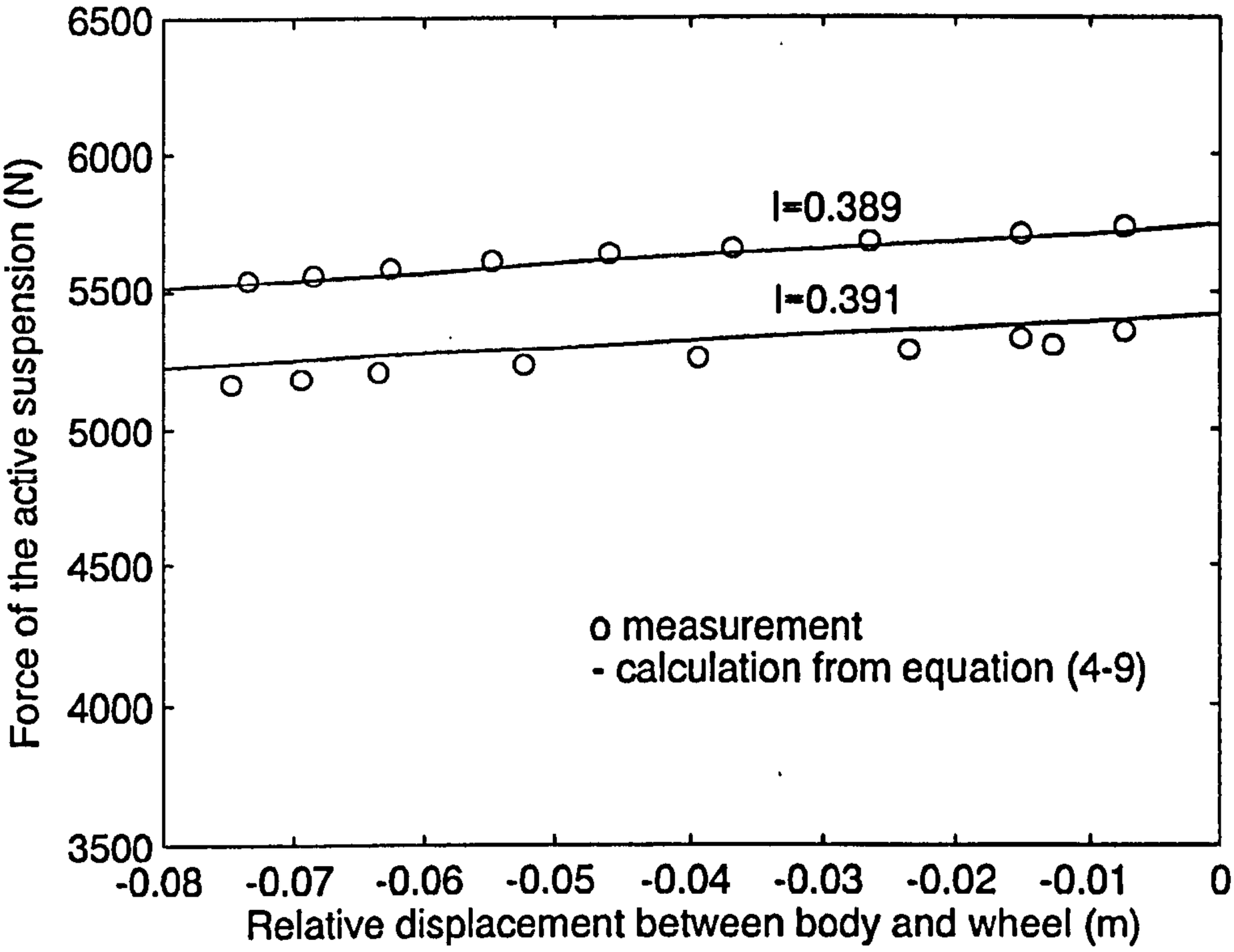

Figure 4-4 Measured and calculated force of the active suspension.

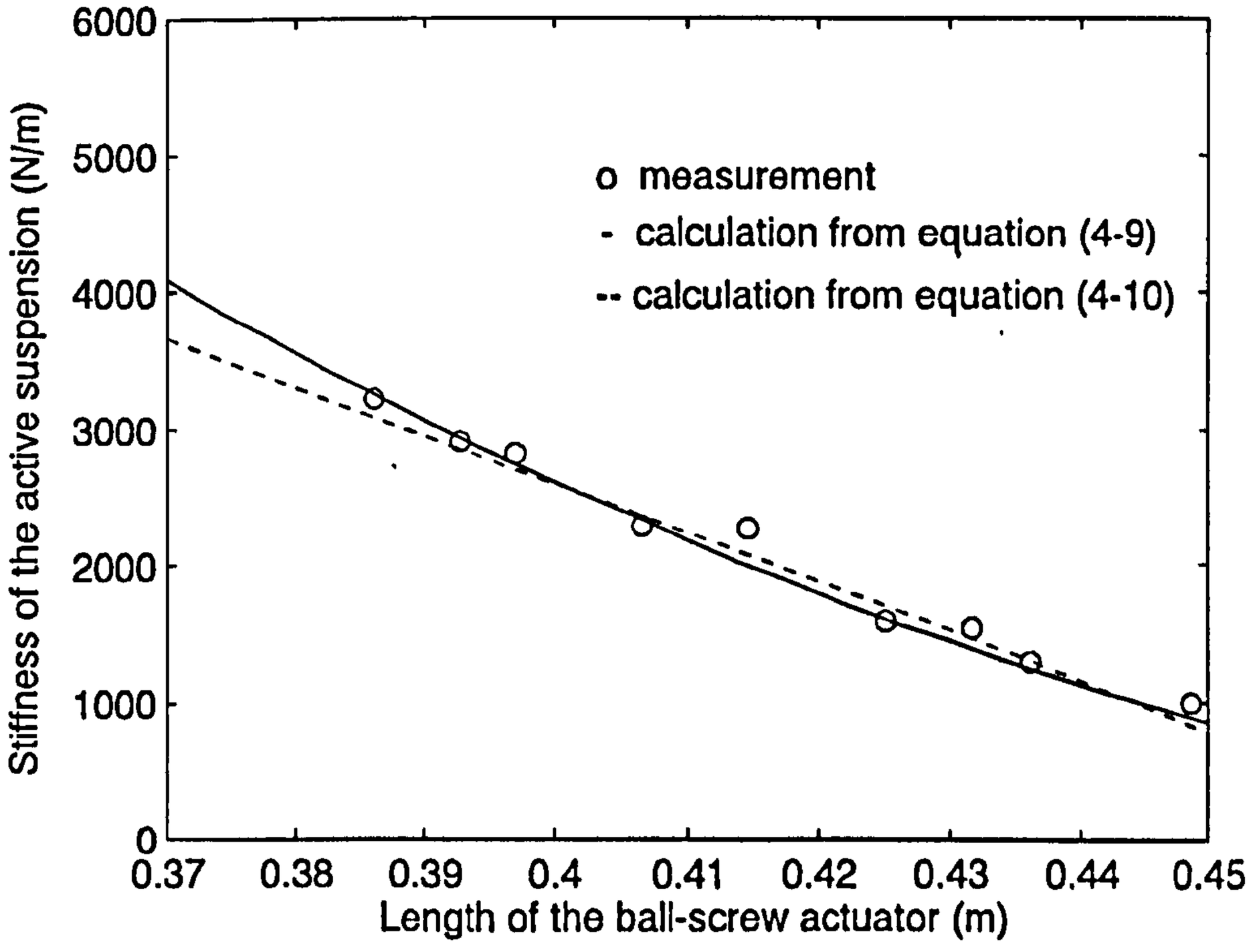

Figure 4-5 Comparison of measured and predicted stiffness of the actuator system.

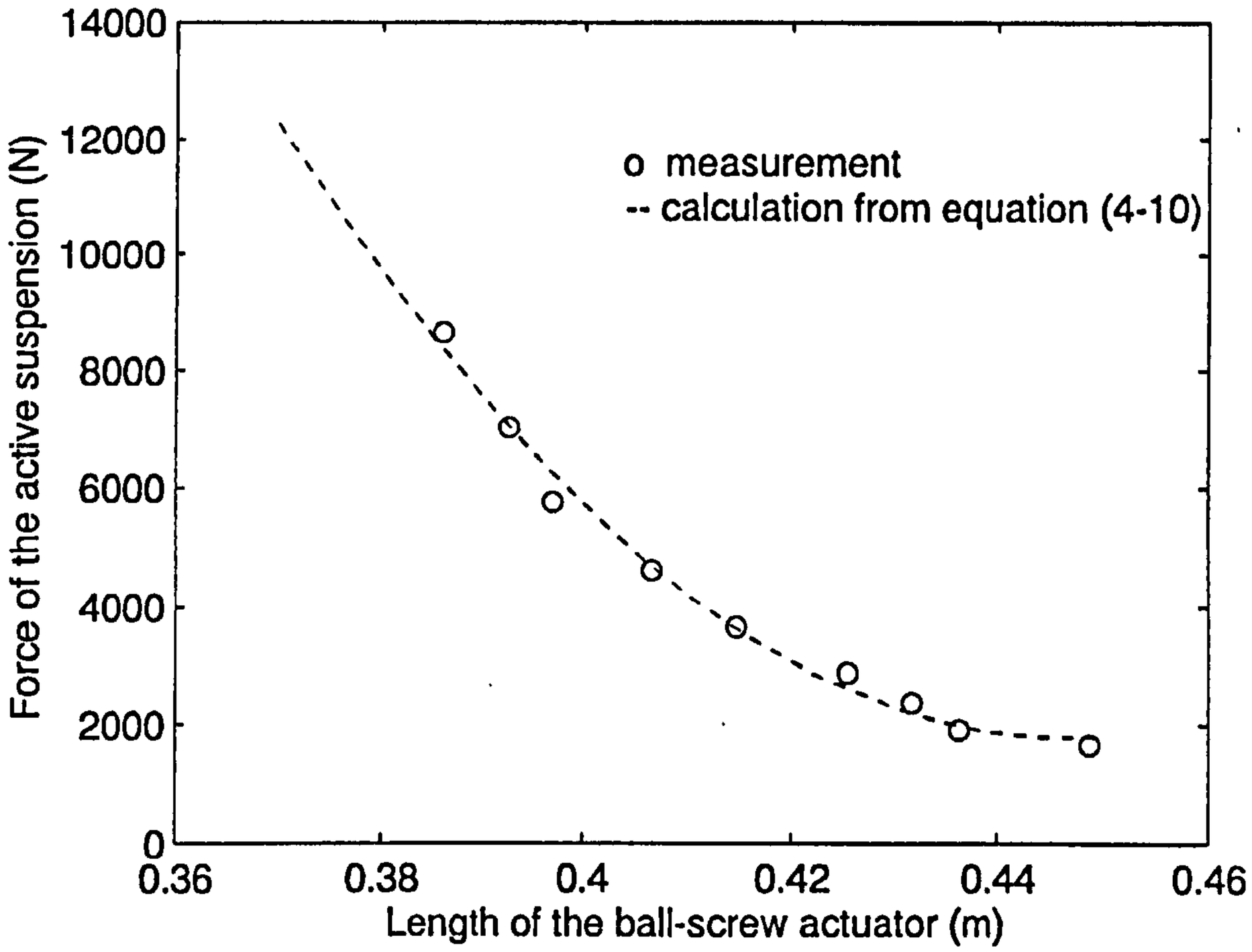

Figure 4-6 Force of the active suspension from experiment and prediction for y_t=0

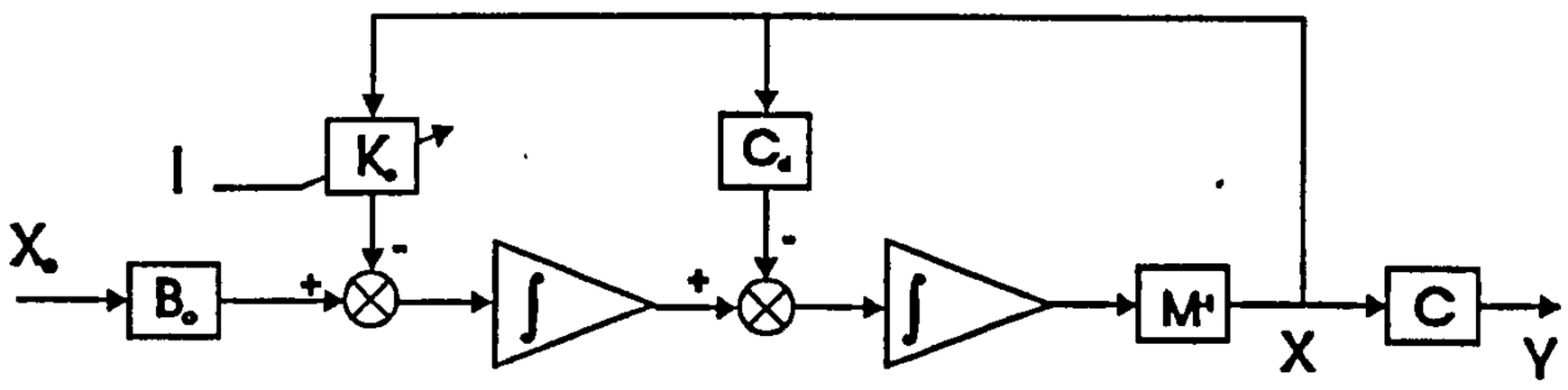

Figure 4-7 Block diagram of the open-loop control system.

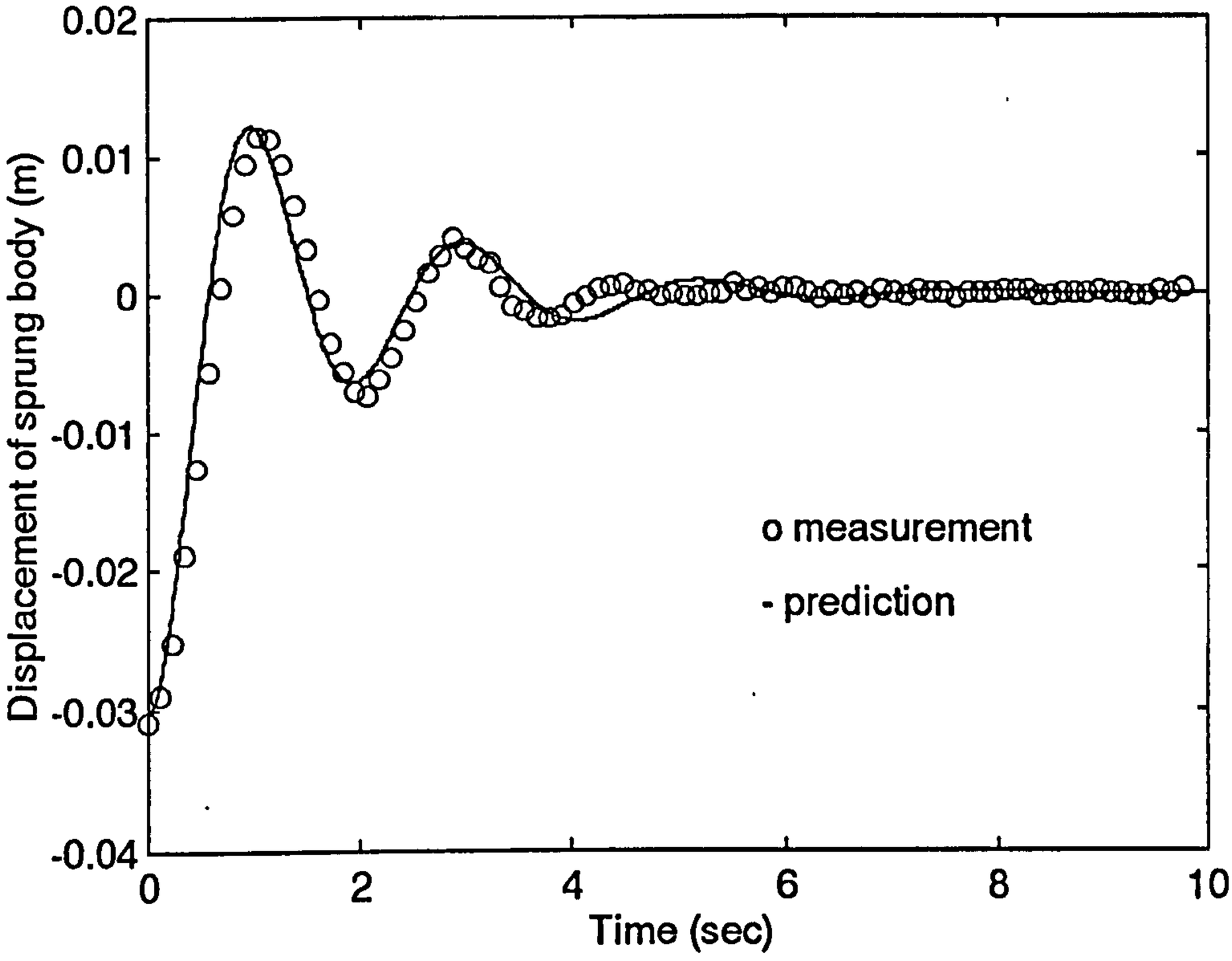

Figure 4-8 Predicted and measured free vibration of the trailer body at l=0.453m

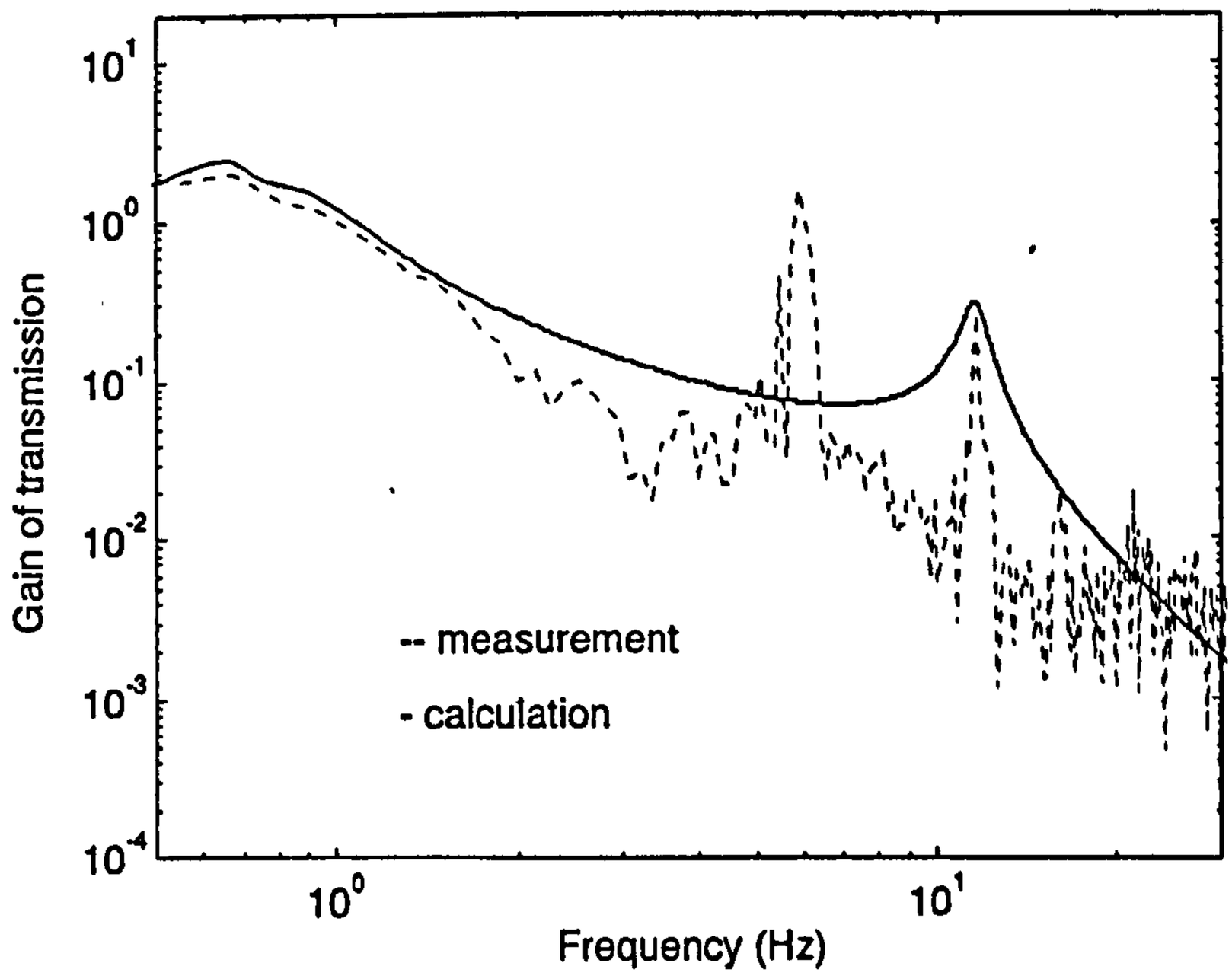

Figure 4-9 Frequency response function of the right side of the body from the right wheel

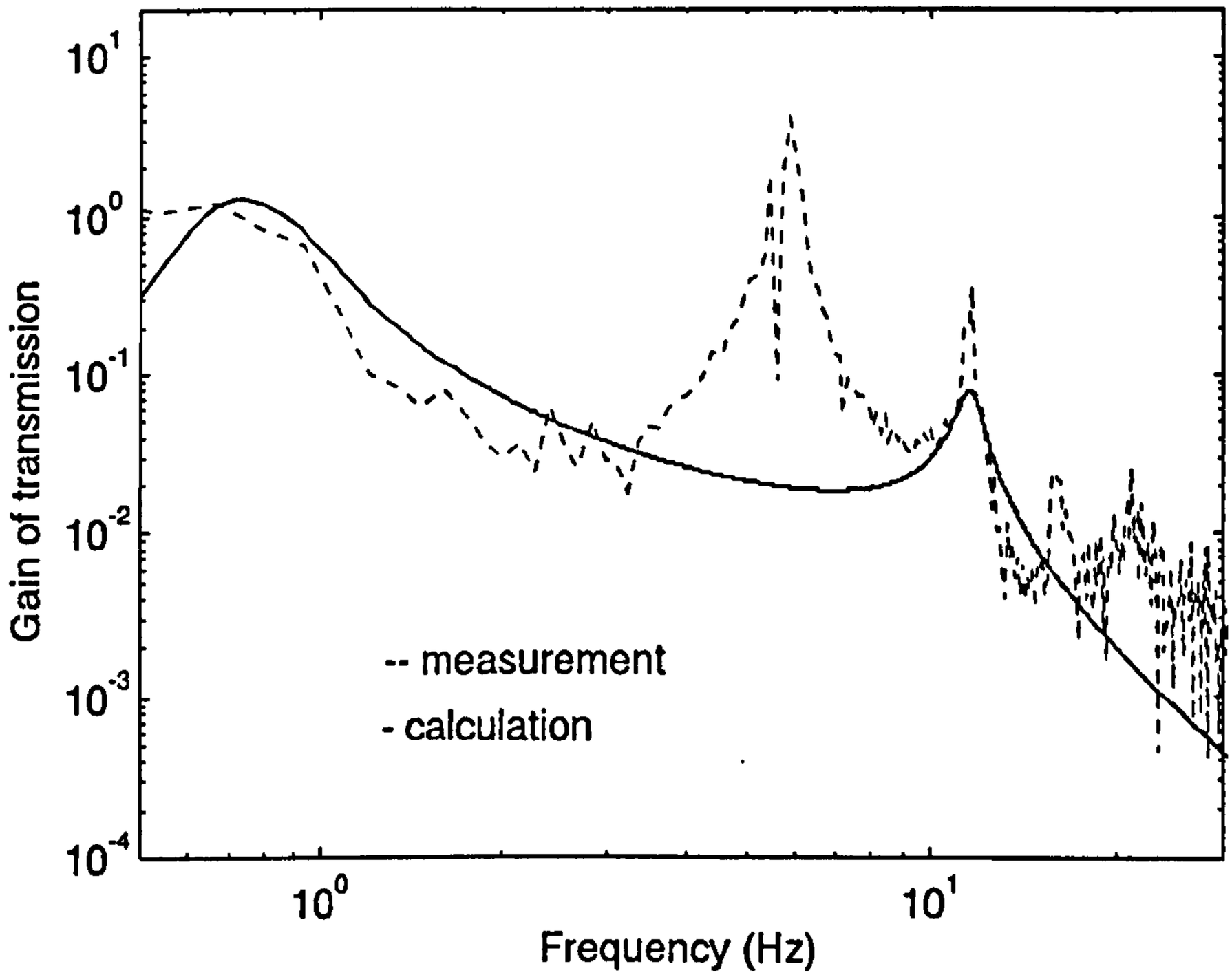

Figure 4-10 Frequency response function of the right side of the body from the left wheel

Chapter 5

Nonlinear Behaviour of the Active Zero Rate Suspension with PD Controller

5.1 Introduction

At present, most of the studies dealing with the analysis and design of active suspensions consider a linear suspension model: the suspension components are linearized around the operating point and control laws are derived using linear model-based control methods such as optimal LQ or H_∞ robust control etc. Although these control methods are of simple implementation, they do not allow full exploitation of the active control resources when they are applied to nonlinear active suspensions.

This chapter presents initial work based on the nonlinear quarter-car model of the active zero rate suspension. The operation of a PD controller for ride height control and vibration isolation is investigated both theoretically and experimentally. In this initial work, a quarter car model was employed. In the next chapter, a half car model will be used to allow the design of a more appropriate controller for the prototype.

5.2 Quarter-car Model with Nonlinear Control Force over Low-pass Bandwidth

The quarter-car model to be used is shown in figure 5-1. Here, the coupling between height and roll motions of the sprung mass is ignored because only vertical motion is taken into account. The motion equation of the system can be derived below by means of Lagrange's equation.

$$M\ddot{X} + C_d\dot{X} + KX = B_c X_c + BU + G \qquad (5\text{-}1)$$

where

the mass matrix $M=diag\{m_0, m_t\}$

the damping matrix $C_d = \begin{bmatrix} c_0 & -c_0 \\ -c_0 & c_0 + c_t \end{bmatrix}$

the stiffness matrix $K = \begin{bmatrix} 0 & 0 \\ 0 & k_t \end{bmatrix}$

the excitation matrix $B_c = \begin{bmatrix} 0 & 0 \\ c_t & k_t \end{bmatrix}$

the control matrix $B = \begin{bmatrix} 1 \\ -1 \end{bmatrix}$

the static load matrix $G = \begin{bmatrix} -m_0 g \\ -m_t g \end{bmatrix}$

the state vector $X = \begin{Bmatrix} x_0 \\ x_t \end{Bmatrix}$

the excitation vector $X_c = \begin{Bmatrix} \dot{x}_c \\ x_c \end{Bmatrix}$

the control vector $U = \{F_a(l, x_0, x_t)\}$

here m_0 is the mass of half the trailer body and m_t is the mass of the wheel. k_t and c_t denote the stiffness and the damping of the tyre respectively and c_0 denotes the conventional damping such as friction. The static load is considered here because the height is affected by the force due to gravity.

F_a is the force produced by the active zero rate suspension, which is a function of the length of the ball-screw actuator (l), the displacement of the trailer body (x_0) and the wheel (x_t). According to the analysis of the last chapter, the simplified expression of this force is

$$F_a = a_0 + a_1 l + a_2 l^2 + (a_3 + a_4 l)(x_0 - x_t) \qquad (5\text{-}2)$$

where a_j (j=0, ..., 4) are the coefficients from the Taylor's expansion. From the results of the validation, equation (5-2) is the simplest form for the nonlinear actuator force.

The ball screw length is set by a DC servo motor with position and velocity feedback and analogue control electronics. This may be modelled most simply as a first order system with a transfer function of:

$$l = \frac{G_{DC}}{1 + s/\omega_0} v \tag{5-3}$$

where ω_0 is the cut-off frequency, G_{DC} is the DC input/output gain, and v is the input voltage. For convenience, the input v can be transferred to $u=G_{DC}v$ with a length dimension and the equation (5-3) can be expressed by a time domain differential equation as follows

$$\dot{l} + \omega_0 l = \omega_0 u \tag{5-4}$$

The value of ω_0 was established by testing the physical actuator system and 'best-fitting' a first order response. This identified a cut off frequency of 5Hz. The comparison between the measurement and model is shown in figure 5-2. The quite good agreement demonstrates that such a model adequately describes the actuator system. The bandwidth of the actuator system is thus around 5Hz, and this effectively limits the bandwidth of the entire suspension system.

The combination of equations (5-1), (5-2) and (5-4) gives the mathematical description of the quarter-car model with nonlinear control force and a limited bandwidth.

From the actual installation of the sensors on the prototype, namely a vertical accelerometer on the body and a body to hub displacement transducer, the observation equation can also be obtained, i.e.

$$Y = C X \tag{5-5}$$

where the observation matrix

$$C = \begin{bmatrix} 1 & 0 \\ 1 & -1 \end{bmatrix}$$

the output vector $$Y = \begin{Bmatrix} y_0 \\ y_1 \end{Bmatrix}$$

where y_0 is same as x_0, the height of the trailer body and y_1 is the relative height of trailer body height to wheel. This system can be described by means of the block diagram shown in figure 5-3. The nonlinear element is caused by the mechanical relationship of the zero rate suspension and the filter element is produced by the electrical circuits for the actuator. The next step is to design a feedback controller from output variables Y to the actuator input u.

5.3 Design of a Two Term Controller

As the initial work, a two term controller with proportional and derivative (PD) actions is introduced here for the height and vibration control. The controller effectively simulates a conventional spring and damper. The feedback equation is listed below:

$$u = ky_1 + c\dot{y}_1 = k(x_0 - x_t) + c(\dot{x}_0 - \dot{x}_t) \qquad (5\text{-}6)$$

where k and c are the gains for the displacement and the velocity (proportional gain and derivative, or velocity gain). Spring force and damping force can be effectively provided through gains k and c respectively, hence these parameters are named 'software spring rate' and 'software damping rate' through this chapter. There are many sophisticated methods to determine both factors for a linear system (e.g. Friedland, 1986). For this prototype, there are some special requirements, i.e.

- The proportional gain should produce appropriate displacements of the sprung body under various load conditions, i.e. the software spring rate must be sufficient to support the body weight.
- The gains should keep the closed-loop system stable to prevent control induced oscillations.
- The proposed body height should be reached from the original position when the system is turned on.
- The gains should provide good vibration suppression to the sprung body.

These requirements will be investigated individually.

5.3.1 Steady state height and stability

The Liapunov stability theory can be applied to not only a linear system but also a nonlinear system (Casti, 1985). The theory will be applied here.

On introducing the controller, the body height in steady state can be determined by using stability analysis. The stability of a possible body height depends on the eigenvalues of the linearized equation about this height for the nonlinear system. If all the eigenvalues of the linearized equation have negative real parts then the body height may be implemented. If one of the eigenvalues has positive real part then the body height can never be realised.

Combining equations (5-4) and (5-6) produces an equation describing the closed loop system response:

$$\dot{i} = \omega_0 (k(x_0 - x_t) + c(\dot{x}_0 - \dot{x}_t) - l) \qquad (5\text{-}7)$$

The body and wheel heights can be obtained by equating the accelerations, the velocities and the dynamic excitation to zero in equations (5-1), (5-2) and (5-7). Because equation (5-2) is second order nonlinear, there are two sets of solutions for the heights, i.e.

$$\begin{cases} x_0^{(1)} = \dfrac{-(a_1 k + a_3) + \sqrt{(a_1 k + a_3)^2 - 4k(a_0 - m_0 g)(a_2 k + a_4)}}{2(a_2 k^2 + a_4 k)} \dfrac{g}{k_t}(m_0 + m_t) \\ x_t^{(1)} = \dfrac{g}{k_t}(m_0 + m_t) \end{cases} \qquad (5\text{-}8)$$

and

$$\begin{cases} x_0^{(2)} = \dfrac{-(a_1 k + a_3) - \sqrt{(a_1 k + a_3)^2 - 4k(a_0 - m_0 g)(a_2 k + a_4)}}{2(a_2 k^2 + a_4 k)} \dfrac{g}{k_t}(m_0 + m_t) \\ x_t^{(2)} = \dfrac{g}{k_t}(m_0 + m_t) \end{cases} \qquad (5\text{-}9)$$

By using the Routh-Hurwitz criterion on the eigenvalue equations of the linearized system for equations (5-1), (5-2) and (5-7), it can be established that the heights $\{x_0^{(2)}, x_t^{(2)}\}$ can be realised when the control parameters k and c are in the stable region as shown in figure 5-4, but $\{x_0^{(1)}, x_t^{(1)}\}$ cannot. This stable region is obtained from the linearised equation of this system. This means that for the parameters in this region, the steady state heights $\{x_0^{(2)}, x_t^{(2)}\}$, obtained from the nonlinear equation, can only be stable when the initial state of the motion starts from a sufficiently closed point.

From equation (5-9), it can be learnt that the relative height y_1 of the trailer body is affected by its mass m_0 and the software spring rate k. Such effect is illustrated in figure 5-5. It is shown in this figure, that increasing the spring rate k reduces the body height and increasing the mass of the body also reduces its height. The effect of spring rate changes is unconventional, and stems from the effective demanded position of y_1=0 implied by the control algorithm. In the test rig, maximum body height can be about 17cm, which means that the spring rate can not be too low if the body height should not be greater than that value.

When the PD controller is introduced, the whole system changes to the model described by the block diagram shown in figure 5-6. In this figure, the loop from the output y_1 to the input u is connected by means of the PD controller, which lifts the sprung body by balancing the gravity force.

5.3.2 Simulation and reachability of the stable equilibrium

One way of evaluating the performance of a control system is the step response (Since the step response is the body motion when the control system is switched-on initially, it is also called 'starting response' in this thesis). This is particularly appropriate to nonlinear systems and is used here to evaluate the PD controller. The wheel height x_t is independent of the control parameters, so the relative height of the body to the wheel, y_1 may be used to indicate the actual body height and is a more accessible parameter than x_0, the true body height. In this section, y_1 will therefore be referred to as the 'body height'.

The system was simulated using MATLAB software. The model is the two degree-of-freedom quarter car model including the nonlinearility and limited bandwidth of the active suspension. The differential equation is solved numerically by means of the fourth order Runge-Kutta formula.

The simulation results are shown in figures 5-7 and 5-8. There is a high frequency component, which is observed at small values of time in these figures. This component is caused by the coupling of the flexibility of the tyre.

Figure 5-7 is the response of the body height when the software damping rate c=0.04. Changes in software spring rate k cause changes of the steady-state body height and the transient-state motion of the trailer body. It is demonstrated that increasing the spring rate can make the body height lower and cause the transient motion to be less well damped. The rise time from initial position to the steady-state body height does not appear to change significantly with increasing spring rate, which is different from the performance of a usual linear system. This difference will be explained in the next section, the frequency response analysis.

Figure 5-8 is the starting response of the body height when the software spring rate k=0.45. It is shown that decreasing the software damping rate results in a faster rise time and more oscillatory motion while the steady-state height of the trailer body remains the same. These effects are similar to those expected in a linear system.

In a linear system without a limited bandwidth actuator, there is mathematically no limit to the spring rate and damping rate. That is not true in the nonlinear model with the limited bandwidth actuator. It is shown in figure 5-9 that the response becomes unstable when the spring rate changes from 0.50 to 0.55. In other words, the trailer body cannot reach a stable steady-state height at k=0.55. It can be seen in figure 5-10 that the response becomes unstable when the software damping rate changes from 0.35 to 0.38. The control system with higher damping rate c=0.38 does not allow stable motion to the steady-state height.

It is demonstrated from both figures 5-9 and 5-10 that the trailer body can never reach a steady-state height when the control parameters are beyond certain limits, even though this height is stable one according to figure 5-4 which is obtained from the linearised equation of this nonlinear system. In a linear system, increasing damping rate increases stability, but the motion here of the nonlinear system does the opposite suddenly as shown in figure 5-10. This unusual phenomenon is worthy of further discussion.

The motion is determined by the following factors

1) The differential equation governing the motion.
2) The initial state of the motion.

If a system is linear, then the motion will always reach the stable height regardless of the initial state. If a system is nonlinear, then the motion will only attain a stable steady state height if the initial value lies within the same 'stable region' as the final value.

The steady-state height is solved from the nonlinear differential equation. The stability of the body height, the region shown in figure 5-4, is obtained by means of the eigenvalues of the linearized equation for this nonlinear differential equation. That means that when the parameters are in the stable region in figure 5-4, the motion which starts from a point sufficiently close to the steady-state height can achieve this height stably.

In the nonlinear case, the stability of the starting response is strongly related to the initial state. When the stable region in state space encloses the initial state, the response will be stable. Otherwise, the motion approaches a different height or an infinite value. The form and extent of the stable region depends on the value of the control parameters, i.e. the software spring and damping rates in this case. There is no

definitive method for establishing the stable region in both state space and parameter space for a nonlinear system, but a numerical solution can be applied.

A standard technique for a low degree-of-freedom system is numerical phase plane (the state space of one degree-of-freedom) analysis. The boundaries in the phase plane can be calculated by using numerical integration and are shown in figures 5-11, 5-12 and 5-13.

To demonstrate the phenomenon clearly and simply, the figures were obtained from the simpler model in which the limited bandwidth of the actuator, the mass and stiffness of the wheel were neglected, i.e. using one mass quarter car model without the limited bandwidth.

In these figures, the x coordinate denotes the body height and the y coordinate denotes its velocity. The stable regions for the steady state are the areas below those curves which encloses the steady state (final value). When the initial state is in such regions, the starting response will be stable and can reach the steady state body height $y_1^{(2)}$. The origin represents the initial state of the trailer body for the prototype with zero displacement and zero velocity.

It is shown in figure 5-11 how the software spring rate k affects the stability boundary. The stable region is reduced with the spring rate k increasing. The initial state of zero height and zero velocity is originally enclosed in the stable regions. When k=2, finally, the initial state is excluded by the stable region, which means physically that the starting response with this parameter can never reach the steady state body height $y_1^{(2)}$ from the initial state.

The effect of the software damping rate c on the stable boundary is demonstrated in figure 5-12. This figure shows that extreme damping rates can cause the stable region not to enclose the initial state. On one end, when the damping rate decreases from c=0.2, the stable region retreats in both the y direction and the x direction and finally the initial state is excluded by the stable region. On the other end, the stable region becomes smaller with the increase of the velocity gain and finally the initial state point is excluded by the region. On other words, both over large and over small damping rate can cause the steady state to be unreachable from the initial state.

Figure 5-13 illustrates the effect of the mass of the trailer body on the stable boundary. When the mass is reduced, the stable region shrinks and finally excludes the initial state when the mass of the sprung body m=170kg. This shows that a small mass can also cause the steady state height to be unreachable from the initial state.

The nonlinearity is the reason for these stable regions. That obviously limits the control performance for the suspension system. There are two options to reduce the nonlinearity. The first is to modify the structure of the suspension system. The second is to develop a nonlinear controller which, through a compensation system, can linearise the whole control system. The first choice needs more extensive investigation into the mechanical design of this zero rate suspension, which may be costly and time consuming. The second option requires no mechanical changes but it is difficult to determine an appropriate nonlinear controller because there is no general method that can be applied and a great deal of nonlinear analysis is required in advance. Another large obstacle for the second is the implementation of the nonlinear controller because the nonlinear algorithm can increase processing time considerably. Hence both options are extensive projects which can be considered in the future. There might be an option to develop an appropriate controller which can improve the stable regions to make control performance acceptable without reducing the nonlinearity. This could be a practical choice and will be investigated in the next chapter.

By using simulation on the one mass quarter car model, the ranges of the software spring rate k and the software damping rate c for a stable response from the initial state of zero height and zero velocity to the steady state height can also be obtained as shown in figure 5-14. In this figure, the upper curve is the reachable boundary based on the model excluding the limited bandwidth of the actuator system (equation (5-4)) and the lower curve is the reachable boundary obtained from the model with the limited bandwidth. The areas below both curves are the stable regions in which the motion from the initial state can stably reach the steady state height. The large difference between the two curves shows that the limited bandwidth of the actuator system plays a significant role in the stability of the control system and deteriorates the stability considerably. This suggests that actuator bandwidth may be a limiting factor in the performance of the suspension system.

Figures 5-11 to 5-14 were obtained based on the one mass quarter car model (with or without limited bandwidth) in which the basic characteristics in the two mass quarter car model for figures 5-3 to 5-10, the suspension nonlinearity and actuator bandwidth, were retained. Therefore, the conclusions from figures 5-11 to 5-14 can explain the unstable behaviours occurred in those figures from the two mass quarter car model, though the particular curves in the former figures do not apply directly to the latter.

5.3.3 Frequency response analysis

The frequency response of the system is important in the prediction of ride quality, but cannot be readily defined for a nonlinear system. This section describes the application of a linearisation process to determine the frequency response at the normal operating height. The motion around the steady state body height $y_1^{(2)}$ is governed by the following equation which is derived from equations (5-1), (5-2), (5-5) and (5-7):

$$\dot{Z} = AZ + F_z + B_{zc} X_c \qquad (5\text{-}10)$$

where

$$A = \begin{bmatrix} 0 & 0 & 1 & 0 & 0 \\ 0 & 0 & 0 & 1 & 0 \\ 0 & \frac{1}{m_0}(a_3 + a_4 k y_1^{(2)}) & 0 & -\frac{c_0}{m_0} & \frac{1}{m_0}(a_1 + a_4 y_1^{(2)} + 2a_2 y_1^{(2)} k) \\ \frac{k_t}{m_t} & \frac{m_0+m_t}{m_0 m_t}(a_3 + a_4 k y_1^{(2)}) - \frac{k_t}{m_t} & \frac{c_t}{m_t} & -\frac{c_t}{m_t} - c_0 \frac{m_0+m_t}{m_0 m_t} & \frac{m_0+m_t}{m_0 m_t}(a_1 + a_4 y_1^{(2)} + 2a_2 y_1^{(2)} k) \\ 0 & \omega_0 k & 0 & \omega_0 c & -\omega_0 \end{bmatrix}$$

$$F_z = \left\{ 0 \quad 0 \quad \frac{1}{m_0}(a_2 z_5^2 + a_4 z_5 z_2) \quad (\frac{1}{m_0} + \frac{1}{m_t})(a_2 z_5^2 + a_4 z_5 z_2) \quad 0 \right\}^T$$

$$B_{zc} = \begin{bmatrix} 0 & 0 & 0 & -\frac{c_t}{m_t} & 0 \\ 0 & 0 & 0 & -\frac{k_t}{m_t} & 0 \end{bmatrix}^T$$

$$Z = \{ z_1 \quad z_2 \quad z_3 \quad z_4 \quad z_5 \}^T$$

$$= \{ y_0 - y_0^{(2)} \quad y_1 - y_1^{(2)} \quad \dot{y}_0 \quad \dot{y}_1 \quad l - k y_1^{(2)} \}^T$$

Provided only small amplitude vibration is involved, a linearized form of equation (5-10) can be used.

Eigenvalue analysis is one of the most accepted linearisation techniques. When applied to equation (5-10) the natural frequencies of the various elements in the system can be determined. The results of this are shown in figures 5-15, 5-16, 5-17 and 5-18 (where a_0=12255, a_1=-273020, a_2=1777400, a_3=36000, a_4=-3741, c_0=600, ct=2, ω_0=10π, m_0=250, m_t=40, and k_t=3*10^5), which illustrate the effect of the control parameters on the natural frequencies and the damping ratio. Low natural frequencies means that the control system provides good isolation and high damping ratio denotes that it can effectively attenuate body vibration and stabilise body motion.

Figure 5-15 shows the effect of the software spring rate *k* on the natural frequencies. When the spring rate changes, the frequency of the trailer body height mode changes between about 1.5Hz and 3Hz. This algorithm uses the direct feedback relationship between the body displacement to the initial height. This gives rise to the negative slope at low *k* values. If the feedback of the displacement to the steady-state height were used then the curve would slope to much lower natural frequencies at low k values. The frequency due to tyre stiffness remains around 16Hz.

Figure 5-15 also suggests that the software spring rate can only affect the frequencies slightly at the high values of *k* required to maintain body height; at lower values of *k* (not realisable with this algorithm) the natural frequency would drop more rapidly. That is why the rise time of the starting response in figure 5-7 does not appear to change significantly with this parameter.

It is shown in figure 5-16 that the damping ratios of the two modes tend to be smaller when the spring rate increases from 0.12 to 2. When *k* is larger than about 1.2, the body height mode becomes unstable. These gives another point of view for the stability, i.e. the larger spring rate degrades the stability.

The effect of the software damping rate *c* on the natural frequencies is illustrated in figure 5-17. The frequencies of both modes increases with the rate rising. Such effects of the damping rate again, only in the region considered are stronger than those of the spring rate. On the other hand, the damping ratio of the body height mode decreases when the damping rate increases from about 0.05 as shown in figure 5-18, which means physically that increasing the damping rate deteriorates the stability of the motion. These are very different from the characteristics of the damping rate in conventional linear control systems.

For optimum ride quality, a low natural frequency and high damping ratio are required. By synthesising the figures 5-15 to 5-18 and 5-5, the choice of the parameters from this viewpoint for the desired ride quality, is around k=0.4 and c=0.05. The damping ratios and the natural frequencies for this closed-loop system are compared with those for the open-loop system at the same steady state condition in table 5-1. The damping ratio of only the wheel mode is clearly increased by the controller. As the trade-off, the damping ratio of the body mode is decreased slightly and the natural frequencies are increased to 2.2Hz and 16.3Hz. The body mode frequency is too high to give acceptable ride comfort.

The free vibration of both systems are simulated numerically based on the nonlinear equation, as shown in figures 5-19 and 5-20. In the figures, the open-loop input is the

same as the value of the closed-loop system at the steady state, and the initial states and other parameters in both cases are same. It is illustrated in figure 5-19 that the vibration of the trailer body can be attenuated by the PD controller more quickly than by the open-loop with the constant input, because the body mode frequency for closed-loop is much higher than that for open-loop. In figure 5-20, the vibration of the wheel is suppressed by the PD controller in a similar time to that by the open-loop with the constant input. These show that the PD controller can control the vibration characteristics of the zero rate suspension.

The above findings show that the PD controller with relative damping can provide the prototype with the following performances:

1) Able to support the quite various weight of the trailer at an appropriate mean ride height.
2) Able to prevent violent trailer body motion and to damping out oscillation.
3) Able to degrade damping of the body mode slightly.
4) Able to isolate the trailer body from road disturbances with over 2Hz in frequency domain.
5) Does not improve damping significantly of the wheel motion.

The last three items are not what we expected and are important for ride quality and vehicle handling, so the performance needs to be improved with other control strategies.

5.3.4 PD controller with sky-hook damping

The 'sky-hook' damping is an important concept in the area of active suspensions. This technique is believed simple and effective for vehicle suspension control. In this chapter, the feedback relationship is introduced as follows:

$$u = ky_1 + c\dot{y}_0 = k(x_0 - x_t) + c\dot{x}_0 \qquad (5\text{-}11)$$

In the following analysis, the same approaches will be employed, i.e. the same two mass quarter car model, with the same nonlinearity for active zero rate suspension and the actuator with the same limited bandwidth.

By using this controller, the same height as equation (5-9) of the trailer body at steady state can be obtained from equations (5-1), (5-4) and (5-5) because the body height depends on only the software spring rate. This steady state height $y_1^{(2)}$ is stable for the

parameters in the stable region as shown in figure 5-21 obtained from the linearised equation. The stable boundary is calculated by the same method and the same other parameters as that of figure 5-4. Comparison of both the figures suggests that the stability constraint for the sky-hook damping is stronger than that of the relative damping.

The block diagram of the closed-loop system with sky-hook damping is shown in figure 5-22. By applying a similar approach to equations (5-1), (5-2), (5-5) and (5-11), the motion equation around the steady state body height $y_1^{(2)}$ is obtained as follows:

$$\dot{Z} = A_1 Z + F_z + B_{zc} X_c \qquad (5\text{-}12)$$

where

$$A_1 = \begin{bmatrix} 0 & 0 & 1 & 0 & 0 \\ 0 & 0 & 0 & 1 & 0 \\ 0 & \frac{1}{m_0}(a_3 + a_4 k y_1^{(2)}) & 0 & -\frac{c_0}{m_0} & \frac{1}{m_0}(a_1 + a_4 y_1^{(2)} + 2a_2 y_1^{(2)} k) \\ \frac{k_t}{m_t} & \frac{m_0 + m_t}{m_0 m_t}(a_3 + a_4 k y_1^{(2)}) - \frac{k_t}{m_t} & \frac{c_t}{m_t} & -\frac{c_t}{m_t} - c_0 \frac{m_0 + m_t}{m_0 m_t} & \frac{m_0 + m_t}{m_0 m_t}(a_1 + a_4 y_1^{(2)} + 2a_2 y_1^{(2)} k) \\ 0 & \omega_0 k & \omega_0 c & 0 & -\omega_0 \end{bmatrix}$$

Other variables in the equation are the same as those in equation (5-10).

The effect of the control parameters on the natural frequencies and damping ratios of the system can be determined as before and is shown in figures 5-23, 5-24, 5-25 and 5-26. When the software spring rate k increases from 0 to 2, the natural frequency of the trailer body height mode decreases before k=0.15 and then increases from 1Hz to 3Hz, while the natural frequency of the wheel mode increases little around 14Hz, as shown in figure 5-23.

In figure 5-24, the damping ratio of body height mode increases with the spring rate rising before k=0.15. Then the body height damping ratio decreases and finally the motion becomes unstable after k=1.5. The damping ratio of the wheel mode is very small and decreases with the spring rate rising.

In figure 5-25, when the software damping rate c increases from about 0.055, the natural frequency of the body height mode increases sharply from about 2Hz to 11Hz. The frequency of the wheel mode changes little around 14Hz. These show that the effect of the damping rate on the body mode frequencies is stronger than that of the spring rate, which is quite different from the characteristics in conventional linear systems. It is demonstrated in figure 5-26 that the damping ratio of the trailer body

height mode increases before about c=0.06 and then decreases with the damping rate rising. The stability of the wheel mode is strengthened as the damping rate increases.

To obtain the optimum ride quality, low frequencies and high damping ratio, the choice of the parameters can be made by synthesising the figures 5-23 to 5-26 and 5-4, i.e. k=0.4 and c=0.055.

The only difference between both equations (5-10) and (5-12) is the coefficient matrix A and A_1 in which the positions of $\omega_0 c$ are different. This can cause quite different performances for the control system.

Comparing figure 5-24 and 5-16, we can find that for the same spring rate, the body damping ratio for the case of sky hook damping is clearly higher than that for the case of relative damping and the unstable boundary is pushed higher by the sky hook damping. But the damping ratio for the former case is less than the latter. For the same damping rate, the damping ratio in figure 5-26 is clearly higher than that in figure 5-18, which means again that the stability of the body height mode is improved by the sky hook damping.

It can be seen from comparison between figures 5-23 and 5-15 that the introduction of the sky hook damping affects little the natural frequencies of both body and wheel mode for the same spring rate. But the effect of the software damping rate on the body height mode in figure 5-25 for the sky hook damping is stronger than that in figure 5-17; and the effect on the wheel mode frequency in the former is lighter than the latter.

Table 5-2 lists the natural frequencies and the damping ratios for the relative damping controller and the sky-hook damping controller at their individual optimum parameters. It is shown that the natural frequency of the wheel mode for the sky-hook damping is smaller than that of the relative damping though the damping ratio for the sky-hook damping is lower. Compared with the relative damping, the natural frequency of the trailer body height mode is slightly smaller and the damping ratio for the same mode is much higher. Since the body height mode plays an important role in the suspension system, it can be concluded that the whole vibration behaviour is improved by the sky-hook damping with suitable parameters.

The free vibration of the control system with sky-hook damping is simulated and compared with that of the relative damping with same parameters k=0.6 and c=0.04, as shown in figures 5-27 and 5-28. It is shown that the sky-hook damping can produce better vibration suppression for the trailer body but does not improve the damping of the wheel vibration.

From above discussion, it is shown that this PD controller with sky-hook damping can clearly improve damping of the body vibration but still can not reduce the frequency of the trailer body to a satisfactory extent and can also not improve damping of the wheel vibration. These are caused by the constraint applied by body height control. This can easily be overcome by feed forward or integral action which are proposed to be examined at the next stage.

5.4 Experiment Results

The whole control system for the PC based prototype has been described in chapter 2. The block diagram of the control system is shown in figure 2-4 schematically. The signals are collected by the sensors. After going through the analogue anti-alias filters, they are transferred from the analogue form to the digital form by the A/D board. The digital signals are processed in the PC 80386 computer and then the generated control signals are sent to D/A board to be transferred into analogue form. These signals are processed in the analogue control circuits before being amplified in the power amplifier circuits. The final signals are sent to the motors which drive the zero rate suspension.

The PD algorithm has been implemented and confirms the model's predictions. Both relative damping and the sky-hook damping PD control have been implemented. Figures 5-29 and 5-30 illustrate the starting response of the sprung body in both cases, which shows that the control software is effective. The figures were not calibrated because only the form of the physical motion of interest, so the y coordinate units are not shown.

The effect of the software spring rate on the starting response is demonstrated in figure 5-29, When the gain increases, the steady state height of the trailer body becomes lower and the transient state motion tend to be more violent. The rise time from the initial state to the steady state body height does not change much. This behaviour is consistent with the theoretical analysis in section 5.3.

It is shown, in figure 5-31, that the software damping rate also produces similar performance on the starting response to the theoretical analysis. When the rate increases, the violence of the response is attenuated while the steady state body height is hardly changed. The damping rate provides a slight effect on the rising time of the response.

In the theoretical analysis on stability, the unstable motion approaches infinity. Actually, the unstable motion is just a undecaying oscillation with big amplitude due to the constraints of the mechanical structure. This can be seen in figures 5-32 and 5-33, in which the responses for, k=0.55 and c=0.03, and k=0.48 and c=0.065 are unstable. Both figures illustrate that the over large spring rate and over large damping rate can make the control system unstable. It is shown in figure 5-34 that heavier mass of the sprung body can give rise to more stable response. These phenomena confirm the theoretical prediction in last section.

The vibration attenuation of the PD controller with relative damping is shown in figure 5-35. The input of the open-loop control system is a constant value which is equal to that for the PD controller in steady state. The vibration of the sprung body for both cases is from the same initial state. It is shown that the vibration of the closed-loop system decays more quickly than that of the open-loop system. A drawback of the controller is that it causes a higher body natural frequency. This has been predicted in last section.

Figure 5-36 shows the comparison of the vibration attenuation for the PD controllers with relative damping and with sky-hook damping. It can be seen that the sky-hook damping can suppress the vibration of the sprung body faster than the relative damping. This effect was also predicted theoretically.

The unstable motion occurs in bounce and roll respectively or compositely. The composite motion is shown in figure 5-37. In addition to the reasons having been discussed, there are two other reasons for the instability. The first is a common view that the omission of the coupling between the bounce and roll motion in the quarter car model can undermine the performance of the controller.

The second is the non-identical properties on both sides of the test rig. Because of this, non-identical parameters are used in the control algorithm to achieve optimal performance on each side. In this case, different velocity gains may lead to very different natural frequencies on both sides due to the sensitivity of the latter as shown in section 5.2. This, in turn may cause the motion on both sides to be unstable. This phenomenon is shown in figure 5-38. Compared with figure 5-37, other components besides the primary harmonic in the roll motion are increased.

To improve the stability caused by these reasons, a half car model needs to be applied to design the controller for the prototype.

5.5 Conclusions

The simulation and experiment have shown that the application of the PD controller, with relative or sky-hook damping, to the zero rate active suspension can support the quite various weight of trailer at an appropriate mean ride height, prevent violent trailer body motion, damp out oscillation and provide the stable body height attitude, but cannot isolate the trailer body from road disturbances with less than 2Hz in frequency domain.

The drawbacks are not what we expected and are important for ride quality and vehicle handling. One of the reasons for that is the limitation of the PD controller in which two control parameters can not give a satisfactory combination for so many aspects.

Another cause of the drawbacks is the nonlinearity of the system which results in a limited stable region and constrains the control parameters. It is shown experimentally and numerically that over large software stiffness rate, over large or over small software damping rate, or over small mass of the trailer body can individually give rise to unstable motion of the trailer body.

In the nonlinear control system, the actuator bandwidth plays a significant role in the control performance. It leads to the stable region reducing considerably based on simulation, which means that the actuator bandwidth is the another limiting factor in the control performance.

To improve the performance of the zero rate suspension, three options can be tried.

- Applying other control strategies. The PID can be a candidate.
- Reducing the limitation on low proportional gains by means of the feedback of the displacement to the demanded height of the trailer body instead of the direct feedback of the displacement to the initial height used in this chapter.
- Designing the controllers based on the half car model which has been developed in chapter 4.

	closed-loop with PD control		open-loop with constant input	
	damping ratio	natural frequency(Hz)	damping ratio	natural frequency(Hz)
body mode	0.4770	2.1650	0.4966	0.3818
wheel mode	0.1137	16.2659	0.0873	13.7394

Table 5-1 The comparison between closed-loop and open-loop

	relative damping control		sky-hook damping control	
	damping ratio	natural frequency(Hz)	damping ratio	natural frequency(Hz)
body mode	0.4770	2.1650	0.8486	2.0763
wheel mode	0.1137	16.2659	0.0750	13.8027

Table 5-2 The comparison between sky-hook damping and relative damping

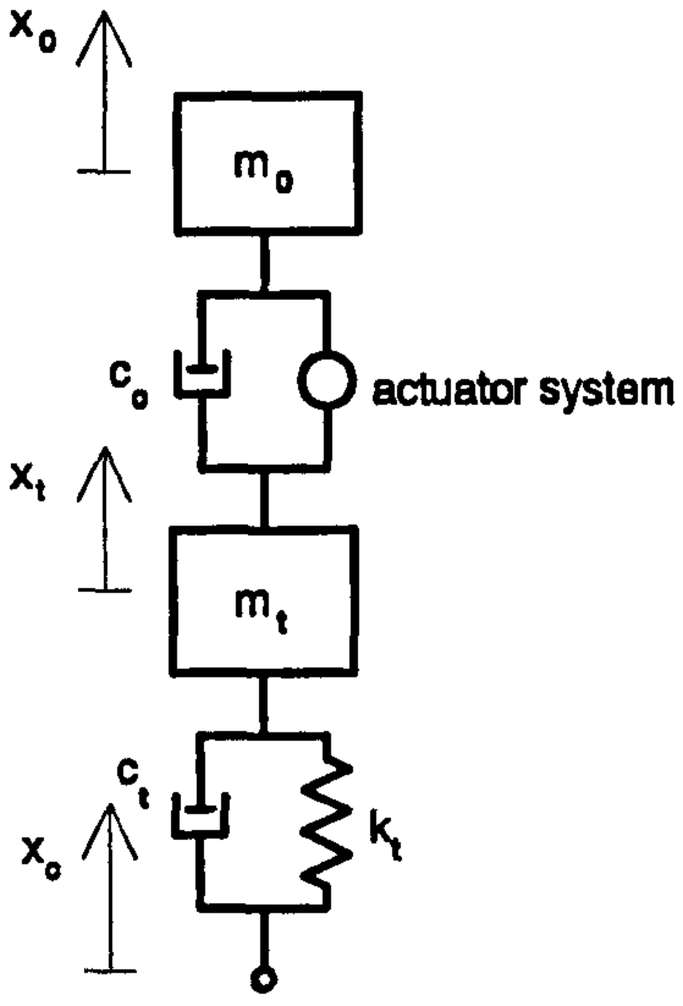

Figure 5-1 The quarter-car model

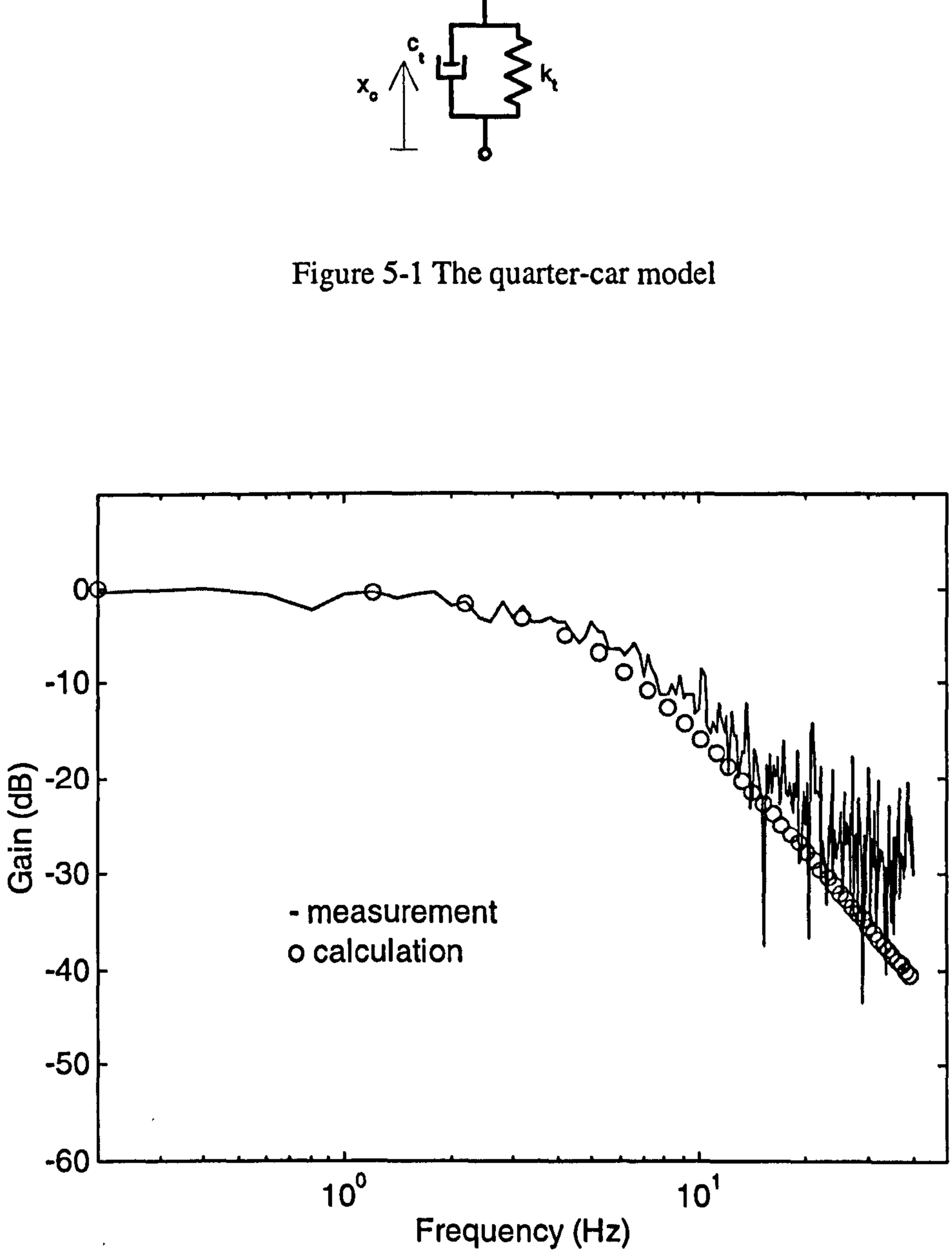

Figure 5-2 Measured and modelled actuator frequency response

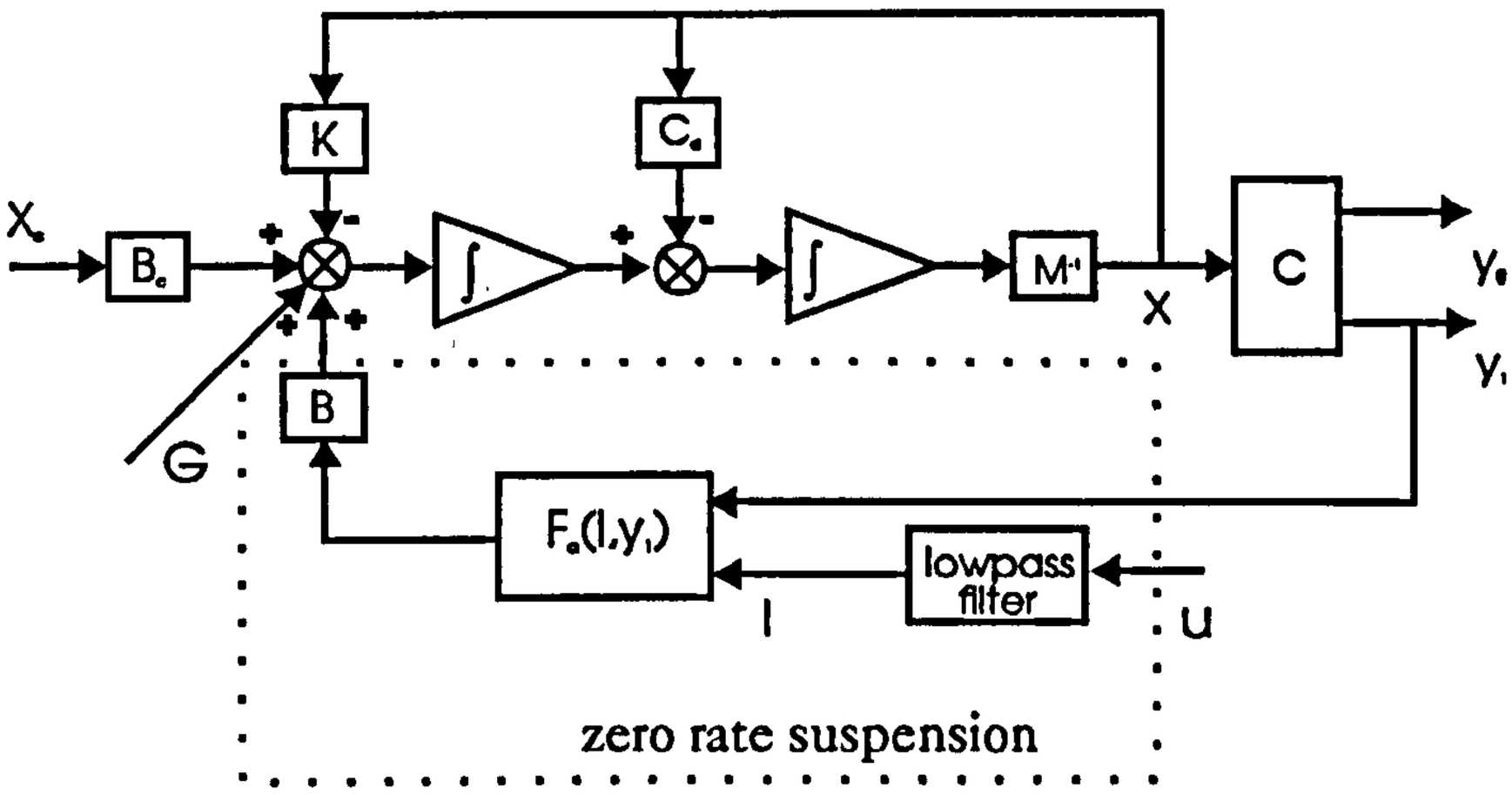

Figure 5-3 Block diagram for the model with open-loop

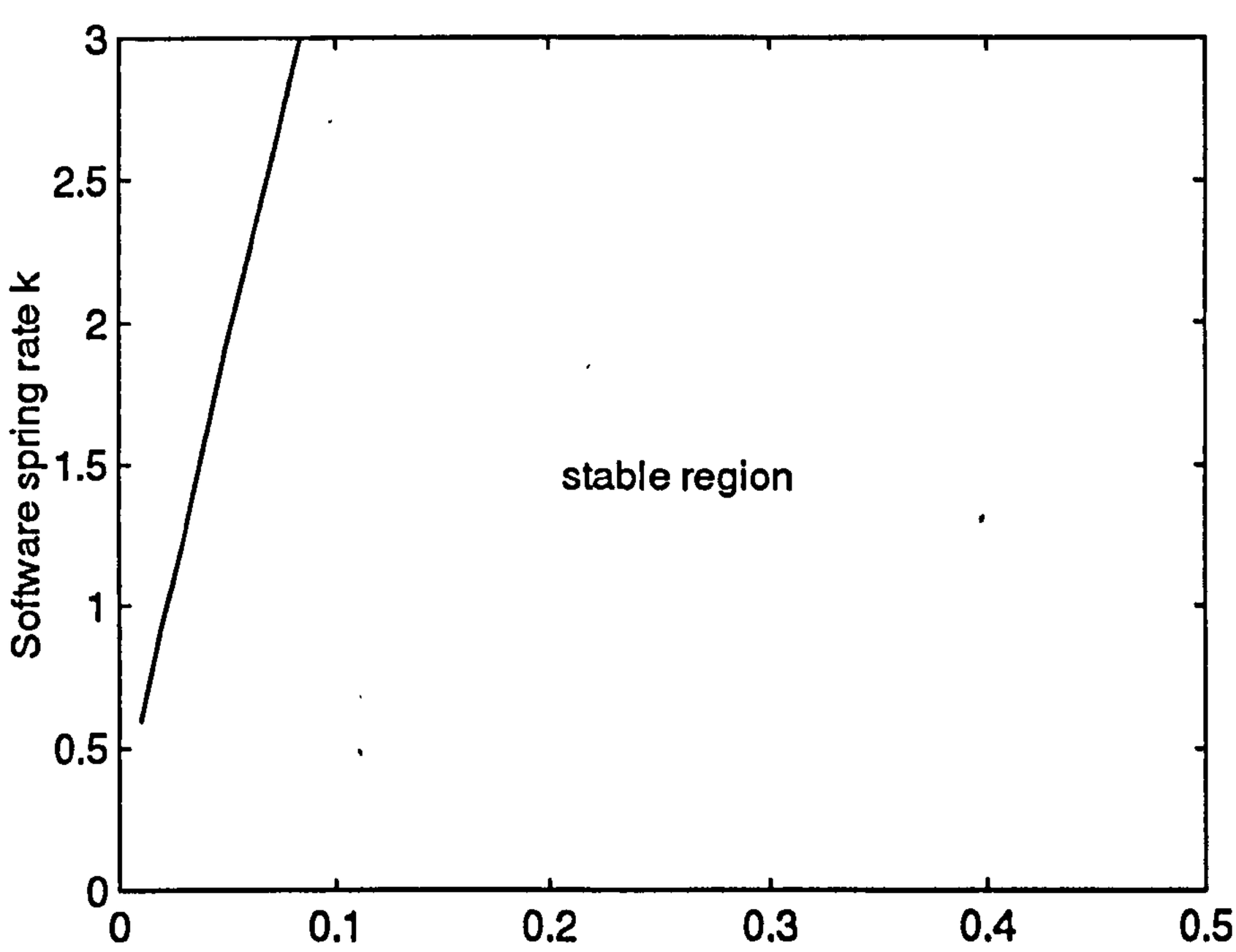

Figure 5-4 Stable region of the equilibrium for the control parameters

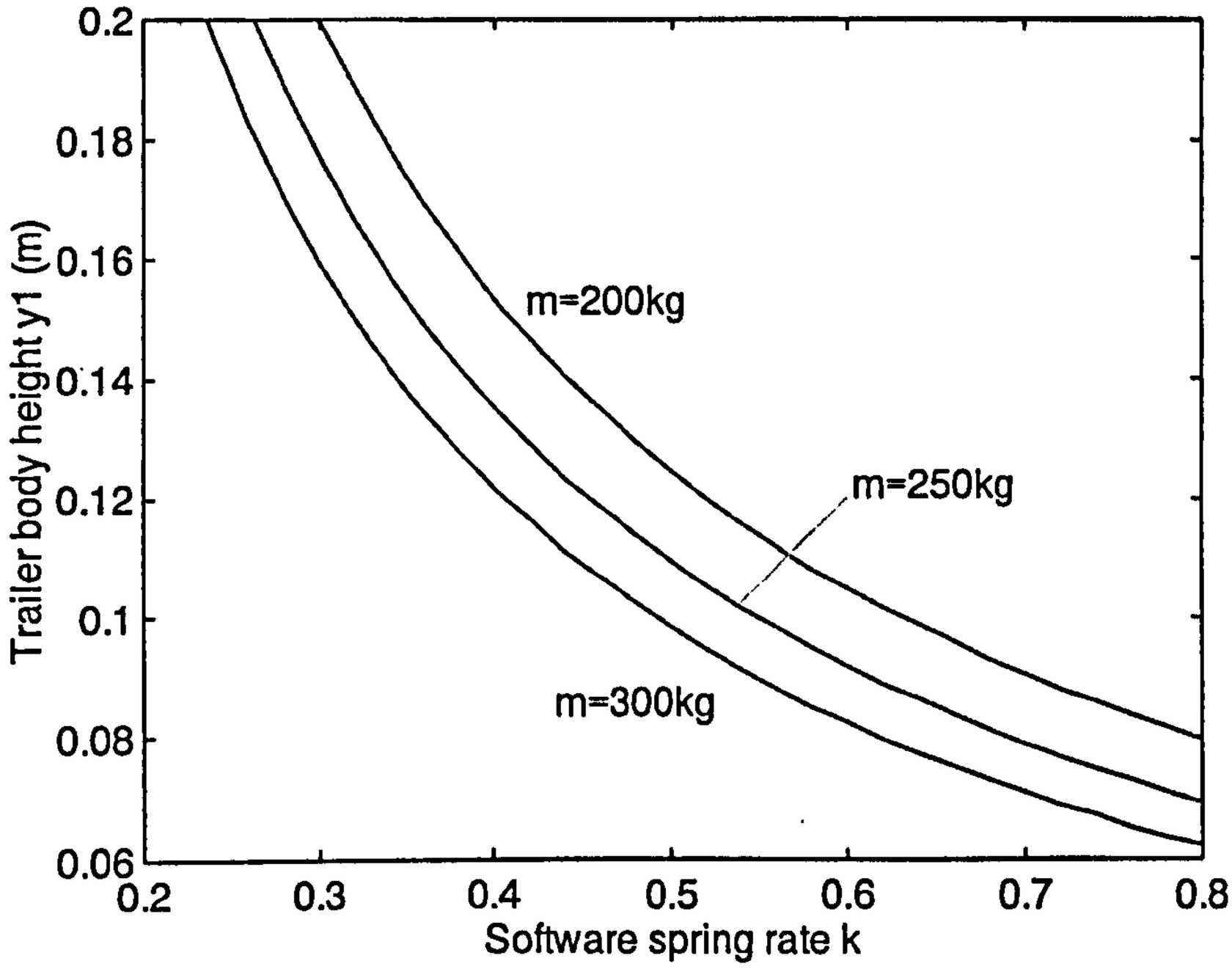

Figure 5-5 Effect of the software spring rate and the mass on the relative height of trailer body in steady state (equilibrium)

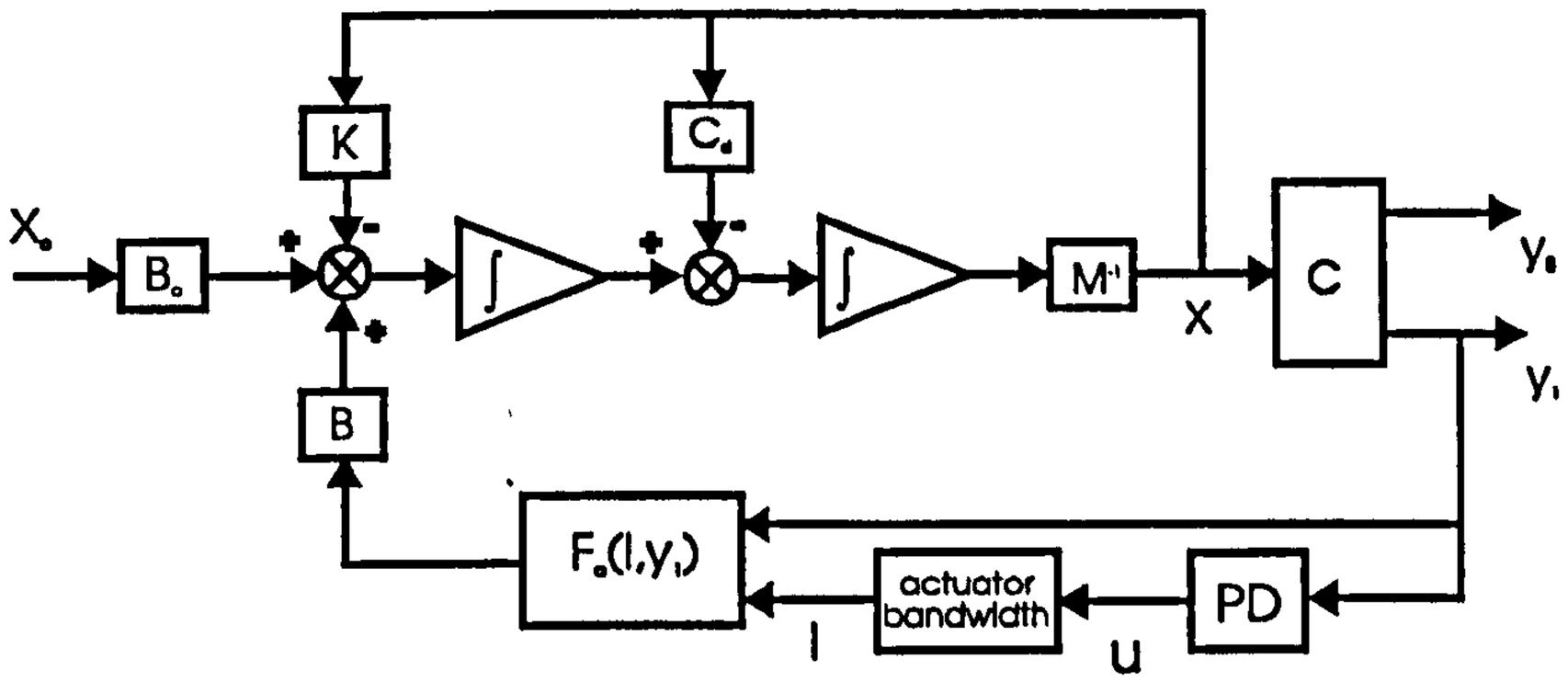

Figure 5-6 Block diagram for the model with PD controller

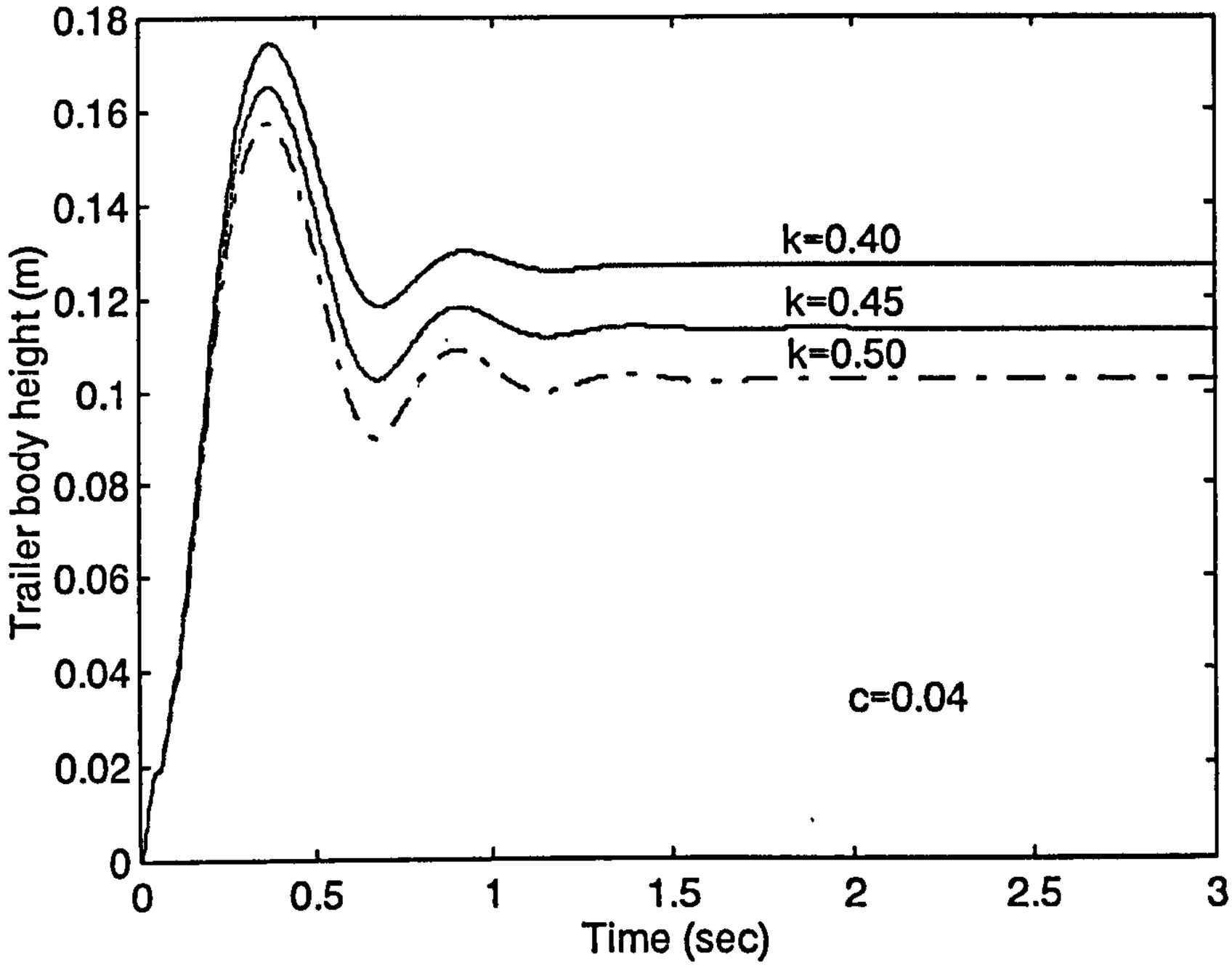

Figure 5-7 Effect of the software spring rate on the starting response

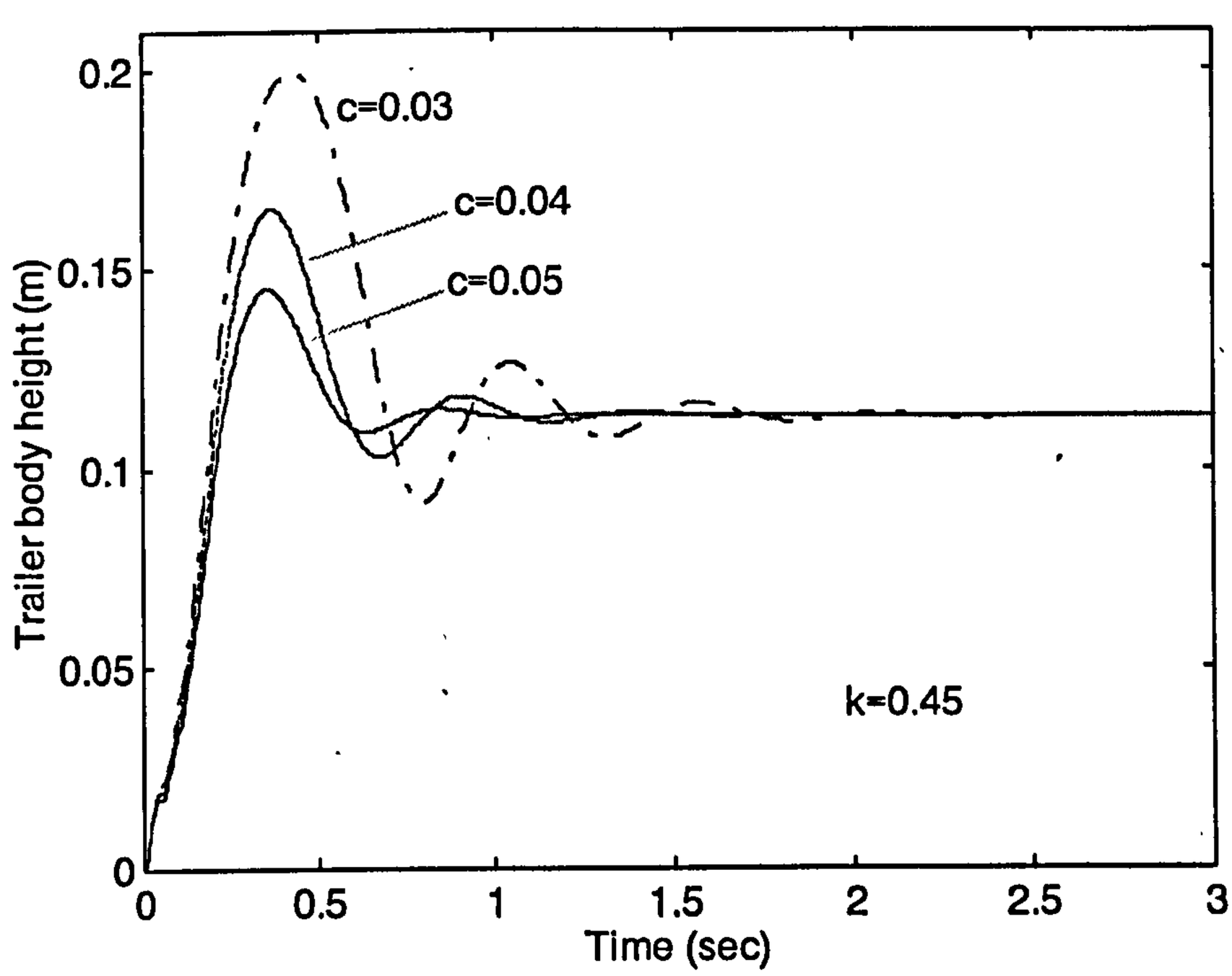

Figure 5-8 Effect of the software damping rate on the starting response

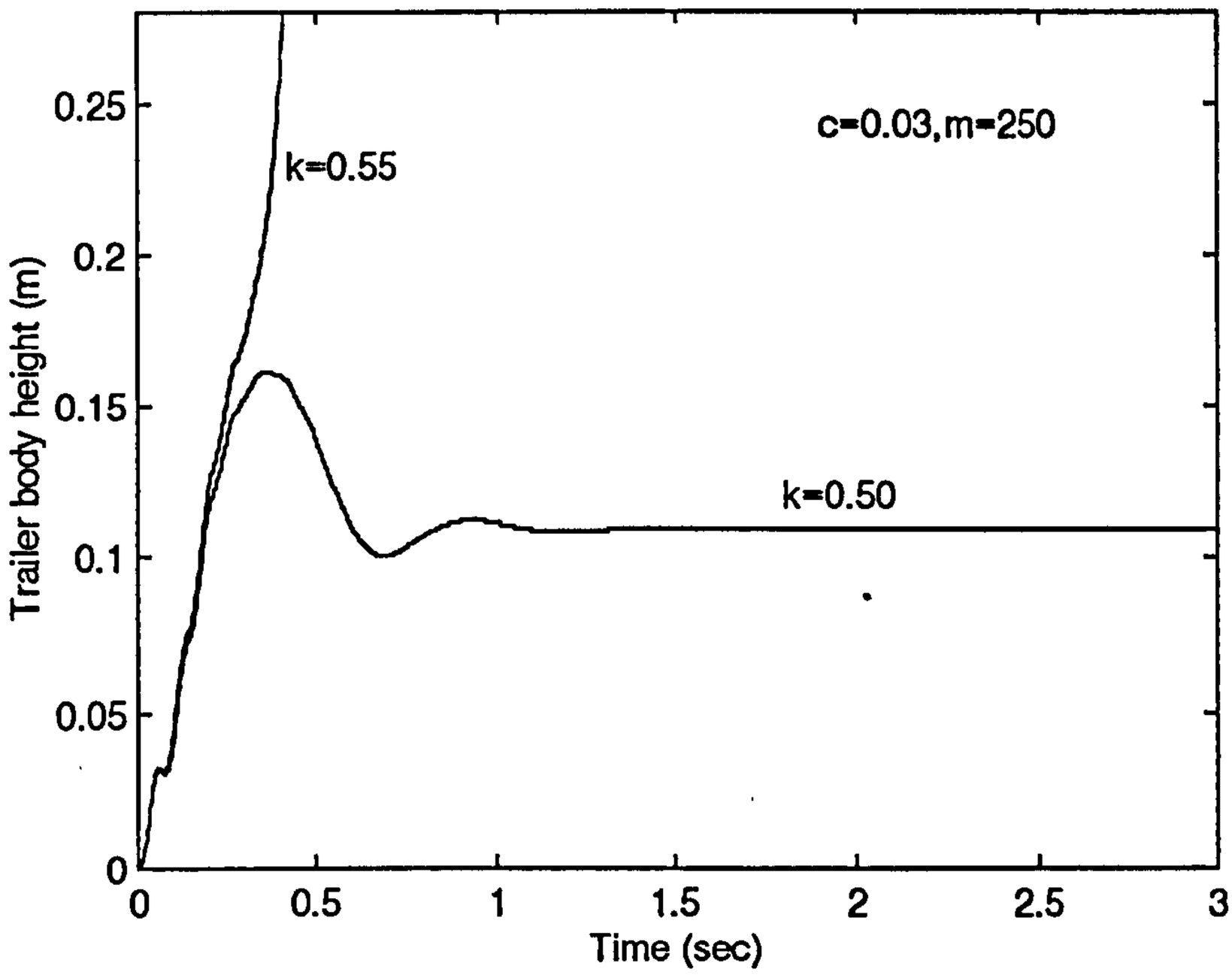

Figure 5-9 Effect of the software spring rate on the stability of the starting response

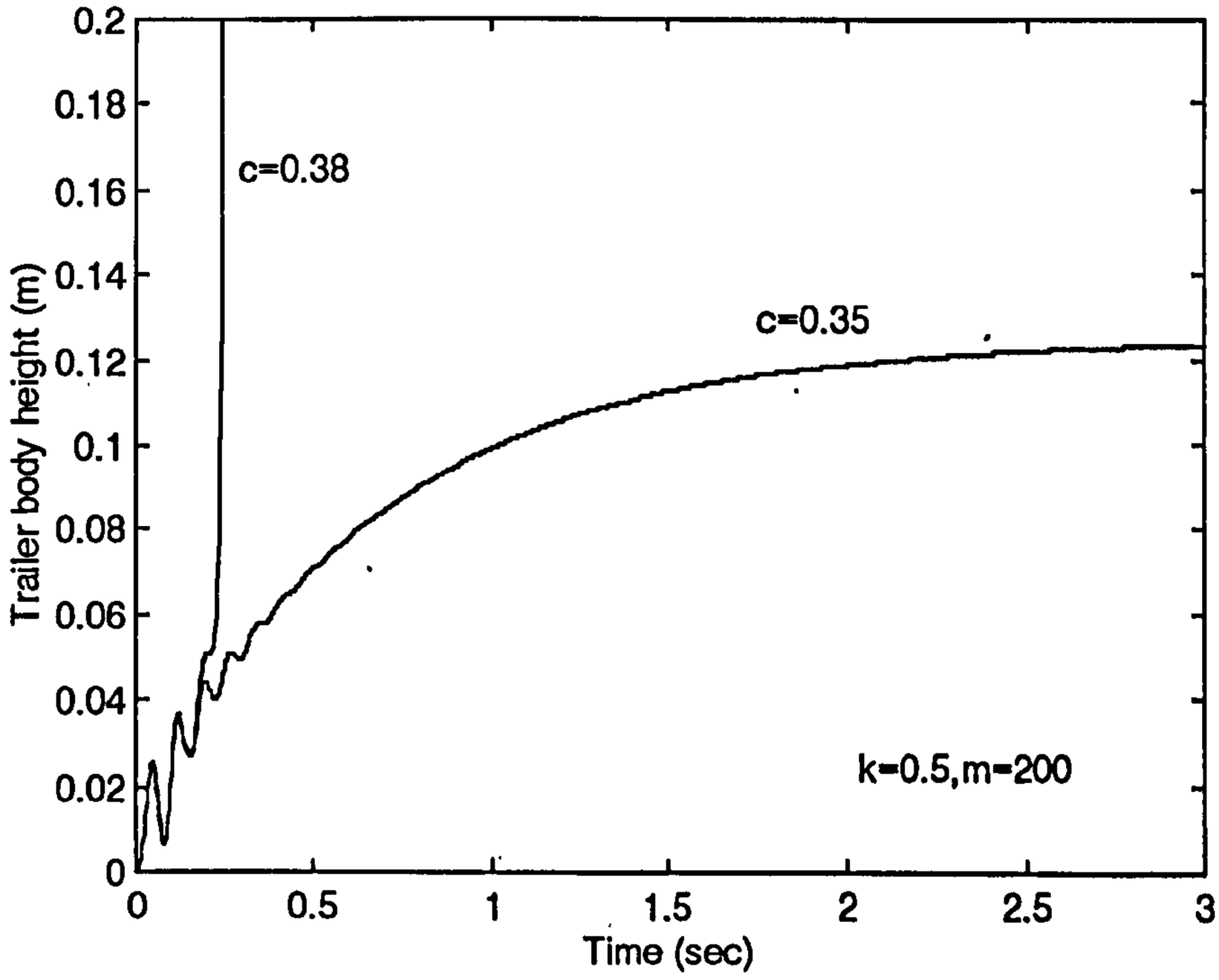

Figure 5-10 Effect of the software damping rate on the stability of the starting response

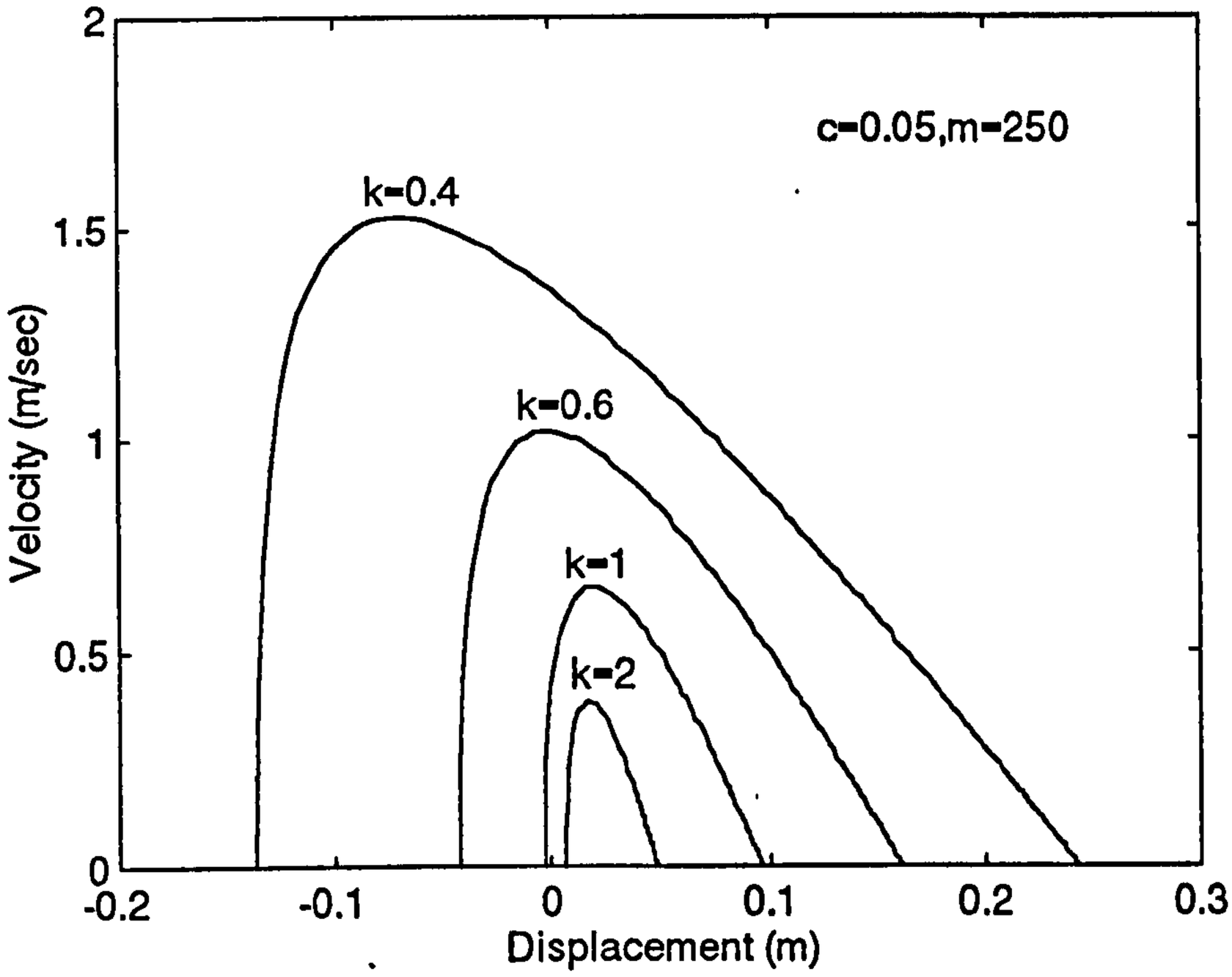

Figure 5-11 Effect of the software spring rate on the stable region in the phase plane based on one mass quarter-car model without limited bandwidth

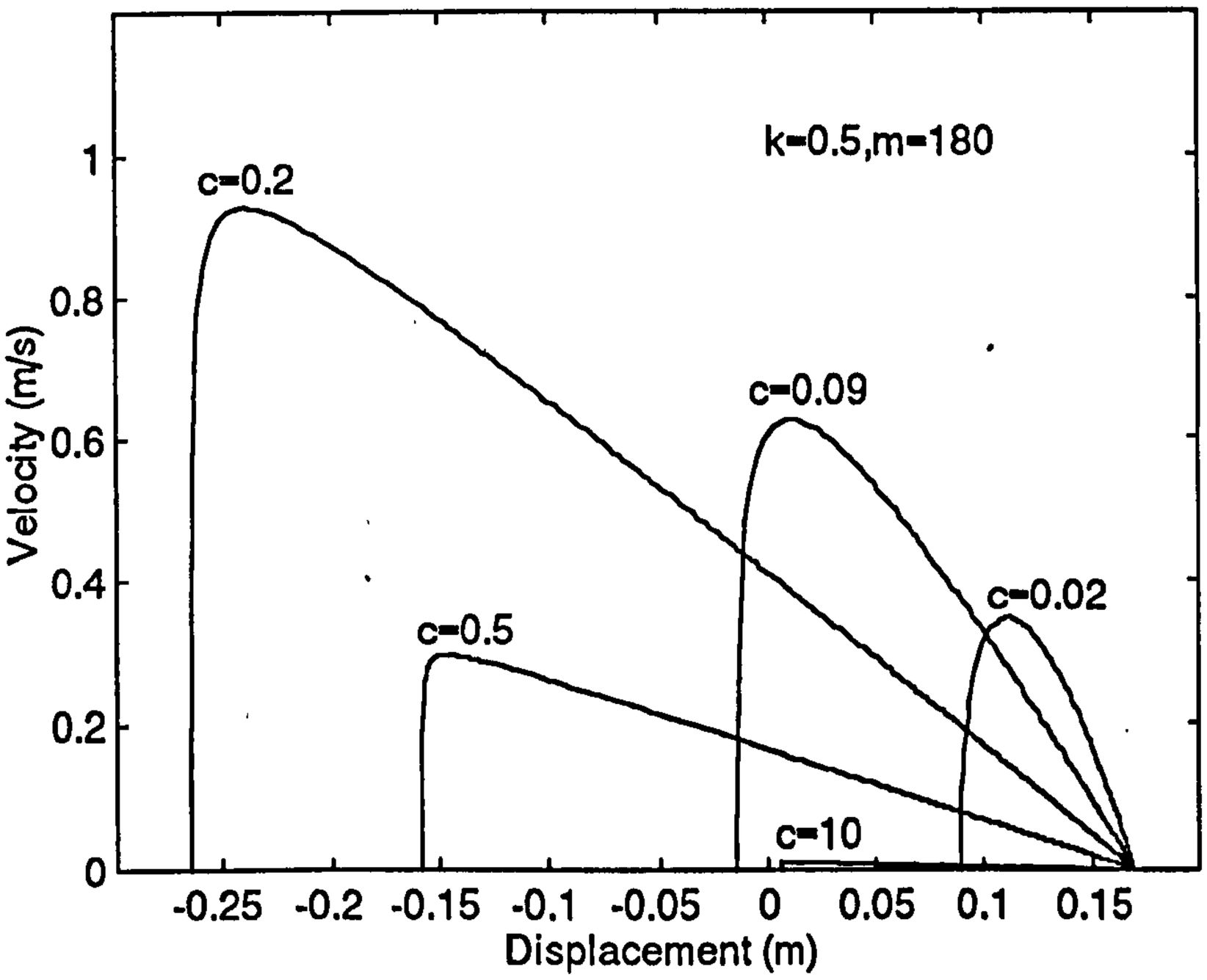

Figure 5-12 Effect of the software damping rate on the stable region in the phase plane based on one mass quarter-car model without limited bandwidth

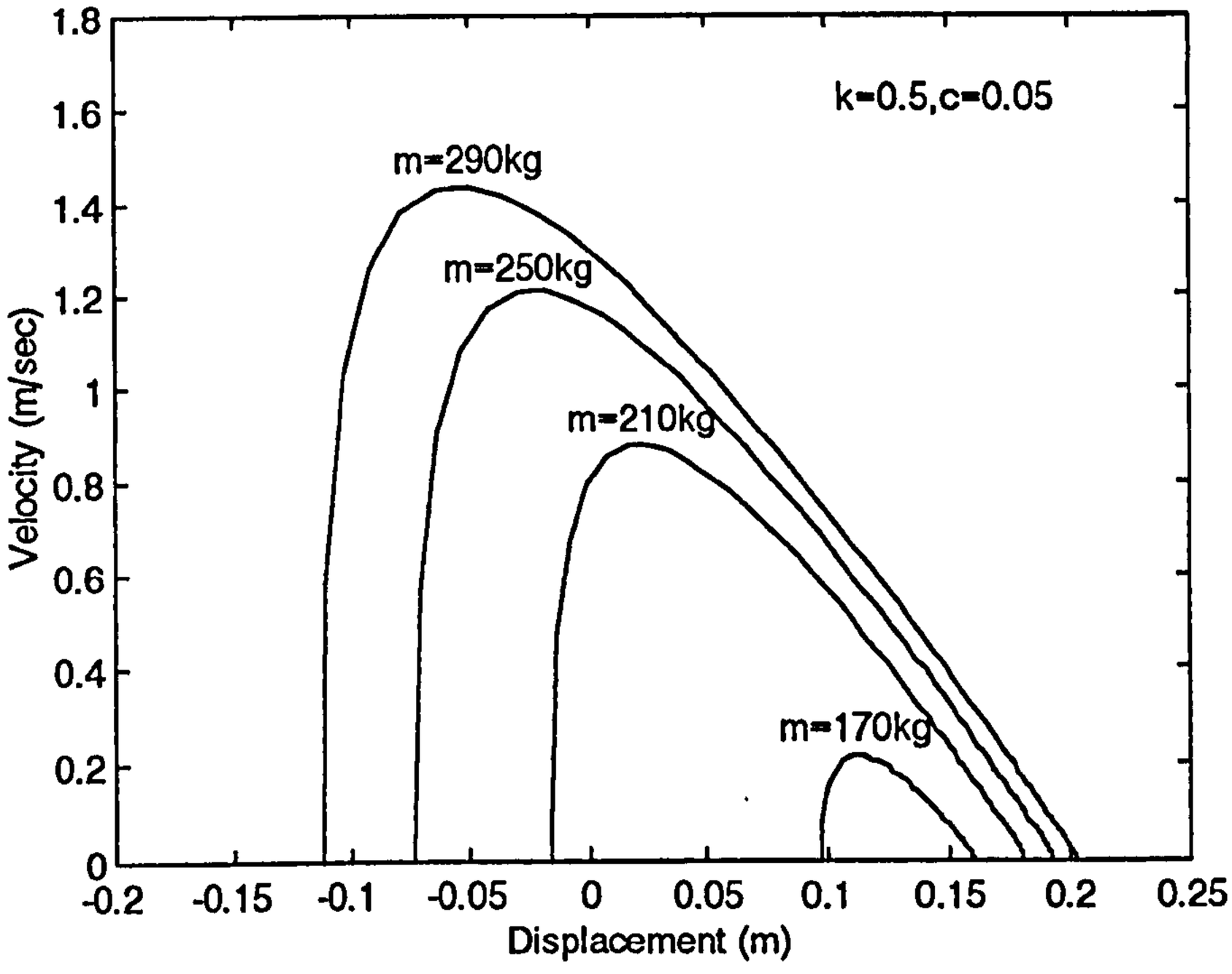

Figure 5-13 Effect of the body mass on the stable region in the phase plane based on one mass quarter-car model without limited bandwidth

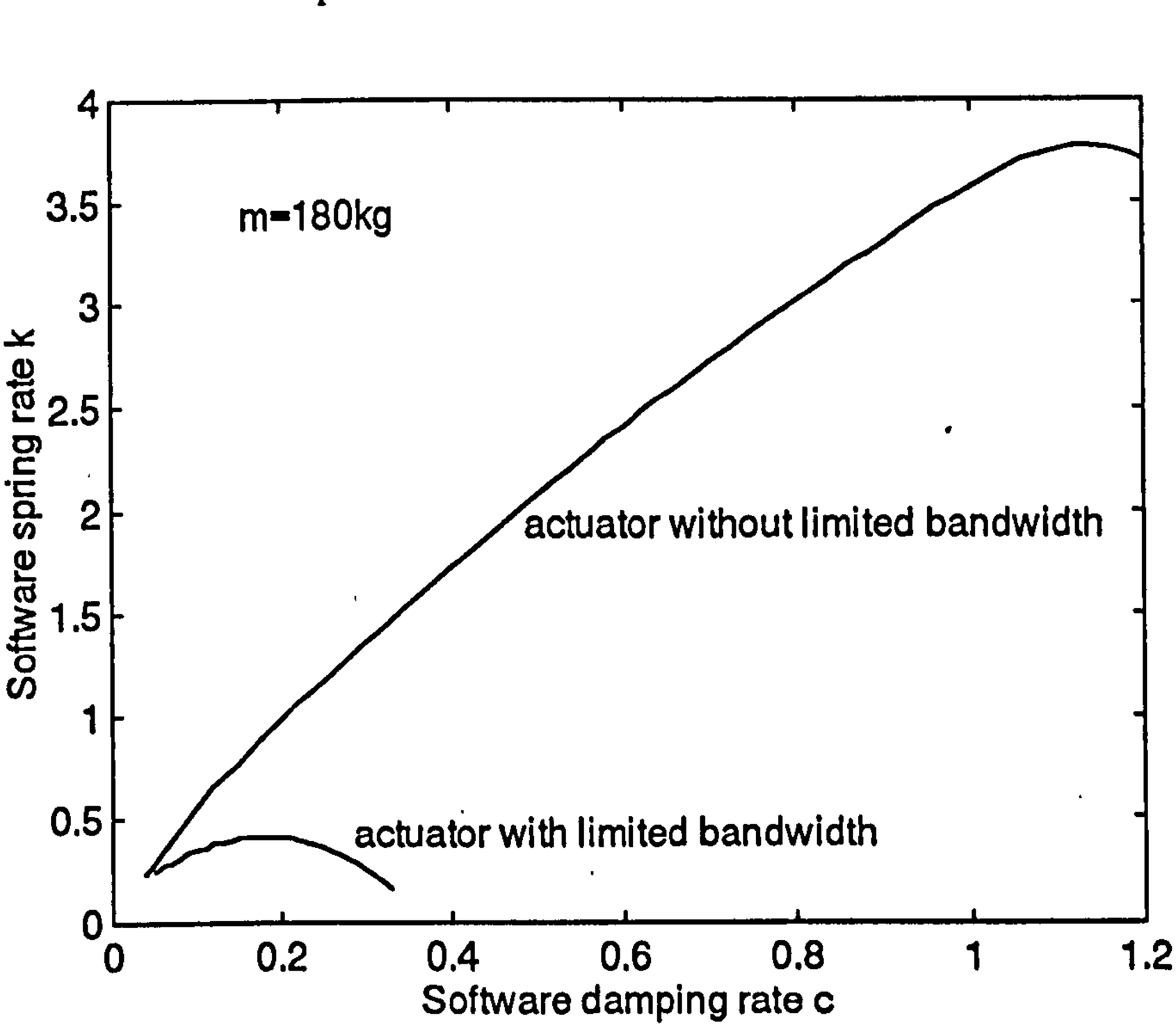

Figure 5-14 Effect of the bandwidth of the actuator force on the reachable region for the software spring rate and damping rate based on one mass quarter-car model

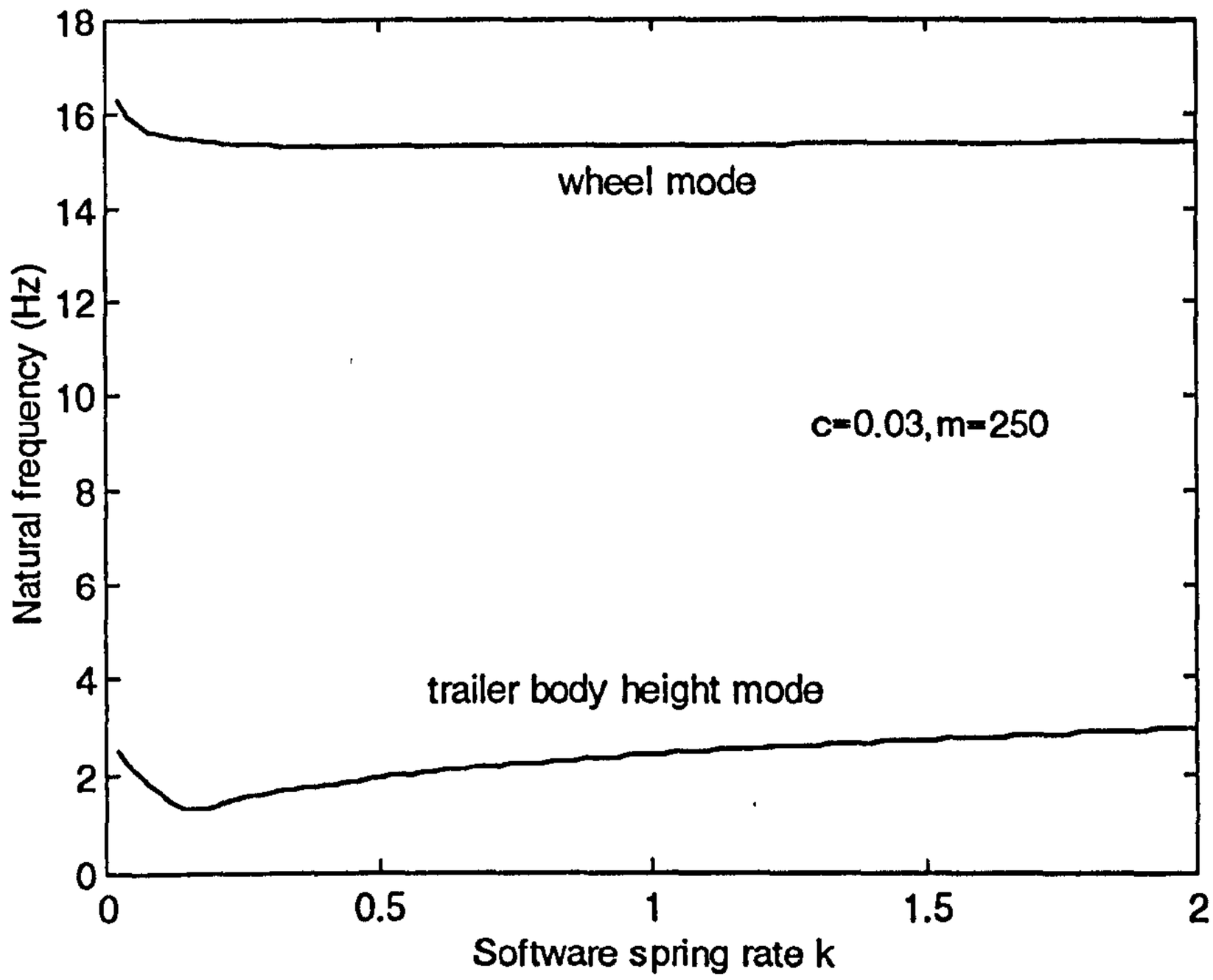

Figure 5-15 Effect of the software spring rate on the natural frequencies

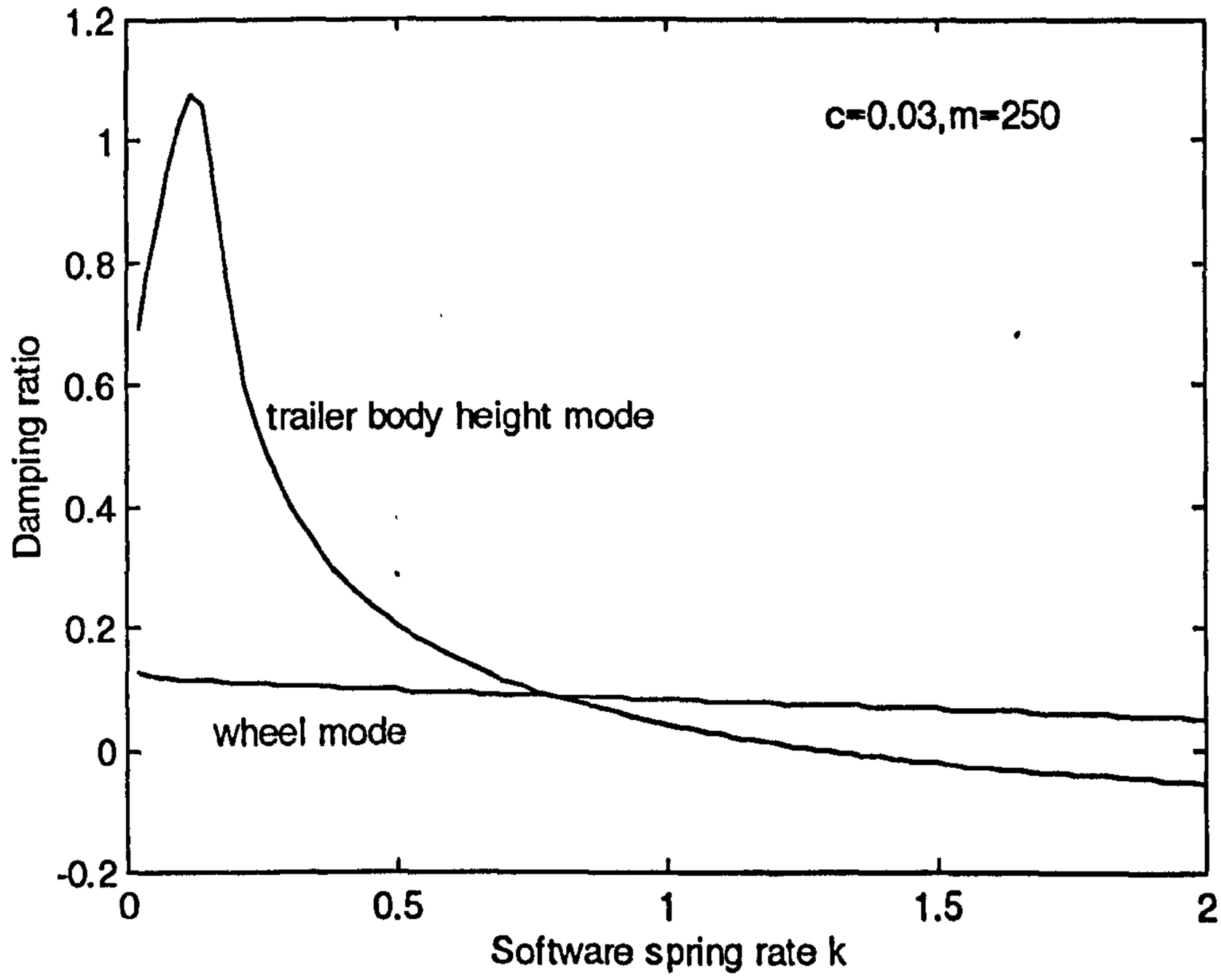

Figure 5-16 Effect of the software spring rate on the damping ratios

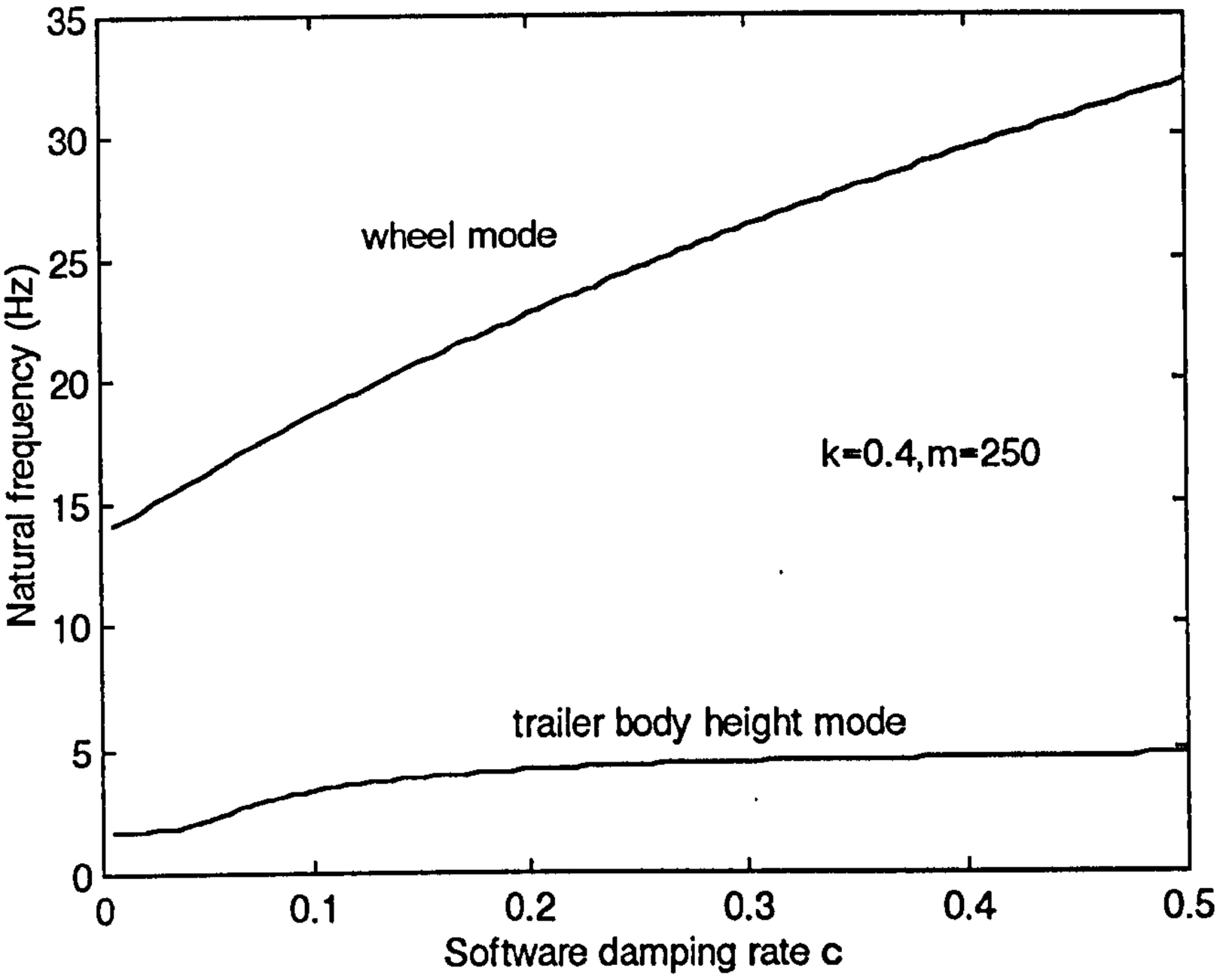

Figure 5-17 Effect of the software damping rate on the natural frequencies

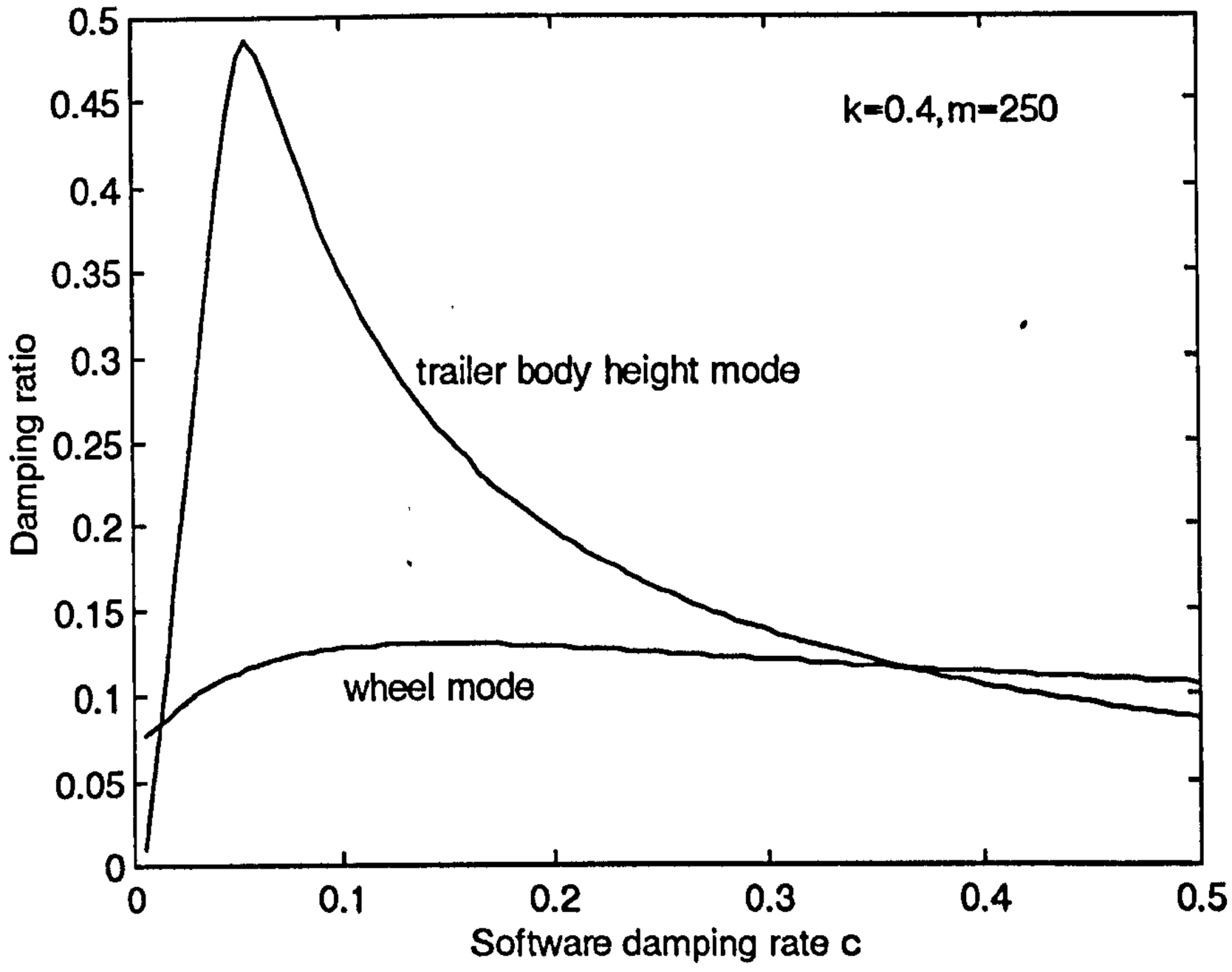

Figure 5-18 Effect of the software damping rate on the damping ratios

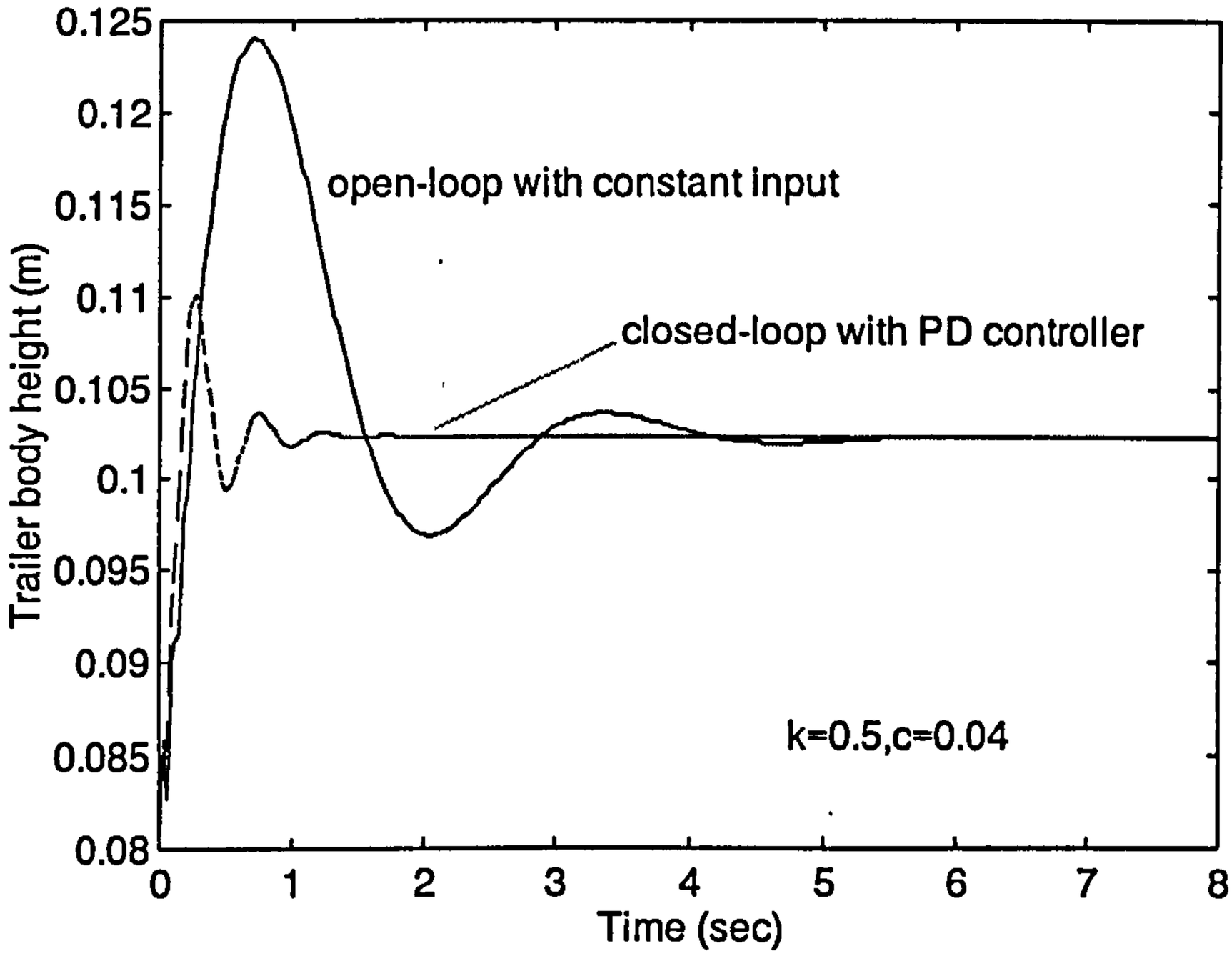

Figure 5-19 Comparison of the closed-loop and the open-loop on vibration decaying

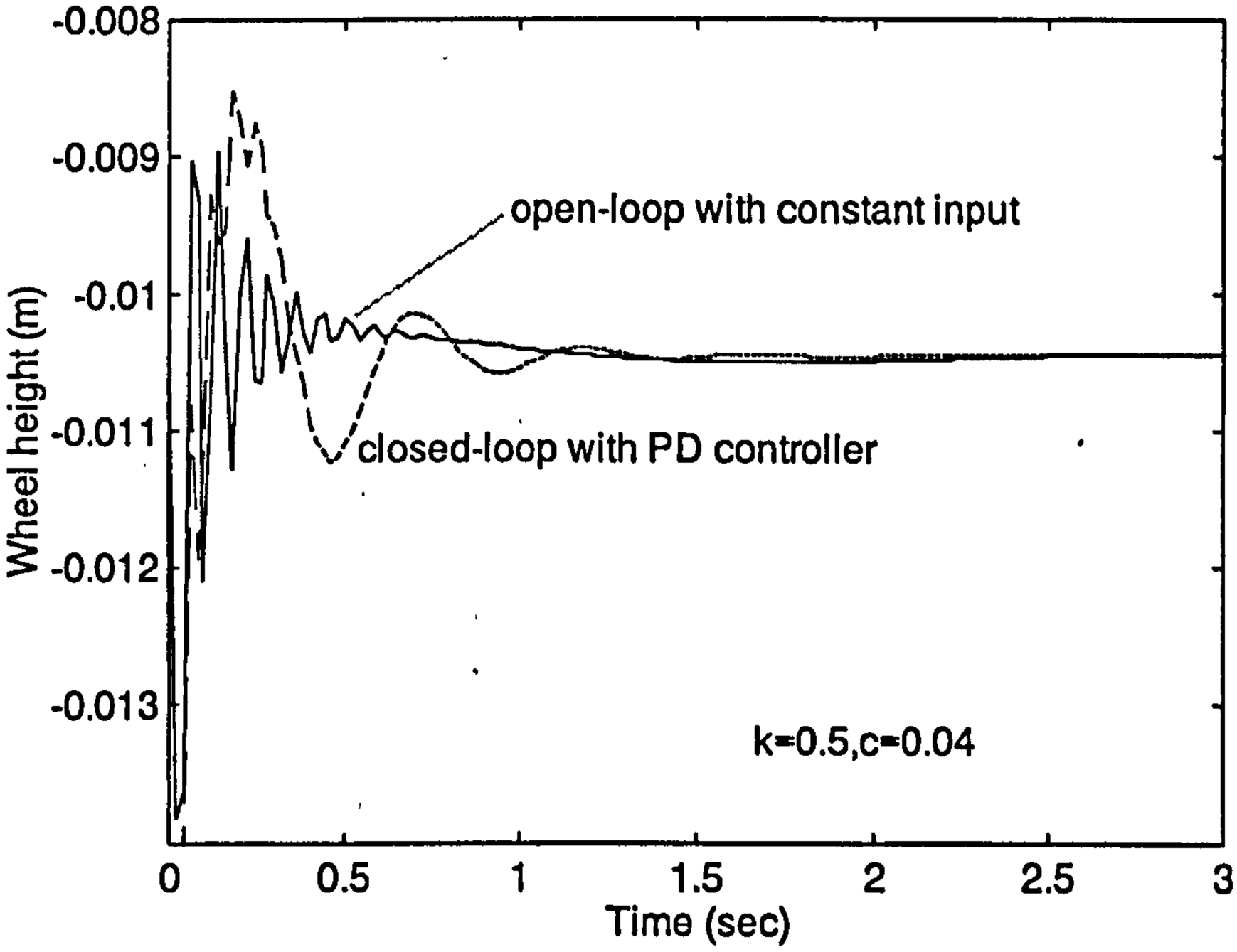

Figure 5-20 Comparison of the closed-loop and the open-loop on vibration decaying

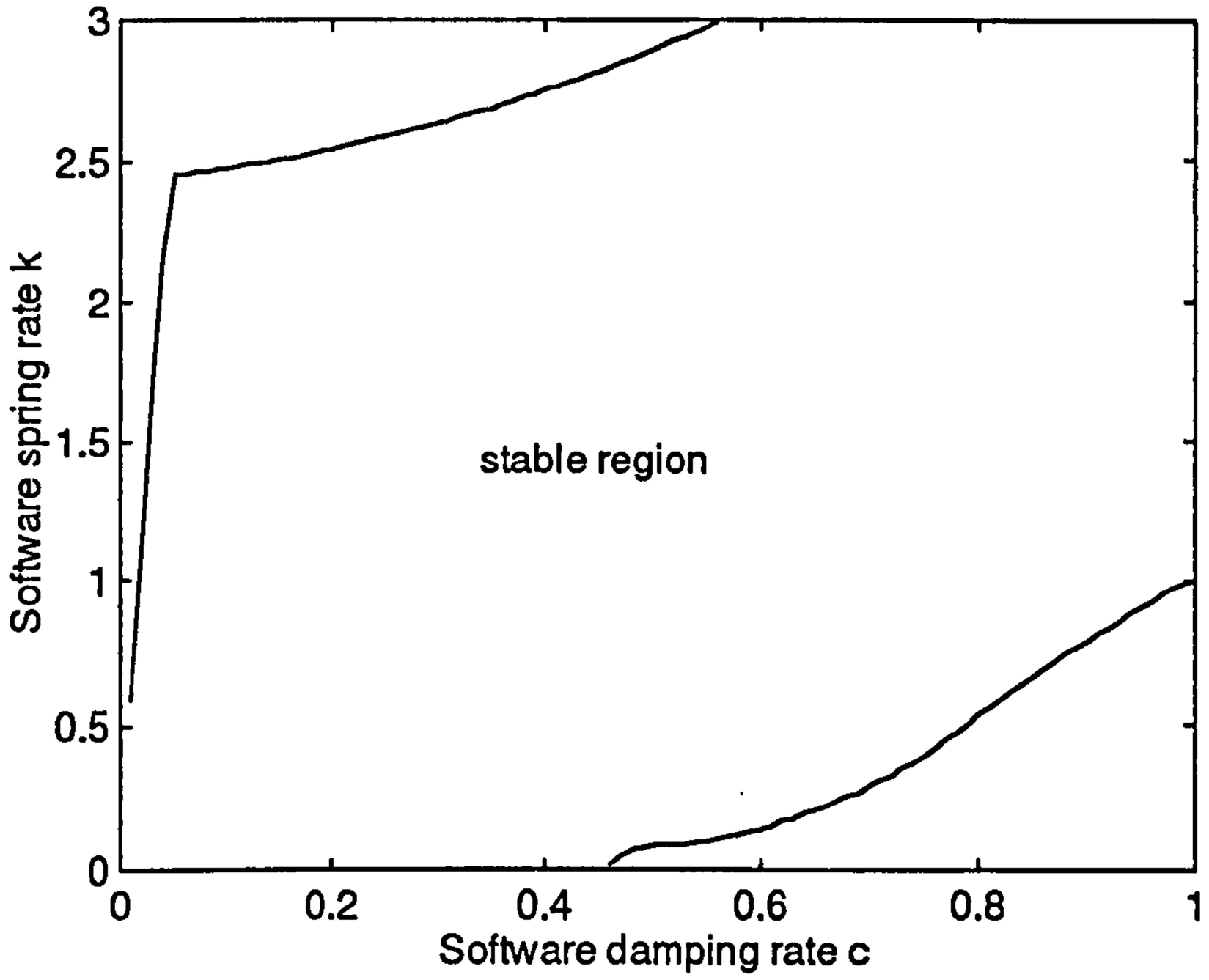

Figure 5-21 Stable region for the control parameters with sky-hook damping

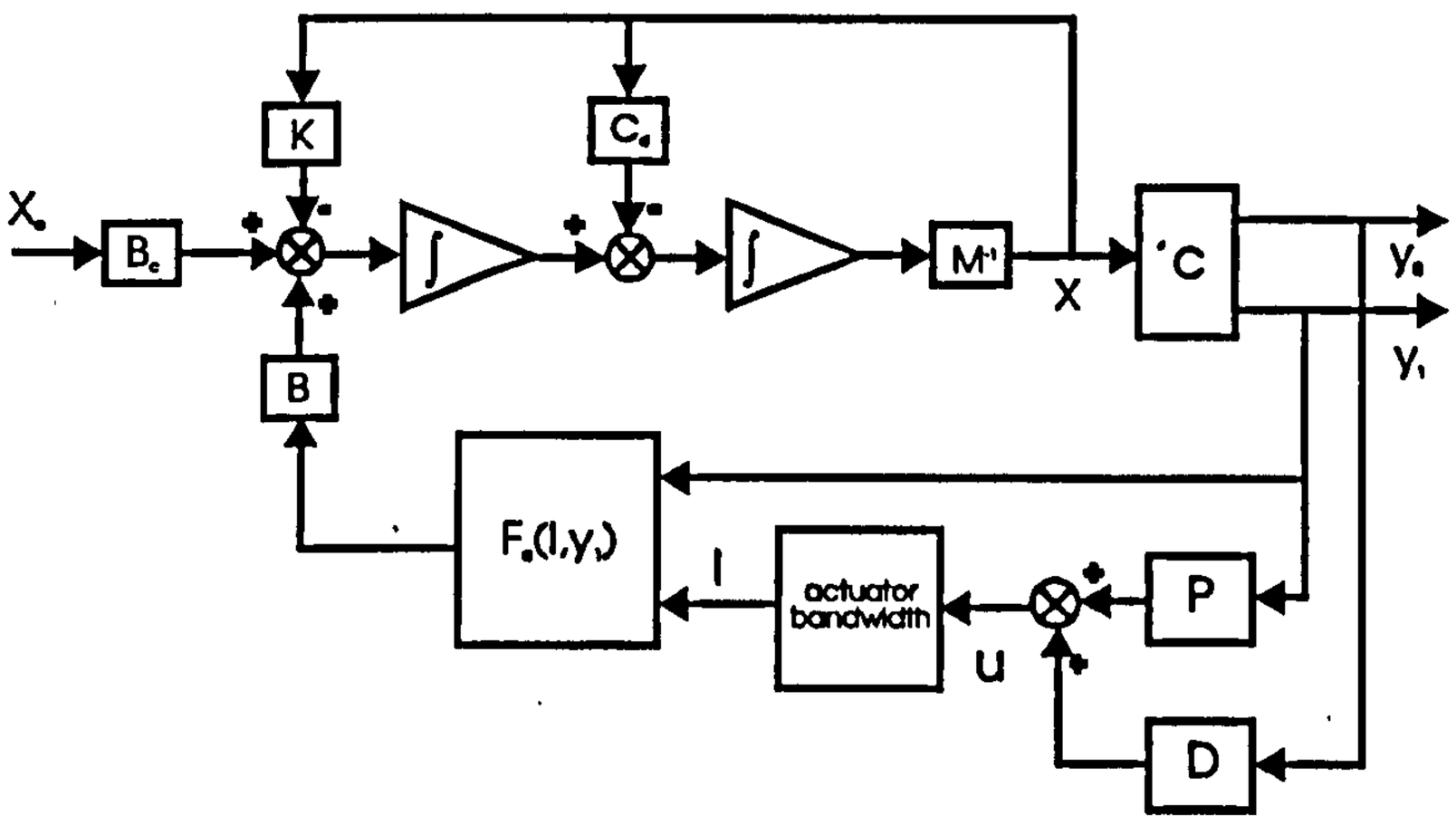

Figure 5-22 Block diagram of the model with sky-hook damping

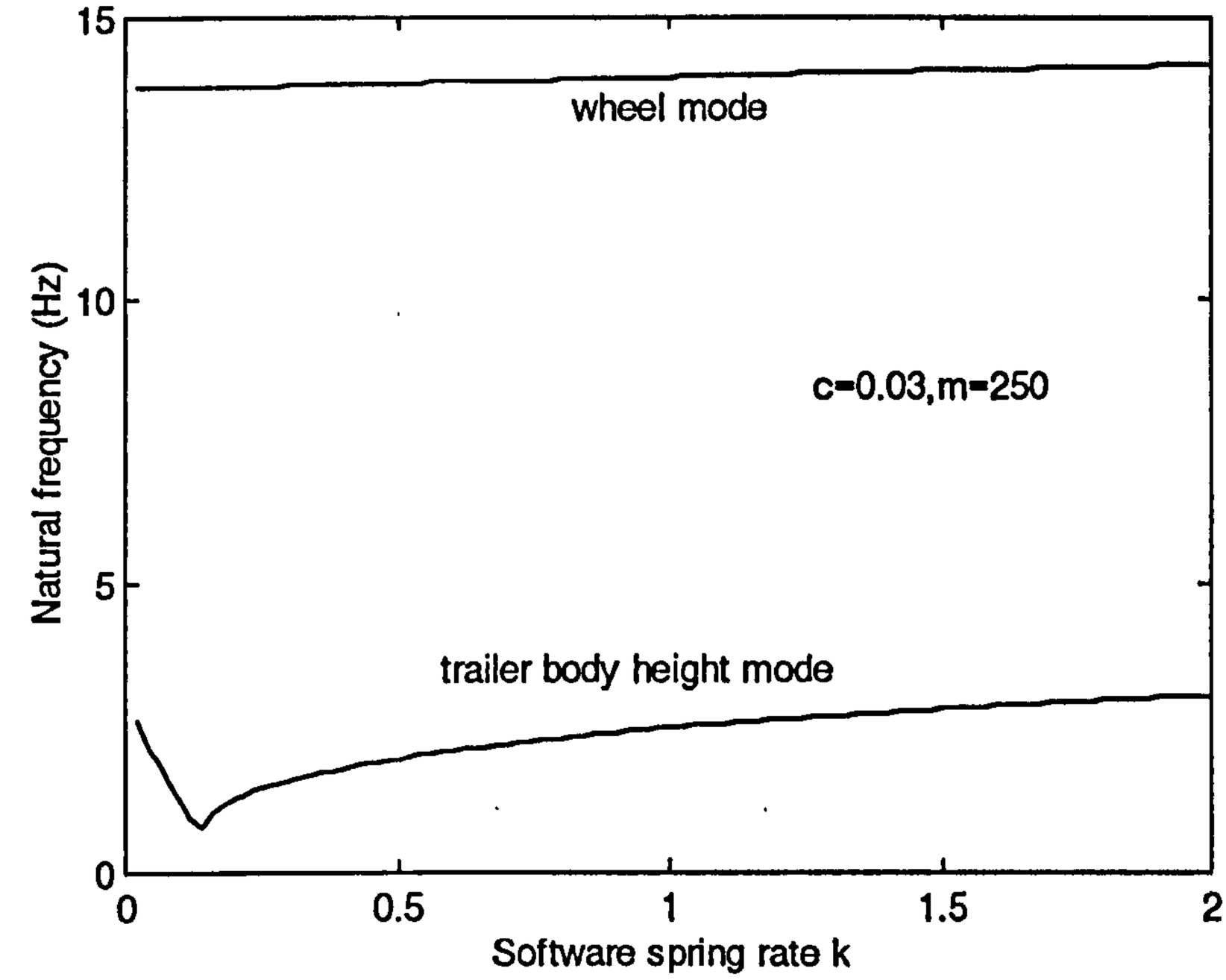

Figure 5-23 Effect of the software spring rate on the natural frequencies

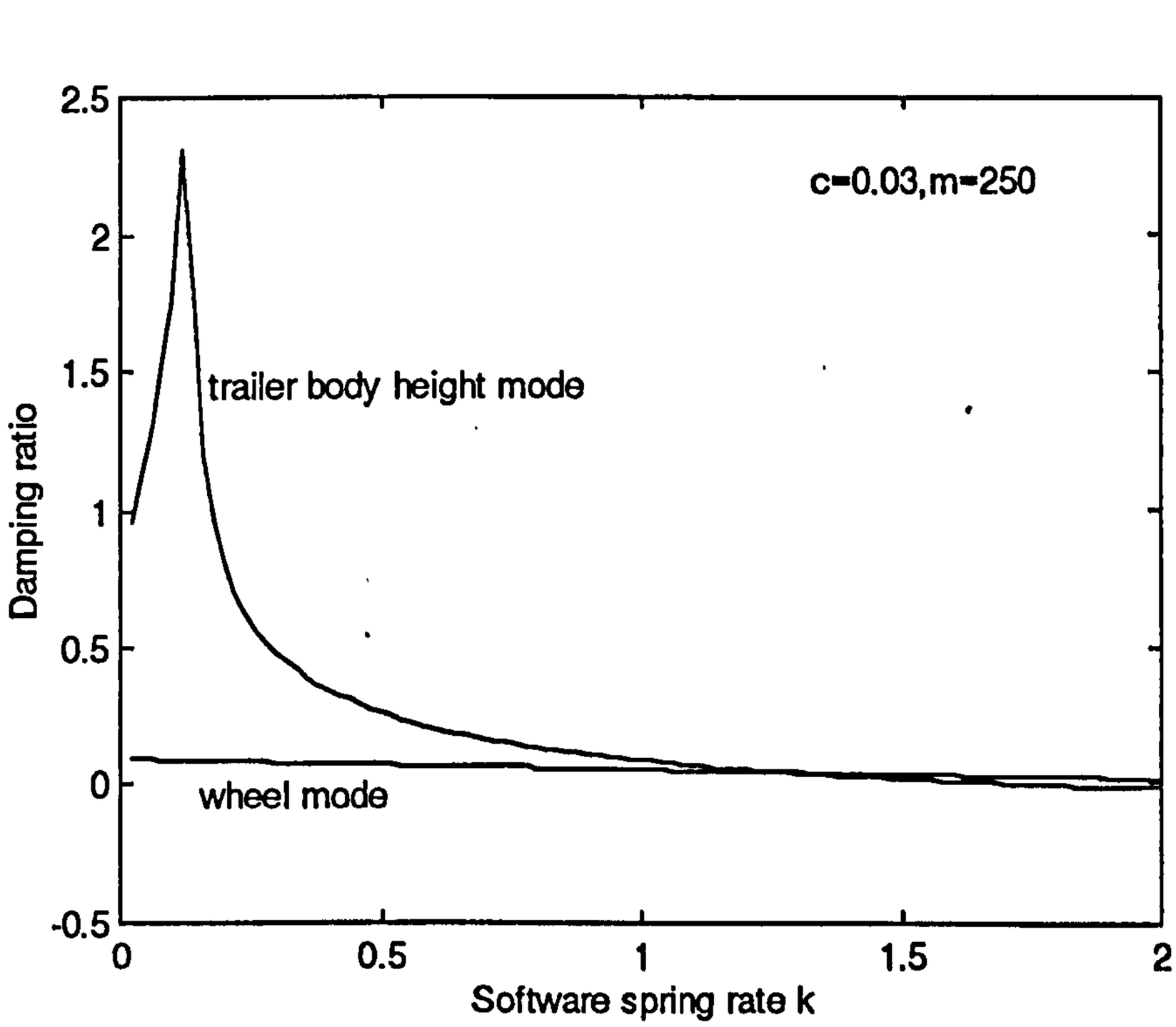

Figure 5-24 Effect of the software spring rate on the damping ratio

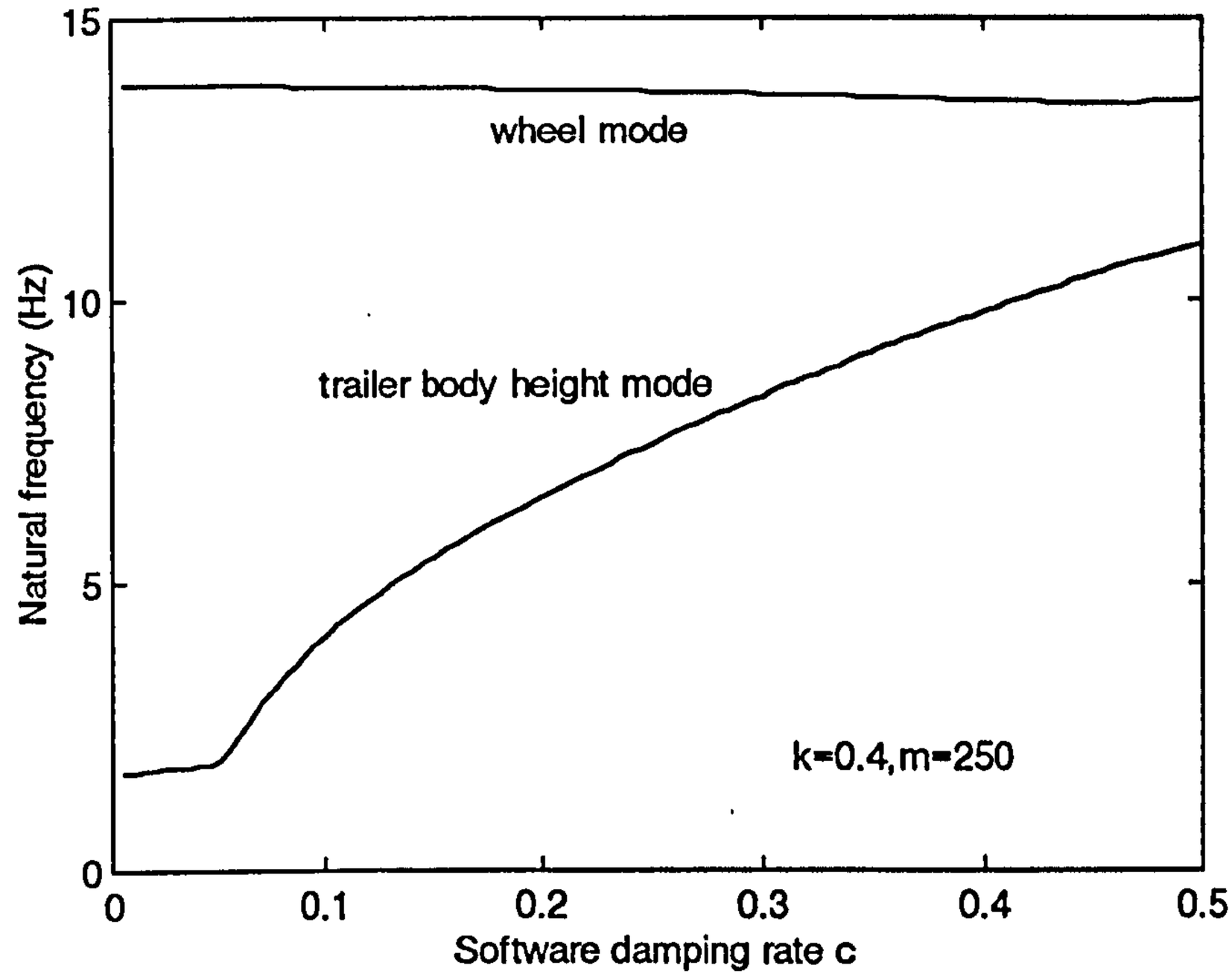

Figure 5-25 Effect of the software damping rate on the natural frequencies

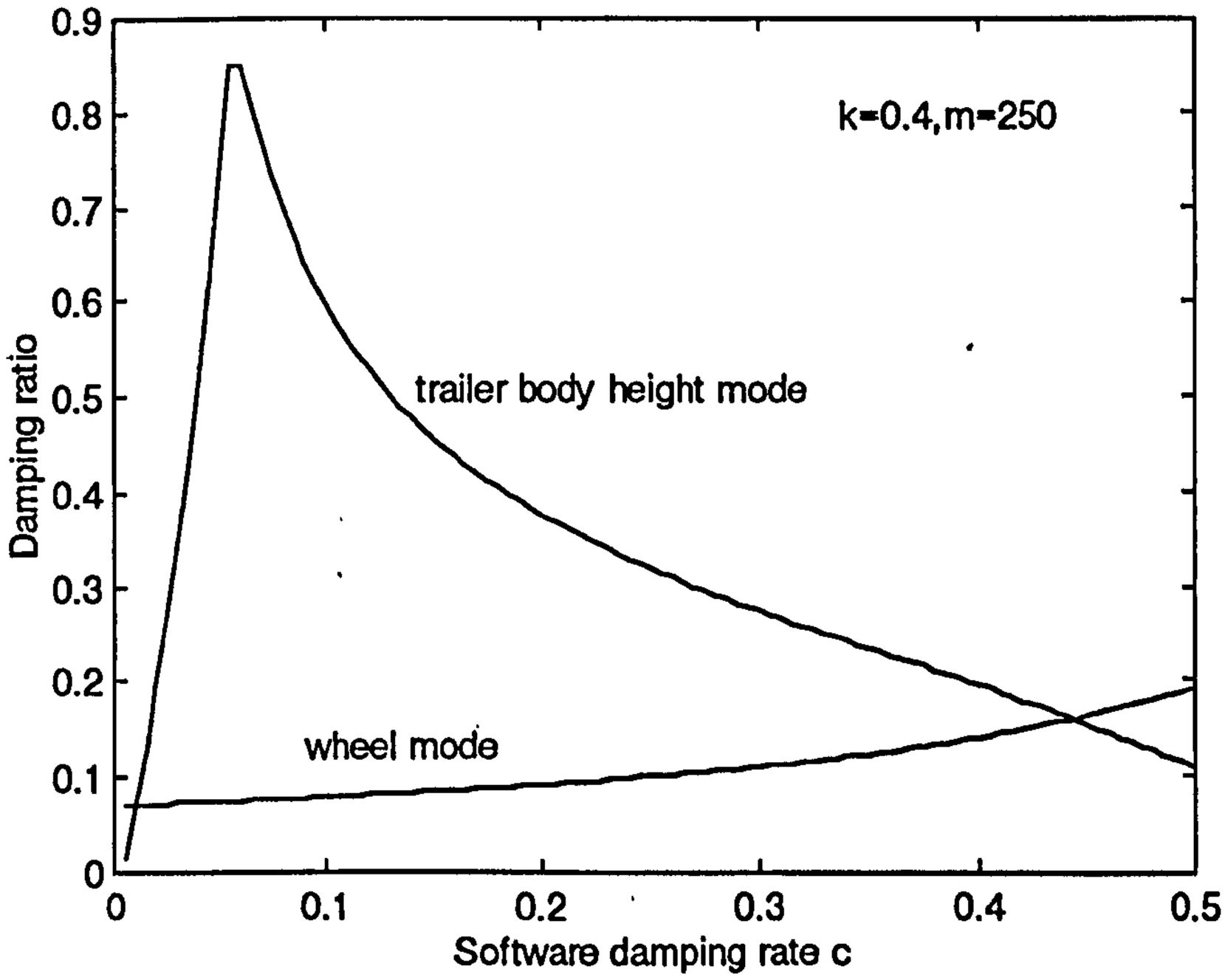

Figure 5-26 Effect of the software damping rate on the damping ratio

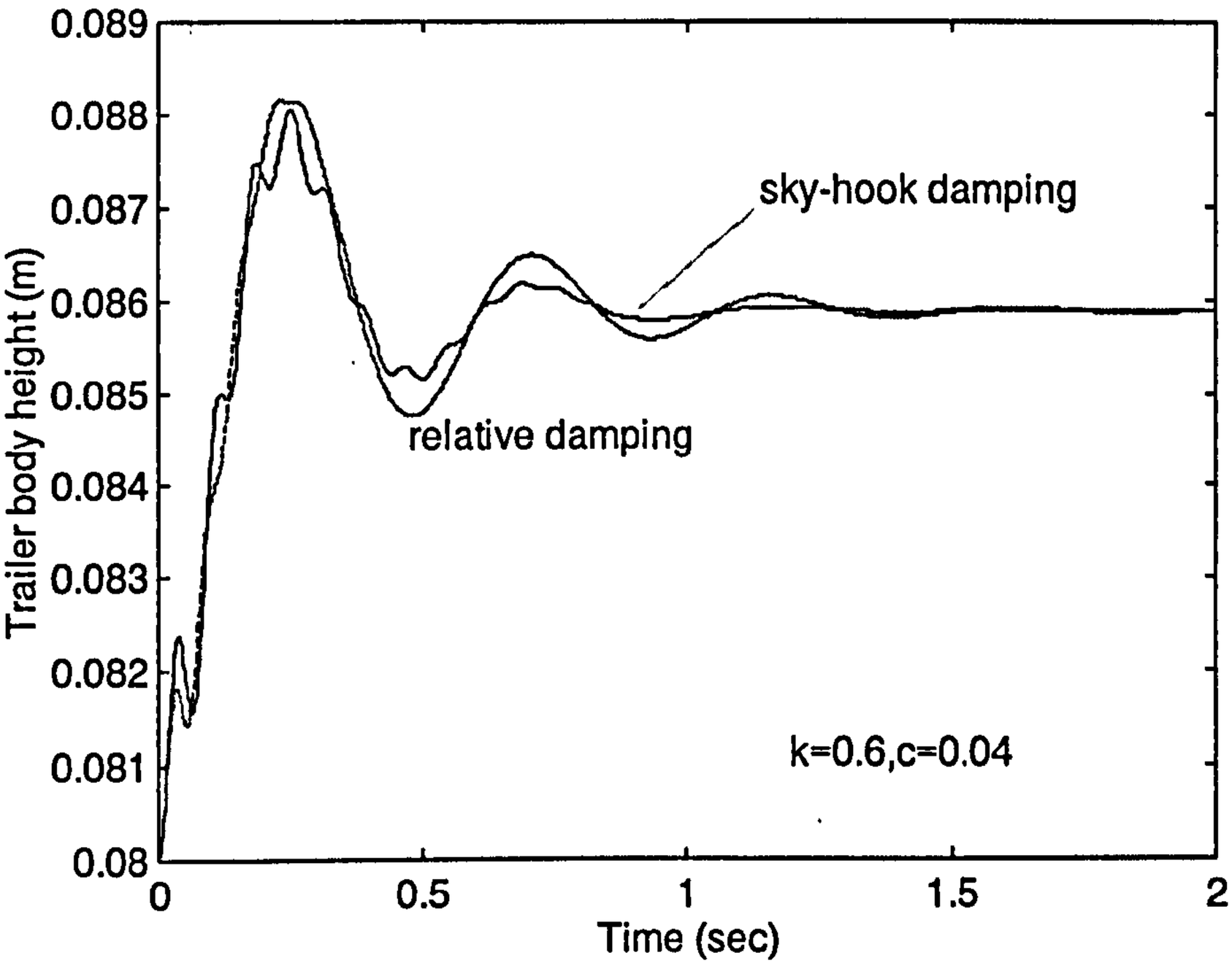

Figure 5-27 Comparison of vibration decaying between sky-hook and relative damping

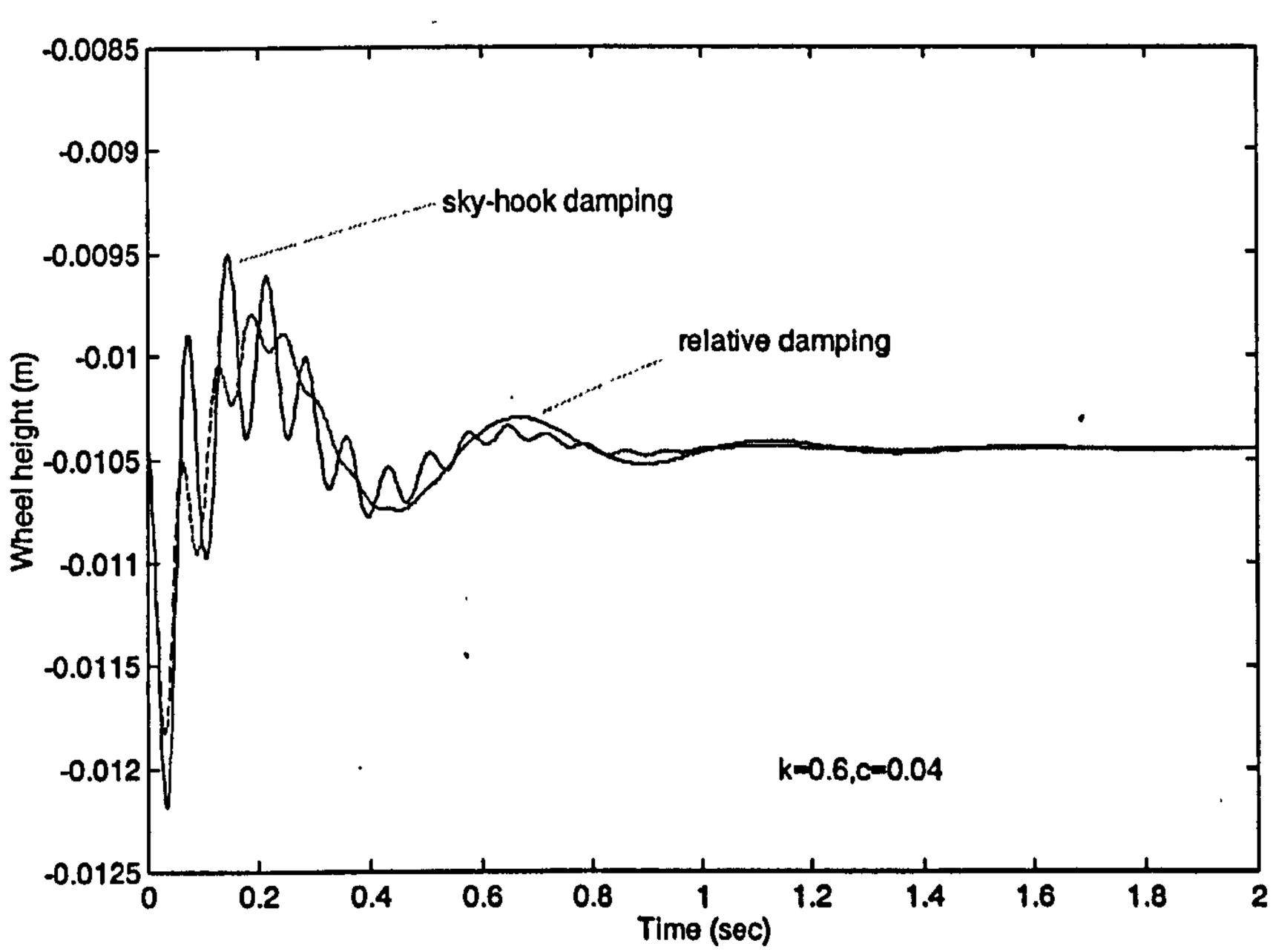

Figure 5-28 Comparison of vibration decaying between sky-hook and relative damping

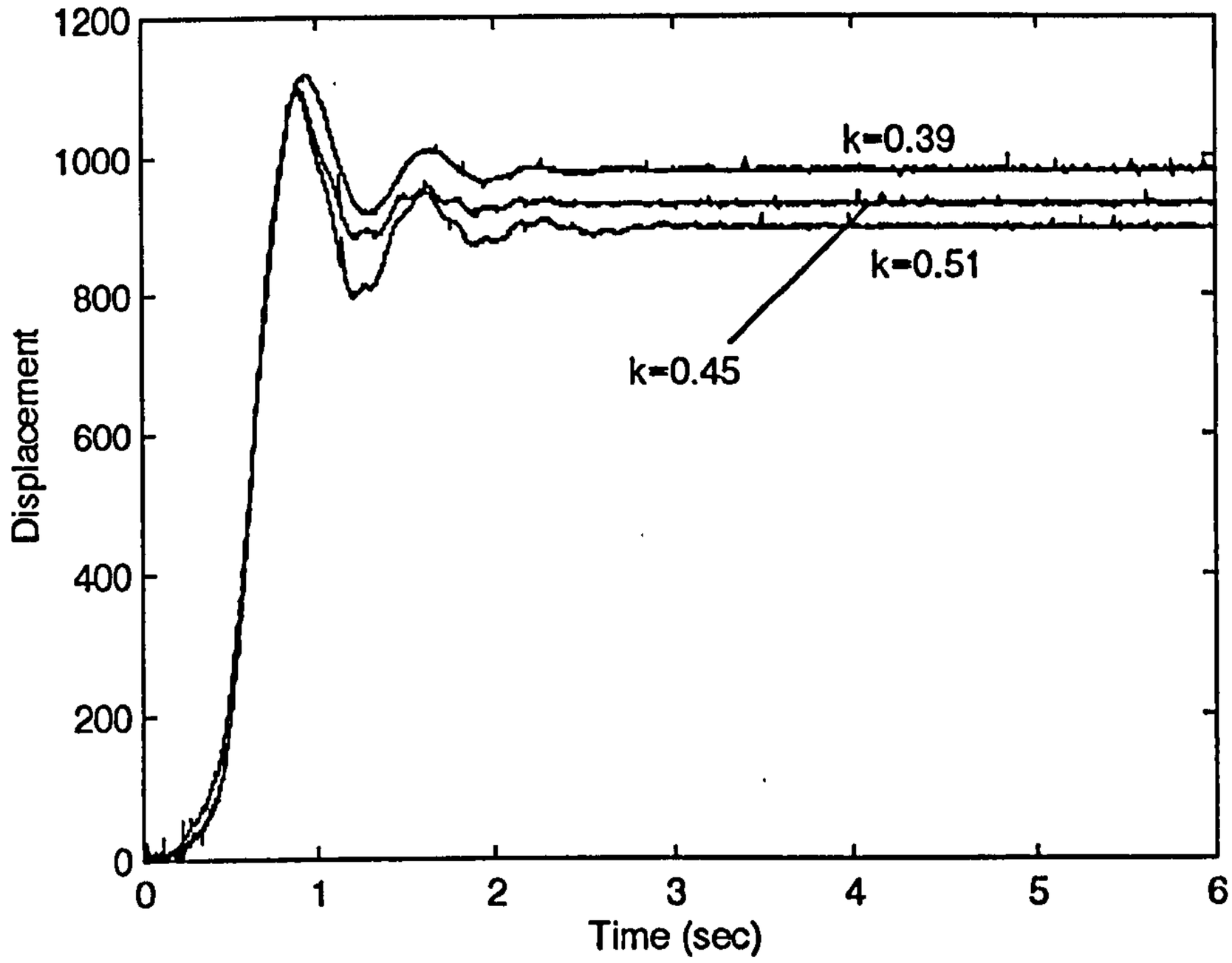

Figure 5-29 Measured starting response for the PD controller with relative damping

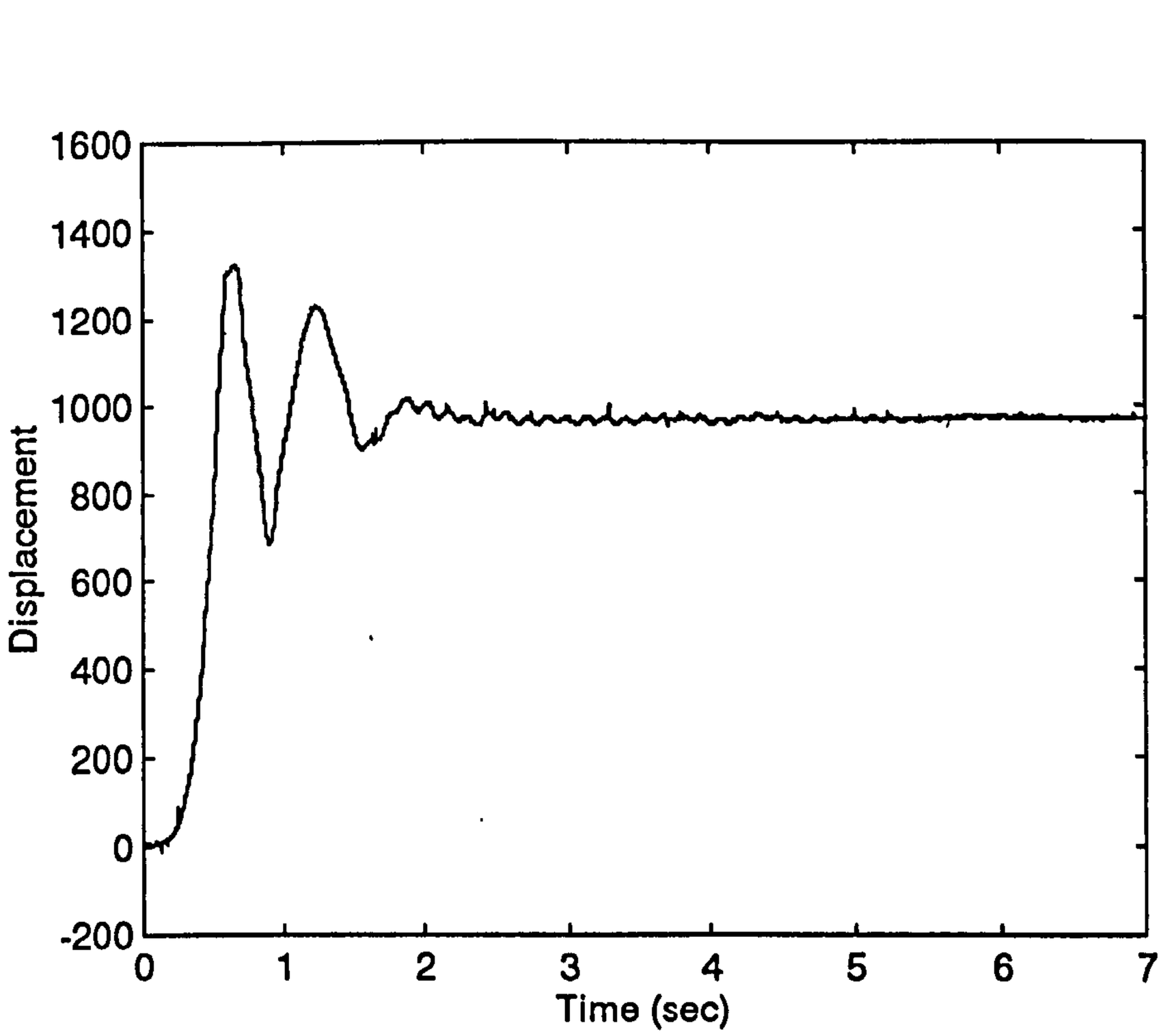

Figure 5-30 Measured starting response for the PD controller with sky-hook damping

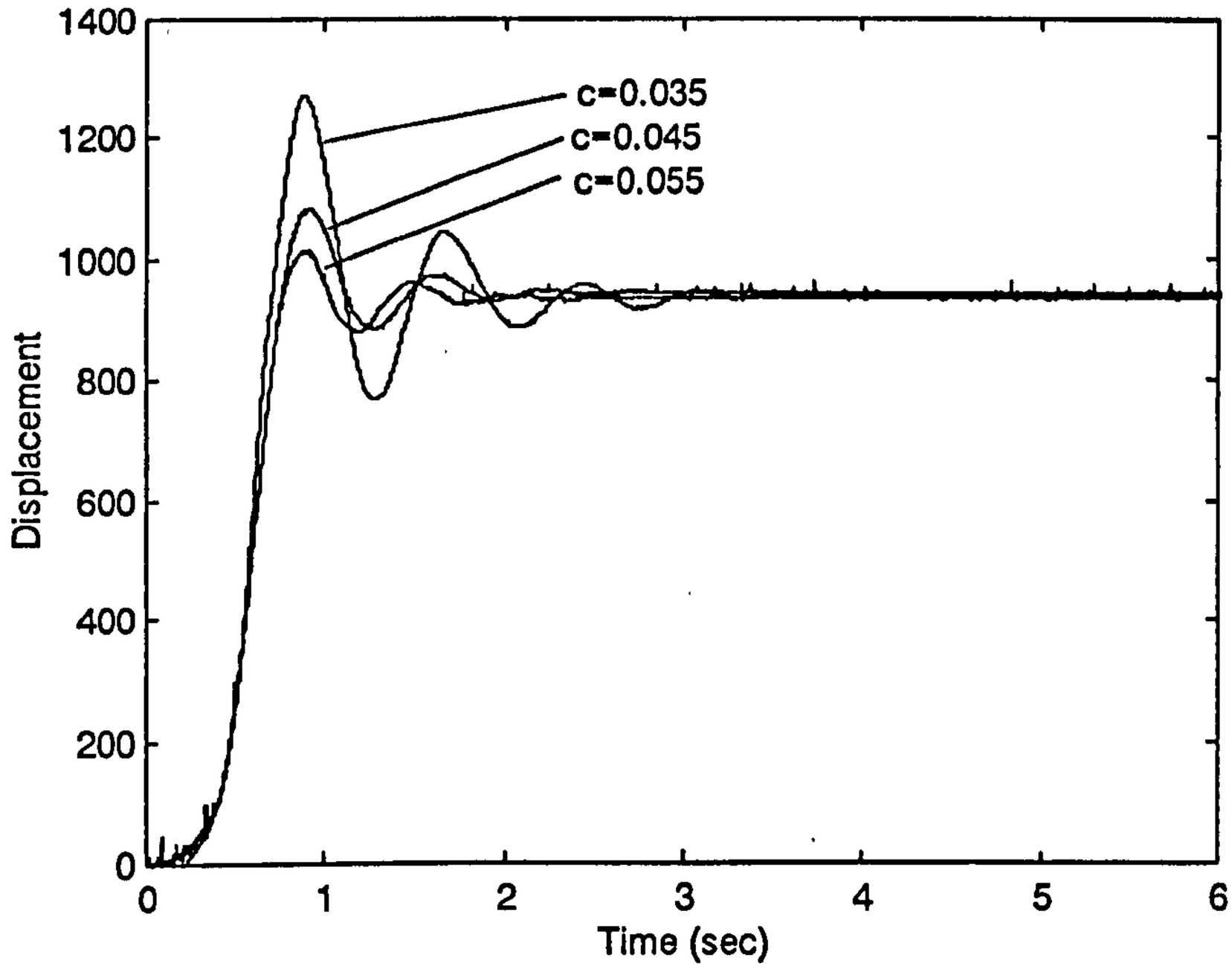

Figure 5-31 Measured starting response for the PD controller with relative damping

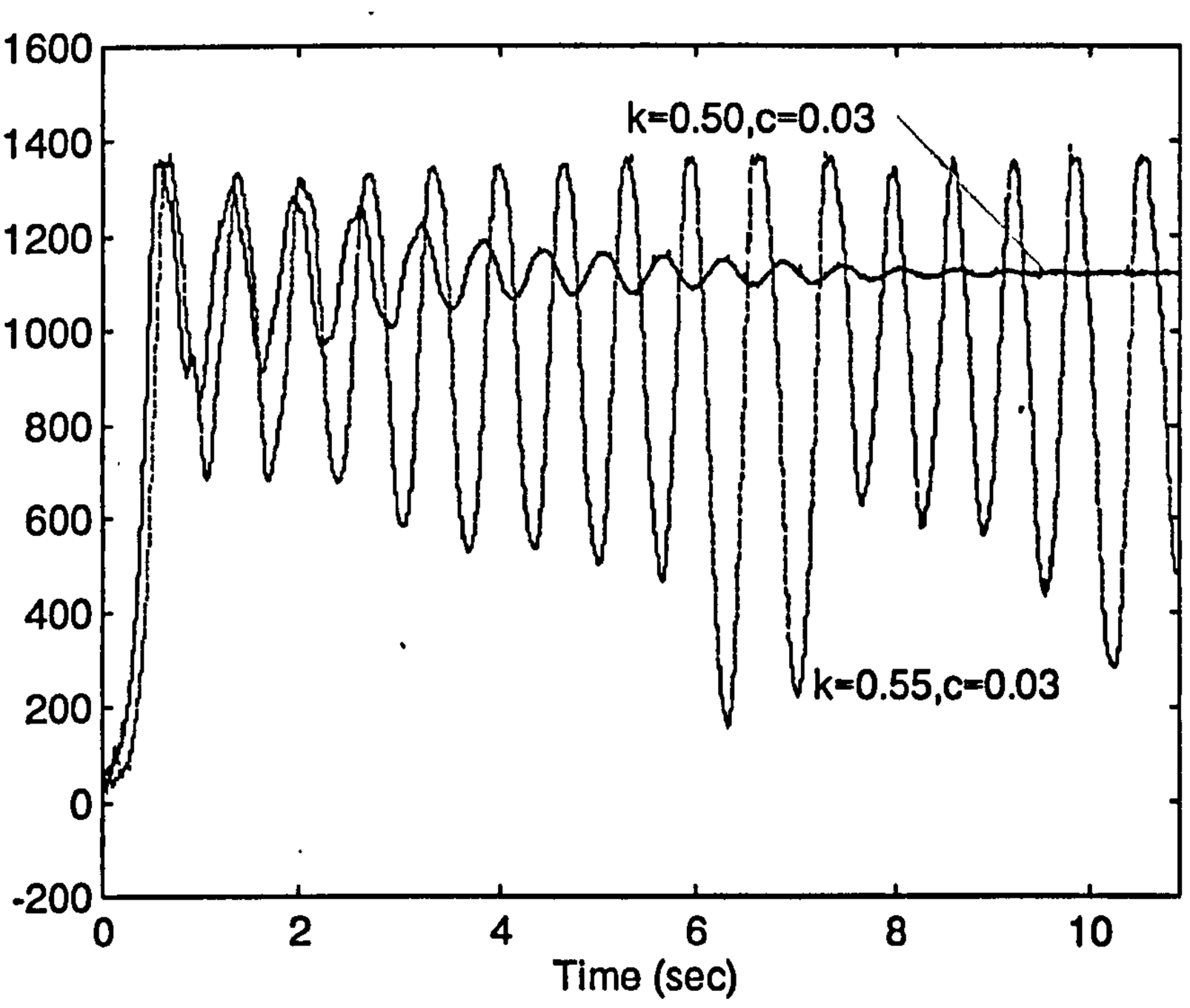

Figure 5-32 Measured effect of software spring rate on stability for relative damping

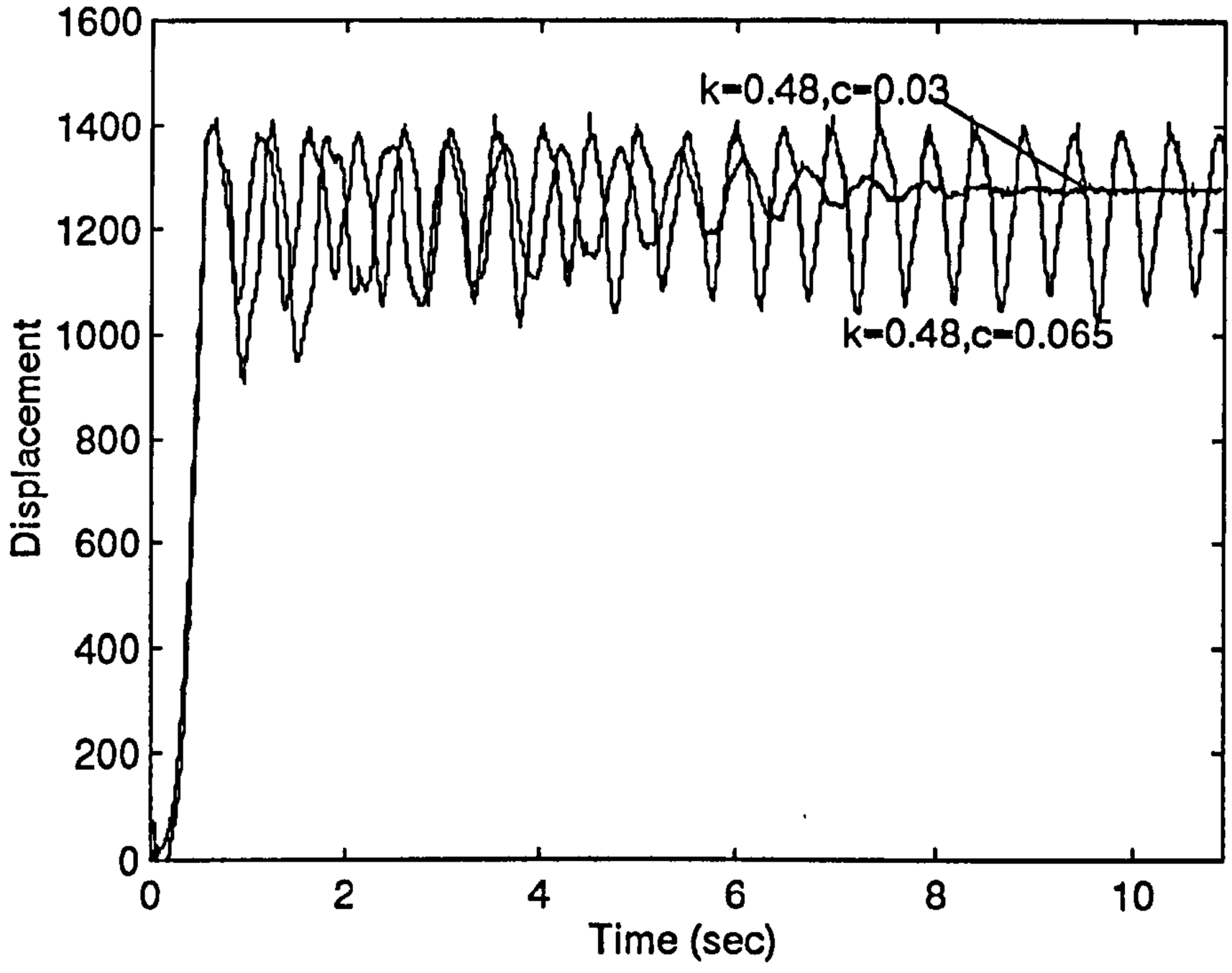

Figure 5-33 Measured effect of software damping rate on stability for relative damping

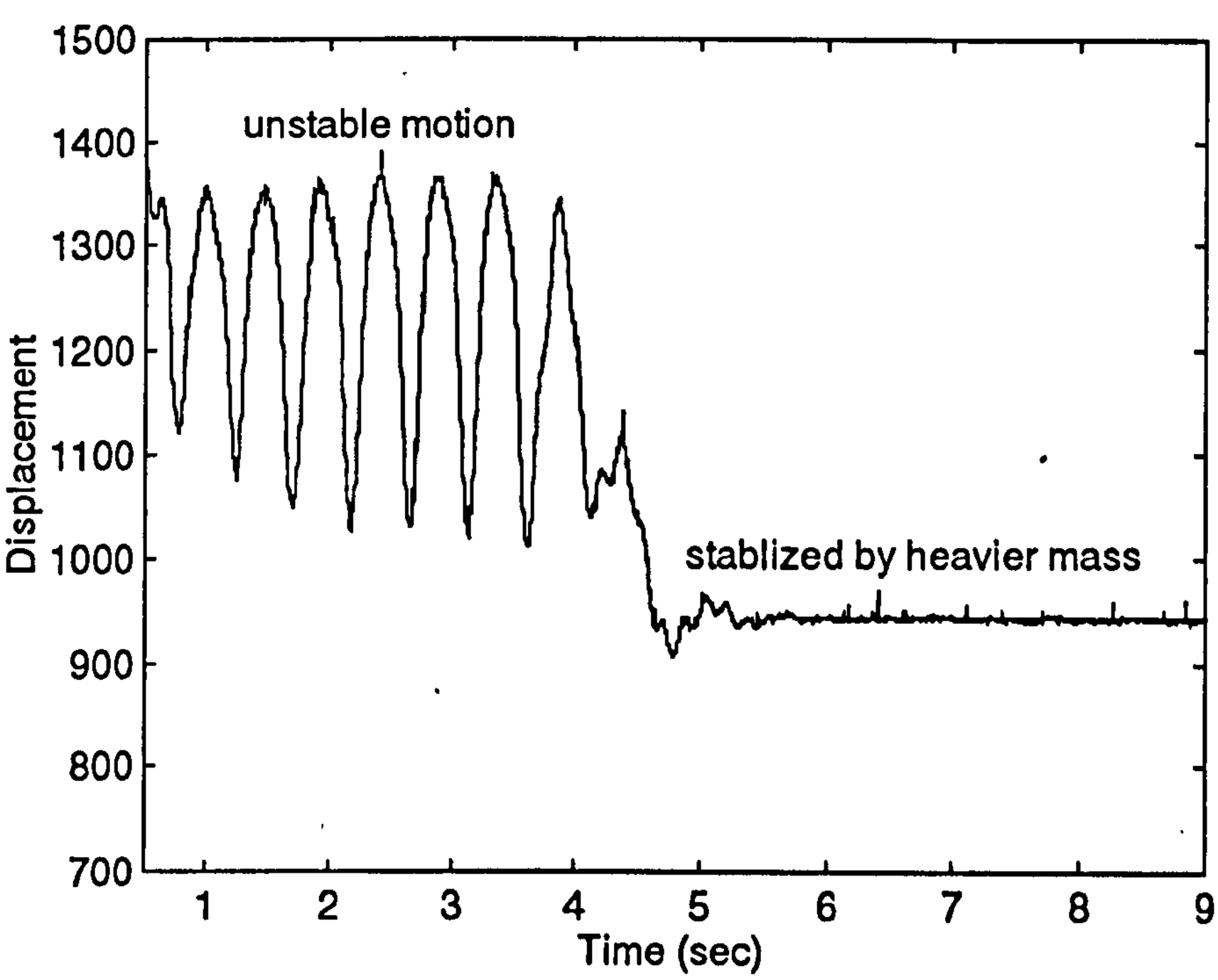

Figure 5-34 Measured effect of the mass on stability for relative damping

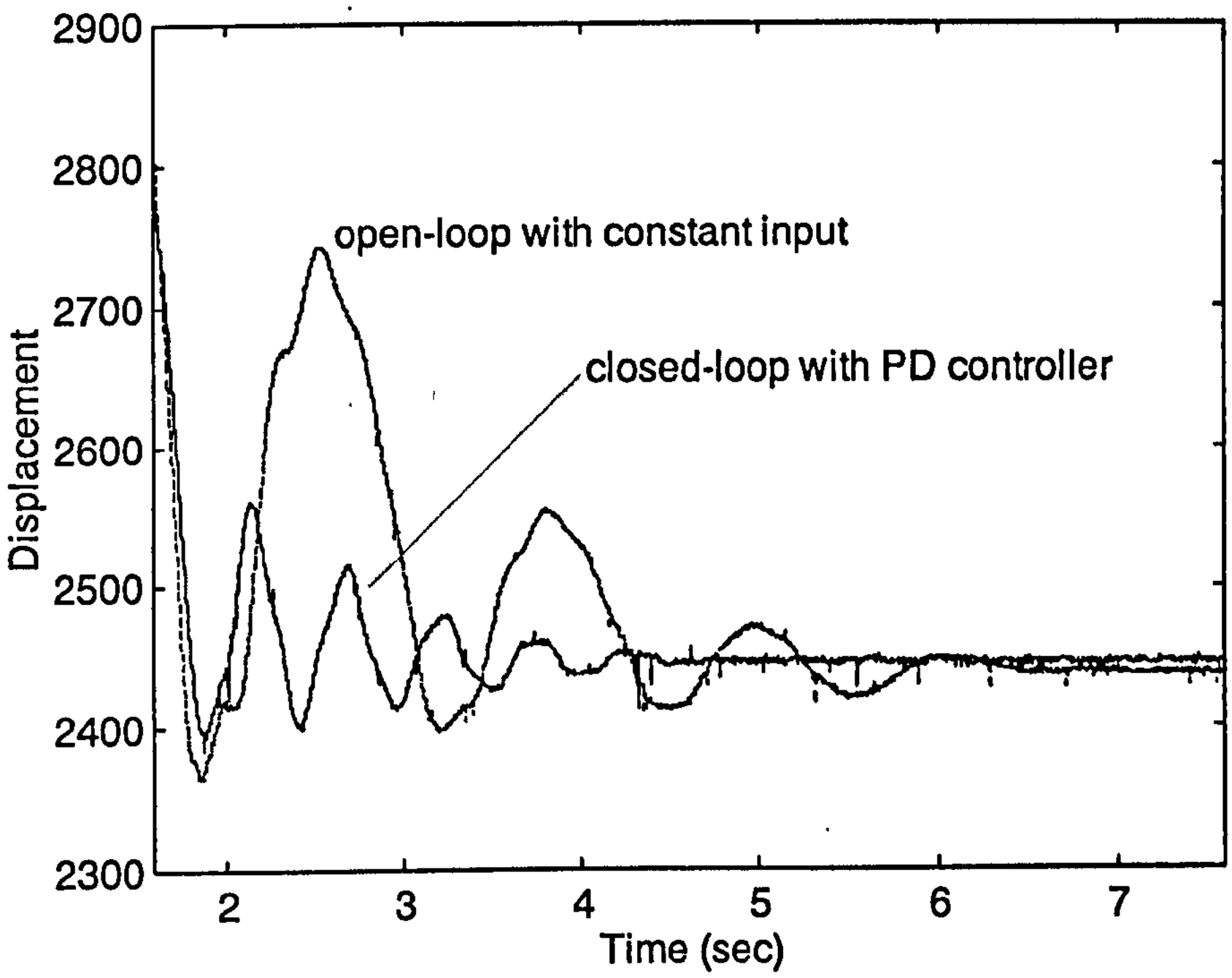

Figure 5-35 Measured vibration for relative damping controller and open-loop system

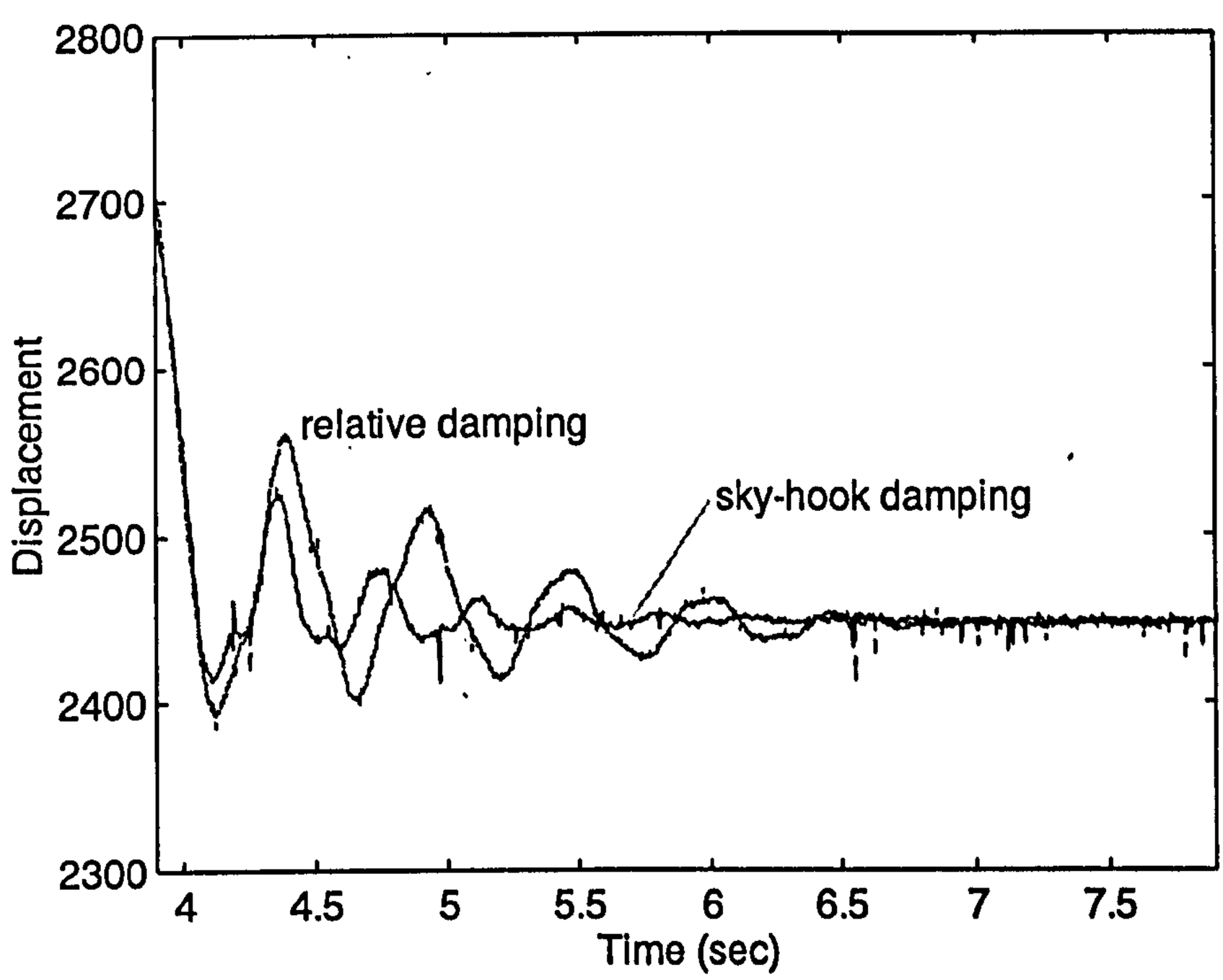

Figure 5-36 Measured vibration for sky-hook damping and relative damping

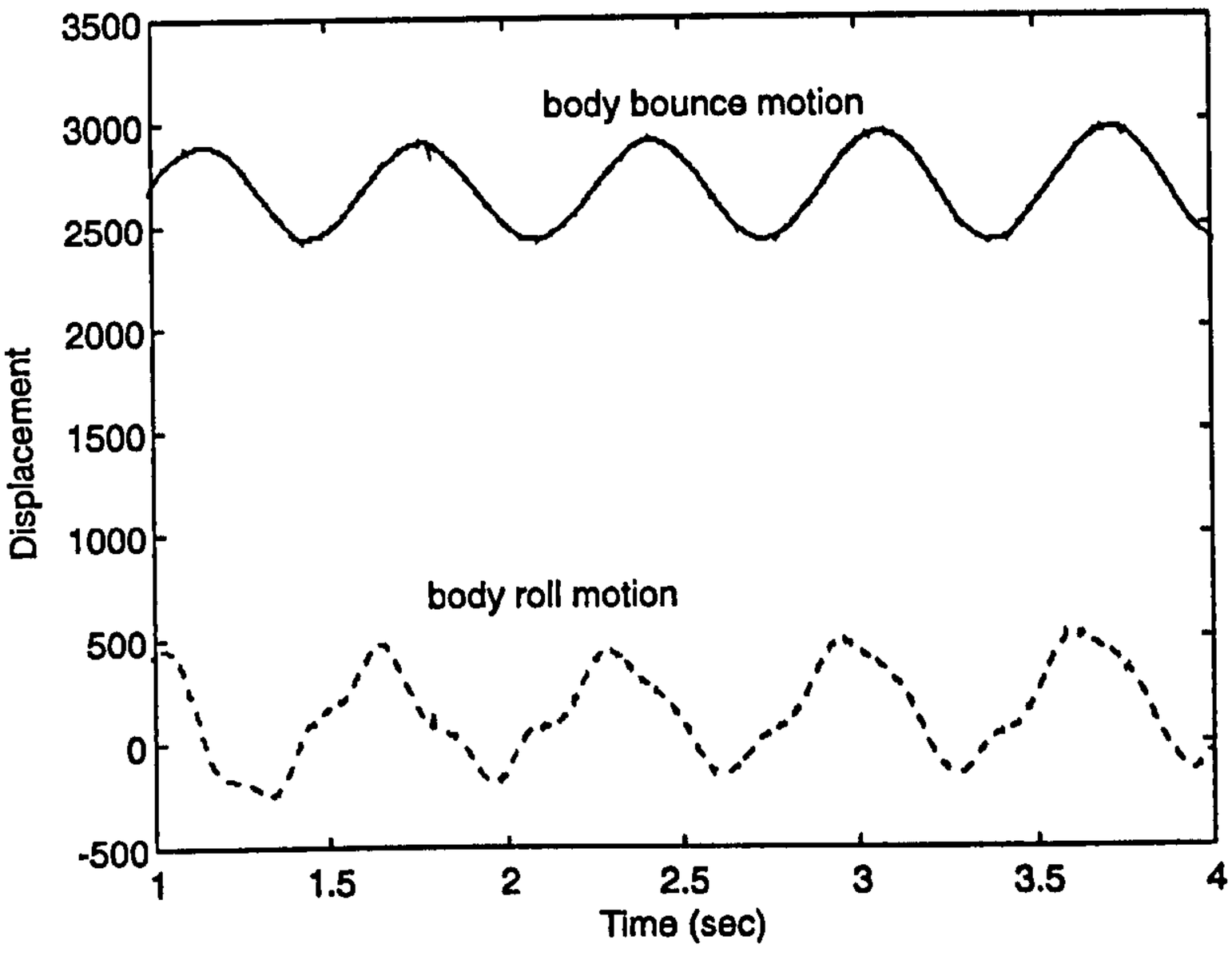

Figure 5-37 Measured unstable motions for same damping rates on both sides

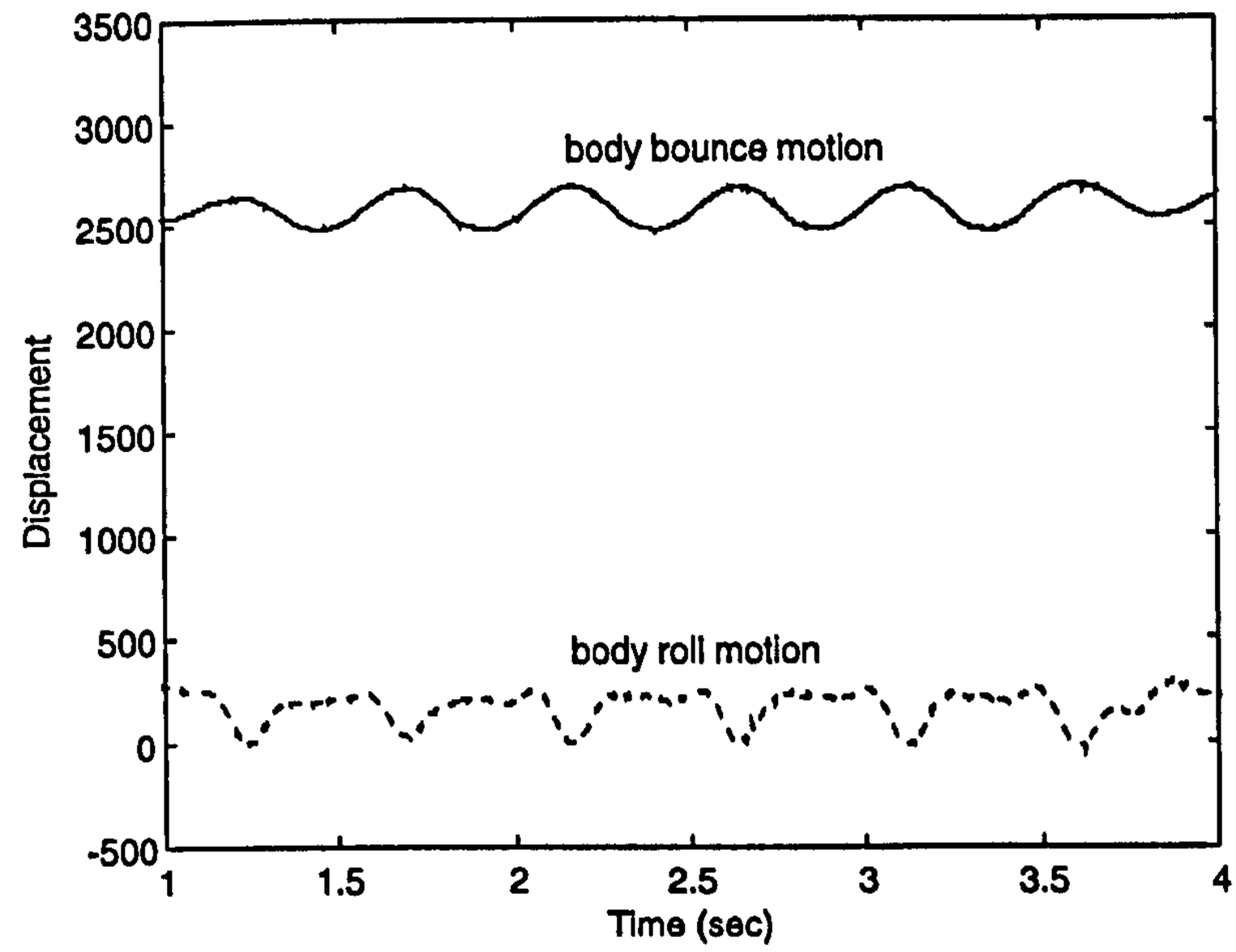

Figure 5-38 Measured unstable motions for different damping rates on both sides

Chapter 6

Performance of MIMO PID Controller for the Active Zero Rate Suspension on the Two Wheeled Trailer

6.1 Introduction

The successful implementation of the PD controller on the prototype is very encouraging though the control performance is not adequate. This at least shows that the developed hardware and software are effective. Based on it, refining the control performance by developing an appropriate algorithm will be carried out.

There is a problem in the implementation of the PD controller, i.e. potential instability. The unstable motion occurs in height and roll respectively or compositely. It has been demonstrated in the last chapter that one of the reasons is the quarter car model being used to design the controller. To improve the stability, a half car model needs to be applied to design the controller for the prototype.

The another problem that occurred in the PD controller is that the demanded position of the sprung body, body frequency and damping cannot be simultaneously achieved. The reason for this is that these factors are related to the proportional and derivative gains, allowing only two parameters to be set, which prevents the simultaneous optimisation of all three characteristics. The solution for this problem is to apply a more sophisticated control strategy. PID control, which has one more term - the integral gain - than PD is a simple option.

PID control is a very popular strategy in industry. It has several advantages such as being simple to implement in real time, easy to understand, and proven to be effective in many situations. It has widely been used for a long time, especially in the single-input and single-output (SISO) systems. In the area of active suspensions with multi-input and multi-output (MIMO), the application of PID has been seldom reported in recent years. The reason for this, in the author's opinion, is that it is difficult to find sophisticated methods to determine a PID controller for MIMO system.

PID control may be very effective in the area of active suspensions because its three terms allow control of position, damping and stiffness, and hence should meet the requirements of self-levelling, good handling and ride comfort. Furthermore, the 'sky-hook' damping can be implemented and PID control of MIMO systems could provide a simple and effective method to controlling the bounce, roll and pitch modes of sprung bodies.

Therefore, this chapter will investigate theoretically and experimentally the performance of the zero rate suspension using MIMO PID control strategy by means of the nonlinear half car model developed in chapter 4.

6.2 Nonlinear Half Car Model with PID Controller

The nonlinear half-car model was developed in chapter 4.

$$M\ddot{X} + C_d\dot{X} + KX = B_c X_c + BU + G \qquad (6\text{-}1)$$

$$Y = CX \qquad (6\text{-}2)$$

where

the mass matrix $M = diag\{ m_0, I, m_{t1}, m_{t2} \}$

the damping matrix

$$C_d = \begin{bmatrix} c_{01}+c_{02} & -c_{01}a+c_{02}b & -c_{01} & -c_{02} \\ -c_{01}a+c_{02}b & c_{01}a^2+c_{02}b^2 & c_{01}a & -c_{02}b \\ -c_{01} & c_{01}a & c_{t1}+c_{01} & 0 \\ -c_{02} & -c_{02}b & 0 & c_{t2}+c_{02} \end{bmatrix}$$

the stiffness matrix $K = diag\{ 0,\ 0,\ k_{t1},\ k_{t2} \}$

the excitation matrix $$B_c = \begin{bmatrix} 0 & 0 & 0 & 0 \\ 0 & 0 & 0 & 0 \\ c_{t1} & 0 & k_{t1} & 0 \\ 0 & c_{t2} & 0 & k_{t2} \end{bmatrix}$$

the control matrix $$B = \begin{bmatrix} 1 & 1 \\ -a & b \\ -1 & 0 \\ 0 & -1 \end{bmatrix}$$

the state vector $$X = \{x_0 \quad \theta \quad x_{t1} \quad x_{t2}\}^T$$

the output vector $$Y = \{y_{01} \quad y_{02} \quad y_{11} \quad y_{12}\}^T$$

the excitation vector $$X_c = \{\dot{x}_{c1} \quad \dot{x}_{c2} \quad x_{c1} \quad x_{c2}\}^T$$

the control vector $$U = \{F_{a1} \quad F_{a2}\}^T$$

the static load vector $$G = \{-m_0 g \; 0 \; -m_{t1} g \; -m_{t2} g\}^T$$

the observation matrix $$C = \begin{bmatrix} 1 & -a & 0 & 0 \\ 1 & b & 0 & 0 \\ 1 & -a & -1 & 0 \\ 1 & b & 0 & -1 \end{bmatrix}$$

Here:

a, b = distances between the centre of mass of the sprung body and the wheels

c_{01}, c_{02} = damping factors between the trailer body and hubs

c_{t1}, c_{t2} = damping of both tyres

F_{a1}, F_{a2} = forces of both actuator systems

I = moment of inertia about the mass centre of trailer body

k_{t1}, k_{t2} = stiffness of both tyres

m_0 = mass of the trailer body

m_{t1}, m_{t2} = masses of both wheels

x_0 = height of the trailer body mass centre

x_{c1}, x_{c2} = excitation of the road in the vertical direction at both wheels

x_{t1}, x_{t2} = vertical displacement of both wheels

y_{01}, y_{02} = height of the trailer body on left and right side

y_{11}, y_{12} = relative height of the trailer body to the hubs on the same side
θ = roll angle of the trailer

F_{a1} and F_{a2} are the forces produced by the active zero rate suspensions on both sides. According to the analysis of chapter 4, the simplified expression of the forces are

$$\begin{aligned} F_{a1} &= a_0 + a_1 l_1 + a_2 l_1^2 + (a_3 + a_4 l_1)(x_0 - a\theta - x_{t1}) \\ &= a_0 + a_1 l_1 + a_2 l_1^2 + (a_3 + a_4 l_1) y_{11} \end{aligned} \tag{6-3}$$

$$\begin{aligned} F_{a2} &= a_0 + a_1 l_2 + a_2 l_2^2 + (a_3 + a_4 l_2)(x_0 + b\theta - x_{t2}) \\ &= a_0 + a_1 l_2 + a_2 l_2^2 + (a_3 + a_4 l_2) y_{12} \end{aligned} \tag{6-4}$$

where a_j (j=0, ..., 4) are the coefficients from the Taylor's expansion, which have been obtained in chapter 4 and employed in chapter 5. Equations (6-3) and (6-4) imply that the suspensions on both sides have the same relationship between suspension force, actuator length (l_j $(j=1,2)$) and relative height. In the real test rig, this is not true. To simplify the problem, the assumption is used here. Some non-identical properties on both sides will be considered latter.

The limited bandwidth of the actuator systems was taken into account again and the same first order model as chapter 5 was applied in the form of time domain.

$$\dot{l}_1 + \omega_{01} l_1 = \omega_{01} u_1 \tag{6-5}$$

$$\dot{l}_2 + \omega_{02} l_2 = \omega_{02} u_2 \tag{6-6}$$

where ω_{01} and ω_{02} denote the cut off frequencies on both sides; and u_1 and u_2 are the inputs of the actuator systems. The measurement has shown that there is about 20% difference between the cut off frequencies. The investigation in chapter 5 illustrated that the cut off frequency affects the performance of the suspension significantly, so the difference will be considered in the subsequent investigation.

The combination of equations (6-1), (6-2), (6-3), (6-4), (6-5) and (6-6) gives the mathematical description of the half-car model with nonlinear control force and a limited bandwidth. The whole model is shown schematically in figure 6-1.

The output vector Y is measured by two vertical accelerometers on the trailer body and two body to hub displacement transducers on both sides of the trailer. The input for each actuator, u_1 and u_2, needs to be determined by appropriate controllers. Because of complexity of the suspension, it is not easy to understand the relationship

in the system only using figure 6-1. The block diagram, figure 6-2 can be more clear for this open loop system.

In chapter 5, the PD controller was considered only between the input and output on the same side and also the dynamic coupling between both sides was ignored. In this chapter, however, the coupling will be taken into account and PID controller will be developed between the whole input vector $\{u_1\ u_2\}$ and the whole output vector $\{y_{01}\ y_{02}\ y_{11}\ y_{12}\}$.

As is well known, a PID controller has three terms, i.e. proportional (P), integral (I) and derivative (D) control, which effectively simulate conventional springs, position compensators and dampers respectively. The requirements for its control performance are the same as those in chapter 5, i.e. appropriate body height and attitude, stability, reachability, high body damping and low body frequency. The integral term can fulfil the first requirement, in which the demanded height and attitude can be specified. The others can obtained by selecting the parameters of the three terms.

An effective method for good body damping is 'sky-hook' damping which is related to the absolute velocity of the vehicle body. In this prototype, the output variables $\{y_{01}\ y_{02}\}$ will be used for the derivative controller. The other two output variables will not be applied because the relative damping has been shown to be less effective than the 'sky-hook' damping. These two output variables $\{y_{11}\ y_{12}\}$, body to hub height, will be employed in the proportional controller, which simulate two springs between body and hubs. These two variables will also be used in the integral controller. The feedback equation is listed below:

$$\begin{Bmatrix} u_1 - u_1^* \\ u_2 - u_2^* \end{Bmatrix} = K_P \begin{Bmatrix} y_{11} - y_{11}^* \\ y_{12} - y_{12}^* \end{Bmatrix} + K_D \begin{Bmatrix} \dot{y}_{01} \\ \dot{y}_{02} \end{Bmatrix} + K_I \int \begin{Bmatrix} y_{11} - y_{11}^* \\ y_{12} - y_{12}^* \end{Bmatrix} dt \qquad (6\text{-}7)$$

where

the proportional matrix: $K_P = \begin{bmatrix} P_{11} & P_{12} \\ P_{21} & P_{22} \end{bmatrix}$

the derivative matrix: $K_D = \begin{bmatrix} D_{11} & D_{12} \\ D_{21} & D_{22} \end{bmatrix}$

the integral matrix: $K_I = \begin{bmatrix} I_{11} & I_{12} \\ I_{21} & I_{22} \end{bmatrix}$

and the demanded heights $\{y_{11}^* \quad y_{12}^*\}$ on both sides are given as demand inputs and $\{u_1^* \quad u_2^*\}$ denote the actuator inputs when the system is in steady state.

The closed loop system is formed with the PID feedback unit, as shown in figure 6-3. Because of the mechanism of the zero rate suspension, the forces $\{F_{a1} \; F_{a2}\}$ are nonlinear functions of the actuator lengths and the body-to-hub displacements. The system therefore is a nonlinear multivariable system, for which there is not a sophisticated and effective method to design the PID controller.

This PID controller is shown in the block diagram of figure 6-4. Comparing with the PD in chapter 5, the PID here is much more complicated. The whole feedback unit uses the information from four output variables $\{y_{01} \quad y_{02} \quad y_{11} \quad y_{12}\}$ and processes the control signals for two input variables $\{u_1 \quad u_2\}$ through the PID. The unit needs four pre-set inputs $\{y_{11}^* \quad y_{12}^*\}$ and $\{u_1^* \quad u_2^*\}$ where the latter two are dominated by the former, so the actual independent pre-set inputs are the former. This point will be explained next.

The steady state inputs $\{u_1^* \quad u_2^*\}$ can be determined by the system model and the demanded heights. When the system is in steady state, the body attitude and height are in the demanded state, and the velocities and accelerations in the system are equal to zero, and the lengths of actuators $\{l_1^* \quad l_2^*\}$ and their inputs $\{u_1^* \quad u_2^*\}$ are corresponding to this state. From equations (6-5) and (6-6), we can obtain

$$\begin{Bmatrix} u_1^* \\ u_2^* \end{Bmatrix} = \begin{Bmatrix} l_1^* \\ l_2^* \end{Bmatrix} \tag{6-8}$$

From equations (6-1), (6-2), (6-3) and (6-4), we can get the lengths of the actuators for the demanded heights.

$$\begin{cases} l_1^* = \dfrac{-1}{2a_2}\left((a_1 + a_4 y_1^*) + \sqrt{(a_1 + a_4 y_1^*)^2 - 4a_2(a_0 + a_3 y_1^* - \dfrac{b}{a+b} m_0 g)}\right) \\ l_2^* = \dfrac{-1}{2a_2}\left((a_1 + a_4 y_2^*) + \sqrt{(a_1 + a_4 y_2^*)^2 - 4a_2(a_0 + a_3 y_2^* - \dfrac{a}{a+b} m_0 g)}\right) \end{cases} \tag{6-9}$$

This equation is illustrated in figure 6-5 in which the length of actuator changes with the demanded height on the same side for various vehicle body mass.

It is shown in figure 6-5 that the steady state actuator length has to be decreased when the demanded body height on the same side is increased. The more the body mass is, the less the actuator length is. Actually, the steady state input of the actuator length does not need to be given precisely because the integral controller can compensate for the input error which results from a change of body mass. This point can be illustrated by the simulation.

Figure 6-6 illustrates two starting response (step response) curves for two different steady state input actuator lengths 0.04 and 0.06. The small difference between the curves shows that the steady state input of actuator length does not much affect on the system response.

In the simulation in this chapter, the y coordinate is different from that in chapter 5. In that chapter, the initial position is at the origin. Here, the demanded height is at the origin because a coordinate transfer (i.e. the feedback of the displacement to the demanded height) has been introduced.

6.3 Stability and Reachability

The whole system including the PID controller is modelled within MATLAB. By means of this, the stability and reachability can be investigated through eigenvalues and step responses. There are 12 parameters in the PID controller, so the investigation is an extremely big job. To simplify the problem, the symmetry of parameters across the trailer is assumed, i.e. $P_{11}=P_{22}$, $P_{12}=P_{21}$, $I_{11}=I_{22}$, $I_{12}=I_{21}$, and $D_{11}=D_{22}$, $D_{12}=D_{21}$.

Figures 6-7 to 6-12 are the stable region for various parameters of the PID controller. These regions were obtained by analysing the eigenvalues of the state matrix of the linearised equation for the whole closed loop system near the steady state position (i.e. the demanded height $\{y_{11}^* \quad y_{12}^*\}$).

The stable region for the proportional gains of the P controller is illustrated in figure 6-7. It is shown that the coupled proportional gain (P_{12} and P_{21}) can not be over large for the stable demanded height for the system. The limit of the coupled proportional gain is slightly above of the main proportional gain (P_{11} and P_{22}).

Figure 6-8 demonstrates the stable region for the derivative gains of the D controller. It is shown that the coupled derivative gain (D_{12} and D_{21}) can not be larger than the

main derivative gain (D_{11} and D_{22}) to obtain a stable demanded height for the control system.

The integral gains of the I controller has the similar stable region as the D controller, as shown in figure 6-9. To keep the demanded height stable, the coupled integral gain (I_{12} and I_{21}) can not be larger than the main integral gain (I_{11} and I_{22}).

The stable region was calculated for the main proportional gain and the main derivative gain as shown in figure 6-10. It is illustrated that the main derivative gain can not be over large or over small to obtain a stable demanded height for the control system. Compared with figure 5-21 where the coupled gains and integral gains are zero, the upper limit for derivative gain has been shown to be caused by the 'sky hook' damping. Figure 5-21 is a particular case for PID here, so the upper boundary is caused by the 'sky hook' property. From figure 6-8, it is easy to find that the lower boundary results from the use of the coupled derivative gain. The main proportional gain can not be less than a value which is related to the coupled proportional gain, as having been shown in figure 6-7.

Figure 6-11 illustrates the stable region for the main derivative gain and the main integral gain. There are upper and lower boundaries for the main derivative gain. The lower boundary is related to the coupled derivative gain and the proportional gains, and the upper boundary changes with the main proportional gain. The integral gain can not be over small, which is caused by the coupled integral gain, as having been shown in figure 6-9.

From figure 6-12, we can find the stable region for the main proportional gain and the main integral gain. For the interested range of the parameters, there are no upper boundaries for both gains. The lower boundary of the main integral gain depends on the coupled integral gain and the lower boundary of the main proportional gain results from the coupled proportional gain. This result is obtained from the linearised equation of the nonlinear system, so it does not mean that there is no limit for the parameters in the test rig, which can be shown in the simulation afterwards.

The effect of the control parameters on the stability shown above is based on the eiganvalues of the linearised system. The behavior for other parameters is similar to the case shown in figures 6-7 to 6-12. These stability characteristics can only determine the property of the system position at steady state (i.e. the demanded height). Because the whole closed loop system is nonlinear, the problem becomes

more complicated. Sometimes the real motion of the system does not follow the behaviour predicted by the linearised approach.

It has been suggested in chapter 5 that the real motion of system depends on two factors, one is the differential equation and another is the initial state of the system. If a system is linear, then the motion will always reach the stable position regardless of the initial states. If a system is nonlinear, then the motion will only attain a stable steady state position if the initial value lies within the same 'stable region' in the state space as the final value. This point has also been demonstrated by the numerical phase plane analysis in the chapter.

Next we will present how the nonlinearity affects the reachability of the closed loop system for the PID controller. In this chapter, numerical analysis is still in use.

Figures 6-13 to 6-18 illustrate the effect of the parameters of the PID controller on the starting responses (step responses). For the parameters used in the responses, the steady state position (the demanded height) of the system is stable according to the eigenvalues of the linearised system. But the starting responses can be either stable or unstable from the initial state. A difference between this chapter and the last is that the zero height and zero angle represent the steady state while the zero height represented the initial state in chapter 5. Because it is the stability that is of interest, only the bounce responses were shown in these figures, which is sufficient for the purpose.

The starting response of the body bounce motion is shown in figure 6-13. There are two curves, stable and unstable, in the figure, which correspond to two different main derivative gains. It is shown that the over large main derivative gains can cause the body bounce motion to become unstable, although the eigenvalue analysis for the linearised system has indicated that the steady state should be stable for both parameters. The reason for this is that the nonlinearity in the system results in the initial state lying in a different region from the stable steady state in the state space, as demonstrated by using phase plane analysis in chapter 5.

Figure 6-14 illustrates the starting response of the body bounce motion. The stable response corresponds to coupled derivative gain, D_{12} and D_{21}=0.15, and the unstable response is for the zero coupled derivative gain. That means physically that the coupled derivative gain can improve the reachability which is caused by nonlinearity. This property is very valuable. If the unstable motion occurs due to nonlinearity when you increase the main derivative gain to obtain high damping, you can make it stable

by increasing the coupled derivative gains, though this also gives rise to a increased lower limit for the main derivative gain according to the eigenvalue analysis.

The effect of the main proportional gain on the reachability is shown in figure 6-15. The starting response of the body bounce motion is stable when the main proportional gains P_{11} and P_{22} are 0.3. The response is unstable when the gains are all 0.4, though the eigenvalue analysis has demonstrated the steady state to be stable. That means that the over large main proportional gain can give rise to the starting response not reaching the steady state because of nonlinearity.

Figure 6-16 illustrates that the starting response of the body bounce motion is unstable for the coupled proportional gains P_{12} and P_{21} being 0.1 and stable for the zero coupled proportional gain. The instability is also caused by the nonlinearity because the steady state is stable according to the eigenvalue analysis. It is shown that the coupled proportional gain can not only result in a lower limit for the main proportional gain for the steady state stability but also the deterioration of the reachability of the nonlinear system.

It is illustrated in figure 6-17 that the starting response of the body bounce motion is affected by the main integral gain. The response is stable when the main integral gain is 0.3 and unstable when it equals to 0.2. That means that the over small main integral gain leads to the steady state not being reachable which is caused by the nonlinearity because the eigenvalue analysis has proved the steady state is stable for the main integral gain of 0.2. This suggests that reachability can be improved through increasing the main integral gain.

The coupled integral gain has a similar effect to the main integral gain on the starting response of the body bounce motion, as shown in figure 6-18. In the figure, the response is stable for the coupled integral gain of 0.12 and unstable for 0.08. The reason for the unstable response is the nonlinearity because the steady state is stable based on the linearised system. The effect implies that increasing the coupled integral gain can also improve the reachability.

The symmetry of the prototype can also affect the reachability to the demanded height of the closed loop system because of the nonlinearity. Here we will investigate the effect of the position of vehicle body mass centre and the difference of the actuator bandwidth on both sides.

In figure 6-19, there are two starting responses of the body bounce motion for two different positions of the body mass centre. One response is stable when the mass

centre is 5cm from the geometric centre and the other is unstable when the mass centre is at 8cm. The unstable response is caused by the nonlinearity because the eigenvalue analysis has shown that the steady state is stable. It implies that unsymmetrical mass distribution can deteriorate the reachability of the demanded height.

The starting response has been predicted in two figures, one is for the identical actuator bandwidth on both sides as shown in figure 6-20 and the other is for different bandwidth as shown in figure 6-21. In figure 6-20, the starting response of the body bounce motion is stable for the higher actuator bandwidth of 4.281Hz and unstable for the lower actuator bandwidth of 4.265Hz. This means that the lower actuator bandwidth can degrade the reachability of the system with identical actuators.

In figure 6-21, the same responses were predicted. One case is stable for the actuator bandwidth of 5Hz on both sides and another is unstable for the actuator bandwidth of 5Hz at left and 4.78Hz at right. The difference of the cut-off frequencies of the actuators on both sides is only about 4.4% and also the unstable value for this case is higher than that for the case of the identical actuators by 12.1%. That means physically that non-identical actuators give rise to more chance for the lower cut-off frequencies of their bandwidth to deteriorate the reachability. It has been mentioned that the actual difference between the two actuator bandwidths is about 20% from the measurement. That therefore is one of the reasons why the actual prototype tends to be unstable. This property is also caused by the nonlinearity because the eigenvalue analysis has shown the steady state to be stable for all cases in figures 6-20 and 6-21.

6.4 On Control Performance

The stability and reachability of the closed loop system with a PID controller have been investigated in last section. This section will discuss the effect of the parameters on the control performance. The starting responses are still in use for the investigation. The predicted responses are shown in figures 6-22 to 6-27 for various values of parameters. To simplify the analysis, the symmetrical parameters are still assumed. To examine the roll motion and coupled gains, unsymmetrical mass distribution is considered.

In figures 6-22(a), (b) and (c), the starting responses were predicted for three different main proportional gains, 0.15, 0.2 and 0.25. It is shown in figure 6-22(a) that increasing the main proportional gain can increase the over shoot and decrease rising

time of the body bounce response. In 6-22(b), the body roll vibration becomes more violent for the higher main proportional gain. Increasing the main proportional gain can degrade the damping for the hub and cause more violent hub vibration, as shown in figure 6-22(c). These behaviours are similar to those in a conventional system.

The starting responses are illustrated in figures 6-23(a), (b) and (c) for the body bounce, body roll and hub vertical motion with different coupled proportional gains, 0, 0.02 and 0.04. In figure 6-23(a), the over shoot increases and rising time decreases with the coupled proportional gain increasing. But increasing the coupled proportional gain can deteriorate damping for the body roll and the hub vertical motion, make their vibration more violent and delay their tending to the steady state, as shown in figures 6-23(b) and (c).

Figures 6-24(a), (b) and (c) illustrate the starting responses for the body bounce, body roll and hub vertical motion with various main derivative gains, 0.04, 0.06 and 0.08. It is shown in figure 6-24(a) that increasing the main derivative gain can increase the over shoot (which is abnormal to a conventional system) and rising time for the body bounce motion. Oscillation did not occur here for small main derivative gains because of the combination of the other control parameters. In figure 6-24(b), increasing the main derivative gain can attenuate the vibration and increase the frequency for the body roll motion. In figure 6-24(c), it can be seen that the damping on hub vibration is degraded by increasing the main derivative gain. This behaviour is caused by the 'sky hook' damping which is supposed to 'take care' only of the vehicle body motion.

The effect of the coupled derivative gain on the starting responses are demonstrated in figures 6-25(a), (b) and (c) for the body bounce, body roll and hub vertical motion. It is shown in figure 6-25(a) that the over shoot and rising time of the body bounce response can be decreased through decreasing the coupled derivative gain. More violent vibration and lower frequency of the body roll motion can be caused by larger coupled derivative gain, as shown in figure 6-25(b). In figure 6-25(c), the damping of the hub vertical response is deteriorated by the increase of the coupled derivative gain, which is also caused by the 'sky hook' damping.

With various main integral gains, 0.04, 0.08 and 0.12, the starting responses are predicted in figures 6-26(a), (b) and (c) for the body bounce, body roll and hub vertical motion. From figure 6-26(a), it can be seen that the over shoot of the body bounce response increases and the rising time decreases slightly with the main integral gain increasing. It is shown in figure 6-26(b) that increasing the main integral gain can

make the body roll response more violent. The change of the main integral gain can give rise to little difference for the hub vertical responses, as shown in figure 6-26(c).

The effect of the coupled integral gain on the starting responses is quite similar to that of the main integral gain, as shown in figures 6-27(a), (b) and (c) for the body bounce, body roll and hub vertical motion. It is demonstrated in figure 6-27(a) that increasing the coupled integral gain can increase the over shoot and decrease the rising time for the body bounce response. In figure 6-27(b), however, increasing the coupled integral gain can make the body roll vibration less violent. It is also shown that increasing the coupled integral gain does not change the hub vibration significantly.

6.5 Experiment Results

The MIMO PID controller has been implemented in the prototype. The code of the control software is written in C++. The structure of this program is shown schematically in the block diagram (figure 6-28). The source code for the PID control algorithm is shown in Appendix C. To change the control parameters on line, the interrupt technique (Adamson, 1990) has been employed in the program. The test results have shown that the implementation is successful.

The effect of the control parameters on the starting responses has been investigated in the test. The results have been shown in figures 6-29 to 6-34. In these figures, the bounce and roll motion were directly obtained through the body to hub displacement transducers. This implies that the measured displacements are with respect to the hubs. The only difference between the relative displacement of the body and the absolute displacement is the high frequency component which is caused by the wheel stiffness. These measurement results were not calibrated for their displacement which is sufficient for the investigation here, so the y coodinate in the figures do not show the units.

It is shown, in figures 6-29(a) and (b), that the main proportional gain also produces similar performance on the starting response to the theoretical analysis. When the gain increases, the responses for both bounce and roll motion become more violent and the rising time decreases, but the steady state keeps nearly unchanged.

The effect of the coupled proportional gain is demonstrated in figures 6-30(a) and (b). It is shown that when the coupled proportional gain increases, both the bounce and roll response move violently and the rising time of bounce motion decreases. These behaviours are similar to those in the theoretical analysis.

Figures 6-31(a) and (b) illustrate the effect of the main derivative gain on the starting responses. When the gain is increased, the rising time of the bounce motion decreases, the over shoot of the bounce motion increases and the roll motion becomes less violent. These characteristics are consistent with the analytical results in last section. However, it should be noted that these characteristics are different from those in a conventional linear system.

As shown in figures 6-32(a) and (b), the coupled derivative gain has similar effect on the starting responses to the theoretical analysis. The rising time and the overshoot of the body bounce motion increase slightly with the increase of the coupled derivative gain. The vibration of the roll motion becomes violent with the increase of the gain, in other words, the equivalent roll damping decreases.

It is illustrated in figures 6-33(a) and (b) that the main integral gain has similar effect on the starting responses to the predicted results. When the main integral gain increases, the rising time decreases and the overshoot of the body bounce motion increases. The roll motion becomes more violent. The steady state for both body motions becomes more achievable.

The effect of the coupled integral gain on the starting responses for the bounce and roll motion is shown in figures 6-34(a) and (b), which also validated the prediction. The rising time decreases and the over shoot for the bounce motion increases with the increase of the coupled integral gain. The roll motion becomes less violent. The bounce motion tends to achieved the steady state more quickly but the roll motion more slowly.

In the theoretical analysis on stability, the unstable motion approaches infinity. Actually, the unstable motion is just an undecaying oscillation with big amplitude for a particular mode due to the constraints of the mechanical structure. This can be seen in figures 6-35 to 6-39, in which the roll motions are shown for both stable and unstable. It has been seen that unstable roll motion can occur due to a number of inappropriate parameters.

In figure 6-35, the stable roll motion corresponds to the main proportional gain $P_{11}=P_{22}=0.3$ and the unstable motion to $P_{11}=P_{22}=0.7$. This means that over large main proportional gain tends to lead to roll motion instability. The test also demonstrated that over large coupled proportional gain causes the suspension to fail to lift the body or to move extremely violently. The test result for this case therefore was not taken for illustration.

In figure 6-36, the roll motion is stable for a main derivative gain $D_{11}=D_{22}=0.085$ and is unstable for $D_{11}=D_{22}=0.11$, which means that over large main derivative gain can cause roll motion instability. In figure 6-37, the roll motion is stable when the coupled derivative gain $D_{12}=D_{21}=0.04$ and is unstable when $D_{12}=D_{21}=0.02$. This means that over small coupled derivative gain also causes roll motion instability.

In figures 6-38 and 6-39, the motions are all unstable but the extent of the instability for the cases is quite different. In figure 6-38, the oscillation amplitude of the roll motion for the main integral gain $I_{11}=I_{22}=0.16$ is less than that for $I_{11}=I_{22}=0.08$, which means that increasing the main integral gain can improve the stability of the body motion. In figure 6-39, the oscillation amplitude of the roll motion for the coupled integral gain $I_{12}=I_{21}=0.06$ is less than that for $I_{12}=I_{21}=0.03$, which demonstrates that the small coupled integral gain tends to degrade the stability of the body motion.

The test results shown in figures 6-35 to 6-39 have confirmed the theoretical prediction for the stability and reachability in section 6.3.

In the real application, the equivalent natural frequencies and damping ratios for various body motions are often referred by engineers as the evaluation of a suspension performance. These characteristics were estimated for the prototype with the implemented MIMO PID controller. The method used here is that the values equal to those from a single degree-of-freedom PID system which is best fitting the measured step response when the proportional gains were changed from 0.1 to 0.5 and the derivative gains from 0.03 to 0.11. This method is not as effective as using a sophisticated instrument which unfortunately is not available.

The results are shown in figures 6-40(a) and (b) in which the equivalent damping ratios are against the equivalent frequencies. It is shown that the trade-off relationship between damping ratio and natural frequency still exists for this approach. In other words, large damping ratio corresponds to a small natural frequency. It can be seen in figure 6-40(a) that the body bounce mode can achieve about 0.5Hz frequency and 0.7 to 0.8 damping. In figure 6-40(b), the body roll mode can achieve approximately from 0.2Hz to 1.4Hz frequency and damping ratio from 0.5 to 0.8. The best achieved combination is the bounce mode with about 0.55Hz frequency and 0.72 damping ratio and the roll mode with about 0.99Hz frequency and 0.80 damping ratio which are quite satisfactory for ride comfort.

6.6 Conclusions

The MIMO PID has been applied to the nonlinear multivariable system presented by the zero rate suspension prototype. The controller designed for the half car model has been successfully implemented in a PC based physical system. The effect of the control parameters on the control performance and stability have been investigated theoretically and experimentally.

It is shown experimentally and numerically that increasing the main or coupled proportional gain results in shorter rising time and bigger over shoot for bounce motion, and worse stability for both body bounce and roll motion. Increasing the main derivative gain gives rise to longer rising time and bigger over shoot for body bounce motion and better damping for body roll motion, but over large main derivative gain can cause unstable roll motion. Increasing the coupled derivative gain can improve such an roll motion instability but can degrade the equivalent damping for the roll motion. These characteristics of the derivative gains are quite different from those in a conventional linear system. Increasing the main or coupled integral gain can also improve the roll motion instability and speed of both motions to the steady state, but results in worse damping and bigger over shoot.

The instability for the system is largely caused by the nonlinearity. In addition to the effect of the above parameters, other factors can also degrade the stability. The mass symmetry of the trailer body, the matching of the two suspensions and the cut off frequency of the actuator bandwidth belong to this category.

The measured results have shown that the trade-off relationship between damping ratio and natural frequency still occurs for the zero rate suspensions with the MIMO PID controller. This approach can provide the trailer body with 0.55Hz frequency and 0.72 damping ratio for bounce motion and the 0.99Hz frequency and 0.80 damping ratio for roll motion. This is quite satisfactory for ride comfort.

The experiment demonstrated that the MIMO PID can improve the stability caused by the nonlinearity and provide better control performance as follows.

- Able to support the trailer body at any demanded ride height within mechanical constraints.
- Enable the ride height to adapt to the change of the body mass and its distribution.
- Able to provide more smooth transient motion to the demanded attitude.

- Able to prevent the violent trailer body motion and to damp out oscillation.
- Able to provide stable body height and attitude.
- Able to isolate the trailer body from road disturbances.
- Does not improve damping of the wheel.

The last item, the drawback, is caused by the 'sky hook' damping in the PID controller, which is proposed to be solved by using an active tuneable vibration absorber.

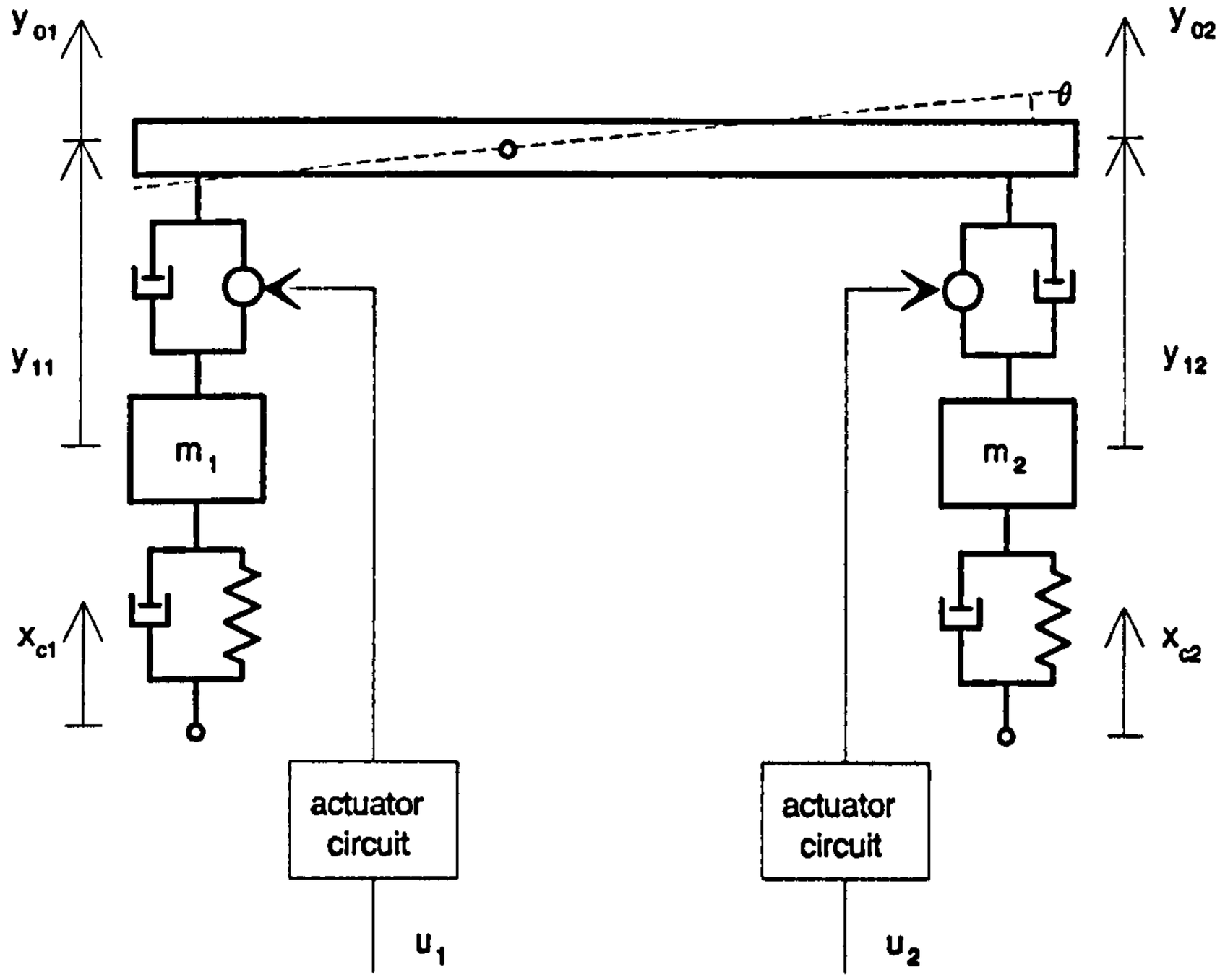

Figure 6-1 Half car model with the inputs and outputs

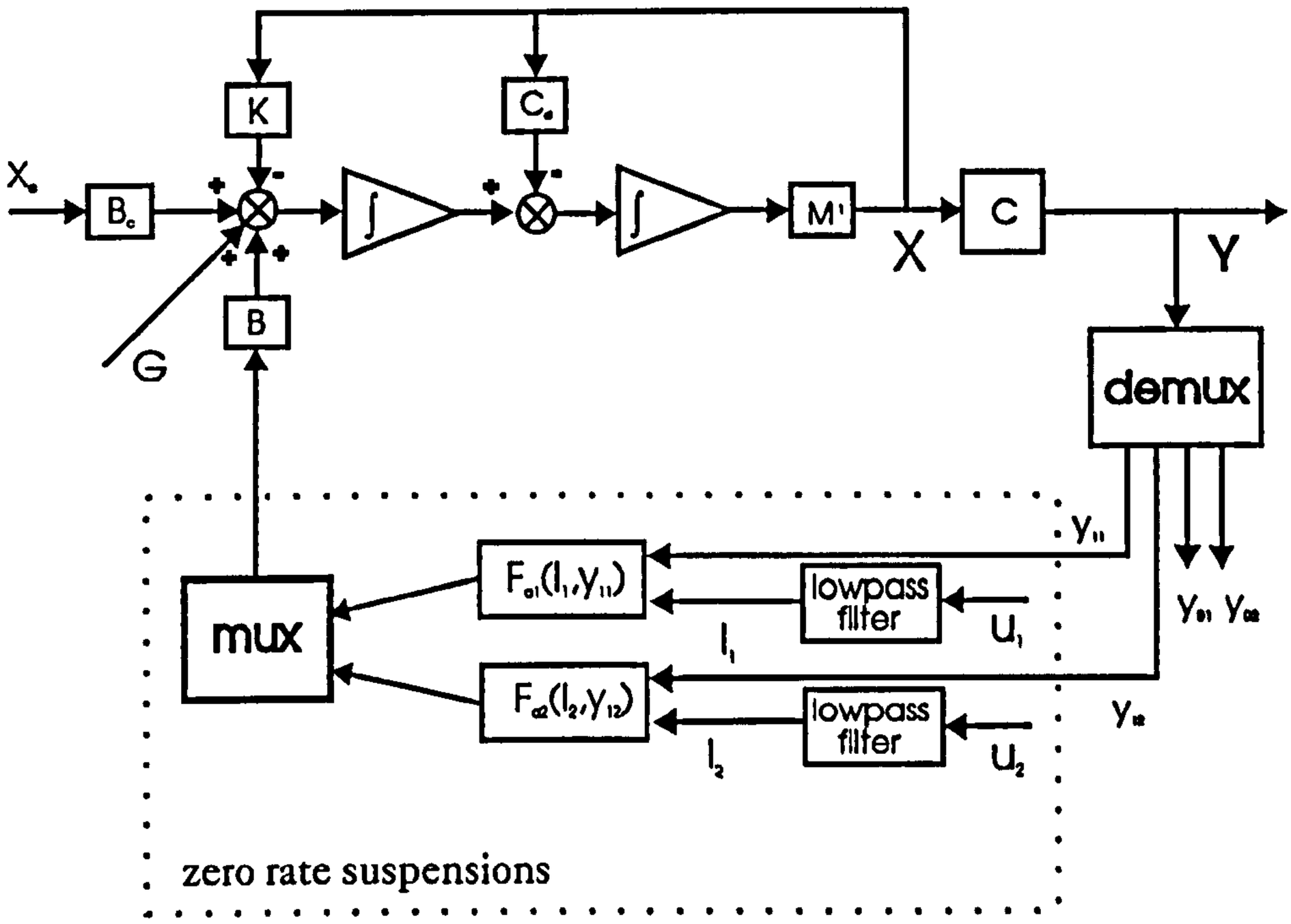

Figure 6-2 Block diagram of the open loop system for the half car model

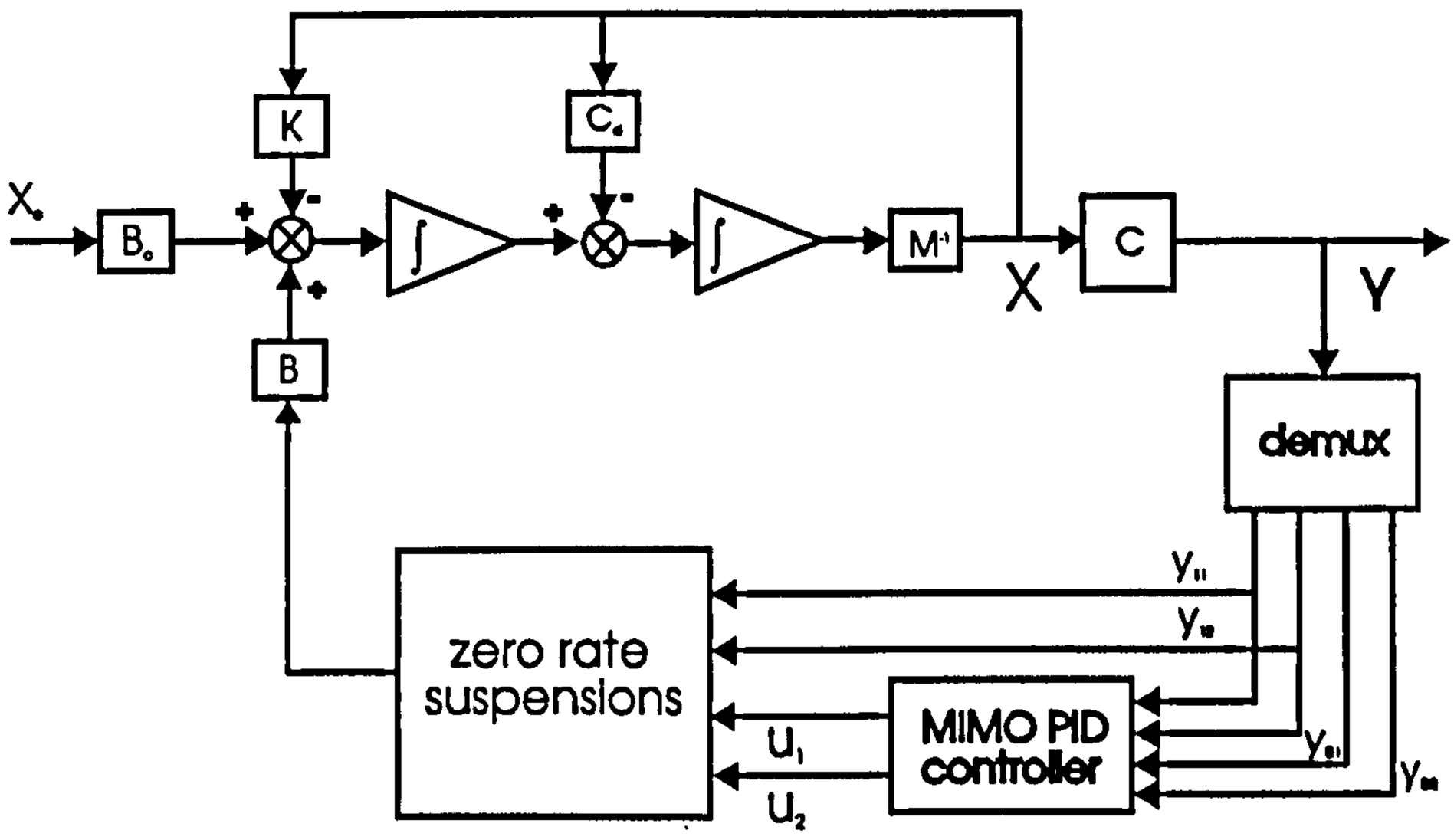

Figure 6-3 Block diagram for the closed loop system with the PID controller

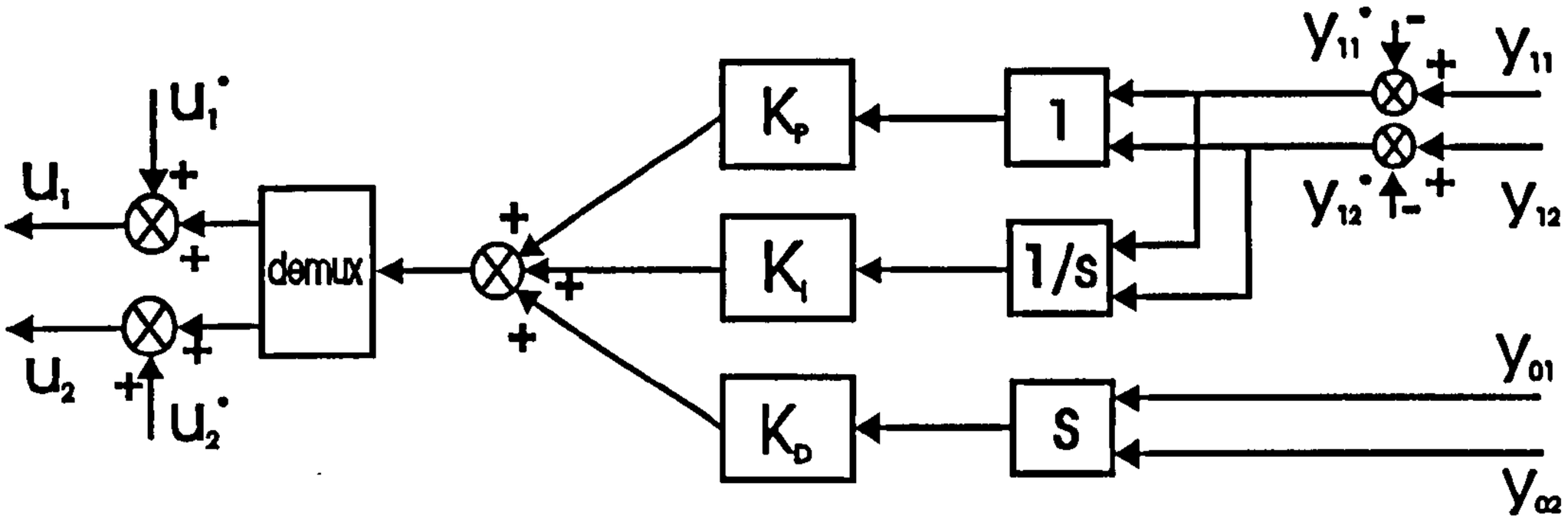

Figure 6-4 Block diagram for the MIMO PID controller

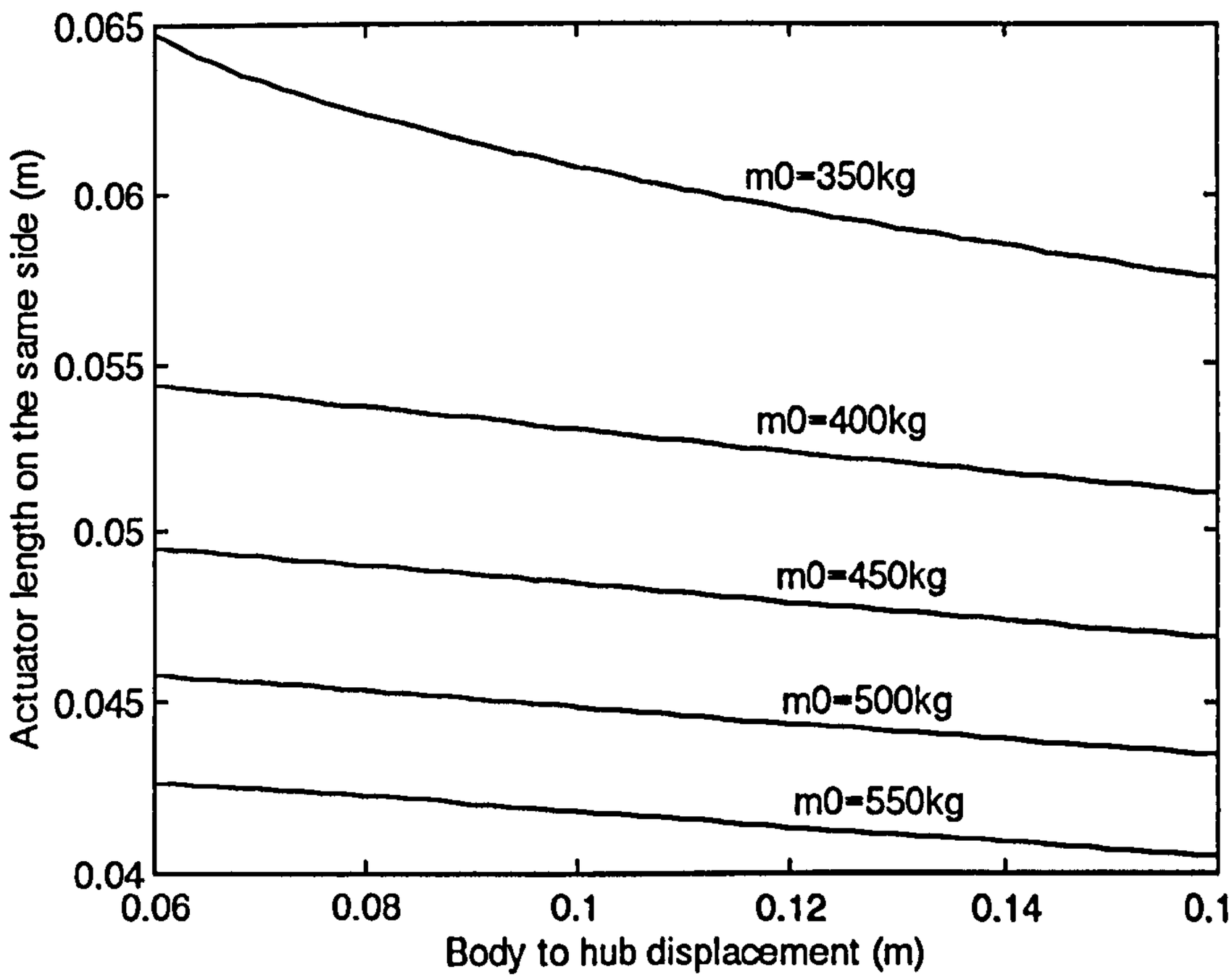

Figure 6-5 The relationship between demanded body to hub displacement and actuator length on the same side with various body masses

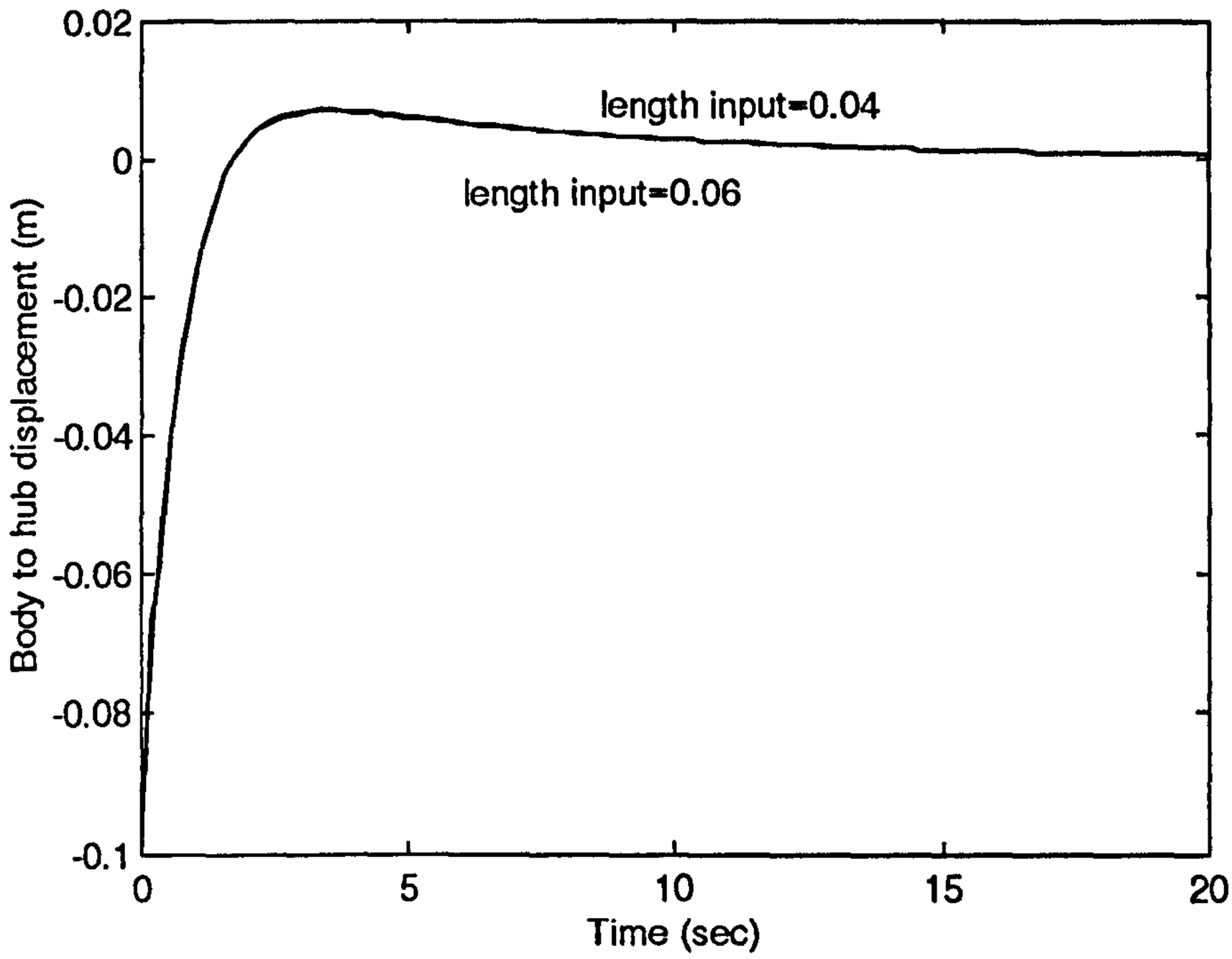

Figure 6-6 The effect of the steady state input for actuator length on the system starting response

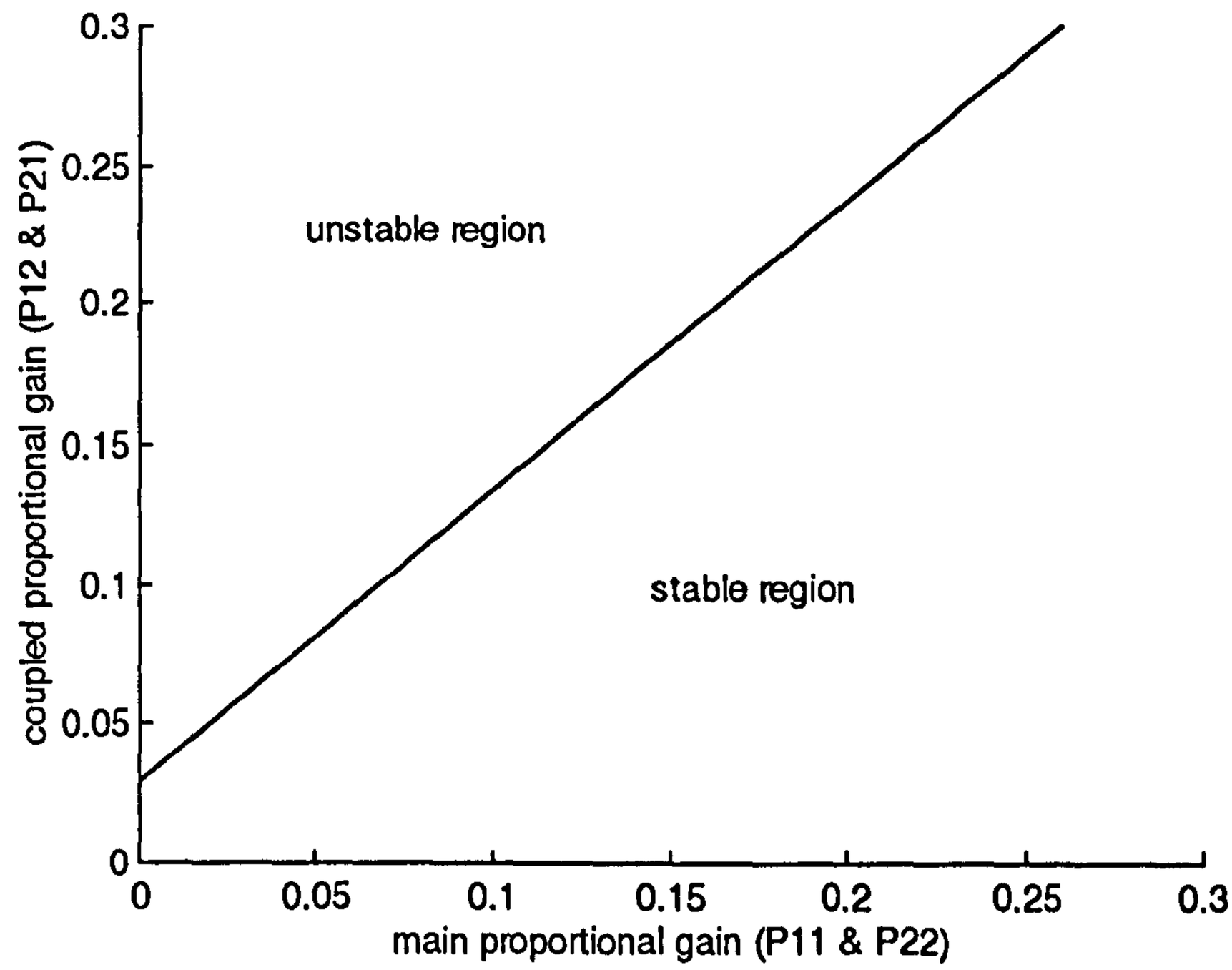

Figure 6-7 The stable region for the coupled proportional gain against the main proportional gain for $D_{11}=D_{22}=0.3$, $D_{12}=D_{21}=0.05$, $I_{11}=I_{22}=0.1$, and $I_{12}=I_{21}=0.08$.

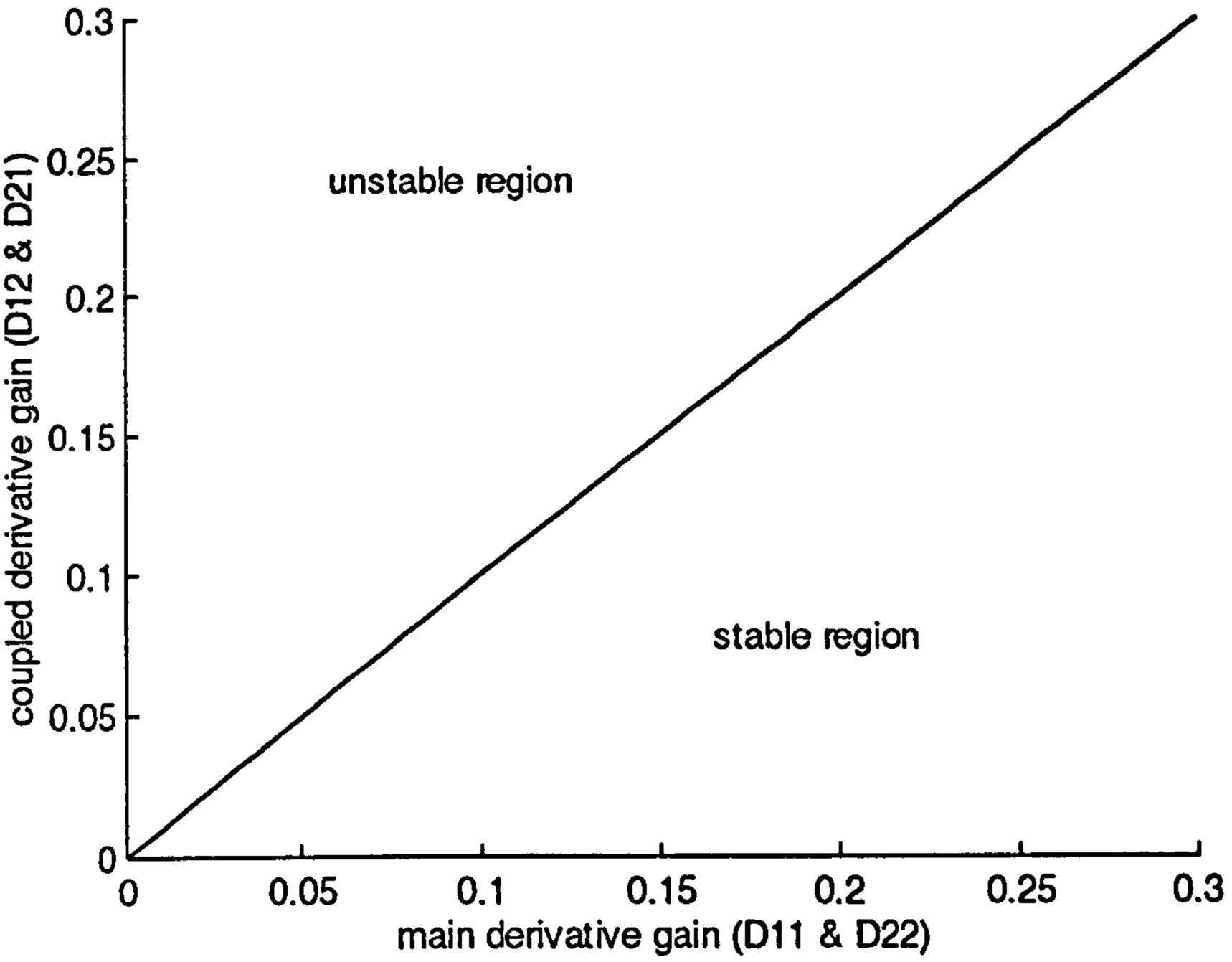

Figure 6-8 The stable region for the coupled derivative gain against the main derivative gain for $P_{11}=P_{22}=0.3$, $P_{12}=P_{21}=0.1$, $I_{11}=I_{22}=0.1$, and $I_{12}=I_{21}=0.08$.

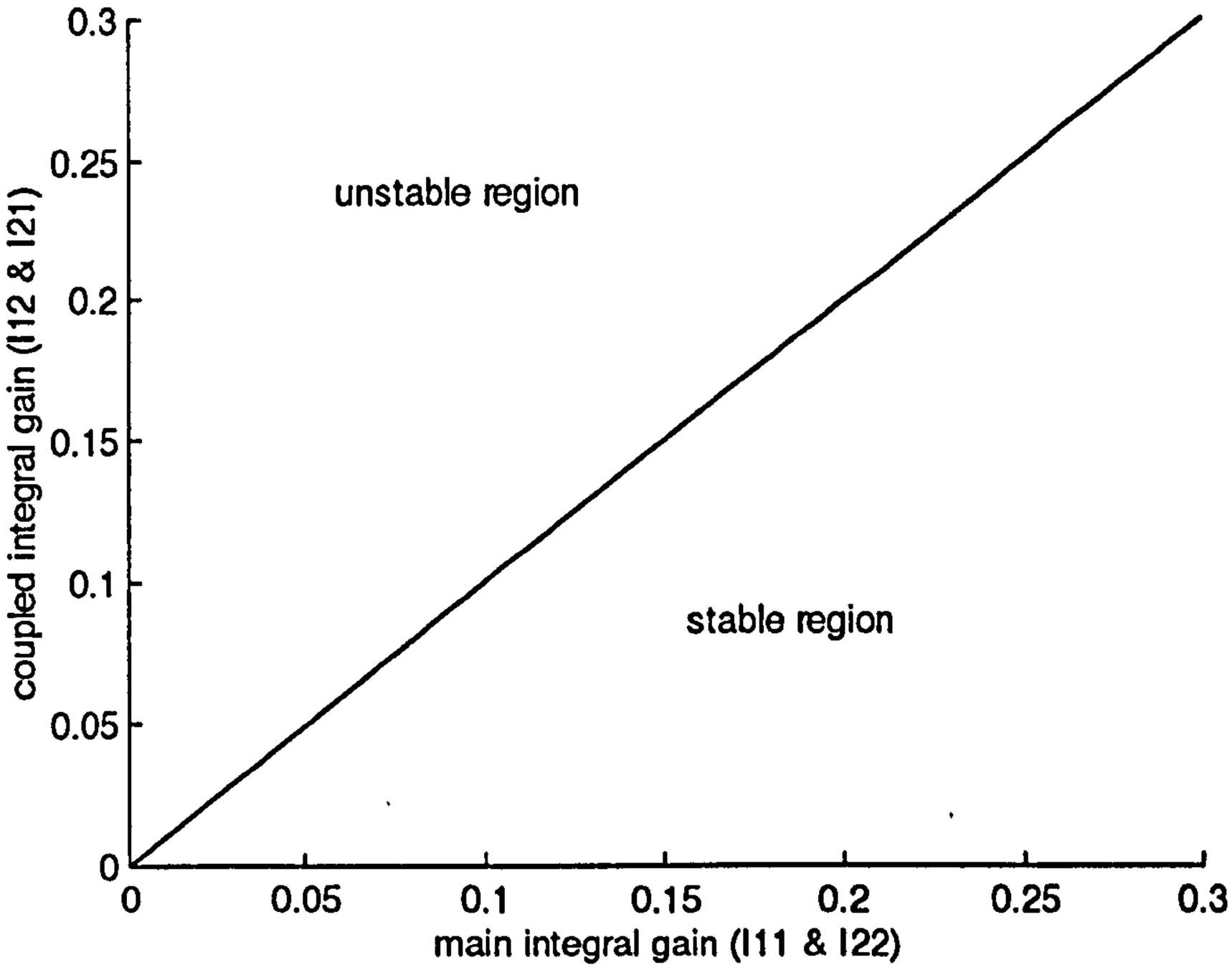

Figure 6-9 The stable region for the coupled integral gain against the main integral gain for $D_{11}=D_{22}=0.3$, $D_{12}=D_{21}=0.05$, $P_{11}=P_{22}=0.3$, and $P_{12}=P_{21}=0.1$.

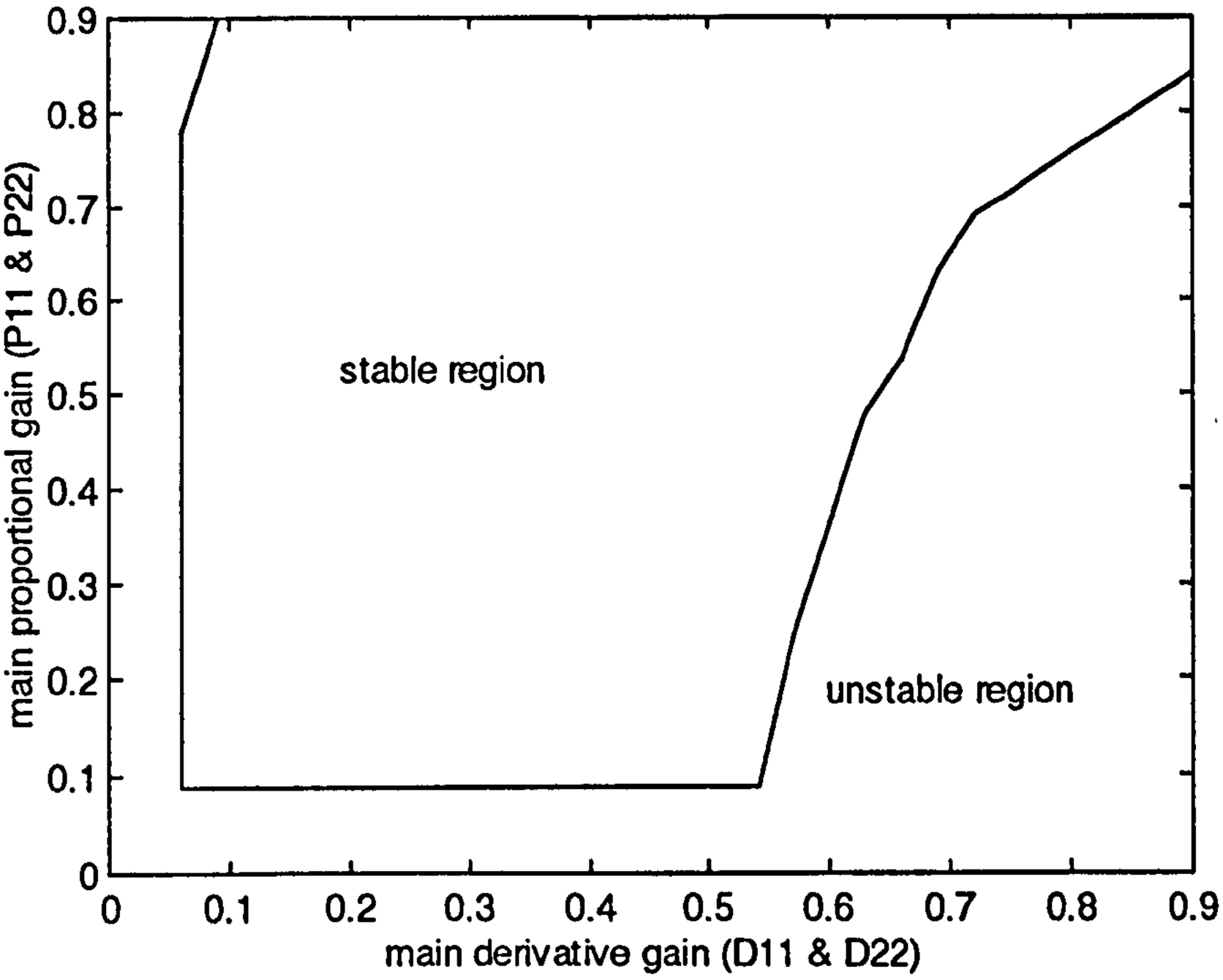

Figure 6-10 The stable region for the main proportional gain against the main derivative gain for $P_{12}=P_{21}=0.1$, $D_{12}=D_{21}=0.05$, $I_{11}=I_{22}=0.1$, and $I_{12}=I_{21}=0.08$.

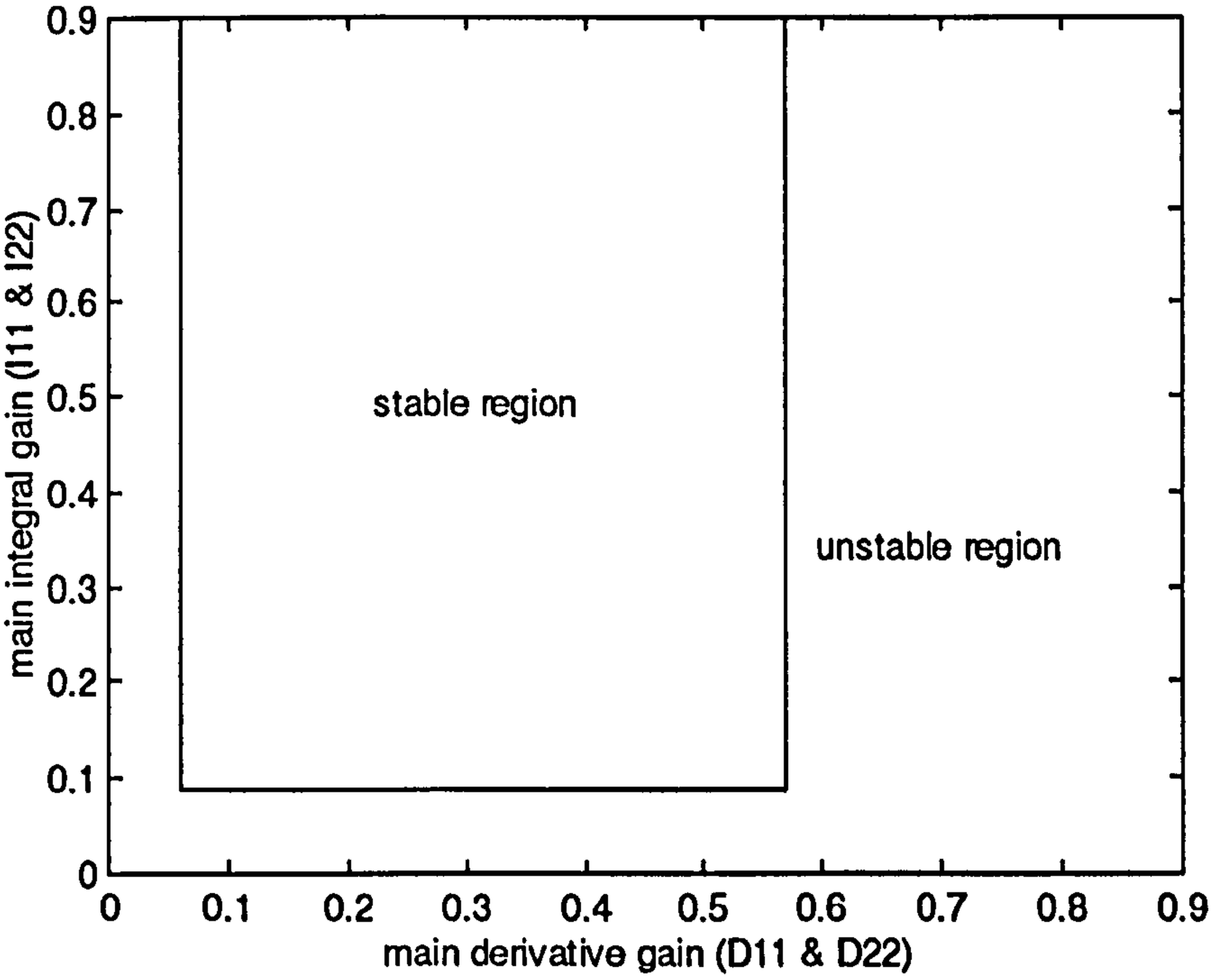

Figure 6-11 The stable region for the main integral gain against the main derivative gain for $P_{11}=P_{22}=0.3$, $P_{12}=P_{21}=0.1$, $D_{12}=D_{21}=0.05$, and $I_{12}=I_{21}=0.08$.

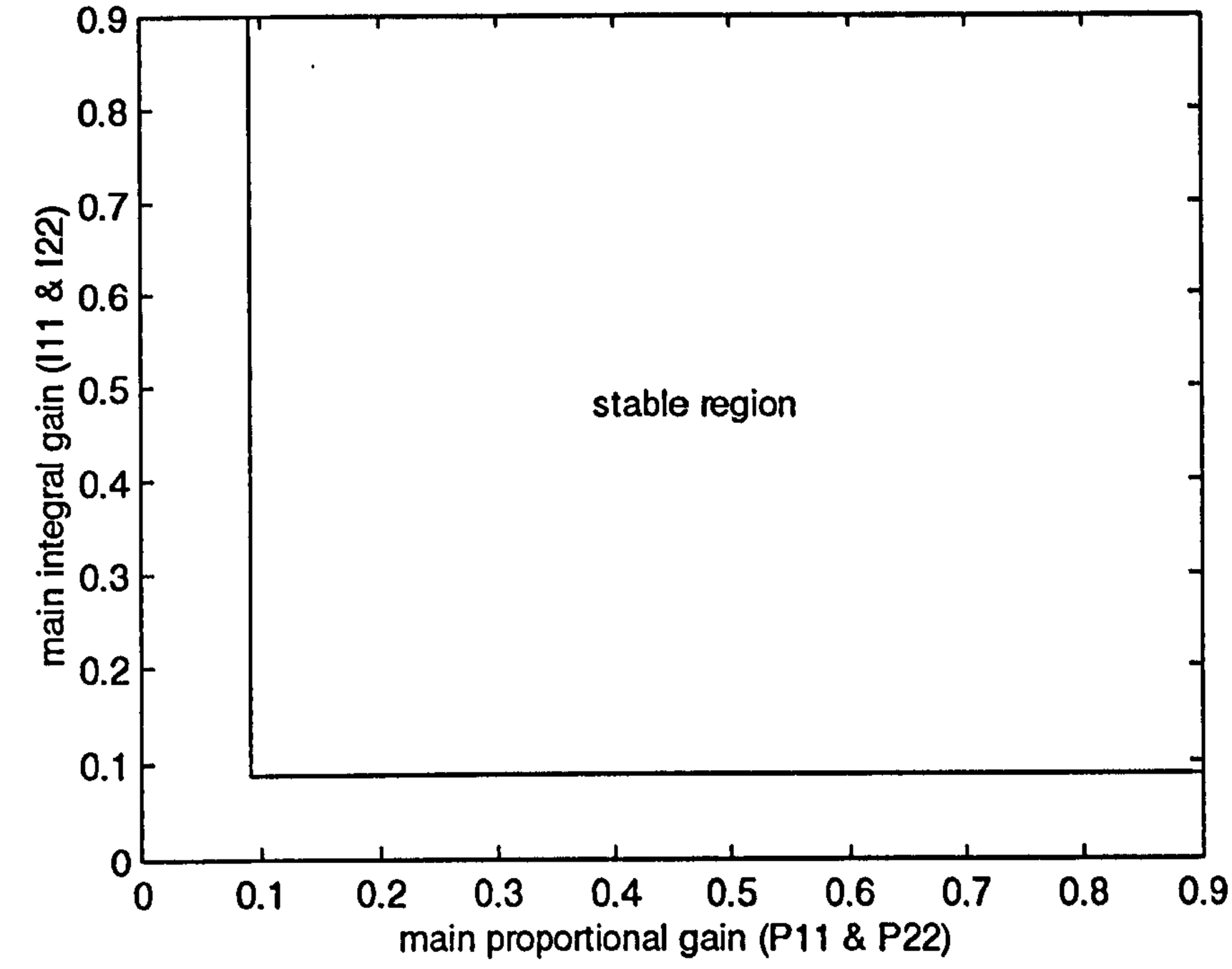

Figure 6-12 The stable region for the main integral gain against the main proportional gain for $D_{11}=D_{22}=0.3$, $D_{12}=D_{21}=0.05$, $P_{12}=P_{21}=0.1$, and $I_{12}=I_{21}=0.08$.

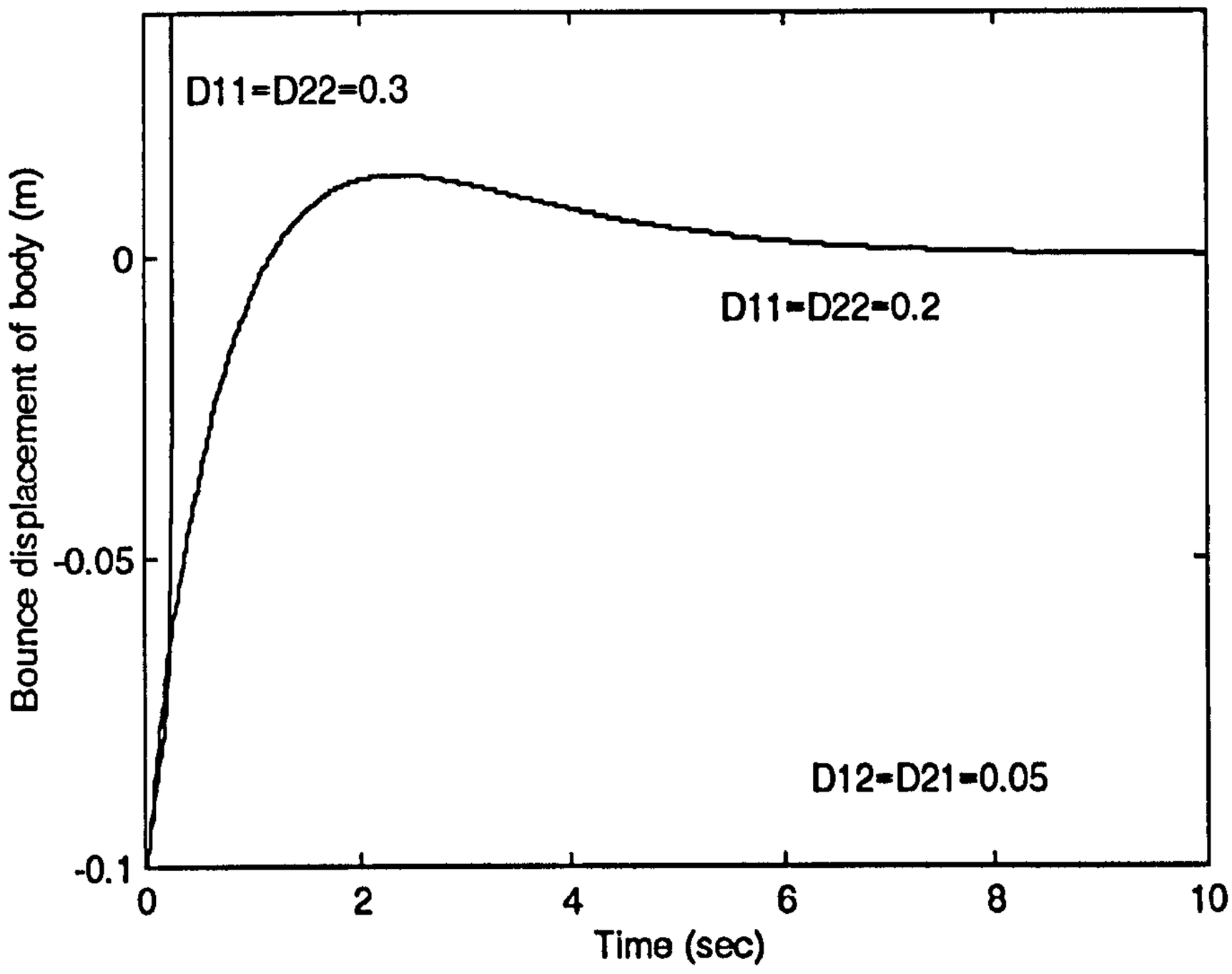

Figure 6-13 Effect of the main derivative gain on stability of the starting response for body bounce motion for $P_{11}=P_{22}=0.3$, $P_{12}=P_{21}=0.1$, $I_{11}=I_{22}=0.1$, and $I_{12}=I_{21}=0.08$.

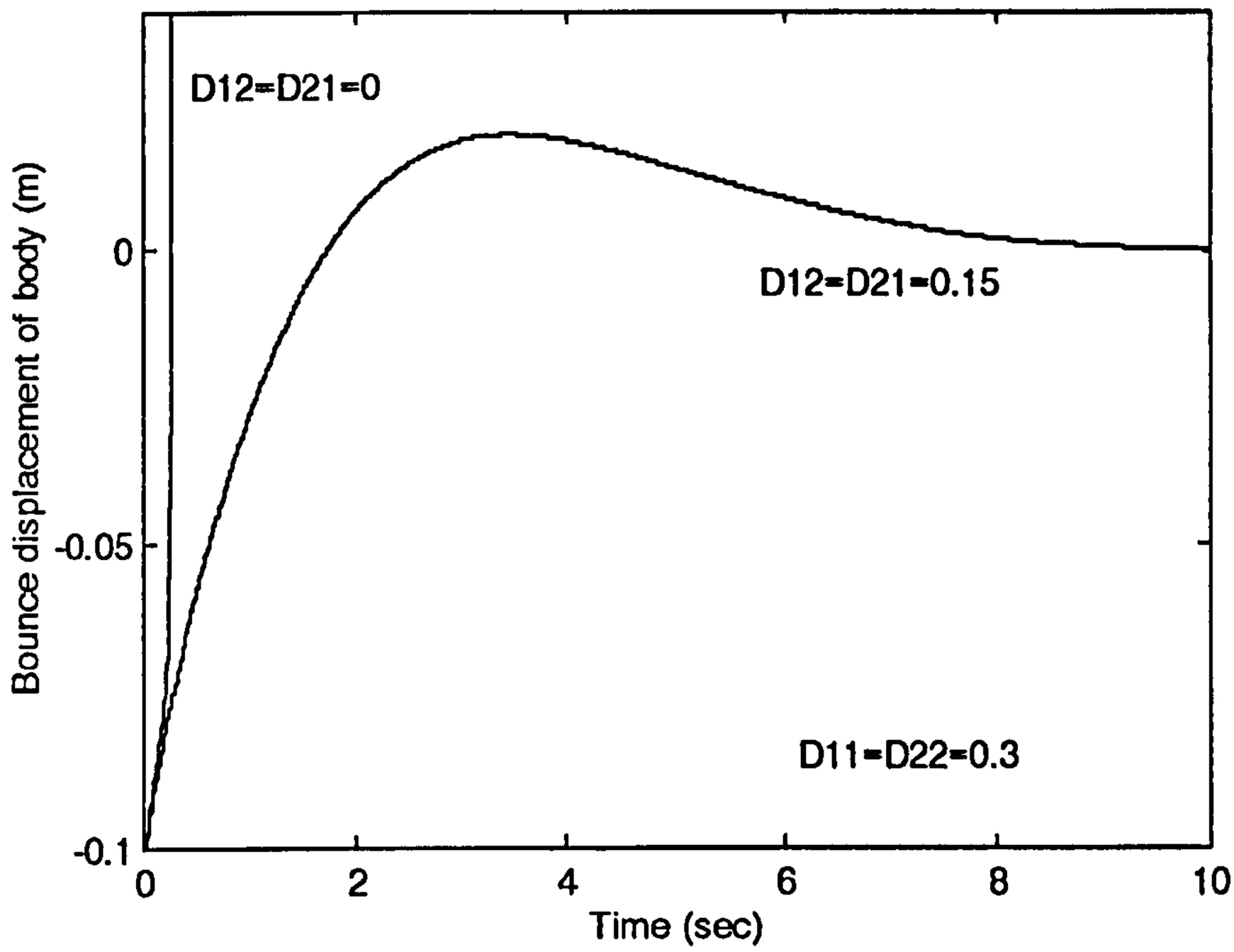

Figure 6-14 Effect of the coupled derivative gain on stability of the starting response for body bounce motion for $P_{11}=P_{22}=0.3$, $P_{12}=P_{21}=0.1$, $I_{11}=I_{22}=0.1$, and $I_{12}=I_{21}=0.08$.

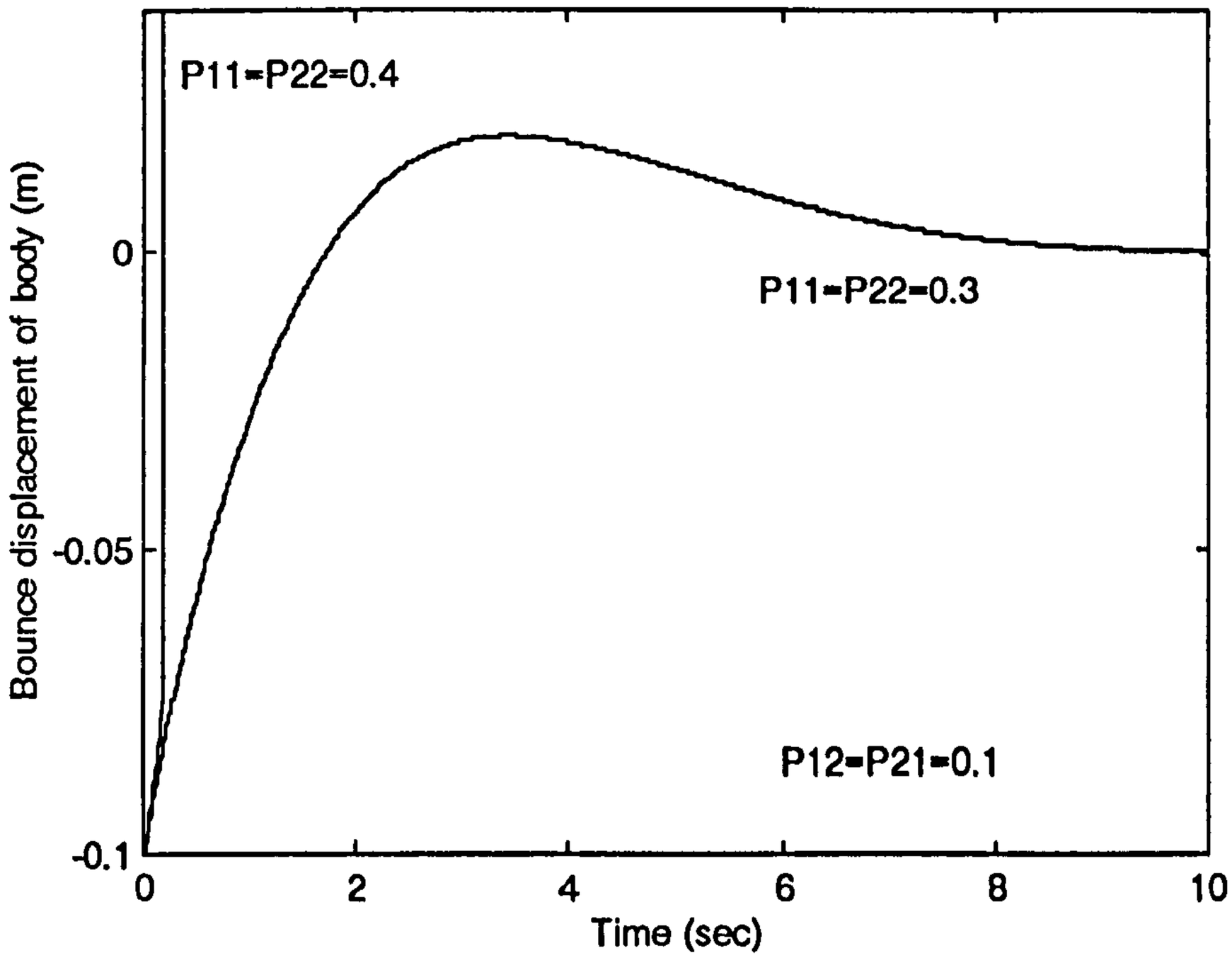

Figure 6-15 Effect of the main proportional gain on stability of the starting response for body bounce motion for $D_{11}=D_{22}=0.3$, $D_{12}=D_{21}=0.15$, $I_{11}=I_{22}=0.1$, and $I_{12}=I_{21}=0.08$.

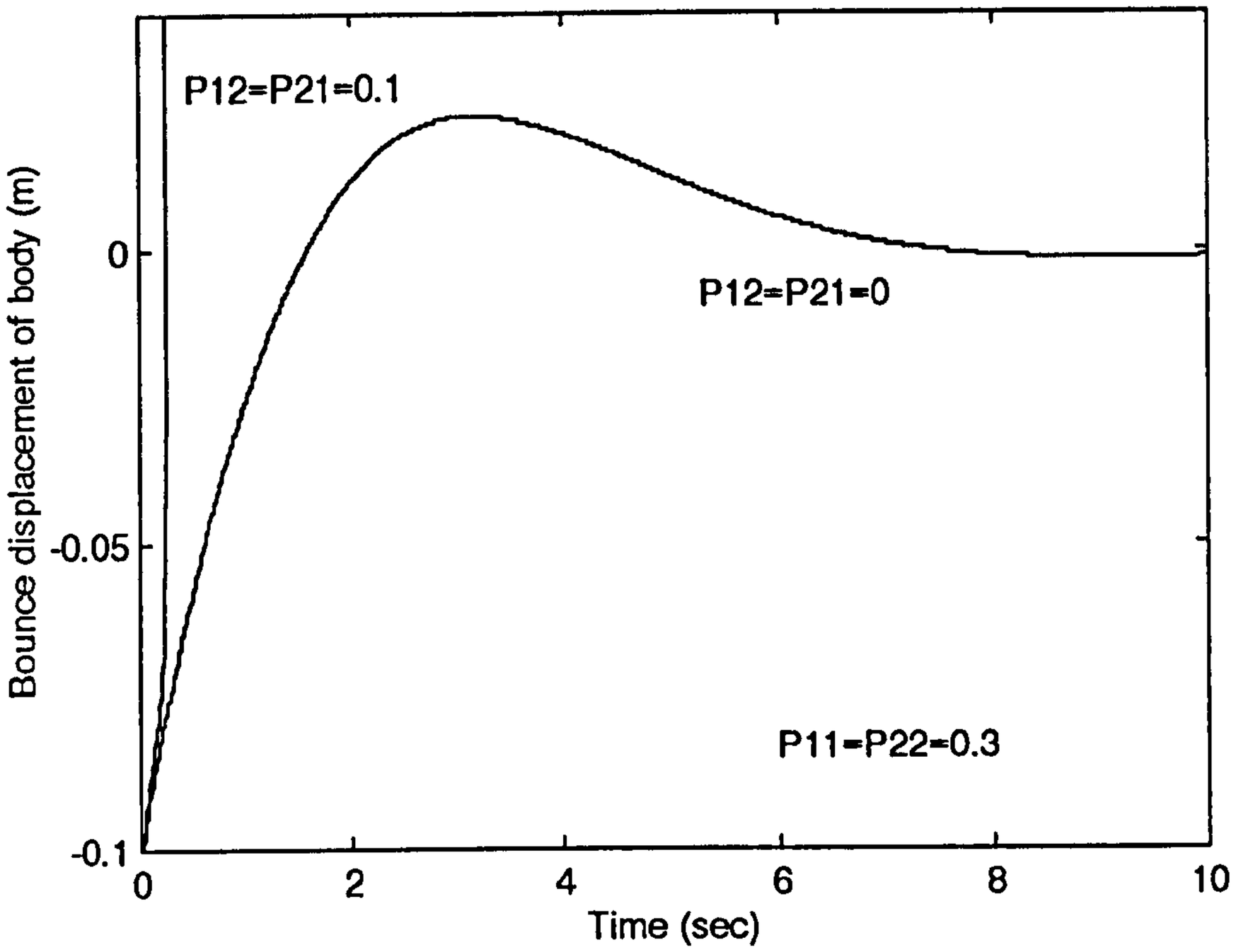

Figure 6-16 Effect of the coupled proportional gain on stability of the starting response for body bounce motion for $D_{11}=D_{22}=0.3$, $D_{12}=D_{21}=0.05$, $I_{11}=I_{22}=0.1$, and $I_{12}=I_{21}=0.08$.

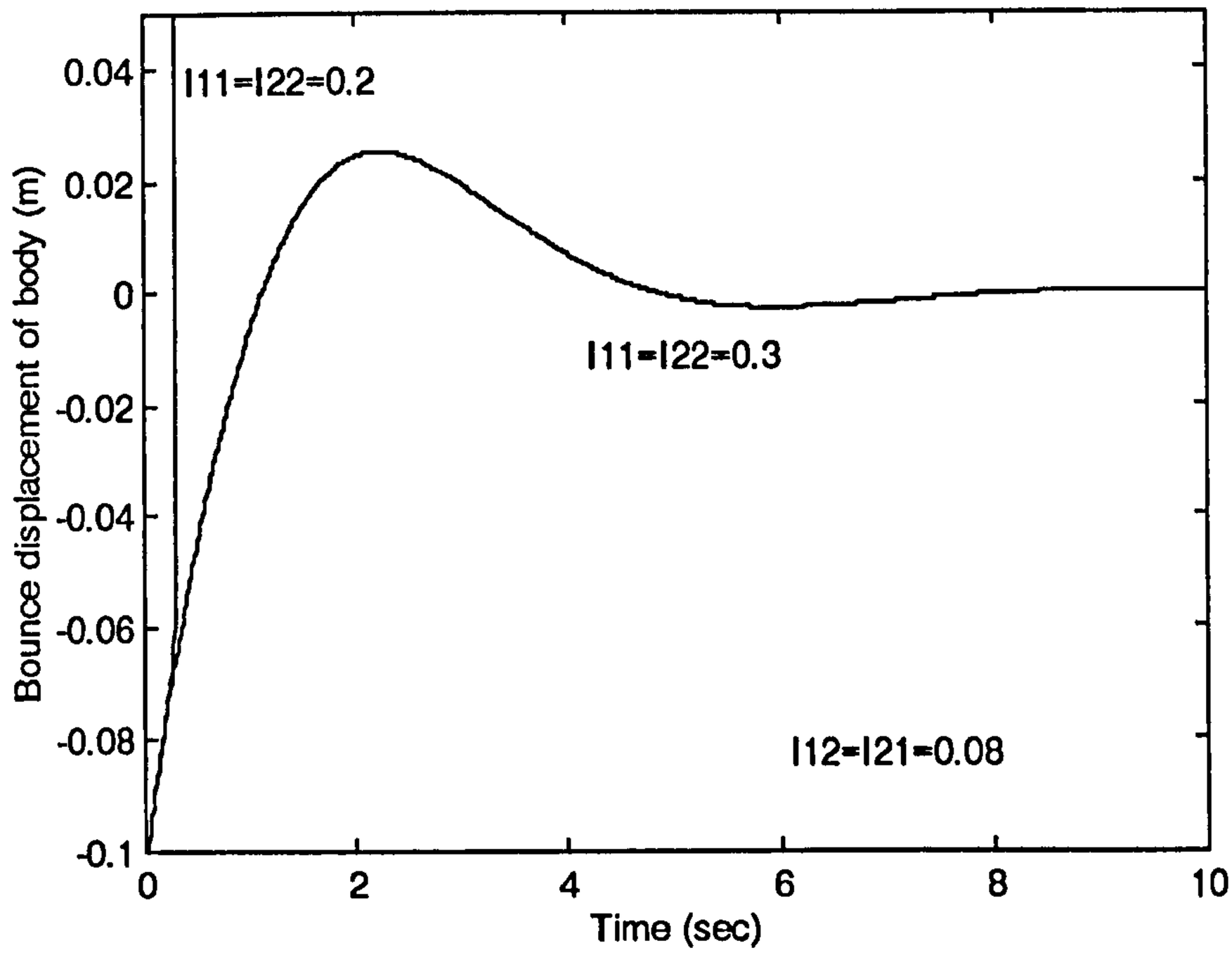

Figure 6-17 Effect of the main integral gain on stability of the starting response for body bounce motion for $D_{11}=D_{22}=0.3$, $D_{12}=D_{21}=0.05$, $P_{11}=P_{22}=0.3$, and $P_{12}=P_{21}=0.1$.

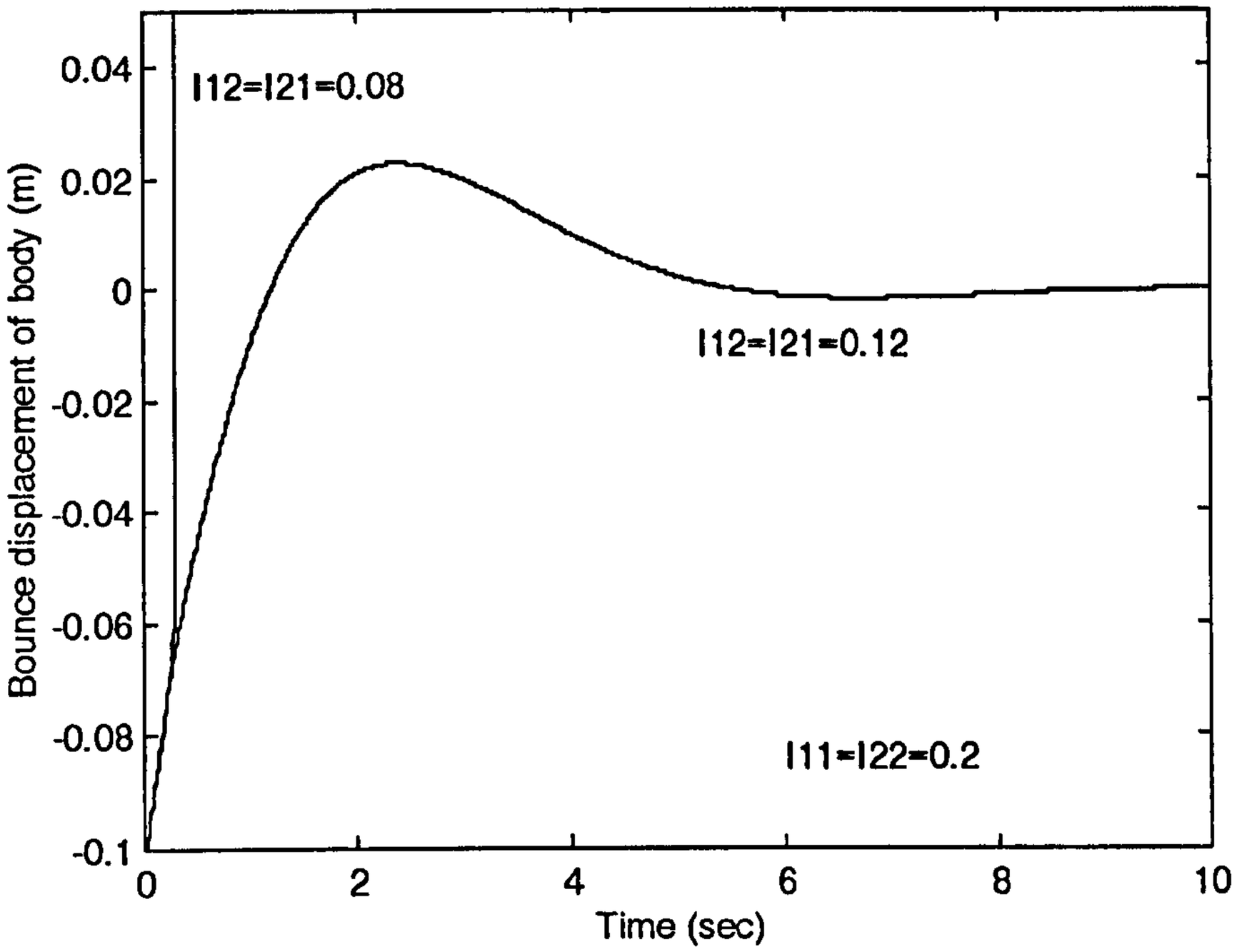

Figure 6-18 Effect of the coupled integral gain on stability of the starting response for body bounce motion for $D_{11}=D_{22}=0.3$, $D_{12}=D_{21}=0.05$, $P_{11}=P_{22}=0.3$, and $P_{12}=P_{21}=0.1$.

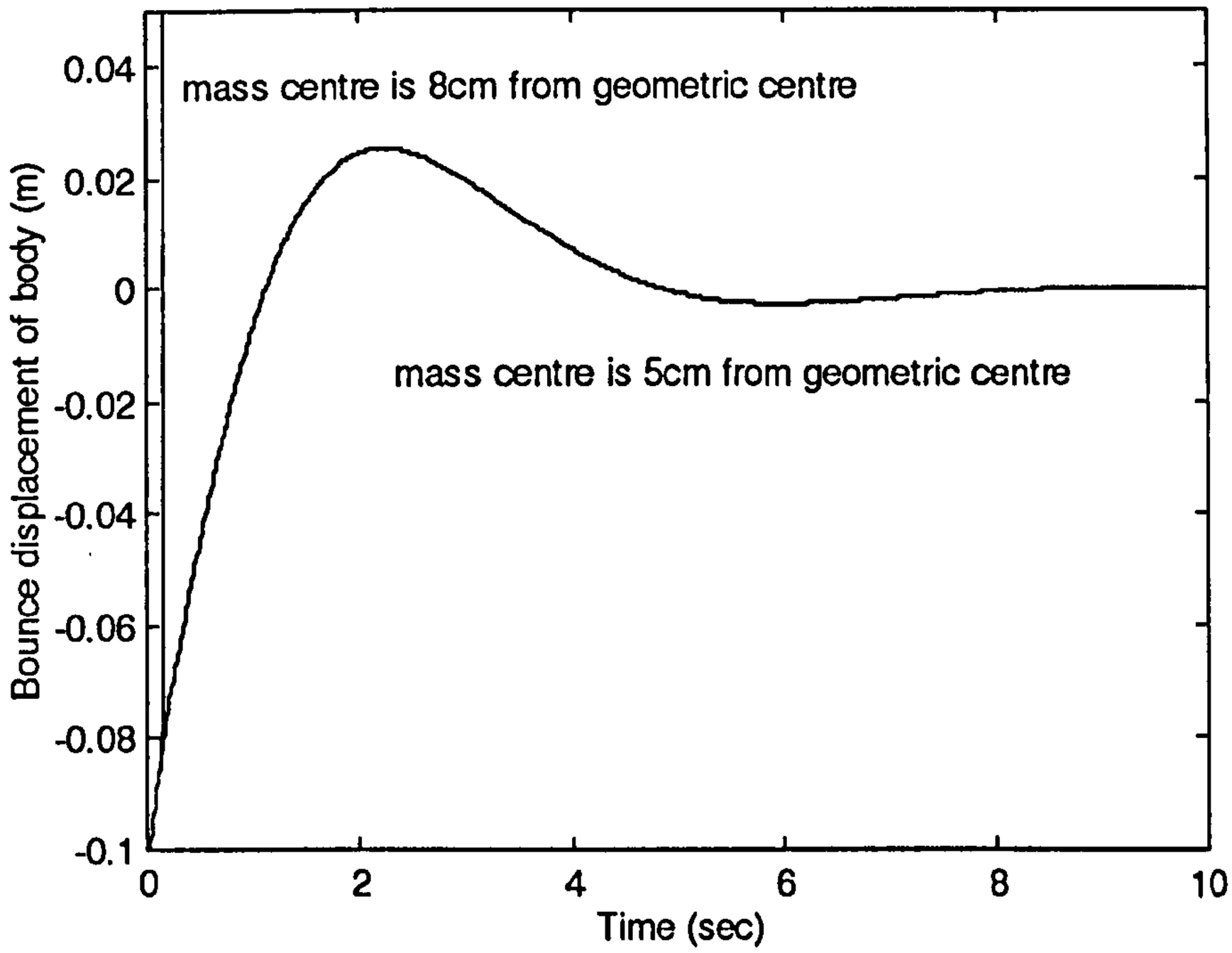

Figure 6-19 Effect of the body mass distribution on stability of the starting response for body bounce motion for $D_{11}=D_{22}=0.3$, $D_{12}=D_{21}=0.05$, $P_{11}=P_{22}=0.3$, $P_{12}=P_{21}=0.1$, $I_{11}=I_{22}=0.3$, and $I_{12}=I_{21}=0.08$.

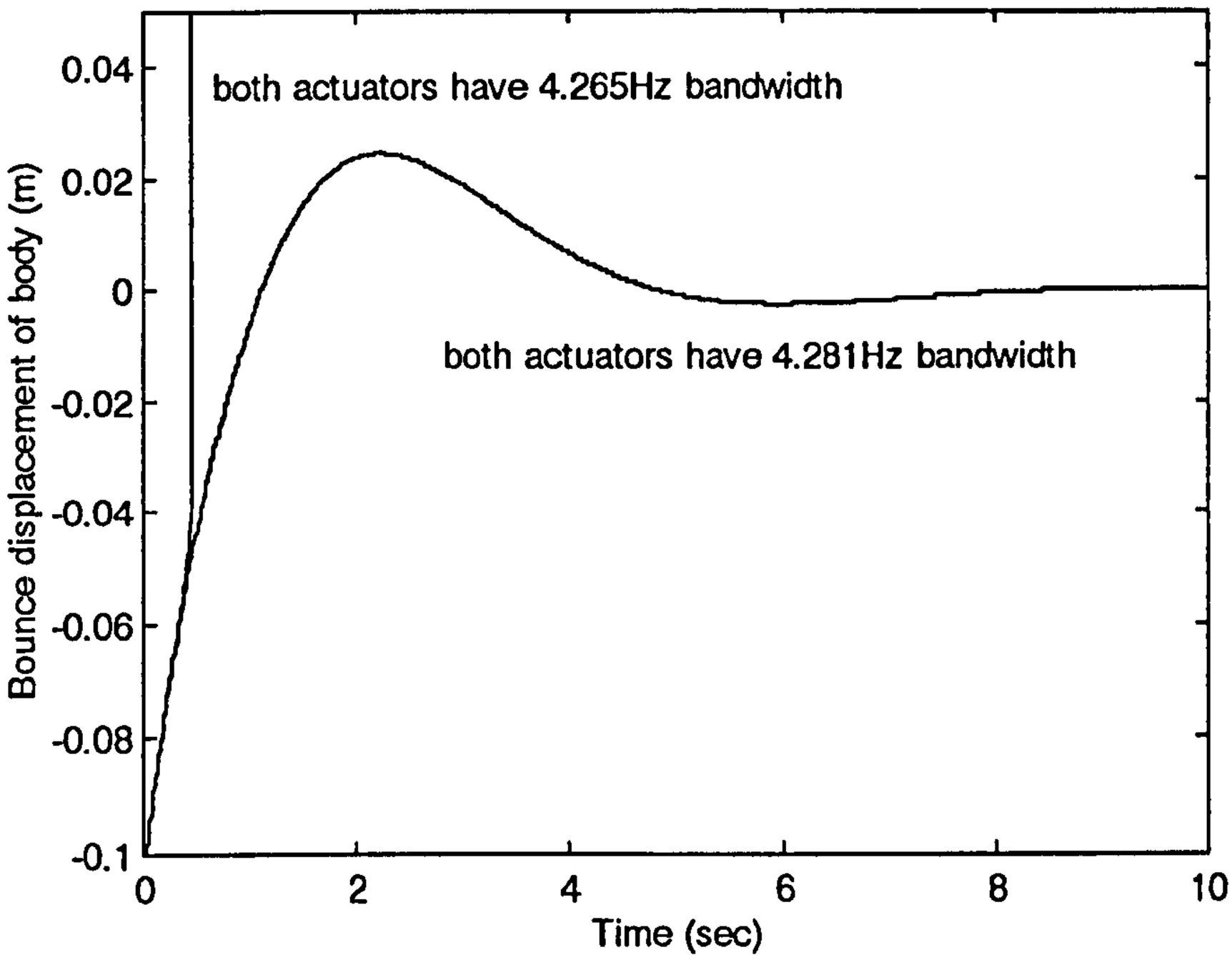

Figure 6-20 Effect of the bandwidth of the identical actuators on both sides on stability of the starting response for body bounce motion for $D_{11}=D_{22}=0.3$, $D_{12}=D_{21}=0.05$, $P_{11}=P_{22}=0.3$, $P_{12}=P_{21}=0.1$, $I_{11}=I_{22}=0.3$, and $I_{12}=I_{21}=0.08$.

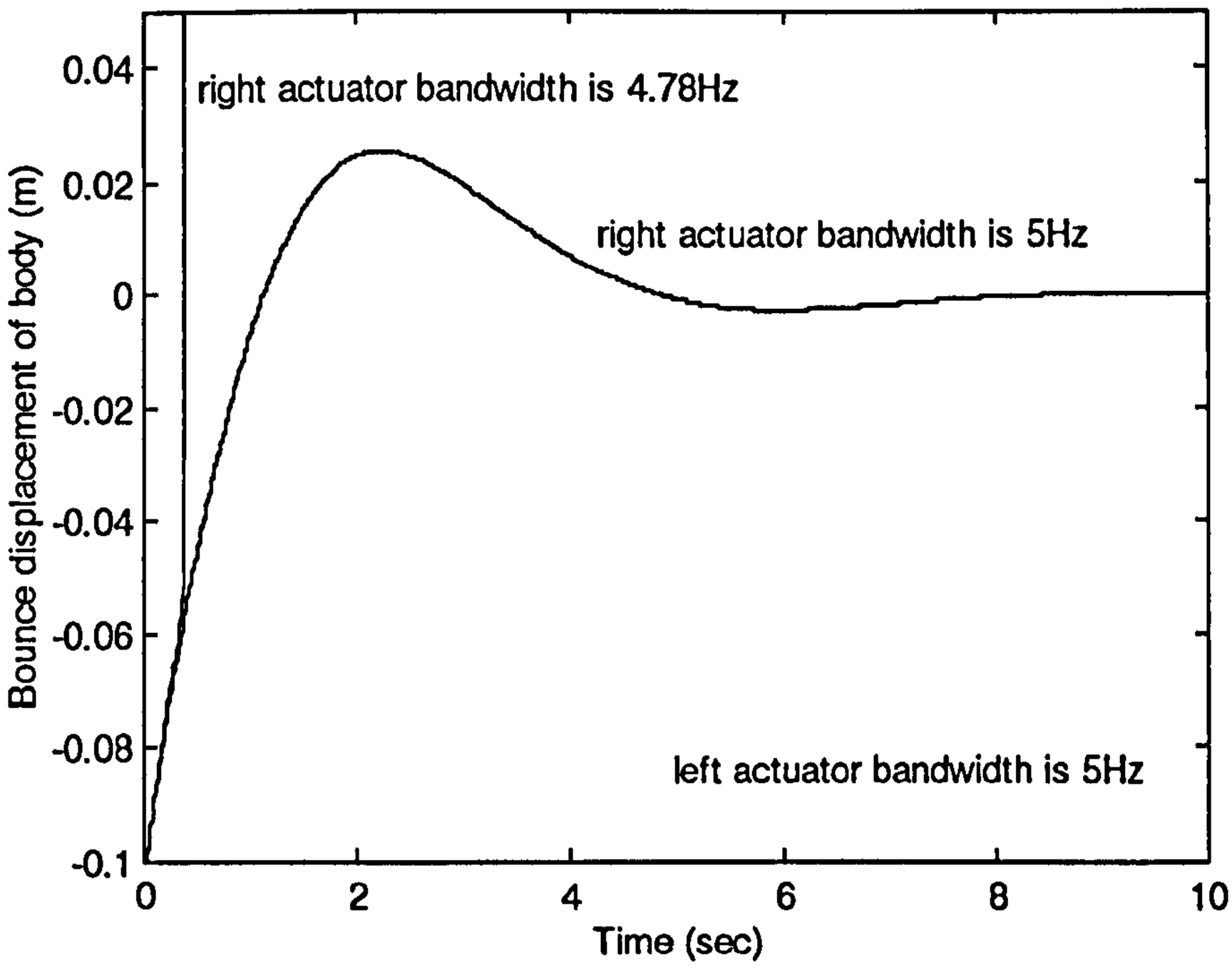

Figure 6-21 Effect of the bandwidth difference of the identical actuators on both sides on stability of the starting response for body bounce motion for $D_{11}=D_{22}=0.3$, $D_{12}=D_{21}=0.05$, $P_{11}=P_{22}=0.3$, $P_{12}=P_{21}=0.1$, $I_{11}=I_{22}=0.3$, and $I_{12}=I_{21}=0.08$.

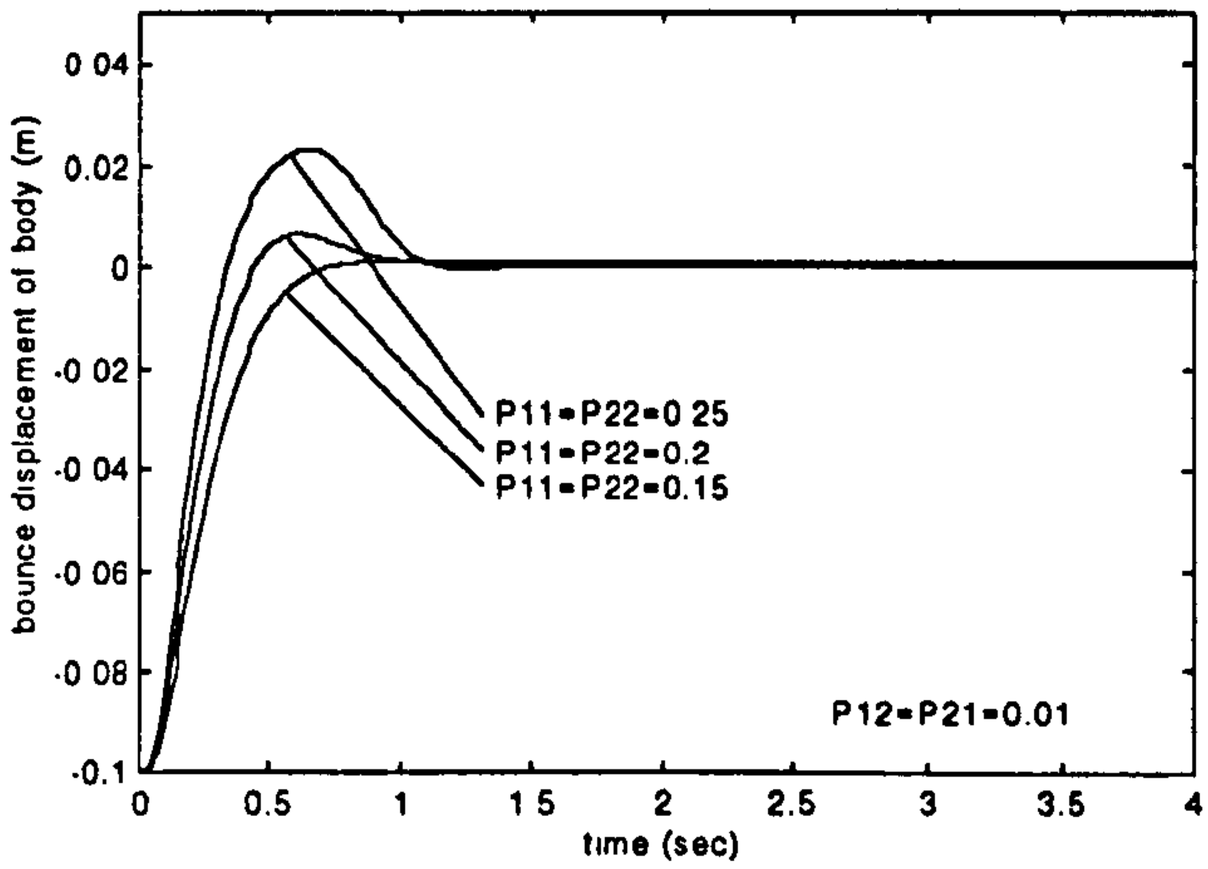

Figure 6-22(a) The effect of the main proportional gain on the body bounce starting response for $D_{11}=D_{22}=0.04$, $D_{12}=D_{21}=0.01$, $I_{11}=I_{22}=0.01$, and $I_{12}=I_{21}=0$.

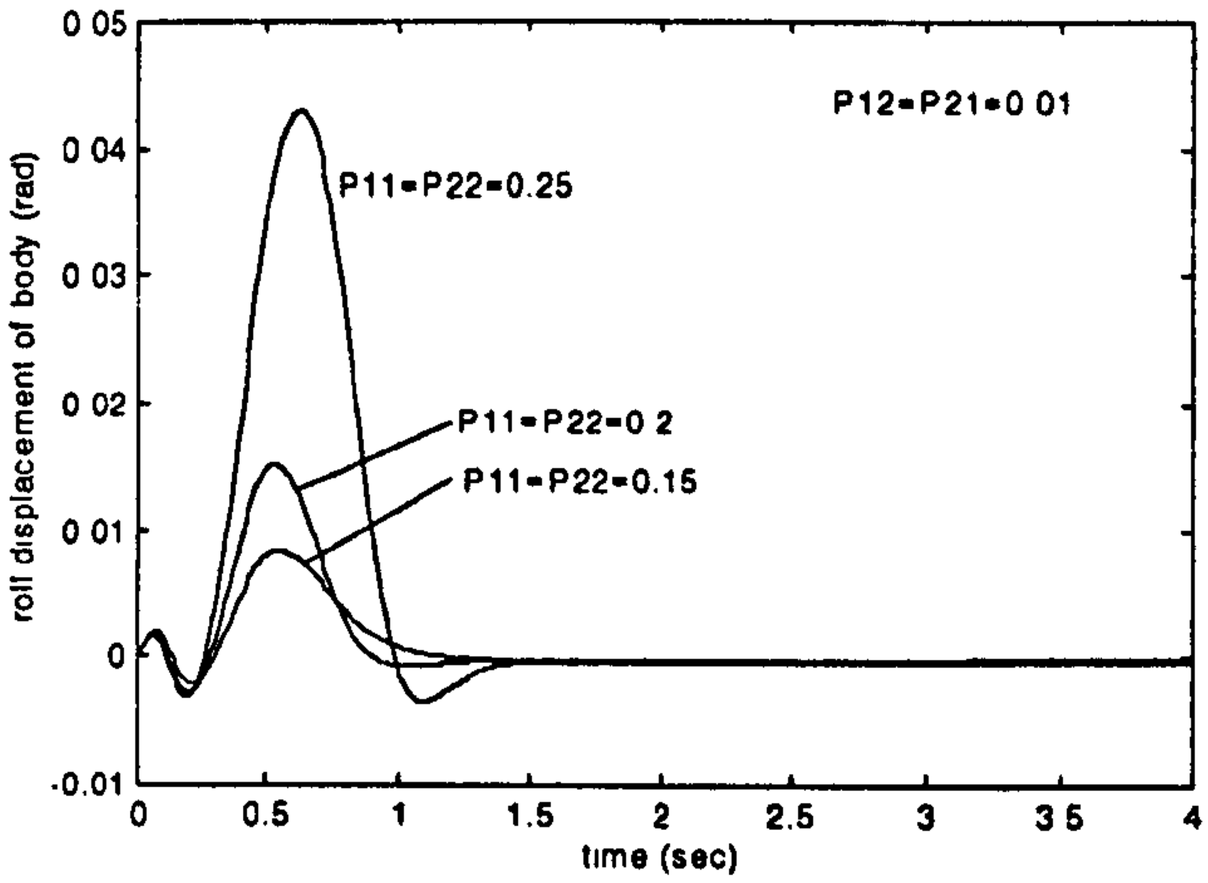

Figure 6-22(b) The effect of the main proportional gain on the body roll starting response for $D_{11}=D_{22}=0.04$, $D_{12}=D_{21}=0.01$, $I_{11}=I_{22}=0.01$, and $I_{12}=I_{21}=0$.

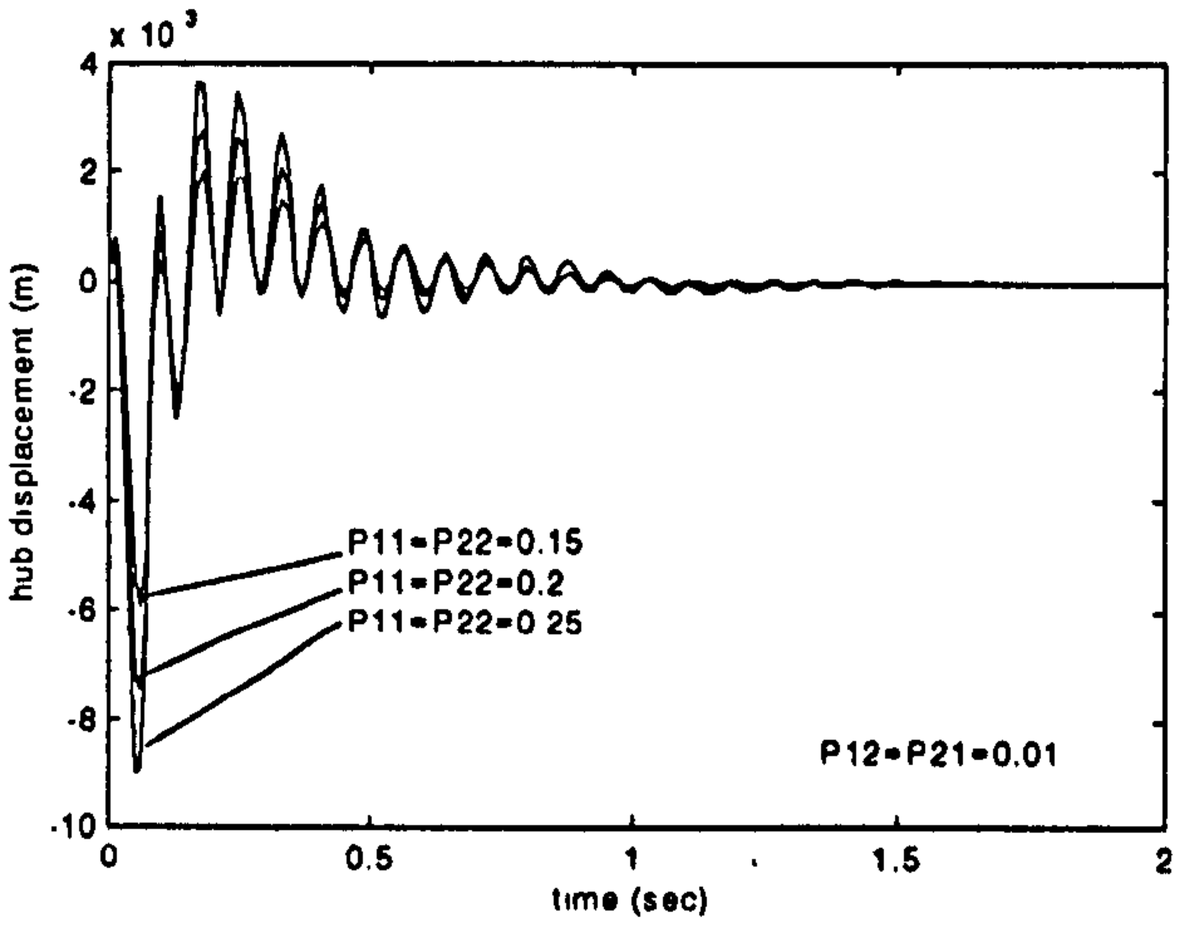

Figure 6-22(c) The effect of the main proportional gain on the wheel vertical starting response for $D_{11}=D_{22}=0.04$, $D_{12}=D_{21}=0.01$, $I_{11}=I_{22}=0.01$, and $I_{12}=I_{21}=0$.

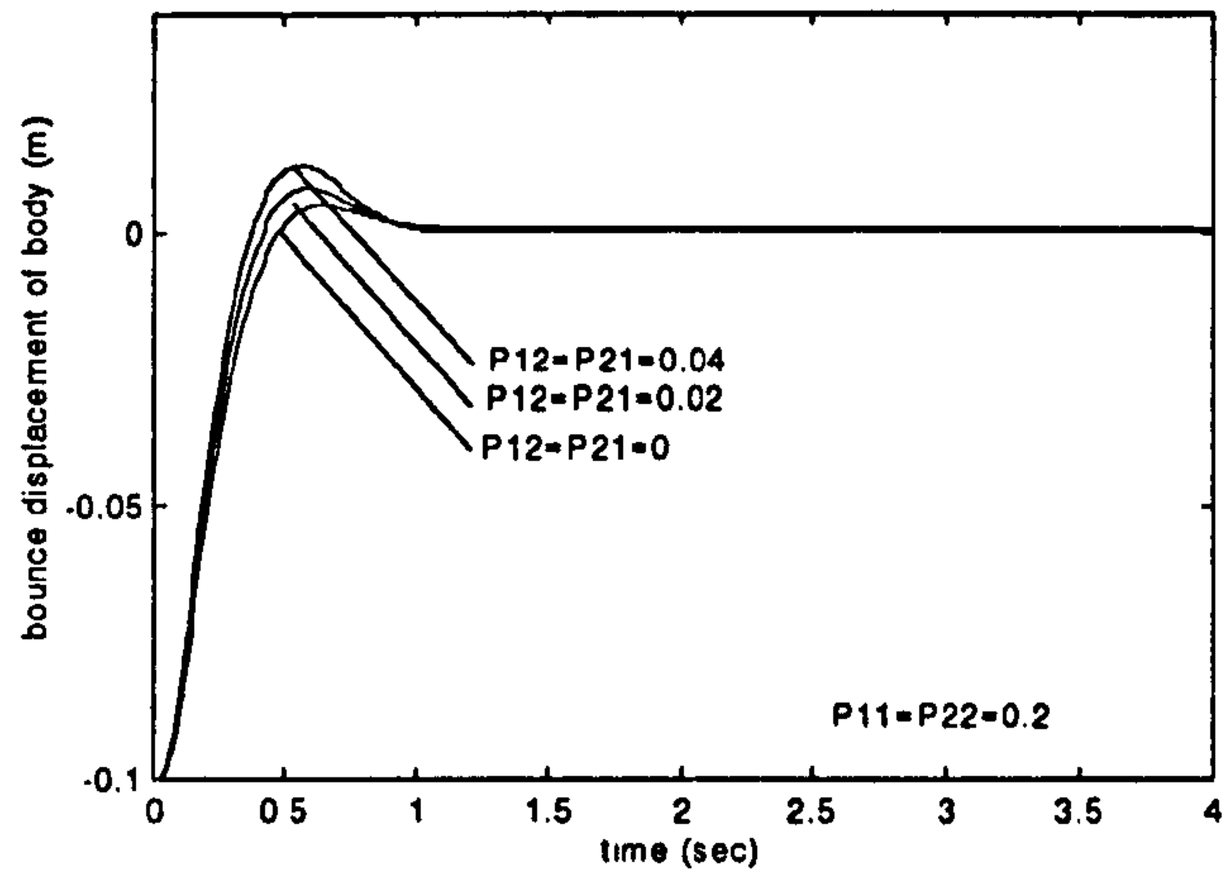

Figure 6-23(a) The effect of the coupled proportional gain on the body bounce starting response for $D_{11}=D_{22}=0.04$, $D_{12}=D_{21}=0.01$, $I_{11}=I_{22}=0.01$, and $I_{12}=I_{21}=0$.

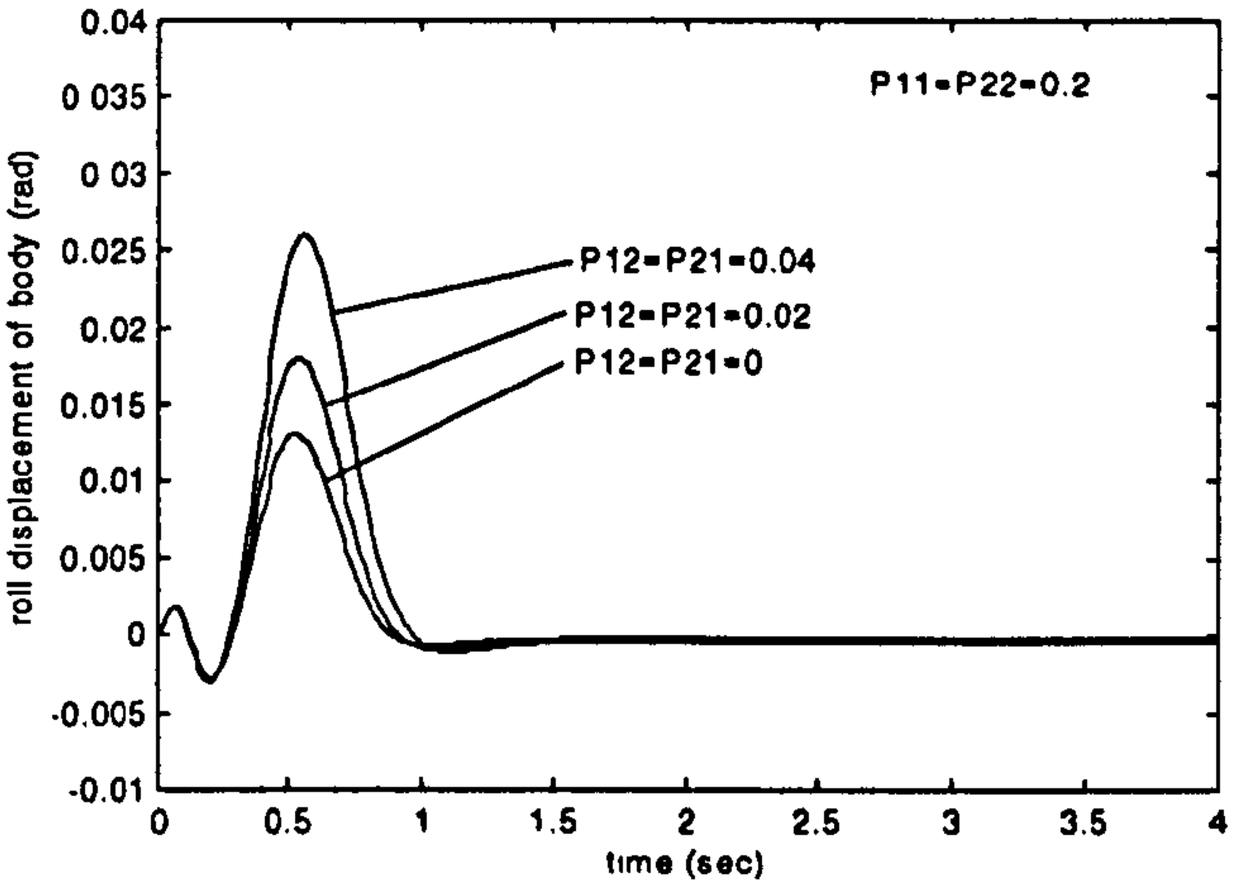

Figure 6-23(b) The effect of the coupled proportional gain on the body roll starting response for $D_{11}=D_{22}=0.04$,.$D_{12}=D_{21}=0.01$, $I_{11}=I_{22}=0.01$, and $I_{12}=I_{21}=0$.

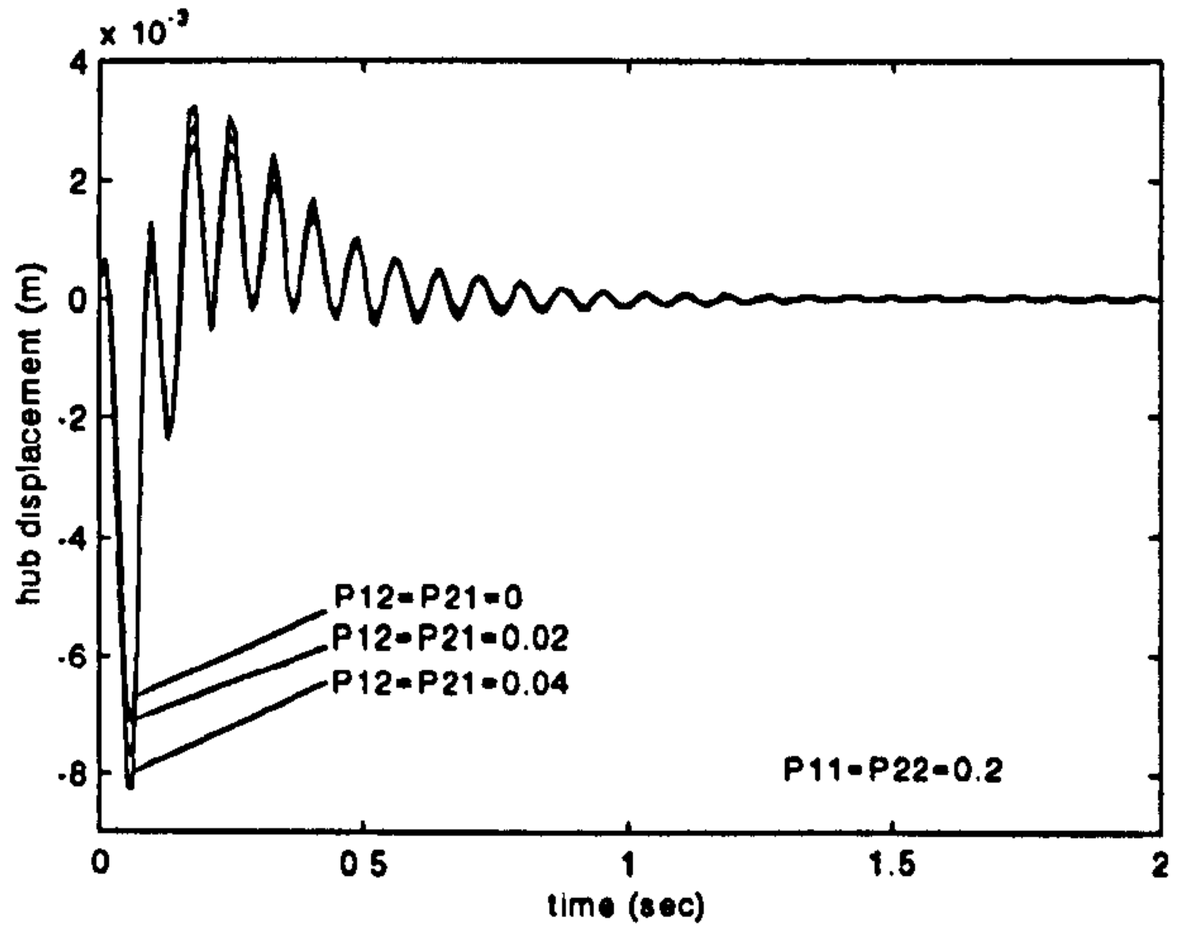

Figure 6-23(c) The effect of the coupled proportional gain on the wheel vertical starting response for $D_{11}=D_{22}=0.04$, $D_{12}=D_{21}=0.01$, $I_{11}=I_{22}=0.01$, and $I_{12}=I_{21}=0$.

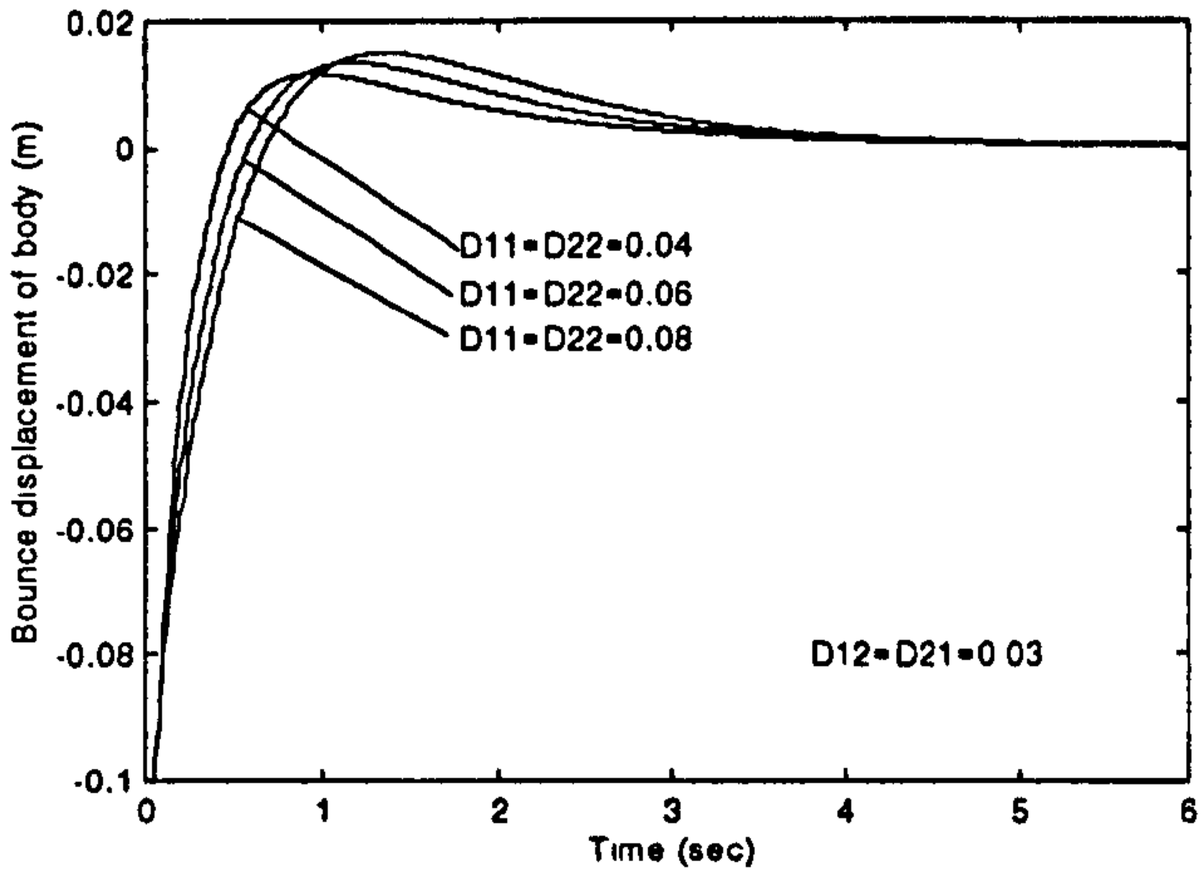

Figure 6-24(a) The effect of the main derivative gain on the body bounce starting response for $P_{11}=P_{22}=0.2$, $P_{12}=P_{21}=0.1$, $I_{11}=I_{22}=0.12$, and $I_{12}=I_{21}=0.11$.

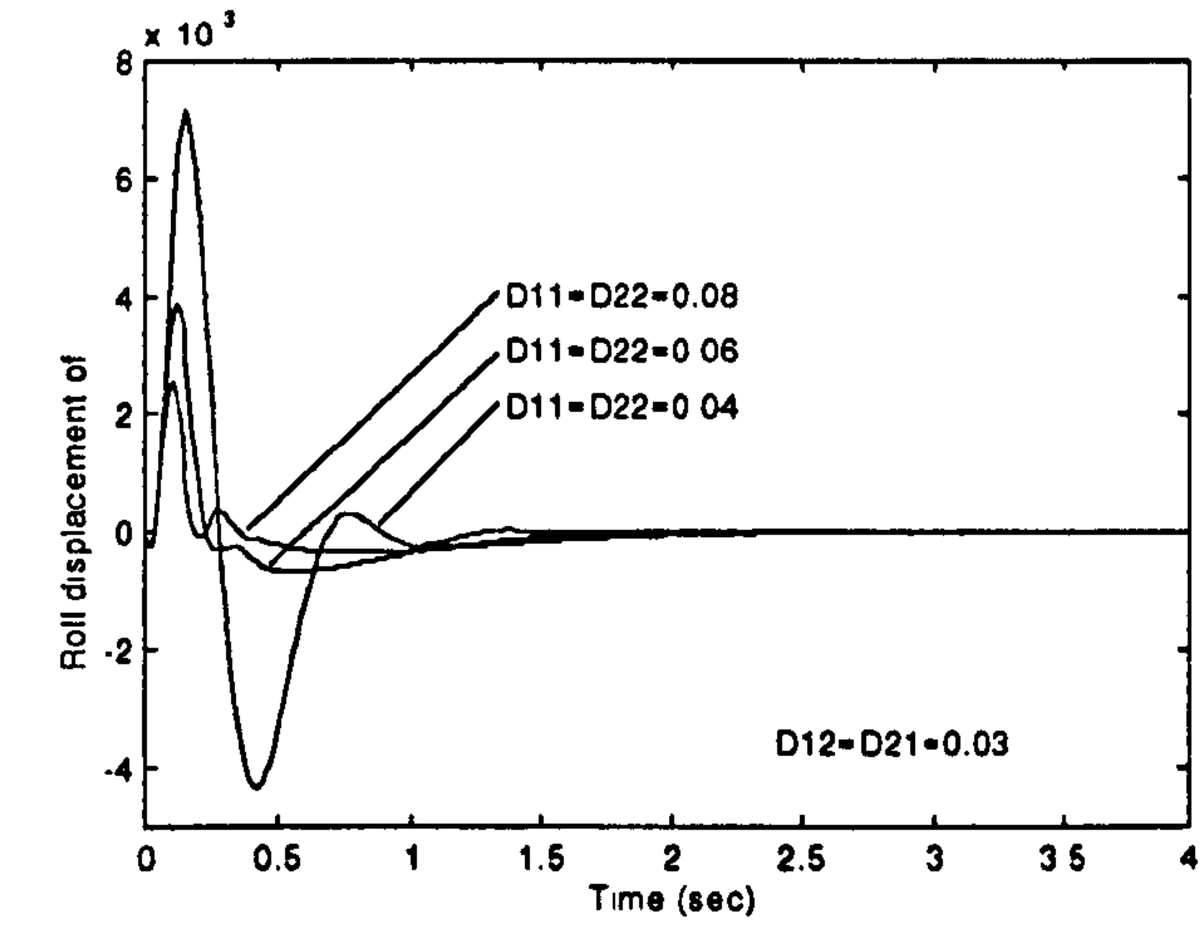

Figure 6-24(b) The effect of the main derivative gain on the body roll starting response for $P_{11}=P_{22}=0.2$, $P_{12}=P_{21}=0.1$, $I_{11}=I_{22}=0.12$, and $I_{12}=I_{21}=0.11$.

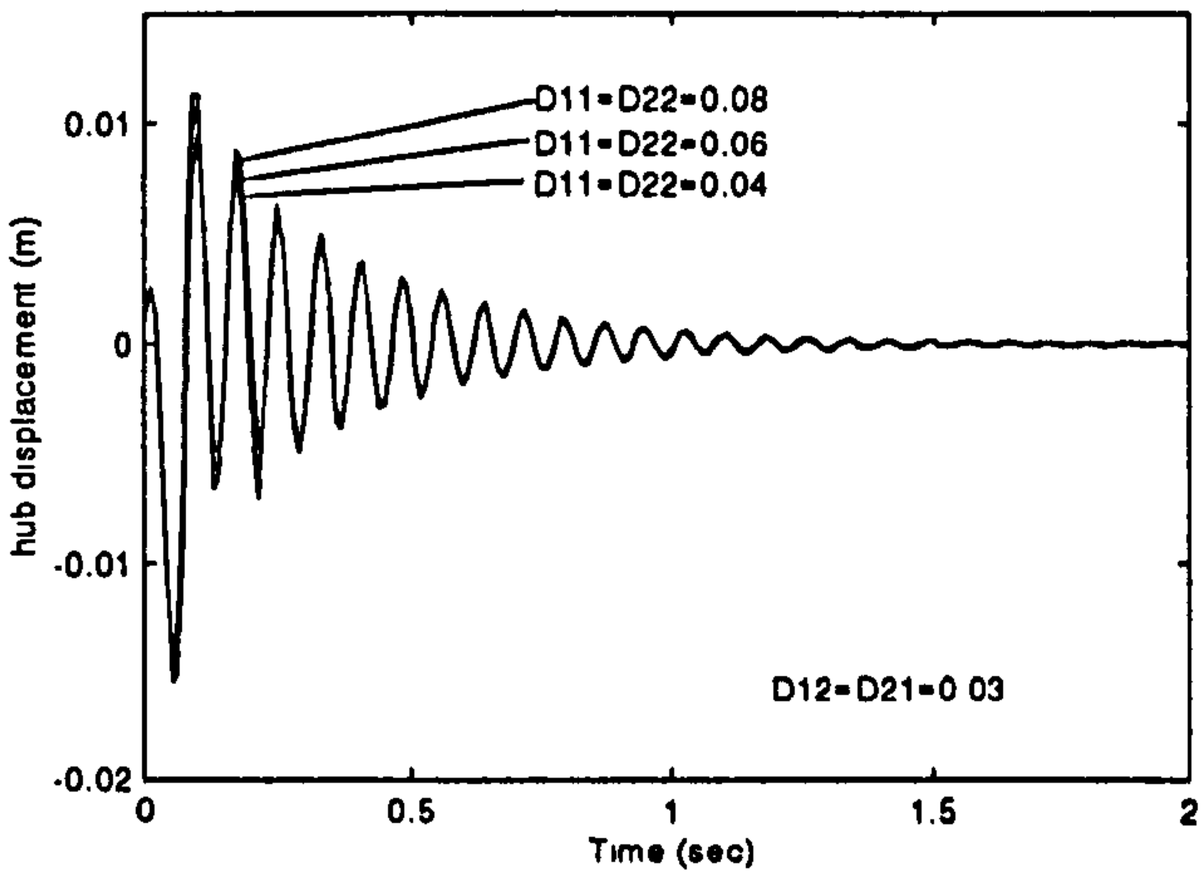

Figure 6-24(c) The effect of the main derivative gain on the wheel vertical starting response for $P_{11}=P_{22}=0.2$, $P_{12}=P_{21}=0.1$, $I_{11}=I_{22}=0.12$, and $I_{12}=I_{21}=0.11$.

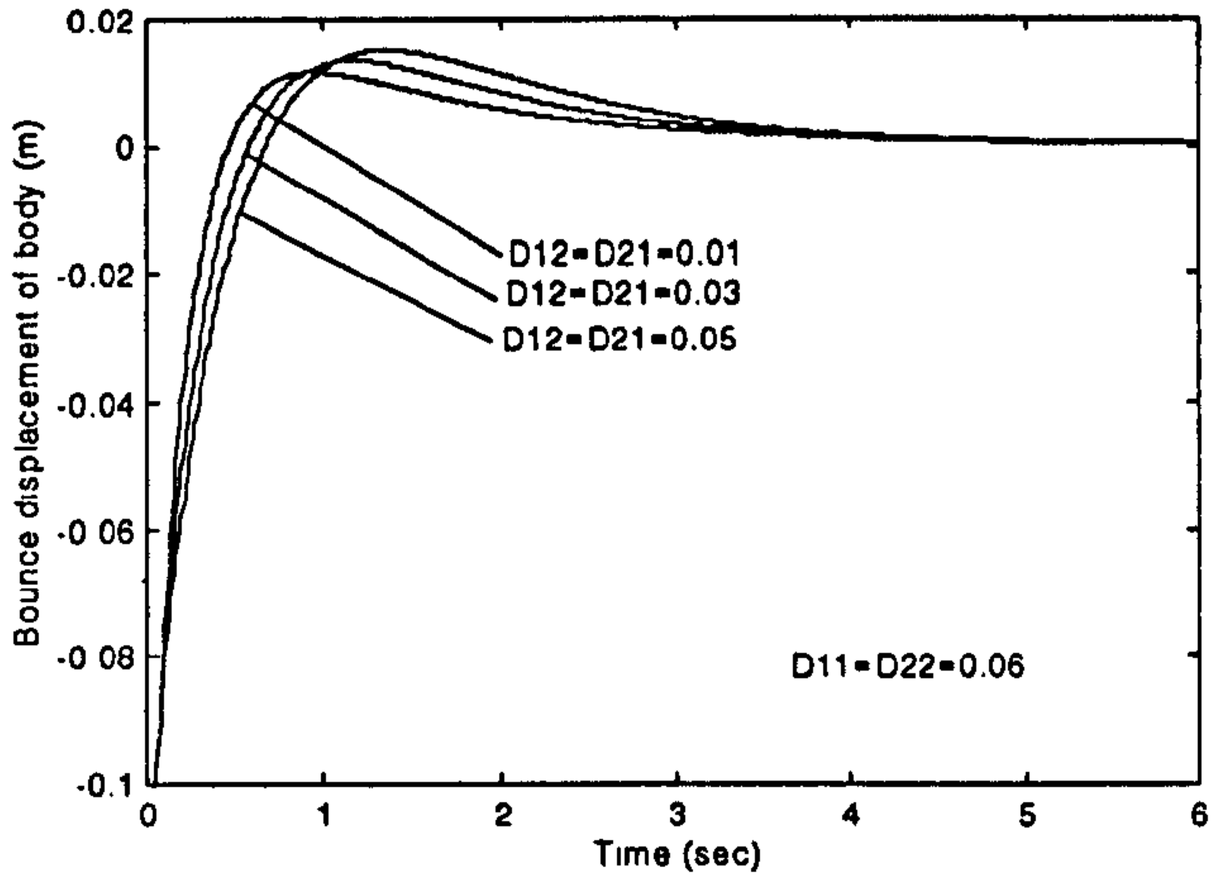

Figure 6-25(a) The effect of the coupled derivative gain on the body bounce starting response for $P_{11}=P_{22}=0.2$, $P_{12}=P_{21}=0.1$, $I_{11}=I_{22}=0.12$, and $I_{12}=I_{21}=0.11$.

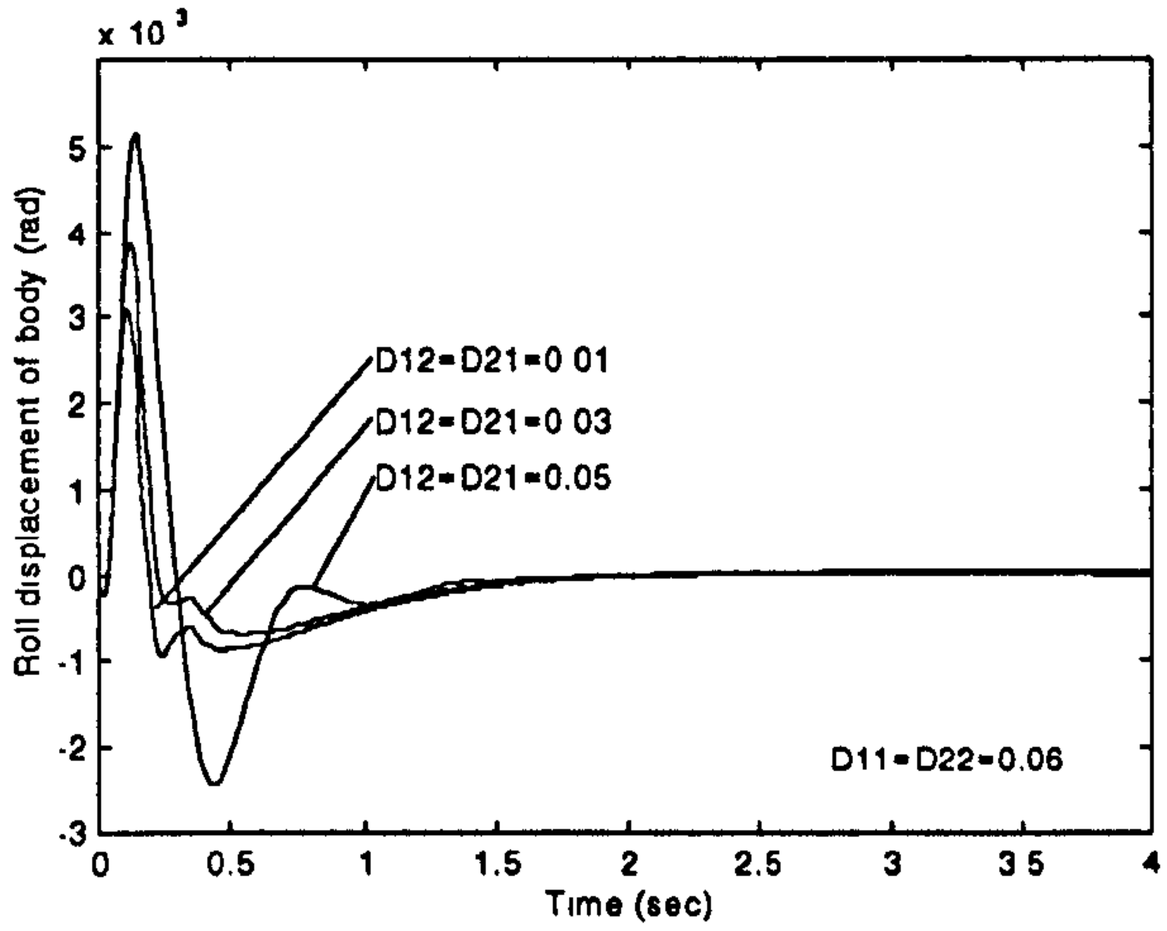

Figure 6-25(b) The effect of the coupled derivative gain on the body roll starting response for $P_{11}=P_{22}=0.2$, $P_{12}=P_{21}=0.1$, $I_{11}=I_{22}=0.12$, and $I_{12}=I_{21}=0.11$.

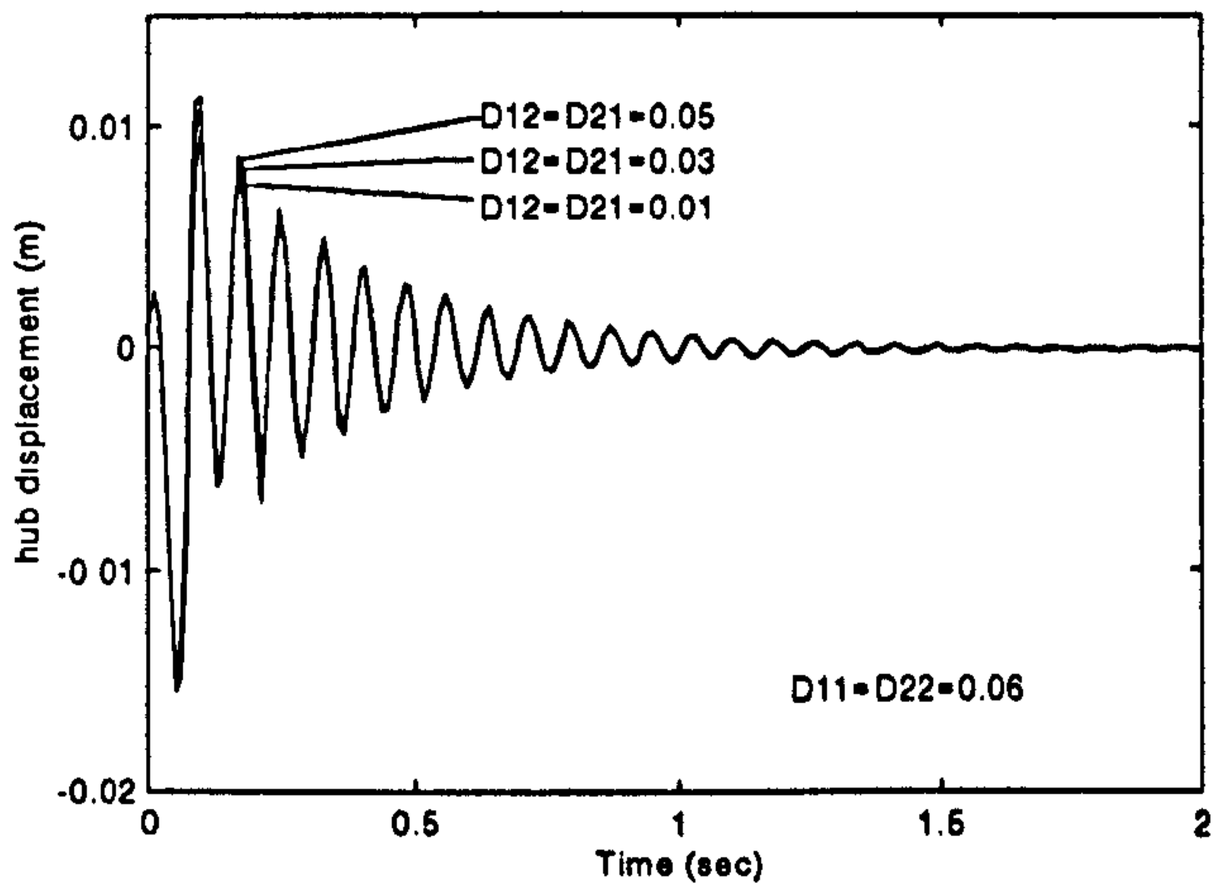

Figure 6-25(c) The effect of the coupled derivative gain on the wheel vertical starting response for $P_{11}=P_{22}=0.2$, $P_{12}=P_{21}=0.1$, $I_{11}=I_{22}=0.12$, and $I_{12}=I_{21}=0.11$.

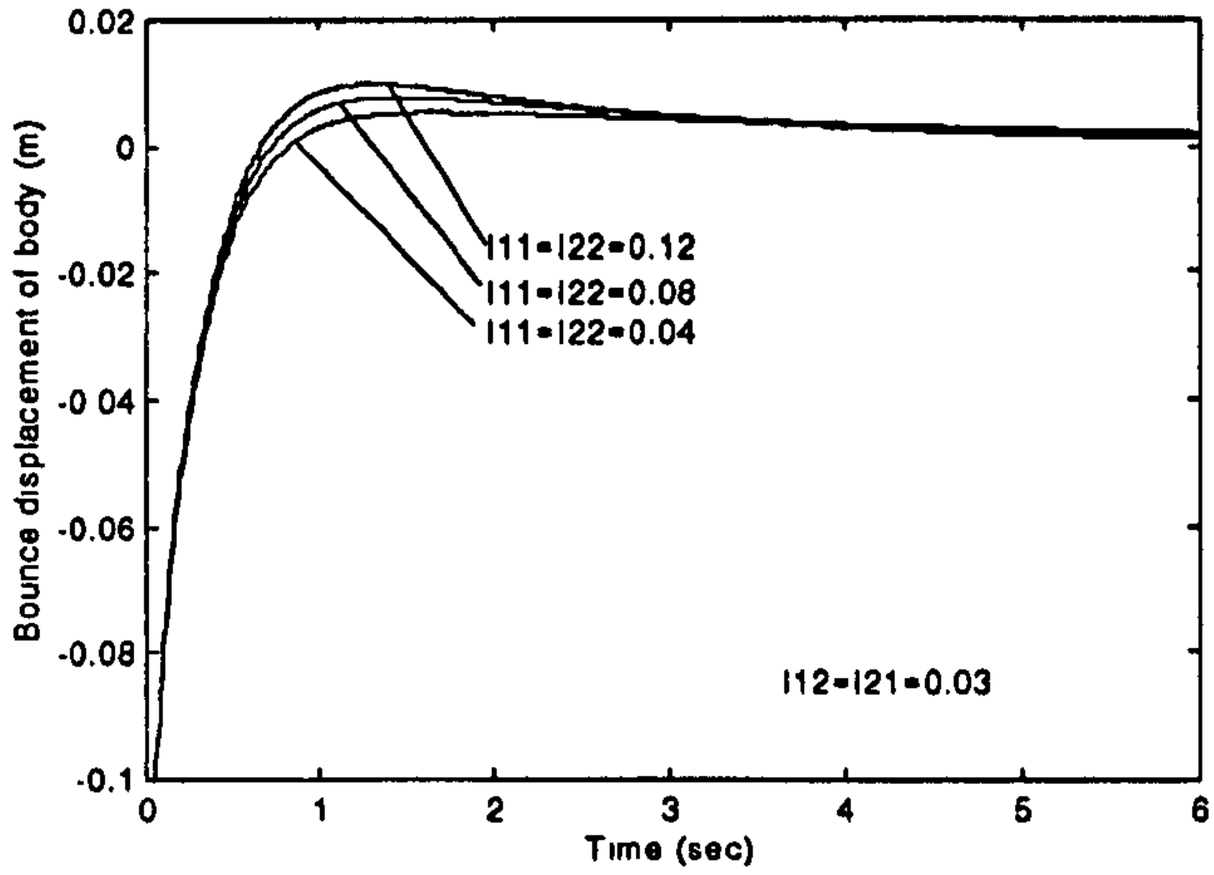

Figure 6-26(a) The effect of the main integral gain on the body bounce starting response for $P_{11}=P_{22}=0.2$, $P_{12}=P_{21}=0.1$, $D_{11}=D_{22}=0.06$, and $D_{12}=D_{21}=0.03$.

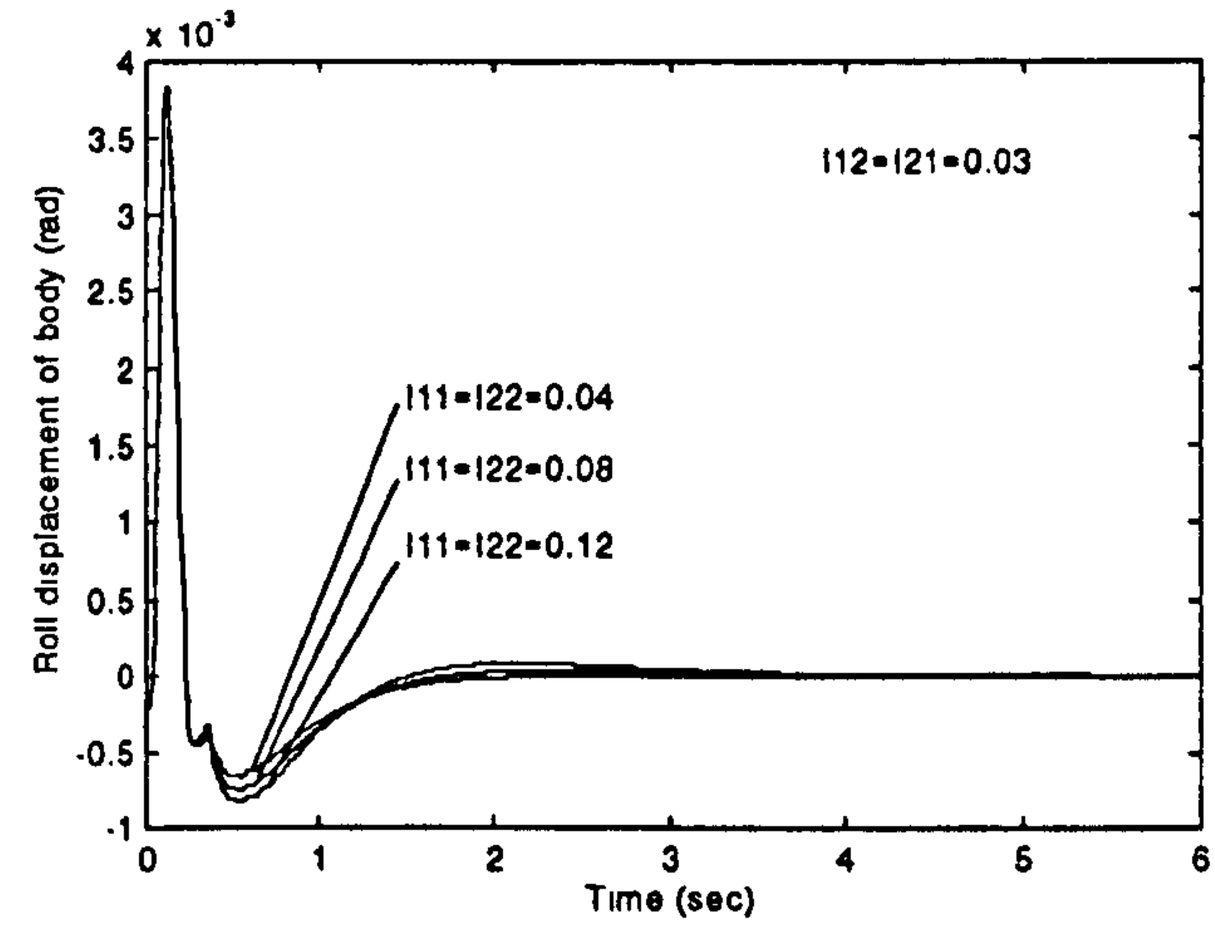

Figure 6-26(b) The effect of the main integral gain on the body roll starting response for $P_{11}=P_{22}=0.2$, $P_{12}=P_{21}=0.1$, $D_{11}=D_{22}=0.06$, and $D_{12}=D_{21}=0.03$.

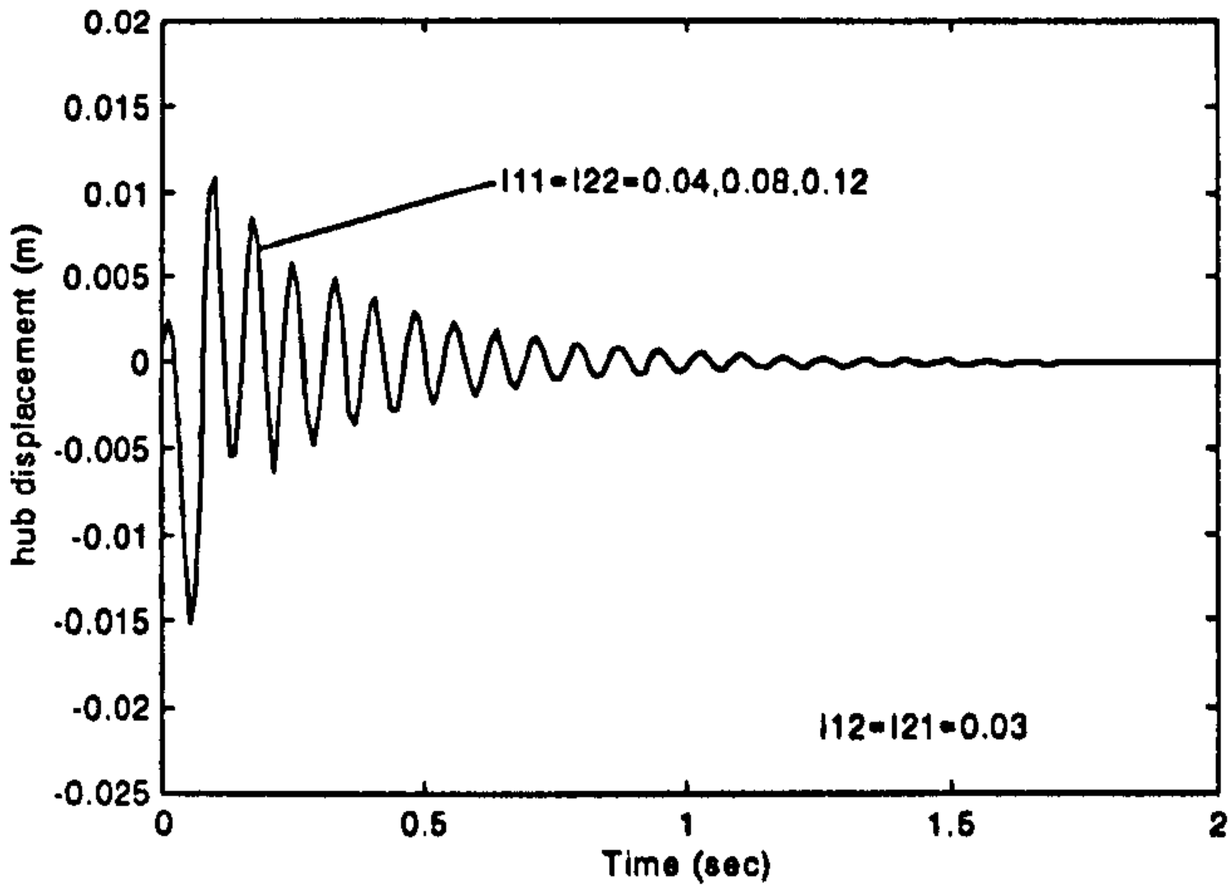

Figure 6-26(c) The effect of the main integral gain on the wheel vertical starting response for $P_{11}=P_{22}=0.2$, $P_{12}=P_{21}=0.1$, $D_{11}=D_{22}=0.06$, and $D_{12}=D_{21}=0.03$.

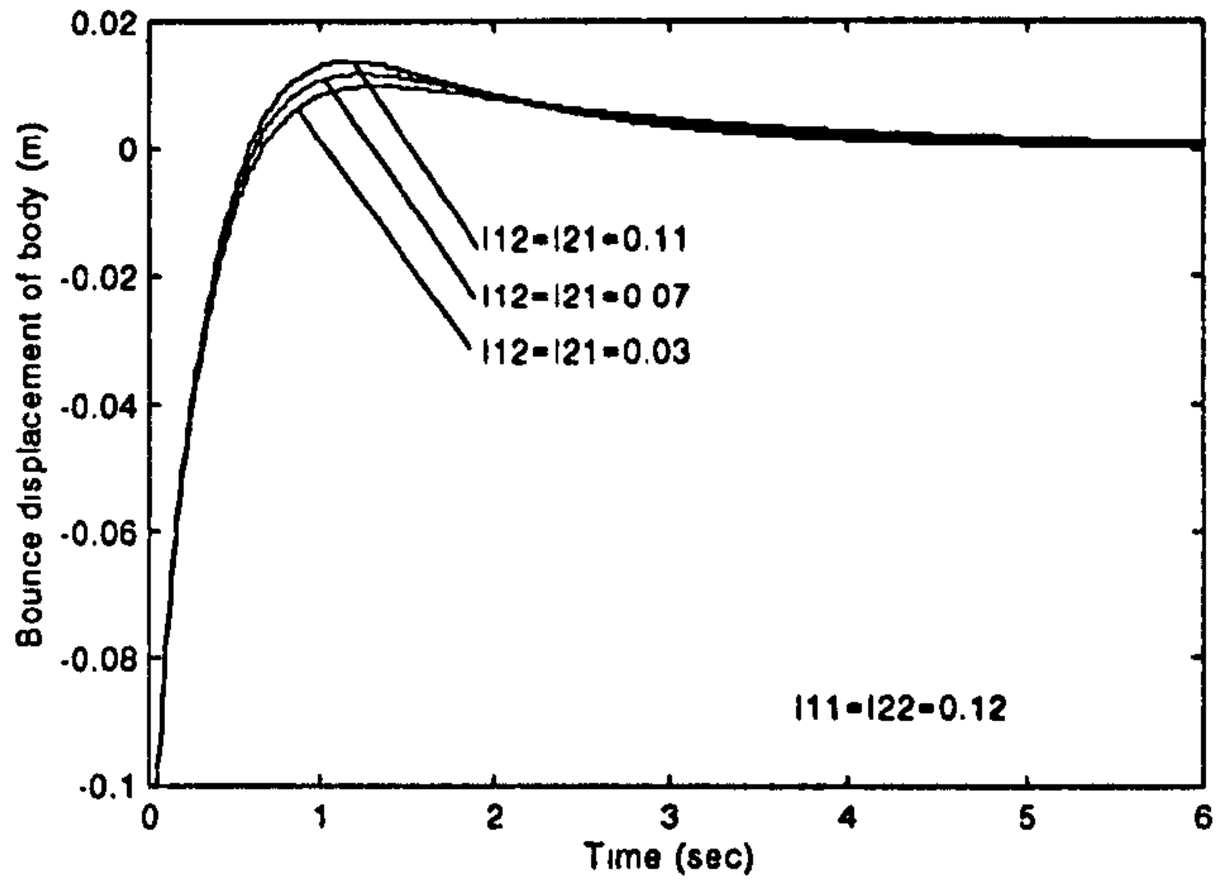

Figure 6-27(a) The effect of the coupled integral gain on the body bounce starting response for $P_{11}=P_{22}=0.2$, $P_{12}=P_{21}=0.1$, $D_{11}=D_{22}=0.06$, and $D_{12}=D_{21}=0.03$.

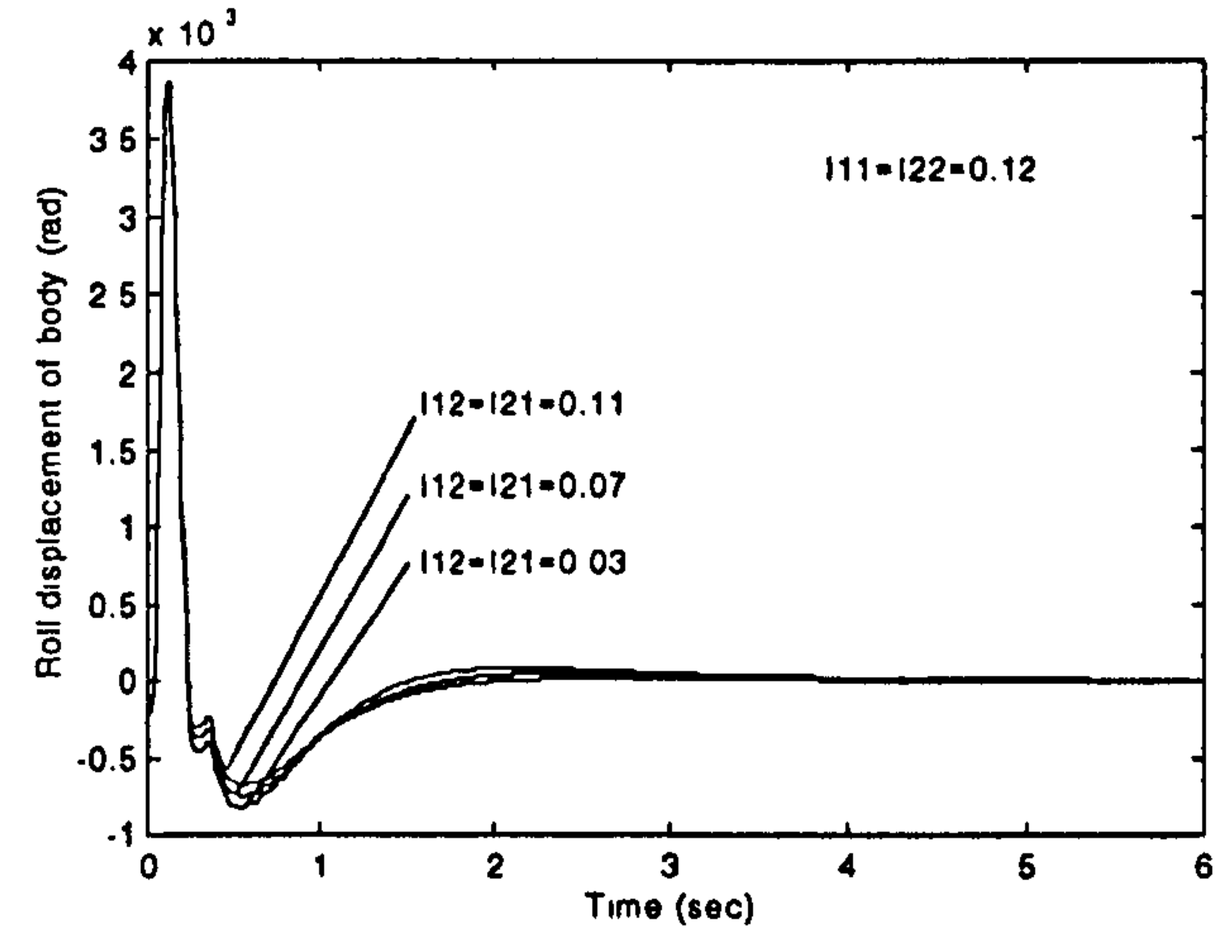

Figure 6-27(b) The effect of the coupled integral gain on the body roll starting response for $P_{11}=P_{22}=0.2$, $P_{12}=P_{21}=0.1$, $D_{11}=D_{22}=0.06$, and $D_{12}=D_{21}=0.03$.

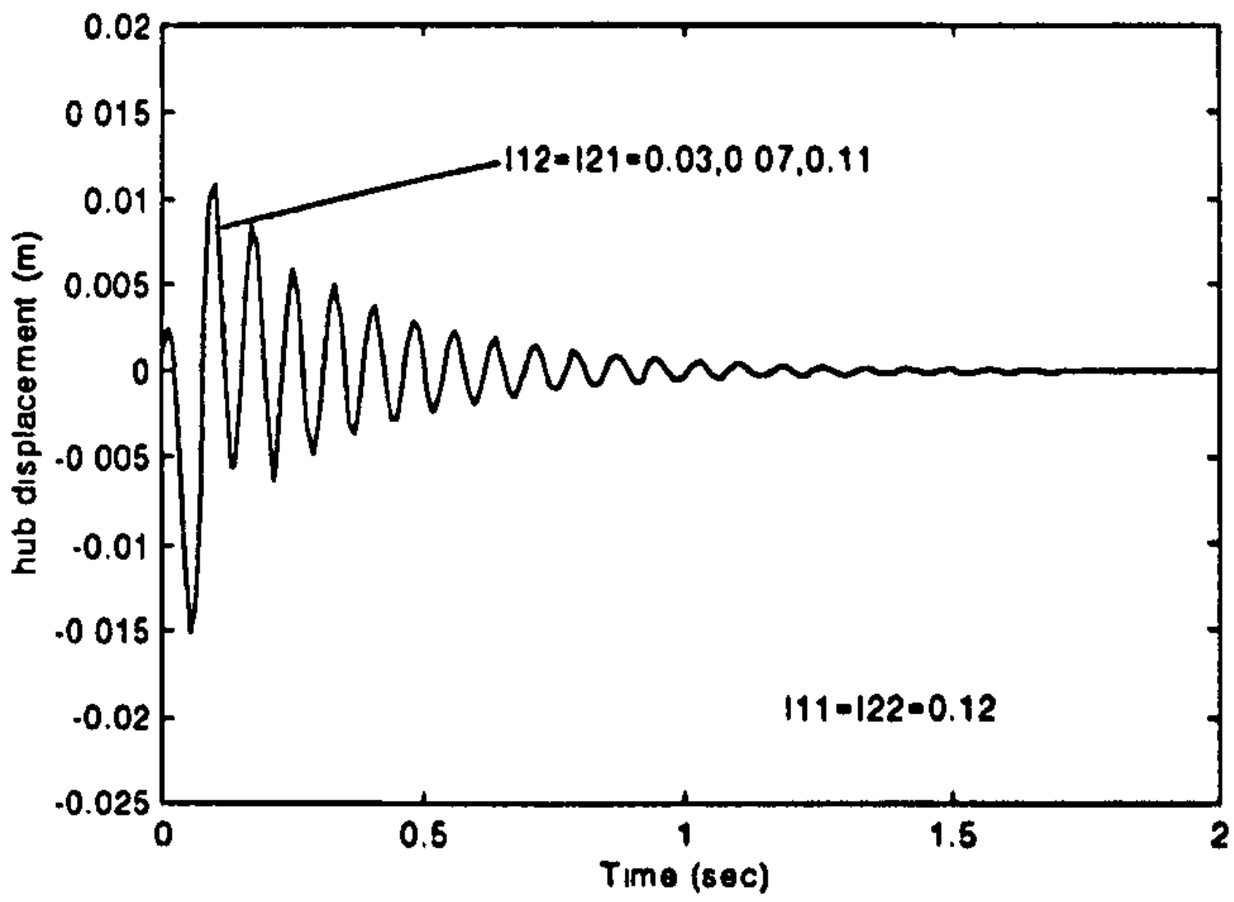

Figure 6-27(c) The effect of the coupled integral gain on the wheel vertical starting response for $P_{11}=P_{22}=0.2$, $P_{12}=P_{21}=0.1$, $D_{11}=D_{22}=0.06$, and $D_{12}=D_{21}=0.03$.

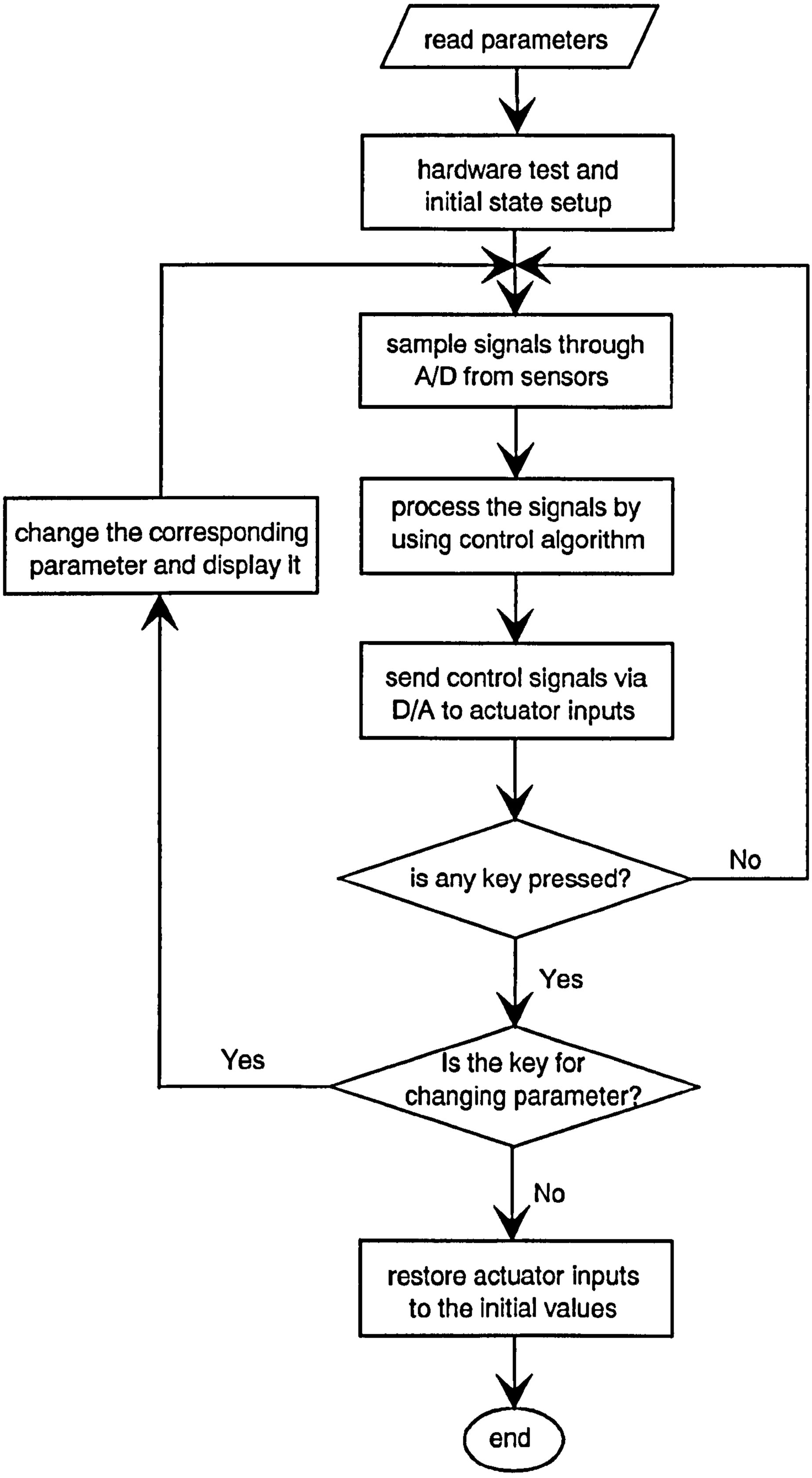

Figure 6-28 Block diagram for the control software

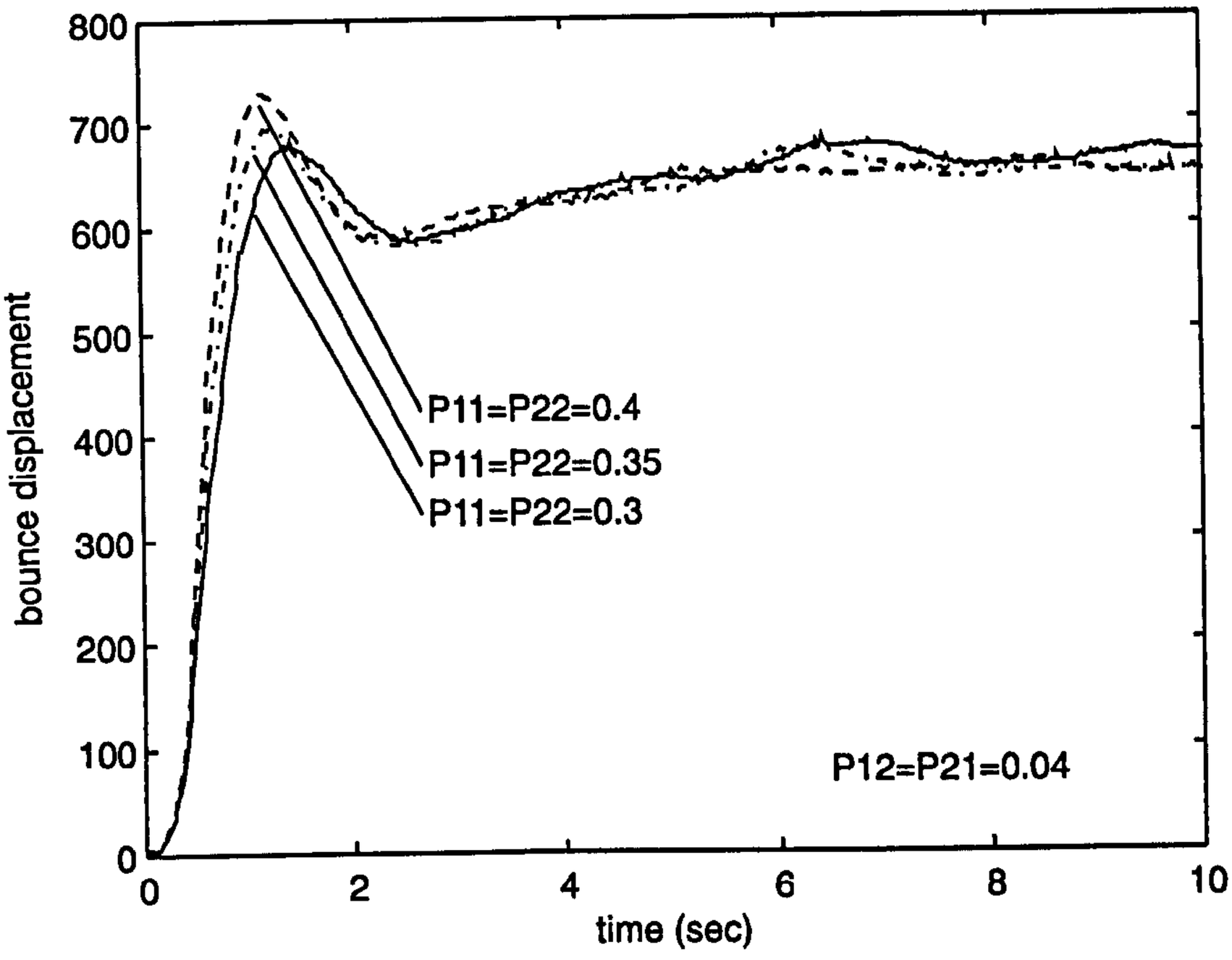

Figure 6-29(a) Measured starting response for the body bounce motion with the effect of the main proportional gain

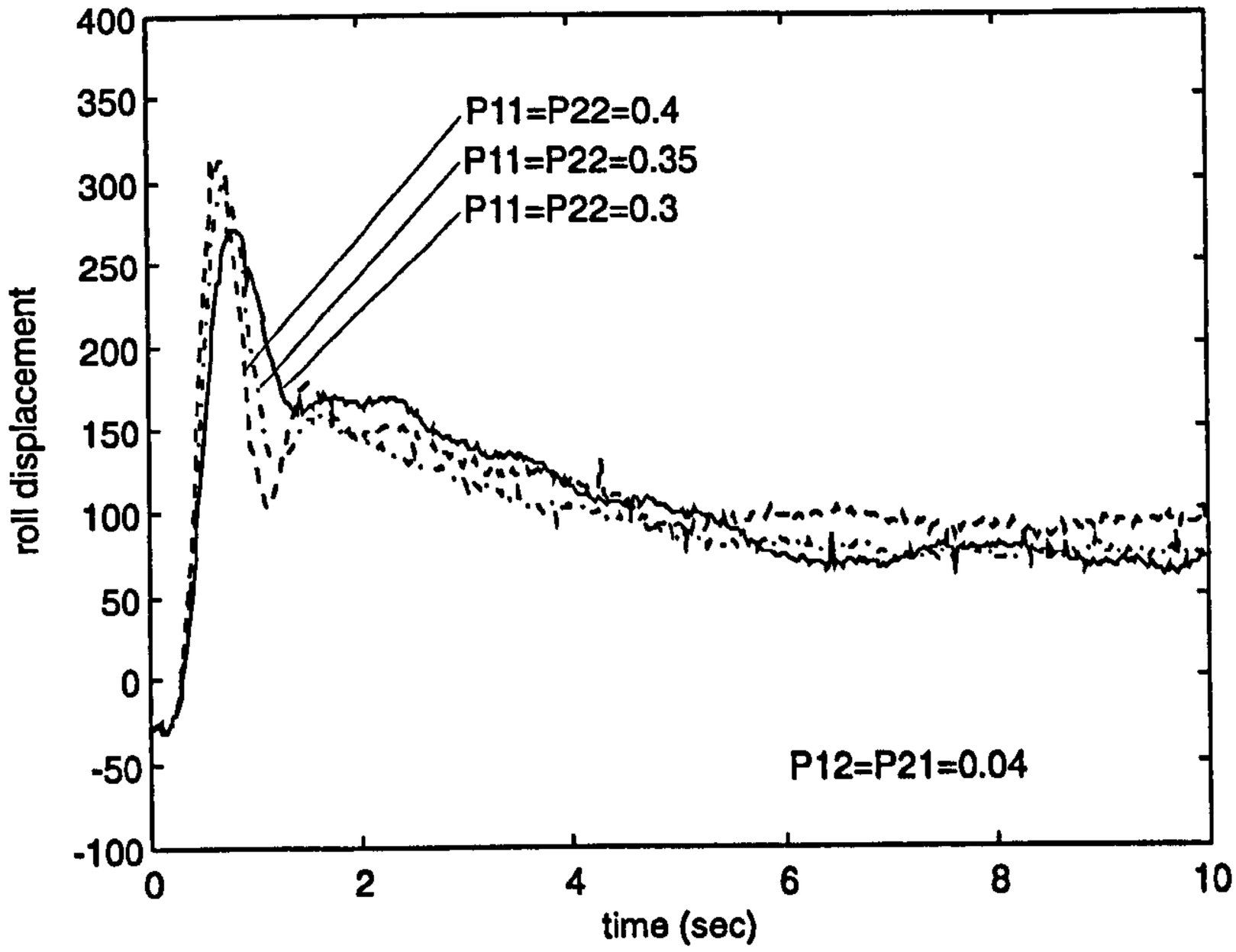

Figure 6-29(b) Measured starting response for the body roll motion with the effect of the main proportional gain

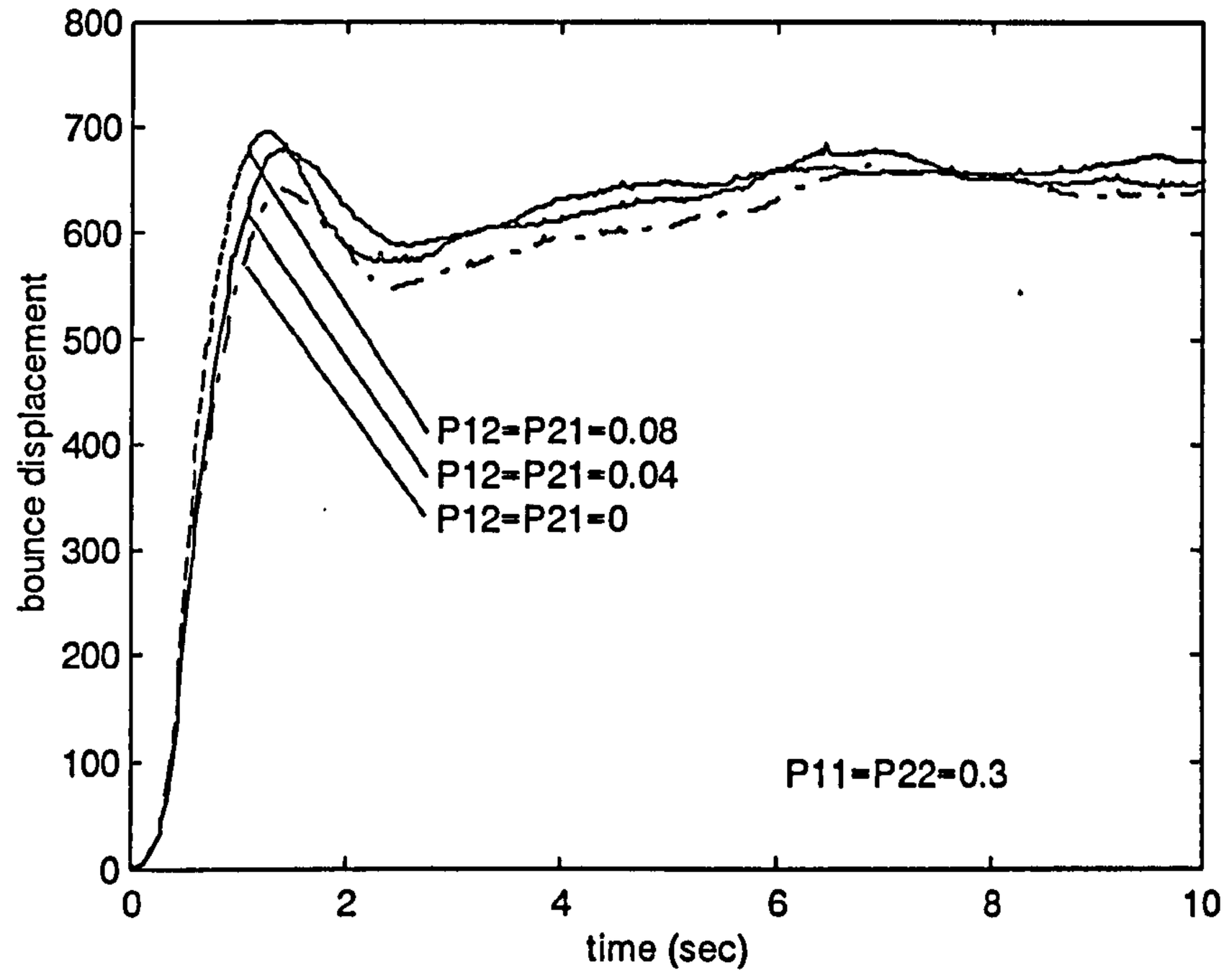

Figure 6-30(a) Measured starting response for the body bounce motion with the effect of the coupled proportional gain

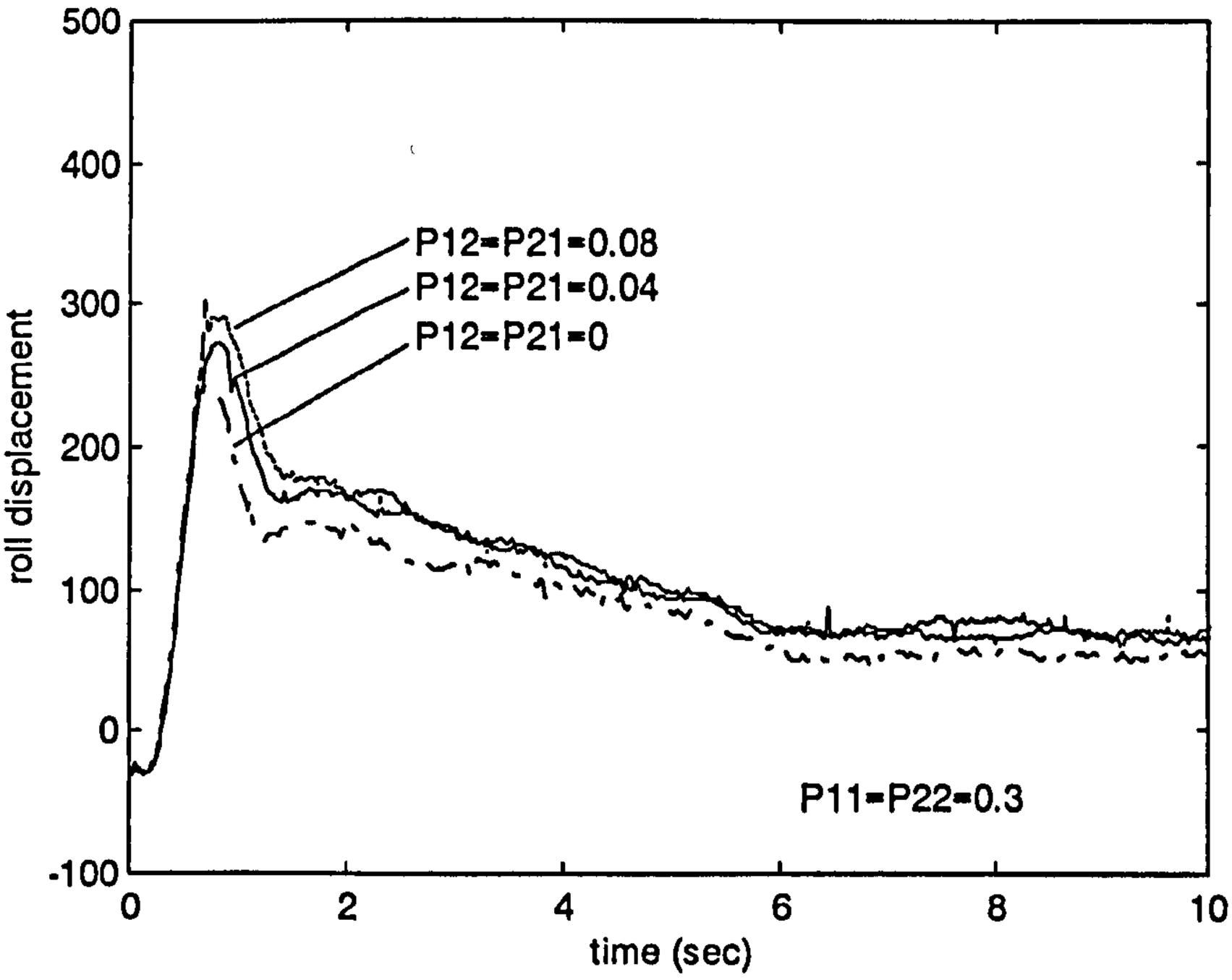

Figure 6-30(b) Measured starting response for the body roll motion with the effect of the coupled proportional gain

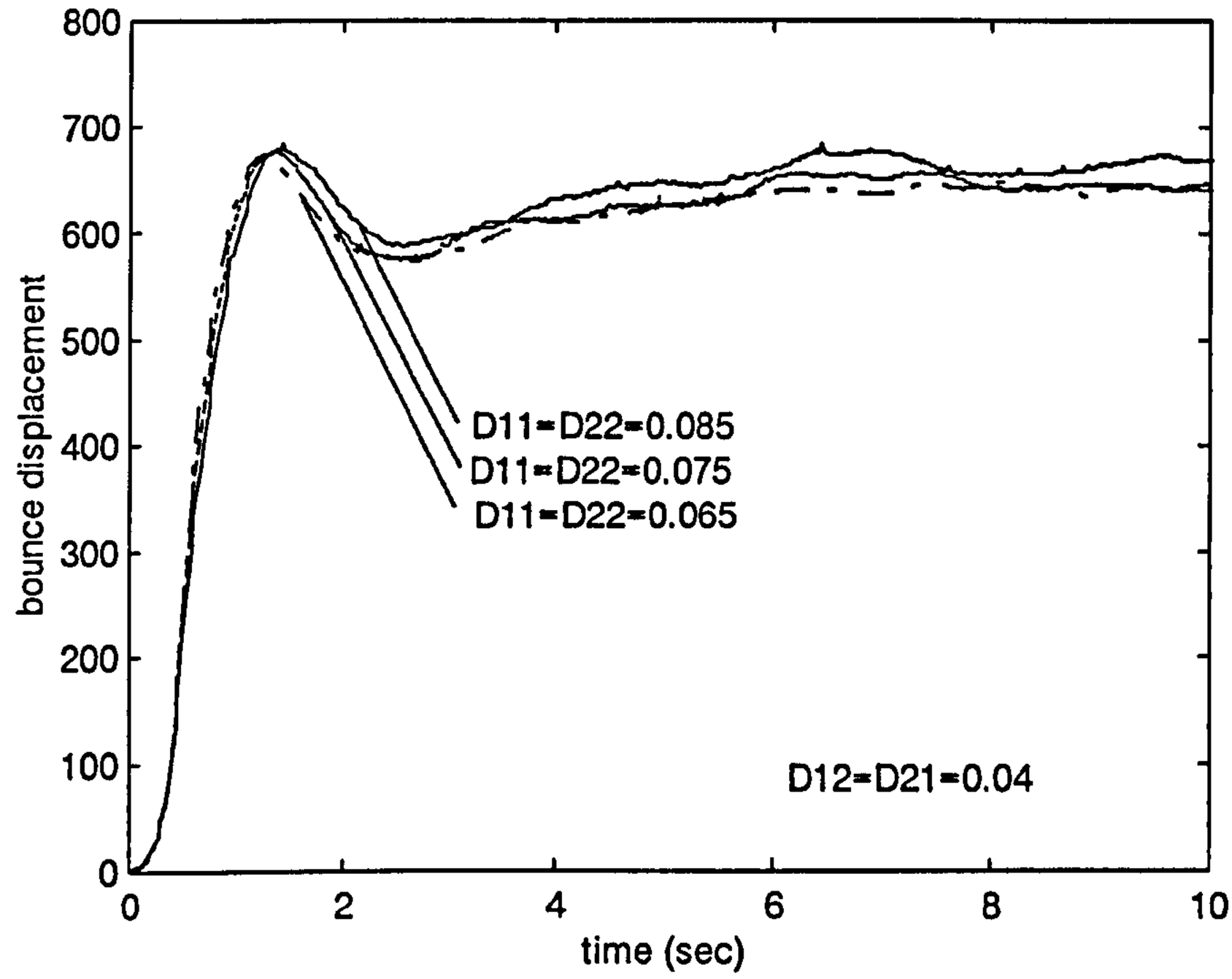

Figure 6-31(a) Measured starting response for the body bounce motion with the effect of the main derivative gain

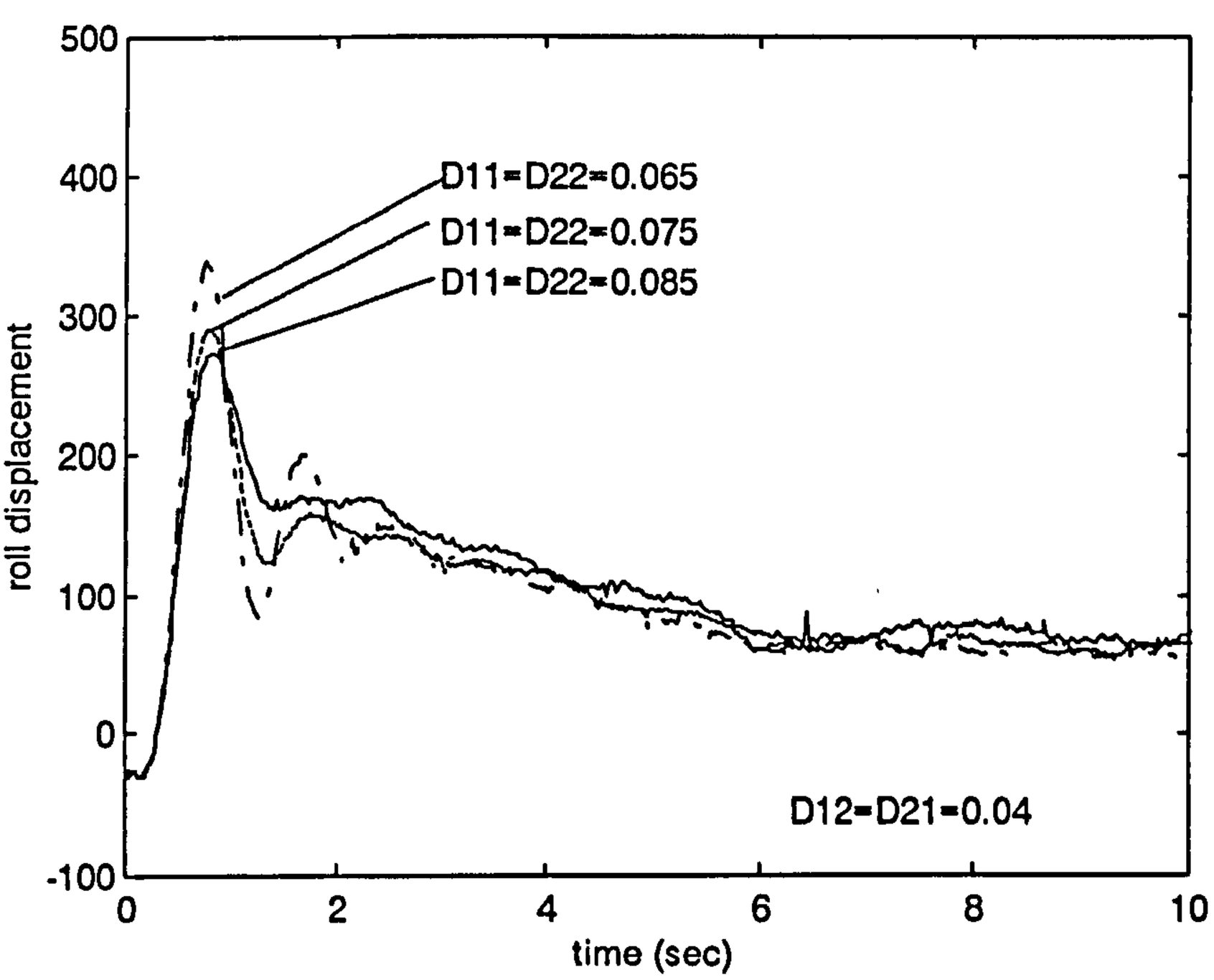

Figure 6-31(b) Measured starting response for the body roll motion with the effect of the main derivative gain

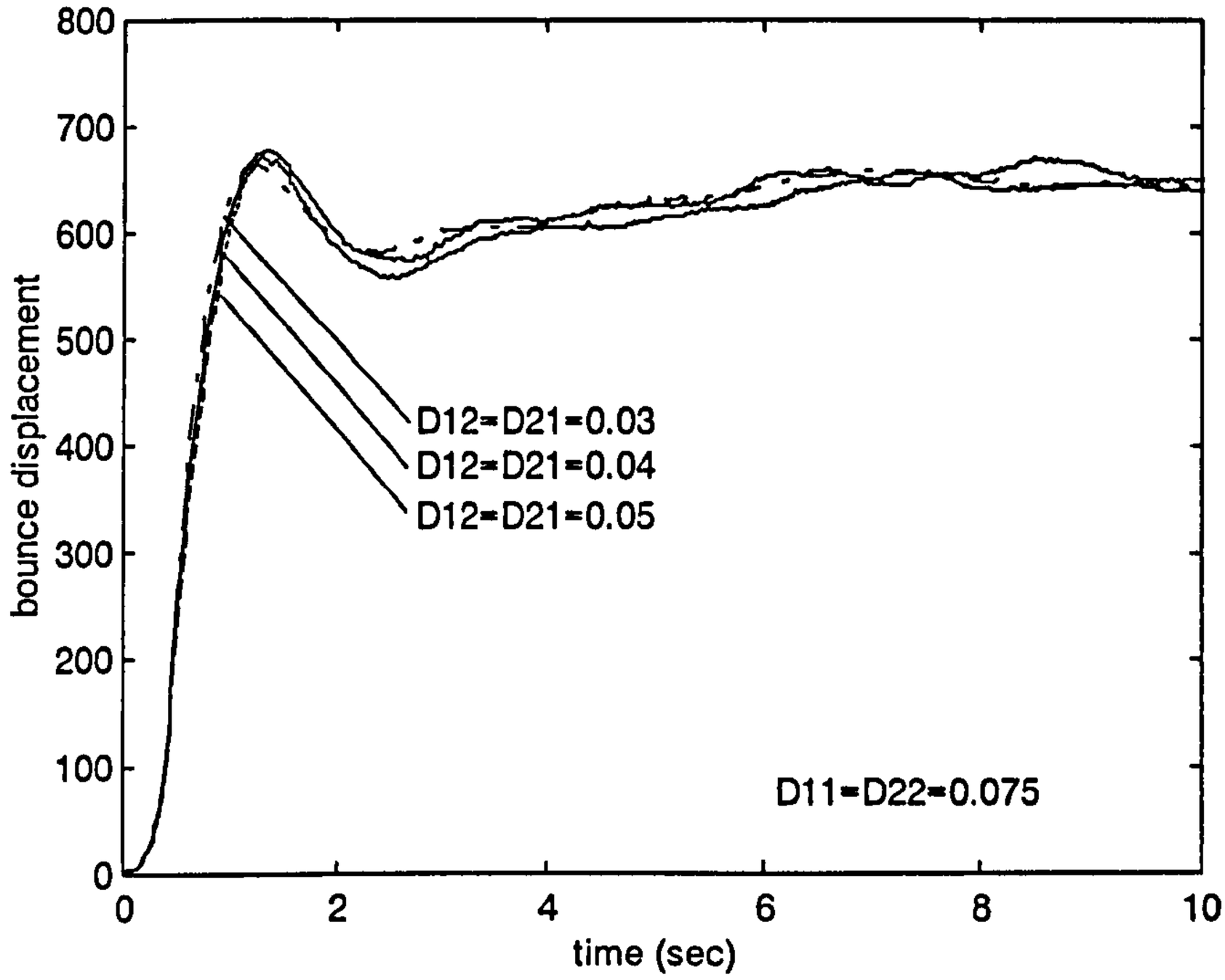

Figure 6-32(a) Measured starting response for the body bounce motion with the effect of the coupled derivative gain

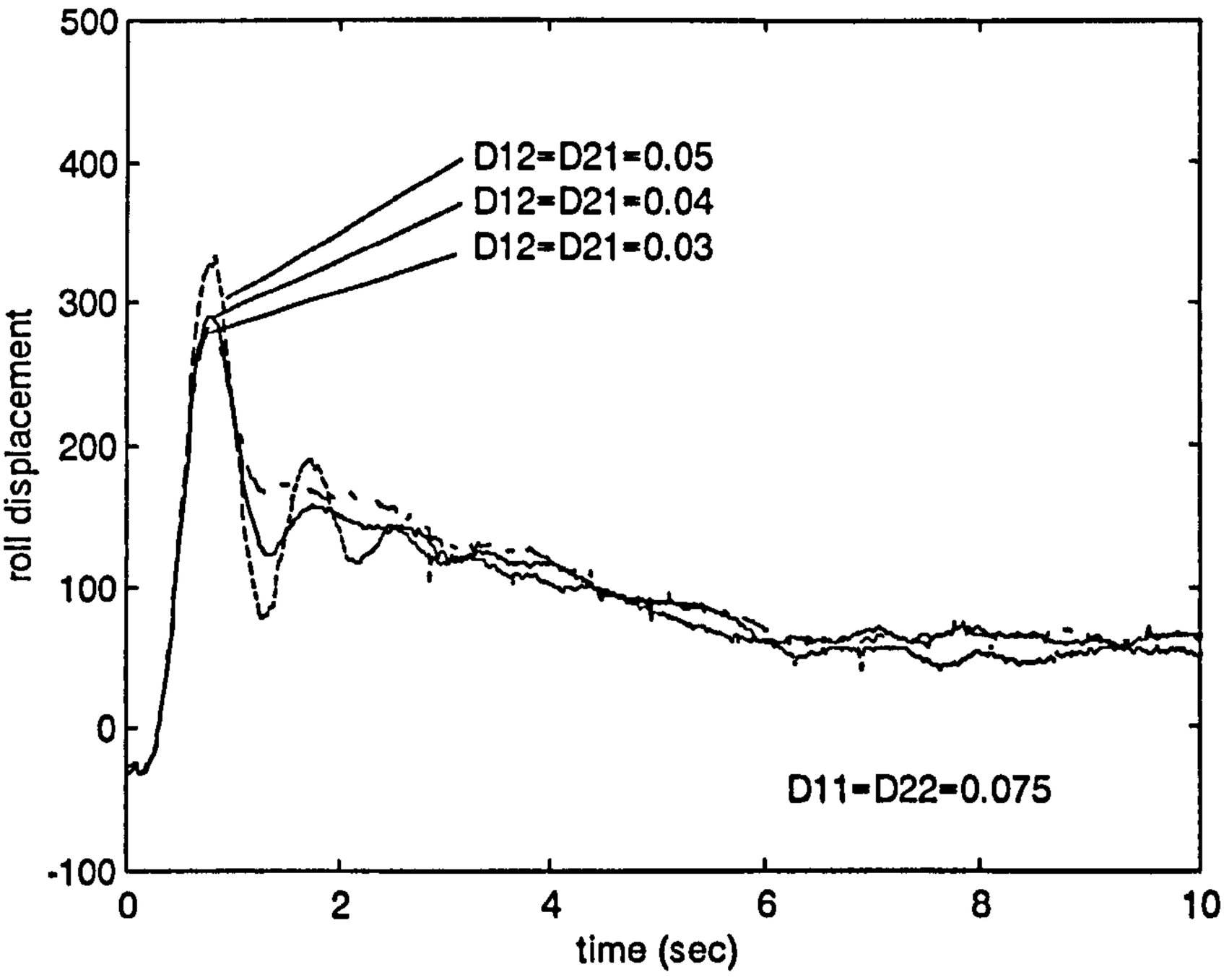

Figure 6-32(b) Measured starting response for the body roll motion with the effect of the coupled derivative gain

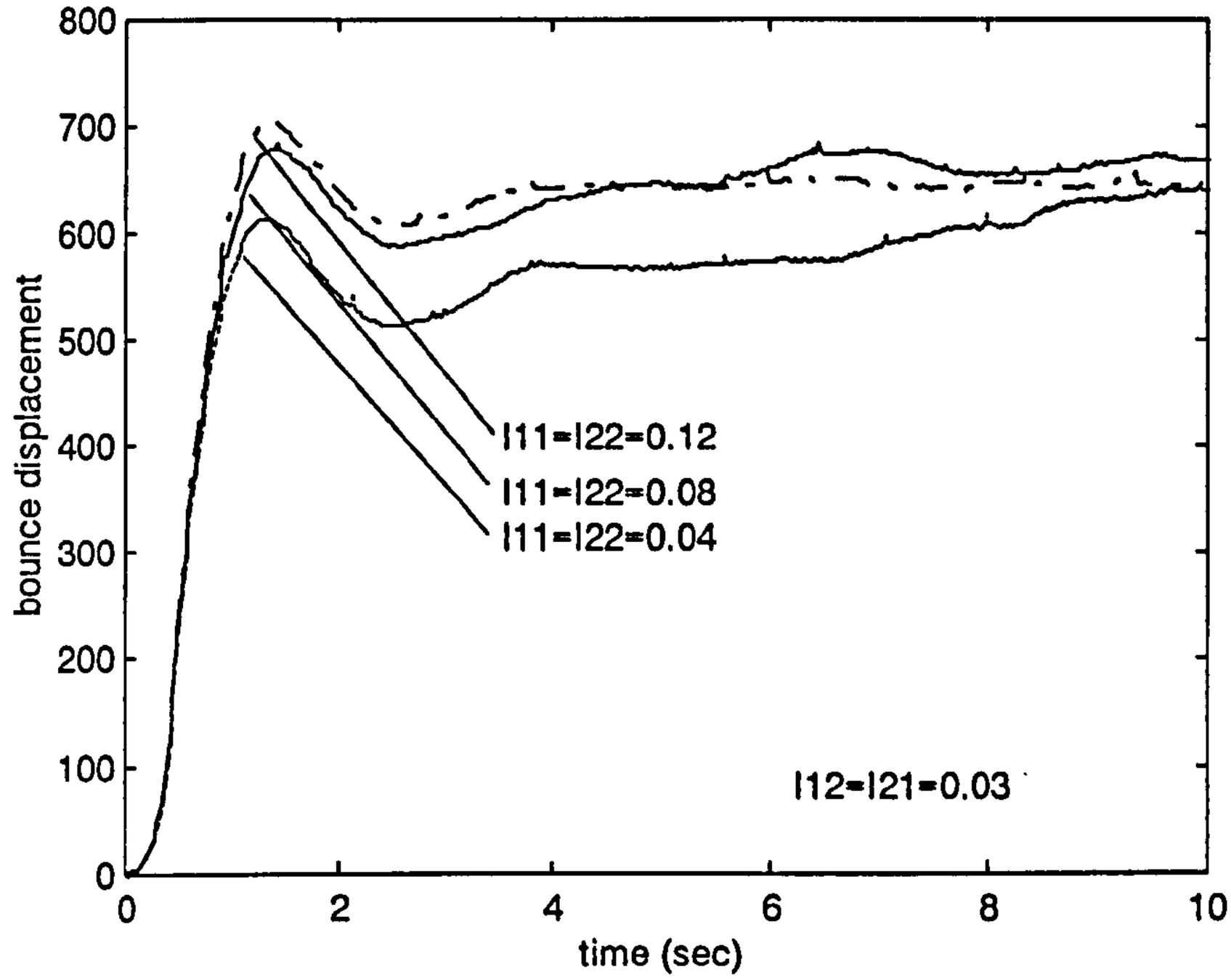

Figure 6-33(a) Measured starting response for the body bounce motion with the effect of the main integral gain

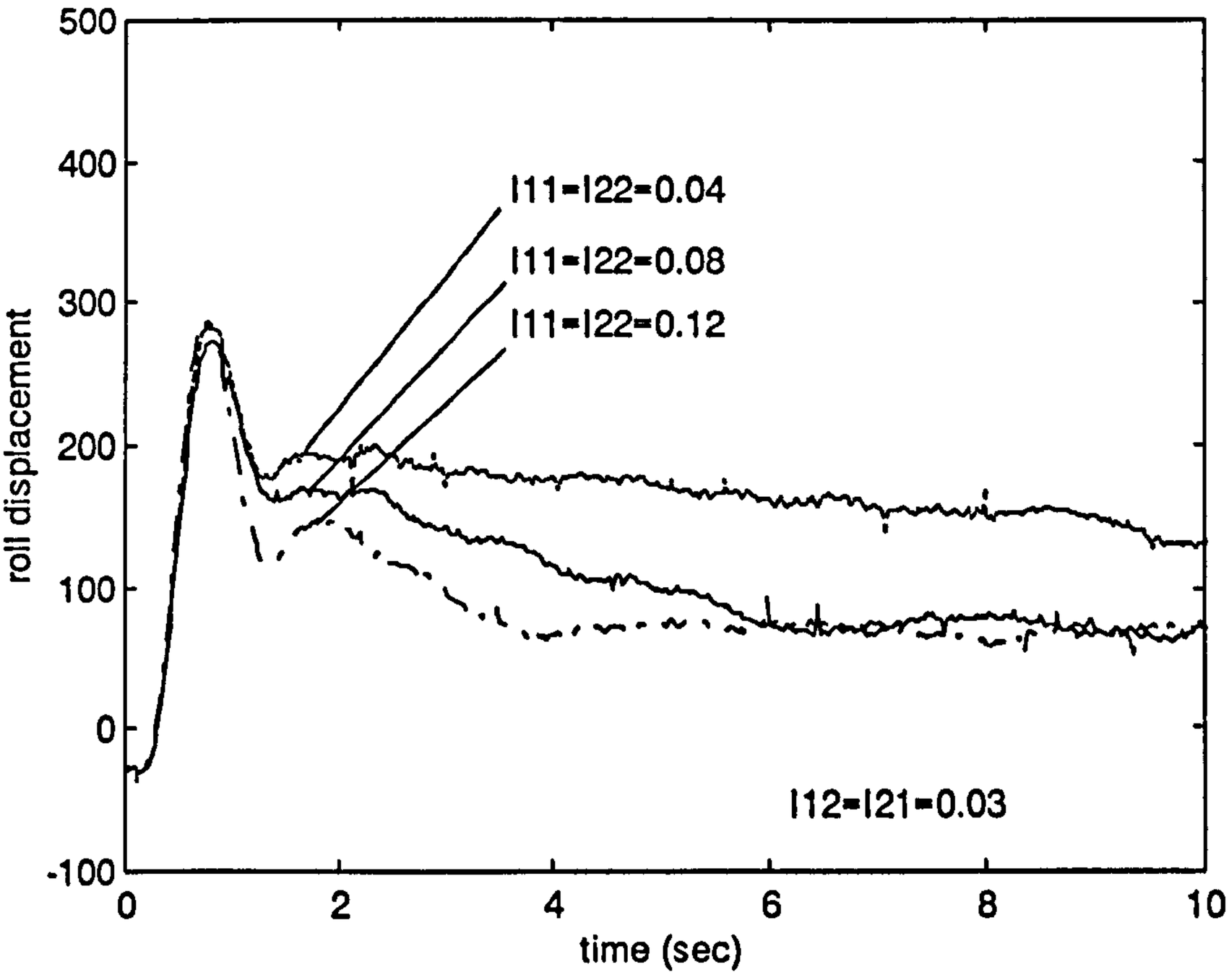

Figure 6-33(b) Measured starting response for the body roll motion with the effect of the main integral gain

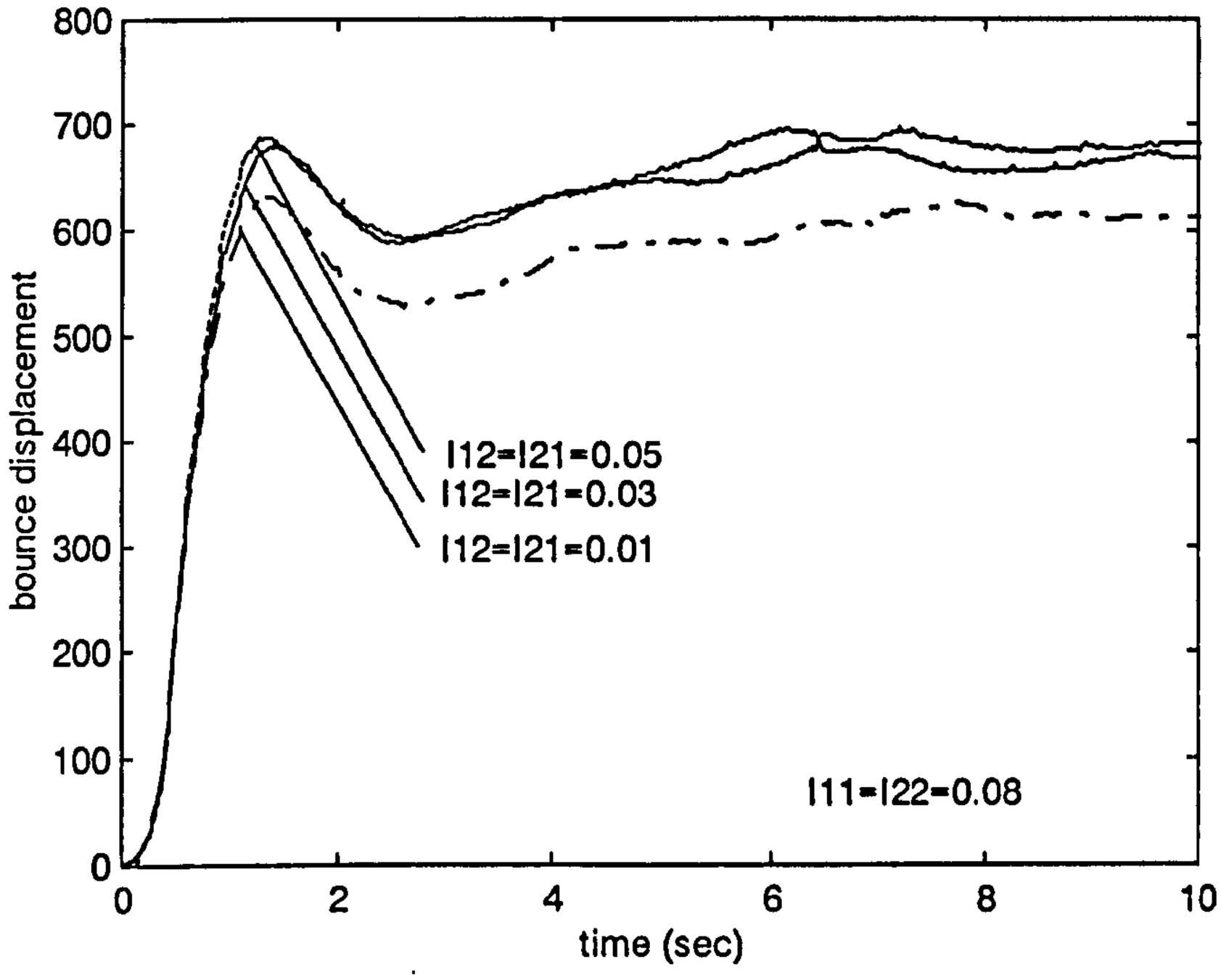

Figure 6-34(a) Measured starting response for the body bounce motion with the effect of the coupled integral gain

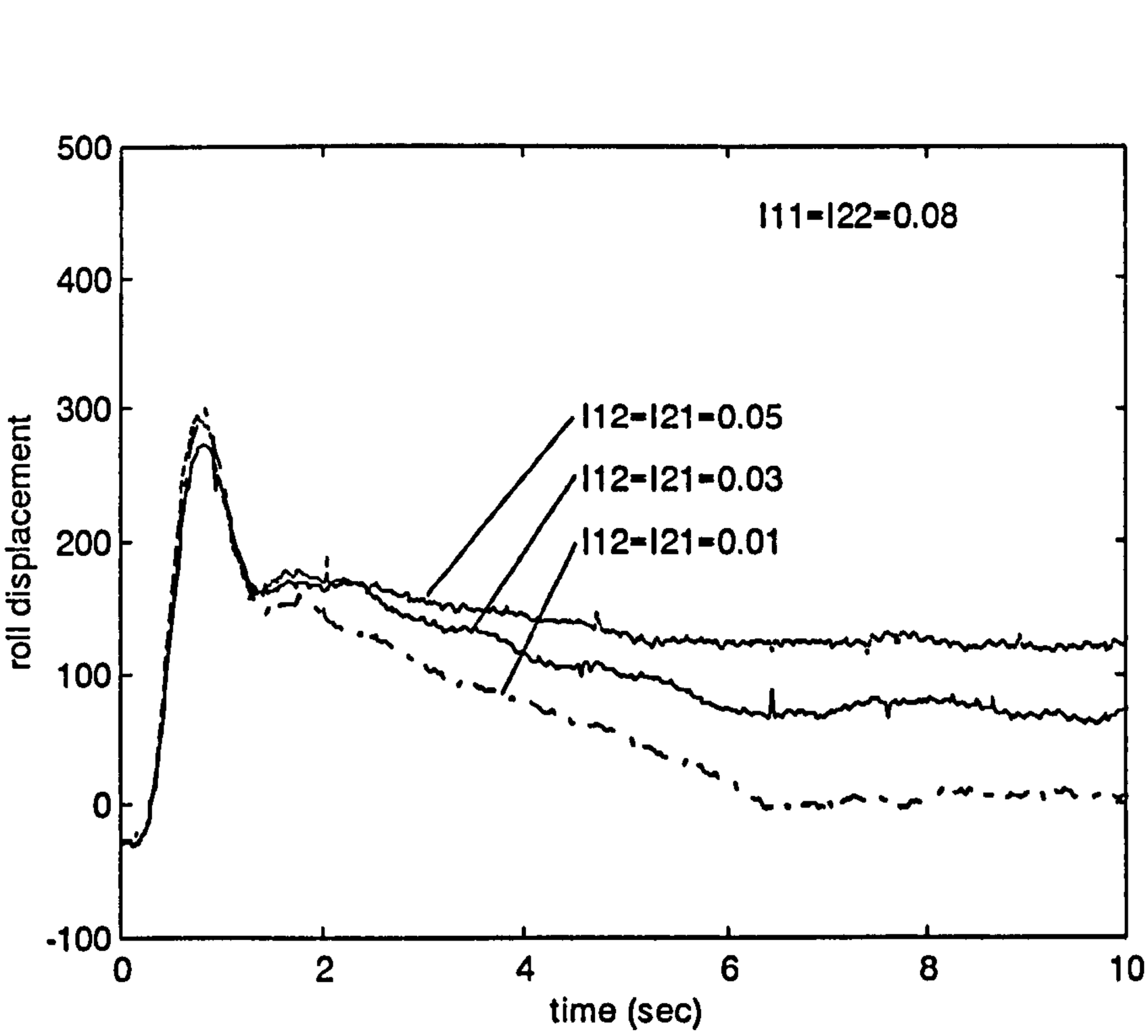

Figure 6-34(b) Measured starting response for the body roll motion with the effect of the coupled integral gain

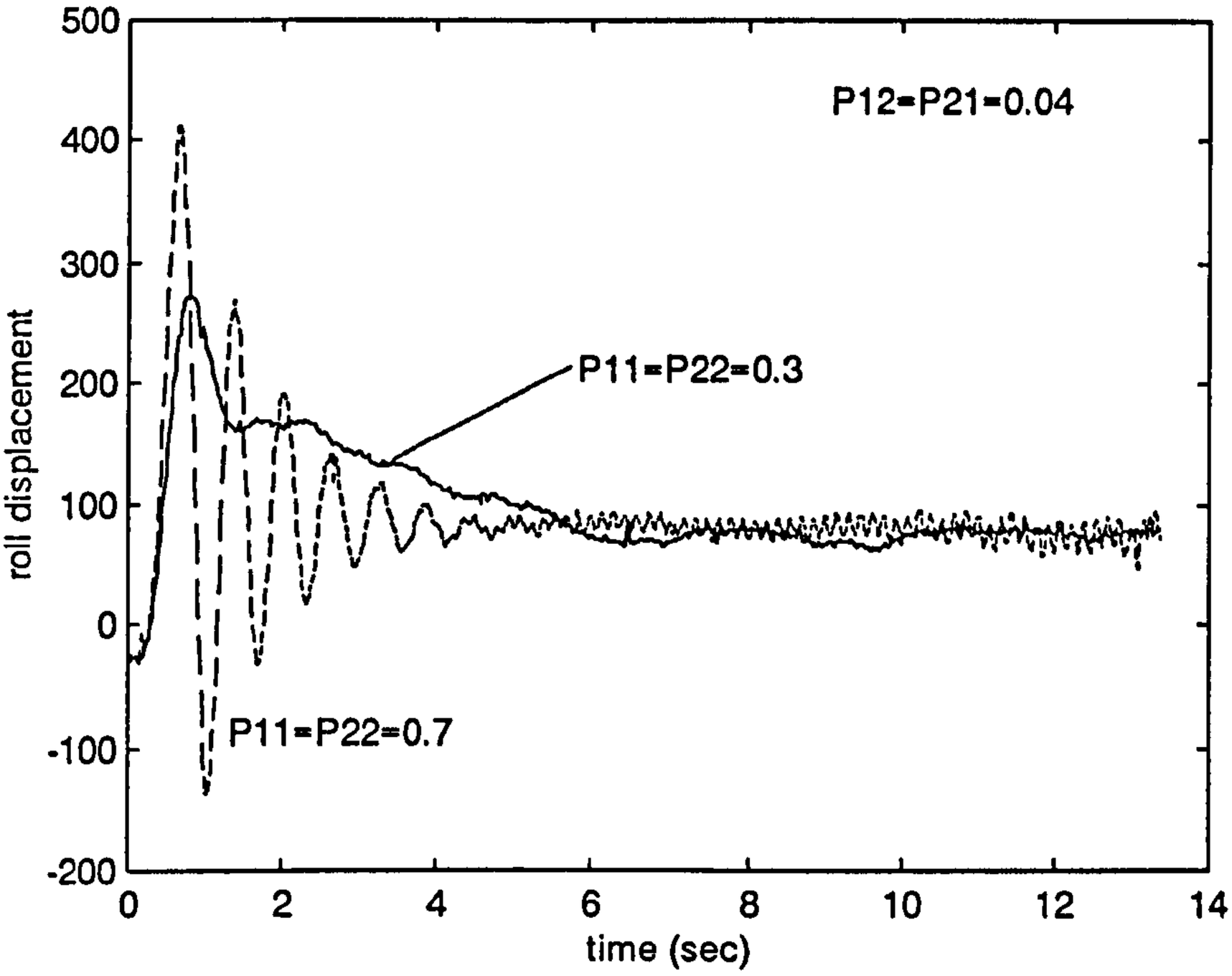

Figure 6-35 The measured effect of the main proportional gain on stability for the body roll motion

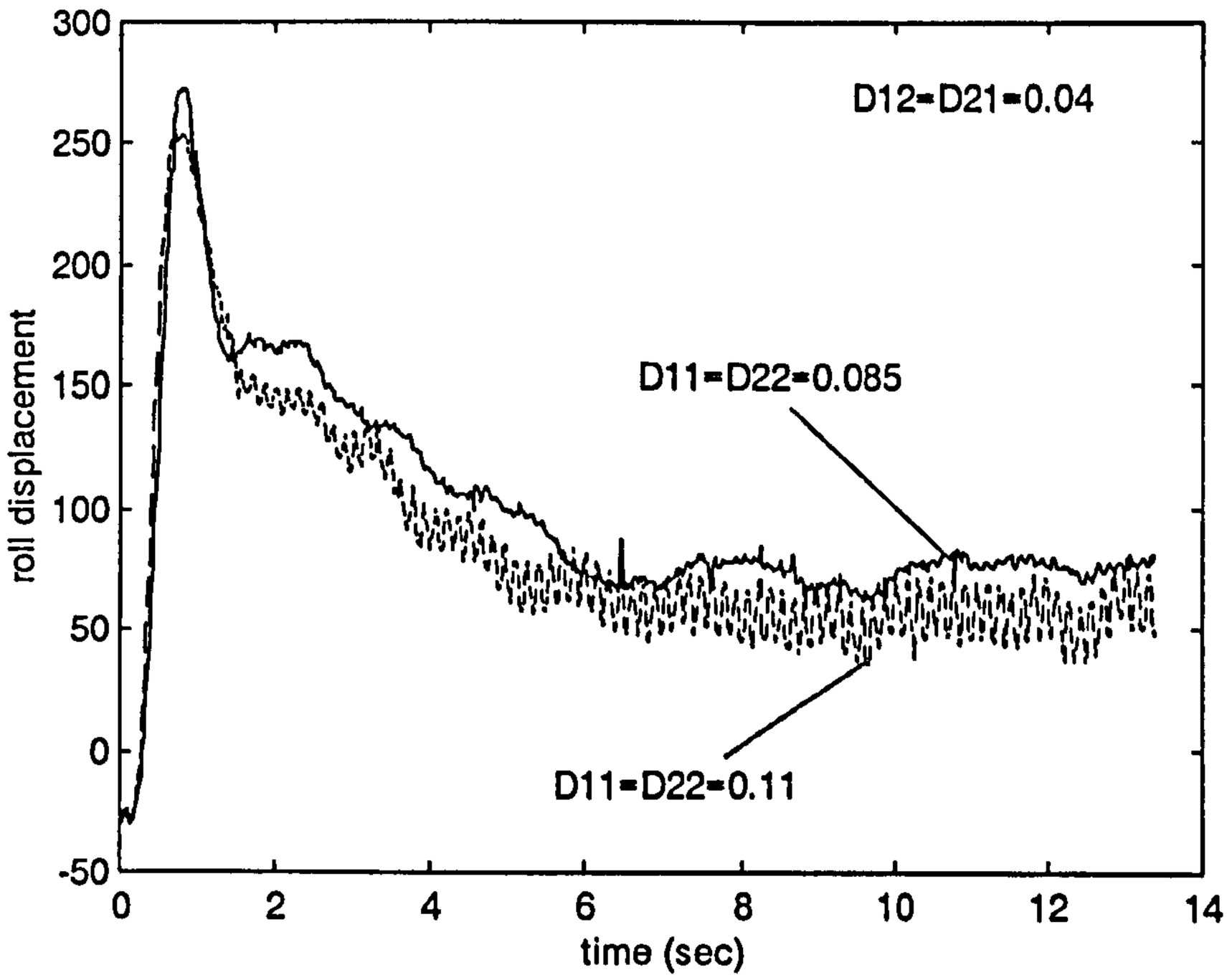

Figure 6-36 The measured effect of the main derivative gain on stability for the body roll motion

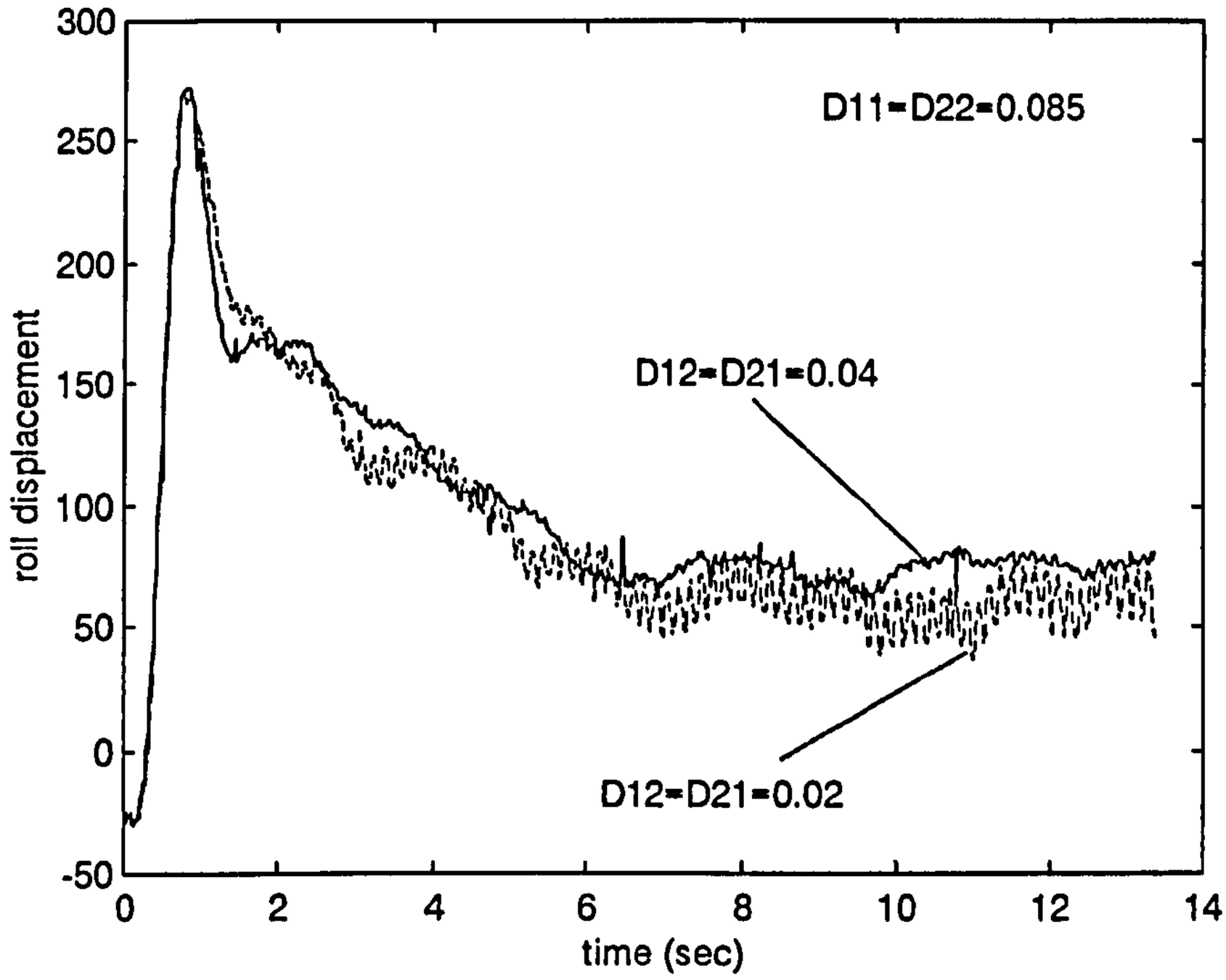

Figure 6-37 The measured effect of the coupled derivative gain on stability for the body roll motion

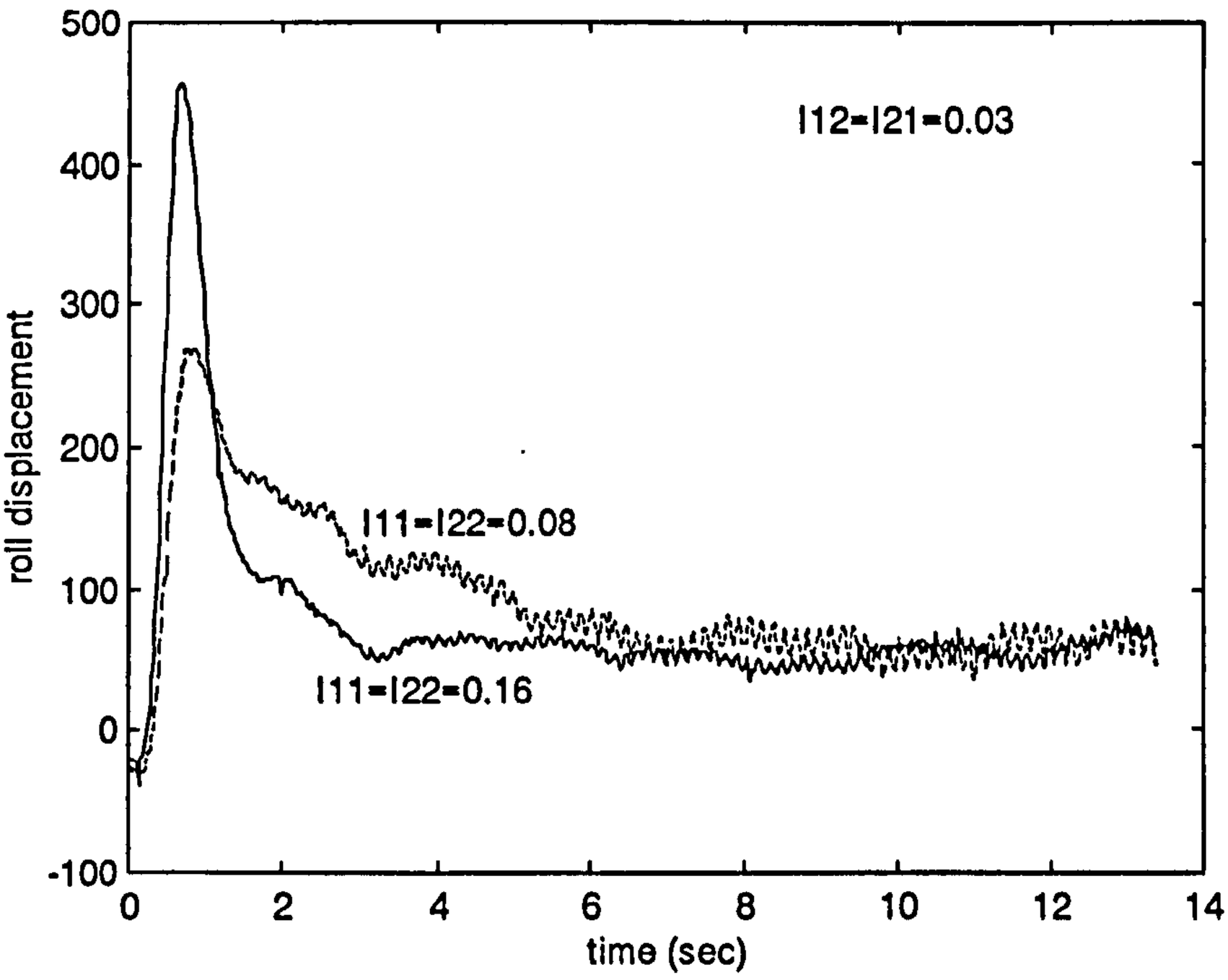

Figure 6-38 The measured effect of the main integral gain on stability for the body roll motion

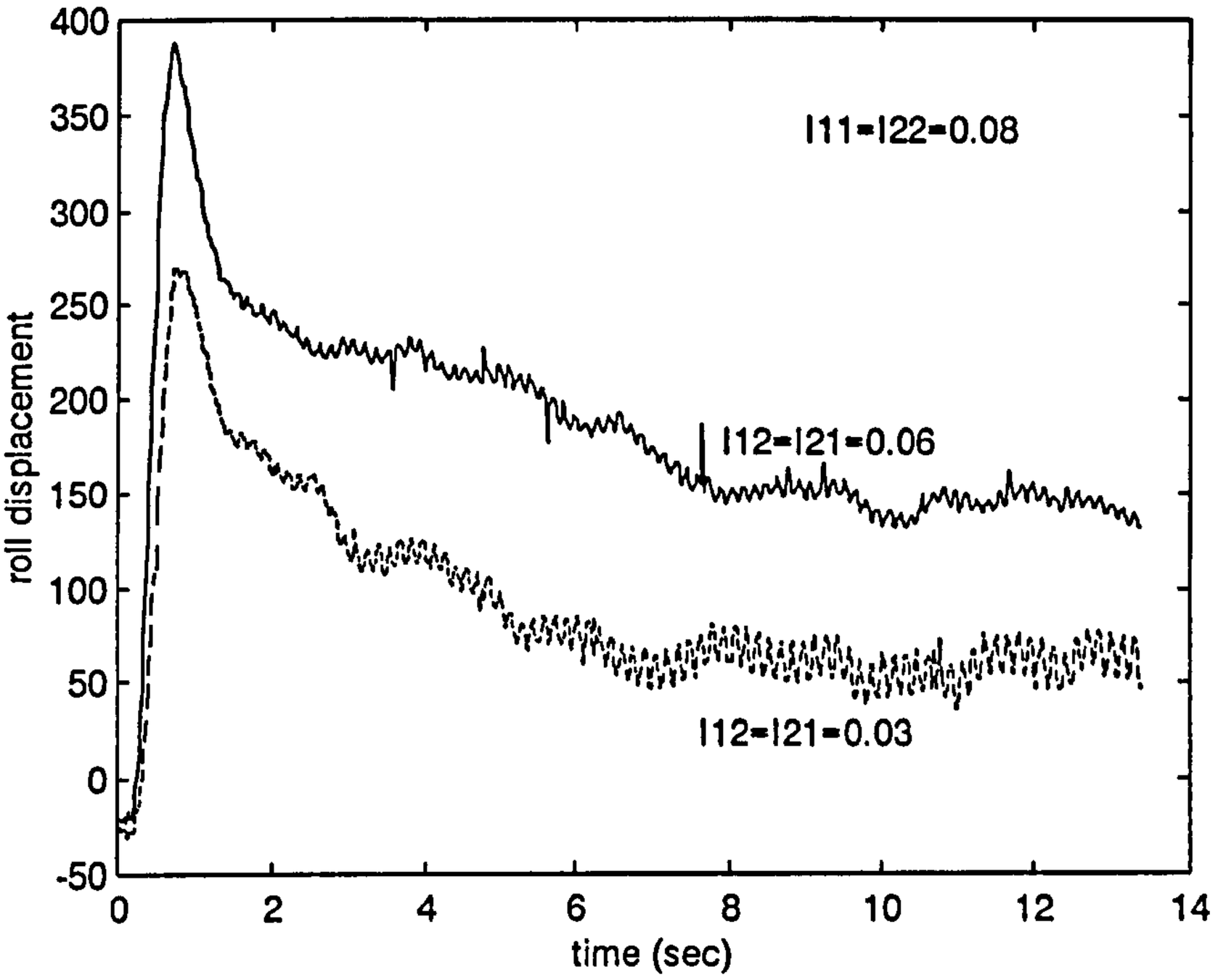

Figure 6-39 The measured effect of the coupled integral gain on stability for the body roll motion

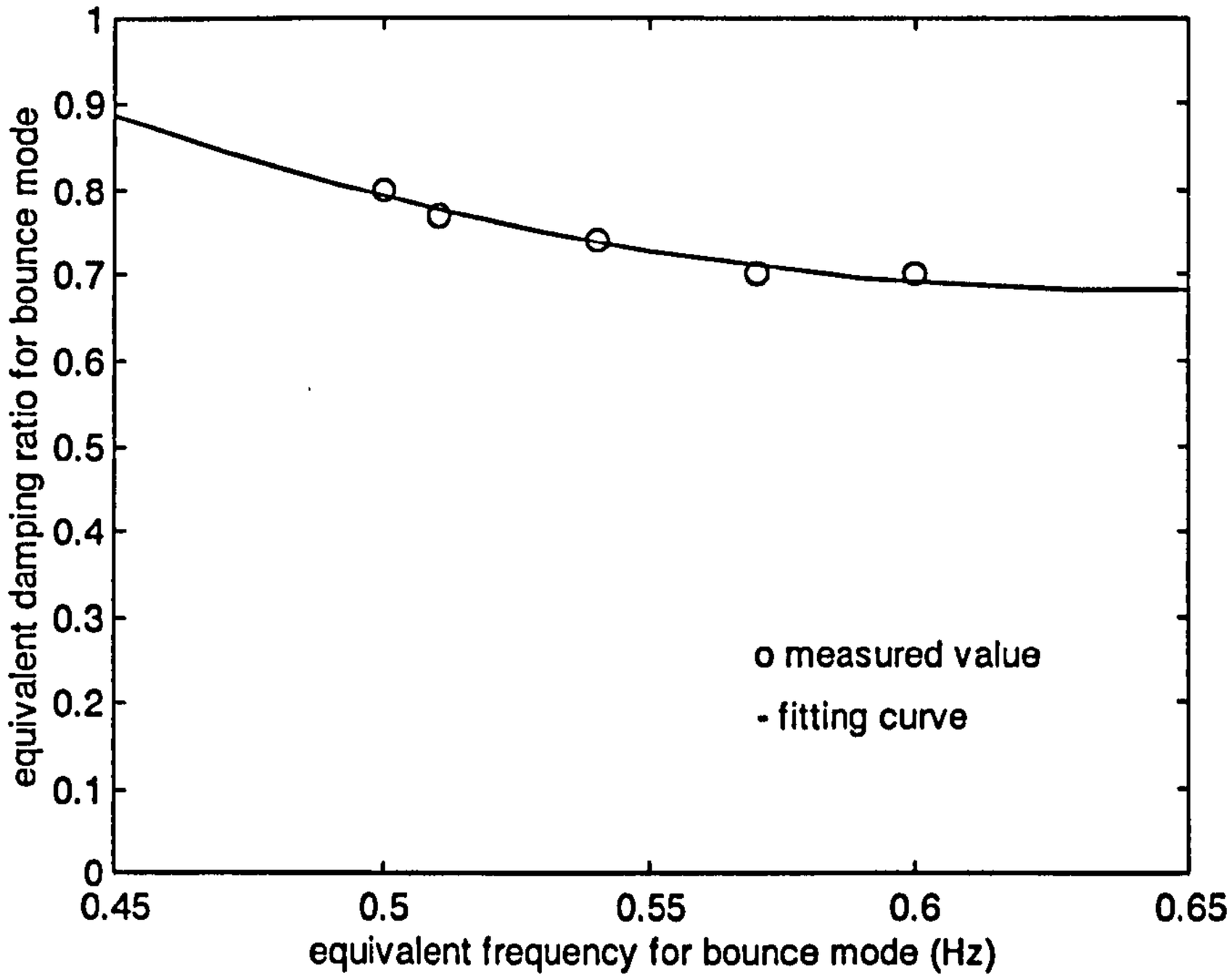

Figure 6-40(a) Measured equivalent damping versus frequency for body bounce mode

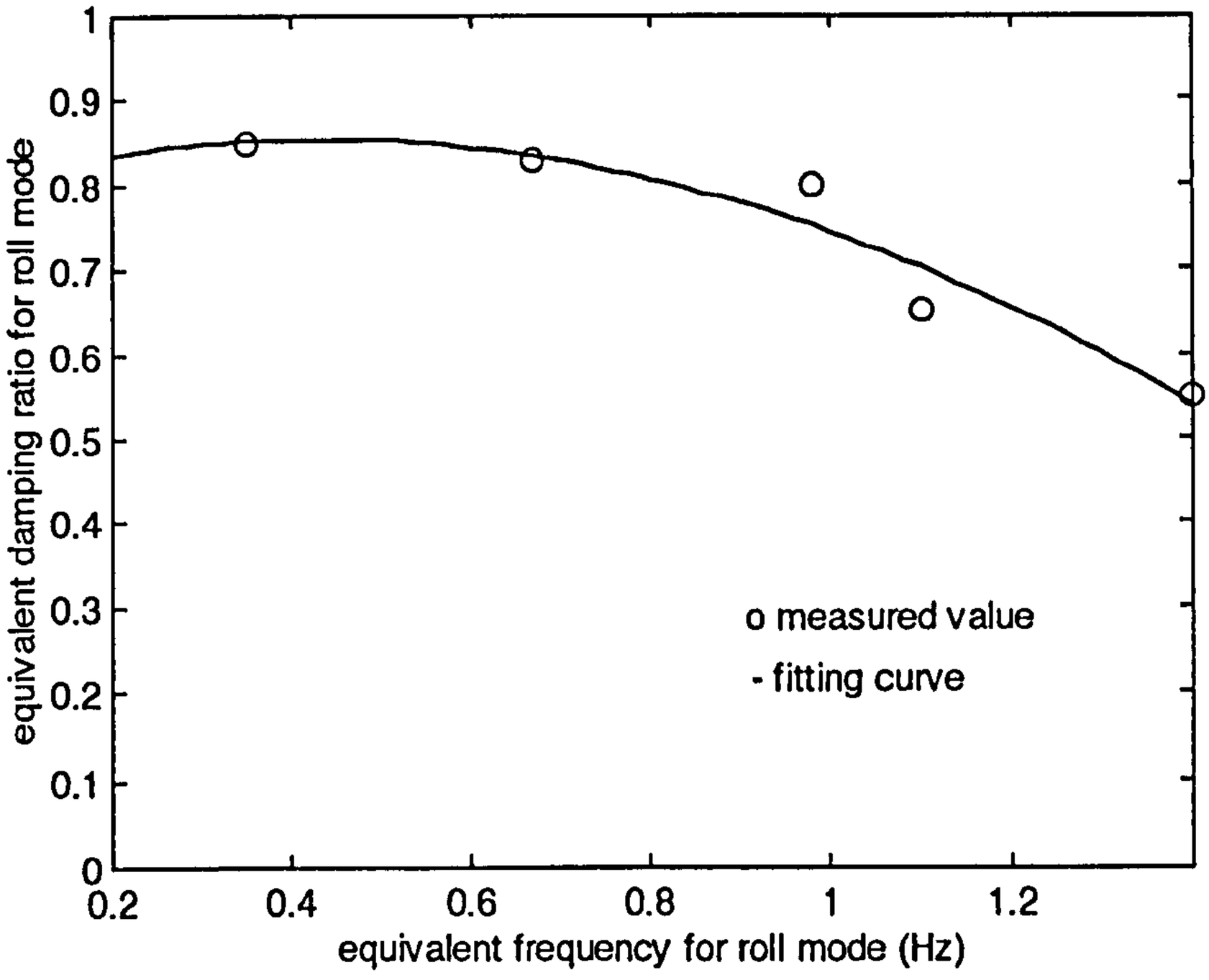

Figure 6-40(b) Measured equivalent damping versus frequency for body roll mode

Chapter 7

Applications of Other Control Strategies and Performance Comparison for the Prototype

7.1 Introduction

Various control strategies have been investigated in the area of active suspension systems for decades. These strategies include LQ optimum techniques, robust optimum control such as H_∞, fuzzy logic, neural network and adaptive control, etc. However, most of the reported investigations have concentrated on theory and simulation. Few applications have been reported in physical prototypes. Of course, theoretical analysis and numerical simulation are both very important but the physical implementation can be more persuasive for a particular system.

In this chapter, fuzzy logic and LQG optimum control strategies are implemented using the active zero rate suspension system hardware. Tests have shown that the implementation for both algorithms is successful though the control performance is not entirely satisfactory. MIMO PID, Fuzzy Logic and LQG optimum controllers are compared with each other for this particular application.

7.2 Application and Implementation of Fuzzy Logic Control on the Active Zero Rate Suspension

As an initial test, fuzzy logic control will be applied to the prototype through a relatively simple model, the quarter car model. The model that will be used in this section is still the same quarter car model as that in chapter 5, i.e.

$$M\ddot{X} + C_d\dot{X} + KX = B_c X_c + BU + G \qquad (7\text{-}1)$$

$$Y = CX \qquad (7\text{-}2)$$

$$F_a = a_0 + a_1 l + a_2 l^2 + (a_3 + a_4 l) y_l \qquad (7\text{-}3)$$

$$\dot{l} + \omega_0 l = \omega_0 u \qquad (7\text{-}4)$$

where the motion equation (7-1), the observation equation (7-2), the equivalent suspension force (7-3) and the actuator bandwidth (7-4) are totally the same as equations (5-1), (5-5), (5-2) and (5-4) respectively. The variables, matrices, coefficients and the block diagram for the open loop system are also the same.

For this quarter car model of the prototype, the body to hub displacement (y_1) and the velocity ($\dot{y}_0$) of the sprung body are employed as the inputs of the fuzzy logic controller and the actuator input signal (u) is the output of the controller, because appropriate body height, stiffness and damping need to be achieved through adjusting the actuator length. The purpose of this two input and one output fuzzy logic controller is to make the sprung body rest at the demanded height with zero velocity and to provide damping to the body. The controller is illustrated in figure 7-1.

The closed loop system with the fuzzy logic controller is shown in figure 7-2. The controller uses the output of the trailer assembly, the error of the body to hub displacement (Δy_1) and the trailer body velocity ($\dot{y}_0$), from which the incremental change of the zero rate suspension input (Δu) is calculated. The displacement error and incremental input change are defined as follows:

$$\Delta y_1(t) = y_1(t) - y_1^* \qquad (7\text{-}5)$$

$$\Delta u(t) = u(t) - u(t-T) \qquad (7\text{-}6)$$

where y_1^* denotes the demanded height of the sprung body, t denotes the time and T is the sampling period.

A fuzzy logic controller is based on a set of rules constructed by logical functions, as in conventional rule-based control; however, fuzzy logic rules are non precise in that they involve linguistic variables. As a result, each variable comparison is with a linguistic term and not a numerical value, so the output is a measure of truth of the comparison as opposed to a binary true or false result.

The block diagram in figure 7-1 has three parts, namely fuzzification, fuzzy logic control rules and defuzzification. For our application, the inputs are in the form of precise measured data, and the controller output is required to be a precise actuator signal. To accommodate this, processes known as fuzzification and defuzzification are added to the controller, which are the conversion between precise input and outputs

and fuzzy sets. In other words, the design of the fuzzy logic controller goes through three stages, i.e. fuzzification, control rules and defuzzification.

In the fuzzification stage, the inputs of the controller are fuzzified into a (finite) number of fuzzy sets with possible membership functions as shown in figures 7-3(a) and (b). The linguistic values for the variables are defined via the fuzzy sets and their associated membership functions. The membership function assigns a number between zero and one to the range of possible values of the variable, called the grade of membership of that value, where zero indicates it is not a member and one represents a complete member. The function can be any shape and can be a continuous function or a set of discrete points. For simplicity in this case, the membership functions were all the same shape -- the triangle.

The body to hub displacement error is described by seven fuzzy sets; these are, Negative Large (NL), Negative Medium (NM), Negative Small (NS), Zero (Z), Positive Small (PS), Positive Medium (PM) and Positive Large (PL). The trailer body velocity is described by three fuzzy sets referred to by Negative (N), Zero (Z) and Positive (P).

The suspension actuator input error (Δu) is fuzzified into seven fuzzy sets with possible membership as shown in figure 7-3(c). The seven fuzzy sets are the same as those of the body to hub displacement error (Δy_1). The defuzzification is done according to this figure.

In figures 7-3(a), (b) and (c), the constants l_{y1}, l_{y2}, l_{y3}, m_{y1}, m_{y2}, m_{y3}, s_{y1}, s_{y2}, s_{y3}, z_{y1}, z_{y2}, n_1, n_2, n_3, p_1, p_2, p_3, z_1, z_2, l_{u1}, l_{u2}, l_{u3}, m_{u1}, m_{u2}, m_{u3}, s_{u1}, s_{u2}, s_{u3}, z_{u1} and z_{u2} used in the definition of the fuzzy sets are chosen according to known information on the ranges of the signals for particular incremental changes to the controller output. These are fixed after practical tests.

Based on these chosen membership functions and the heuristic knowledge gained from the previous research, the fuzzy control rules can be formulated. These are summarised in table 7-1 for various fuzzy controller inputs. Using these, the fuzzy logic controller will give the incremental changes needed for the suspension actuator input ($\Delta u(t)$); this can be added to the previous actuator input ($u(t-T)$) to give the next actuator input using the relation shown in equation (7-6).

It is assumed that the suspension system and controller are required to regulate the body height at set-points for each within a range between 0 to 17cm where the 10cm height is the demanded body position. The actuator input is assumed to be within -5v

to -1.5v. From table 7-1, we can see that there 21 permutations of the fuzzy errors sets for each fuzzy logic controller output. This needs Zadeh's logic 'AND' and 'OR' operations (Virk, 1996) in order to calculate the required incremental control values to maintain the demanded height.

There are seven membership functions of fuzzy output for the actuator input signals and the required fuzzy rules need to be as follows: Rules R_1, R_2, R_3, R_4, R_5, R_6 and R_7 are for determining whether the increment for the actuator input Δu is Negative Large (NL), Negative Medium (NM), Negative Small (NS), Zero (Z), Positive Small (PS), Positive Medium (PM) or Positive Large (PL) respectively.

These rules can be presented as logical statements, for example, R_1 can be written as: **The increment of the actuator input Δu, is Negative Large if Δy_1 is PL AND $\dot{y}_0$ is Z, OR, Δy_1 is PM AND $\dot{y}_0$ is P, OR, Δy_1 is PL AND $\dot{y}_0$ is P.**

These rules mean physically that the actuator input needs to increase or decrease an appropriate amount when the body height is not as demanded and the velocity is not zero.

These rules can be translated into mathematical forms by using fuzzy set theory (Virk, 1996). The 'AND' and 'OR' operations are defined by

$$\mu_A \textbf{ AND } \mu_B = \textbf{min}\{\mu_A, \mu_B\} \quad \text{and} \quad \mu_A \textbf{ OR } \mu_B = \textbf{max}\{\mu_A, \mu_B\} \qquad (7\text{-}7)$$

for any two membership values μ_A and μ_B on the fuzzy subsets A and B respectively.

The defuzzification of the controller output set can be achieved in a number of ways. Two of these are often used. The first is to take the value with the maximum membership value, and the mean of maxima when the maximum is not unique. The second is to take the value at which the membership function has its centroid. The second method was employed here.

The closed loop system with the designed fuzzy logic controller was simulated in terms of the starting response as shown in figure 7-4. This figure illustrates the effect of the sprung body mass on the starting responses. For the heavier mass, the controller leads to bigger over shoot, more steady state error, more delayed starting and shorter rising time.

The centroid defuzzification which was in use sometimes causes steady state error because the precise value of the actuator input does not change when the fuzzy value is 'Z' due to the property of the centroid technique. This resultant error, however, can

be controlled in a small range which is acceptable to the prototype, by adjusting the range of the 'Z' fuzzy member for the body to hub displacement.

The delayed starting results from the unchanged increment for the 'PL' fuzzy control input member. To achieve the stable operation, this increment should be reasonably small, This can give rise to the actuator moving slowly which causes the sprung body with large mass to take time to start moving.

The designed fuzzy logic controller was implemented in the two wheeled trailer with the active zero rate suspension. Figure 7-5 illustrates the measured starting responses on the two sides of the trailer body. It is shown that the implemented fuzzy logic controller can stably lift the trailer body and make it achieve the demanded position with acceptable over shoot. In other words, the implementation has been successful.

Of course, from figure 7-5, it can be seen that the performance of this controller is not ideal. Firstly, the trailer body starting response was delayed for a few seconds, which is consistent with the simulation results. The reason for this has been explained in the simulation analysis.

Secondly, the response starting point for the two body sides are significantly different. In figure 7-5, the left side started moving about 3 seconds earlier than the right side did. This can result in not only a undesirable bounce motion of the trailer body but also a big roll motion in the initial stage, as shown in figures 7-6 and 7-7. The difference can also give rise to the interference between responses on both sides. In figure 7-5, the motion on the left side was excited to an oscillation by the right side starting though the left side has nearly achieved to its steady state.

There are three reasons for the undesirable difference. Firstly, the fuzzy logic controller was designed based on a quarter car model which ignores the roll motion of the trailer body. Secondly, the actual prototype has two sets of suspension systems which do not have identical performance according to measurement results. Finally, the mass distribution of the trailer body is not symmetrical.

It is demonstrated in figure 7-6 that the transient motion of the body bounce was not smooth because of the difference of the starting point on both sides. It can also be found that the damping for the bounce motion was low which is again undesirable. In figure 7-7, it is shown that the trailer body kept a slanting attitude for about 2 seconds due to the starting point difference. The oscillation shows that the damping for the roll motion was even lower than that of the bounce.

As an initial application of fuzzy logic control strategy, the successful implementation in the zero rate suspension is encouraging. Though some aspects of the performance are not ideal, an important factor is that the controller might be a way to overcome the stability boundary due to the coupling between nonlinearity and actuator bandwidth for this prototype. It is still worth investigating the application further because the potential of the fuzzy logic controller has not been fully revealed in this particular test.

To improve the performance, the following modifications are proposed.

- Designing the controller based on the half car model, which will introduce more complexity and more processing time.
- Optimising the fuzzy logic algorithm design.
- Paying more attention to increasing the damping provided by the controller.
- Improving the robustness of the control to asymmetry of the actuator system and mass distribution.

These will require an very extensive investigation of fuzzy logic theory, simulation and experiment for this system.

7.3 Application and Implementation of LQG Controller for the Active Zero Rate Suspension

Optimum control techniques have been successfully applied to control problems in aeronautics and aerospace. One of the distinct approaches is the LQG optimum control strategy. Its application has been investigated extensively for automotive active suspensions but few physical implementation have been reported as mentioned in chapter 1.

Here the half car model shown in equations (6-1) to (6-6) in chapter 6 is still in use. Before using LQG, the mathematical model has to be changed into the standard form because the LQG control theory is based on linear state space equations with some random disturbances and measurement noise.

The first change is that the nonlinear model has to be linearised around an appropriate position. The steady state position -- the demanded body position, can be a good one because the system normally works around this position. That can be realised by introducing two independent local integral controllers, which can result in the trailer

body achieving the required position. Whilst the local controllers can not ensure the stability of the steady state, controllability and observability can still be retained, which allows the added overall controller to stabilise the system. The local integral controllers are shown as follows.

$$u_1 = I_1 \int (y_{11} - y_{11}^*) dt + \bar{u}_1 \tag{7-8}$$

$$u_2 = I_2 \int (y_{12} - y_{12}^*) dt + \bar{u}_2 \tag{7-9}$$

where I_1 and I_2 are the local integral gains. The first terms on the right side is the local controller and $\bar{u}_1$ and $\bar{u}_2$ denote the control input to be produced by the added overall controller. The system with the local controllers is illustrated in the block diagram of figure 7-8.

The equations (6-1) to (6-6) and (7-8) and (7-9) can be linearised about the steady state $\{(y_{11}^* b + y_{12}^* a)/l,\ (y_{12}^* - y_{11}^*)/l,\ 0,\ 0,\ l_1^*,\ l_2^*\}$ where l_1^* and l_2^* are the lengths of the actuators corresponding to the demanded body heights as shown in equation (6-9). To make the model more consistent with the real system, random measurement noise was introduced in the measurement equation. The resultant equations can be written as first order differential equations in the standard state space form, i.e.

$$\begin{cases} \dot{\mathcal{X}} = A\mathcal{X} + B\mathcal{U} + J\mathcal{V} \\ \mathcal{Y} = C\mathcal{X} + \mathcal{W} \end{cases} \tag{7-10}$$

where the state vector

$$\mathcal{X} = \left\{ x_0 \ -\frac{y_{11}^* b + y_{12}^* a}{l} \ \ \theta \ -\frac{y_{12}^* - y_{11}^*}{l} \ \ x_{11} \ \ x_{12} \ \ \dot{x}_0 \ \ \dot{\theta} \ \ \dot{x}_{11} \ \ \dot{x}_{12} \ \ l_1 - l_1^* \ \ l_2 - l_2^* \ \ z_1 \ \ z_2 \right\}^T$$

the output vector

$$\mathcal{Y} = \{ y_{11} - y_{11}^* \ \ y_{12} - y_{12}^* \ \ \dot{y}_{01} \ \ \dot{y}_{02} \ \ l_1 - l_1^* \ \ l_2 - l_2^* \}^T$$

the input vector $\mathcal{U} = \{ \bar{u}_1 \ \ \bar{u}_2 \}^T$

the disturbance vector $\mathcal{V} = \{ \dot{x}_{c1} \ \ \dot{x}_{c2} \ \ x_{c1} \ \ x_{c2} \}^T$

the measurement noise vector

$$\mathcal{W} = \{ w_1 \ \ w_2 \ \ w_3 \ \ w_4 \ \ w_5 \ \ w_6 \ \ w_7 \ \ w_8 \}^T$$

the state space matrix is a 12 by 12 array

$$\mathcal{A} = \begin{bmatrix} 0 & E & 0 & 0 \\ M^{-1}(-K + BF_y B^T) & -M^{-1}C_d & M^{-1}BF_l & 0 \\ 0 & 0 & D & -DK_I \\ B^T & 0 & 0 & 0 \end{bmatrix}$$

the control matrix is a 12 by 2 array $\mathcal{B} = \begin{bmatrix} 0 \\ -D \\ 0 \end{bmatrix}$

the observation matrix is a 6 by 12 array

$$\mathcal{C} = \begin{bmatrix} 1 & a & -1 & 0 & 0 & 0 & 0 & 0 & 0 & 0 & 0 & 0 \\ 1 & b & 0 & -1 & 0 & 0 & 0 & 0 & 0 & 0 & 0 & 0 \\ 0 & 0 & 0 & 0 & 1 & -a & 0 & 0 & 0 & 0 & 0 & 0 \\ 0 & 0 & 0 & 0 & 1 & b & 0 & 0 & 0 & 0 & 0 & 0 \\ 0 & 0 & 0 & 0 & 0 & 0 & 0 & 0 & 1 & 0 & 0 & 0 \\ 0 & 0 & 0 & 0 & 0 & 0 & 0 & 0 & 0 & 1 & 0 & 0 \end{bmatrix}$$

the disturbance matrix is a 12 by 4 array $\mathcal{F} = \begin{bmatrix} 0 \\ M^{-1}B_c \\ 0 \end{bmatrix}$

here

$$F_l = \begin{bmatrix} a_1 + 2a_2 l_1^* + a_4 y_{11}^* & 0 \\ 0 & a_1 + 2a_2 l_2^* + a_4 y_{12}^* \end{bmatrix}$$

$$F_y = \begin{bmatrix} a_3 + a_4 l_1^* & 0 \\ 0 & a_3 + a_4 l_2^* \end{bmatrix}$$

$$D = \begin{bmatrix} -\omega_{01} & 0 \\ 0 & -\omega_{02} \end{bmatrix}$$

$$K_I = \begin{bmatrix} I_1 & 0 \\ 0 & I_2 \end{bmatrix}$$

and E is a 4*4 unit matrix and 0 can be zero or a zero matrix with appropriate size; the matrices M, K, C_d, B, B_c and other variables are the same as those in chapter 6.

The disturbance $\mathcal{V}$ actually represents the excitation from the road profile at the wheels. The measurement noise $\mathcal{W}$ denotes the random electromagnetic disturbance in the measurement components and circuits. Both $\mathcal{V}$ and $\mathcal{W}$ can be looked on as white

noise processes with Gaussian probability density function. Because of the physics of $\mathcal{V}$ and $\mathcal{W}$, they can be thought to be uncorrelated. Then equation (7-10) is the model for designing the LQG controller. The system can described by the typical block diagram of figure 7-9.

The zero state of equation (7-10) corresponds to the demanded trailer body position. In other words, the trailer body achieving the demanded position can be represented through the motion of equation (7-10) approaching to the zero state. Next we will seek a LQG law such that a performance index is minimised.

The most popular performance index is the integral of a quadratic form in the state $\mathcal{X}$ plus a second quadratic form in the control $\mathcal{U}$ (Friedland, 1986), i.e.

$$V = \int_t^{t_p} [\mathcal{X}^T(\tau) Q \mathcal{X}(\tau) + \mathcal{U}^T(\tau) R \mathcal{U}(\tau)] d\tau \qquad (7\text{-}11)$$

where Q and R are symmetric matrices which are often called the state weighting matrix and control weighting matrix respectively. The lower integral limit t is identified as the present time and the upper limit t_p is the terminal time, or final time of the control process.

In the performance index defined by (7-11) two terms contribute to the integrated cost of control: the quadratic form $\mathcal{X}^T Q \mathcal{X}$ which represents a penalty on the deviation of the state $\mathcal{X}$ from the demanded body position and the term $\mathcal{U}^T R \mathcal{U}$ which represents the 'cost of control'. The minimisation of the index means that the total deviation of the state to the demanded position and the total cost of control energy are the minimum during the control process.

The LQG controller is a linear control law, i.e.

$$\mathcal{U}(t) = -\mathcal{G}\mathcal{X}(t) \qquad (7\text{-}12)$$

where $\mathcal{G}$ is a suitable gain matrix. The design of the controller for the state equation (7-10) is to seek a gain matrix in equation (7-12) to minimise a specified performance index V in equation (7-11). B. Friedland (1986) has mentioned the relevant derivation and proof extensively so repetition of these is not needed. Only the main results are presented here.

The optimum control feedback gain for the performance index (7-11) is proved to be

$$\mathcal{G} = R^{-1} \mathcal{B}^T \mathcal{M} \qquad (7\text{-}13)$$

This gives the optimum gain matrix in terms of the solution to the differential equation, i.e.

$$-\dot{\mathcal{M}} = \mathcal{M}\mathcal{A} + \mathcal{A}^T\mathcal{M} - \mathcal{M}\mathcal{B}R^{-1}\mathcal{B}^T\mathcal{M} + Q \qquad (7\text{-}14)$$

This matrix differential equation, one of the most famous in the literature of modern control theory -- the Riccati equation, gives the matrix $\mathcal{M}$ which, using (7-13), gives the optimum gain matrix $\mathcal{G}$.

Equations (7-13) and (7-14) imply that the control weighting matrix R has to be non-singular. That means that all the magnitudes of the control signal $\mathcal{U}$ have to be limited by using the control weighting matrix in the performance index; otherwise the design that emerges is liable to generate control signals that cannot be achieved by the actuators; such 'optimum' result therefore cannot be obtained.

In the application in which the control interval is finite, the gain matrix $\mathcal{G}$ will generally be time-varying even when the matrices $\mathcal{A}$, $\mathcal{B}$, Q and R are all constant, because the solution matrix $\mathcal{M}(t,t_p)$ of the matrix Riccati equation will not be constant. If the control interval is infinite, the terminal time t_p is infinite, so the integration of (7-11) will either converge to a constant matrix $\mathcal{M}^*$ or grow without limit. If it converges to a limit, the derivative $\dot{\mathcal{M}}$ tends to zero. Hence for an infinite terminal time the optimum performance index is

$$V^* = \mathcal{X}^T\mathcal{M}^*\mathcal{X} \qquad (7\text{-}15)$$

where $\mathcal{M}^*$ satisfies the algebraic quadratic equation (sometimes called the algebraic Riccati equation)

$$0 = \mathcal{M}^*\mathcal{A} + \mathcal{A}^T\mathcal{M}^* - \mathcal{M}^*\mathcal{B}R^{-1}\mathcal{B}^T\mathcal{M}^* + Q \qquad (7\text{-}16)$$

and the optimum gain in the steady state is given by equation (7-13) using $\mathcal{M}^*$. The resultant optimum gain is the steady state solution.

The above method to obtain the optimum controller is for the approach of state feedback control. If the state variables can be fully measured, the method can be a good one. In a actual system, however, the state variables cannot often be measured completely, so the mentioned method can not be applied directly. Unfortunately the test rig for this project belongs to this category. According to modern control theory, an appropriate observer has to be developed to estimate the state variables by using output variables.

Because of the measurement noise and the road disturbance, the measured output variables are often noisy. One of the effective estimation methods for this is the Kalman filter which gives the optimum observer and is well known.

The observer can be obtained by

$$\dot{\hat{x}} = A\hat{x} + Bu + K(y - C\hat{x}) \qquad (7\text{-}17)$$

with the observation y given by (7-10) and the control u given by

$$u = -G\hat{x} \qquad (7\text{-}18)$$

where K is the observer gain and $\hat{x}$ is the state vector to be estimated. In a similar way to the control feedback gain, the observer gain can be obtained through optimisation.

We still want to minimise

$$J = E\left\{\int_t^{t'} [x^T Q x + u^T R u] d\tau\right\} \qquad (7\text{-}19)$$

where the difference between (7-11) and (7-19) is that the latter has considered the random disturbances of the measurement and road excitation through the expected value. The performance index (7-19) is minimised by selecting the gain as the Kalman filter gain

$$K = \hat{P} C^T R^{-1} \qquad (7\text{-}20)$$

where $\hat{P}$ is given by the corresponding Riccati equation

$$\dot{\hat{P}} = \hat{P} A^T + A\hat{P} - \hat{P} C^T \hat{W}^{-1} C\hat{P} + F\hat{V}F^T \qquad (7\text{-}21)$$

here $\hat{W}$ and $\hat{V}$ are the spectral densities of the road disturbance and the measurement noise respectively.

For steady state solution, $\hat{P}$ is a constant matrix, the solution of the algebraic Riccati equation, i.e.

$$0 = \hat{P} A^T + A\hat{P} - \hat{P} C^T \hat{W}^{-1} C\hat{P} + F\hat{V}F^T \qquad (7\text{-}22)$$

The Kalman filter is illustrated in the block diagram of figure 7-10. The estimate of the state variables is obtained from the control input and the measurement output.

The design of the LQG controller of the linear system (7-10) has three main points for a steady state solution:

- Using the control law (7-18) and the state vector $\hat{x}$ is the result of the linear observer (7-17).
- Finding the control gain matrix G as the solution of the corresponding deterministic optimum control problem, i.e. through equations (7-13) and (7-16).
- Obtaining the observer gain matrix K as the optimum gain for the corresponding Kalman filter, i.e. through equations (7-20) and (7-22).

The controller and observer can be designed separately, because the separation principle has ensured that an observer designed for a known input can serve to estimate the state of the process for the purpose of the generating the control input. The whole closed loop system is illustrated in figure 7-11. The combination of the observer and controller is called the compensator of the plant -- the original system.

For the particular model of this prototype, the LQG controller can be easily obtained by MATLAB Control System Toolbox when the model is determined. The controller can be given by the function '**lqr**' and the observer can be given by the function '**lqe**'.

The designed controller and observer were connected into the nonlinear system as shown in figure 7-12, which simulates the real prototype. The simulation results are shown in figures 7-13(a) and (b). It can be seen that the controller can produce low frequency to the body bounce and roll motion for the system. The over shoot for the bounce motion is not quite desirable. The design of the controller depends on the selection of the weightings matrices Q and R. How these weightings affect the control performances is very complicated and indirect, a fully understanding of which needs a more extensive investigation into the relationship.

The designed LQG compensator was implemented on the physical test rig. Figures 7-14(a) and (b) illustrate that the prototype with the LQG compensator basically works. The trailer body achieved the demanded position, which means that the introduction of the local integral controllers works to some extent. A low frequency of both the body bounce and roll motion can be achieved by the LQG compensator.

In the implementation and experiment, many drawbacks have been found for the LQG compensator. The first is that the damping for both the body bounce and roll motion is very small, which can be clearly seen in figures 7-14(a) and (b). The reason for this is that the relationship between the control performance and the weighting matrices have

not been fully understood. It is very difficult to do so. The designed controller which showed good damping in simulation could not often be implemented stably.

The second is that robustness of the LQG is not good enough for the actual application. In the experiment, instability often occurred when the weights were not put properly on the trailer or a parameter was changed a little bit. The reason for this is that the design of the LQG controller and observer is based on a pure linear model with a high rank which makes the resultant compensator very sensitive to the change of a parameter. The difference between the linear model and the actual nonlinear system can also give rise to the poor robustness.

The third is that the body height can only compensate for weight change over a very limited range which is not acceptable for real world applications. The problem is caused by the 'cost of control' in the optimum performance index (7-11). To achieve a stable implementation large values in the control weighting matrix have to be used, which results in reduced response to the control input.

The basic functioning of the LQG compensator shows that the methodology of the design and implementation has been correct but it seems from the experimental results that the encouraging predicted performance of the LQG strategy could not be realised with this particular active suspension system. In the author's opinion, the standard performance index (7-11) for the optimum LQG design should be evaluated again to confirm its appropriateness to the actual requirement of automotive suspensions and identify possible improvements.

7.4 Control Performance Comparison on the Prototype

So far, three control strategies, MIMO PID, Fuzzy Logic and LQG optimum control, have been applied to the two wheeled trailer with active zero rate suspension. The methodology for the applications and implementations has been proved experimentally to be correct. Of course, the performance of these control strategies vary considerably.

The evaluation standard for the comparison is the vital requirement of automotive suspensions, i.e. the damping for the body bounce and roll motions and the vibration transmission from the road input to the trailer body. The comparison will be based on the measured results.

Figure 7-15 illustrates the free vibration of the trailer body bounce motion measured for the three control strategies. It can be seen that the PID can provide the biggest damping of the body bounce motion. The fuzzy logic can produce less damping of the bounce motion than the PID and the LQG control gives the smallest damping. This means that the MIMO PID controller can make the zero rate suspension attenuate most effectively the body bounce which is caused by steering, acceleration or other excitations.

Figure 7-16 demonstrates the measured free vibration of the trailer body roll motion for the three control strategies. It is shown that the MIMO PID controller can again provide the biggest damping of the body roll motion. And again, the fuzzy logic controller can give less damping of the body roll motion than PID. The damping produced by the LQG control in the body roll motion is even worse than that in the bounce motion for the same control strategy. This shows that the MIMO PID controller can make the zero rate suspension damp out most effectively the body roll vibration for the same reasons as the bounce motion.

The vibration transmission from road excitation input to the trailer body via the wheel and suspension is another primary ride comfort performance of a suspension. The transmission can be evaluated by means of the frequency response functions. These have been measured for the three control strategies by using the developed transfer function identification system.

The frequency response functions for the trailer have been measured using the developed frequency response measurement technique presented in chapter 3. These real results are shown in figures 7-17 and 7-18. Figures 7-17 shows the resultant frequency response functions for the vibration transmission from the road input on the right wheel to the right side of the trailer body. It can be seen that the fuzzy logic controller gives equivalent transmission gain to the PID controller but the LQG results in about 5dB higher vibration gain due to its much lower damping when the excitation frequency is below about 1Hz. When the excitation frequency is between about 2.5Hz and 6Hz, the transmission gains for both fuzzy logic and LQG are 8dB higher than that of the PID. When the excitation is between about 8Hz and 12Hz (the wheel mode is in this region), the transmission gain of the PID is 15dB lower than those of the fuzzy logic and the LQG controllers.

The lateral mode at about 6Hz always exists for the three controllers. The only difference is the peak of the mode occurs at the slightly different frequencies. The height of the peak for the PID is the highest which is about 7dB higher than that for

the LQG and is about 3dB higher than that for the fuzzy logic. These peaks are not insignificant, but were not included in the model used to develop the controllers. This lateral mode is considered worthy of further investigation because of its significant effect on vibration transmission.

When the excitation frequency is between about 1Hz and 2.5Hz, the transmission gain for the fuzzy logic is about 8dB higher than those for both the PID and LQG. The reason for this is that the low level of damping resulted in the trailer body shaking for quite long time on the rubbers in the mechanical components during the measurement of the frequency response. So this does not mean very much for the transmission performance of the fuzzy logic controller. This phenomenon also occurred in the measurement of the frequency response function for the vibration transmission from the road input on the left wheel to the right side of the trailer body, as shown in figure 7-18, which resulted in the transmission gain of the fuzzy logic being higher than those of the PID and the LQG between about 1Hz and 2.5Hz.

In figure 7-18, the transmission gain for the LQG is about 12dB higher than that of the PID and 9dB higher than that of the fuzzy logic when the excitation frequency is below about 1Hz. The reason for this is the poor body roll mode damping produced by the LQG controller. When the excitation frequency is between about 2.5Hz and 6Hz, the transmission gains for both the LQG and fuzzy logic controllers are about 12dB higher than that of the PID. When the excitation frequency is between about 8Hz and 12Hz (the wheel mode is in this region), the transmission gain for the PID is about 15dB lower than those of the LQG and fuzzy logic.

Around the frequency of the lateral mode, the peaks of this mode occur at slightly different frequencies. The gain of the peak for the PID is about 3dB higher than that of the fuzzy logic and 5dB higher than that of the LQG. In a similar way to the right to right transmission in figure 7-17, the lateral mode at about 6Hz still affects the left to right transmission performance significantly. The reason for this is again that the controller based model did not include the lateral mode.

Ease of implementation is another factor in the evaluation of a control strategy. The related characteristics are shown in table 7-2 for the three control strategies. It can seen that the memory which the executable control program and the input parameters take up are equivalent for the controllers. The memory for the PID controller is slightly higher than those of others because the control program for the PID has the capability for on-line parameter adjustment by using interrupt techniques. If this were

not present, the memory requirement for the PID program would be less than for the others.

The execution time lasting for the control signal processing loop presented in table 7-2 for the three controllers. The time for the PID is about 1.1ms, the fuzzy logic 2.2ms and the LQG 7.8ms. The short execution time per loop means that you can use the processor with a low CPU speed because normally the suspension requires only about 10ms sampling period. This therefore can reduce the cost of the control hardware. From this point of view, the PID performs the best and the fuzzy logic is better than the LQG.

On-line parameter adjustment has been implemented in the PID control software by using the interrupt technique. This feature could also be added into the software for the fuzzy logic control if necessary, but for the LQG control program, on-line parameter adjustment can not be included because the parameters are only indirectly related to the control performance and the compensator has to be created by a complicated program. This makes its engineering application inconvenient.

The robustness of the PID controller is very good. The parameters in the PID can be changed over a large range with the suspension remaining stable and reasonable changes in the mass or its distribution do not significantly affect the stability. The stable parameter region for the fuzzy logic is not as large as that of the PID. The LQG controller has the worst robustness. The suspension often becomes unstable even when the body mass or its distribution changes very little. Sometimes the suspension with the LQG which had worked well would become unstable after few weeks became unstable necessitating redesign of the controller and observer. This behavior therefore makes the implementation of the LQG control much more difficult than for the others.

The suspension with the PID controller can keep the trailer body in the demanded position with a range of mass and mass distribution. When the mass or its distribution changes, the body responds very little, quickly and smoothly. The suspension with the fuzzy logic can keep the demanded position as well but the transient motion of the body is not satisfactory because the body mode damping and frequency results in the body responding slowly with large amplitude. The suspension with the LQG control acts nearly as a passive low stiffness spring, which results in the suspension failing to maintain the same position. This poor level of adaptiveness for the LQG is not acceptable in real applications.

On the whole, it has been shown that the PID controller provides the best performance for the zero rate suspension. Fuzzy logic needs more extensive investigation to obtain better performance. The LQG, however, has not been shown to have any benefits worthy of further investigation.

7.5 Conclusions

The fuzzy logic and LQG control strategies have been applied and implemented on the two wheeled trailer with the active zero rate suspension. The experimental results have shown that the implementation is successful though there are some performance shortcomings in both control systems. That at least demonstrates that the methodology and control software were correct for the application.

The zero rate suspension with fuzzy logic control can achieve the demanded position for various mass and mass distribution stably and with low body mode frequencies, but can not produce high damping in the body modes. The other main drawback is that the body lifting was delayed for a unacceptably long time. However, this is only an initial application so the potential performance has not been fully revealed. To develop its encouraging points, the application of the fuzzy logic needs to be investigated extensively for this particular application.

The LQG control strategy applied to the zero rate suspension did not show merit. The controller results in the suspension working nearly like a passive spring with low stiffness which can only produce a low natural frequency in the body modes but can not provide high damping and adaptive body position to the change of mass or mass distribution. The robustness of this controller is poor and the implementation is difficult and inconvenient. The results of applying LQG on the prototype have not yet shown any point from which the investigation is worth continuing.

Performance and implementation comparison for the MIMO PID, LQG and fuzzy logic control strategies has been made in this chapter for the zero rate suspension. It has been shown that the PID controller provides the best performance, good vibration isolation and quite high damping and good adaptiveness to the mass change, and the easiest implementation due to its good robustness and simple algorithm. The PID therefore can be a good candidate for the real application in the prototype.

		body to hub displacement error						
		NL	NM	NS	Z	PS	PM	PL
sprung body velocity	N	Δu=PL	PL	PM	PS	Z	NS	NM
	Z	PL	PM	PS	Z	NS	NM	NL
	P	PM	PS	Z	NS	NM	NL	NL

Table 7-1 Fuzzy logic control rules for the controller output errors

	memory for program and input data	execution time per loop	parameter adjustment	robustness	adaptiveness to mass change
PID	125kb	1.1ms	on-line	very good	very good
fuzzy logic	103kb	2.2ms	can be on-line	quite good	quite good
LQG	107kb	7.8ms	off-line	poor	poor

Table 7-2 The implementation performance for the three control strategies

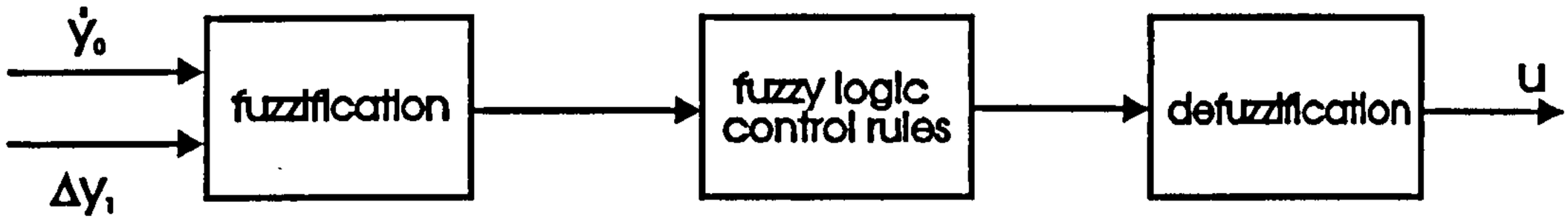

Figure 7-1 The architecture of fuzzy logic controller

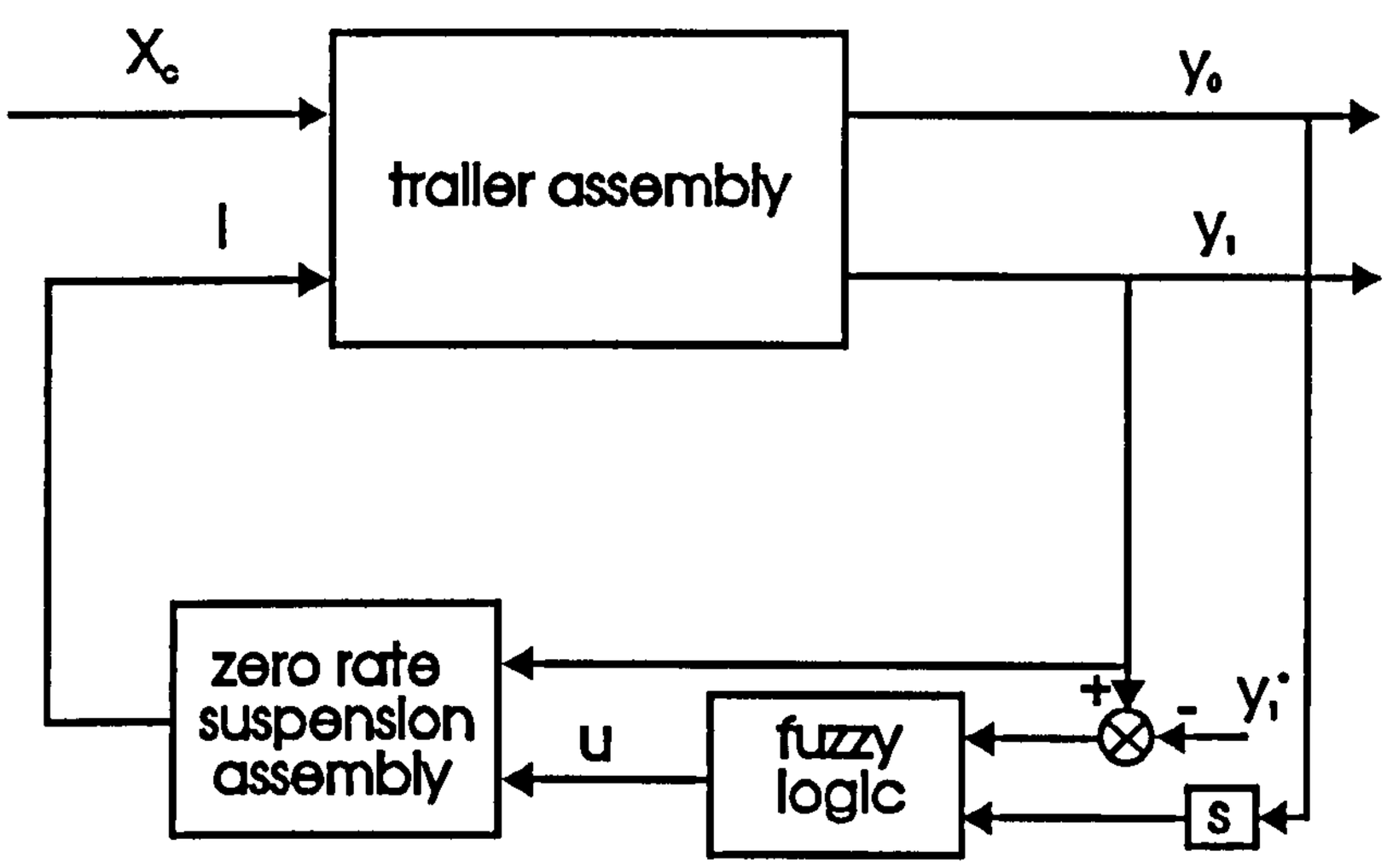

Figure 7-2 The block diagram of the closed loop system for the prototype with the fuzzy logic controller

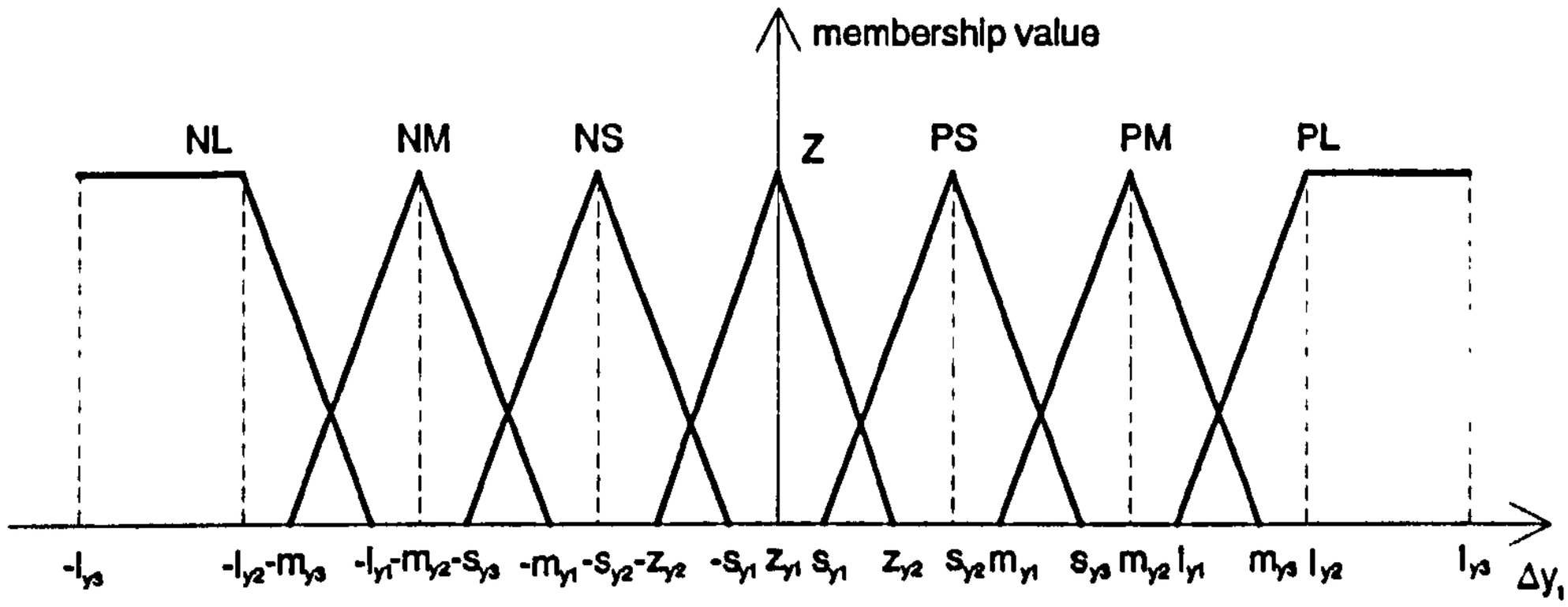

Figure 7-3(a) Fuzzy subset for incremental displacement

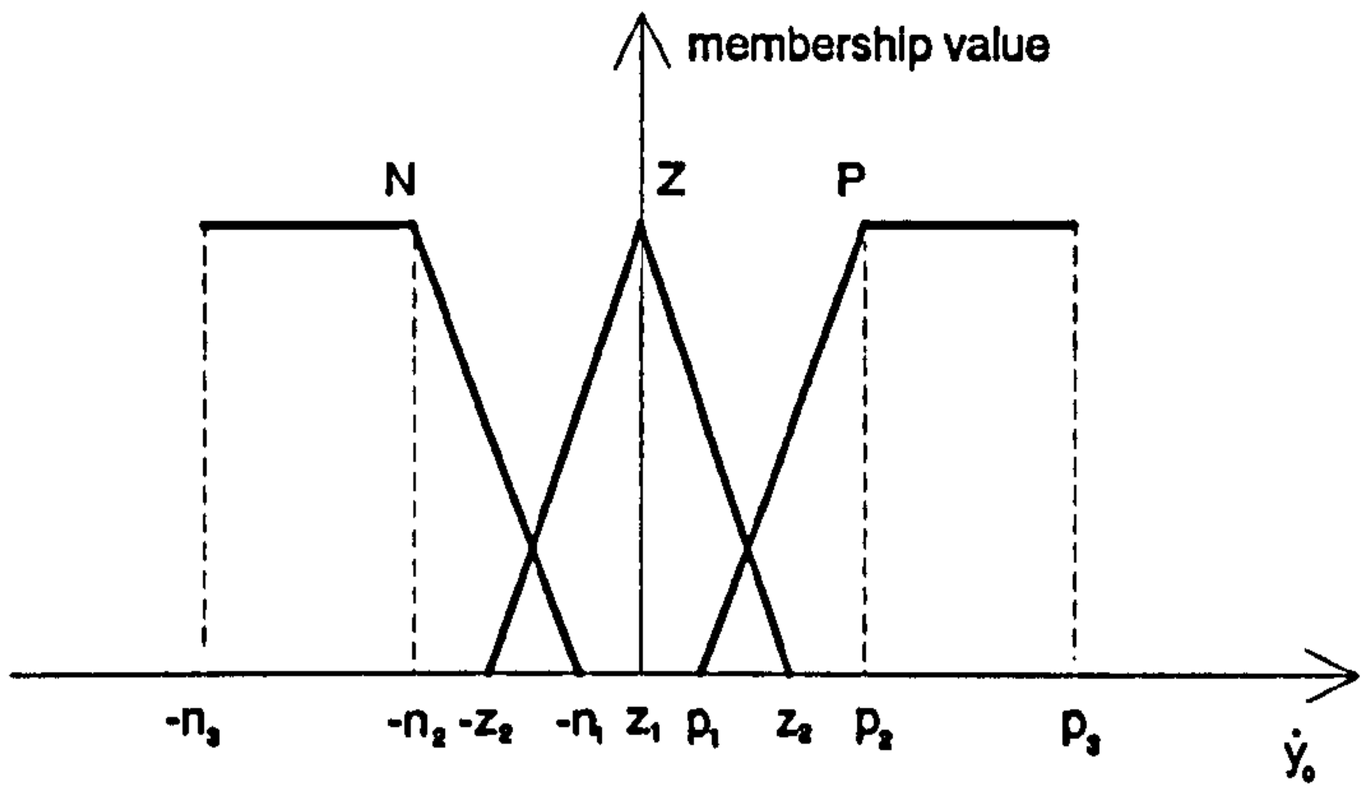

Figure 7-3(b) Fuzzy subset for body velocity

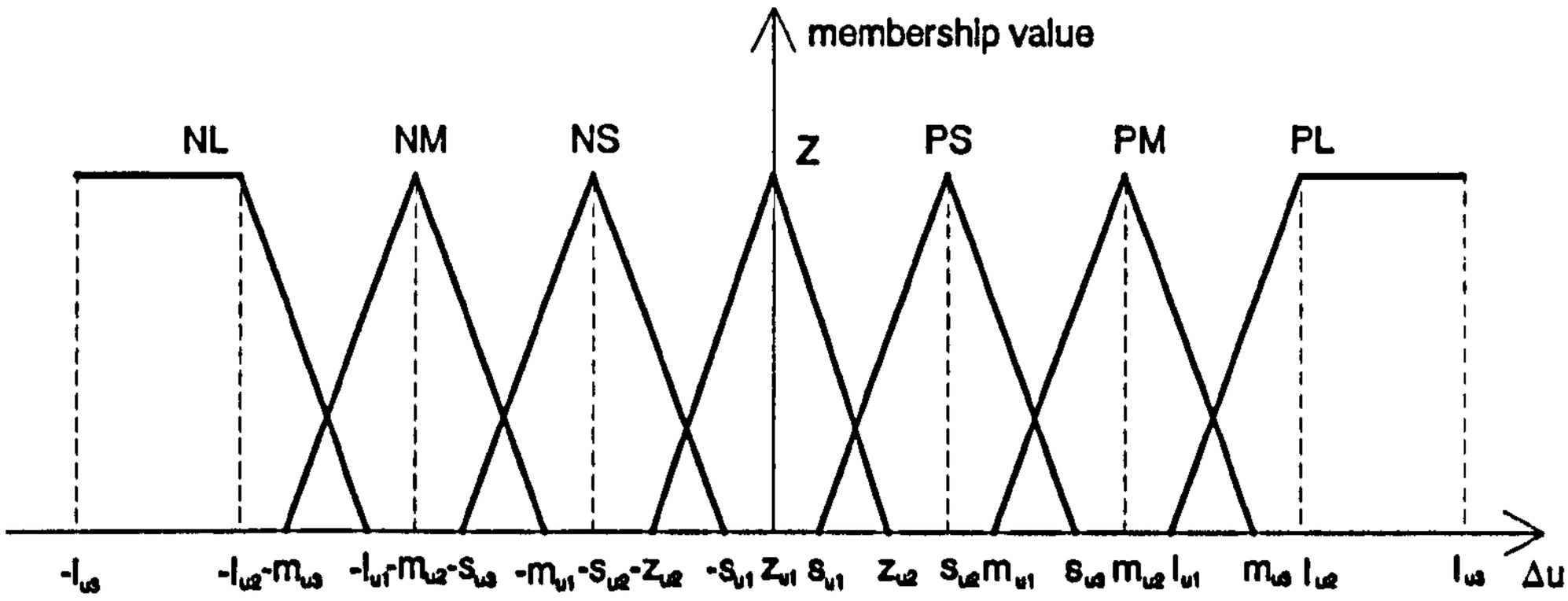

Figure 7-3(c) Fuzzy subset for incremental control input

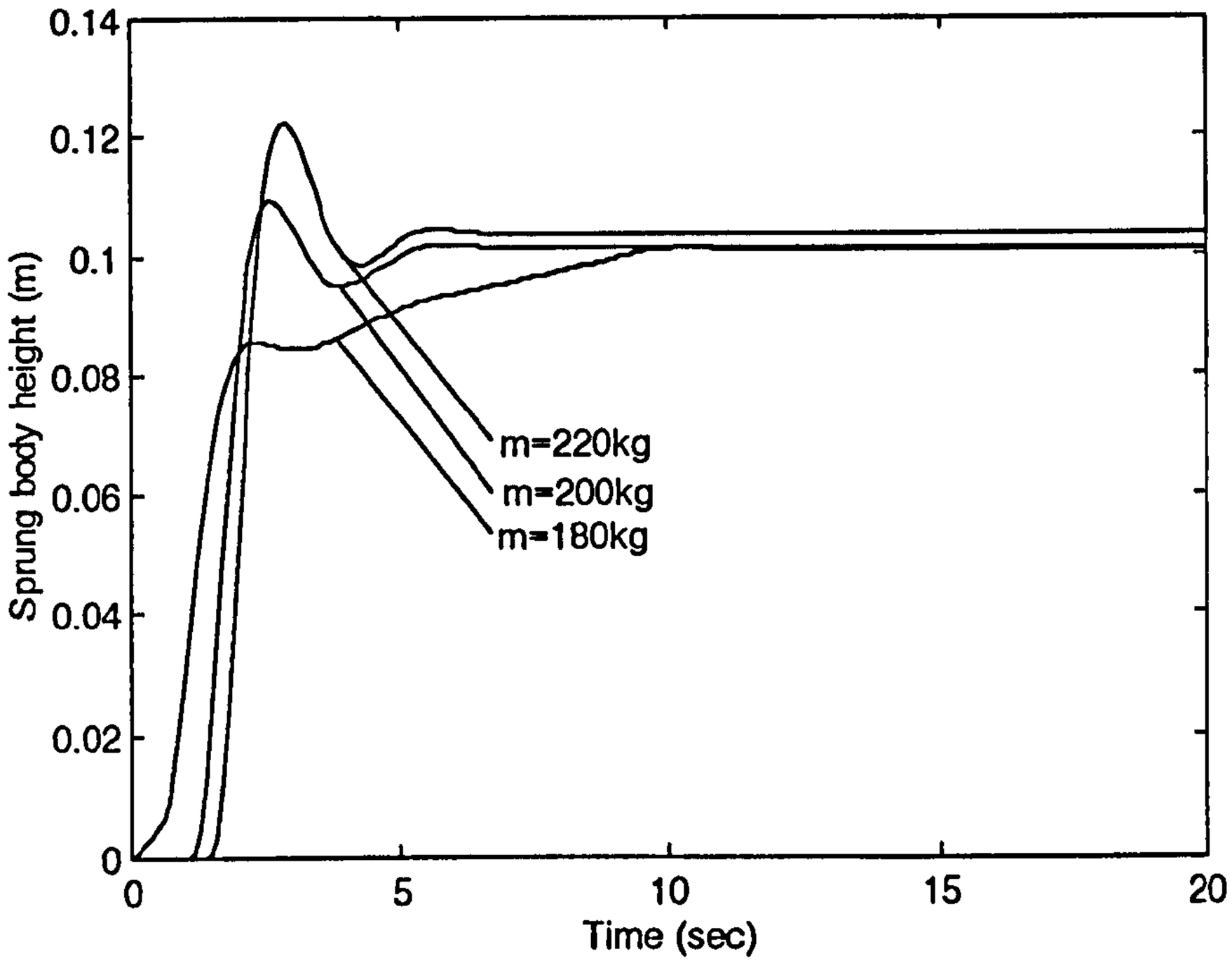

Figure 7-4 The simulated starting response of the fuzzy logic controller for various sprung body masses

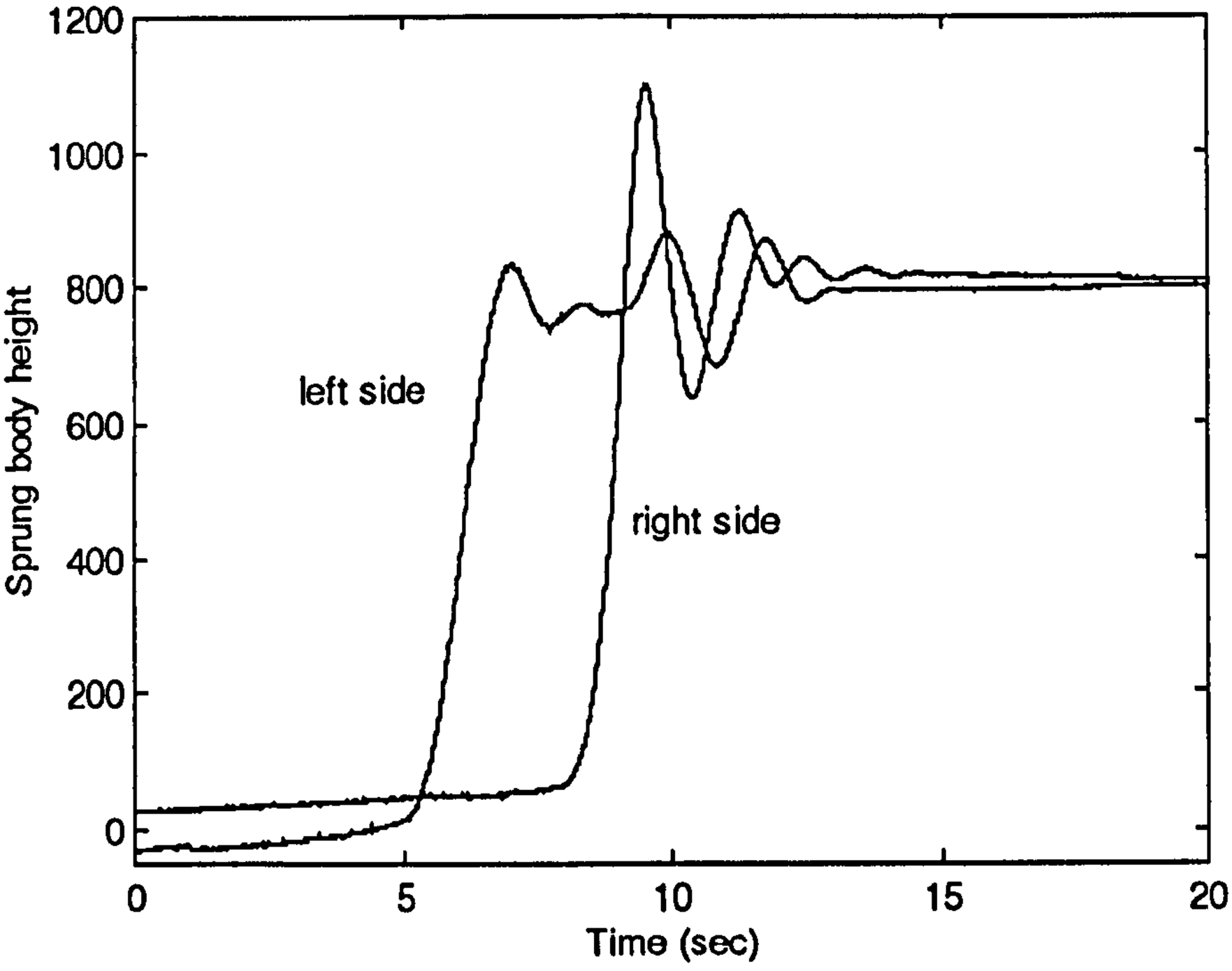

Figure 7-5 The measured starting response on two trailer body sides for the fuzzy logic controller

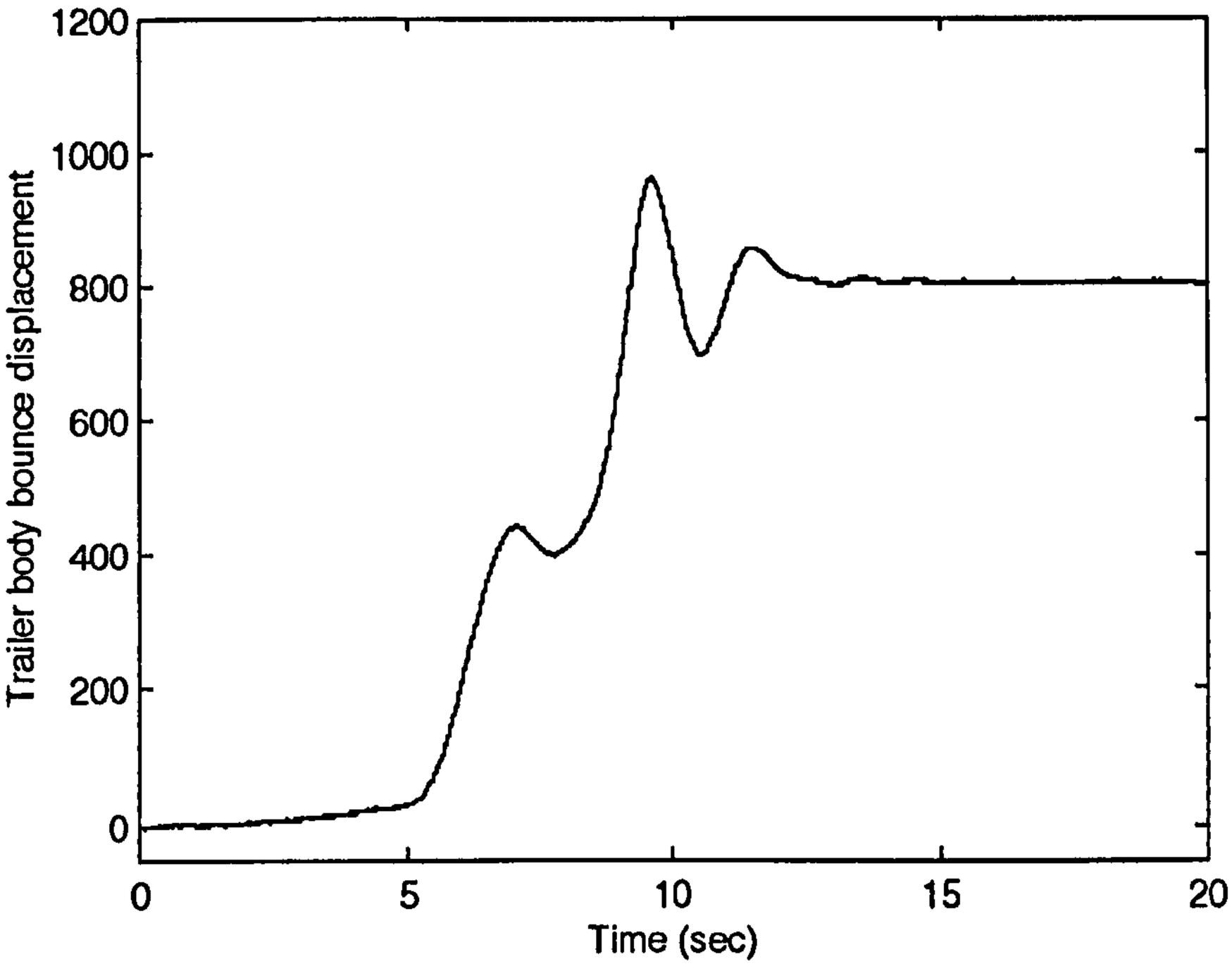

Figure 7-6 The measured starting response of the trailer bounce motion for the fuzzy logic controller

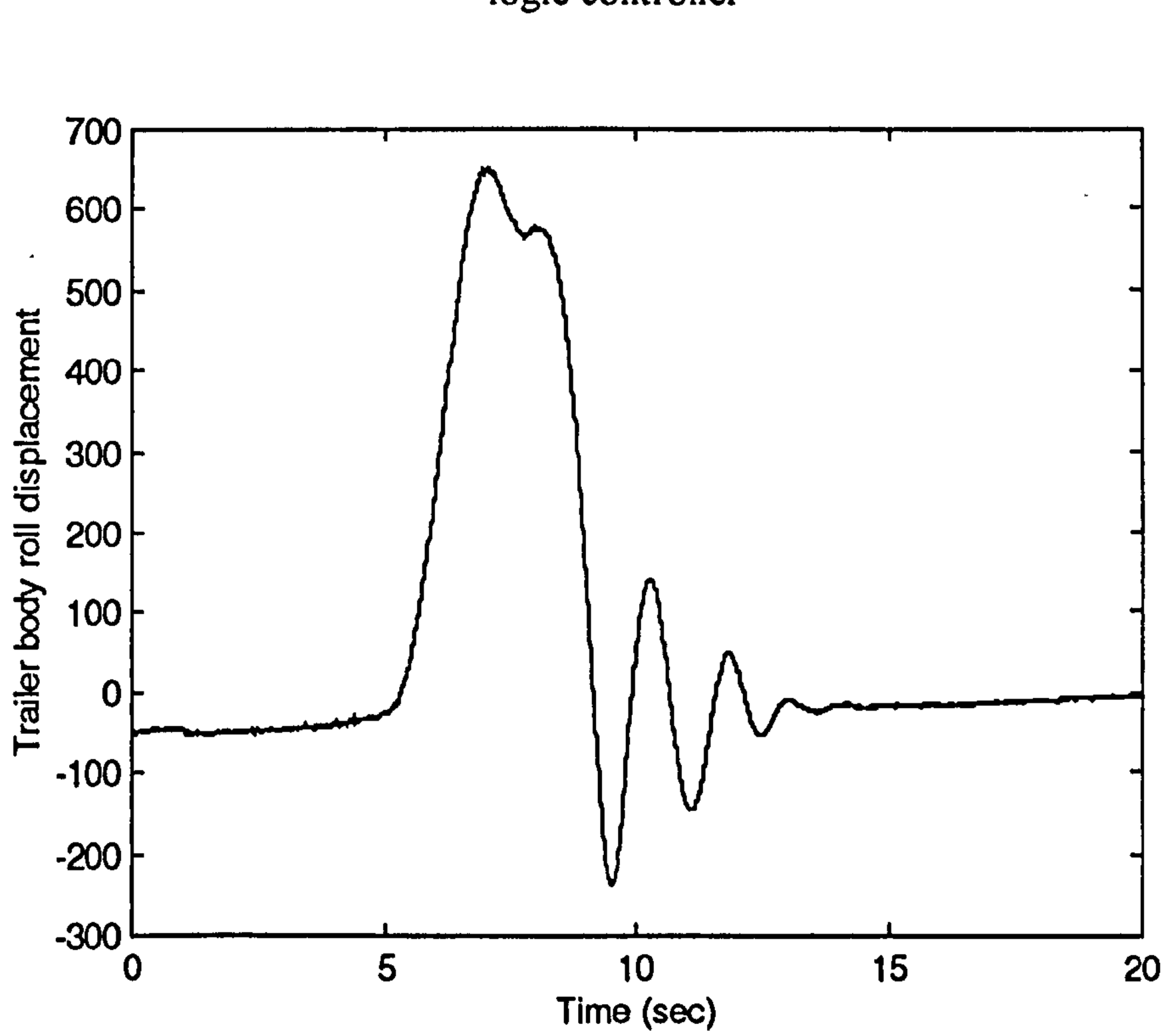

Figure 7-7 The measured starting response of the trailer roll motion for the fuzzy logic controller

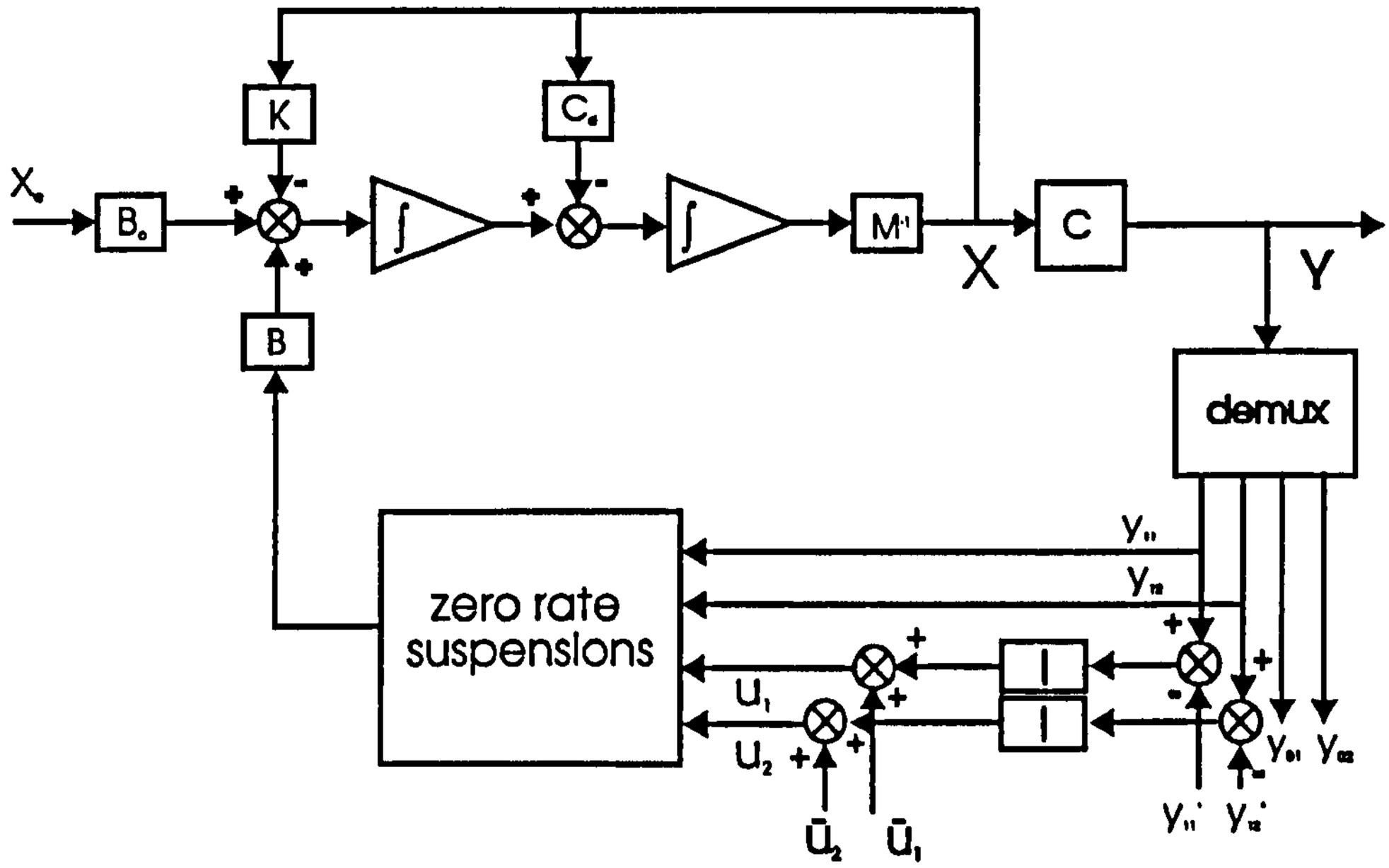

Figure 7-8 Block diagram of the system with local integral controllers

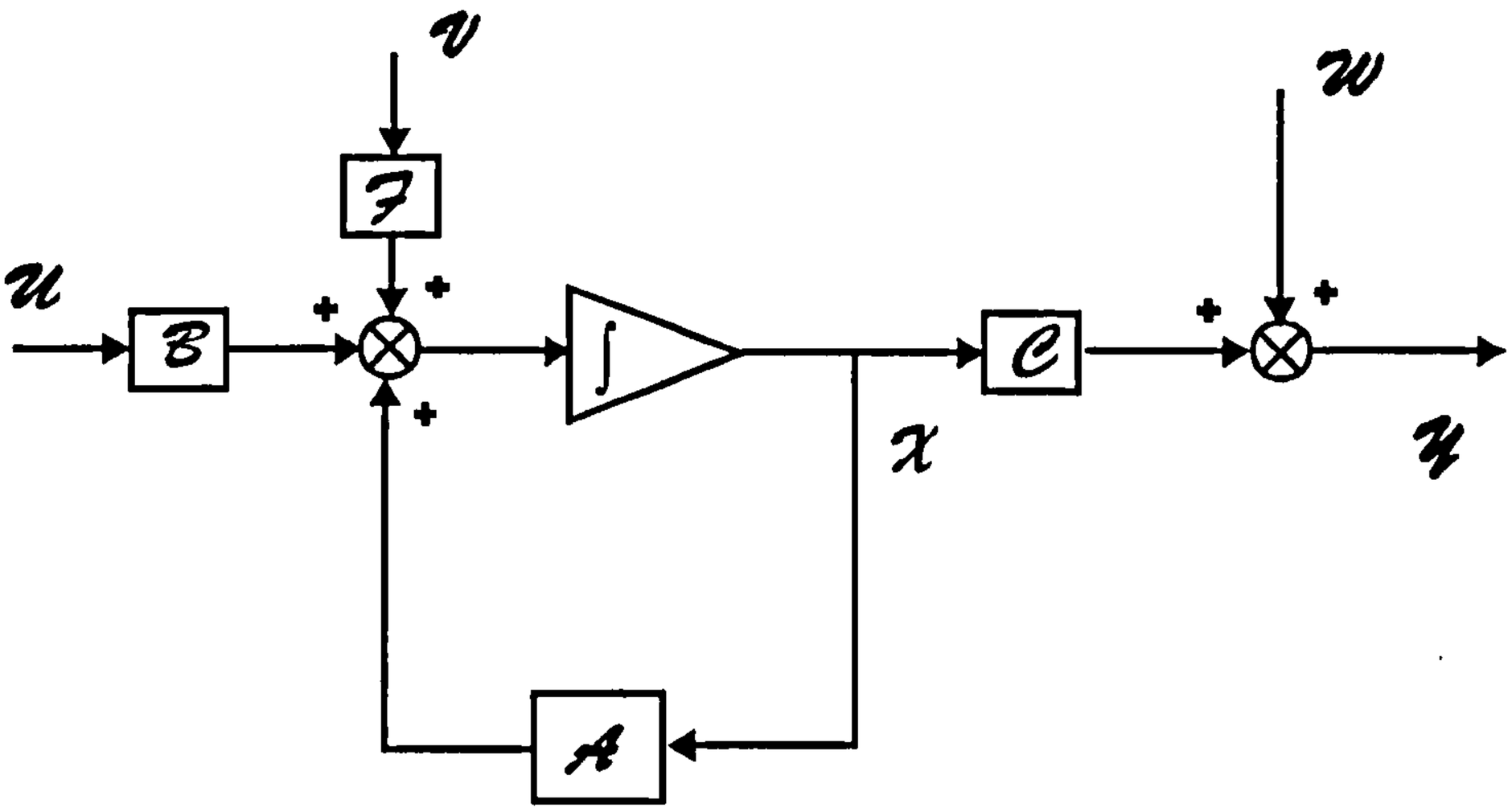

Figure 7-9 Block diagram of the standard state space expression for the linearised system with local integral controller

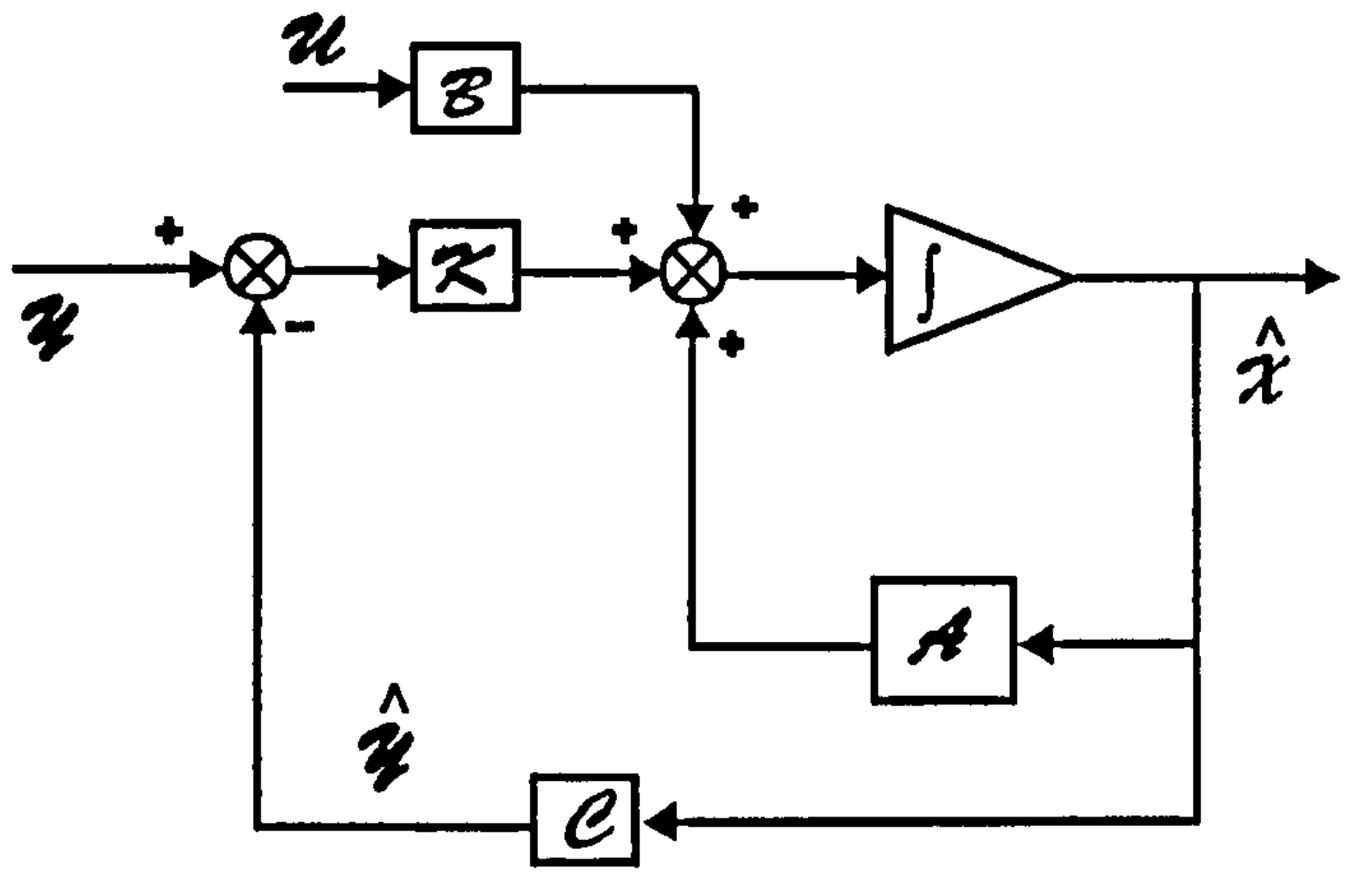

Figure 7-10 Block diagram of the optimum observer -- Kalman filter

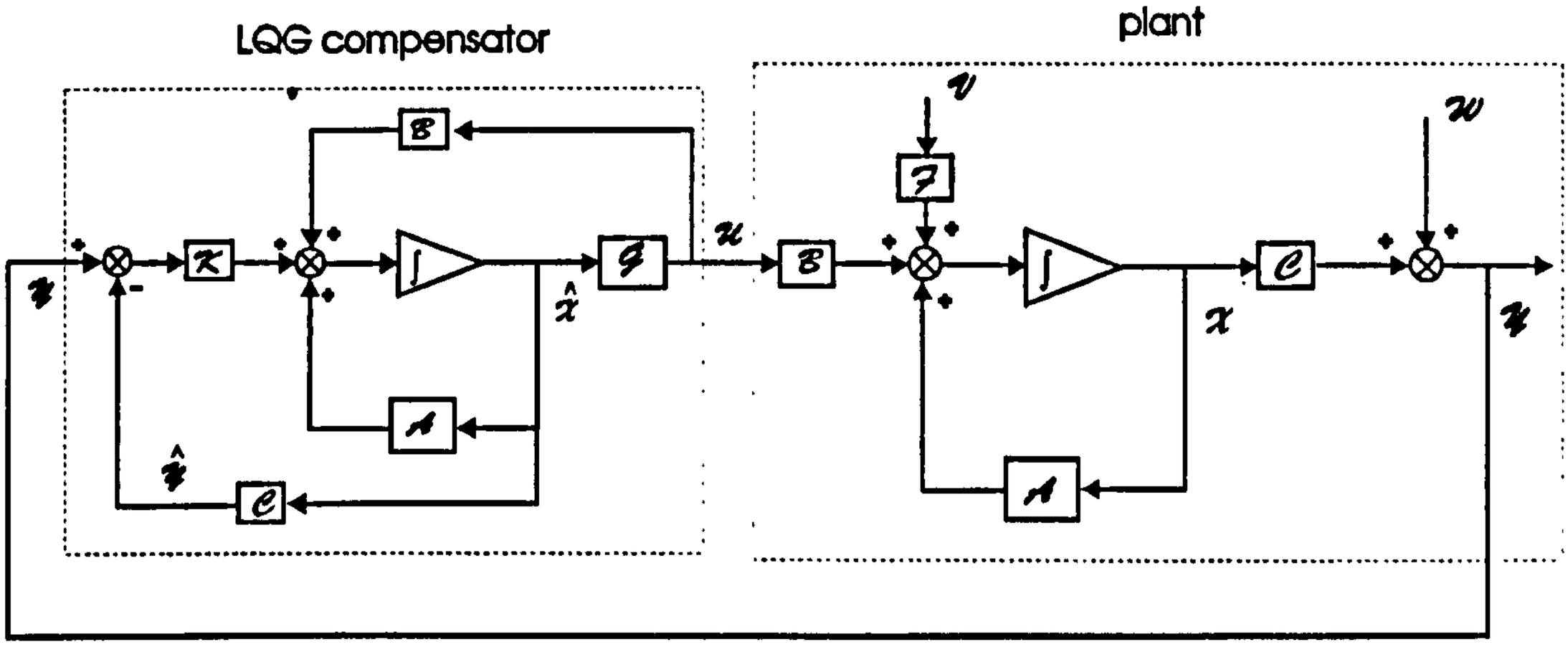

Figure 7-11 Block diagram of the closed loop system with LQG compensator

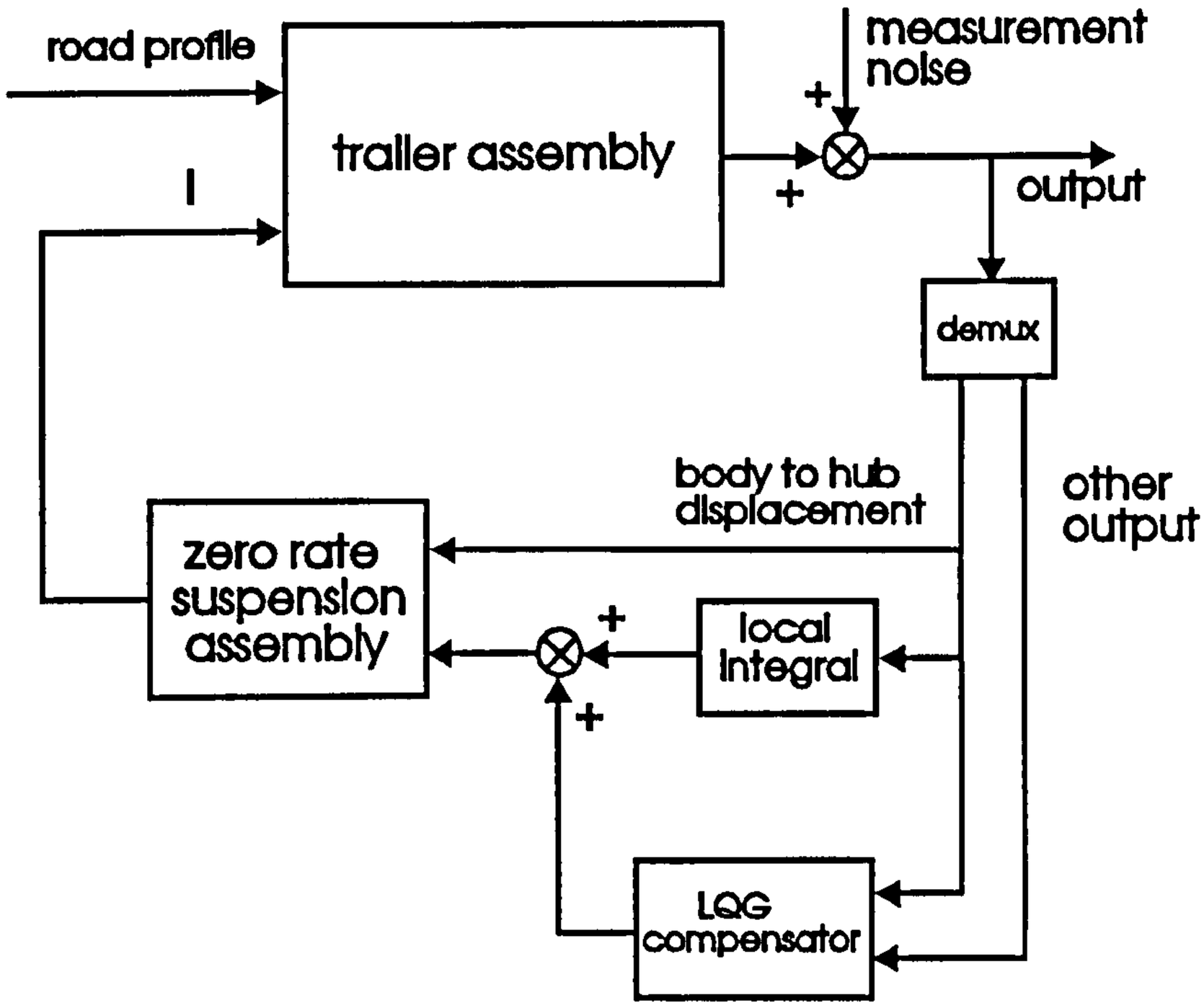

Figure 7-12 Block diagramof the nonlinear prototype with local integral controllers and the overall LQG compensator

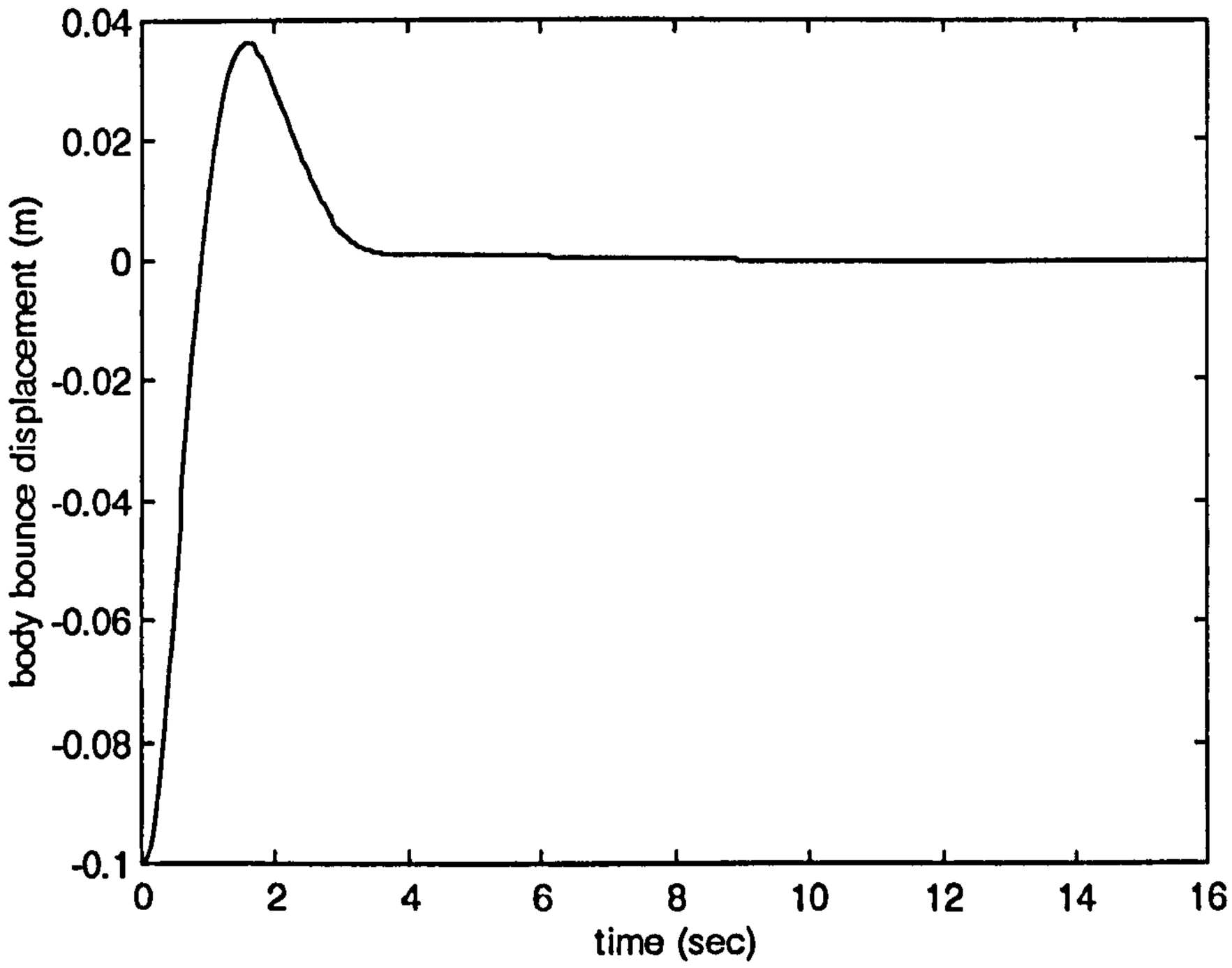

Figure 7-13(a) The starting response for the body bounce motion with LQG compensator

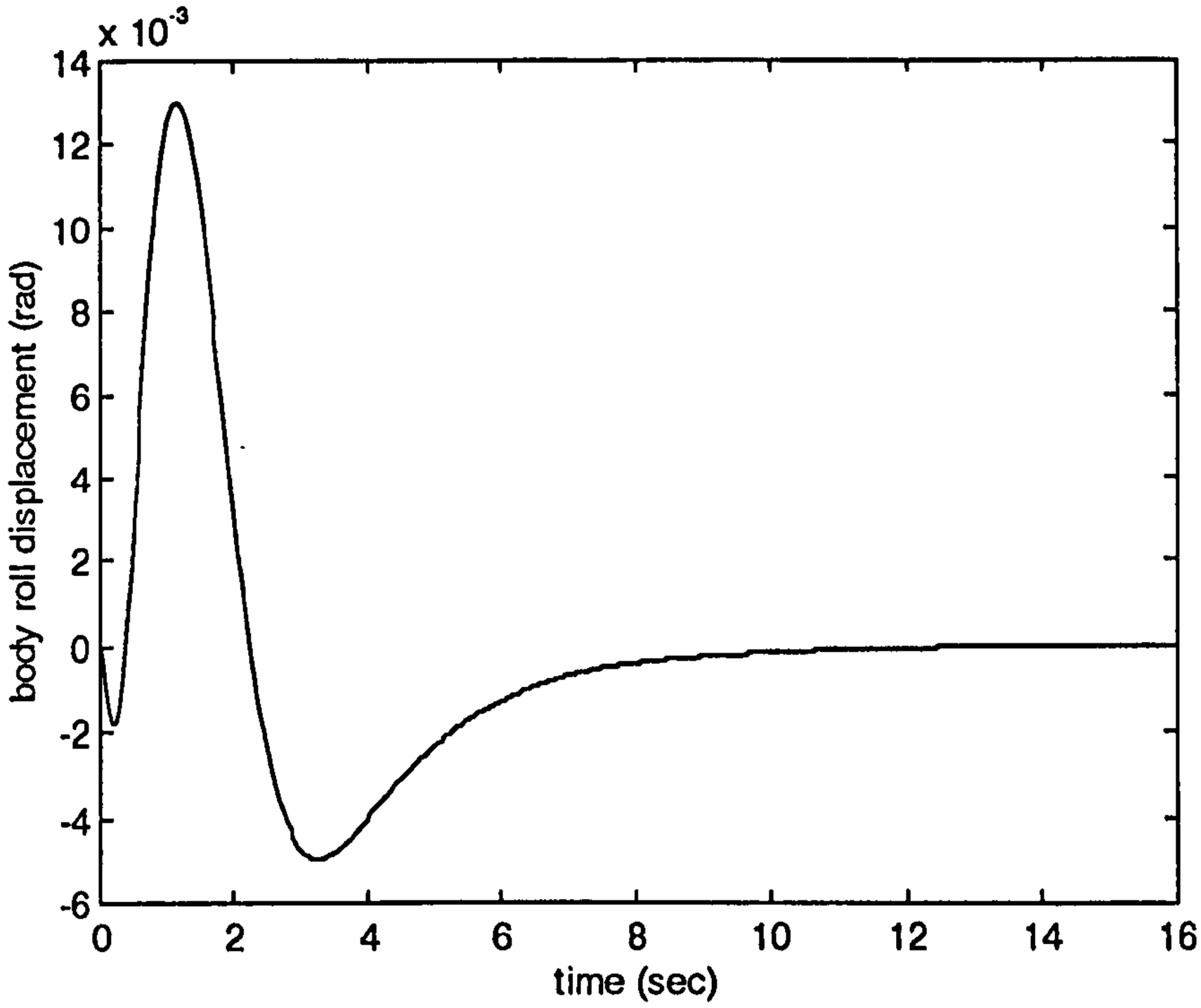

Figure 7-13(b) The starting response of the body roll motion with LQG compensator

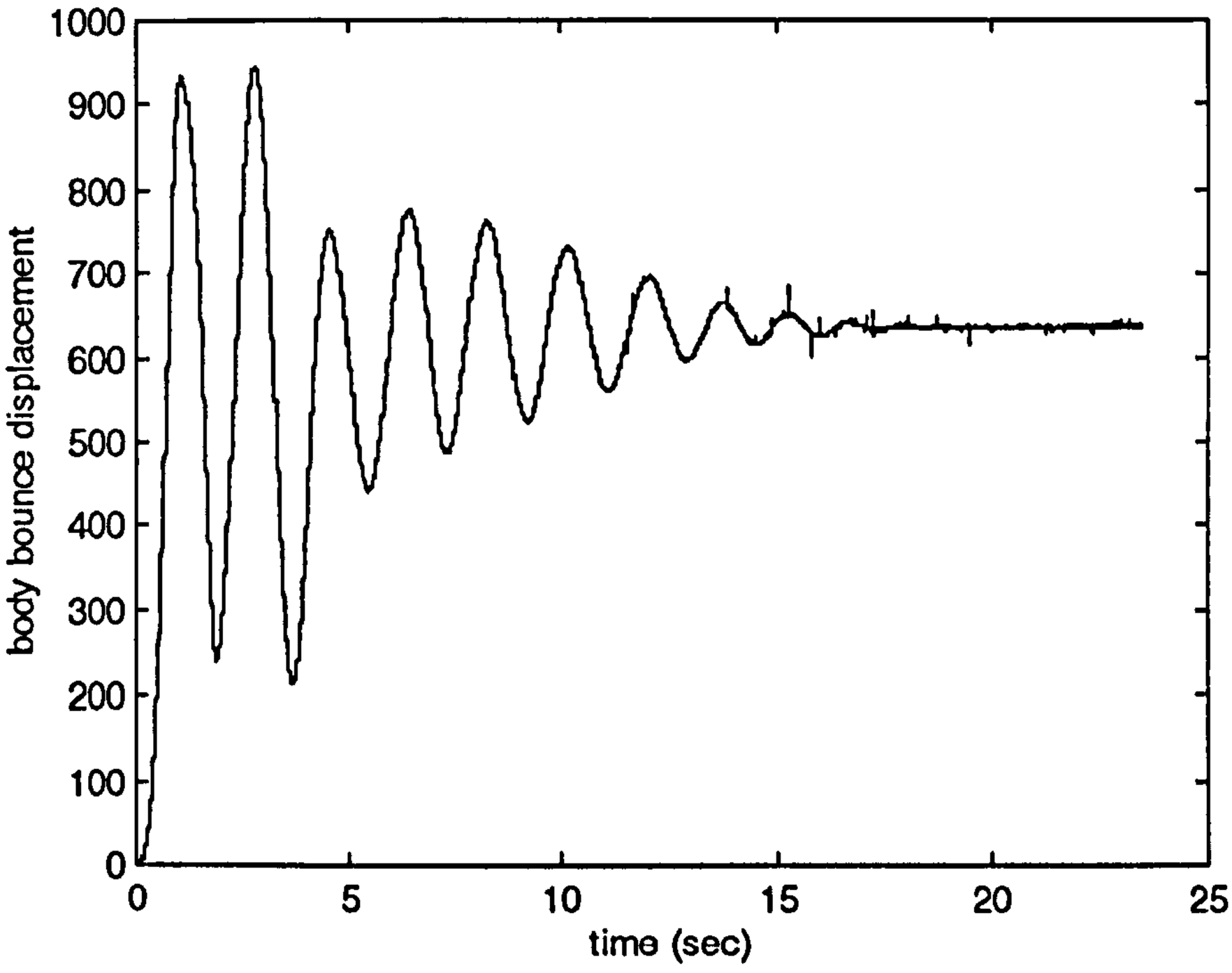

Figure 7-14(a) The measured starting response for the body bounce motion with LQG controller

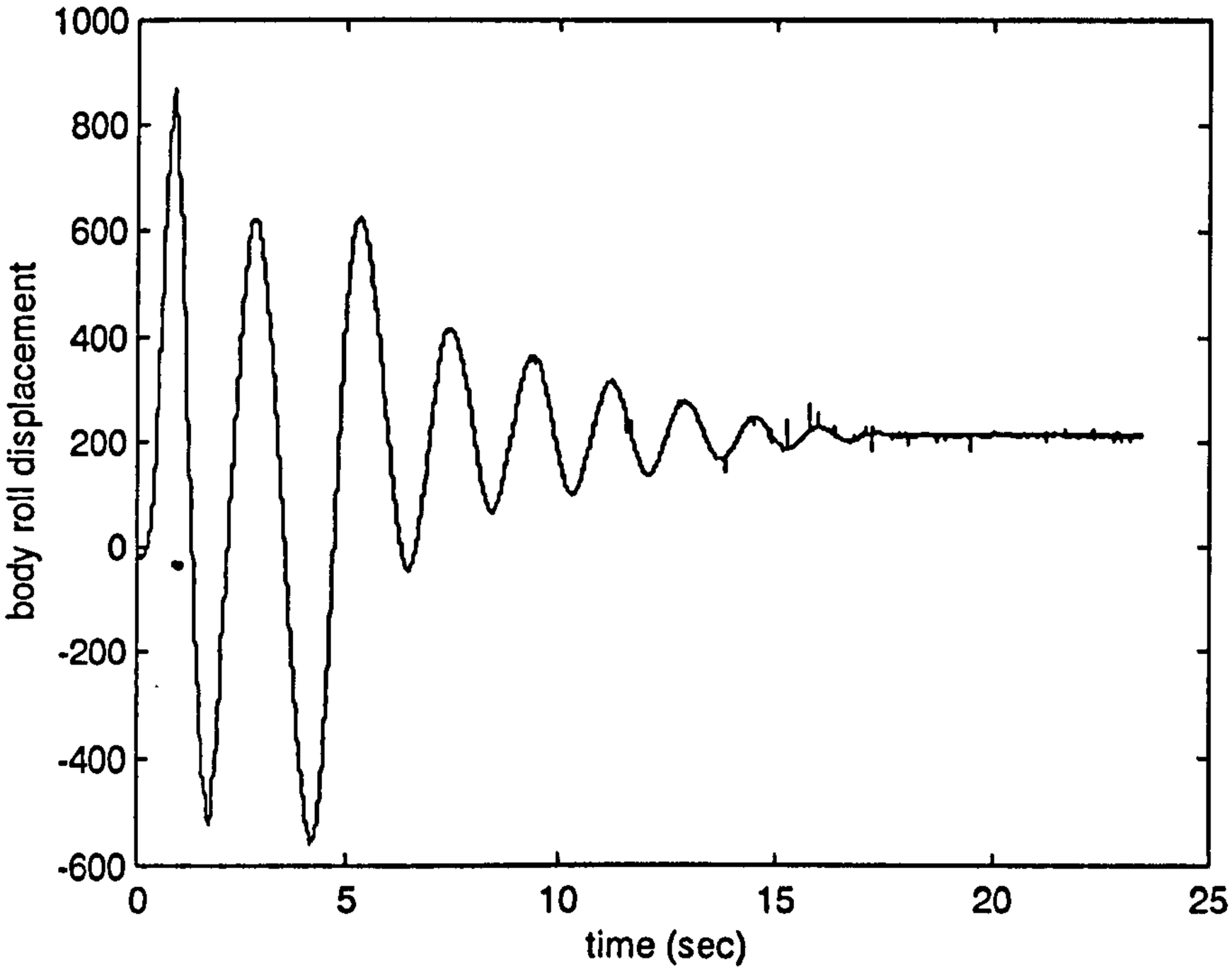

Figure 7-14(b) The measured starting response for the body roll motion with LQG controller

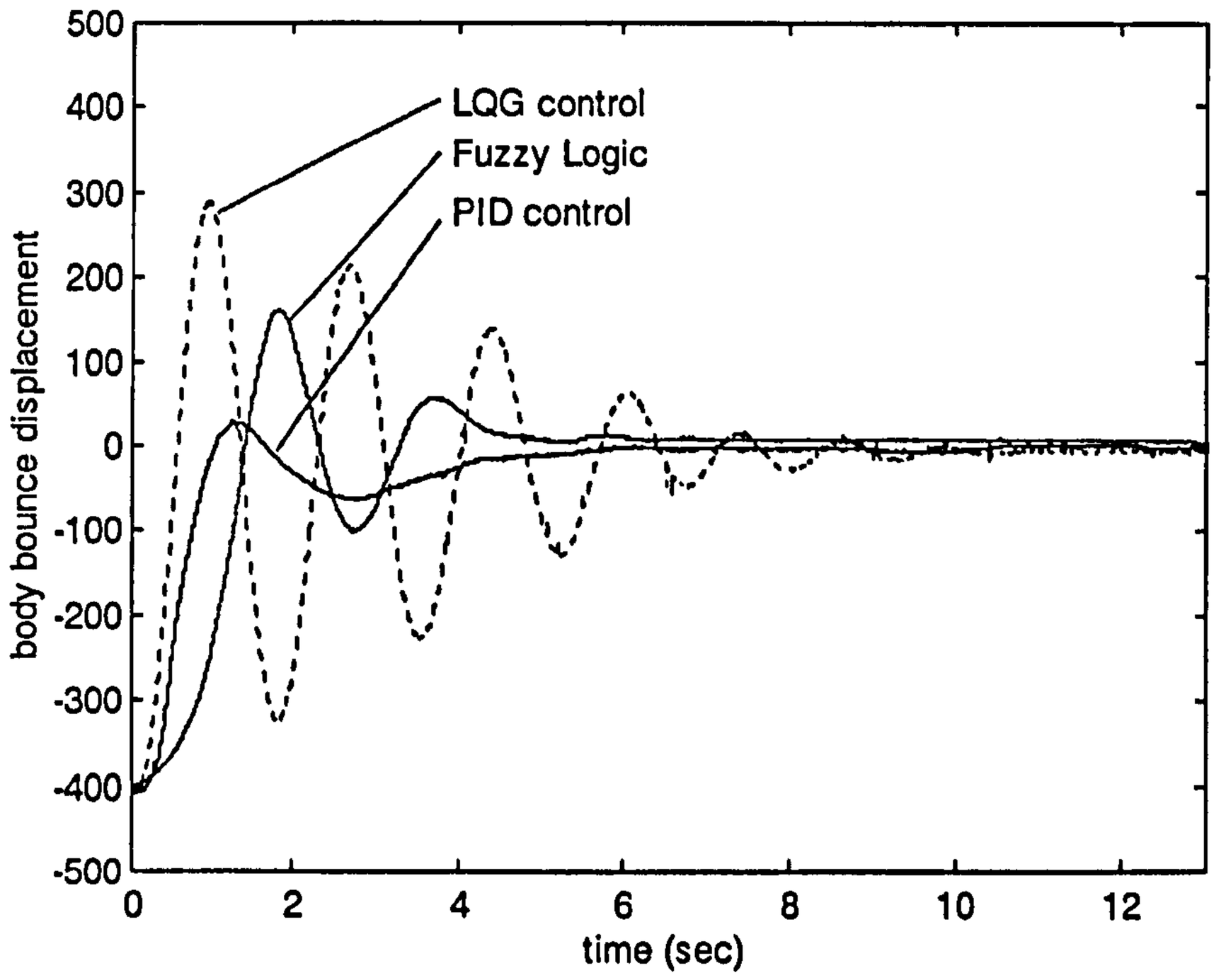

Figure 7-15 The measured body free bounce vibration for different controllers

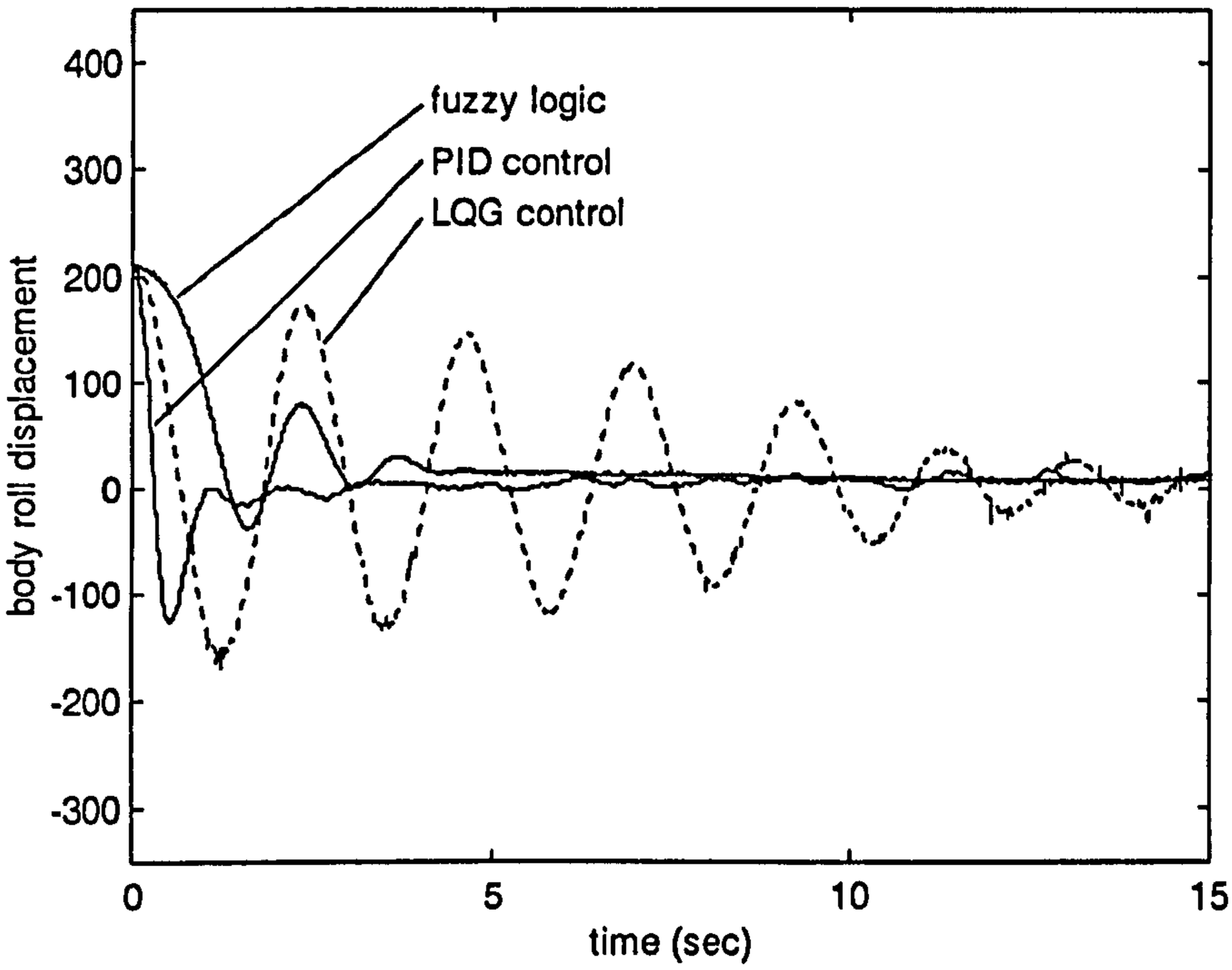

Figure 7-16 The measured body roll free vibration around for different controllers

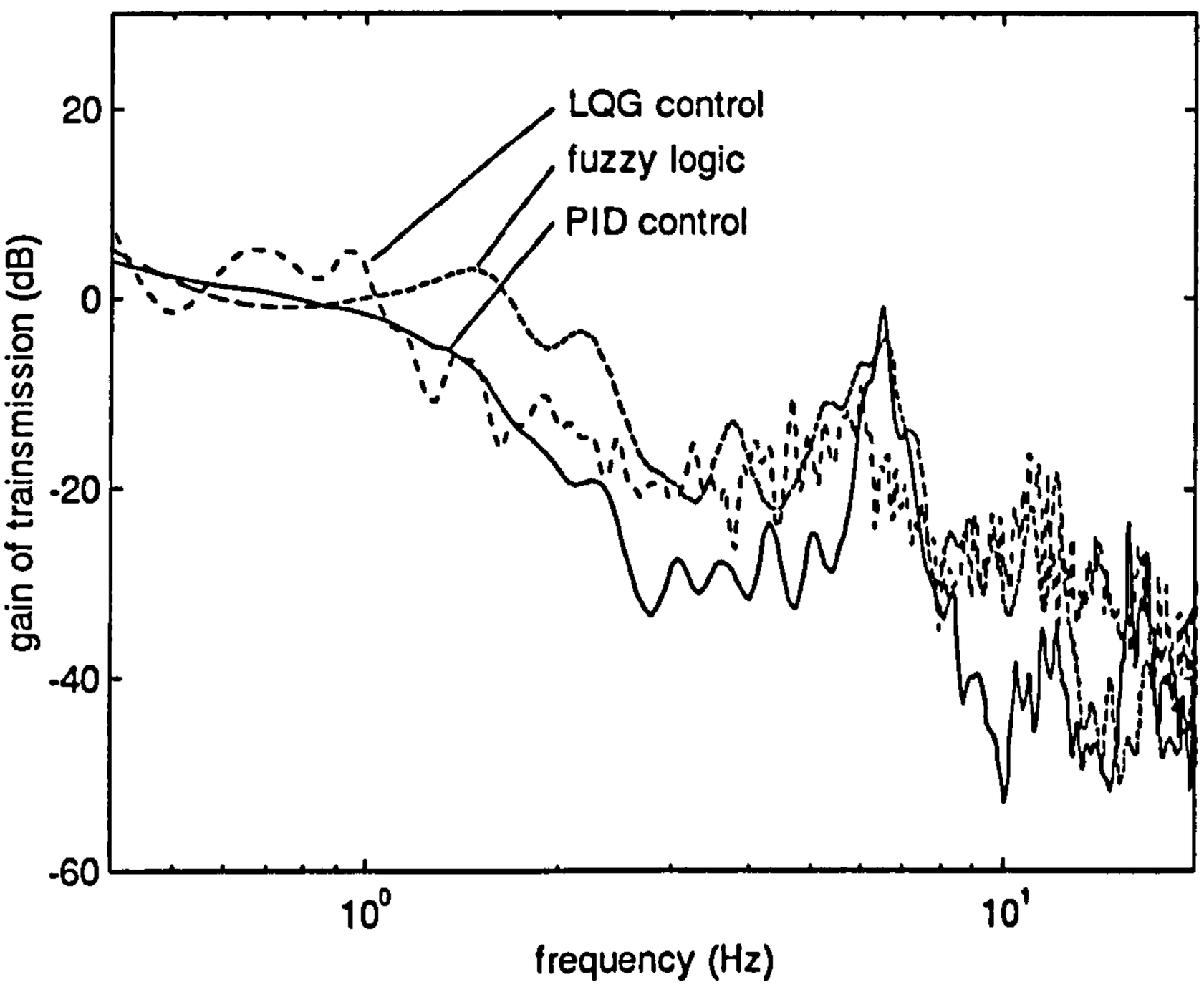

Figure 7-17 Frequency response function of the vibration transmission of the right side of the body from the road input on the right wheel for different controllers

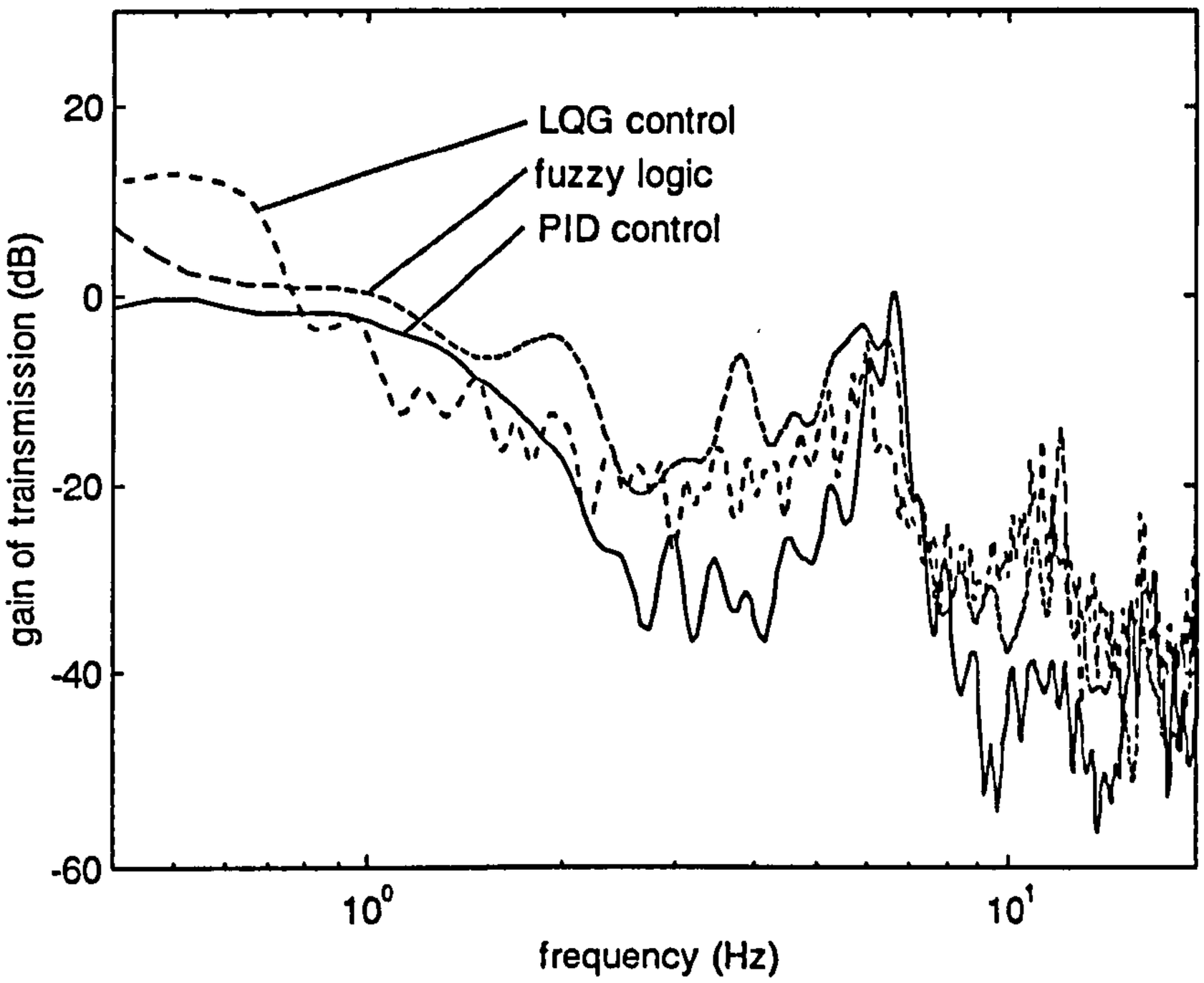

Figure 7-18 Frequency response function of the vibration transmission of the right side of the body from the road input on the left wheel for different controllers

Chapter 8

Active Tuneable Vibration Absorber for Automotive Suspension Applications

8.1 Introduction

The vibration absorber was invented nearly one century ago. The approach provides a low cost and effective method for vibration attenuation. It has been widely used in many fields. The application of vibration absorbers have been investigated by many researchers for suspension systems as shown in chapter 1.

To demonstrate the effect of the vibration absorber, an example is discussed first, then the effect of the parameters of the absorber on the vibration attenuation performance is investigated for selecting the tuning parameter of an active tuneable vibration absorber (ATVA). Finally a control strategy for an ATVA is presented and evaluated by simulation.

8.2 Effect of Vibration Absorber on Suspension Performance

To demonstrate the behavior of the suspension and absorber clearly, a simple example is employed. This example is a linear quarter car model which is used by many researchers. The comparison will be made between the model with an absorber on the unsprung mass and without the absorber. Both the models are shown in figures 8-1(a) and (b).

The motion equation for the quarter car model without the absorber can be derived as follows:

$$M\ddot{X} + C_d\dot{X} + KX = B_c X_c + BU + G \qquad (8\text{-}1)$$

where

the mass matrix $M=diag\{m_0, m_t\}$

the damping matrix $C_d = \begin{bmatrix} c_0 & -c_0 \\ -c_0 & c_0 + c_t \end{bmatrix}$

the stiffness matrix $K = \begin{bmatrix} 0 & 0 \\ 0 & k_t \end{bmatrix}$

the excitation matrix $B_c = \begin{bmatrix} 0 & 0 \\ c_t & k_t \end{bmatrix}$

the control matrix $B = \begin{bmatrix} 1 \\ -1 \end{bmatrix}$

the static load vector $G = \begin{bmatrix} -m_0 g \\ -m_t g \end{bmatrix}$

the state vector $X = \begin{Bmatrix} x_0 \\ x_t \end{Bmatrix}$

the excitation vector $X_c = \begin{Bmatrix} \dot{x}_c \\ x_c \end{Bmatrix}$

U is the force of the active suspension between the sprung and unsprung mass and the other parameters are the same as those in chapter 5. Because we are testing the effect of the vibration absorber, the simple model, i. e. the linear force and the sky-hook PD controller are considered in this chapter.

The controller for the suspension shown as follows

$$U = -\begin{bmatrix} k & -k \end{bmatrix} \begin{Bmatrix} x_0 \\ x_t \end{Bmatrix} - \begin{bmatrix} c & 0 \end{bmatrix} \begin{Bmatrix} \dot{x}_0 \\ \dot{x}_t \end{Bmatrix} \qquad (8\text{-}2)$$

is introduced into equation (8-1). After the coordinate transformation, the resultant equation is obtained below

$$M\ddot{X} + C_{d1}\dot{X} + K_1 X = B_c X_c \qquad (8\text{-}3)$$

where the damping matrix is

$$C_{d1} = \begin{bmatrix} c_0 + c & -c_0 \\ -c_0 - c & c_0 + c_t \end{bmatrix}$$

and the stiffness matrix is

$$K_1 = \begin{bmatrix} k & -k \\ -k & k + k_t \end{bmatrix}$$

The transfer function for the road excitation can be derived from equation (8-3), i.e.

$$X = (Ms^2 + C_{d1}s + K_1)^{-1} B_c \begin{Bmatrix} s \\ 1 \end{Bmatrix} x_c \qquad (8\text{-}4)$$

This function can be used to evaluate the performance of the vibration isolation.

The motion equation for the quarter car model with the vibration absorber on the unsprung mass can also be derived, i.e.

$$\hat{M}\ddot{\hat{X}} + \hat{C}_d\dot{\hat{X}} + \hat{K}\hat{X} = \hat{B}_c\hat{X}_c + \hat{B}\hat{U} + \hat{G} \qquad (8\text{-}5)$$

where

the mass matrix $\hat{M} = diag\{m_0 \quad m_t \quad m_a\}$

the damping matrix $\hat{C}_d = \begin{bmatrix} c_0 & -c_0 & 0 \\ -c_0 & c_0 + c_t + c_a & -c_a \\ 0 & -c_a & c_a \end{bmatrix}$

the stiffness matrix $\hat{K} = \begin{bmatrix} 0 & 0 & 0 \\ 0 & k_t + k_a & -k_a \\ 0 & -k_a & k_a \end{bmatrix}$

the excitation matrix $\hat{B}_c = \begin{bmatrix} 0 & 0 \\ c_t & k_t \\ 0 & 0 \end{bmatrix}$

the control matrix $\hat{B} = \begin{bmatrix} 1 \\ -1 \\ 0 \end{bmatrix}$

the static load vector $\hat{G} = \begin{bmatrix} -m_0 g \\ -m_t g \\ -m_a g \end{bmatrix}$

the state vector $$\hat{X} = \begin{Bmatrix} x_0 \\ x_t \\ x_a \end{Bmatrix}$$

the excitation vector $$\hat{X}_c = \begin{Bmatrix} \dot{x}_c \\ x_c \end{Bmatrix}$$

here x_a denotes the displacement of the absorber mass. m_a, c_a and k_a represent the mass, damping and stiffness of the absorber. The sky-hook damping PD controller

$$\hat{U} = -\begin{bmatrix} k & -k & 0 \end{bmatrix} \begin{Bmatrix} x_0 \\ x_t \\ x_a \end{Bmatrix} - \begin{bmatrix} c & 0 & 0 \end{bmatrix} \begin{Bmatrix} \dot{x}_0 \\ \dot{x}_t \\ \dot{x}_a \end{Bmatrix} \qquad (8\text{-}6)$$

is introduced in equation (8-7), which results in

$$\hat{M}\ddot{\hat{X}} + C_{d2}\dot{\hat{X}} + K_2\hat{X} = \hat{B}_c\hat{X}_c \qquad (8\text{-}7)$$

where the damping matrix

$$C_{d2} = \begin{bmatrix} c_0 + c & -c_0 & 0 \\ -c_0 - c & c_0 + c_t + c_a & -c_a \\ 0 & -c_a & c_a \end{bmatrix}$$

the stiffness matrix $$K_2 = \begin{bmatrix} k & -k & 0 \\ -k & k_t + k_a + k & -k_a \\ 0 & -k_a & k_a \end{bmatrix}$$

The transfer function for the road excitation can be derived into

$$\hat{X} = (\hat{M}s^2 + C_{d2}s + K_2)^{-1}\hat{B}_c \begin{Bmatrix} s \\ 1 \end{Bmatrix} x_c \qquad (8\text{-}8)$$

for the quarter car model with the vibration absorber on the unsprung mass.

The two equations (8-4) and (8-8) are used to evaluate the vibration transmission performance for both corresponding systems. The calculation results have been obtained and are shown in figures 8-2 to 8-5. In these figures, three cases were considered, namely the conventional passive suspension, the active suspension with sky-hook PD controller and the combination of the active suspension with sky-hook PD and the absorber on the hub. The values of active stiffness and damping are the same as the passive suspension.

It is shown in figure 8-2 that the combination of the sky-hook PD controller and the absorber can provide the best transmission for the body. Its vibration transmission gain can be reduced by about 6dB to 26dB lower than that of the passive suspension in the frequency range of 1Hz to 20Hz and by about 28dB at around 10Hz (the wheel mode) than that of the single active suspension with sky-hook PD controller. It is demonstrated that the sky-hook damping can provide low vibration transmission for the body only at the frequencies outside the wheel mode region.

In figure 8-3, it can be seen that the conventional passive suspension can provide the lowest vibration level for the hub. Around the frequency of the wheel mode, its vibration transmission is about 10dB lower than that of the combination of the absorber and sky-hook damping and about 37dB lower than that of the sky-hook damping.

Figures 8-4 and 8-5 illustrate similar behaviour to the above. The former two figures are the case of the zero conventional damping ($c_0=0$) between body and hub and the latter two are for the large conventional damping ($c_0=300$Ns/m). In figures 8-4 and 8-5, The body vibration transmission for the combination of sky-hook damping and absorber can be reduced by about 6dB to 14dB from that of the passive suspension in the frequency region from 1Hz to 20Hz and by about 10dB from that of the sky-hook damping alone at around 10Hz (the wheel mode). The hub transmission for the passive suspension can be decreased by about 8dB from that of the combination of the sky-hook and absorber and by about 17dB from that of the only sky-hook damping around the wheel mode.

Obviously, the improvement of the transmission for the combination of the sky-hook damping and absorber in figure 8-4 is not as significant as that in figure 8-2, because the existence of the conventional damping degrades the body vibration transmission. The body transmission gain for the absorber approach is increased by the conventional damping at frequencies over 2Hz, at worst by about 12dB. The transmission for the sky-hook damping alone increases the same for the frequencies beyond the wheel mode but decreases by about 15dB at the frequency of this mode. The transmission for the passive suspension does not change much due to the conventional damping.

The hub transmission around the wheel mode for the three approaches are decreased to differing extents by the conventional damping. For the absorber combination, the transmission is reduced by only 3dB.

The system damping ratios for the three approaches are shown in the tables 8-1. It can be seen that the sky-hook damping alone can provide quite a high level of damping to the body mode but a poor damping to the wheel mode. The introduction of the absorber can increase the wheel mode damping significantly, which means that good vehicle handling can be provided by the vibration absorber on hub.

From the above discussion, we can conclude that the conventional damping in a passive suspension can provide good wheel mode damping and body mode damping but poor body vibration transmission; active suspension with sky-hook damping can provide only good body mode damping but the very poor wheel mode damping and poor body transmission around the frequency of the wheel mode; the combination of the sky-hook damping and absorber can provide good body mode damping, quite good wheel mode damping and very good body vibration transmission. In other words, the introduction of the absorber into the sky-hook damping active suspension can improve both ride comfort and handling significantly.

8.3 Effect of Absorber Parameters on Vibration Attenuation

As is well known, a vibration absorber has three parameters, namely the mass, stiffness and damping. How these parameters affect the behaviour of the system is investigated in this section. The model shown in figure 8-1(b) is still employed and equation (8-8) is used to predict the vibration transmission.

Figure 8-6 illustrates the frequency response function of the body vibration transmission with the effect of the absorber natural frequency. It is shown that different natural frequencies can lead to quite different body transmission around the wheel mode frequency. The height of the two peaks at the composite natural frequencies corresponding to the absorber and wheel mode can be changed to an optimum value by tuning the absorber frequency.

The similar phenomenon can be found in the hub vibration transmission as shown in figure 8-7. The height of the two peaks at the composite natural frequencies corresponding to the absorber and wheel mode is more sensitive to the change of the absorber frequency than that of the body transmission. When the absorber frequency is 9Hz, the wheel vibration transmission gain is about 12dB. When the absorber

frequency is tuned by about 6.4% lower than 9Hz, the wheel vibration transmission gain around the wheel mode region can be reduced by about 4dB.

Figure 8-8 demonstrates the effect of the absorber damping on the body vibration transmission via the frequency response function. When the absorber is tuned properly, the absorber damping can be the next important parameter for the optimum transmission. When the absorber damping is 1000Ns/m, the frequency response (body transmission) has only one peak being -21dB high around the wheel mode region due to the high damping. When the absorber damping is reduced to 300, the body transmission can be decreased about 7dB. In this case, the one peak becomes the lower two peaks. When the absorber damping is reduced further to 100 or 30, the body transmission will become higher than the optimum state corresponding to $c_a=300$.

In figure 8-9, the absorber damping has the similar effect on the hub vibration transmission. Over large damping leads to a high transmission peak and over small damping results in two high transmission peaks. The worst case transmission can be 16dB higher than that with the absorber damping set to $c_a=300$.

The body vibration transmission is presented via the frequency response function for various absorber to wheel mass ratios in figure 8-10. When the mass ratio equals to 0.25, the absorber provides the best vibration transmission to the sprung body. Over small mass ratio can result in a high transmission to the body. Over large mass ratio can give rise to two high peaks at the composite natural frequencies corresponding to the absorber and wheel mode, which also degrades the body transmission. This effect is due to reduced damping ratio of the absorber.

The hub vibration transmission is illustrated via the frequency response function for various absorber to wheel mass ratios in figure 8-11. A similar phenomenon can be seen in this figure. A mass ratio of 0.25 produces the best vibration transmission. Over small mass ratio causes the vibration transmission gain to be up to 30dB higher. For over large mass ratio, the transmission gain of the first peak around the wheel mode is 5dB higher than that of the best one though the transmission in the middle is 10dB lower.

When the absorber frequency and damping have suitable values, the transmission to both the body and hub can simultaneously optimised. Figures 8-12 and 8-13 illustrate the optimum vibration transmission for both the body and hub with various absorber parameters. It is shown that the extent of the optimum transmission is determined by

the absorber to wheel mass ratio. Because a high absorber mass results in high dynamic force on the hub, close coupling between the absorber and hub can result. That means that a large mass absorber can exert a large influence on the hub vibration.

The absorber frequency and damping for optimum transmission are changed with the absorber to wheel mass ratio. When the mass ratio is increased, the frequency should be decreased and the damping should be increased. The optimum parameter combination changes when the other parameters of the vehicle system, such as wheel stiffness and damping, etc. change. Normally, the absorber to wheel mass ratio can not be changed very much. To obtain the optimum transmission, the absorber frequency and damping have to be tuned properly.

In figures 8-12 and 8-13, it can be seen that the optimum body vibration transmission has the same absorber parameter combination as the optimum hub transmission. In other words, the optimum transmission for both body and hub transmission can achieve the optimum state at the same tuned absorber parameter combination.

It is also demonstrated in figures 8-12 and 8-13 that optimum transmission is more sensitive to the absorber frequency than to the absorber damping. When the hub transmission around the wheel mode frequency decreases from about 18dB to 6dB, the absorber frequency is reduced only 31.4%, but the absorber damping is increased by 50 times.

8.4 Control Strategy of the Active Absorber

As is well known, the change of the air pressure in a tyre or its temperature, which often occurs in practice, can result in a change of the wheel stiffness. A passive vibration absorber on the hub can not adapt to such changes. A mistuned absorber may cause degraded performance because the vibration attenuation is very sensitive to the absorber frequency as discussed in last section. In addition, the change of other parameters of the primary system (vehicle body and wheel), such as wheel damping, can also give rise to the degradation of the vibration attenuation for the absorber. These changes can be adapted to when an active absorber is introduced.

Because the change of the primary system parameters is not very fast, to reduce cost and increase reliability, the absorber can be the active tuneable type. The simplest and cheapest way for this is to use the absorber with only one tuneable parameter. The

selection of tuneable parameter can be made based on the results of the previous section.

It has been found that the absorber to wheel mass ratio can affect the optimum parameters of the absorber, but the wheel mass normally changes very little and it is difficult to implement variable mass in the absorber. Tuning absorber stiffness and damping can be much easier than tuning the mass, so the mass can excluded as a tuning parameter. It has also been shown that the vibration attenuation performance is much more sensitive to the absorber frequency than to the absorber damping. The absorber stiffness therefore is the best candidate as a tuning parameter if a practical and easy way of implementing can be found.

The next issue is to determine the objective for tuning stiffness. To maintain optimum performance, the stiffness has to be tuned to adapt to changes in the primary system parameters. The optimum state has been illustrated in figures 8-12 and 8-13. It has been shown that the optimum state for the body transmission occurs at the same absorber parameters as that for hub transmission. This means that we can monitor only the vibration transmission to the hub and optimise this by tuning the absorber stiffness.

The frequency response function in figure 8-13 has told us what the optimum state is, i.e. the two peaks at the composite frequencies corresponding to the absorber and wheel mode have the approximately same height. In other words, the objective for the tuneable absorber is to keep the heights of the hub transmission gain approximately the same at both composite frequencies in frequency domain.

Because it is very difficult to directly measure the road profile, it is not easy to identify the transfer function from the road profile to the hub. Road excitation is often modelled as white noise with some bandwidth by many researchers. If the bandwidth covers the frequency region for the composite frequencies corresponding to the absorber and wheel mode, the objective of the tuneable absorber can be simplified further. The frequency spectrum for the hub vibration can be directly employed to substitute the transfer function from the road excitation to the hub as the tuning objective. Because of the white noise excitation, the frequency spectrum for hub vibration has the same characteristic, two peaks at the composite frequencies corresponding to the absorber and hub modes with the approximately same height, as the road profile to the hub transmission.

The control strategy for the tuneable absorber is summarised in figure 8-14. This shows that the control procedure is: sampling hub vibration signals, analysing the

signals by FFT, seeking the peaks of the resultant frequency spectrum curve at both composite frequencies corresponding to the absorber and wheel modes, comparing the height of the peaks, adjusting the absorber frequency properly when the height difference is larger than a set amount, keeping the absorber frequency value when the height difference is smaller than the amount, and then repeating the first step -- sampling the hub vibration signals.

The decremental amount of the tuned frequency can be given by the positions of the two peaks in frequency domain and the height difference between the two. The algorithm for this is given as follows

$$\Delta f = \delta(h_1 - h_2)(f_1 - f_2) \qquad (8\text{-}9)$$

where Δf denotes the decremental frequency for the tuneable absorber; f_1 and f_2 are the composite frequencies at the two peaks around the wheel mode; h_1 and h_2 represent the height of the two peaks in the frequency spectrum; δ denotes a coefficient.

The control strategy was simulated on the quarter car model with the ATVA. The results are illustrated in figures 8-15(a) and 8-16(a). Figure 8-15(a) illustrates the frequency spectrum for the hub vibration excited by a white noise road profile before tuning the absorber and figure 8-16(a) illustrates the frequency spectrum after 5 cycles of tuning the absorber. Obviously, the case shown in figure 8-16(a) belongs to the optimum state. It is shown that the control strategy for the ATVA is able to tune the absorber frequency to achieve the optimum state of the vibration attenuation.

The frequency responses for the hub transmission corresponding to the two cases were also calculated respectively by means of equation (8-8) as shown in figures 8-15(b) and 8-16(b). It can be seen that the hub vibration transmission for road profile input can be adjusted to the optimum state at the same time by tuning the absorber. This demonstrates the above discussion that the frequency spectrum for the hub vibration can be directly employed to substitute the hub transmission as the tuning objective for the white noise road excitation with a proper bandwidth.

Figure 8-17 illustrates the change of the absorber frequency being tuned. The frequency starts increasing from 10Hz. It achieves the region neighbouring the ideal optimum value after normally 3 to 6 cycles of tuning and changes around this value stocastically. The reason for the random change is that the control objective is based on the estimated frequency spectrum for the hub vibration excited by the white noise road input, which may cause some random errors.

8.5 Conclusions

It has been shown that using the combination of a vibration absorber and active suspension with sky-hook damping can provide better performance for both the vehicle body and hub than using only the suspension. The active vibration absorber can further enhance the performance by being adaptive to changes in system parameters.

A variable stiffness absorber is applied in this chapter. A control strategy has been proposed and tested by simulation on a quarter car model. The simulated results have shown that the control strategy and algorithm are effective.

	sky-hook damping	sky-hook damping and absorber	conventional passive damping
body mode	0.7169	0.7168	0.6923
wheel mode	0.0038	0.1065	0.4148
absorber mode	-	0.1078	-

Table 8-1 The system damping ratios resulted in by different assemblies for zero original body to hub damping

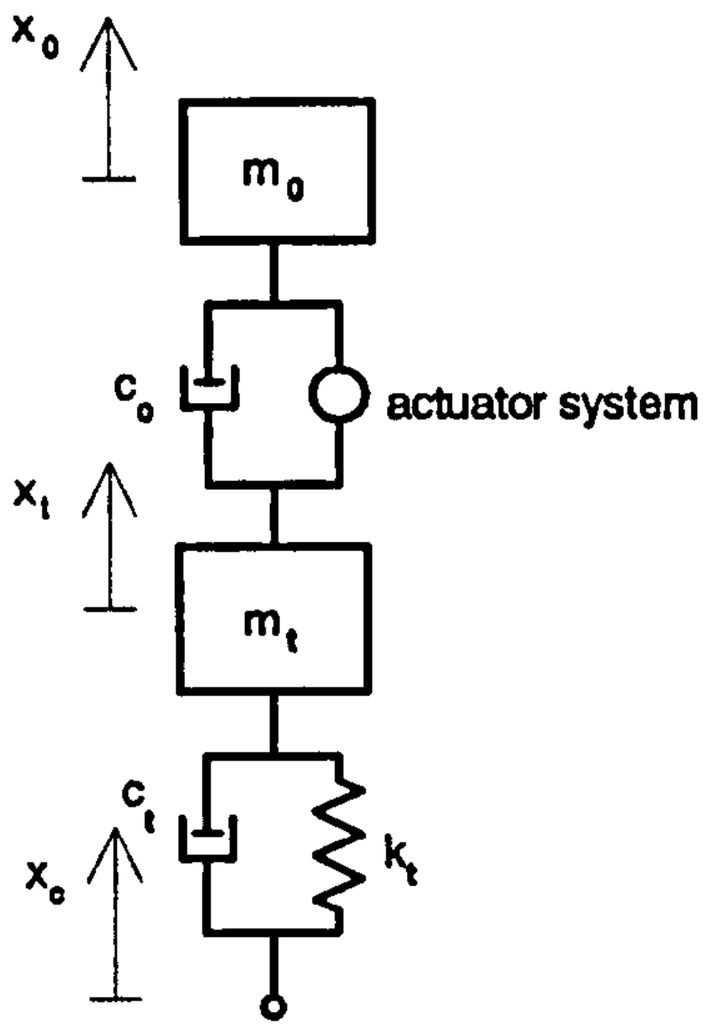

Figure 8-1(a) The quarter car model

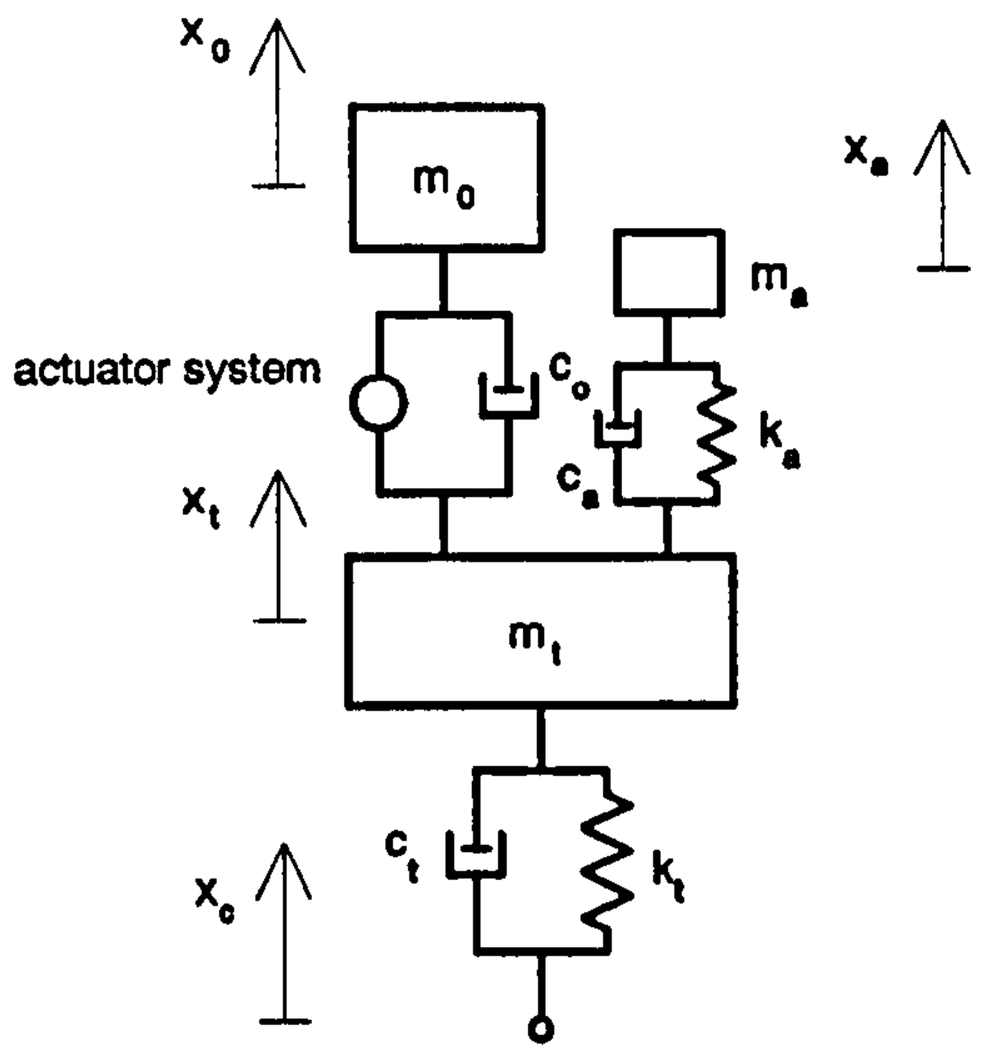

Figure 8-1(b) The quarter car model with the vibration absorber

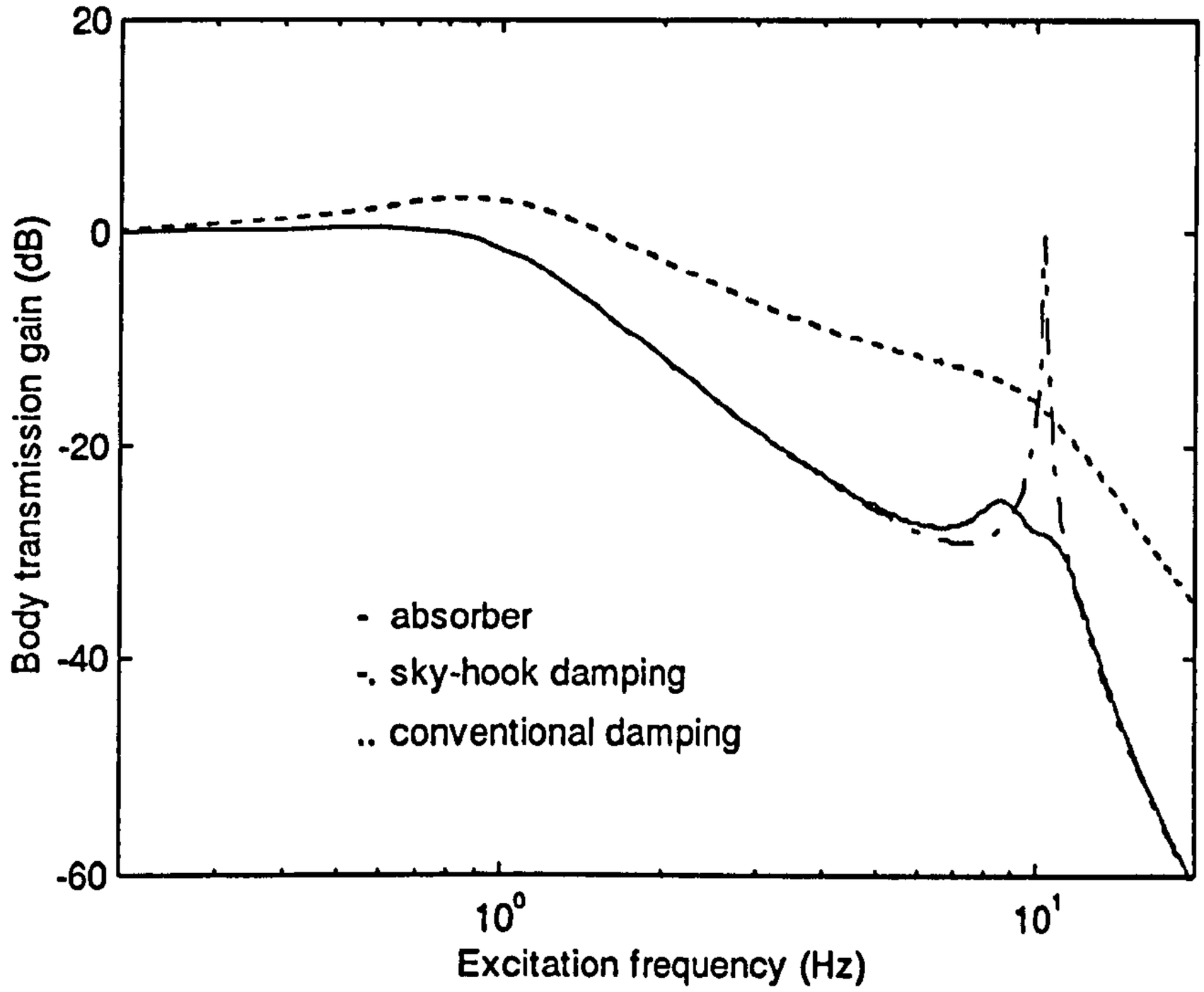

Figure 8-2 The frequency response function for the transmission of the body from the road profile for the zero original passive damping between the body and hub

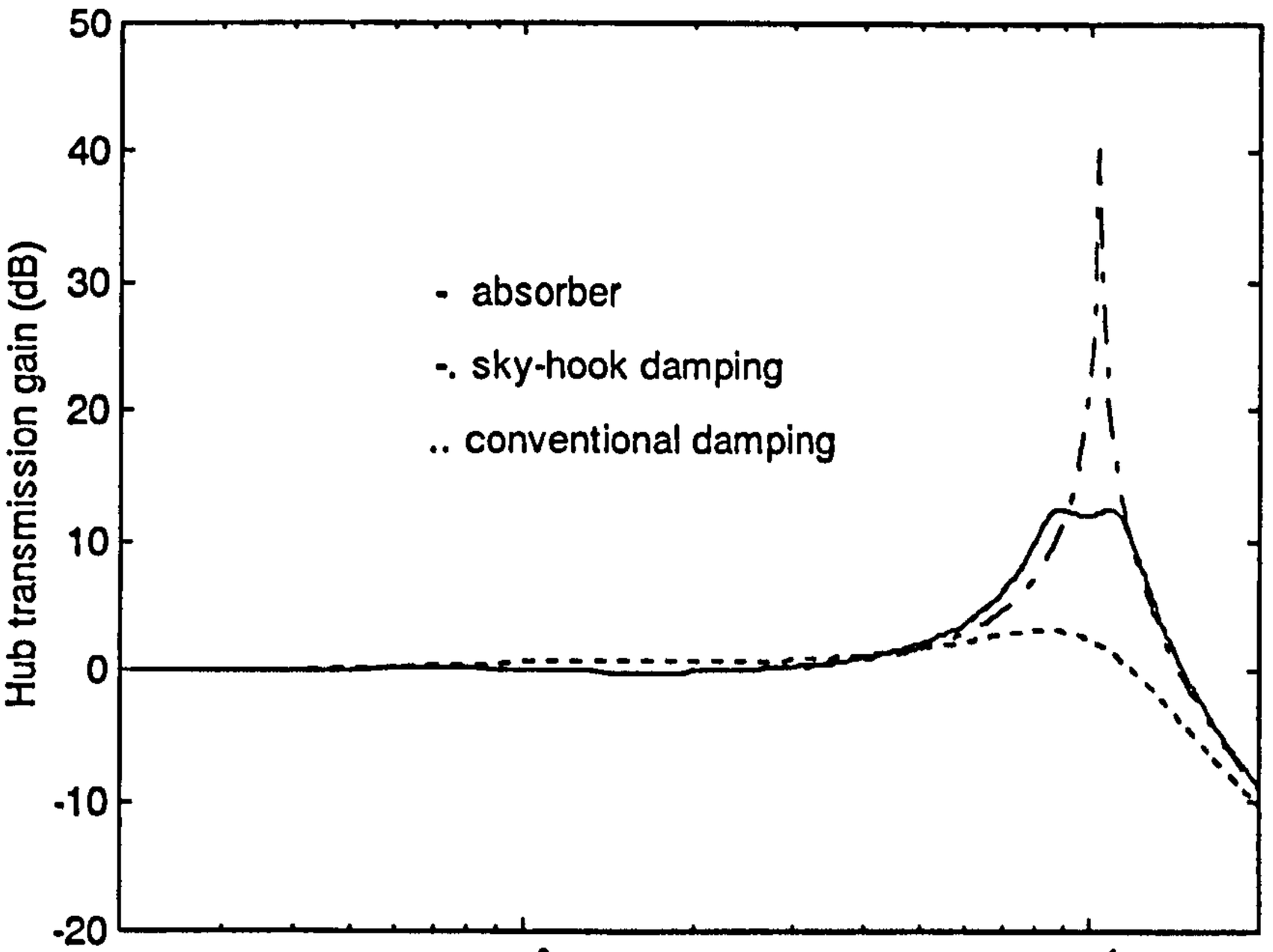

Figure 8-3 The frequency function response for transmission of the hub from the road profile for the zero original passive damping between the body and hub

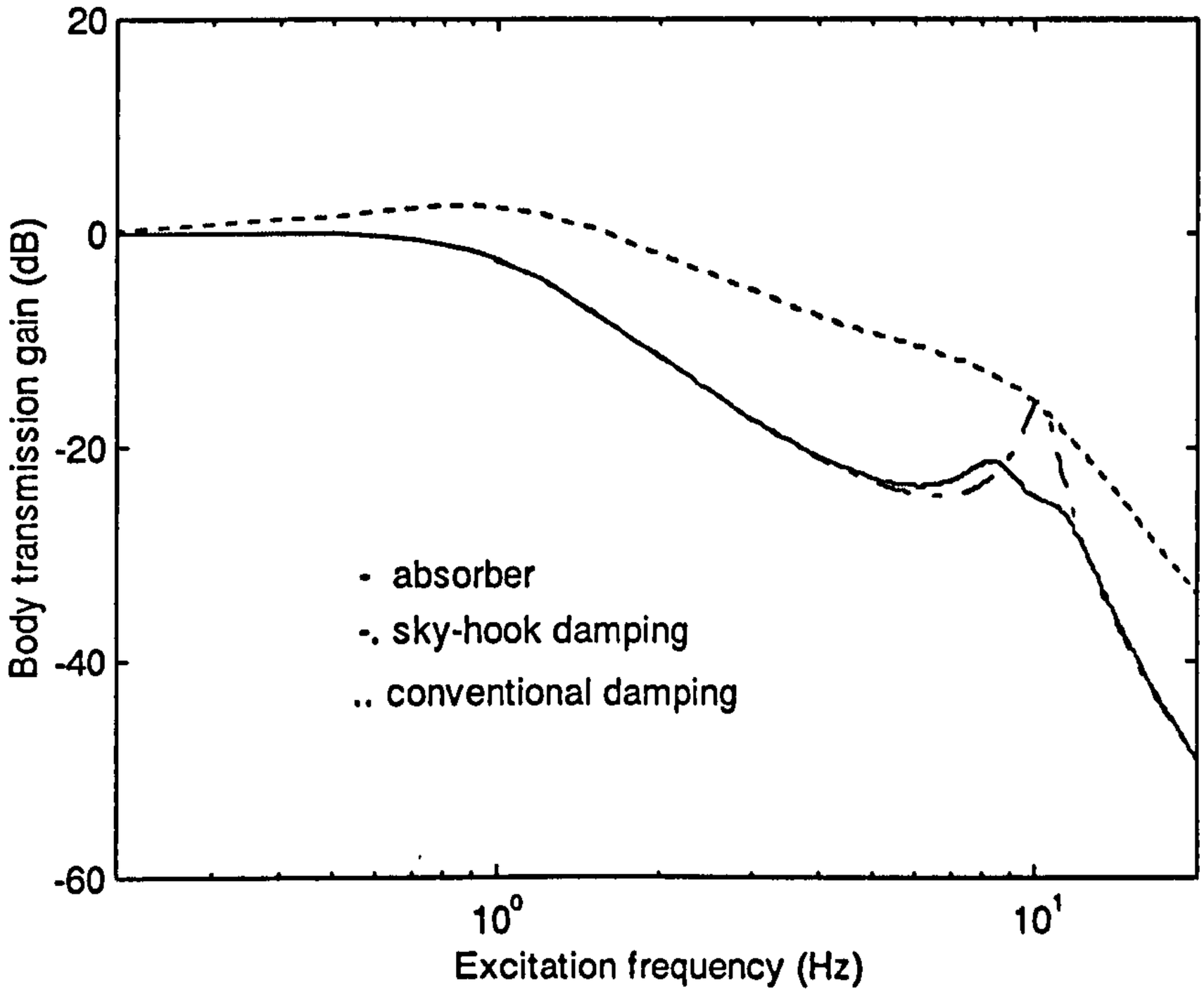

Figure 8-4 The frequency response function for the transmission of the body from the road profile for the large original passive damping between the body and hub

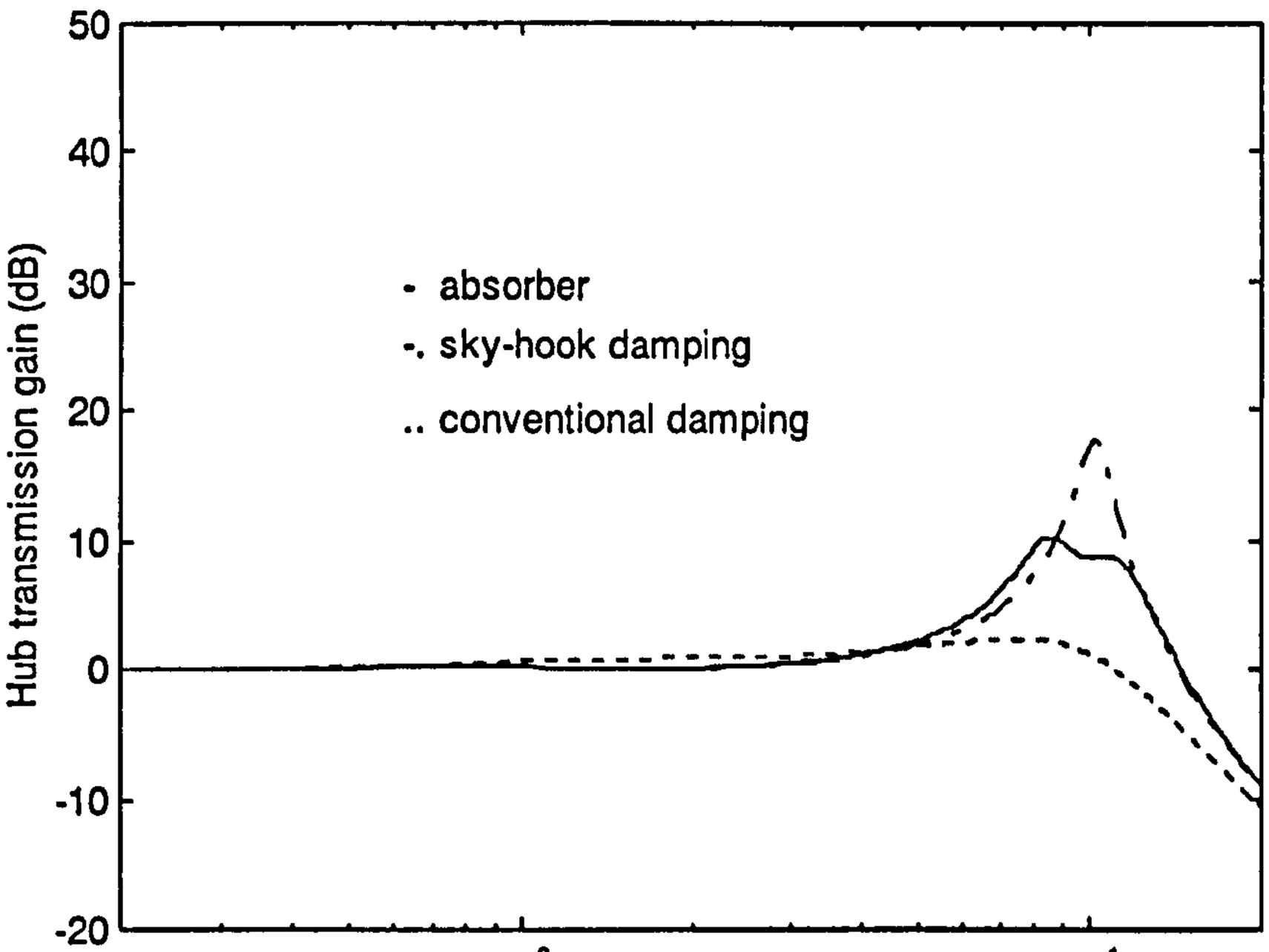

Figure 8-5 The frequency function response for transmission of the hub from the road profile for the large original passive damping between the body and hub

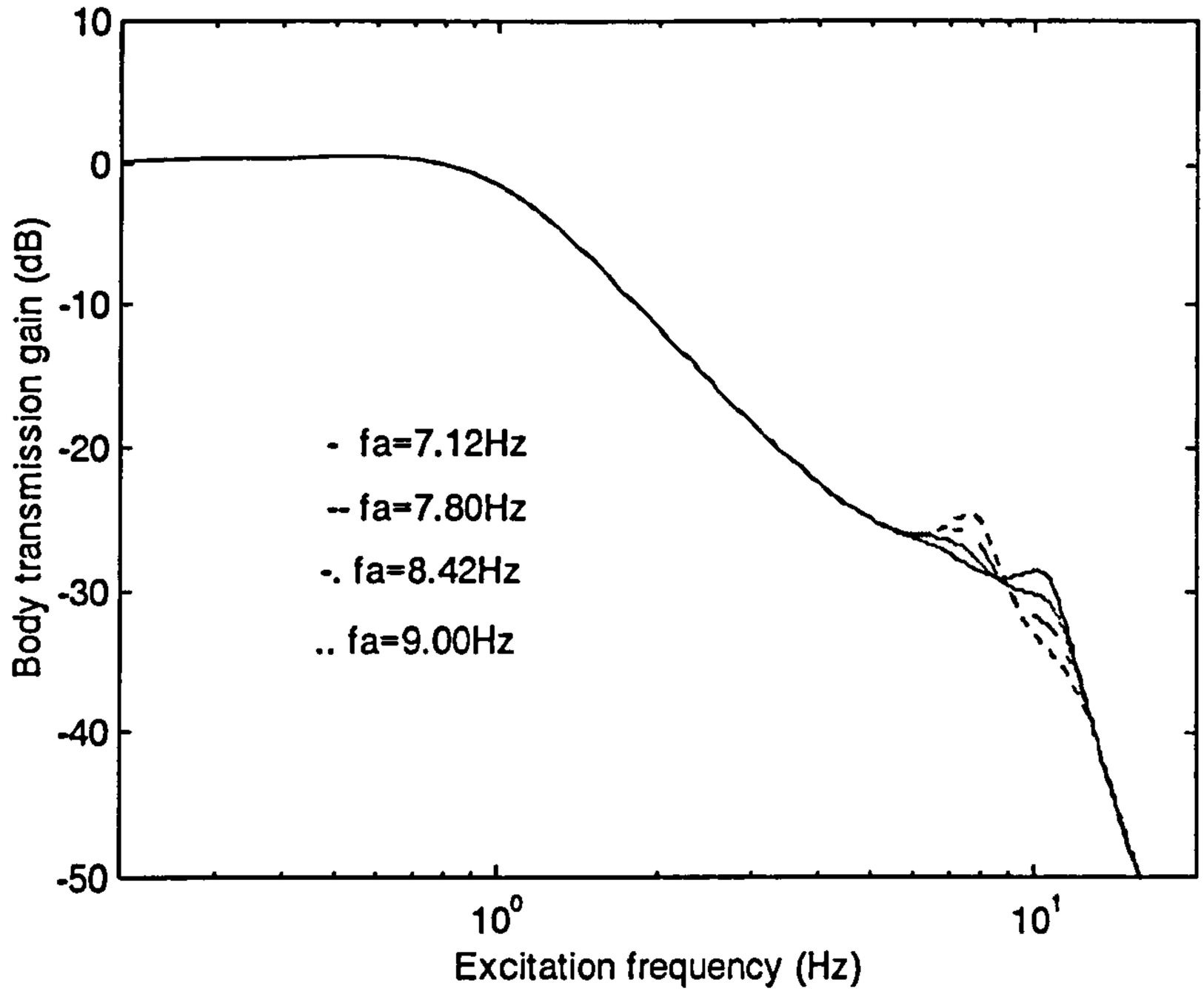

Figure 8-6 Frequency response function of the body vibration transmission with various absorber frequencies for $m_a/m_t=0.25$ and $c_a=300$

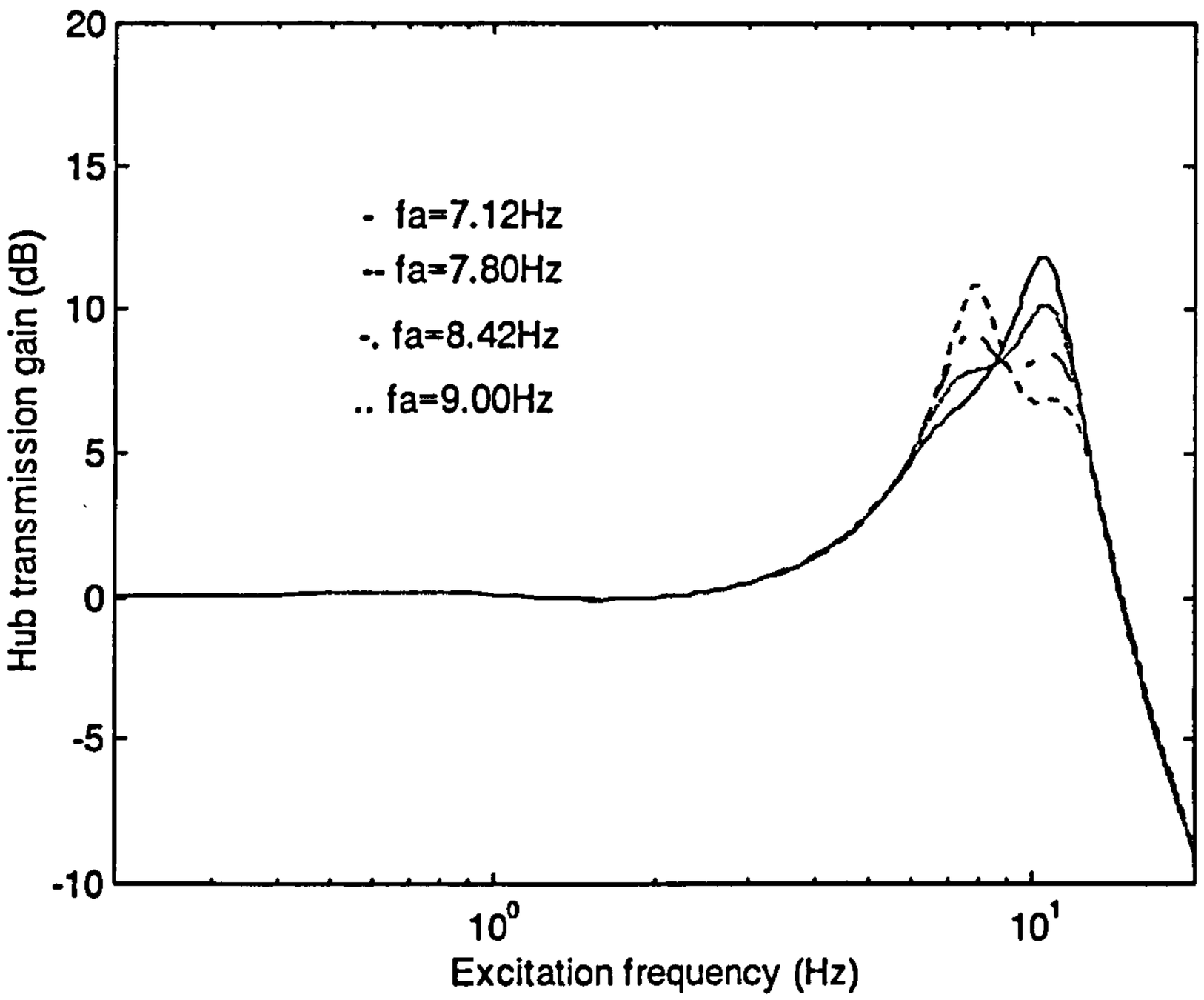

Figure 8-7 Frequency response function of the hub vibration transmission with various absorber frequencies for $m_a/m_t=0.25$ and $c_a=300$

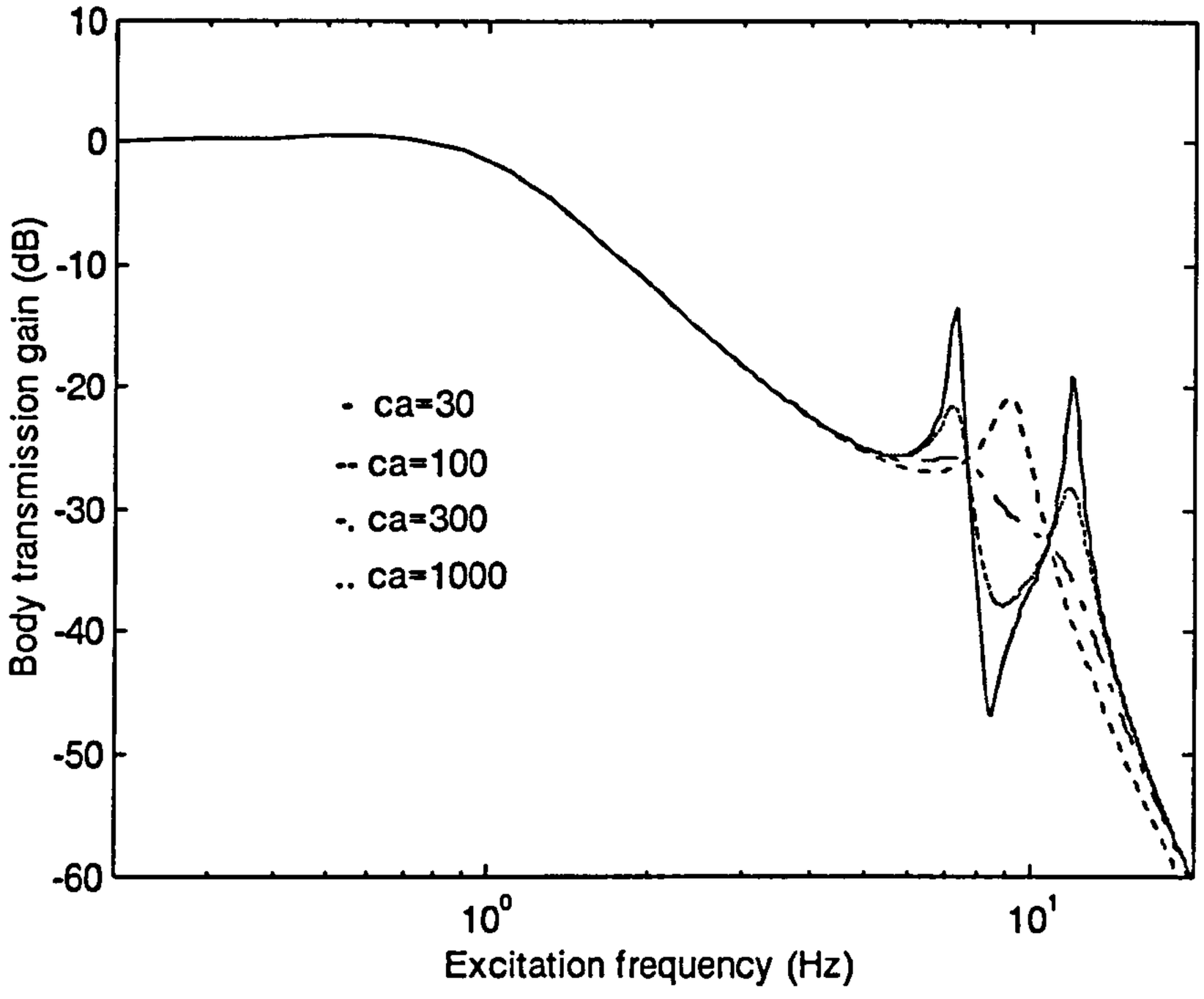

Figure 8-8 Frequency response function of the body vibration transmission with various absorber damping for $m_a/m_t=0.25$ and $f_a=8.42Hz$

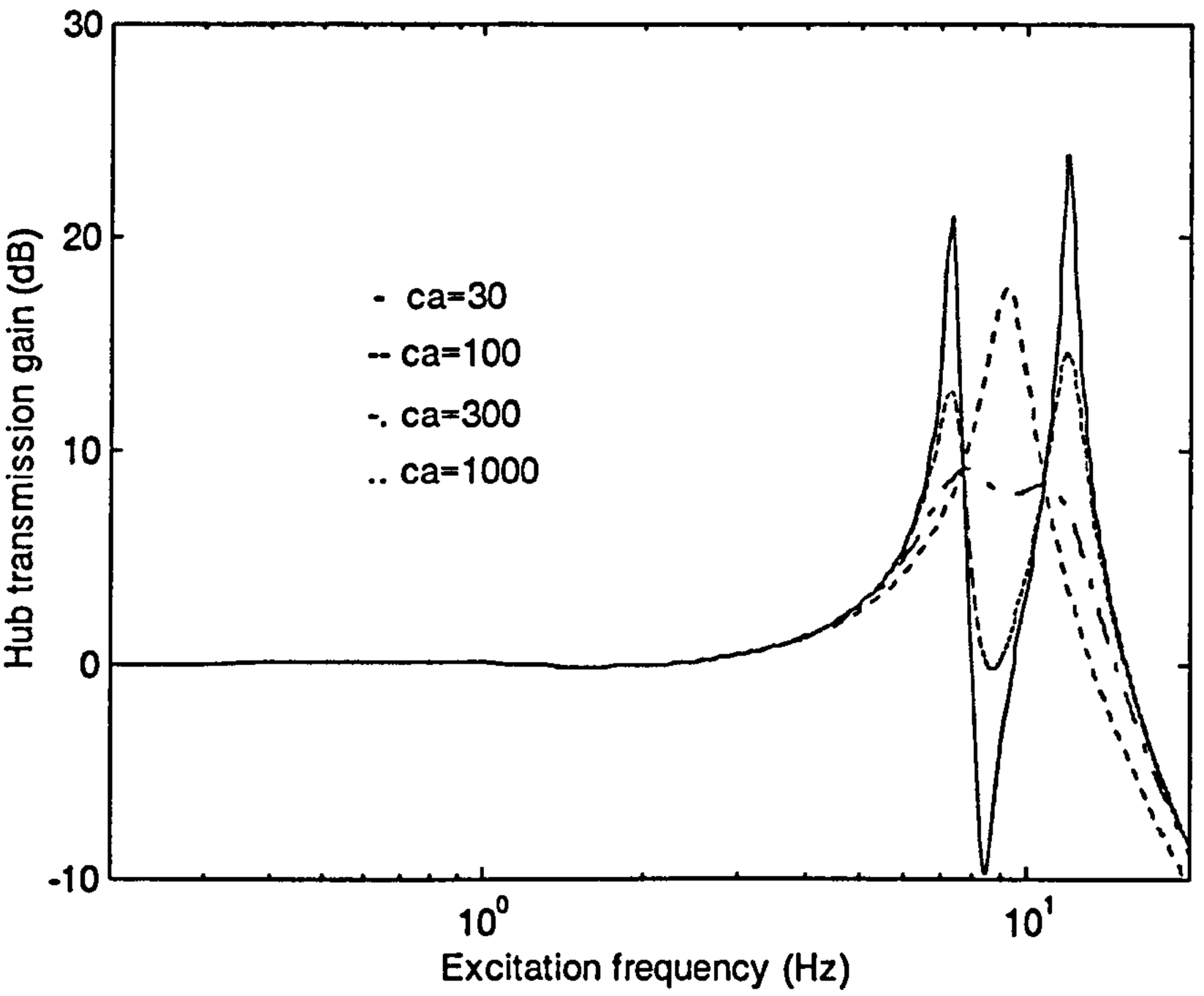

Figure 8-9 Frequency response function of the hub vibration transmission with various absorber damping for $m_a/m_t=0.25$ and $f_a=8.42Hz$

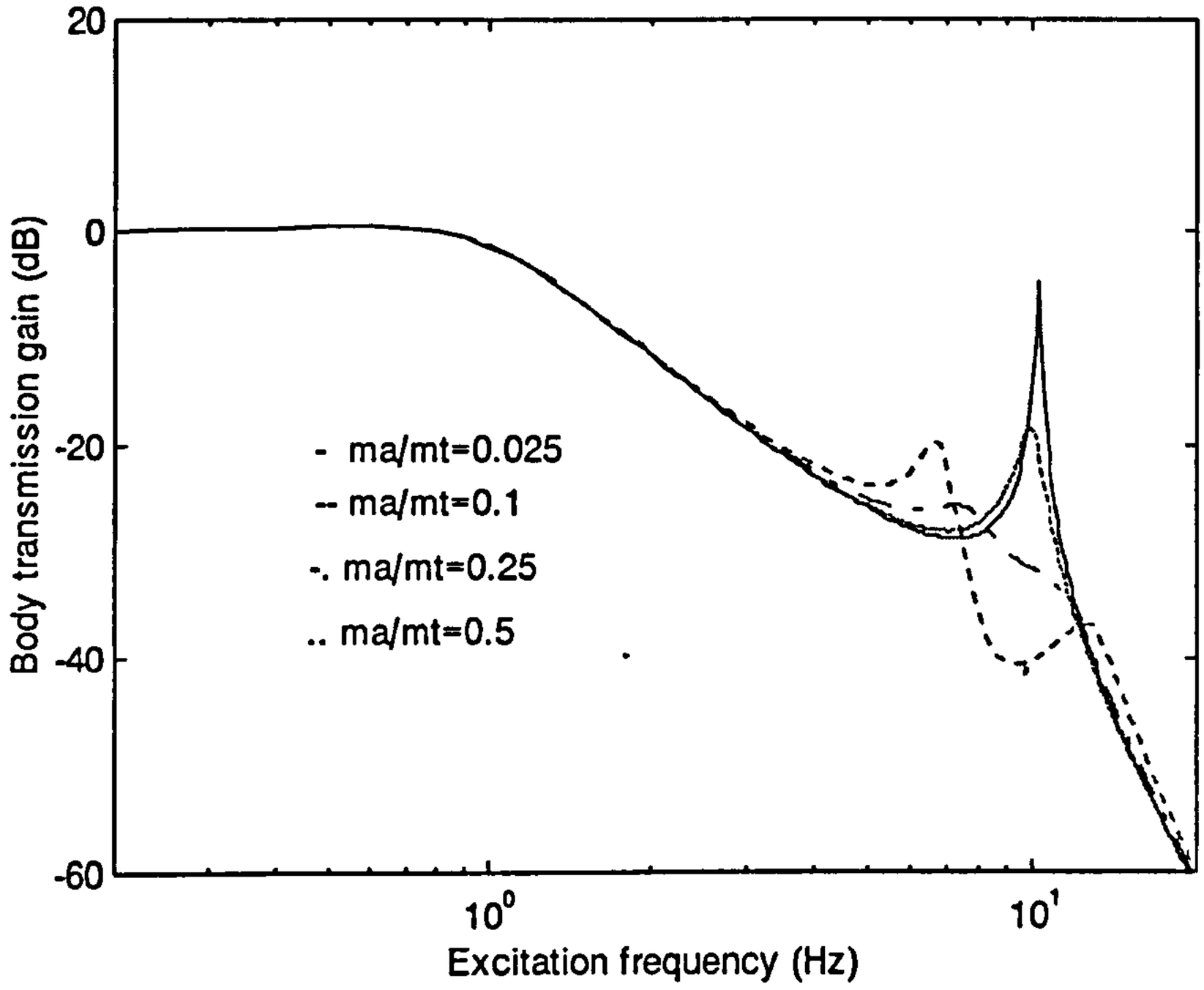

Figure 8-10 Frequency response function of the body vibration transmission with various absorber to wheel mass ratios for c_a=*300* and f_a=*8.42Hz*

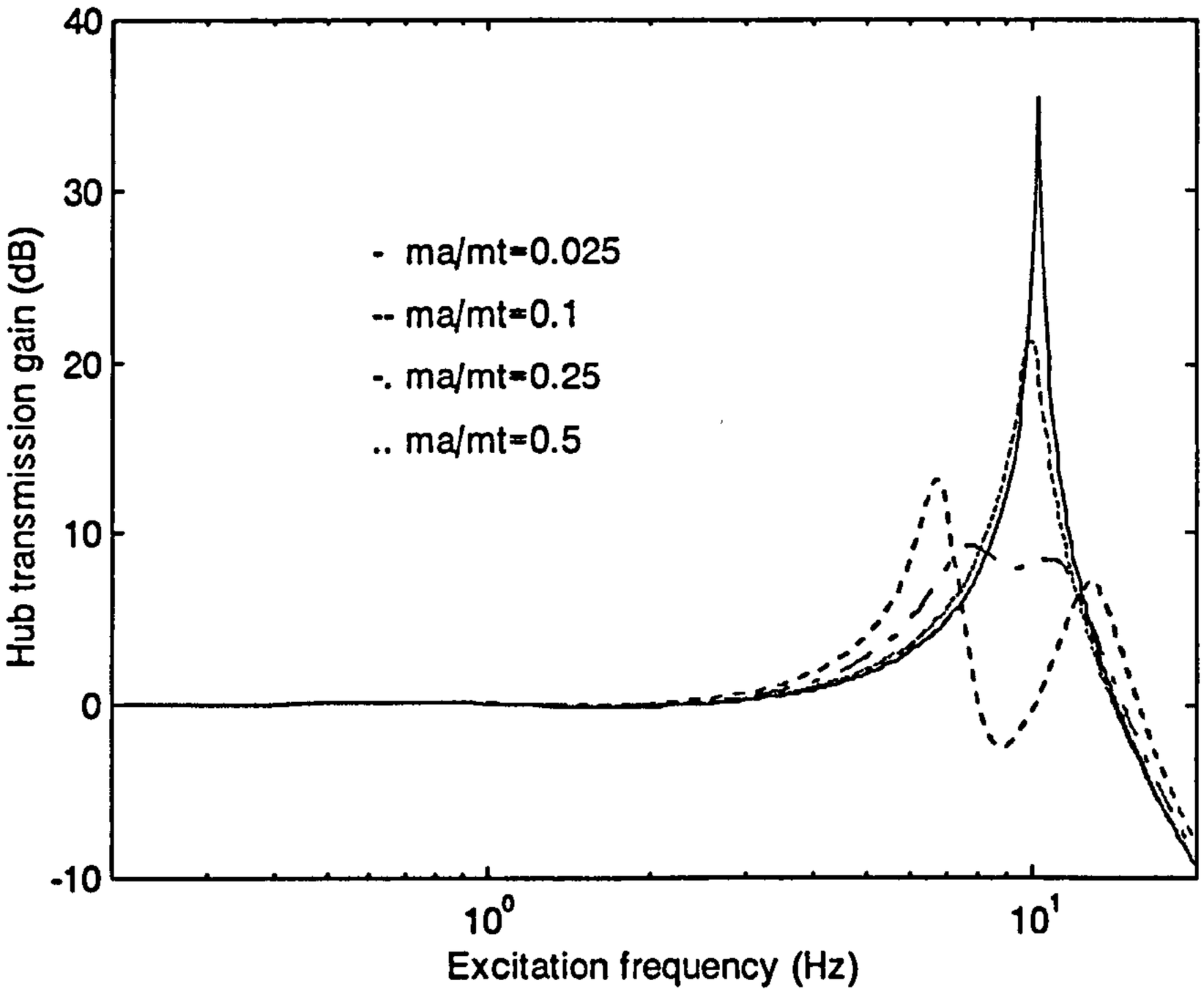

Figure 8-11 Frequency response function of the hub vibration transmission with various absorber to wheel mass ratios for c_a=*300* and f_a=*8.42Hz*

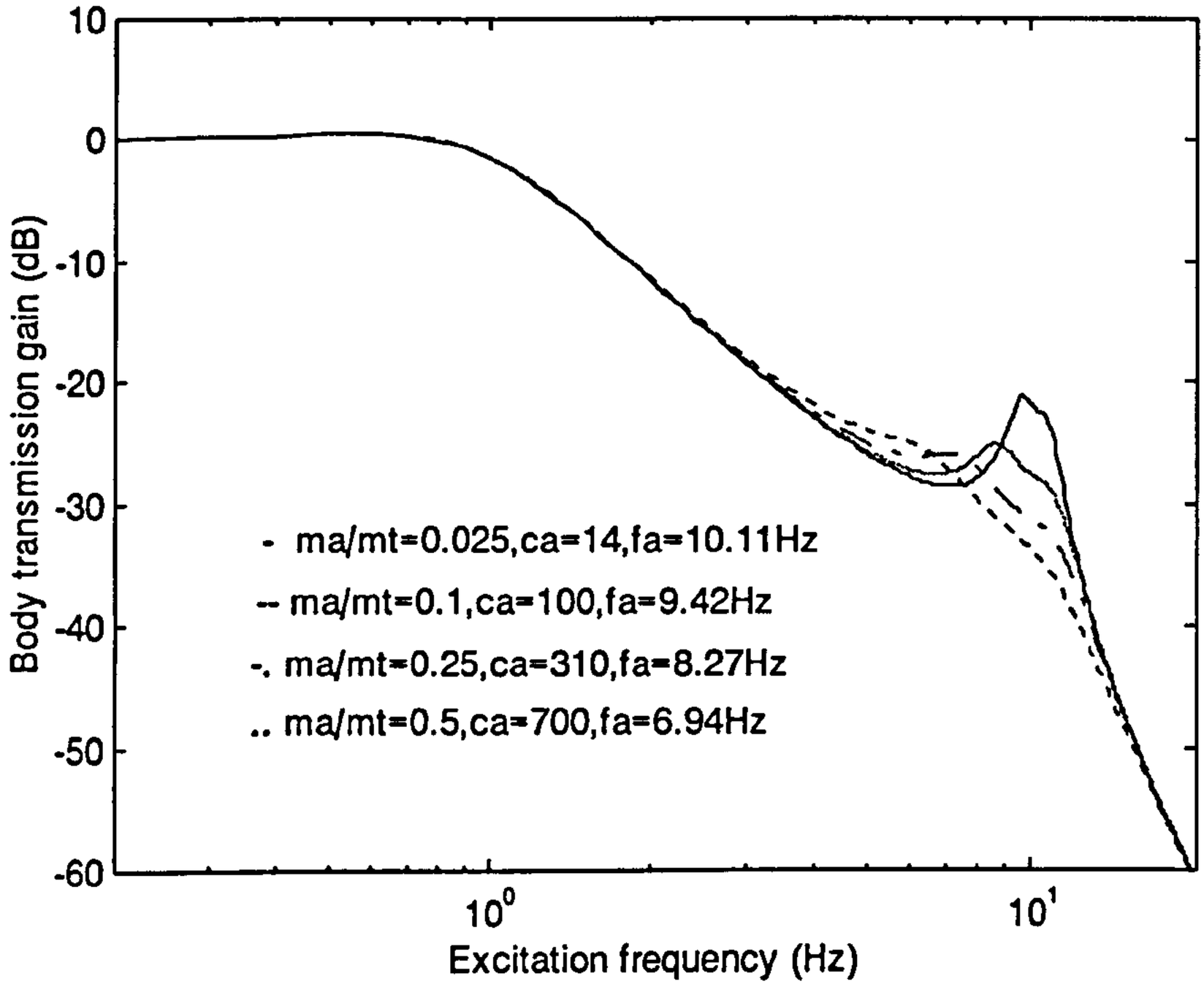

Figure 8-12 Frequency response function of the body vibration transmission for optimum absorber parameter combinations with various absorber masses

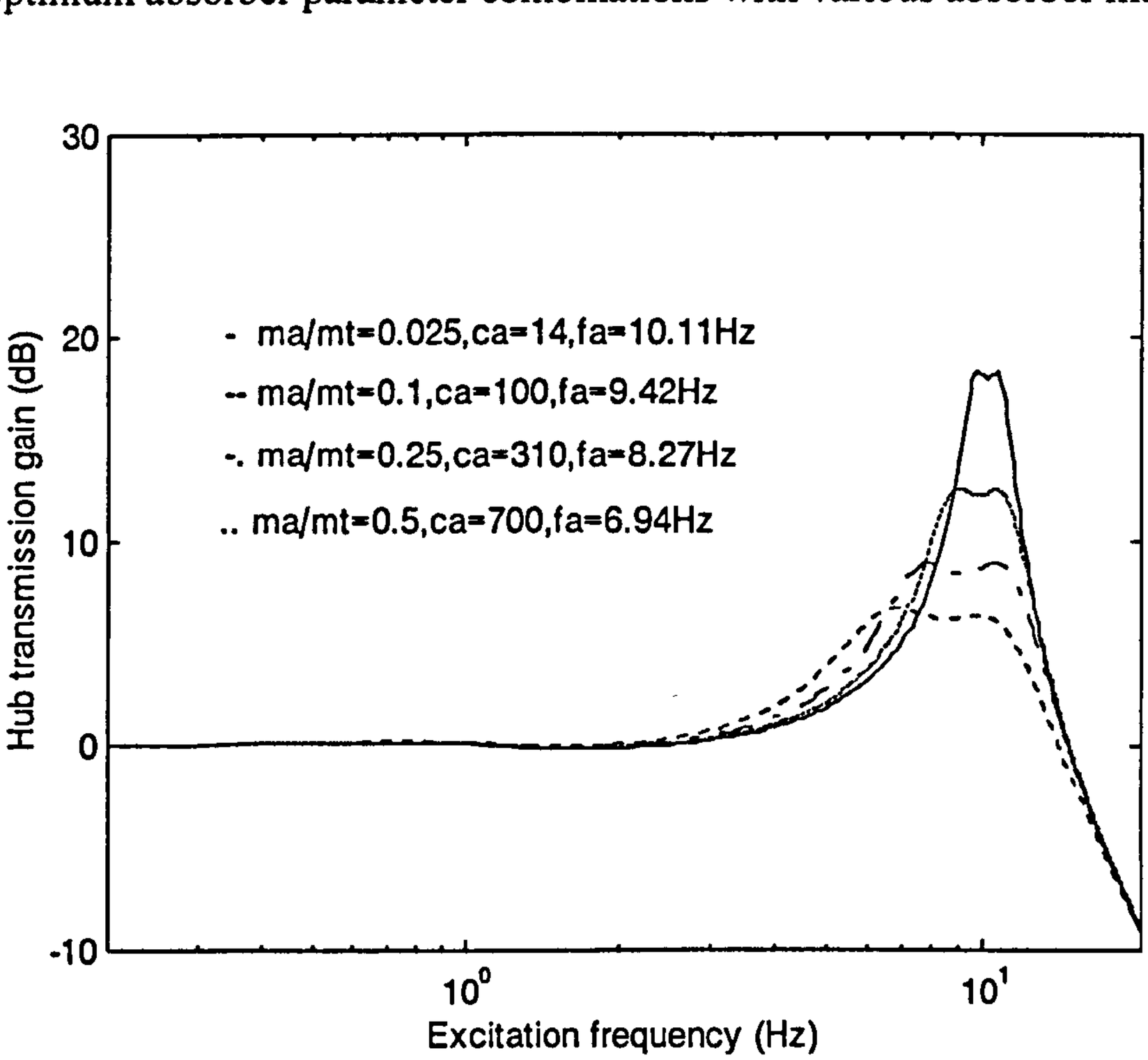

Figure 8-13 Frequency response function of the hub vibration transmission for optimum absorber parameter combinations with various absorber masses

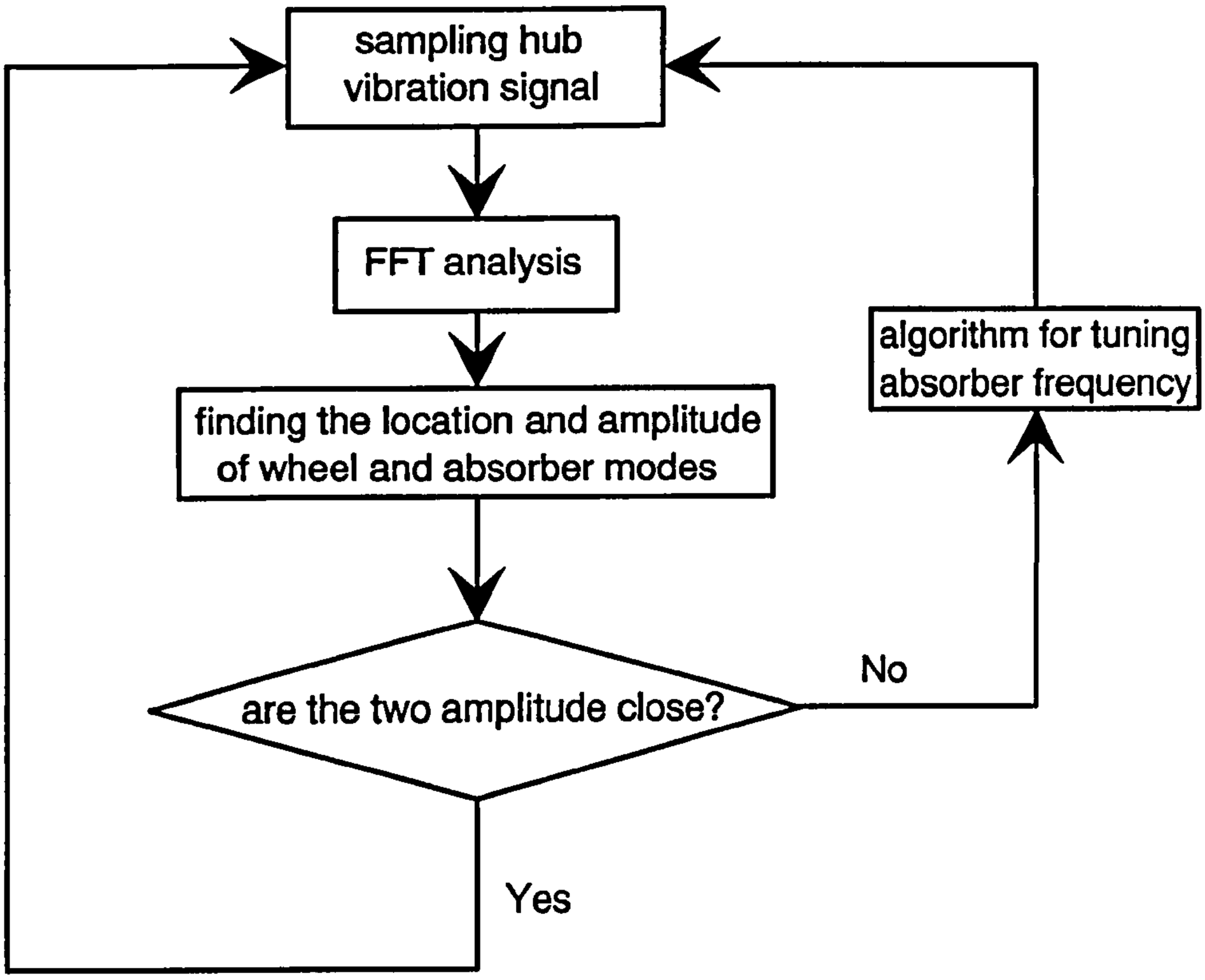

Figure 8-14 The control strategy for the active tuneable absorber

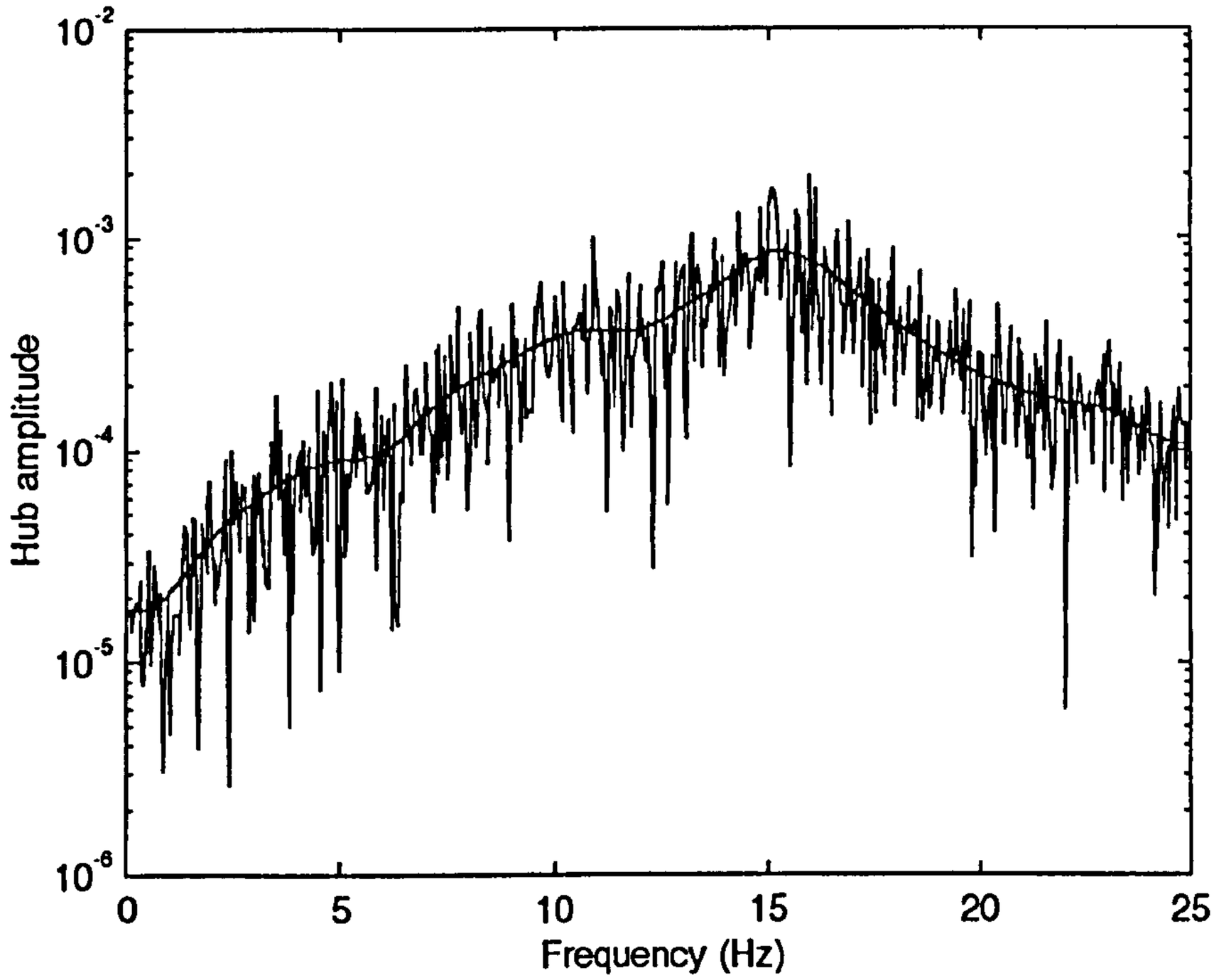

Figure 8-15(a) The initial frequency spectrum for hub vibration excited by white noise road profile before the absorber frequency being tuned

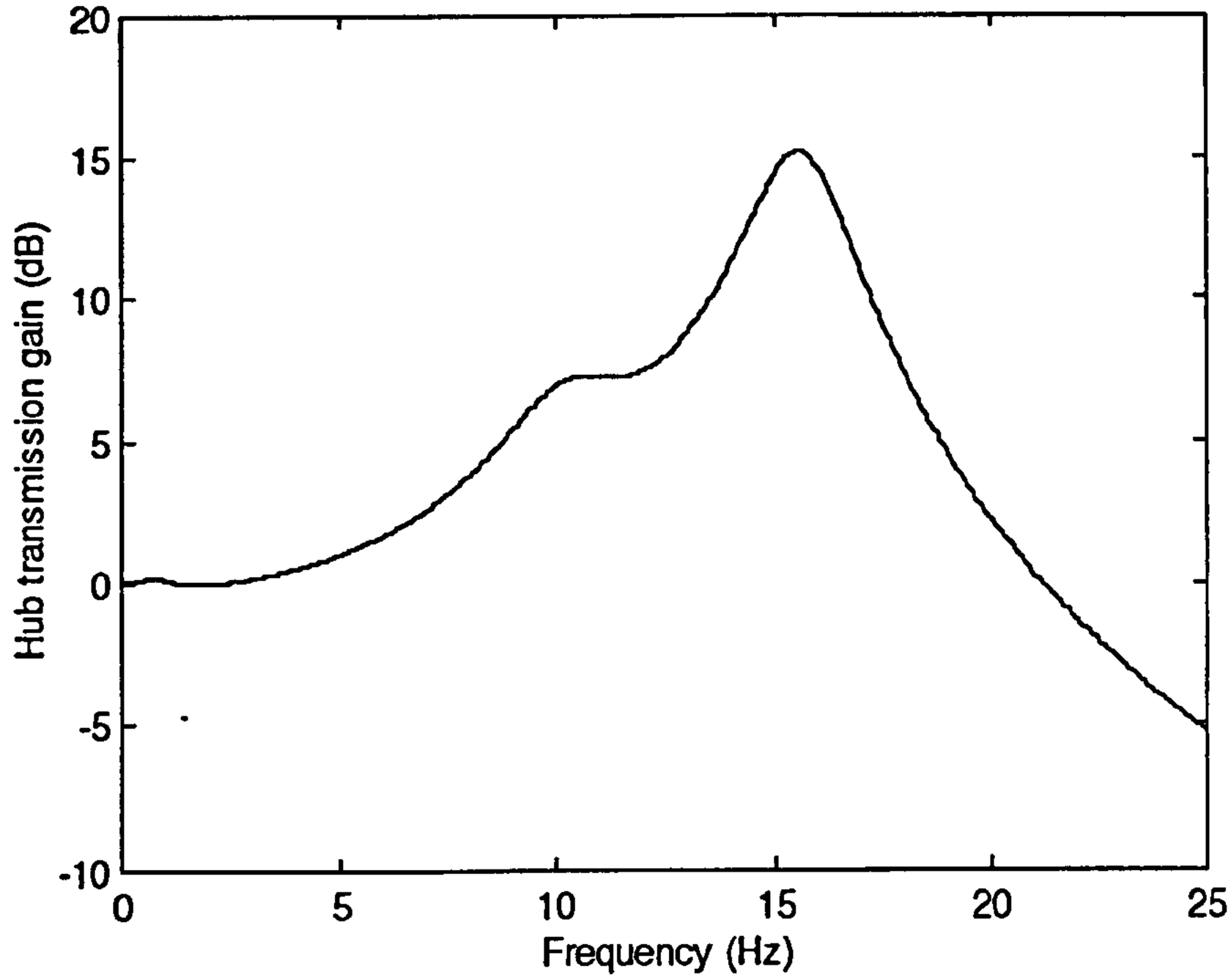

Figure 8-15(b) The initial corresponding hub transmission before the absorber frequency being tuned

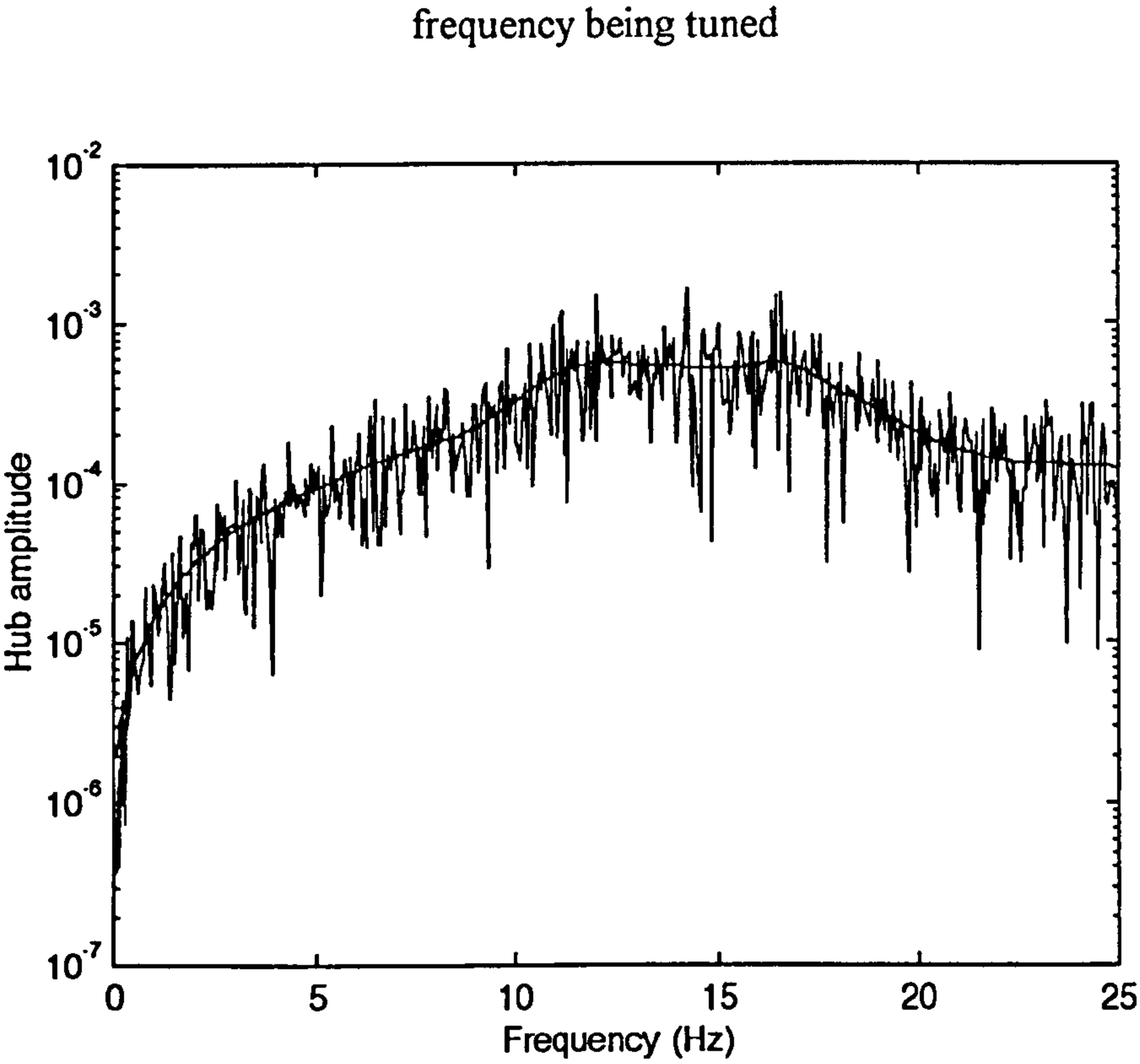

Figure 8-16(a) The frequency spectrum for hub vibration excited by white noise road profile after a few times of tuning the absorber frequency

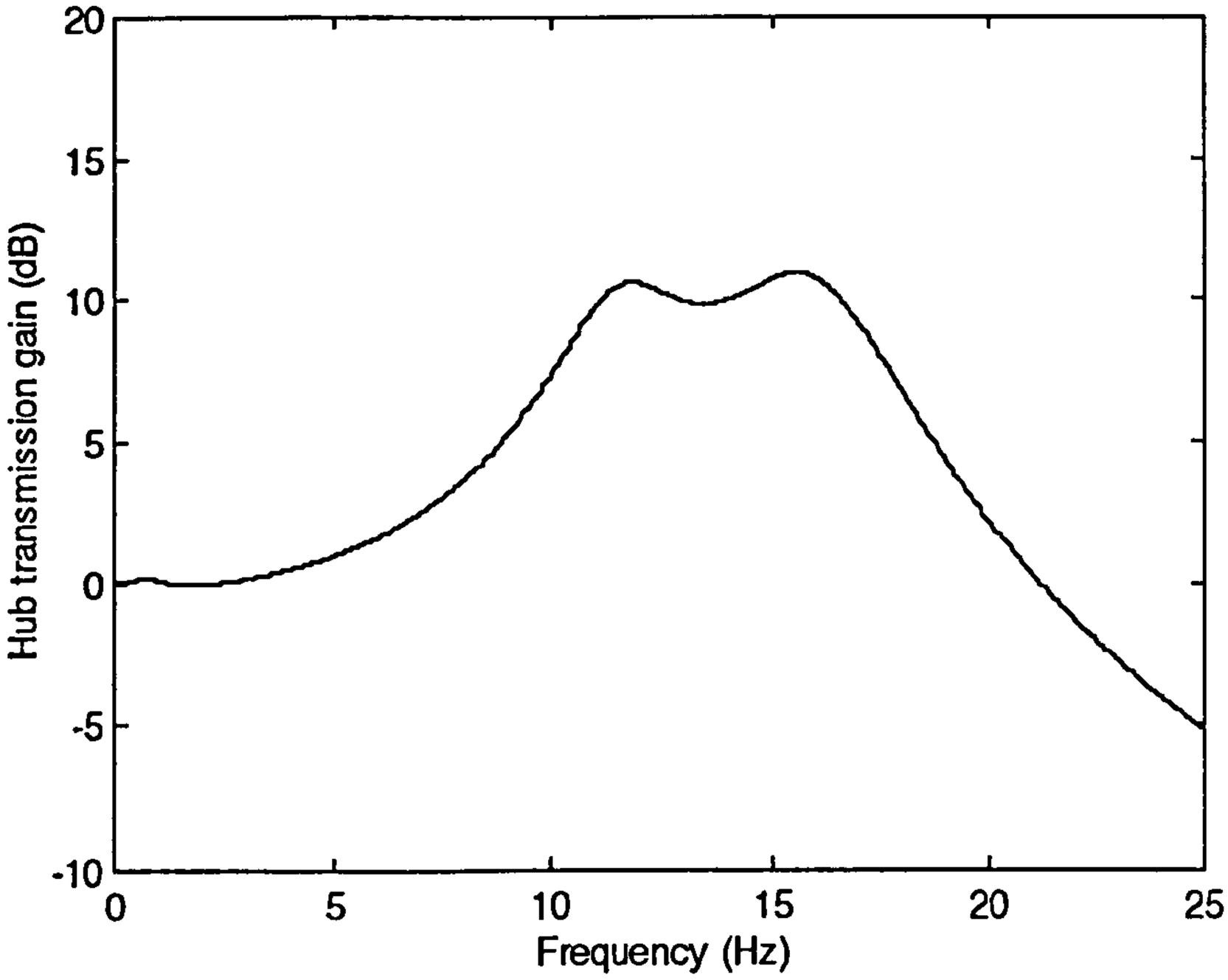

Figure 8-16(b) The corresponding hub transmission after a few cycles of tuning the absorber frequency

Figure 8-17 The procedure of the absorber frequency being tuned

Chapter 9

Implementation of the Active Tuneable Vibration Absorber and Measurement Results

9.1 Introduction

It has been demonstrated in the last chapter that a vibration absorber on the hub is effective at reducing vibration transmission to the body and attenuating the hub vibration. The ATVA can adapt to changes in the primary system. The proposed control strategy has been demonstrated to work well for the ATVA.

To validate the results obtained from the simulation, a quarter car test rig and prototype for the ATVA have been developed and built. It is shown by experiment that the implementation is successful and the ATVA works well. In this chapter, the implementation and experimental results will be presented.

9.2 Description of the Quarter Car Test Rig

In order to demonstrate the performance of the developed absorber, a quarter car test rig has been built in the Engineering Division at the University of Wolverhampton. This rig is built from a used car wheel and suspension. Two rig arrangements are shown in figures 9-1 and 9-2.

The wheel and suspension are the front assembly of a Triumph Dolomite. The damper and spring were not used but the wheel and wishbones were kept. The double wishbone is installed on two steel bars which are fixed on a pair of vertical steel channels. The wheel can move along the constraint of the wishbone. On the hub, there is a pedestal for the accelerometer which is the same type as that on the trailer body and can measure the vertical acceleration of the hub. There is also a position for the developed absorber assembly on the hub.

Two methods for measuring the vibration transmission of the hub from the road profile have been used on the test rig. The first is a standard method which is shown in figure 9-1. Under the wheel, there is a vibrator which is driven by a DC motor. This vibrator can vertically provide a sine wave excitation to the wheel. The excitation covers the frequency domain from about 2Hz to 30Hz. Both the motions on the hub and vibrator are measured through two accelerometers respectively. The vibration transmission at each frequency can be obtained from the ratio of the hub amplitude over the excitation amplitude for the corresponding frequency. The vibration transmission over the whole frequency range can be produced by sweeping the excitation frequency. Because this rig is a demonstrator only for the absorber, the frequencies from 5Hz to 20Hz are investigated.

The second method, which has been introduced in Chapter 3, is used again for the quarter car test rig as shown in figure 9-2. The measurement platform is put under the wheel. A set of pre-loaded springs are connected from the wishbone to ground. There are two purposes for this; to simulate static load of the vehicle body and to keep the wheel from bouncing off the platform during the test.

The relevant signals are sampled by a PC computer for both methods. The computer is still the Apricot 80386sx. The other hardware such as A/D board, is also the same as that in Chapter 2. The analysis of the signals for the second method is the same as that in Chapter 3.

9.3 Implementation of the ATVA

A prototype of the ATVA has been developed in the Engineering Division, University of Wolverhampton. This ATVA is a PC based mechatronic system as shown in figure 9-3. The system includes four primary parts, namely the tuneable absorber, the measurement system, the computer control system, and the actuator system, which will be introduced individually.

The tuneable absorber consists of a spring which is made of a steel beam, a pneumatic cylinder which works as a damper, a weight which can be moved along the beam, and a frame which supports the spring and damper and can be mounted on the hub, as shown in figure 9-4.

This is a tuneable stiffness approach. The stiffness tuning is implemented by changing the position of the weight along the beam. If the approach is modelled as a massless

cantilever beam with a concentrated load as shown in figure 9-5, the natural frequency will be

$$f_a = \frac{1}{2\pi}\sqrt{\frac{3EI_a}{m_a x_a^3}} \qquad (9\text{-}1)$$

where E is the Young's modulus and I_a is the area moment of inertia of beam cross section.

Comparison between the prediction of equation (9-1) and experimental results is made in figure 9-6. It is shown that there is a big difference between them. The reasons for this are that the actual prototype has three primary differences from the ideal cantilever beam model. The first is that the beam is fixed on the frame by only two screws, which is not the ideal fixed constraint. The second is that the beam has considerable mass and the physical size of the weight is large, which is significantly different from a concentrated mass on a massless beam. The third is that the frame is not an ideal rigid structure, which can further degrade 'the fixed end constraint'. All of these points result in the real natural frequency being much less than that predicted by equation (9-1). If the real prototype was modelled as precisely as possibly, the resultant equation would be much more complicated than equation (9-1).

It can be seen in figure 9-6 that the actual natural frequency for the tuneable absorber can be changed in the range from about 11Hz to 19Hz which covers the normal requirement for the particular wheel.

The measurement system consists of an accelerometer on the hub and a corresponding signal conditioning device. The vibration of the hub can be measured through the accelerometer. The measured signals are used to analyse the state of the hub and then to determine the state of the absorber. The signal conditioning is an analogue anti-alias filter which can avoid aliasing caused by high frequency noise.

The actuator system is a linear stepping motor with its drive board. The specification of the stepping motor and the drive board are shown in tables 9-1 and 9-2 respectively. The body of the motor is mounted on the absorber mass as shown in figure 9-4. One end of the motor lead screw is fixed on the end of the spring beam. When the motor operates, the motor body and the weight will move along the beam. Power for the stepping motor comes from the drive board.

The clock input for the drive board is a 1Hz-25kHz pulse. The frequency of the input pulses determines the stepping speed of the motor and the number of pulses

determines the displacement of the motor. In the absorber application, the displacement of the motor is significant, but its speed needs only to be set to a reasonable value. The input pulses are produced by the computer control system.

The computer control hardware is the Apricot 80386sx PC computer with the AD1200 A/D and D/A board. The measured signals are transferred from the analogue form to the digital form by the A/D board and sampled into the PC computer. After appropriate processing, the control signals are created in the computer and are sent to the actuator system via the digital output port of the AD1200 board.

The control software is written in C++. The structure of the software is illustrated in the block diagram in figure 9-7. The control strategy presented in last chapter is included in this software.

The clock - control pulse can be produced by sending '0' and '1' through the digital output port at an appropriate rate. The number of the pulses depends on how far the absorber mass is to be moved. According to the measured relationship between the mass position and natural frequency in figure 9-6, the distance can be determined from the frequency required. A method for determining the tuned frequency has been given in the control strategy discussed in the last chapter.

Within the processing loop, the keyboard is monitored. There are two purposes for this. The first is that the control system has to wait for the hub vibration to be excited because there is no excitation facility in this quarter car test rig to simulate the random road profile. The method being used is to hammer the wheel, which can simulate the wheel going over a stone swiftly. This method of course is not ideal because repetitive hammering may mislead the controller. The second purpose is to allow the control program to be interrupted.

To avoid the need for a position transducer on the absorber mass an initialisation procedure ensures the mass starts at the extreme end on the beam. From this point all incremental changes are summed to maintain absolute position data. Similarly when the algorithm ends the mass is returned to the extreme end of the beam.

In table 9-2, it can be seen that stepper motor drive board has four inputs. Two of them, direction and clock, are necessary for the application of the ATVA. Every input only takes up one bit of the digital output port. In other words, the application needs at most four and at least two digital output bits. When the computer determines the direction and amount of the movement for the absorber mass, it will send the suitable

binary number to the direction bit whilst sending the '0' and '1' the appropriate number of times to the clock bit.

Because the level '1' for the AD1200 board is only 4.3V but the level '1' for the stepper motor drive board needs to be 12V, a voltage amplifier had to be installed between the two boards.

9.4 Experimental Results for the ATVA

The developed ATVA was tested on the quarter car test rig. Some encouraging experimental results have been obtained. The performance of the ATVA has been observed in two respects. The first is the vibration attenuation performance and the another is the frequency tuning control performance.

Figure 9-8 illustrates the measured hub vibration transmission obtained by the method of the sine sweep based on the rig shown in figure 9-1. The two curves correspond to hub without the absorber and with the well-tuned absorber respectively. It is shown that the well-tuned absorber can attenuate the hub vibration by about 9dB around the wheel mode frequency. The biggest attenuation achieved is about 13dB.

Figure 9-9 was obtained by the developed measurement system for identifying suspension transfer functions as shown in figure 9-2. The measured hub vibration transmission correspond to the same cases as those in figure 9-8. It is shown again that the well-tuned absorber can reduce the hub vibration by about 9dB near the region of the wheel mode frequency.

Comparing figures 9-8 and 9-9, it can be seen that the two different measurement methods have given similar results for the hub vibration attenuation performance. Both methods give similar peaks of the composite natural frequencies for the wheel and absorber modes for the two cases. It is shown that both measurement methods can produce basically the same results for the vibration transmission. This comparison is the second validation of the developed measurement system for identifying suspension transfer functions.

By using the first measurement system shown in figure 9-1, the acceleration of the hub response can be measured for the sine road excitation. Figure 9-10 illustrates the time domain response of the hub acceleration for the case with no absorber. At 13.66Hz excitation frequency, the response amplitude is more than four times the road

excitation. When the well-tuned absorber is mounted on the hub, as shown in figure 9-11, the hub response amplitude is nearly the same as that of the road excitation at the same excitation frequency. It is shown, from the time domain point of view, that the well-tuned developed absorber can provide a significant vibration attenuation performance to the hub.

The control strategy developed in chapter 8 for the ATVA has been implemented in the prototype. Figures 9-12 and 9-13 are the test results for the control performance. There are two curves in each figure. The dash line is obtained directly from the measured acceleration and the solid line is the fitting curve of the spectrum.

Figure 9-12 shows the frequency spectrum of the hub vibration acceleration before the absorber frequency is tuned. At this stage, the peak at the higher composite frequency is higher than that at the lower composite frequency. That means that the absorber was not well tuned to the appropriate state. The control system was turned on. After normally 5 cycles of measuring the hub acceleration, FFT analysis and tuning absorber frequency, the frequency spectrum of the hub vibration acceleration was obtained as shown in figure 9-13. It can be found in this figure that the two peaks have the nearly same height, which means that the absorber frequency has been well tuned.

Figures 9-14 and 9-15 illustrate the hub vibration responses excited by sine road input at 14Hz before and after the absorber being tuned. The two figures are corresponding to the cases shown in figures 9-12 and 9-13 respectively. In figure 9-14, the amplitude of the response is about 1.8 times of the excitation. In 9-15, the amplitude of the response is less than 1.1 times of the excitation. The hub vibration was reduced by about 55% after the absorber being tuned, which means that the tuned absorber is effective and necessary.

To demonstrate the adaptive performance to parameter shifting in the primary system, the operation of the ATVA was examined for a change in the air pressure in the tyre. Figures 9-14 and 9-15 are for the tyre air pressure of 2bar and the absorber mass is the position of 11.5cm for the case in figure 9-15. When the air pressure was changed to 1.5bar, the frequency spectrum was measured as shown in figure 9-16 in which the absorber position is the same as that in figure 9-15. Obviously, the absorber needs to be tuned again. After several cycles of tuning, the measured frequency spectrum became the well-tuned state shown in figure 9-17. In this state, the position of the absorber mass is at 12.3cm. That means that the ATVA can automatically adjust its optimum state with changes in the tyre air pressure.

These results show that the developed control strategy for the ATVA is effective and works well in the prototype.

9.5 Conclusions

The development of an active tuneable vibration absorber has been presented in this chapter. The developed control strategy for the ATVA has been implemented in a physical prototype. Experimental results have shown that the ATVA can attenuate the hub vibration transmission by about 9dB and the control system can automatically adjust the absorber frequency to keep the hub vibration at a low level. That means that the concept, design and implementation for the ATVA and its control system have been successful.

In the author's opinion, two points still need to be improved for the prototype. The first is that the mechanical design for the absorber should be made more sophisticated, even though the current prototype is small enough for real use. The second is that the period of tuning the absorber frequency is about four minutes which may be too long for the actual application. This problem can be solved through improving the algorithm, software and hardware in the control system. If both problems can be solved satisfactorily, the ATVA will be a good candidate for the real applications.

Starting force	125N
Step	0.025mm
Travel (max)	170mm
Motor (4-phase unipolar)	12V d.c., 25Ω
Lead screw length	225mm
Lead screw termination	M4
Step accuracy	±0.005mm
Accuracy of repetition	±0.01mm

Table 9-1 The technical specification for the standard stepping linear motor

Size	standard Euro card 168*100*15
Mating edge connector	standard 32-way DIN 41612 socket e.g. RS 471-503 or 467-453
Supply (board and motor)	15-30V d.c. +10% max. unregulated smoothed
Current consumption: a) board only	60mA
b) motor windings	dependent on motor used-up to 2A/phase max.
On-board auxiliary output	12V d.c. 50mA max. regulated
Switch logic control	Level '0' 0V Level '1' 12V } CMOS and open collector T.T.L. compatible
inputs: a) full/half step	Level '1' full step, Level '0' half step
b) direction	
c) clock	1Hz-25kHz, 10μs min. pulse width negative edge triggered
d) preset	Active Level '0' sets motor drive states to Q1 & Q2 OFF, Q2 & Q4 ON (full step mode). Q1, Q2 & Q3 OFF, Q4 ON (half step mode)

Table 9-2 The specification for the 4-phase unipolar stepper motor drive board

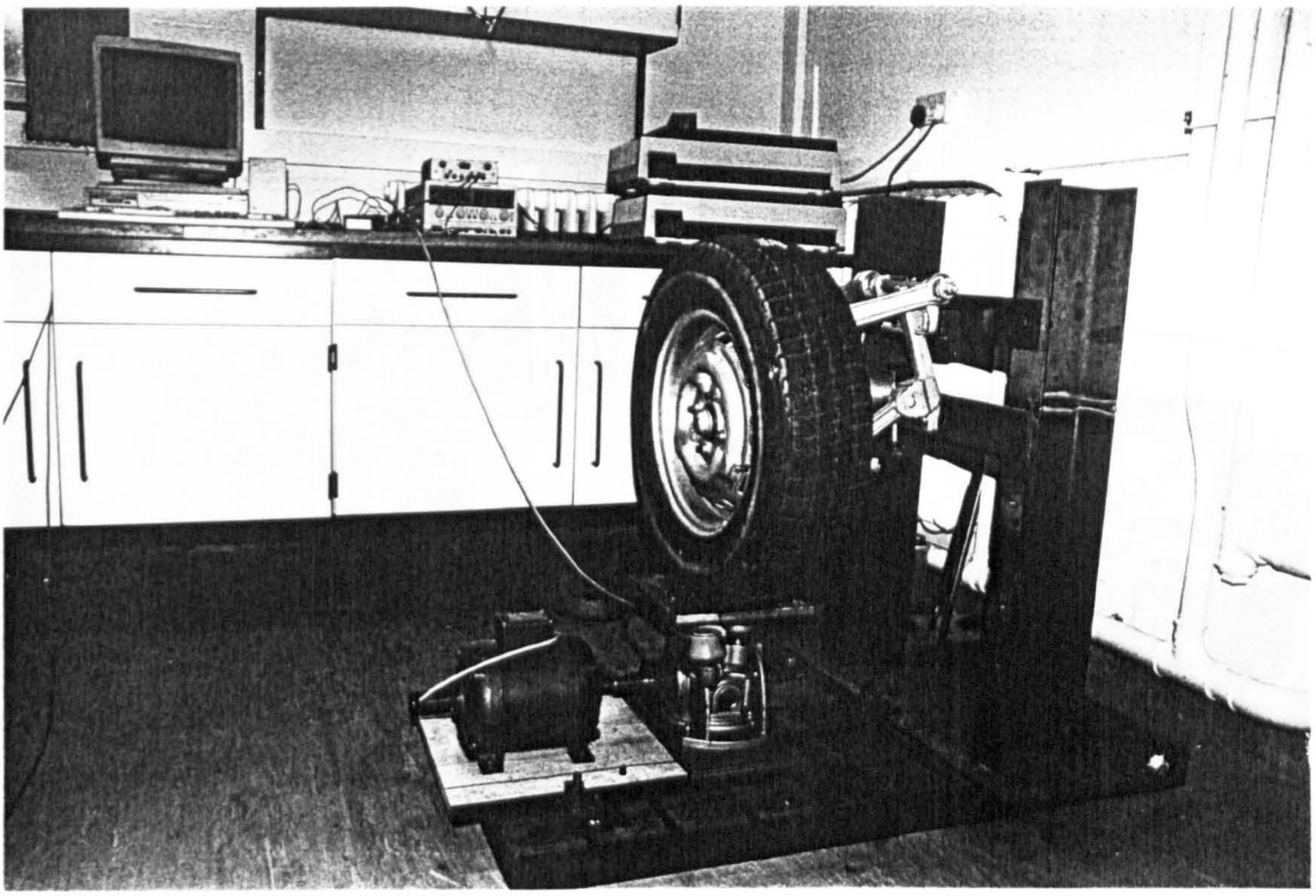

Figure 9-1 The quarter car test rig with sine road excitation

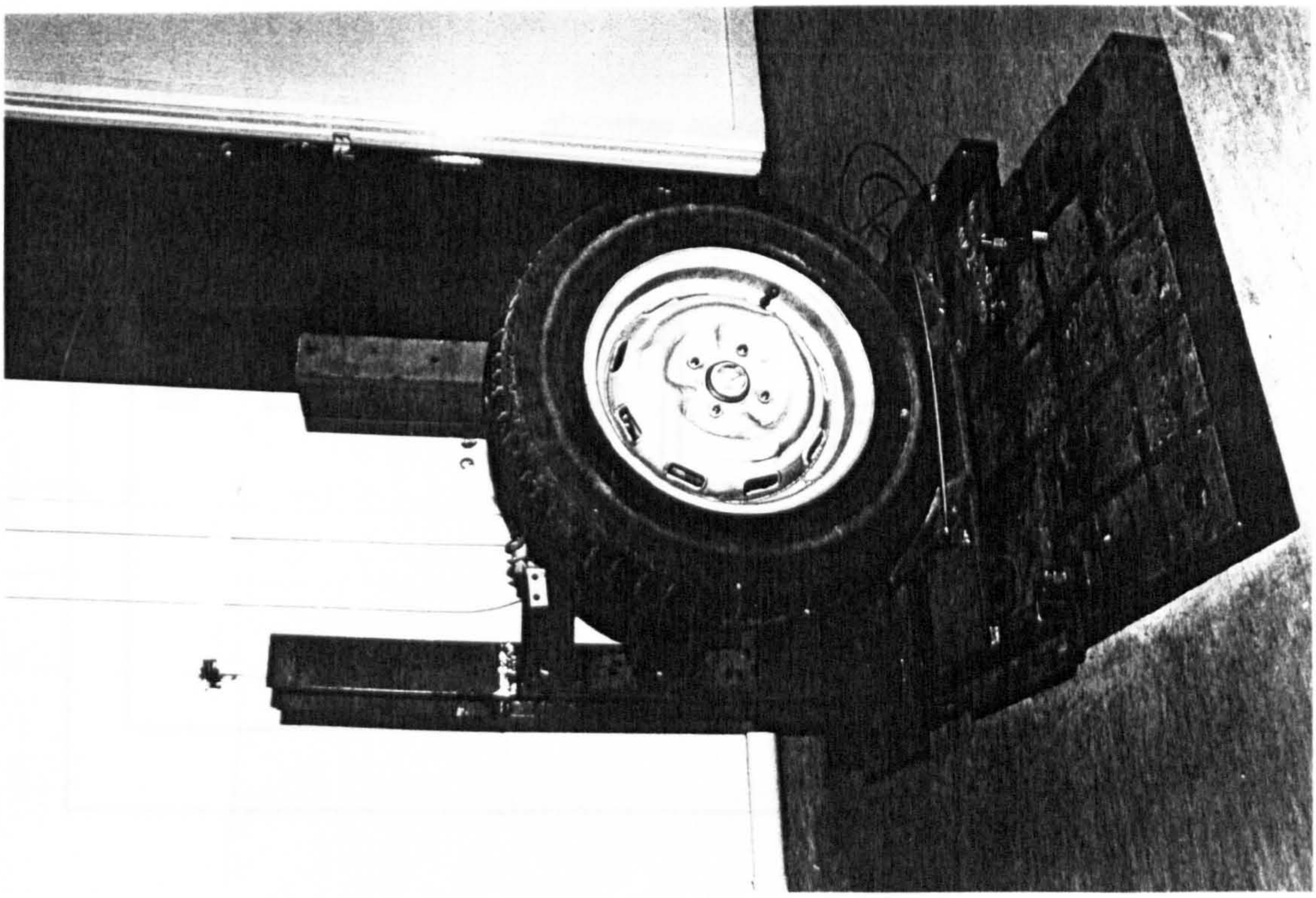

Figure 9-2 The quarter car test rig with the developed measurement system for identifying suspension transfer function

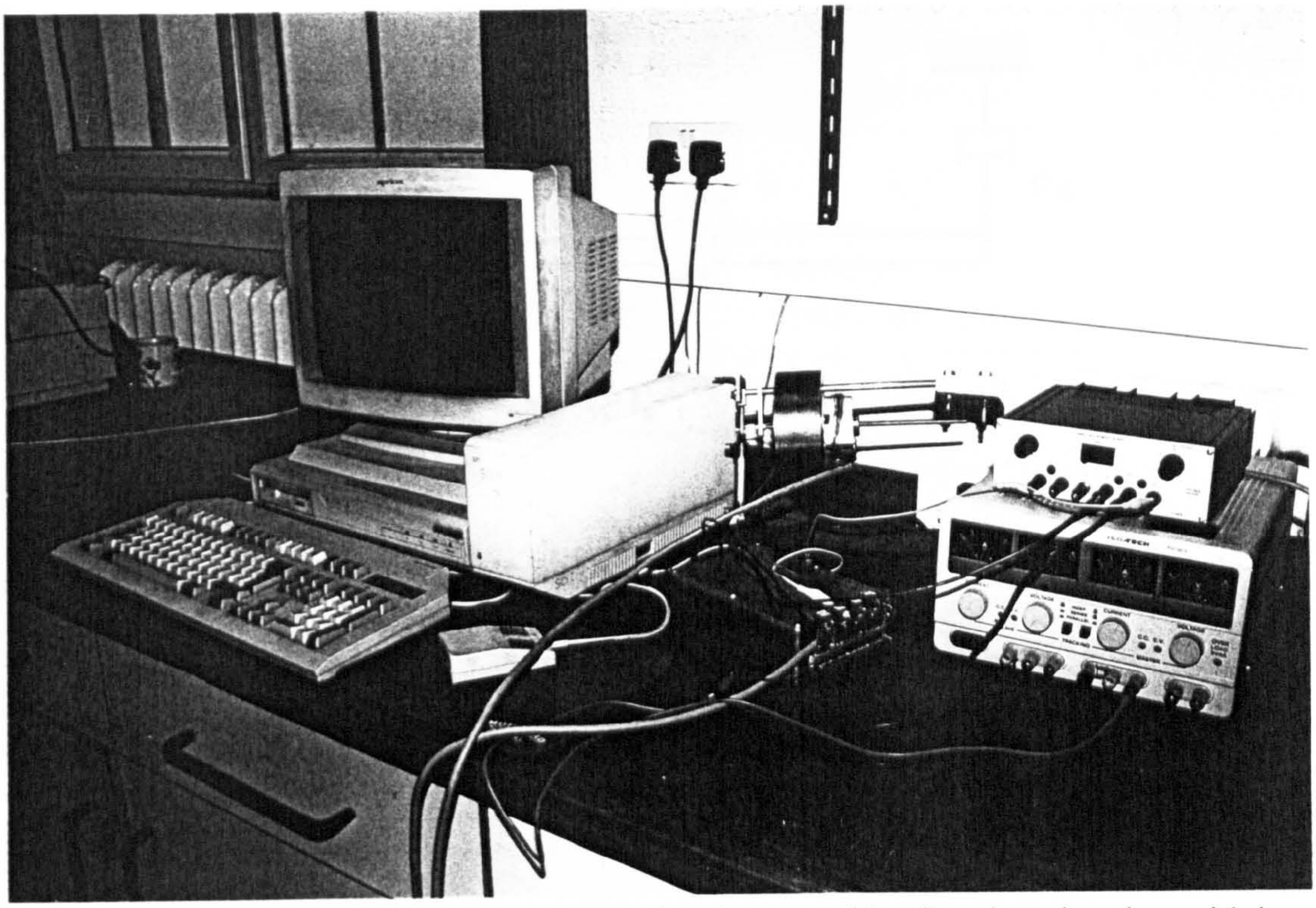

Figure 9-3 The prototype of the developed active tuneable vibration absorber with its control system and interfaces

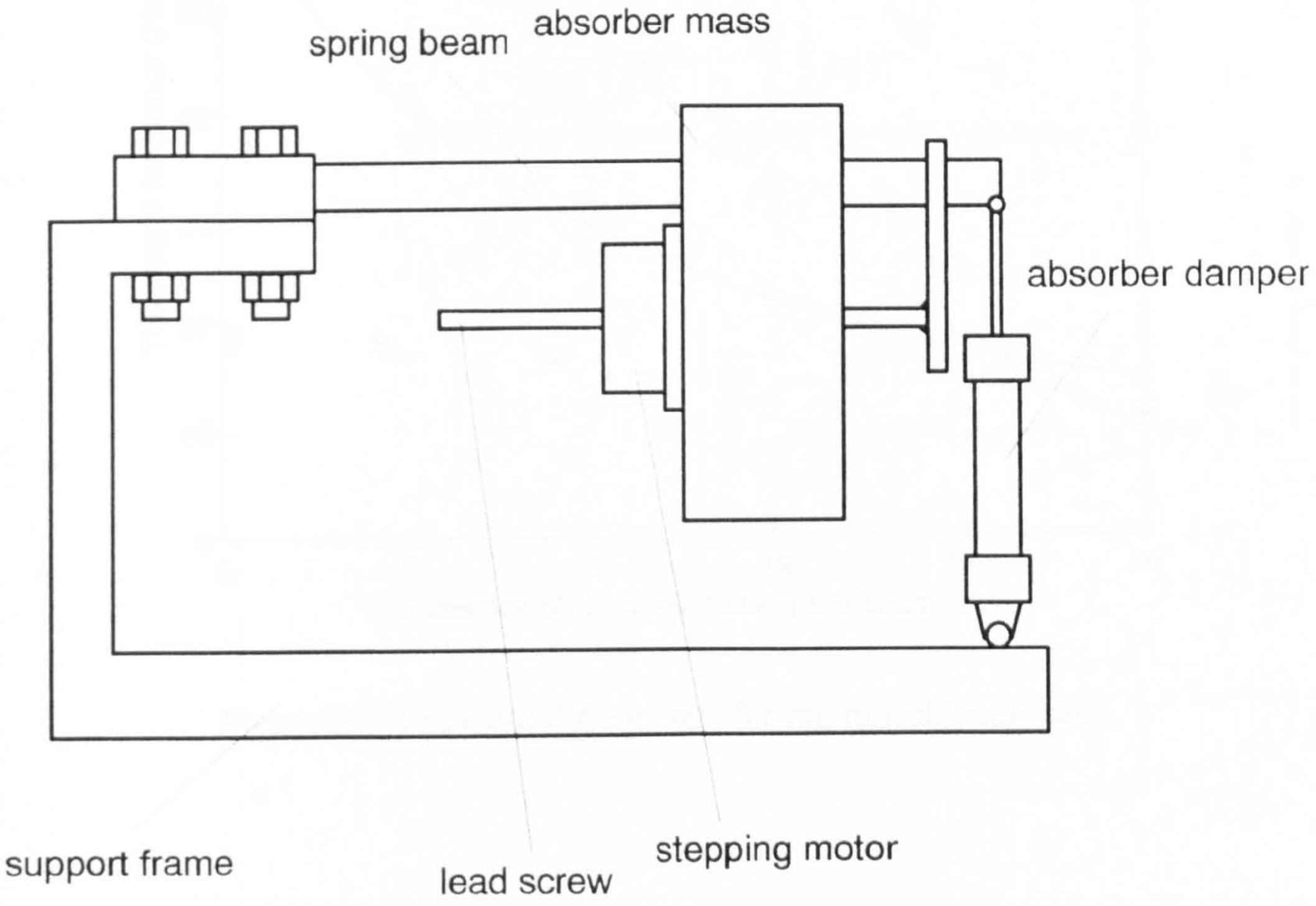

Figure 9-4 The mechanical set-up of the developed ATVA

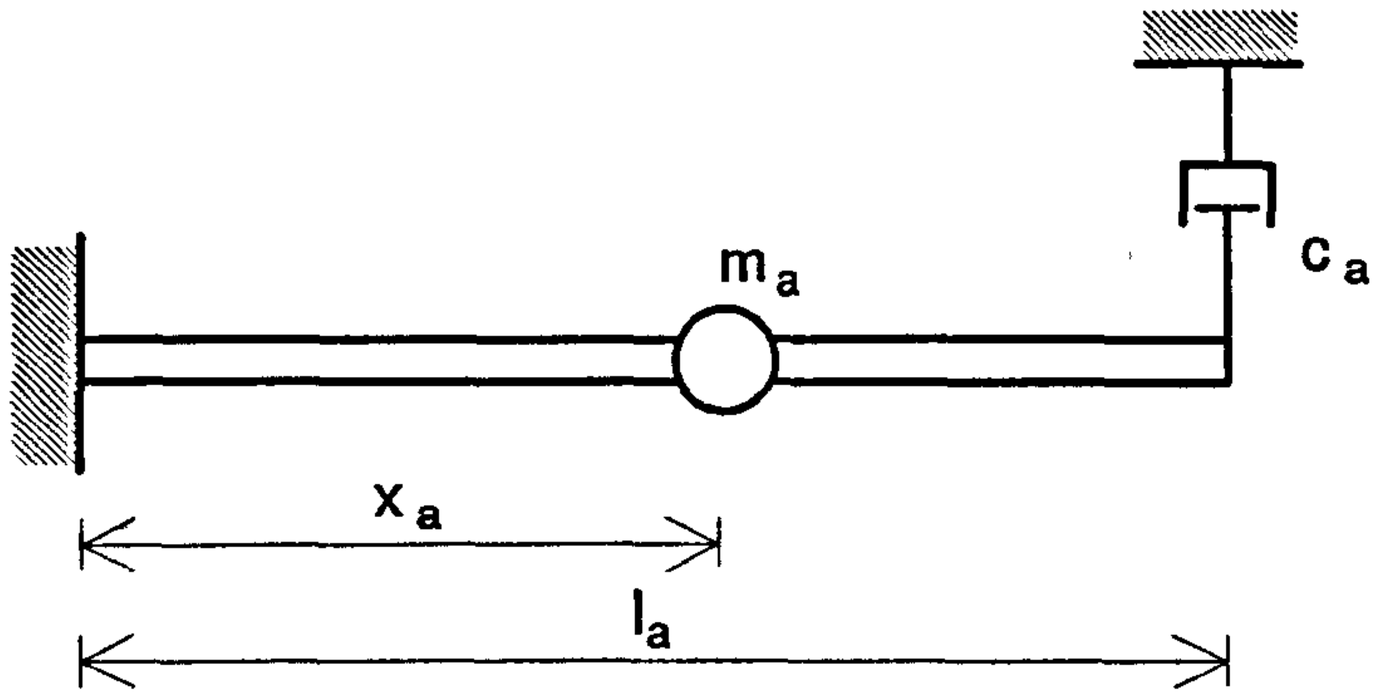

Figure 9-5 The ideal cantilever beam model

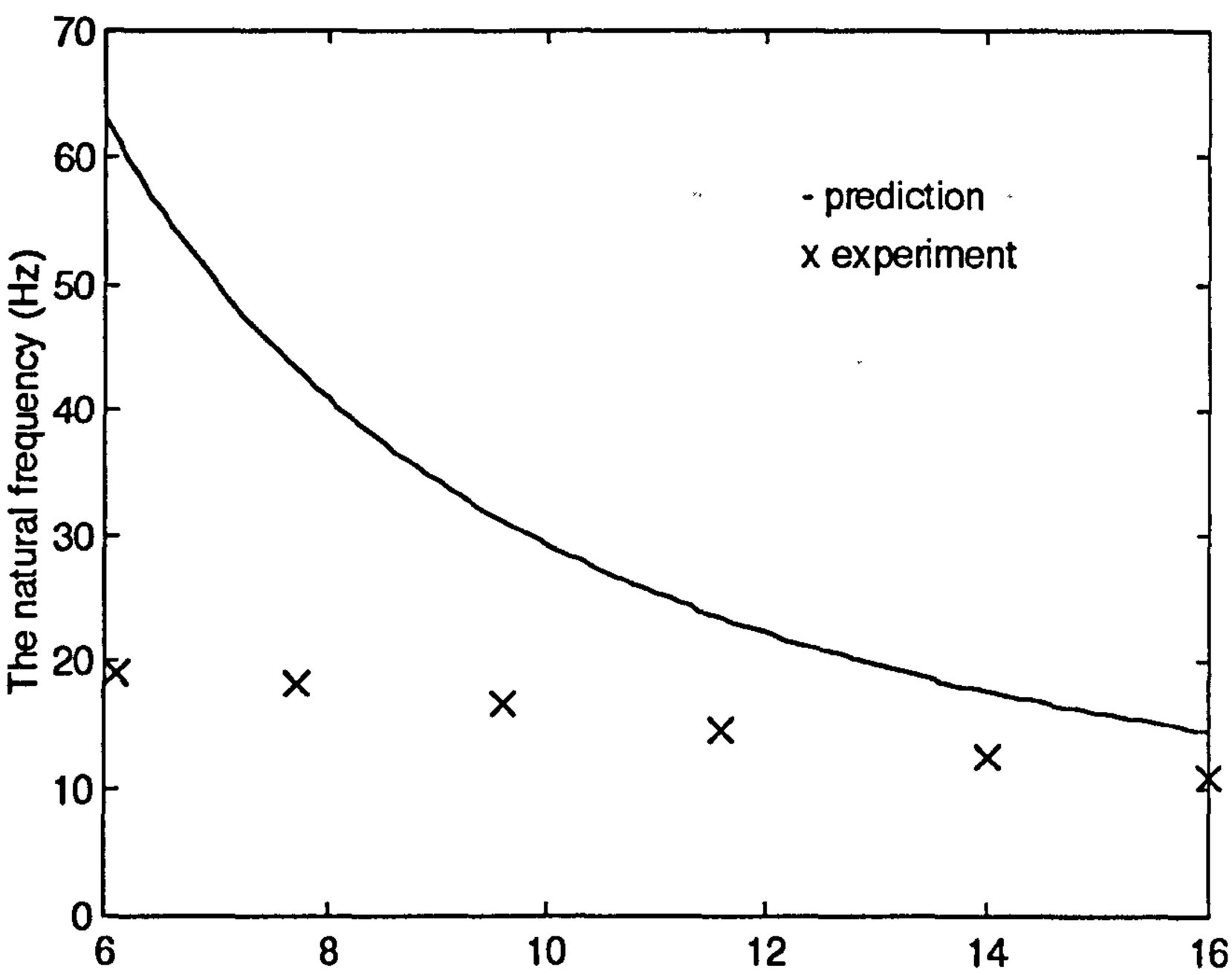

Figure 9-6 The natural frequency for the tuneable absorber

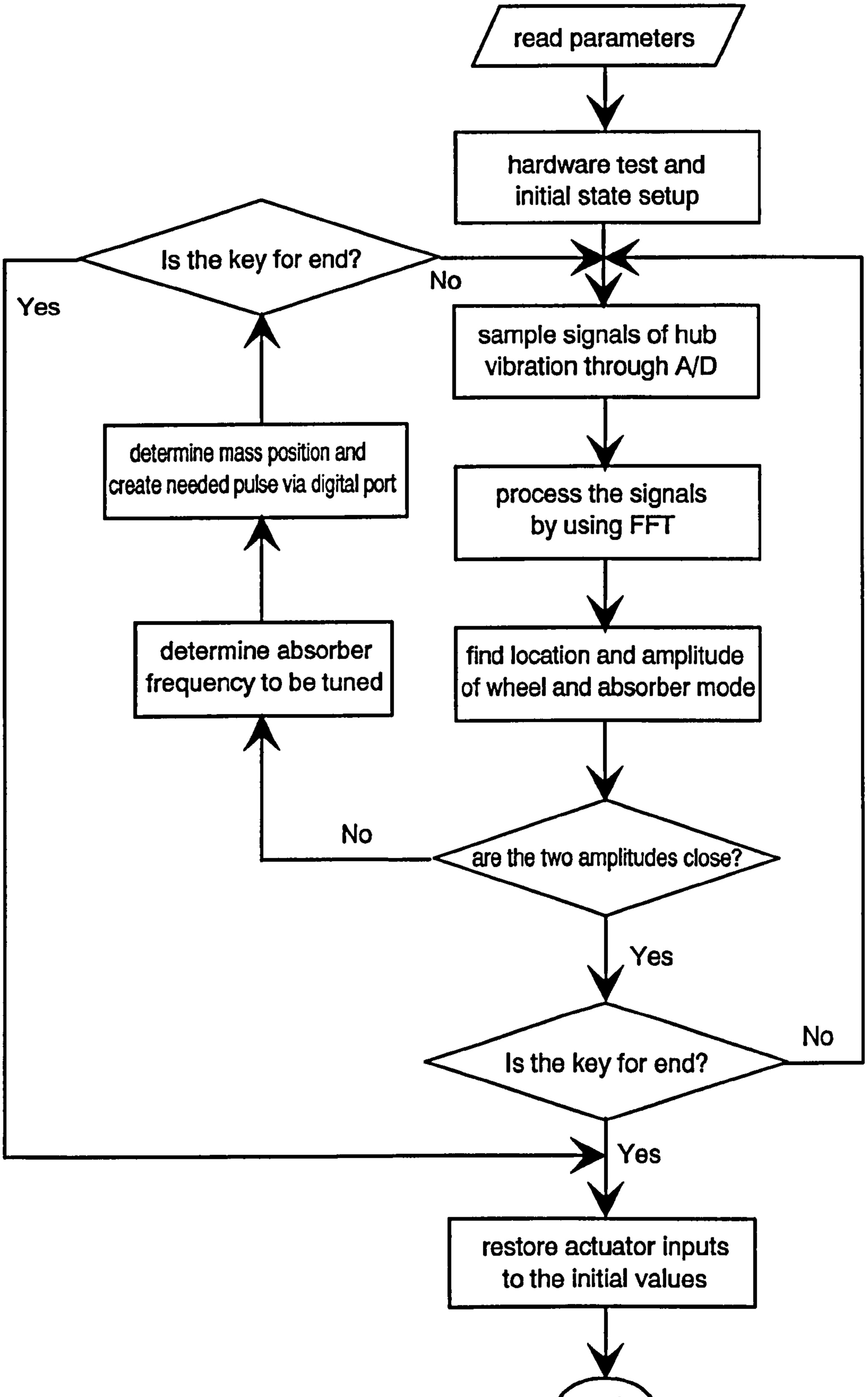

Figure 9-7 The block diagram for the tuneable absorber control software

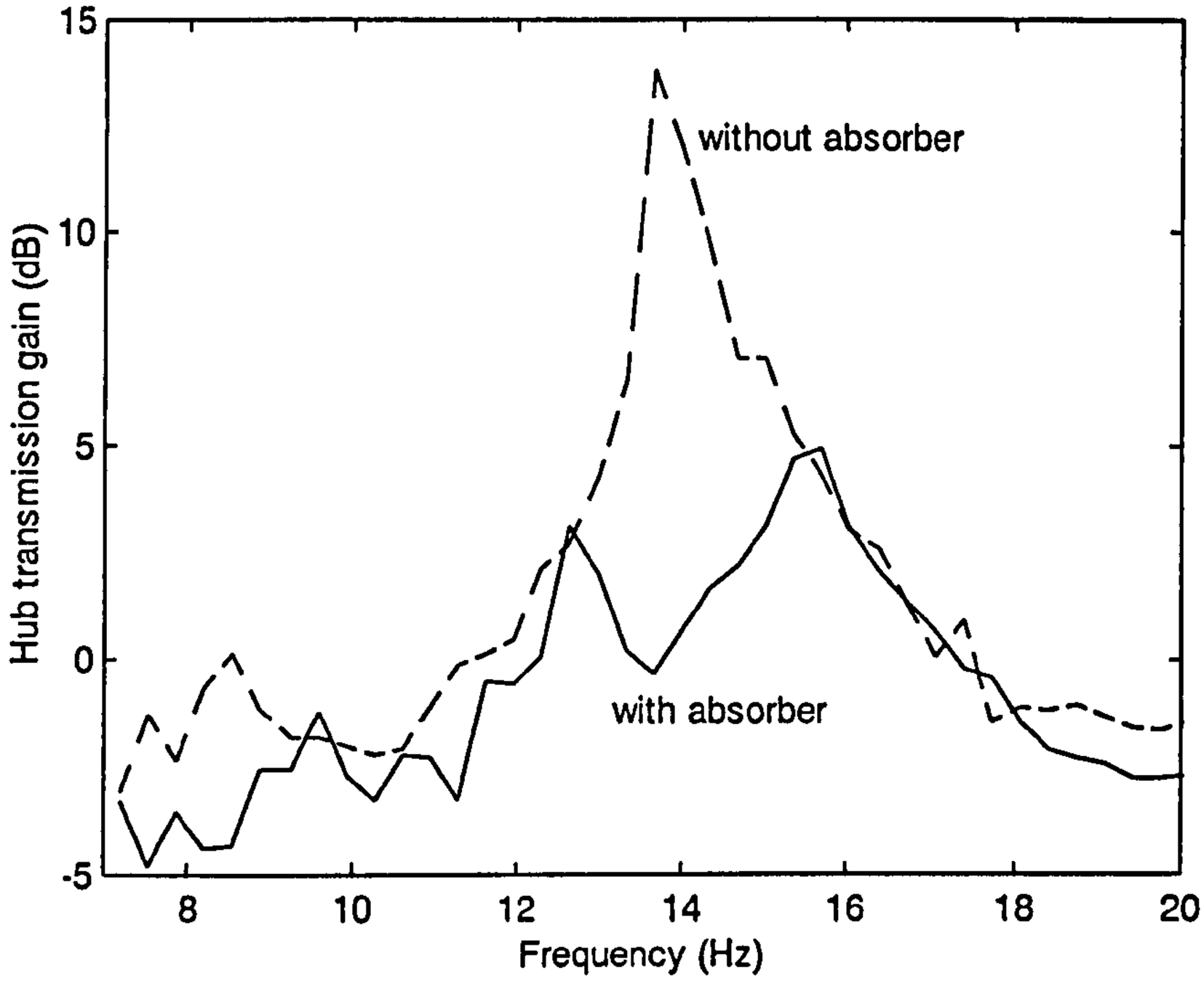

Figure 9-8 The measured hub vibration transmission obtained by sine sweep

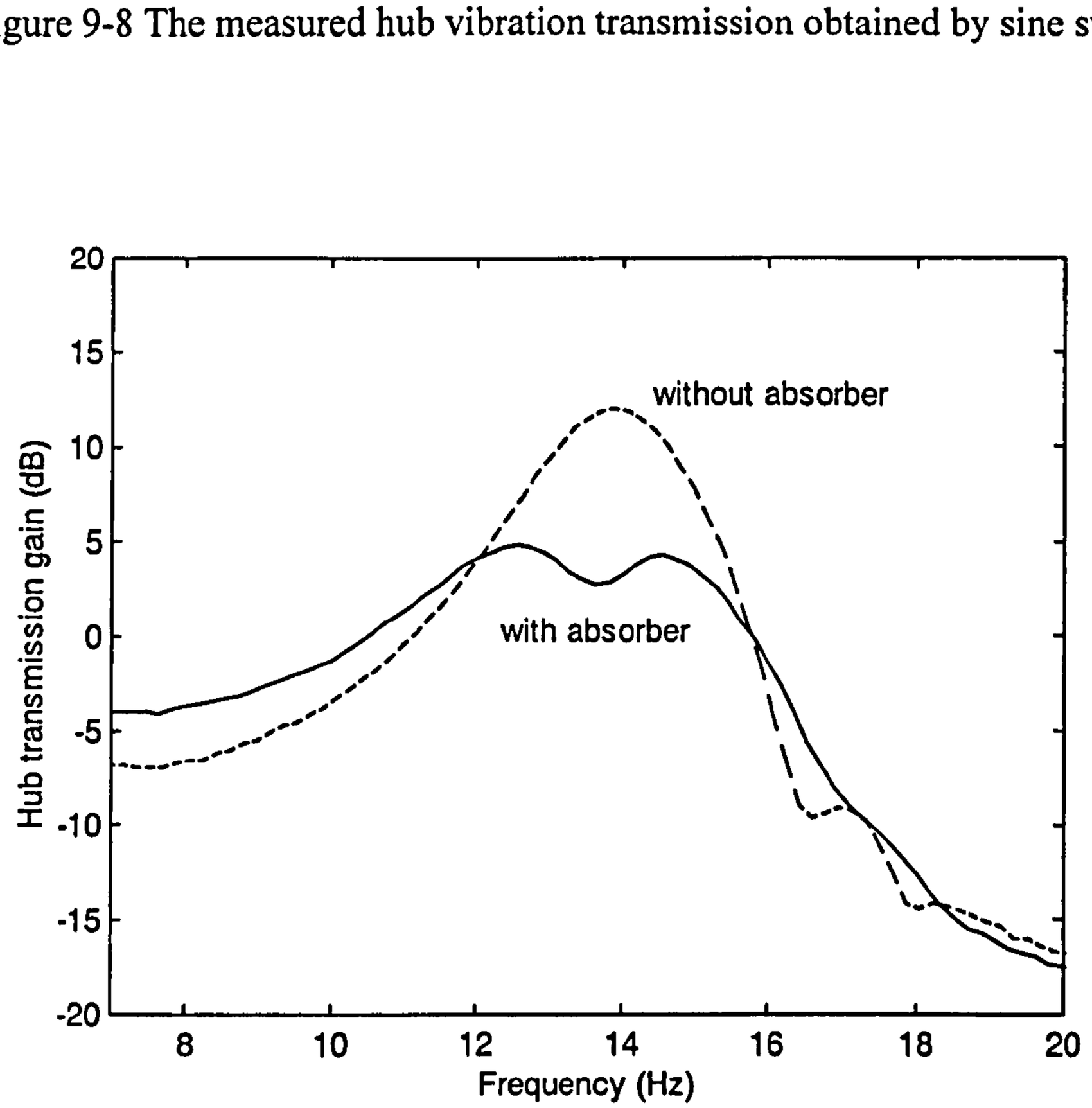

Figure 9-9 The measured hub vibration transmission obtained by the developed measurement platform

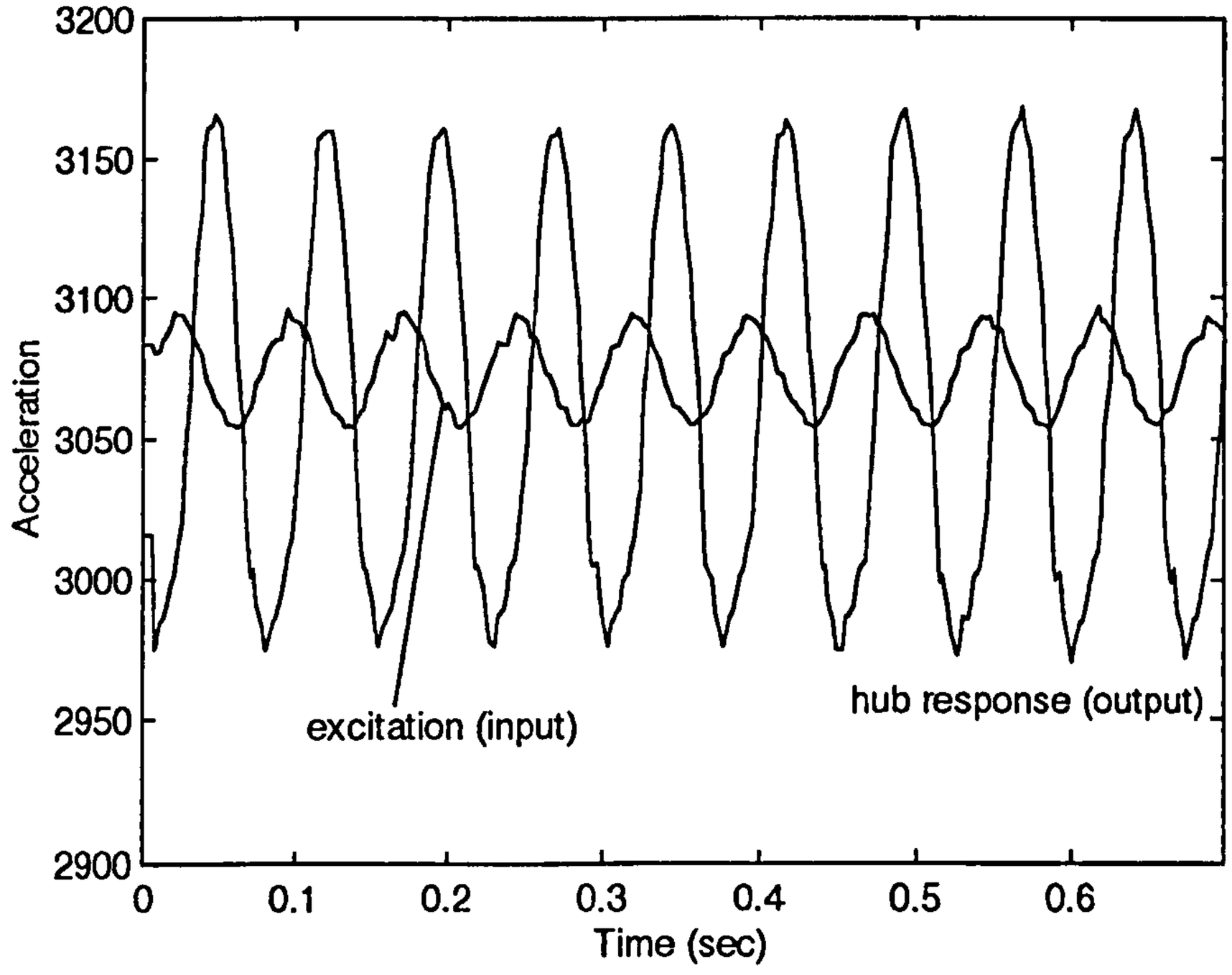

Figure 9-10 The hub response excited by sine road input at 13.66Hz when there is not the absorber on the hub

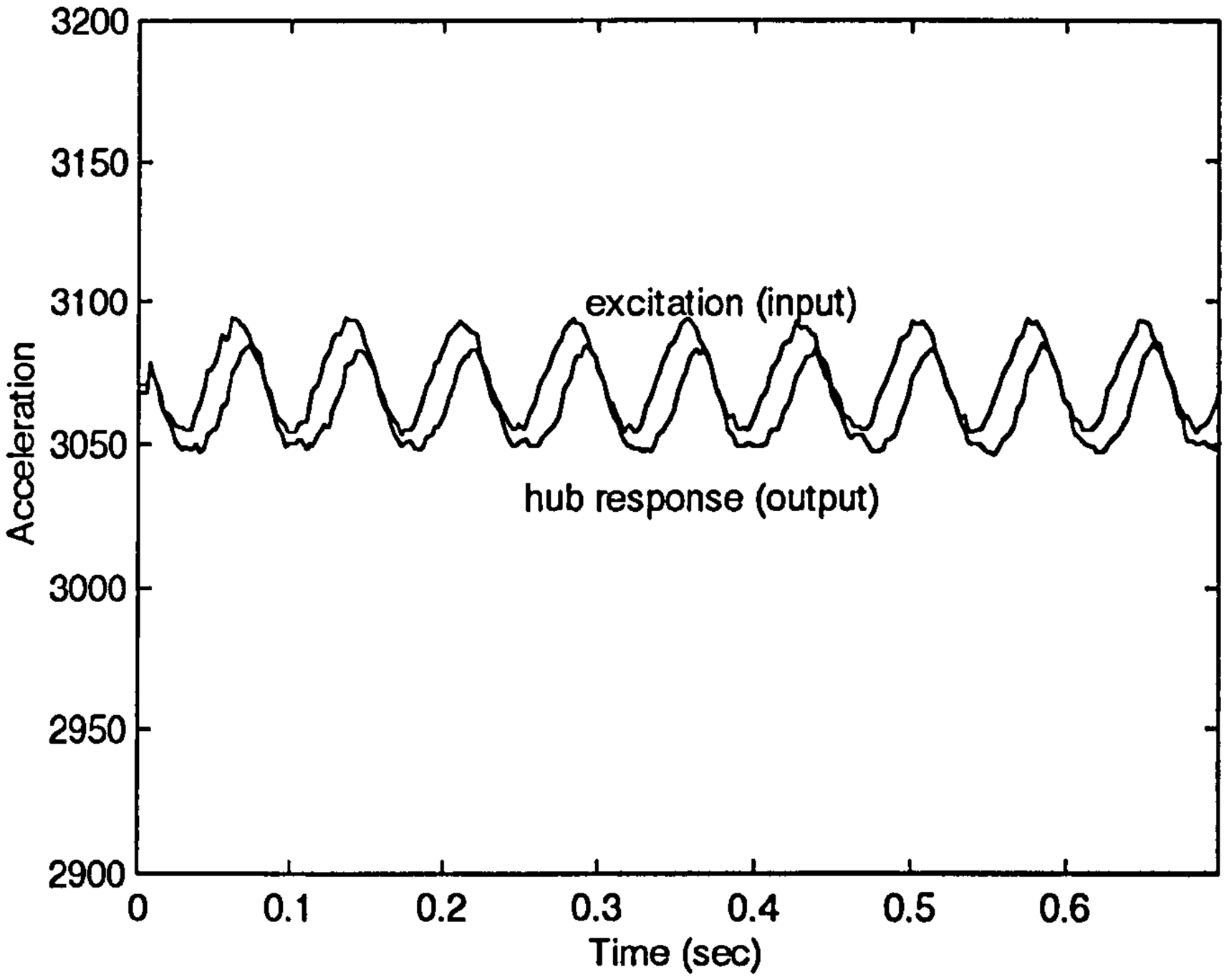

Figure 9-11 The hub response excited by sine road input at 13.66Hz when the well-tuned absorber is installed on the hub

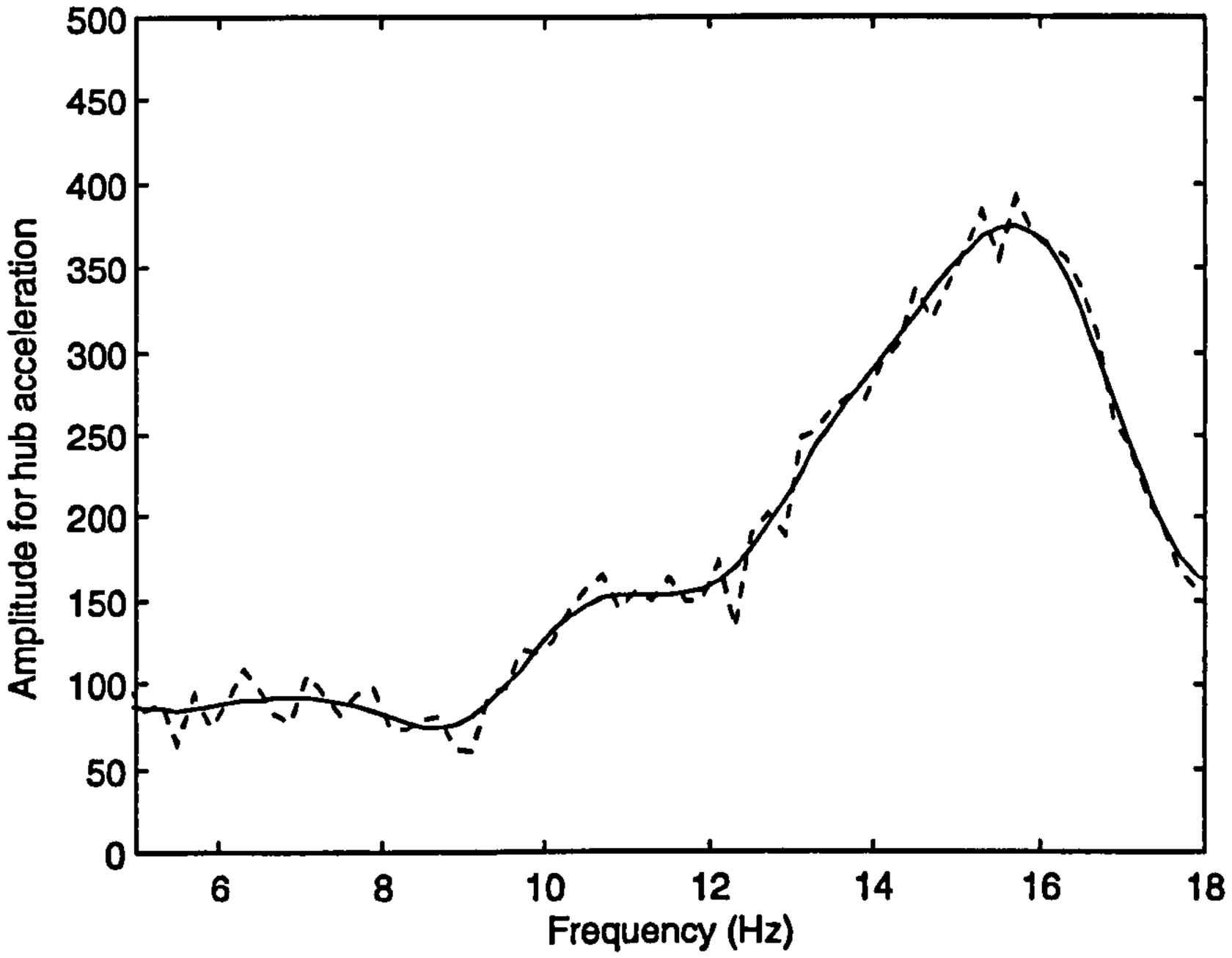

Figure 9-12 The measured frequency spectrum for the hub acceleration before the absorber being tuned

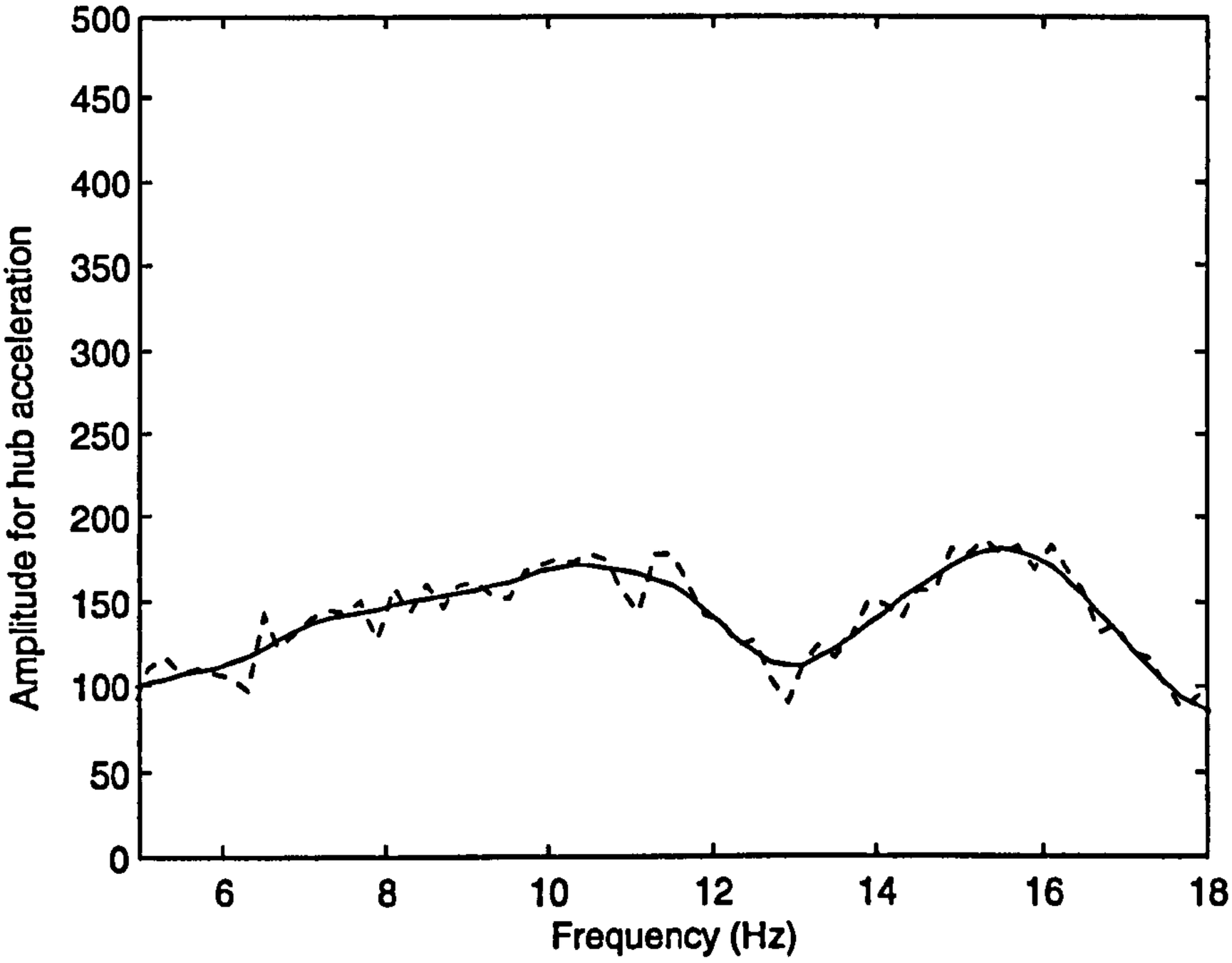

Figure 9-13 The measured frequency spectrum for the hub acceleration after the absorber being tuned for several times

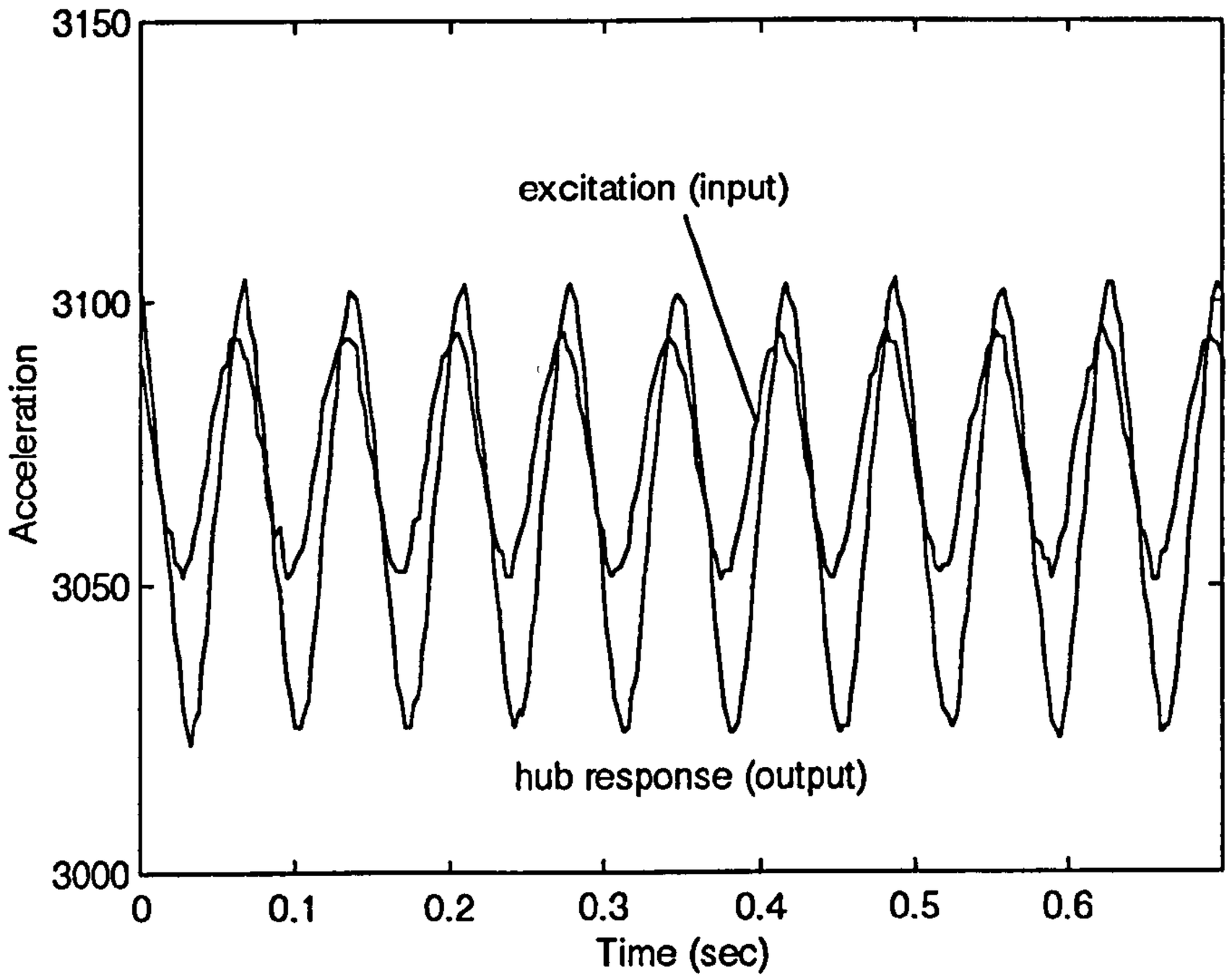

Figure 9-14 The hub response excited by sine road input at 14Hz before the absorber being tuned

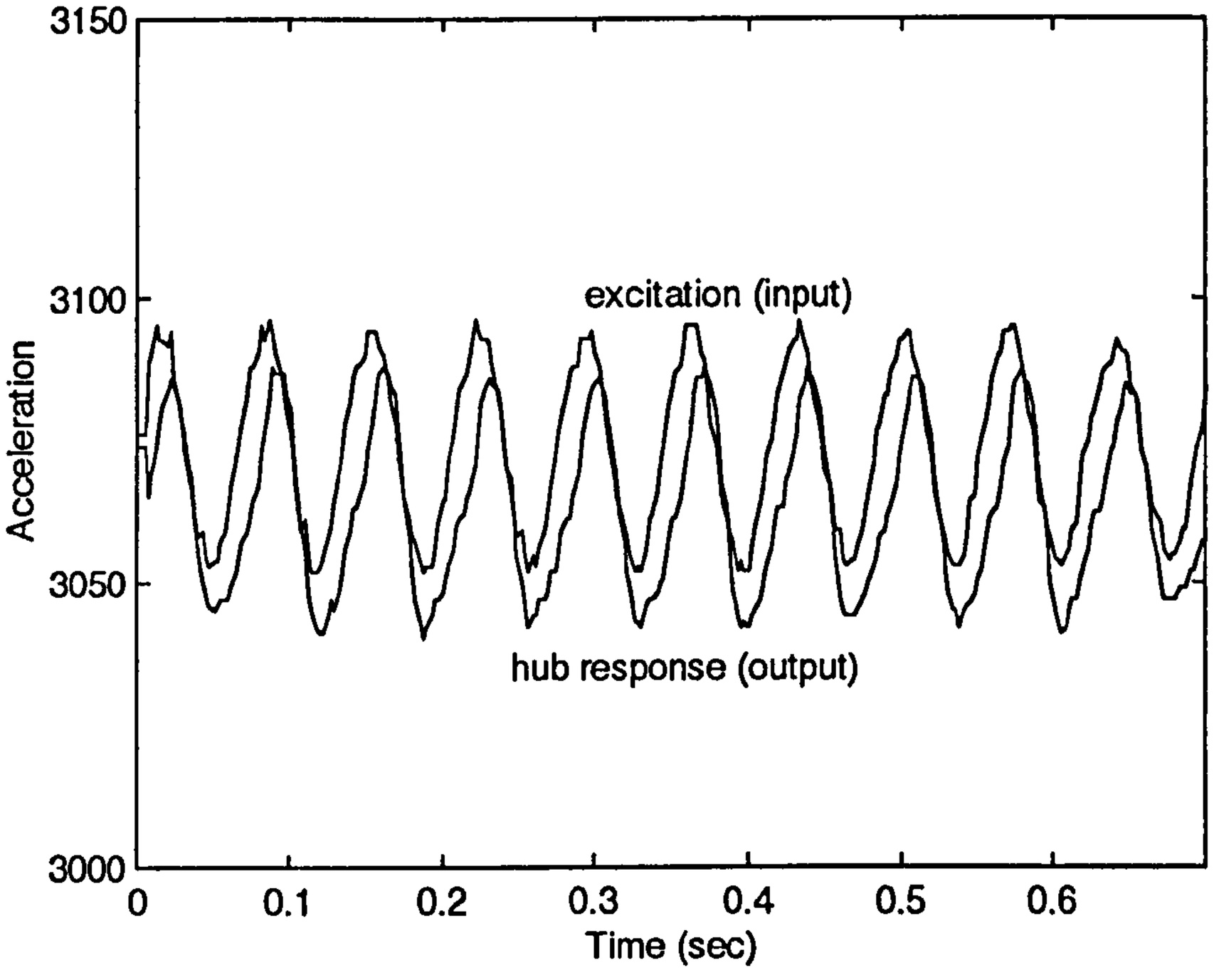

Figure 9-15 The hub response excited by sine road input at 14Hz after the absorber being tuned for several times

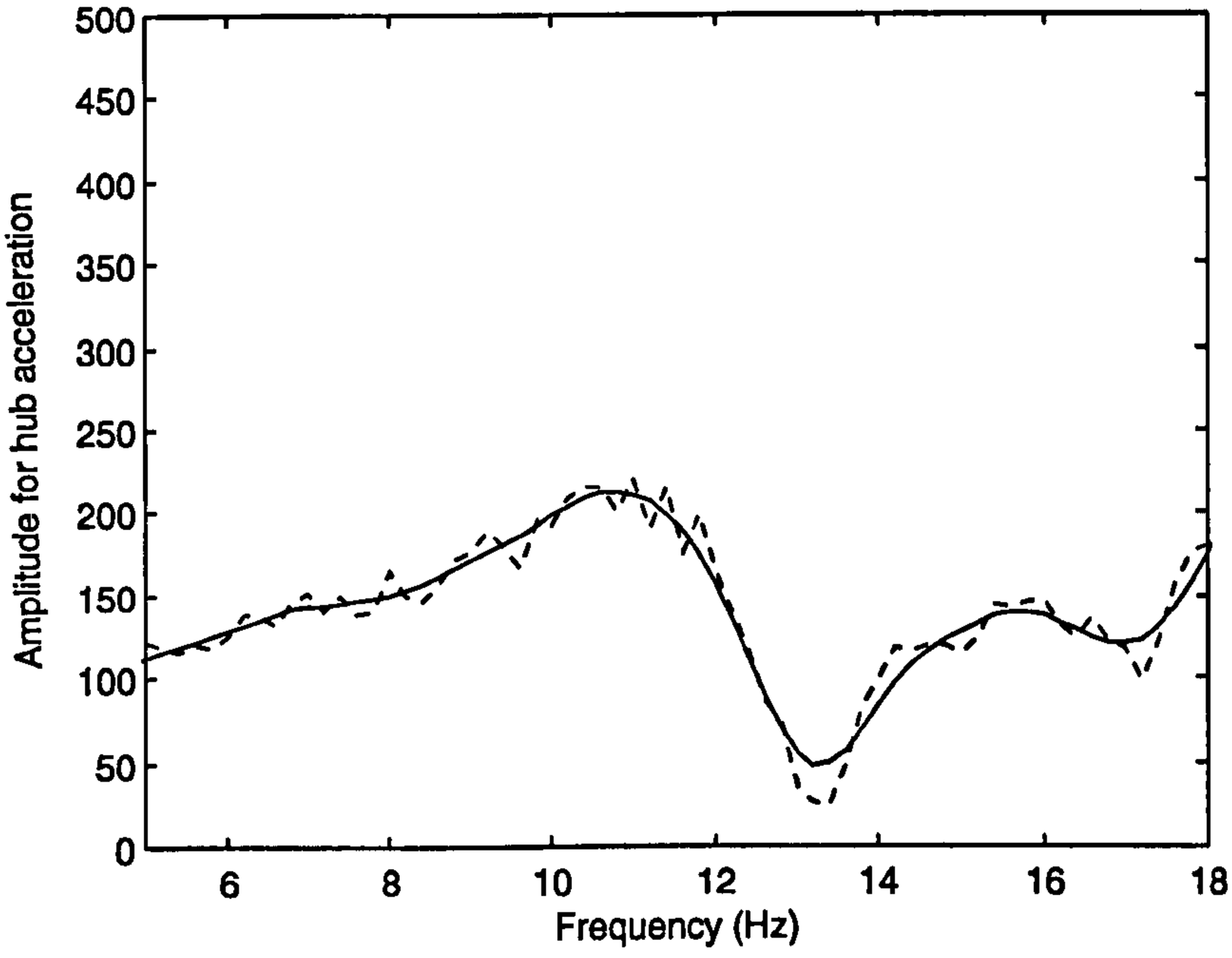

Figure 9-16 The measured frequency spectrum of the hub acceleration when the air presure in the tyre was changed from 2bar to 1.5bar

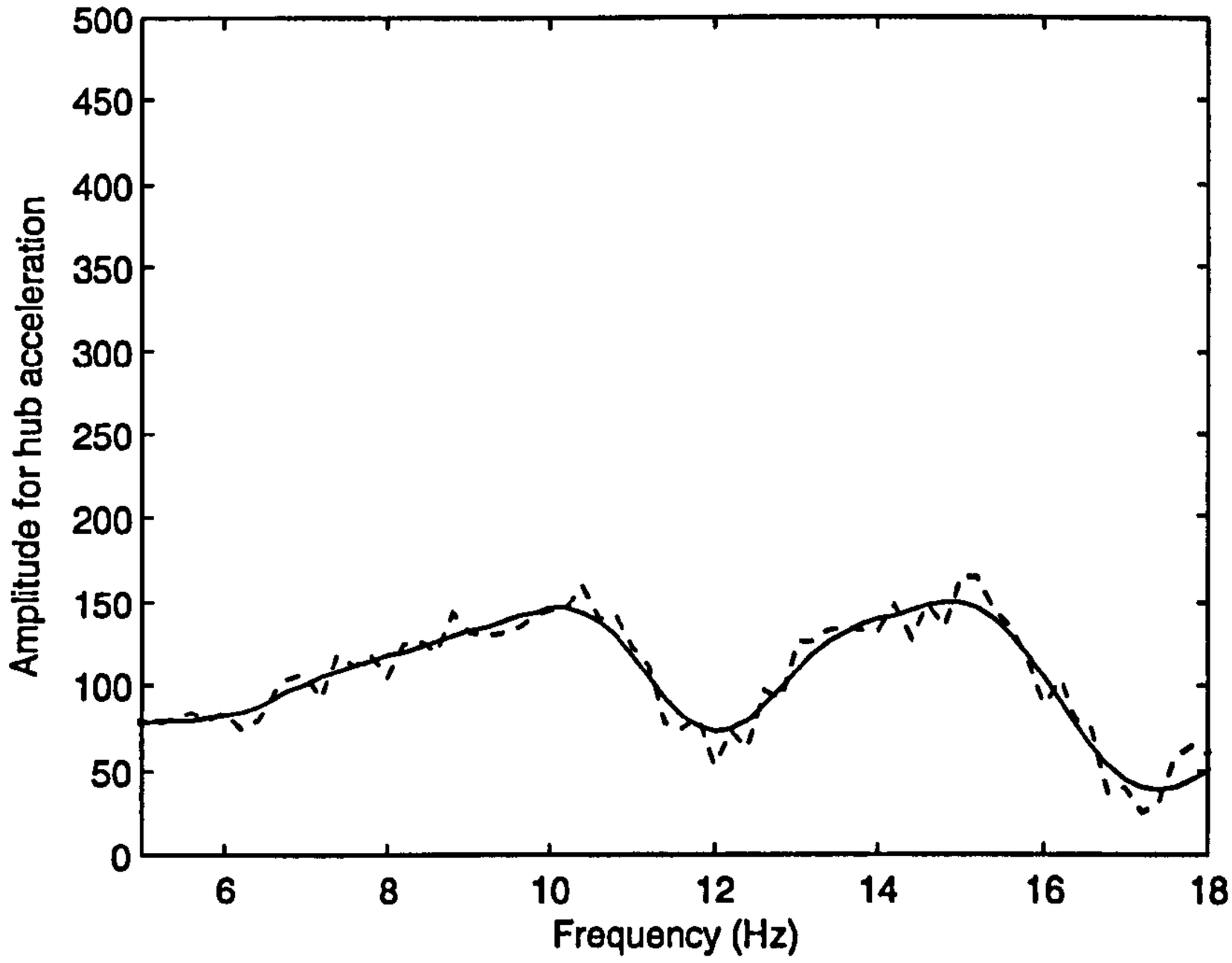

Figure 9-17 The measured frequency spectrum of the hub acceleration after the absorber being well tuned for 1.5bar air pressure in the tyre

Chapter 10

Performance Prediction for the Two Wheeled Trailer with the Zero Rate Suspensions and ATVA

10.1 Introduction

Control of the zero rate suspension has been investigated in chapters 5 to 7. It has been shown that the suspension can provide good ride comfort to the trailer body but cannot reduce the hub vibration. To solve this problem, the ATVA was investigated and implemented in chapters 8 and 9. It has been shown that the developed ATVA prototype is effective for this purpose.

In chapter 8, it was proved by simulation that the combination of the ATVA and the active linear suspension with sky hook damping can provide both good ride comfort and good hub damping. But the combined performance of the ATVA and the zero rate suspension has not been investigated because the suspension is a nonlinear system. This will be considered in this chapter.

10.2 Modelling of the Two Wheeled Trailer with Zero Rate Suspensions and ATVA

The model used is illustrated in figure 10-1. This is still a half car model. The difference from the model in chapter 4 is that there are two active tuneable absorbers on the two unsprung masses. Similarly to chapter 4, the motion equation for this model can be obtained as follows.

$$M\ddot{X} + C_d\dot{X} + KX = B_c X_c + BU + G \qquad (10\text{-}1)$$

where

the mass matrix $M = diag\{m_0 \quad I \quad m_{t1} \quad m_{t2} \quad m_{a1} \quad m_{a2}\}$

the stiffness matrix $$K=\begin{bmatrix} 0 & 0 & 0 & 0 & 0 & 0 \\ 0 & 0 & 0 & 0 & 0 & 0 \\ 0 & 0 & k_{t1}+k_{a1} & 0 & -k_{a1} & 0 \\ 0 & 0 & 0 & k_{t2}+k_{a2} & 0 & -k_{a2} \\ 0 & 0 & -k_{a1} & 0 & k_{a1} & 0 \\ 0 & 0 & 0 & -k_{a2} & 0 & k_{a2} \end{bmatrix}$$

the damping matrix

$$C_d=\begin{bmatrix} c_{01}+c_{02} & -c_{01}a+c_{02}b & -c_{01} & -c_{02} & 0 & 0 \\ -c_{01}a+c_{02}b & c_{01}a^2+c_{02}b^2 & c_{01}a & -c_{02}b & 0 & 0 \\ -c_{01} & c_{01}a & c_{01}+c_{t1}+c_{a1} & 0 & -c_{a1} & 0 \\ -c_{02} & -c_{02}b & 0 & c_{02}+c_{t2}+c_{a2} & 0 & -c_{a2} \\ 0 & 0 & -c_{a1} & 0 & c_{a1} & 0 \\ 0 & 0 & 0 & -c_{a2} & 0 & c_{a2} \end{bmatrix}$$

the excitation matrix $$B_c=\begin{bmatrix} 0 & 0 & 0 & 0 \\ 0 & 0 & 0 & 0 \\ c_{t1} & 0 & k_{t1} & 0 \\ 0 & c_{t2} & 0 & k_{t2} \\ 0 & 0 & 0 & 0 \\ 0 & 0 & 0 & 0 \end{bmatrix}$$

the control matrix $$B=\begin{bmatrix} 1 & -a & -1 & 0 & 0 & 0 \\ 1 & b & 0 & -1 & 0 & 0 \end{bmatrix}^T$$

the state vector $$X=\{x_0 \quad \theta \quad x_{t1} \quad x_{t2} \quad x_{a1} \quad x_{a2}\}^T$$

the excitation vector $$X_c=\{x_{c1} \quad x_{c2} \quad \dot{x}_{c1} \quad \dot{x}_{c2}\}^T$$

the control vector $$U=\{F_{a1} \quad F_{a2}\}^T$$

the static load vector $$G=\{-m_0g \quad 0 \quad -m_{t1}g \quad -m_{t2}g \quad -m_{a1}g \quad -m_{a2}g\}^T$$

The other equations can also be obtained, i.e., the observation equation:

$$Y=CX \tag{10-1}$$

where the observation matrix is $C = \begin{bmatrix} 1 & -a & 0 & 0 & 0 & 0 \\ 1 & b & 0 & 0 & 0 & 0 \\ 1 & -a & -1 & 0 & 0 & 0 \\ 1 & b & 0 & -1 & 0 & 0 \end{bmatrix}$

the output vector $y = \{y_{01} \quad y_{02} \quad y_{11} \quad y_{12}\}^T$;

the equivalent force for the zero rate suspension:

$$\begin{cases} F_{a1} = a_0 + a_1 l_1 + a_2 l_1^2 + (a_3 + a_4 l_1) y_{11} \\ F_{a2} = a_0 + a_1 l_2 + a_2 l_2^2 + (a_3 + a_4 l_2) y_{12} \end{cases} \tag{10-3}$$

the limited bandwidth:

$$\begin{cases} \dot{l}_1 + \omega_{01} l_1 = \omega_{01} u_1 \\ \dot{l}_2 + \omega_{02} l_2 = \omega_{02} u_2 \end{cases} \tag{10-4}$$

In equation (10-1), x_{a1} and x_{a2} are the displacement of the absorber weights; m_{a1} and m_{a2} denote the mass of the absorber weights on both sides; k_{a1} and k_{a2} represent the stiffness of the absorber springs; and c_{a1} and c_{a2} are the damping of the absorber dampers. Other parameters and variables in equations (10-1) to (10-4) are the same as those in equations (6-1) to (6-6) of chapter 6.

The MIMO PID controller with 'sky-hook' damping is employed for the suspension system because was shown to have good performance. The same feedback equation as equation (6-7) is employed, i.e.

$$\begin{Bmatrix} u_1 - u_1^* \\ u_2 - u_2^* \end{Bmatrix} = K_P \begin{Bmatrix} y_{11} - y_{11}^* \\ y_{12} - y_{12}^* \end{Bmatrix} + K_D \begin{Bmatrix} \dot{y}_{01} \\ \dot{y}_{02} \end{Bmatrix} + K_I \int \begin{Bmatrix} y_{11} - y_{11}^* \\ y_{12} - y_{12}^* \end{Bmatrix} dt \tag{10-5}$$

where the parameters and variables are all the same as those in chapter 6. The simulation will be pursued for this controller.

The absorbers on the unsprung masses are the active tuneable vibration absorbers, in which the absorber stiffness can be adjusted through analysing the hub motion. The developed ATVA in chapters 8 and 9 is applied to this system.

The whole system is illustrated in the block diagram shown in figure 10-2. The block diagram of the trailer dynamics looks different from that in figure 6-3. Actually, they are equivalent apart from the ATVA controller. The layout has been changed in the figure 10-2 to more clearly present the ATVA and PID controller; the only difference

between figures 10-2 and 6-3 is that the absorber stiffness is tuned by the ATVA controller which gets information from the hub acceleration.

10.3 Simulation Results

As before, MATLAB is used to analyse the model. To demonstrate the effect of the combination of the PID controller with sky hook damping and ATVA, the trailer with only the PID controller was simulated as a reference. The model for this case has been shown in chapter 6.

To simulate the road profile excitation, a white noise signal was employed. Generally excitations under the two wheels are independent though they are believed to have the same property, i.e. white noise with normal distribution.

Figures 10-3(a) and (b) illustrate the excitation for the trailer without the ATVA. The predicted response of the trailer body on its two sides are shown in figures 10-3(c) and (d) under these road excitations. It can be seen that the transmission of road excitation to the trailer body can be attenuated significantly by the zero rate suspension controlled by the MIMO PID with sky hook damping, which has been demonstrated in chapters 6 and 7. The response of the two hubs shown in figure 10-3(e) and (f), however, do not give the desirable results. The peak-peak amplitude for both hubs is increased by about 3 times, compared to the road amplitude.

Figures 10-4(a) to (f) are for the case of the trailer with the ATVA. The road excitation in this case, shown in figures 10-4(a) and (b), is similar to that in figure 10-3(a) and (b). The effect of the zero rate suspension also appears to be similar to that in the case without the ATVA in terms of the trailer body response in figures 10-4(c) and (d). In this case, however, the vibration attenuation for the hubs is improved considerably. The peak-peak amplitude of the hubs with the ATVA is about 40% bigger than that of the excitations whereas without ATVA the corresponding figure was about 200% bigger than the excitation. This means that the ATVA can provide improved vibration attenuation at the hubs.

The vibration transmission for the combination of the ATVA and PID with sky hook damping were investigated through the estimated frequency response as shown in figures 10-5. Because the prototype is a nonlinear system, there is no general method to get a precise frequency response. The method used here is the use of the ratio of the

response to the road excitation at each frequency in frequency domain. Because the resultant frequency response was very noisy, to compare the curves clearly, curve fitting was employed. The results of this method can be quite different due to the nonlinearity, but the results for very small displacement should not be changed much since the model for the trailer was validated for small deflection in chapter 4.

The frequency response from the left wheel to the left body is illustrated in figure 10-5(a) for with and without ATVA. It is shown that the left-left body transmission was decreased by ATVA by about 6dB to 10dB when the excitation frequency is over 10Hz. The frequency response from the left wheel to the left hub is shown in figure 10-5(b). It can be seen that the left-left hub vibration transmission was reduced by ATVA by about 2dB to 16dB when the excitation is higher than 10Hz. Only in a small range around 9Hz, is the transmission gain with ATVA larger than that without ATVA. These mean that the body and hub vibration transmission can be improved considerably by ATVA.

10.4 Conclusions

The simulation results have shown that the application of ATVA on the trailer can attenuate the hub vibration significantly. The estimated frequency response also shows that the body and hub vibration transmission can be improved considerably by ATVA. The combination of ATVA and active zero rate suspension controlled by the MIMO PID with sky hook damping can provide both the ride comfort and handling. Therefore, the implementation of this combination is worthy of further investigation and implementation.

Based on the previous experimental work, the implementation of this combination can possibly be achieved for the current trailer and its hardware. It has been shown that the zero rate suspension needs 6 channels of A/D input and 2 channels of D/A output, and each ATVA needs 1 channel of A/D input and 4 bits of the digital output. The current AD board AD1200 has 8 channels of differential A/D input (16 channels of single A/D input), 2 channels of D/A output and 8 bits of the digital output. These are sufficient to the application of the zero rate suspension and the two ATVA. In the control software for the MIMO PID, the sampling speed can be increased by about another two times. This means that the CPU has a certain potential time for other jobs. The addition of the control for the two ATVA to the PID control software therefore is

possible. Of course, that is not a easy job. In the author's opinion, how to distribute the computing time to the suspension and absorbers will be a key problem.

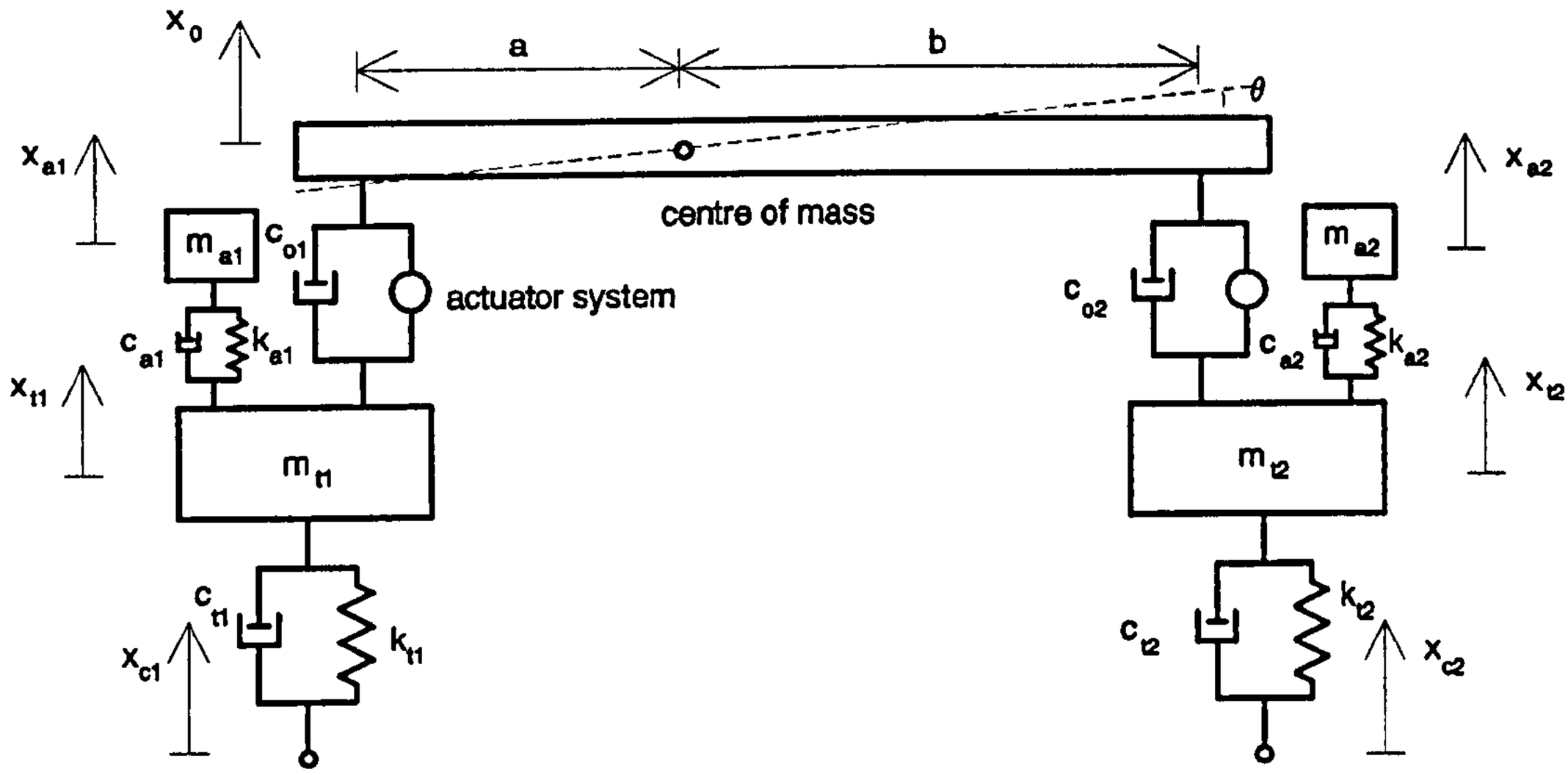

Figure 10-1 The half car model of the trailer with ATVA on hubs

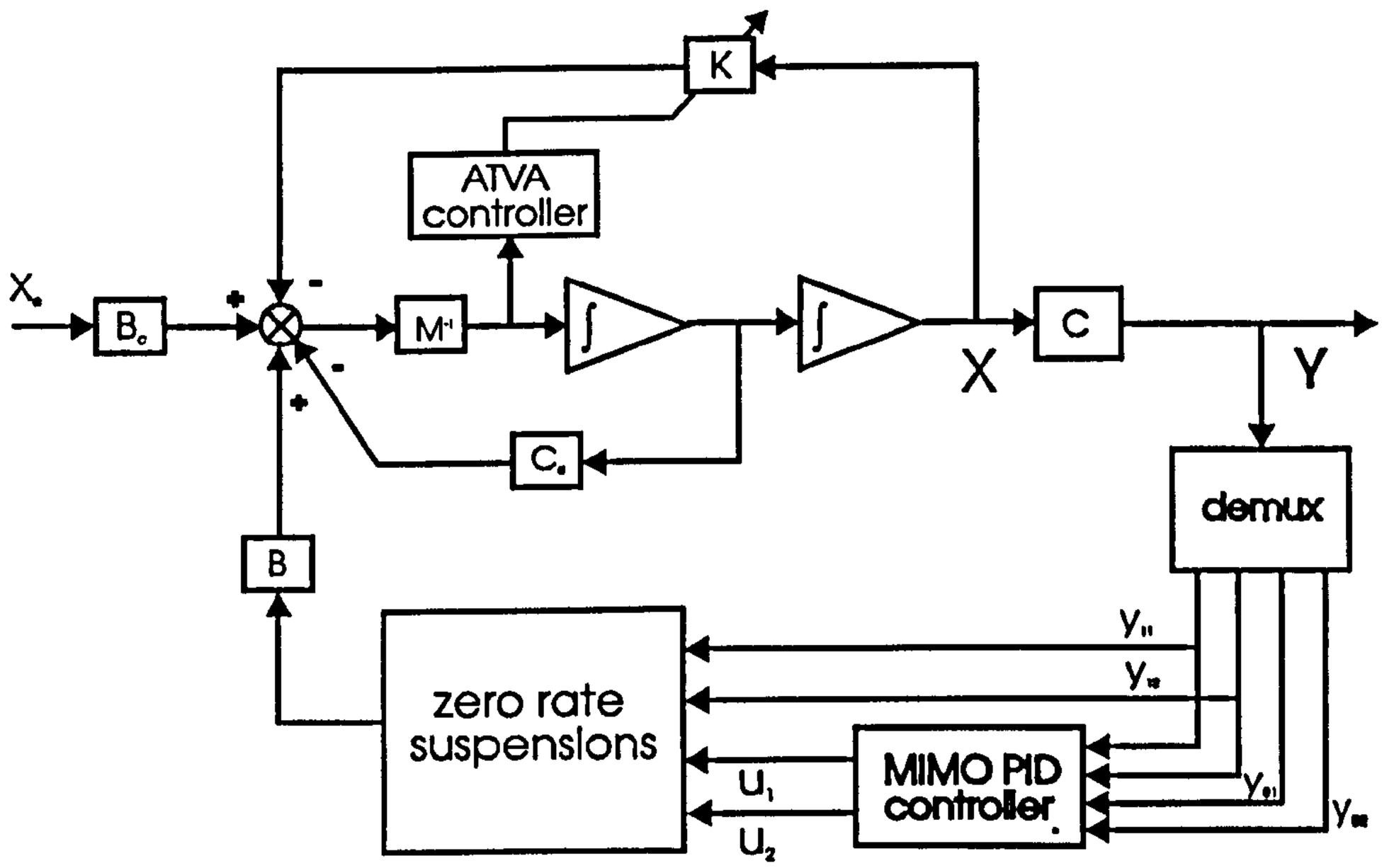

Figure 10-2 The block diagram for the two wheeled trailer with the ATVA and the zero rate suspension controlled by MIMO PID

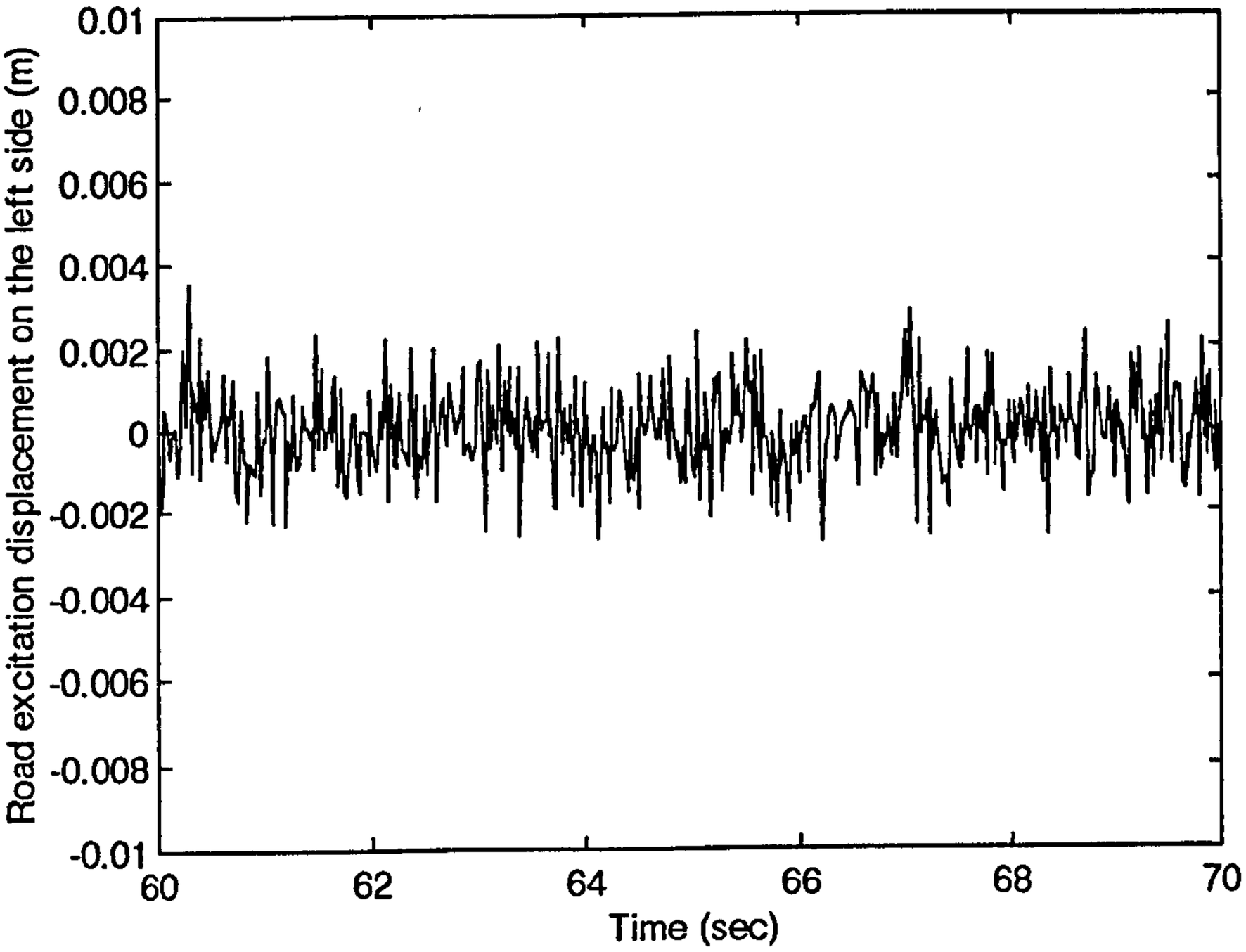

Figure 10-3(a) The white noise road excitation under the left wheel

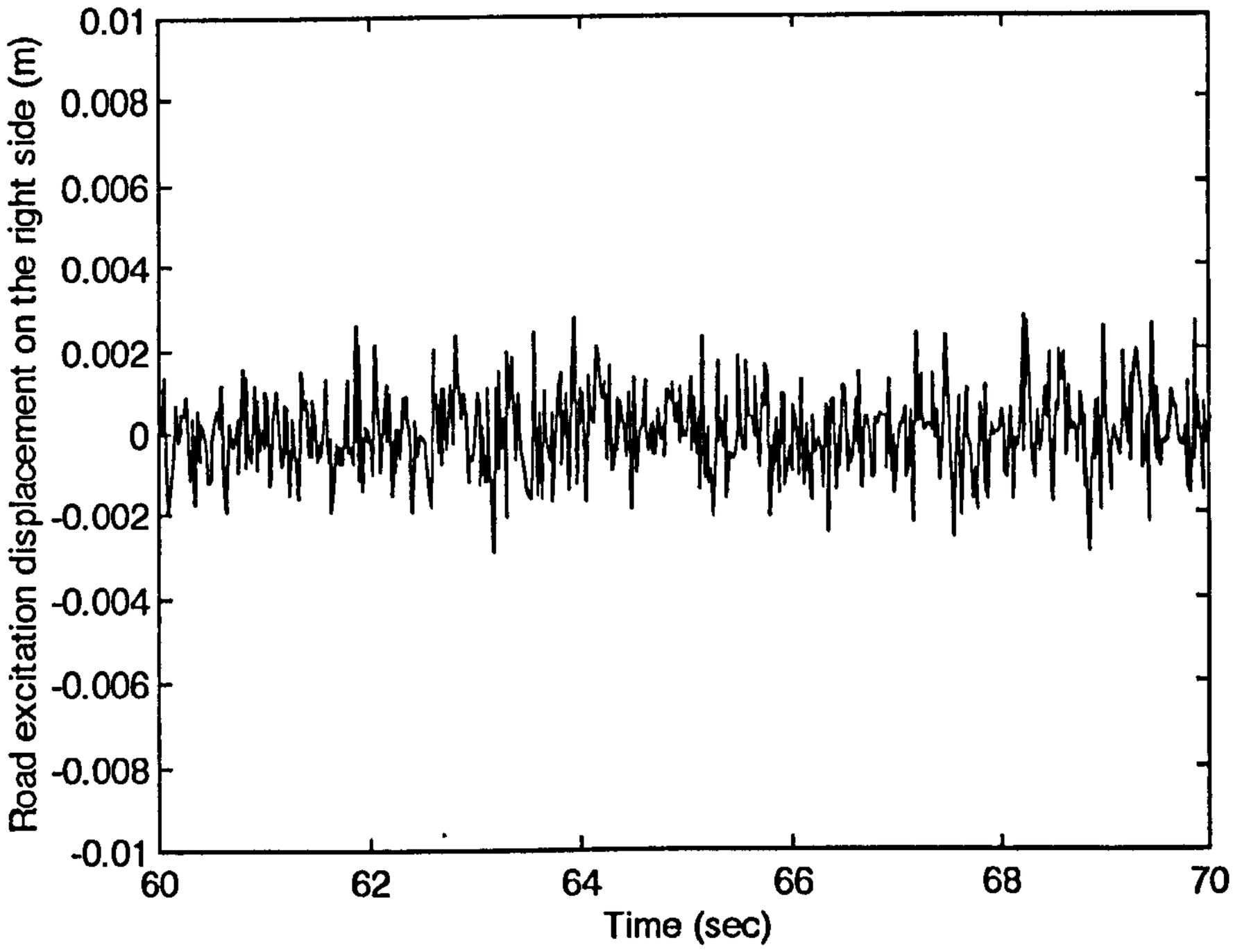

Figure 10-3(b) The white noise road excitation under the right wheel

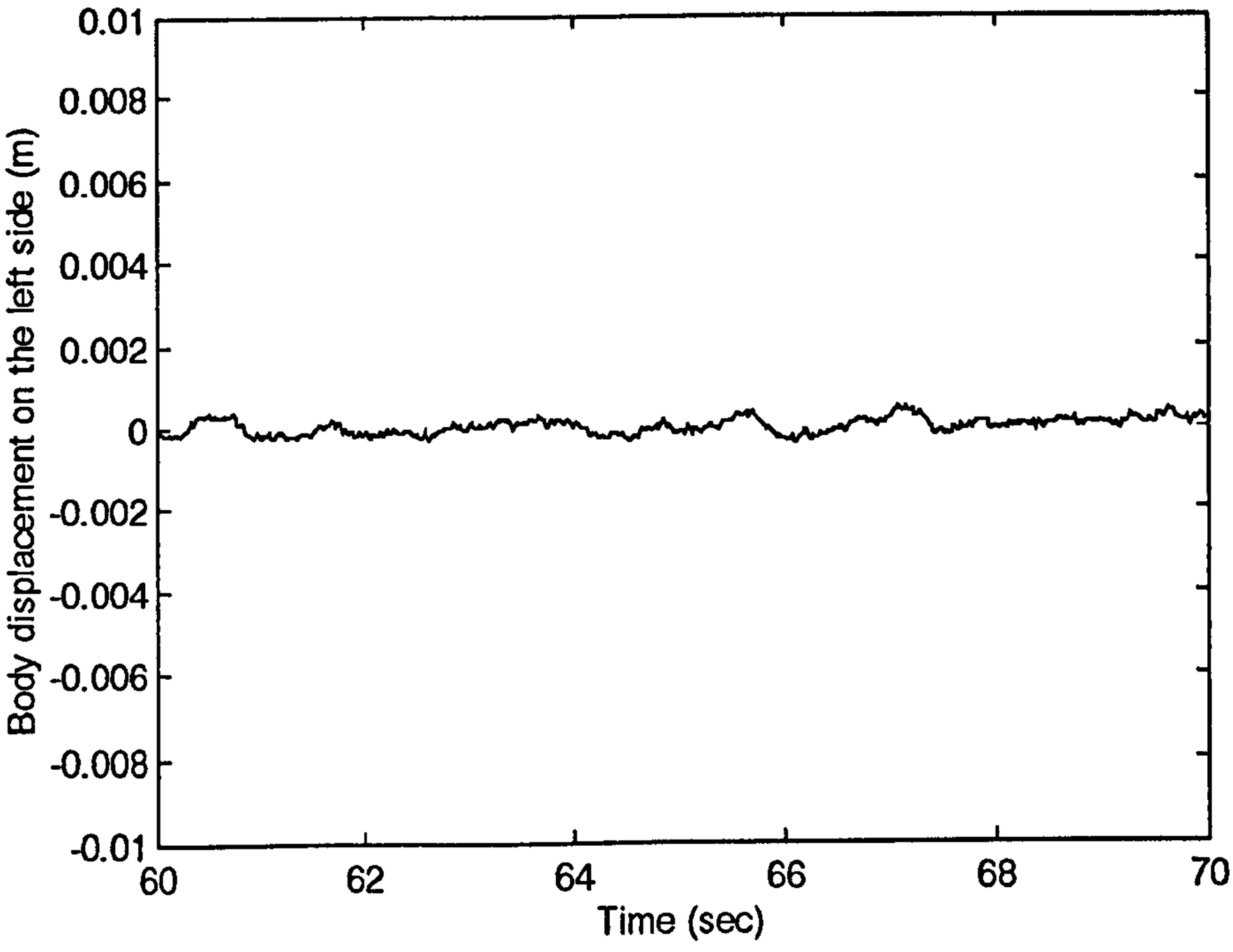

Figure 10-3(c) The trailer body response on the left side when ATVA is not in use

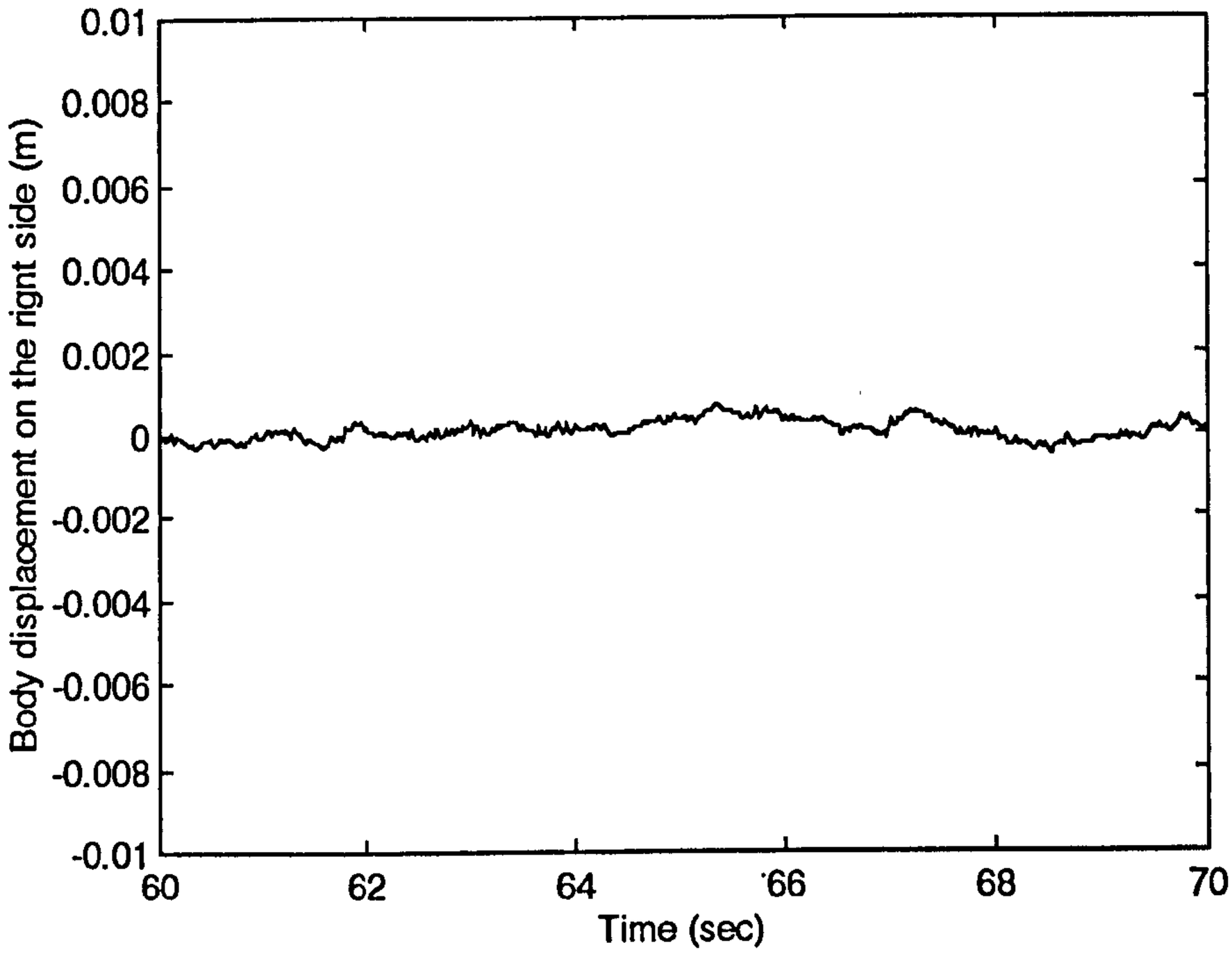

Figure 10-3(d) The trailer body response on the right side when ATVA is not in use

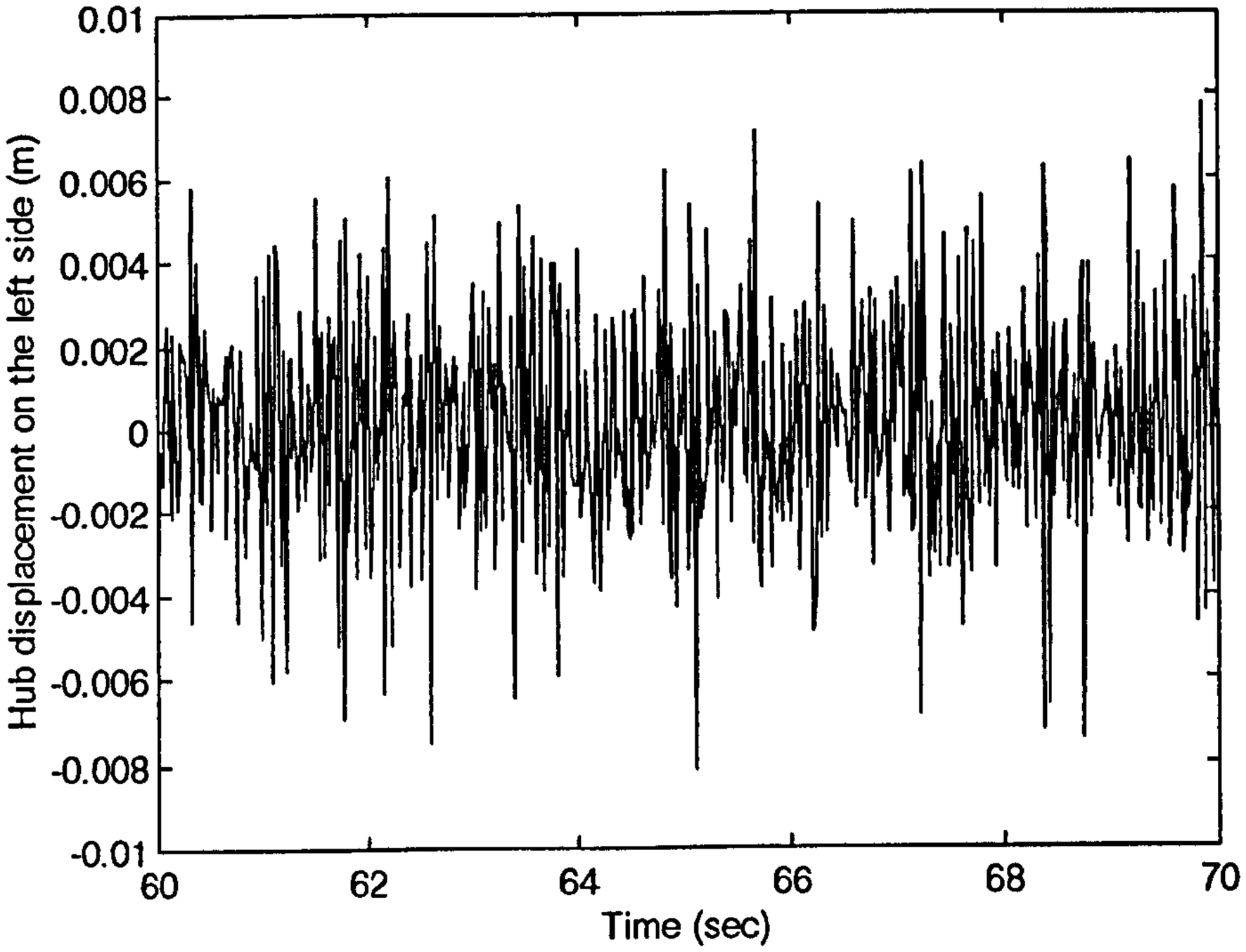

Figure 10-3(e) The left hub response when ATVA is not in use

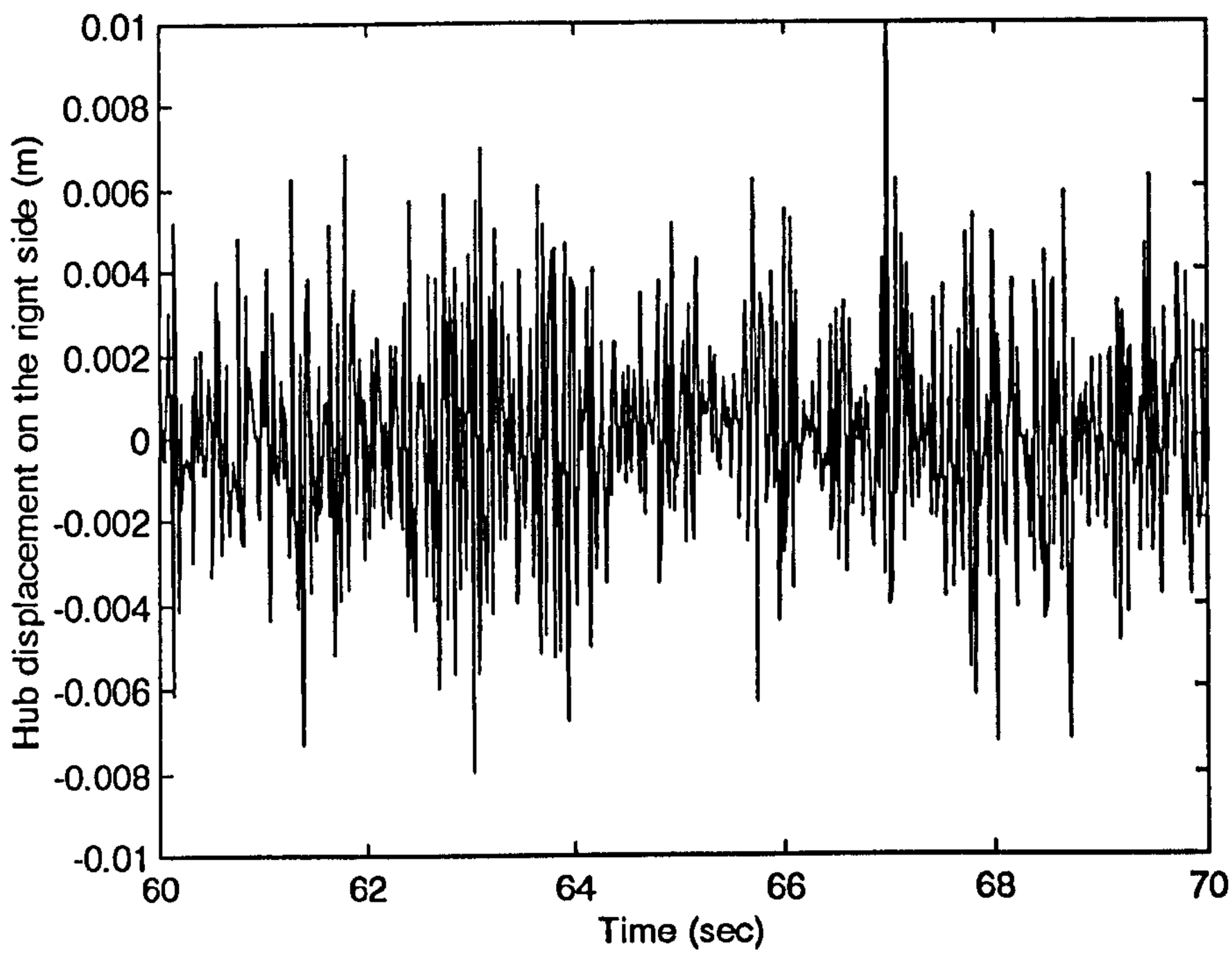

Figure 10-3(f) The right hub response when ATVA is not in use

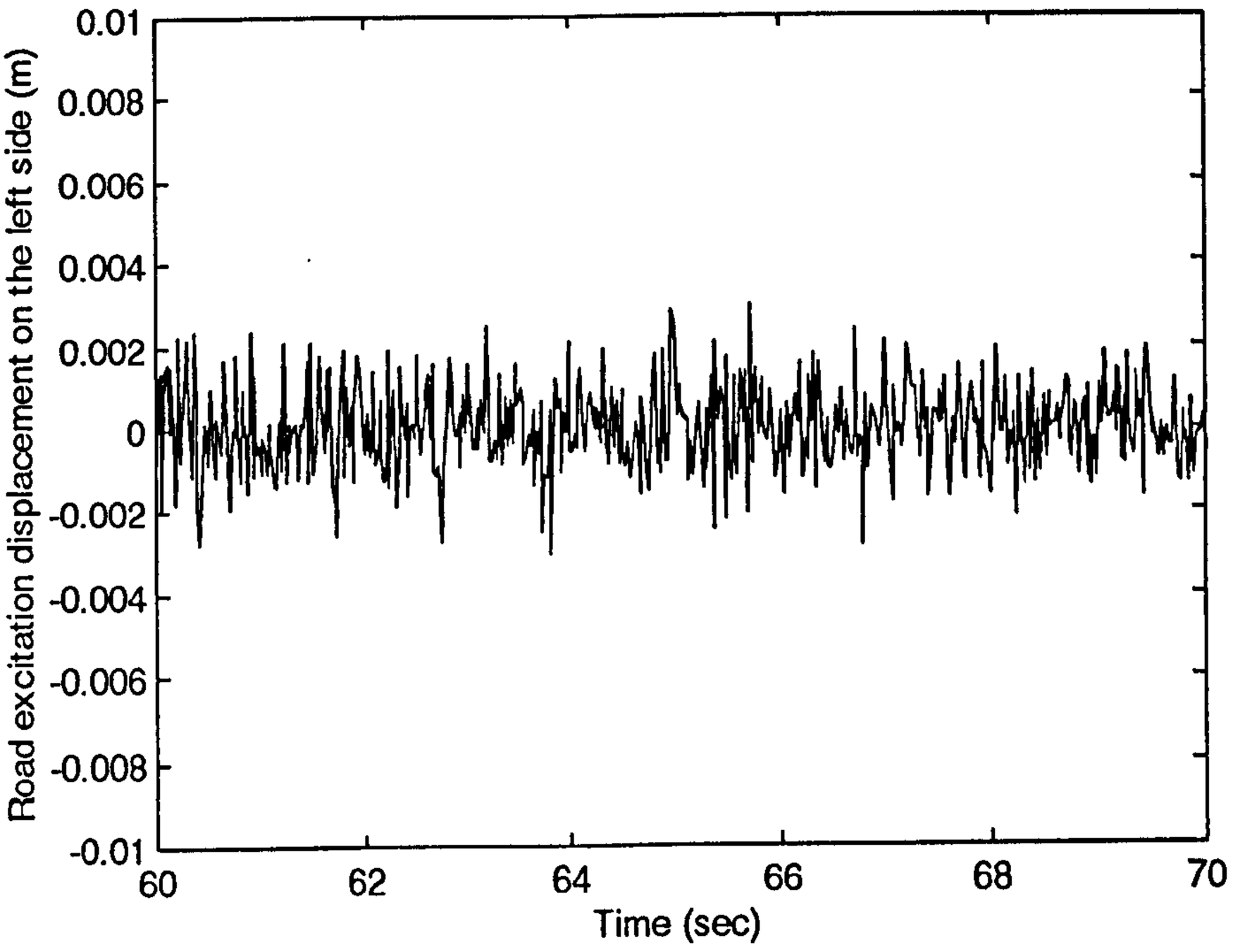

Figure 10-4(a) The white noise road excitation under the left wheel

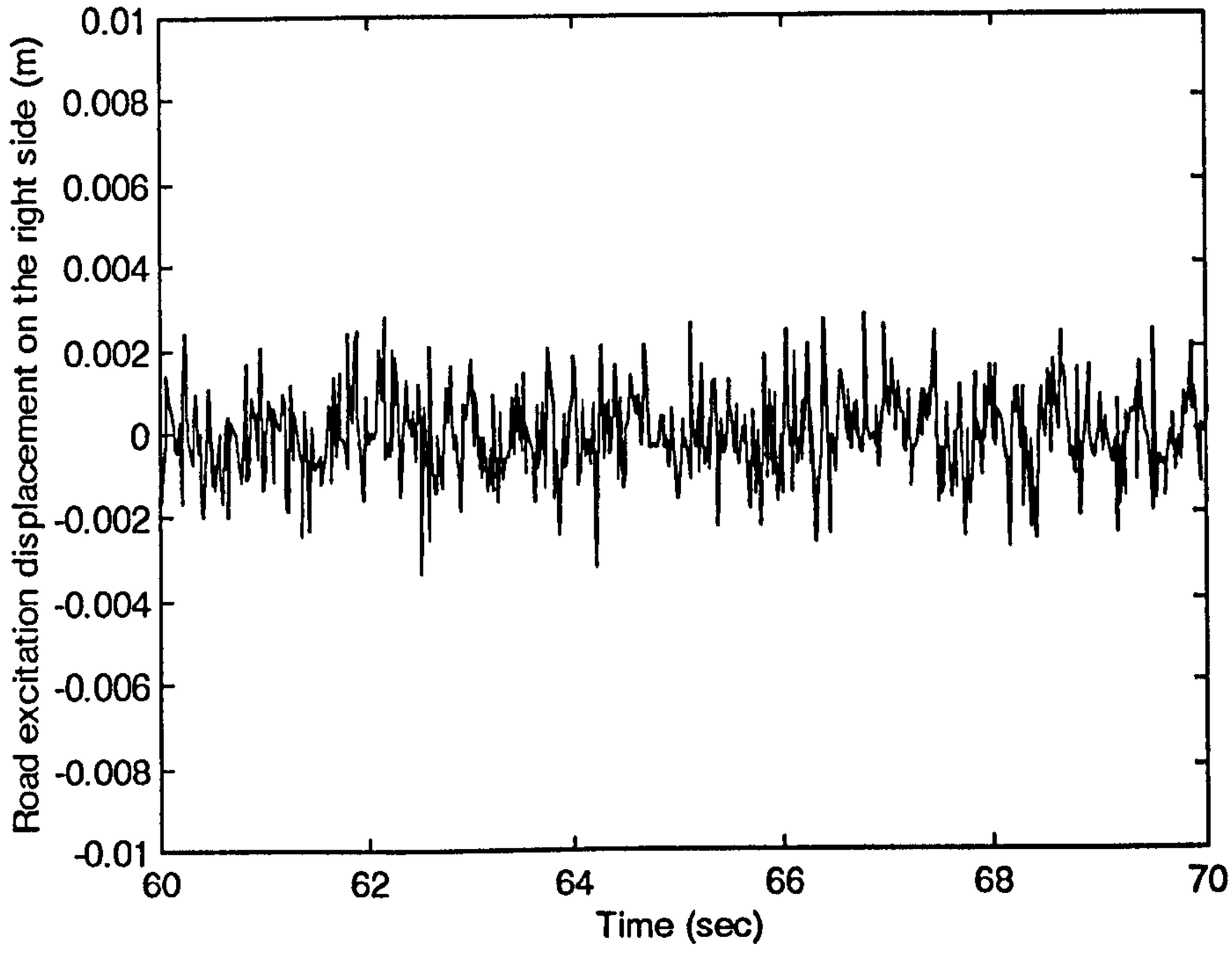

Figure 10-4(b) The white noise road excitation under the right wheel

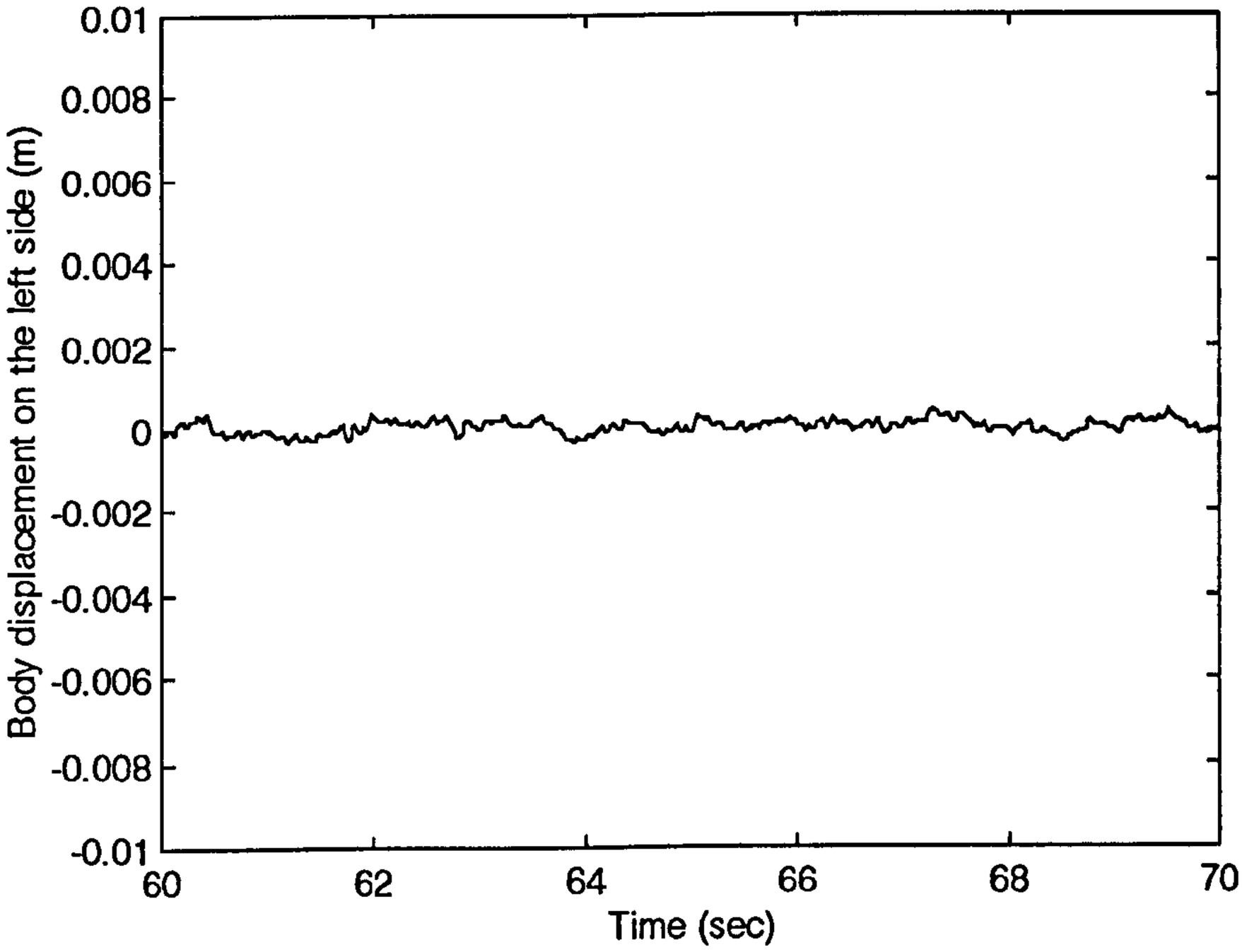

Figure 10-4(c) The trailer body response on the left side when ATVA is employed

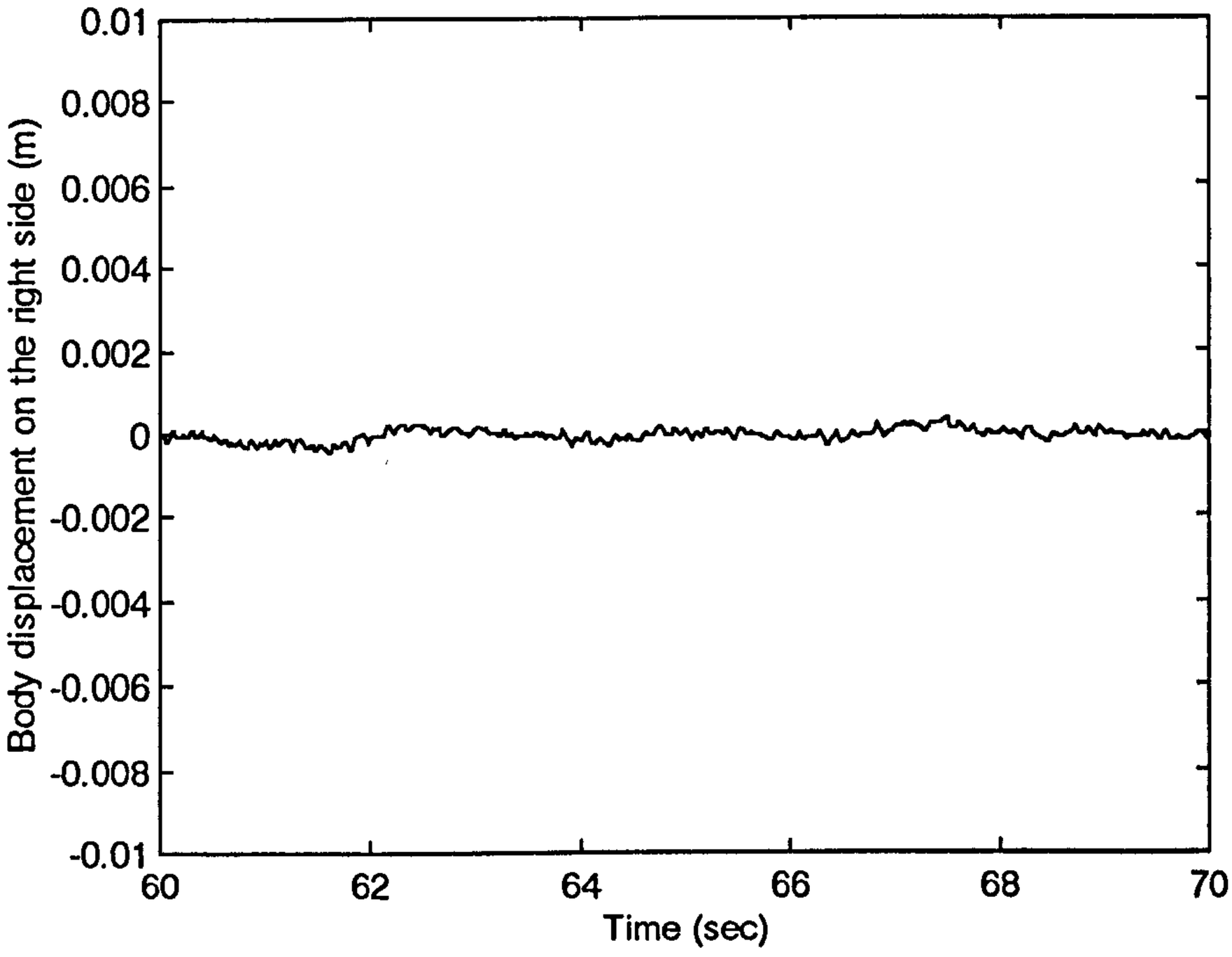

Figure 10-4(d) The trailer body response on the right side when ATVA is employed

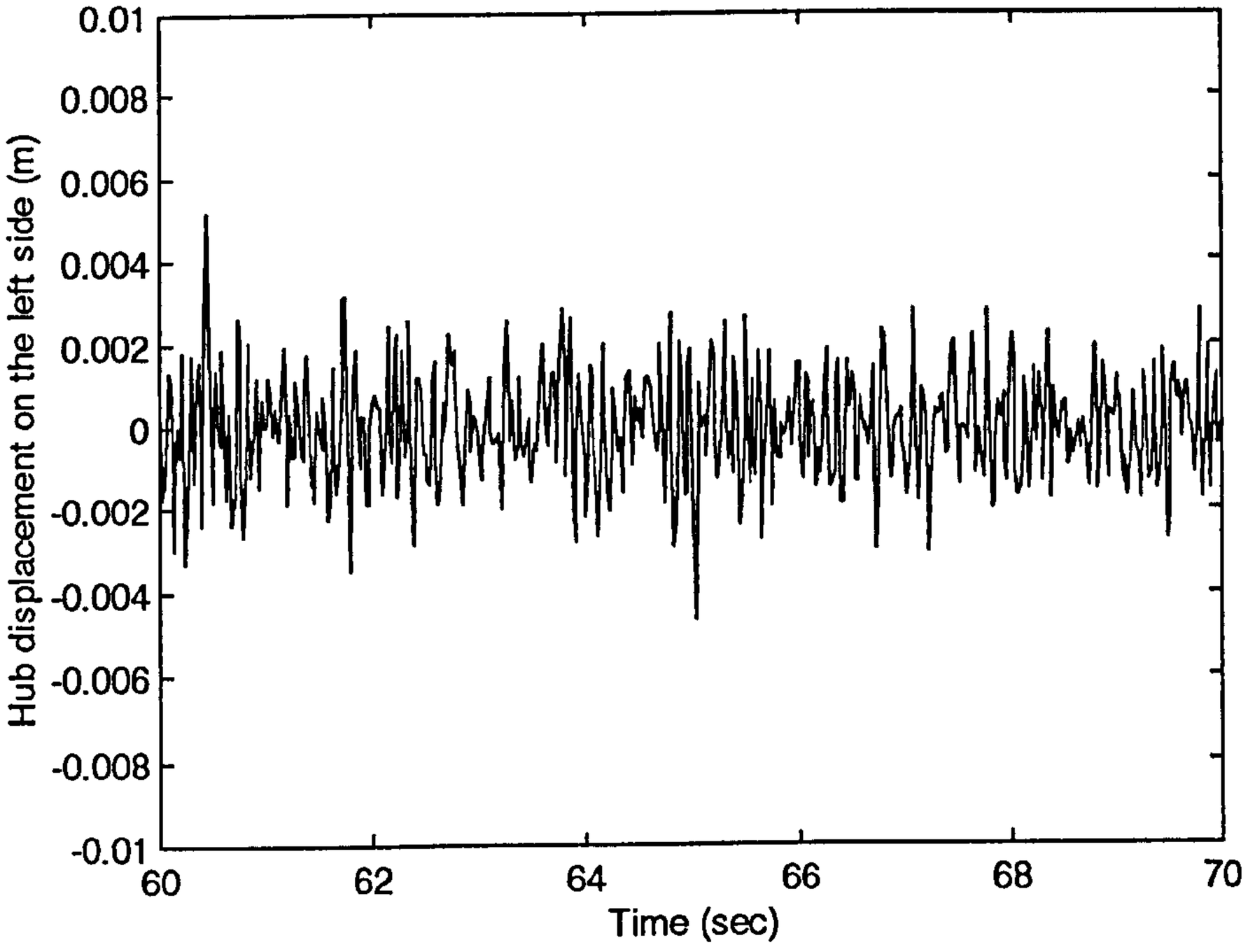

Figure 10-4(e) The left hub response when ATVA is employed

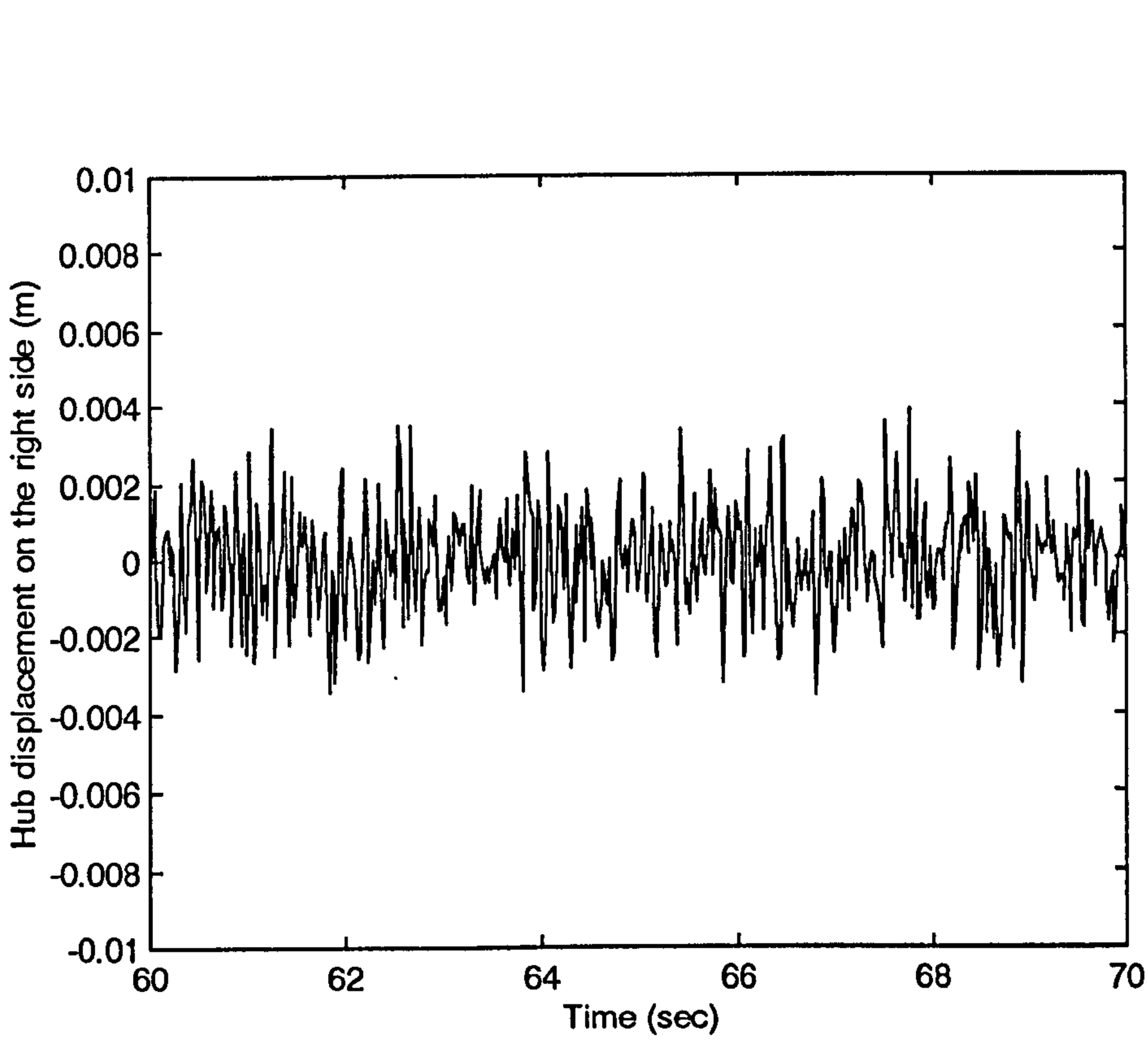

Figure 10-4(f) The right hub response when ATVA is employed

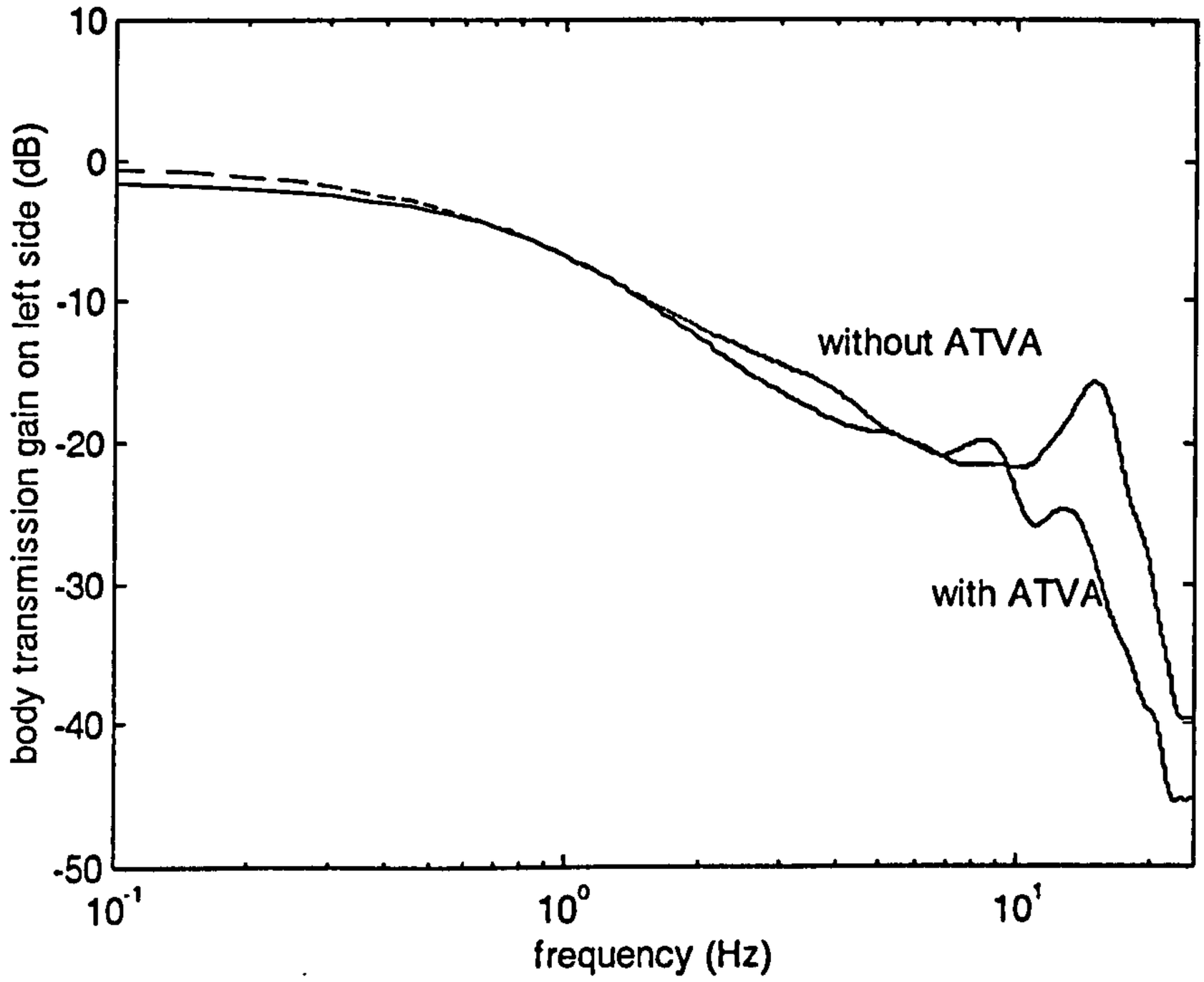

Figure 10-5(a) Estimated frequency response for vibration transmission from the left wheel to the left side of the trailer body using random response

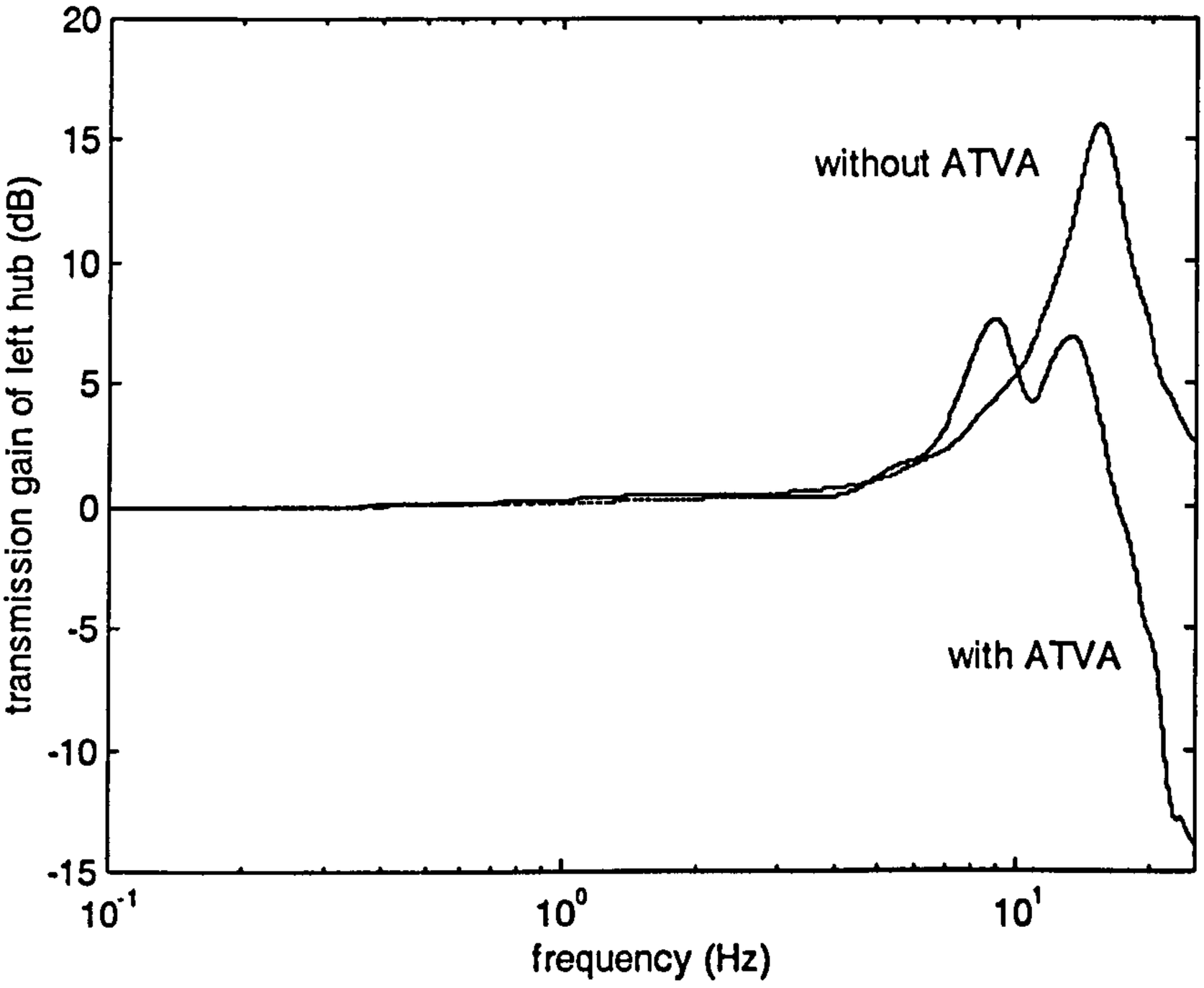

Figure 10-5(b) Estimated frequency response for vibration transmission from the left wheel to the left hub using random response

Chapter 11

Conclusions

11.1 Summary of Work Completed

In this thesis, both theoretical and experimental research work has been carried out in the area of active suspensions for automotive application. The following activities have been completed.

- Recent literature in the area of automotive active suspensions has been collected and reviewed.

- A PC-based digital control system and interfaces to the existing trailer with zero rate suspensions, sensors and electronics have been developed. The required software has been written in C++ for control implementation. Experimental results have shown that the whole system functions correctly.

- A nonlinear half car model has been established for the two wheeled trailer with zero rate suspension. Limited bandwidth of the actuators has been included in the analytical multi-input/multi-output model. This model has been validated by measurement on the test rig.

- Various control strategies, namely PD, MIMO PID, LQG and Fuzzy Logic, have been applied to the trailer with the active zero rate suspension. These controllers were simulated in the nonlinear models and implemented in the test rig. Experimental results have validated the methodology for these applications.

- Performance of the above control strategies has been investigated mathematically and experimentally for the particular test rig, in terms of ride comfort and handling.

- The effects of the nonlinearity and limited bandwidth of actuators on the instability of the test rig were also investigated based on the nonlinear model. The stable regions in the phase plane was obtained and employed to explain the instability.

- A PC-based active tuneable vibration absorber (ATVA) has been developed and built from concept to prototype. This system includes an accelerometer on the hub, an absorber tuned by a stepping motor, a PC computer and the relevant interfaces. The corresponding control strategy and software have also been developed for the ATVA. Experiment and simulation have been used to evaluate the performance of the ATVA. It has been shown that the whole developed system including hardware, software and algorithm is effective.

- A quarter car unsprung mass test rig has been built for testing the developed ATVA and its performance measured.

- Performance of the combination of the zero rate suspension and the ATVA has been predicted by simulating the trailer response under road profile inputs. The nonlinear half car model with MIMO PID controllers and ATVA under white noise excitation was employed for this purpose.

- In addition to the originally planned work, a PC-based measurement system for identifying the transfer function of vehicle suspensions has been developed from concept to prototype. This work includes designing and building the measurement platform and interfaces to the PC computer, writing software for signal sampling and processing, and developing the test method and algorithm. Its test results have been validated with two standard methods. The first used the hydraulic shaker at the University of Birmingham and the second used the quarter car test rig with sine wave sweeping excitation. The developed system has been proved to function correctly.

11.2 Conclusions

- The PD controller with relative or sky hook damping for the zero rate suspension can support a range of weights of trailer at an appropriate mean ride height, prevent violent trailer body motion, damp out oscillation and provide a stable body height attitude, but cannot isolate the trailer body from road disturbance of less than 2Hz in the frequency domain.

- The nonlinearity of the system results in a limited stable region and constrains the control parameters. Excessive proportional gain, excessive or insufficient derivative gain, or insufficient trailer body mass can individually give rise to

unstable motion of the trailer body. The reason for this is that the stable region in the state space is decreased to exclude the initial state. In the nonlinear system, the actuator bandwidth plays a significant role in the control performance. It leads to considerable reduction of the stable region (based on simulation), which means that the actuator bandwidth is the another limiting factor in the control parameters. Other factors can also degrade the stability, such as the mass symmetry of the trailer body, the matching of the two suspensions and the matching of the cut off frequencies of the actuators bandwidths.

- The multi-input and multi-output PID with sky hook damping can improve stability which may be degraded by the nonlinearity, and provide quite satisfactory control performance and ride comfort. This controller is able to support the trailer body at any demanded ride height within mechanical constraints, enable the ride height to adapt to changes in body mass, provide smoother transient motion to the demanded attitude, prevent violent trailer body motion, damp out its oscillation, provide stable height and attitude and isolate the trailer body from road disturbances. The drawback of the controller is that it does not improve damping of the hub, because of the sky hook damping.

- Fuzzy Logic control can achieve the demanded position, for various mass and mass distribution in a stable manner and offers low body mode frequencies, but cannot produce high damping of the body modes. The other drawback is that body lifting is delayed for an unacceptably long time. However, the potential performance has not been fully revealed because it is an initial application. A further extensive investigation, therefore, is needed for this particular application.

- The LQG control strategy applied to the zero rate suspension, did not show merit. The controller resulted in the suspension working almost as a passive spring with low stiffness which can only produce a low natural frequency in the body modes but could not provide high damping or body position control. The robustness of this controller was poor and the implementation was difficult and inconvenient. The results of applying LQG on the prototype have not yet shown any point from which the investigation is worth continuing.

- The comparison of these controllers has shown that the multi-input and multi-output PID controller provides the best performance, in terms of good vibration isolation and quite high damping, good adaptiveness to mass change and the easiest implementation due to its good robustness and simple algorithm. PID is therefore a good candidate for a prototype controller.

- The developed system for the Active Tuneable Vibration Absorber can reduce the hub vibration transmission by about 9dB and the control system can automatically adjust the absorber to keep the hub vibration at a low level. It is shown that the Active Tuneable Vibration Absorber is a viable candidate to compensate for the drawback of PID with sky hook damping, by damping out the hub vibration. The simulation results have shown that the combination of the Active Tuneable Vibration Absorber and zero rate suspension controlled by the multi-input and multi-output PID with sky hook damping can provide both ride comfort and improved handling.

Chapter 12

Future Work

In spite of the successful and exciting results discussed in previous chapters, there are still several aspects of the system requiring further investigation.

1. **Designing a controller based on the trailer model including the dynamic characteristic of the buckled spring.**

   In the current test rig, the buckled springs are assembled in the trailer by mounting their ends into the individual small grooves without any fixing parts. This mechanism may result in the buckled spring jumping off its location, which is not desirable. This effect can be caused by a type of resonance of the spring itself. The causes of this need to be investigated further. However, the current model for the trailer only includes the buckled spring as a 'zero rate' element with no dynamic characteristics. To address this problem a more substantial model, incorporating spring dynamics, is required.

2. **Reducing the body vibration transmission around the lateral body mode.**

   The measured frequency response functions of the body vibration transmission (figures 4-9, 4-10, 7-17 and 7-18) have shown that a lateral mode exists at a frequency of about 6Hz, around which the mode leads to a significant transmission gain. This phenomenon occurs in various systems that have been measured; open loop and closed loop, controlled by MIMO PID, LQG and Fuzzy Logic. Obviously, the high transmission gain around the lateral mode degrades ride comfort.

   Closed loop systems have shown lower transmission gains around this mode than the open loop system, though the gains for the former can still not be ignored. This means that a control algorithm in a closed loop system can go some way towards reducing the transmission gain. An investigation into the design of a suitable

controller may be worthwhile. In the author's opinion, this should be created, based on a model including, at least, the lateral mode.

It has been found experimentally that the lateral mode is strongly coupled with the roll mode of the trailer body. This may be one of the reasons for such a strong response at the lateral mode. The coupling is caused by the mechanism of the suspension system. This mode can probably be included in a suitable multibody model and will introduce considerable additional complexity.

Using the model with the lateral mode might have another benefit, further revealing the reason for unstable roll motion for the trailer body. The sudden unstable motion caused by increasing the body damping often appears as an oscillation at about 5Hz, which is near that of the lateral mode. This may be caused by the nonlinearity, or caused by the instability of the lateral mode, or caused by coupling between both of these. These interesting problems are worth being investigated based on an extensive model, which might lead to the roll instability problem being solved.

3. **Continuing the application of the Fuzzy Logic control strategy in the test rig.**

Initial application of Fuzzy Logic has shown some encouraging features which suggest that the work in the area is worth continuing. The advantages of Fuzzy Logic have not been fully employed, and these advantages might lead to overcoming the unstable limit on the body roll motion caused by the nonlinearity. Continuing work can include improving the index function and technique for defuzzification, using the half car model and MIMO Fuzzy Logic controller, and trying the combination of Fuzzy Logic and PID control, etc.

4. **Improving the developed ATVA.**

It has been mentioned that there are two drawbacks in the current ATVA. The first is that the mechanical design of the absorber should be made more sophisticated, though the current prototype is probably small enough for real use. The ideal configuration may be a cylinder with mass, stiffness-tuneable spring and damper inside. The implementation of the stiffness-tuneable spring is a key problem. The application of a spring with a suitable nonlinear rate might be a solution.

The second drawback is that the time taken to tune the absorber frequency is about four minutes, which may be too long for the practical application. This problem

can be solved through improving the algorithm, software and hardware in the control system.

If both problems can be resolved satisfactorily, the ATVA will be a good candidate for the practical application.

5. **Implementing the combination of the ATVA and the zero rate suspension, controlled by the MIMO PID with sky hook damping.**

   The simulation results have shown that this combination can provide both ride comfort and good handling, so the implementation is very promising. It has been suggested that the current control hardware is sufficient for the requirements of the zero rate suspension and two ATVAs. Only two accelerometers need to be added to the existing transducers on the trailer. Implementation of the combination is, therefore, possible. The author believes that the key problem is how to distribute the CPU time between the suspension and absorbers. If one processor is shown to be insufficient, two processors should be adequate. The use of parallel processing techniques would play a important role in this case.

It is hoped that these activities will be carried out in the future. The author believes that the solution of the above problems will result in the performance of the suspension and ATVA system being upgraded significantly.

References

[1] Abdel Hady, M. B. A. and Crolla, D. A. (1989). Theoretical analysis of active suspension performance using a four-wheel vehicle model. Proc. of I Mech E. 203(D2), 125-135.

[2] Abe, M.(1994). A study on effects of roll moment distribution control in active suspension on improvement of limit performance of vehicle handling. Inter. J. of Vehicle Design. 15(3-5), 326-336.

[3] Abe, M. (1994). A study on effects of roll moment distribution control in active suspension on improvement of limit performance of vehicle handling. Inter. J. of Vehicle Design. 15(3/4/5), 326-336.

[4] Adamson, T. (1990). Structured C for technology. Merrill Publishing Co. 1990.

[5] Ahmadian, M. (1993). Ride evaluation of a class 8 truck with semiactive suspensions. ASME, Advanced Automotive Technology. DSC-Vol.52, 21-25.

[6] Akatsu, Y., Fukushima, N., Takahashi, K., Satoh, M. and Kawararaki, Y. (1990). An active suspension employing an electrohydraulic pressure control system. Proc. of SAE, 18th FISITA Congress the Promise of New Technology in Automotive Industry. 905123, 949-959.

[7] Allemang, R. J. (1994). Modal analysis - Where do we go from here? *Proc. of the 11th IMAC.*

[8] Alleyne, A., Neuhaus, P. D. and Hedrick, J. K. (1993). Application of nonlinear control theory to electronically controlled suspension. Vehicle System Dynamics. 22(3), 309-320.

[9] Alleyne, A. and Hedrick, J. K. (1993). Adaptive control for active suspensions. ASME, Advanced Automotive Technology. DSC-Vol.52, 7-13.

[10] Alleyne, A. (1994). Multiple surface sliding control. ASME, Dynamic Systems and Control, DSC-Vol.55-1, 93-99.

[11] Alleyne, A. and Hedrick, J. K. (1995). Nonlinear adaptive control of active suspensions. IEEE Trans. Control Systems Tech. 3(1), 94-101.

[12] Amirouche, F., Palkovics, L. and Woodrooffe, J. (1994). Optimal driver seat suspension design for heavy trucks. ASME, Transportation Systems, DSC-Vol.54/DE-Vol.76, 277-291.

[13] Appleyard, M. and Wellstead, P. E. (1995). Active suspensions: some background. IEE Proc. Control Theory Appl. 142(2), 123-128.

[14] Ashokkumar, C. R. and Yedavalli, R. K. (1994). Robust control of quarter car suspension models: A case study with real parameter variations. ASME, Active Control of Vibration and Noise. DE-Vol.75, 511-517.

[15] Automotive Engineer. (1994). Focus on vehicle refinement. April/May, 1994, 16-21.

[16] Automotive Engineering, (1993). Active damping using ERM fluids. June, 1993, 19-23.

[17] Barak, P. (1993). A performance index for bounce, pitch and roll control of an automotive suspension. ASME, Symposium on Mechatronics. DSC-Vol.50/PED-Vol.63, 231-237.

[18] Barbieri, N. (1995). The optimal active suspension systems for an off-road vehicle. Inter. J. Vehicle Design. 16(2/3), 219-228.

[19] Beard, J. E. and Sutherland, J. W. (1993). Robust suspension system design. ASME, Advances in Design Automation, DE-Vol.65-1, 387-395.

[20] Ben Mrad, R., Fassois, S. D. and Levitt, J. A. (1993). On the problem of on-board prediction of power consumption in automobile active suspension systems. ASME, Advanced Automotive Technology. DSC-Vol.52, 27-38.

[21] Ben Mrad, R., Levitt, J. A. and Fassois, S. D. (1994). Nonlinear dynamic modelling of an automobile hydraulic active suspension system. Mechanical Systems and Signal Processing. 8(5), 485-517.

[22] Bender, E. K. (1968). Optimum linear preview control with application to vehicle suspension. Trans. ASME, J. of Basic Eng. 90(2), 213-221.

[23] Besinger, F. H., Cebon, D. and Cole, D. J. (1995). Damper models for heavy vehicle ride dynamics. Vehicle Systems Dynamics. 24(1), 35-64.

[24] Best, M. C. and Gordon, T. J. (1994). A factorial analysis of Kalman filtering for semi-active vehicle suspension control. ASME, Engineering Systems Design and Analysis. PD-Vol.64-6, 125-137.

[25] Blackwood, G. H. and von Flotow, A. H. (1992). Active control for vibration isolation despite resonant base dynamics. ASME, Active control of Noise and Vibration. DSC-Vol.38, 285-294.

[26] Blankenship, G. L., Ghanadan, R., Polyakov, V. and Kwatny, H. G. (1993). Modeling and design tools for control of multibody systems: Nonlinear adaptive control. ASME, Advanced Automotive Technology. DSC-Vol.52, 81-97.

[27] Bullough, W. A., Peel, D. J., Sproston, J. L., Stanway, R. and Rodgers, L. (1994). An ER long-stroke damper for vehicle suspension applications. ASME, Developments in Electrorheologyical Flows and Measurement Uncertainty, FED-Vol.205/AMD-Vol.190, 41-49.

[28] Burland. (1992). Turbo C++ (user guide). Borland International Inc. 1992.

[29] Burton, A. W., Truscott, A. J. and Wellstead, P. E. (1995). Analysis, modelling and control of an advanced automotive self-levelling suspension system. IEE Proc. Control Theory Appl. 142(2), 129-139.

[30] Castiglioni, G., Jaker, K. P., Luckel, J. and Rutz, R. (1992). Active vehicle suspension with an active vibration absorber. Worldwide Passenger Car Conf. and Exposition. SAE Technical Paper Series 923027.

[31] Cebon, D., Besinger, F. H. and Cole, D. J. (1996). Control strategies for semi-active lorry suspensions. Proc. of I Mech E. 210(D2), 161-178.

[32] Cech Ilja. (1994). A full-car model of a vehicle with controlled suspension. Vehicle System Dynamics. 23(7), 467-480.

[33] Chen, S. H., Chou, J. H. and Chao, C. H. (1995). Stability robustness of the LQG active suspensions with disturbance/noise uncertainties and time-varying parametrical perturbations. Inter. J. of Vehicle Design. 16(4/5), 428-440.

[34] Cheok, K. C., Huang, N., Horner, T. G. and Settle, T. (1992). Concurrent real-time simulation and animation of active suspension control systems using digital processor and graphics hardware. ASME, Transportation Systems. DSC-Vol.44, 359-366.

[35] Cherry, A. S. and Jones, R. P. (1995). Fuzzy logic control of an automotive suspension system. IEE, Proc. Control Theory Appl. 142(2), 149-160.

[36] Colinot, J. P., Hernette, V. and Jarri, Ph. (1993). Gyrometer application for a low-frequency active suspension. Sensors and Actuators A. 37-38, 116-120.

[37] Corriga, G. Sanna, S. and Usai, G. (1991). An optimal tandem active-passive suspension system for road vehicles with minimum power consumption. IEEE Trans. on Industrial Electronics. 38(3), 210-216.

[38] Cotsaftis, M. (1992). Anticipative robust control for vehicle suspension. ASME, Transportation Systems. DSC-Vol.44, 129-137.

[39] Crolla, D. A., Horton, D. N. L., Pitcher, R. H. and Lines J. A. (1987). Active suspension control for an off-road vehicle. Proc. of I Mech E. 201(D1), 1-10.

[40] Crolla, D. A. and Abdel-Hady, M. B. A. (1991). Active suspension control; Performance comparisons using control laws applied to a full vehicle model. Vehicle Systems Dynamics. 20(2), 107-120.

[41] Crolla, D. A., Soliman, A., El-Sayed, F. M. and El-Alaily, M. M. (1993). Experimental results from a slow-active suspension system. Inter. J. of Vehicle Design. 14(2/3), 226-245.

[42] Crolla, D. A. (1996). Vehicle dynamics - theory into practice. Proc. of I Mech E. 210(D2), 83-94.

[43] Cucuz, S. (1994). Evaluation of ride comfort. Inter. J. of Vehicle Design. 15(3-5), 318-325.

[44] Darling, J., Dorey, R. E. and Ross-Martin, T. J. (1992). A low cost active anti-roll suspension for passenger cars. Trans. ASME, J. Dyn. Systems, Meas., Control. 114(4), 599-605.

[45] de Benito, C. D. (1990). On-board real-time failure detection and diagnosis of automotive systems. Trans. ASME, J. Dyn. Systems, Meas., Control. 112(4), 769-773.

[46] Demic, M. (1994). Optimization of vehicle elasto-damping elements characteristics from the aspect of ride comfort. Vehicle System Dynamics. 23(5), 351-377.

[47] Demic, M. (1996). Optimisation of characteristics of elastic-damping elements from aspect of oscillatory comfort and vehicle handling. Inter. J. of Vehicle Design. 17(1), 76-91.

[48] Dukkipati, R. V., Osman, M. O. M. and Vallurupalli, S. S. (1993). Adaptive active suspension to attain optimal performance and maintain static equilibrium level. Inter. J. of Vehicle Design. 14(5/6), 471-496.

[49] El-Demerdash, S. M. and Crolla, D. A. (1996). Effect of non-linear components on the performance of a hydro-pneumatic slow-active suspension system. Proc. of IMechE. 210(D2), 23-34.

[50] El-Gindy, M. and Palkovics, L. (1993). Possible application of artificial neural networks to vehicle dynamics and control: a literature review. Inter. J. of Vehicle Design. 14(5/6), 593-614.

[51] Elbeheiry, E. M., Karnopp, D. C., Elaraby, M. E. and Abdelraaouf, A. M. (1995). Advanced ground vehicle suspension systems - A classified bibliography. *Vehicle System Dynamics*. 24(3), 231-258.

[52] Elbeheiry, E. M. and Karnopp, D. C. (1996). Optimal control of vehicle random vibration with constrained suspension deflection. J. Sound and Vibration. 189(5), 547-564.

[53] Foag, W. (1989). A practical control concept for passenger car active suspensions with preview. Proc. of I Mech E. 203(D2), 221-230.

[54] Fodor, M. G. and Redfield, R. (1993). The variable linear transmission for regenerative damping in vehicle suspension control. Vehicle System Dynamics. 22(1), 1-20.

[55] Frahm, H. (1911). Device for damping vibrations of bodies. USA Patent 989958.

[56] Friedland, B. (1986). Control system design. McGraw-Hill, Inc.

[57] Friswell, M. I. and Mottershead, J. E., (editors), (1996). *Proceedings of the International Conference on Identification in Engineering Systems*. Swansea.

[58] Frost, G. P., Howell M. N., Gordon, T. J. and Wu, Q. H. (1996). Dynamic vehicle roll control using reinforcement learning. Proc. of Inter. Conf. on Control'96. Exeter, Sept. 1996. 1107-1112.

[59] Fukami, A., Yano, M., Tokuda, H., Ohki, M. and Kizu, R. (1994). Development of piezo-electric actuators and sensors for electronically controlled suspension. Inter. J. of Vehicle Design. 15(3-5), 348-357.

[60] Goran, M. B., Bachrach, B. I. and Smith, R. E. (1992). The design and development of a broad bandwidth active suspension concept car. IMechE C389/418, 925100, 231-252.

[61] Gordon, T. J., Marsh, C. and Wu, Q. H. (1993). Stochastic optimal control of active vehicle suspensions using learning automata. Proc. of I Mech E. 207(D2), 143-152.

[62] Grobbelaar, B. (1992). An optimization technique for vehicle suspensions with the Vibration Dose Value as optimization parameter. Worldwide Passenger Car Conf. and Exposition. SAE Technical Paper Series 922142.

[63] Hac, A. (1992). Design of disturbance decoupled observer for bilinear systems. Trans. ASME, J. Dyn. Systems, Meas., Control. 114(3), 556-562.

[64] Hac, A. (1995). Decentralised control of active vehicle suspensions with preview. Trans. ASME, J. Dyn. Systems, Meas., Control. 117(4), 478-483.

[65] Hac, A. and Youn, I. (1992). Optimal semi-active suspension with preview based on a quarter car model. Trans. ASME, J. Vib. Acoustics. 114(1), 84-92.

[66] Hac, A. and Youn, I. (1993). Optimal design of active and semi-active suspensions including time delays and preview. Trans. ASME, J. Vib. Acoustics. 115(4), 498-508.

[67] Hac, A., Youn, I. and Chen, H. H. (1994). Control of suspensions for vehicles with flexible bodies: Part I - active suspensions. ASME, Transportation Systems, DSC-Vol.54/DE-Vol.76, 69-91.

[68] Hac, A., Youn, I. and Chen, H. H. (1994). Control of suspensions for vehicles with flexible bodies: Part II - semi-active suspensions. ASME, Transportation Systems, DSC-Vol.54/DE-Vol.76, 93-113.

[69] Hall, B. B. and Gill, K. F. (1987). Performance evaluation of motor vehicle active suspension systems. Proc. of I Mech E. 201(D2), 135-148.

[70] Hall, B. B. and Tang, J. S. (1990). Analysis of active and semi-active vehicle suspensions fitted with a pneumatic self-energizing levelling device. Proc. of I Mech E. 204(D2), 161-171.

[71] Hampo, R. J. (1992). Genetic programming: A new paradigm for control and analysis. ASME, Transportation Systems. DSC-Vol.44, 155-163.

[72] Harris, C. M. and Crede, C. E. (1961). Shock and vibration handbook. Vol.1-3 McGRAW-HILL BOOK Company. 1961.

[73] Harrison, R. F. (1993). Optimal control of vehicle suspension dynamics incorporating front-to-rear excitation delays: An approximate solution. J. Sound Vib. 168(2), 339-354.

[74] Hedrick, J. K. and Butsuen, T. (1990). Invariant properties of automotive suspensions. Proc. of I Mech E. 204(D1), 21-27.

[75] Hedrick, J. K., Rajamani R. and Yi, K. (1994). Observer design for electronic suspension applications. Vehicle System Dynamics. 23(6), 413-440.

[76] Herzog, R. (1994). Active versus passive vibration absorbers. Trans. ASME, J. Dyn. Systems, Meas. Control. 116(3), 367-371.

[77] Hoogterp, F. B. (1995). Active suspension technology for combat vehicles. Proc. of SPIE, Technology for Advanced Land Combat. Vol.C59, 25-48.

[78] Hrovat, D. (1991). Optimal suspension performance for 2-D vehicle models. J. sound Vib. 146(1), 93-110.

[79] Hrovat, D. (1993). Applications of optimal control to advanced automotive suspension design. Trans. ASME, J. Dyn. Systems, Meas., Control. 115(2), 328-342.

[80] Huang, N., Cheok, K. C., Horner, T. G. and Settle, T. (1993). Real-time simulation and animation of suspension control system using TI TMS320C30 digital signal processor. SIMULATION. 61(6), 405-416.

[81] Huisman, R. G. M., Veldpaus, F. E., Voets, H. J. M. and Kok, J. J. (1993). An optimal continuous time control strategy for active suspensions with preview. Vehicle System Dynamics. 22(1), 43-55.

[82] Huisman, R. G. M., Veldpaus, F. E., Van Heck and Kok, J. J. (1993). Preview estimation and control for (semi-) active suspension. Vehicle System Dynamics. 22(3), 335-346.

[83] Ishihama, M., Satoh, S., Seto, K. and Nagamatsu, A. (1994). Vehicle vibration reduction by transfer function phase control on hydraulic engine mounts. JSME Inter. J. Series III, 37(3), 536-541.

[84] ISO International Standard 2631-1974 (E). Guide for evaluation of human exposure to whole-body vibration.

[85] Kadota, H., Tabe, M., Aonuma, T., Mouri, H. and Nishiguchi, K. (1994). Application of electronically controlled suspension to the 'One-Box Car'. Inter. J. of Vehicle Design. 15(3-5), 291-300.

[86] Karnopp, D. (1990). Design principles for vibration control systems using semi-active dampers. Trans. ASME, J. Dyn. Systems, Meas., Control. 112(3), 448-455.

[87] Karnopp, D. (1995). Active and semi-active vibration isolation. Trans. ASME, Special 50th Anniversary Design Issue. 117. 177-185.

[88] Katsuda, T., Hiraiwa, N., Doi, S. and Yasuda, E. (1992). Improvement of ride comfort by continuously controlled damper. Worldwide Passenger Car Conf. and Exposition. SAE Technical Paper Series 920276.

[89] Kim, G. and Singh, R. (1992). Resonance, isolation and shock control characteristics of automotive nonlinear hydraulic engine mounts. ASME, Transportation Systems. DSC-Vol.44, 165-180.

[90] Kim, G. and Singh, R. (1993). A broadband adaptive hydraulic mount system. ASME, Advanced Automotive Technology. DSC-Vol.52, 247-255.

[91] Langlois, R. G. and Anderson, R. J. (1995). Preview control algorithm for the active suspension of an off-road vehicle. Vehicle Systems Dynamics. 24(2), 65-97.

[92] Lee, D. M. A., Pascoe, D. M. and ElMaraghy, W. H. (1993). An analysis of the multi-link independent suspension system. Inter. J. of Vehicle Design. 14(1), 44-58.

[93] Leighton, N. J. (1991). Vehicle technology. GKN Technology. Report No: 5082.

[94] Leighton, N. J. (1994). Application of advanced modelling techniques to reduce prototyping time for a novel active suspension system. IEE Computing and Control Division Colloquium on Automotive Applications of Advanced Modelling and Control. London.

[95] Leighton, N. J. and Pullen, J. (1994). A novel active suspension system for automotive application. Proc. of I Mech E, 208(D4), 243-250.

[96] Levitt, J. A. and Zorka, N. G. (1991). The influence of tire damping in quarter car active suspension models. Trans. ASME, J. Dyn. Systems, Meas., Contrcl. 113(1), 134-137.

[97] Li, W. and Liu, W. (1993). New Methods to raise accuracy for road unevenness measurement. ASME, Advanced Automotive Technologies, DSC-Vol.52, 65-70.

[98] Lieh, J. (1992). Semi-active damping control of vehicle ride. ASME, Active control of Noise and Vibration. DSC-Vol.38, 345-351.

[99] Lieh, J. (1992). Damping control of ride quality for flexible vehicle. ASME, Transportation Systems. DSC-Vol.44, 113-127.

[100] Lieh, J. (1993). Semiactive damping control of vibrations in automobiles. Trans. ASME, J. Vib. Acoustics. 115(3), 340-343.

[101] Lieh, J. (1993). Frequency analysis of active suspensions with optimal Damping control using second-order models. ASME, Advanced Automotive Technology. DSC-Vol.52, 15-19.

[102] Lieh, J. (1993). The effect of bandwidth of semiactive dampers on vehicle ride. Trans. ASME, J. Dyn. Systems, Meas., Control. 115(3), 571-575.

[103] Lin, R. C., Cebon, D. and Cole, D. J. (1996). Optimal roll control of a single-unit lorry. Proc. of I Mech E. 210(D1), 45-55.

[104] Lin, Y. J. and Lu, Y. Q. (1993). Toward better ride performance of vehicle suspension systems via intelligent control. ASME, Intelligent Control Systems. DSC-Vol.48, 105-112.

[105] Lin, Y. J., Lu Y. Q. and Padovan, J. (1993). Fuzzy logic control of vehicle suspension systems. Inter. J. of Vehicle Design. 14(5/6), 457-470.

[106] Lin, Y. and Lu, Y. (1994). Active vehicle suspension systems utilizing intelligent control. ASME, Transportation System, DSC-Vol.54/DE-Vol.76, 29-41.

[107] Lohmann, B. (1995). Application of model order reduction to a hydropneumatic vehicle suspension. IEEE Trans. Control Systems Tech. 3(1), 102-109.

[108] Louam, N., Wilson, D. A. and Sharp, R. S. (1988). Optimal control of a vehicle suspension incorporating the time delay between front and rear wheel inputs. Vehicle Systems Dynamics. 17(6), 317-336.

[109] Mackovjak, J. M. and Martone, C. J. (1995). Dynamic absorber suspension strut. United States Patent. Patent No. 5392882.

[110] Maemori, K. (1995). Alternate optimization of speed control hump for automobiles suspension. JSME Inter. J. Series C. 38(3), 552-557.

[111] Mahajan, S. and Robin, R. (1993). Power distribution in active vibratory systems. ASME, Advanced Automotive Technology. DSC-Vol.52, 289-298.

[112] Mahajan, S. and Redfield, R. C. (1994). Dynamic performance issues in active, energy-efficient vibration control systems. ASME, Transportation Systems, DSC-Vol.54/DE-Vol.76, 53-67.

[113] Mao, Y., Zhu, X., Zhang, J. and Huang, S. The prediction of vehicle ride comfort with consideration of nonlinear suspension. Proc. of 11st Intl. Modal Analysis Conf. 1259-1263.

[114] Michelberger, P., Palkovics, L. and Bokor, J. (1993). Robust design of active suspension system. Inter. J. of Vehicle Design. 14(2/3), 145-164.

[115] Moran, A. and Nagai, M. (1992). Analysis and design of active suspensions by H_∞ robust control theory. JSME Inter. J. Series III, 35(3), 427-437.

[116] Moran, A. and Nagai, M. (1993). Optimal preview control of rear suspension using nonlinear neural networks. Vehicle System Dynamics. 22(3), 321-334.

[117] Naem, A. S. H., Stanway, R., Sproston, J. L. and Bullough, W. A. (1994). A strategy for adaptive damping in vehicle primary suspension systems. ASME, Adaptive Structures and Composite Materials, AD-Vol.45/MD-Vol.54, 395-404.

[118] Nagai, M. (1993). Recent researches on active suspensions for ground vehicles. JSME Inter. J. Series III, 36(2), 161-170.

[119] Nestico, V. (1995). Hybrid electric drive active suspension. Proc. of SPIE, Technology for Advanced Land Combat. Vol.C59, 21-24.

[120] Olgac, N. and Holm-Hansen, B. T. (1993). A new direction in vibration absorption: delayed resonator. ASME, Symposium on Mechatronics. DSC-Vol.50/PED-Vol.63, 15-20.

[121] Olgac, N. and Holm-Hansen, B. T. (1993). Vibration absorbers utilizing only position measurements for time varying excitation frequencies. ASME, Symposium on Mechatronics. DSC-Vol.50/PED-Vol.63, 223-229.

[122] Olgac, N. and Holm-Hansen, B. (1994). Design characteristics of a novel tuneable active vibration absorber. ASME, Active Control of Vibration and Noise, DE-Vol.75, 477-483.

[123] Olgac, N. and Holm-Hansen, B. (1995). Tuneable active vibration absorber: The delayed resonator. Trans. ASME, J. Dyn. Systems, Meas. Control. 117(4), 513-519.

[124] Oueslati, F. and Sankar, S. (1992). A comparative study of active suspension performance with full and limited state feedback controls based on an in-plane vehicle ride model. ASME, Active control of Noise and Vibration. DSC-Vol.38, 353-362.

[125] Oueslati, F. and Sankar, S. (1994). A class of semi-active suspension schemes for vehicle vibration control. J. Sound Vib. 172(3), 391-411.

[126] Palkovics, L., Stepan, G. and Michelberger, P. (1993). Chaotic behaviour of the nonlinear wheel suspension system. Machine Vibration. 2(1), 47-53.

[127] Palkovics, L., El-Gindy, M. and Pacejka, H. B. (1994). Modelling of the cornering characteristics of types on an uneven road surface: a dynamic version of the 'Neuro-Tyre'. Inter. J. of Vehicle Design. 15(1/2), 189-215.

[128] Paterson, C. A., Burnham, K. J., James, D. J. G. and Williams, R. A. (1994). A fixed parameter optimal controller design for an active suspension system -- A sensitivity analysis. Mechatronics. 4(3), 317-329.

[129] Patten, W. N., Sack, R. L. and He, Q. (1996). Controlled semi-active hydraulic vibration absorber for bridges. J. of Structural Engineering. 122(2), 187-192.

[130] Pilbeam, C. and Sharp, R. S. (1993). On the preview control of limited bandwidth vehicle suspensions. Proc. of I Mech E. 207(D2), 185-193.

[131] Pinkos, A., Shtarkman, E. and Fitzgerald, T. (1994). Actively damped passenger car suspension system with low voltage electro-rheological magnetic fluid. ASME, Transportation Systems, DSC-Vol.54/DE-Vol.76, 1-12.

[132] Prokop, G. and Sharp, R. S. (1995). Performance enhancement of limited-bandwidth active automotive suspensions by road preview. IEE Proc. Control Theory App. 142(2), 140-148.

[133] Qin, Z. (1990). Electronics (in Chinese). High Educational Publishing Company. 1990.

[134] Rajamani, R. and Hedrick, J. K. (1995). Adaptive observers for active automotive suspensions: theory and experiment. IEEE Trans. Control Systems Tech. 3(1), 86-93.

[135] Rakheja, S., Afework, Y. and Sankar, S. (1994). An analytical and experimental investigation of the driver-seat-suspension. Vehicle System Dynamics. 23(8), 501-524.

[136] Rakheja, S, Liu, P., Ahmed, A. K. W. and Su, H. (1993). Analysis of an interlinked hydro-pneumatic suspension. ASME, Advanced Automotive Technology. DSC-Vol.52, 279-287.

[137] Ray, L. R. (1992). Robust linear-optimal control laws for active suspension system. Trans. ASME, J. Dyn. Systems, Meas., Control. 114(4), 592-598.

[138] Ray, L. R. (1995). Nonlinear state and tire force estimation for advanced vehicle control. IEEE Trans. Control Systems Tech. 3(1), 117-124.

[139] Rezeka, S. F. and Saafan, A. A. (1994). Adaptive semi-active suspension with combined viscous and dry energy dissipation. ASME, Active Control of Vibration and Noise, DE-Vol.75, 519-525.

[140] Richard, M. J., Bouazara, M. Cheng, L. and Rakheja, S. (1993). The influence of suspension parameters on the response of a vehicle using the vector network method. ASME, Advanced Automotive Technology. DSC-Vol.52, 59-63.

[141] Ryba, D. (1993). Semi-active damping with an electromagnetic force generator. Vehicle Systems Dynamics. 22(2), 79-95.

[142] Salman, M. A., Lee, A. Y. and Boustany, N. M. (1990). Reduced order design of active suspension control. Trans. ASME, J. Dyn. Systems, Meas., Control. 112(4), 604-610.

[143] Sawyer, C. A. (1994). Active or adaptive suspension. Automotive Industries. June, 1994, 59-61.

[144] Sears, K. J. (1990). New suspension system for high performance front wheel drive car. Proc. of SAE, 18th FISITA Congress the Promise of New Technology in Automotive Industry. 905079, 603-608.

[145] Seto, K. and Furuishi, Y. (1991). A study on active dynamic absorber. ASME, Model Analysis, Modelling, Diagnostics, and control -- Analytic and Experimental, DE-Vol.38, 263-270.

[146] Sharp, R. S. (1994). The application of multi-body computer codes to road vehicle dynamics modelling problems. Proc. of I Mech E. 208(D1), 55-61.

[147] Sharp, R. S. and Hassan, S. A. (1987). Performance and design considerations for aissipative semi-active suspension systems for automobiles. Proc. of I Mech E. 201(D2), 149-153.

[148] Sharp, R. S. and Hassan, S. A. (1987). On the performance capabilities of active automobile suspension systems of limited bandwidth. Vehicle Systems Dynamics. 16(4), 213-225.

[149] Sharp, R. S. and Hassan, J. H. (1988). Performance predictions for a pneumatic active car suspension system. Proc. of I Mech E. 202(D4), 243-250.

[150] Shim, J. S., Heo, S. J. and Yoo, Y. M. (1990). Effect of a semi-actively controlled suspension unit on the vehicle dynamic characteristics. Proc. of SAE, 18th FISITA Congress the Promise of New Technology in Automotive Industry. 905040, 279-285.

[151] Shuttlewood, D. W., Crolla, D. A., Sharp, R. S. and Crawford, I. L. (1993). Active roll control for passenger cars. Vehicle System Dynamics. 22(3), 383-396.

[152] Smith, M. C. (1995). Achievable dynamic response for automotive active suspensions. Vehicle Systems Dynamics. 24(1), 1-33.

[153] Soliman, A. M. A., Crolla, D. A. and El-Sayed, F. M. (1993). A comparison of control strategies for the switchable damper suspension system. Inter. J. of Vehicle Design. 14(4), 308-324.

[154] Soltis, M. W. (1987). 1987 thunderbird turbo coupe programmed ride control (PRC) suspension. SAE Technical Paper Series 870540.

[155] Spentzas, C. N. (1993). Optimization of vehicle ride characteristics by means of Box's method. Inter. J. of Vehicle Design. 14(5/6), 539-551.

[156] Spyros, G. T. (1994). Fuzzy systems and fuzzy expert control: an overview. The Knowledge Engineering Review. 9(3), 229-268.

[157] Stenssion, A., Asplund, C. and Karlsson, L. (1994). The nonlinear behaviour of a MacPherson strut wheel suspension. Vehicle System Dynamics. 23(2), 85-106.

[158] Stephens, L. S., Rouch, K. E. and Tewani, S. G. (1991). Theory for an active dynamic vibration absorber. ASME, Structure Vibration and Acoustics, DE-Vol.34, 89-94.

[159] Sun, J. Q., Jolly, M. R. and Norris, M. A. (1995). Passive, adaptive and active tuned vibration absorbers -- A survey. Trans. ASME, Special 50th Anniversary Design Issue. 117, 234-242.

[160] Sun, Y. and Parker, G. A. (1993). A position controlled disc valve in vehicle semi-active suspension systems. Control Engineering Practice. 1(6), 927-935.

[161] Sunwoo, M., Cheok, K. C. and Huang, N. J. (1991). Model reference adaptive control for vehicle active suspension systems. IEEE Trans. on Industrial Electronics. 38(3), 217-222.

[162] The MATH WORKS Inc. (1994). Matlab user's guide (for the main package and its toolboxes).

[163] Thirupathi, S. R. and Naganathan, N. G. (1995). Piezoceramic macromotion actuator: Analytical synthesis and prototype investigations. Smart Structures and Integrated Systems, Proc. of SPIE. Vol. 2443, 771-781.

[164] Tobata, H., Fukuyama, K., Kimura, T. and Fukushima, N. (1993). Advanced control methods of active suspension. Vehicle System Dynamics. 22(3), 347-358.

[165] Truscott, A. J. (1994). Composite active suspension for automotive vehicles. Computing & Control Engineering Journal. June, 149-154.

[166] Truscott, A. J. and Wellstread, P. E. (1995). Adaptive ride control in active suspension systems. Vehicle Systems Dynamics. 24(5), 197-230.

[167] Tseng, H. E. and Hedrick, J. K. (1994). Performance of a semi-active suspension with leading system information. ASME, Transportation Systems, DSC-Vol.54/DE-Vol.76, 115-126.

[168] Tseng, H. E. and Hedrick, J. K. (1994). Semi-active control laws - Optimal and sub-optimal. Vehicle System Dynamics. 23(8), 545-569.

[169] Tsunashima, H. and Abe, M. (1994). Dynamics of the mechanical levitation control system for a maglev transport vehicle. JSME Inter. J. Series III, 37(3), 528-535.

[170] Tsunashima, H., Fujioka, T. and Abe, M. (1994). Dynamics of a mechanically controlled permanent magnet suspension for maglev transport vehicle. ASME, Transportation Systems, DSC-Vol.54/DE-Vol.76, 265-275.

[171] Turner, J. D. (1988). Instrumentation for engineers. MACMILLAN EDUCATION LTD. 1988.

[172] Ulsoy, A. G., Hrovat, D. and Tseng, T. (1994). Stability robustness of LQ and LQG active suspensions. Trans. ASME, J. Dyn. Systems, Meas., Control. 116(1), 123-131.

[173] Vallurupalli, S. S., Osman, M. O. M. and Dukkipati, R. V. (1992). Adaptive control of an active suspension. ASME, Transportation Systems. DSC-Vol.44, 441-452.

[174] Vallurupalli, S. S., Osman, M. O. M. and Dukkipati, R. V. (1993). Adaptive vehicle system that maintains static equilibrium during load shift. ASME, Advanced Automotive Technology. DSC-Vol.52, 175-185.

[175] Vallurupalli, S. S., Dukkipati, R. V. and Osman, M. O. M. (1994). Smart active suspension to counteract on-line parametric variations due to critical maneuvers. ASME, Transportation Systems, DSC-Vol.54/DE-Vol.76, 13-28.

[176] Venhovens, P. J. Th., van der Knaap, A. C. M. and Pacejka, H. B. (1992). Semi-active vibration and attitude control. World-wide Passenger Car Conf. and Exposition. SAE Technical Paper Series 923032.

[177] Venhovens, P. J. Th., van der Knaap, A. C. M. and Pacejka, H. B. (1993). Semi-active attitude and vibration control. Vehicle System Dynamics. 22(3), 359-381.

[178] Venhovens, P. J. Th. (1994). The development and implementation of adaptive semi-active suspension control. Vehicle System Dynamics. 23(3), 211-235.

[179] Virk, G. S., Ghazali, A. B. and Azzi, D. (1996). Fuzzy logic control of building management systems. Proc. of Inter. Conf. on Control'96. Exeter, Sept. 1996. 580-585.

[180] Vu-Quoc, L. and Olsson, M. (1993). High-speed vehicle models based on a new concept of vehicle/structure interaction component: Part 1 -- Formulation. Trans. ASME, J. Dyn. Systems, Meas., Control. 115(1), 140-147.

[181] Wang, N., Fagan, D. J. and Staley S. M. (1993). XBB: A blackboard system for vehicle suspension tuning. ASME, Advances in Design Automation. DE-Vol.65-1, 397-409.

[182] Wang, T. L., Shahawy, M. and Huang, D. Z. (1993). Dynamic response of highway trucks due to road surface roughness. Computer & Structures. 49(6), 1055-1067.

[183] Webb, A. C.; Burnham, K. J.; James; D. J. G. and Williams, R. A. (1995). A comparative study of passive and low bandwidth active suspension systems. J. of Systems Science. 21(4)

[184] Webb, A. C.; Burnham, K. J.; James; D. J. G. and Williams, R. A. (1996). On-line adaptive control of a low bandwidth active suspension system. Proc. of Inter. Conf. on Control'96. Exeter, Sept. 1996. 1154-1159.

[185] Williams, R. A. (1994). Electronically controlled automotive suspension. Computing & Control Engineering Journal. June, 143-148.

[186] Williams, D. E. and Haddad, W. M. (1995). Nonlinear control of roll motion moment distribution to influence vehicle yaw characteristics. IEEE Trans. Control Systems Tech. 3(1), 110-116.

[187] Wu, Q. (1992). Principle of automatic control (in Chinese). Publisher in Tsing Hua University. 1992.

[188] Wu, H. C., Yan, W. Z., Mo, C. and Patten, W. N. (1993). A prototype semisctive damper. ASME, Advanced Automotive Technology. DSC-Vol.52, 51-57.

[189] Wurtenberger, M., Germann St. and Isermann, R.(1992). Modelling and parameter estimation of nonlinear vehicle dynamics. ASME, Transportation Systems. DSC-Vol.44, 53-63.

[190] Xiong, S., Cheng, H. and Zhang, D. (1993). Identification and structural dynamics modification of a nonlinear system. Proc. of 11st Intl. Modal Analysis Conf. 274-277.

[191] Yamaguchi, H., Doi, S. -I., Iwama, N. and Hayashi, Y. (1993). Experimental study of system optimization for suppression of vehicle vibration. Vehicle System Dynamics. 22(3), 299-308.

[192] Yeh, E. C. and Tsao, Y. J. (1994). A Fuzzy preview control scheme of active suspension for rough road. Inter. J. of Vehicle Design. 15(1/2), 166-180.

[193] Yi, K. and Hedrick, K. (1993). Dynamic tire force control by semiactive suspensions. Trans. ASME, J. Dyn. Systems, Meas., Control. 115(3), 465-474.

[194] Yi, K., Wargelin M. and Hedrick K. (1992). Dynamic tire force control by semi-active suspensions. ASME, Transportation Systems. DSC-Vol.44, 299-310.

[195] Yoon, Y. S. and Kim, H. (1996). Feedforward neuro-controlled active suspension using frequency and time-mixed shape performance index. Part 1: Control logic and performance. Inter. J. of Vehicle Design. 17(2), 163-181.

[196] Yoshimura, T., Edokoro, K. and Ananthanarayana, N. (1993). An active suspension model for rail/vehicle systems with preview and stochastic optimal control. J. Sound Vib. 166(3), 507-519.

[197] Youn, I. and Hac, A. (1993). Active preview suspension with integral action. ASME, Advanced Automotive Technology. DSC-Vol.52, 1-5.

[198] Youn, I. and Hac, A. (1995). Semi-active suspensions with adaptive capability. J. Sound and Vibration. 180(3), 475-492.

[199] Young, W. C. (1989). Roark's formulas for stress & strain. 6th edition. McGRAW-HILL BOOK COMPANY. 1989.

Appendix A

Sky Hook Damping

In a mass spring damper system force may be transmitted to accelerate the mass by one of two ways; through the spring or through the damper. The spring force is proportional to its displacement, i.e. in the case of a suspension system to the difference between the vertical displacements of the body and the wheel. The damper force is proportional to the relative velocity of its ends, i.e. in a conventional suspension the difference between the vertical velocity of the body and the wheel.

If a vertical velocity is imparted to the wheel then, until the body attains the same vertical velocity, a force will be generated by the damper and will cause the body to accelerate vertically more rapidly than would have been the case in the absence of a damper. Hence any sudden road inputs result in force being transmitted through the damper to the body. These results in a harshness over high frequency road disturbances.

If it were possible to disconnect the damper from the hub and attach it between the body and a fixed vertical reference point then wheel movements would not give rise to any force being developed in the damper. Body motions would still result in a damper force proportional to the vertical velocity, so the damping ratio of the motion remains unchanged but the ride would be improved, especially over high frequency disturbances. This arrangement is known as 'sky hook' damping and cannot be realised mechanically.

These two scenarios are illustrated in figure A-1.

The difference between the cases can also be seen analytically. Considering first the conventionally damped case, and taking a force balance on the mass it can be seen that:

$$m\ddot{x}_b + c(\dot{x}_b - \dot{x}_w) + k(x_b - x_w) = 0$$

which can be re-arranged to give:

$$m\ddot{x}_b + c\dot{x}_b + kx_b = c\dot{x}_w + kx_w$$

in which the left hand side represents the natural response of the system and the right hand side represents the forcing function, which contains the spring related and the damper related components.

If the 'sky hook' damping case is considered, in which the damper is fixed to an absolute reference, the latter relationship becomes:

$$m\ddot{x}_b + c\dot{x}_b + kx_b = kx_w$$

In this case the only forcing function is that which is spring related.

The effect of this on the frequency response is to reduce the transmission of high frequency components (i.e. those with a high velocity content). This has the effect of reducing the harshness of the ride.

In an active suspension the forces acting on the body are generated by the control algorithm. It is therefore possible to generate 'sky hook' damping forces provided the absolute vertical velocity of the body can be determined. This is possible through the use of a vertical accelerometer, which gives body vertical acceleration which can be numerically integrated to yield the required velocity value. It is the ability to simulate the 'sky hook' damper that gives active systems an unmatchable advantage over conventional suspensions in terms of ride quality.

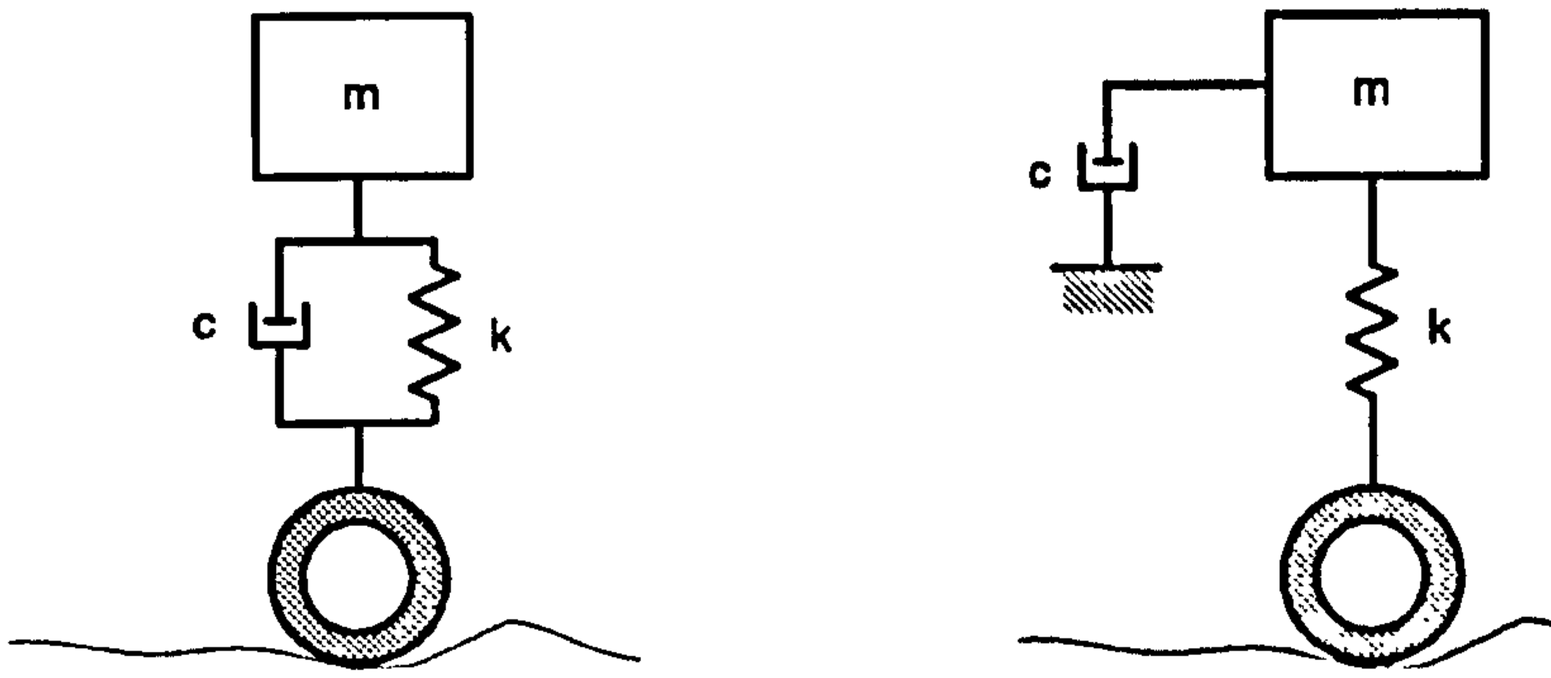

Conventional damping 'sky hook' damping

Figure A-1 Comparison of damping technique

Appendix B

Zero Rate Suspension and Buckled Spring[1]

B.1 The zero rate concept

The concept of a very low spring rate suspension system has existed within GKN Technology for some time. The system incorporates two novel principles which are both required to implement a working system but which may have other applications individually and are thus best considered separately at this stage.

B.1.1 Spring design

The basic characteristic of a conventional spring is one of a constant rate, i.e. a linear load/compression relationship which is not appropriate for a very low rate suspension since the preload required to support a vehicle would result in large initial displacements of the spring. This implies a very long natural length and an associated penalty in weight and cost of the spring as well as dubious practicality. If an initially flat leaf spring is loaded axially the load will not result in any appreciable deflection until the buckling point is reached, at which point the leaf begins to buckle and maintains an nearly constant load over a considerable range of deflections. These two modes of operation are illustrated in figures B-1.

The use of a buckling leaf spring therefore offers a very low effective spring rate but additionally yields an improved material utilisation since no deflection occurs at loads below the buckling point and therefore no initial energy is stored in the spring. This implies that at the static load condition the total potential energy stored in the material of the spring is less than would be the case for a conventional spring of the same rate which in turn indicates that less material is required to contain the energy. Hence for a given application a lighter spring can be employed. This saving can be optimised by designing the spring to distribute the stored energy optimally throughout the material.

---

[1] This appendix is mainly quoted from the technical report written by Dr. N. J. Leighton, 1991.

This is achieved by a leaf spring of constant thickness whose profile is defined by two almost circular arcs (figure B-2).

The use of a very low rate suspension system inherently offers excellent ride comfort and isolation from road inputs as a result of its near zero natural frequency but it offers no control over the ride height of the vehicle and is unable to accommodate variations in vehicle mass. These factors render the system of no use as a vehicle suspension in its own right; some means of varying the force produced is required before a usable system can be realised.

B.1.2 Variable leverage design

If the spring unit of a suspension system is mounted at an angle to the line of action of the vehicle loads (i.e. the vertical) then the spring sees a mechanical disadvantage against the load supporting the vehicle. The magnitude of this mechanical disadvantage depends on the angle between the lines of action of the two forces (figure B-3). If a spring producing an essentially constant force is mounted at an angle to the desired line of action it is therefore possible to change the resultant force along the line of action by varying the angle, i.e. changing the leverage of the spring. This principle allows a constant force spring to produce a variable force at the wheel of a vehicle and thus to adapt to variations in vehicle weight as well as dynamically controlling the ride height.

In the two wheeled trailer test rig, this principle was implemented by moving the opposite end to the hub of the buckled spring along a locus of circular arc on the trailer body. The movement was fulfilled by a ball screw lead driven by a DC motor.

By combining this variable leverage principle with the zero rate spring concept it is therefore possible to envisage a realistic design of vehicle suspension.

B.2 The force of buckled spring

The expression of the force for the spring profile is based on the requirement that for uniform curvature the bending moment M_b at any point along the spring must bear a constant ratio to the geometrical moment of inertia I_s at that point, as shown in Figure B-4. Since I_s is proportional to the width W_x, and M_b to the lateral displacement d_x we have

$$\frac{W_x}{W} = \frac{d_x}{d} = \frac{\cos\theta_x - \cos\theta}{1 - \cos\theta} = \frac{\cos\frac{x}{R} - \cos\frac{l_s}{2R}}{1 - \cos\frac{l_s}{2R}}$$

where R is the bending radius.

As this expression is a function of R it is clear that the spring element will bend along an exact arc only for the particular value of R used to define the profile. By setting R equal to $\frac{3l_s}{2\pi}$ we obtain a circular bending arc of 120° at the point of maximum deflection. The force F_s at this point is readily calculated by applying the standard bending formula

$$M_b = F_s d_x = \frac{EI_s}{R}$$

to the cross section, $d = R(1 - \cos\frac{l_s}{2R})$, and $I_s = \frac{Wl_s^3}{12}$ (where l_s is the thickness of the spring) for a rectangular section on the spring characteristic the bending curve departs from a circular arc. At other points on the spring characteristic the bending curve departs from a circular area, making analysis more difficult. However the departure is small and a good approximation to the force can be obtained by assuming that the spring profile is notionally adjusted, while retaining the same surface area, so as to give a true circular bending arc. We then derive the general expression as follows

$$F_s = \frac{EW_x t_s^3}{3l_s^2} = \frac{EWt_s^3}{3l_s^2} \cdot \frac{\theta^2}{1 - \cos\theta}$$

where θ is half the bending arc angle for the adjusted spring profile. It is determined by

$$\Delta l_s = l_s(1 - \frac{\sin\theta}{\theta})$$

where Δl_s is the longitudinal displacement.

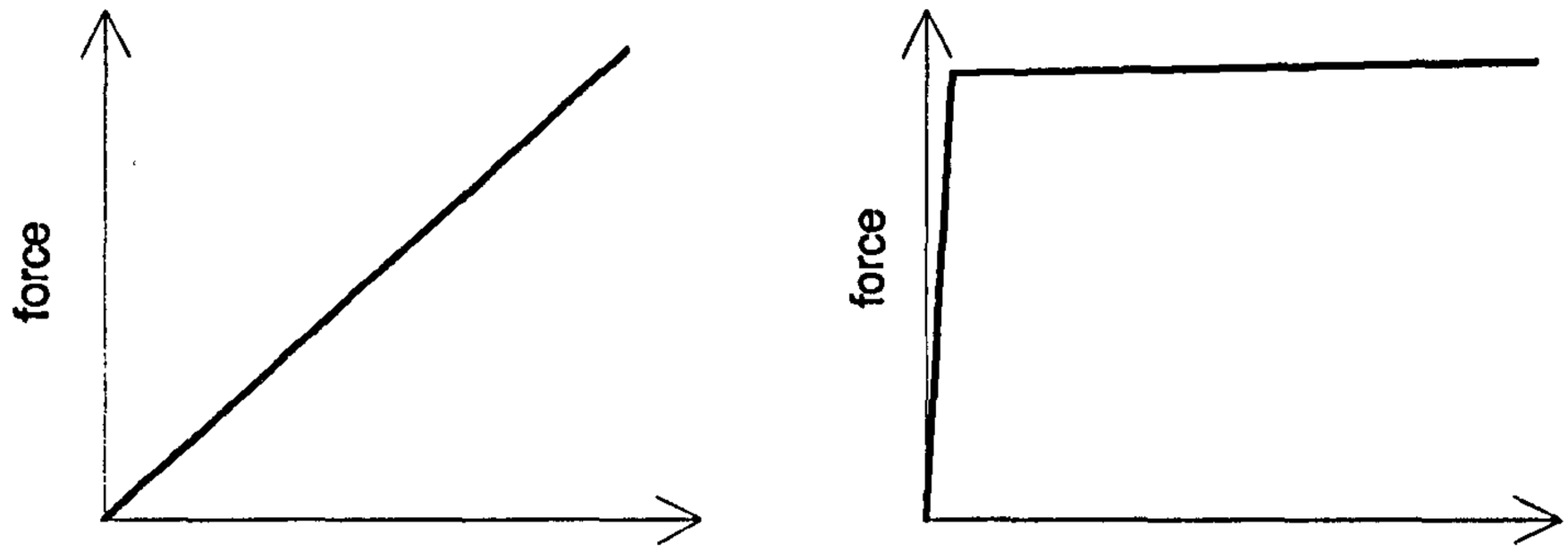

(a) Conventional spring (b) Buckling spring

Figure B-1 Spring characteristics

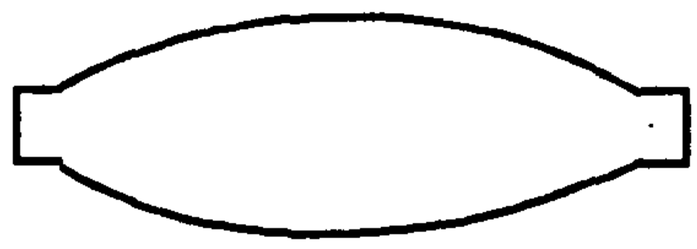

Figure B-2 Optimum spring shape

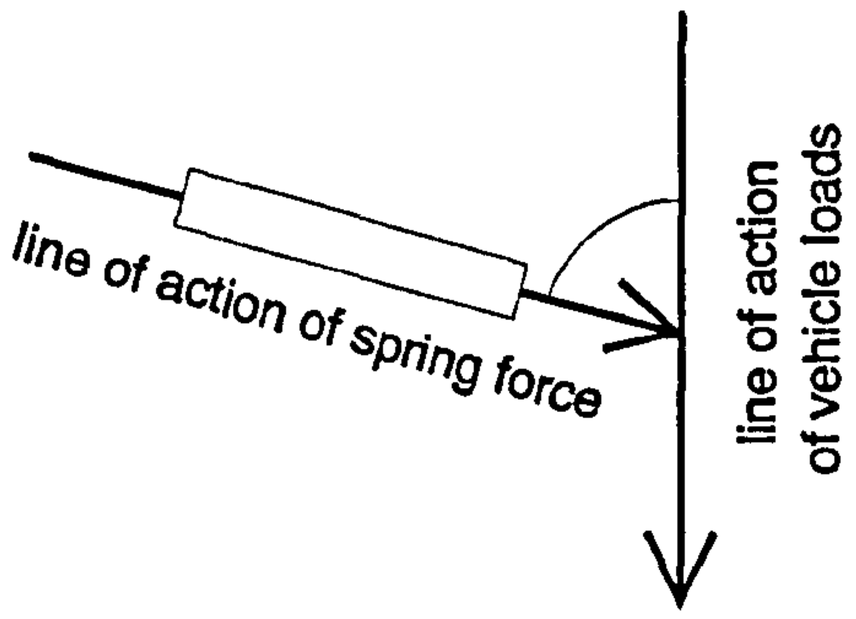

Figure B-3 Variable leverage concept

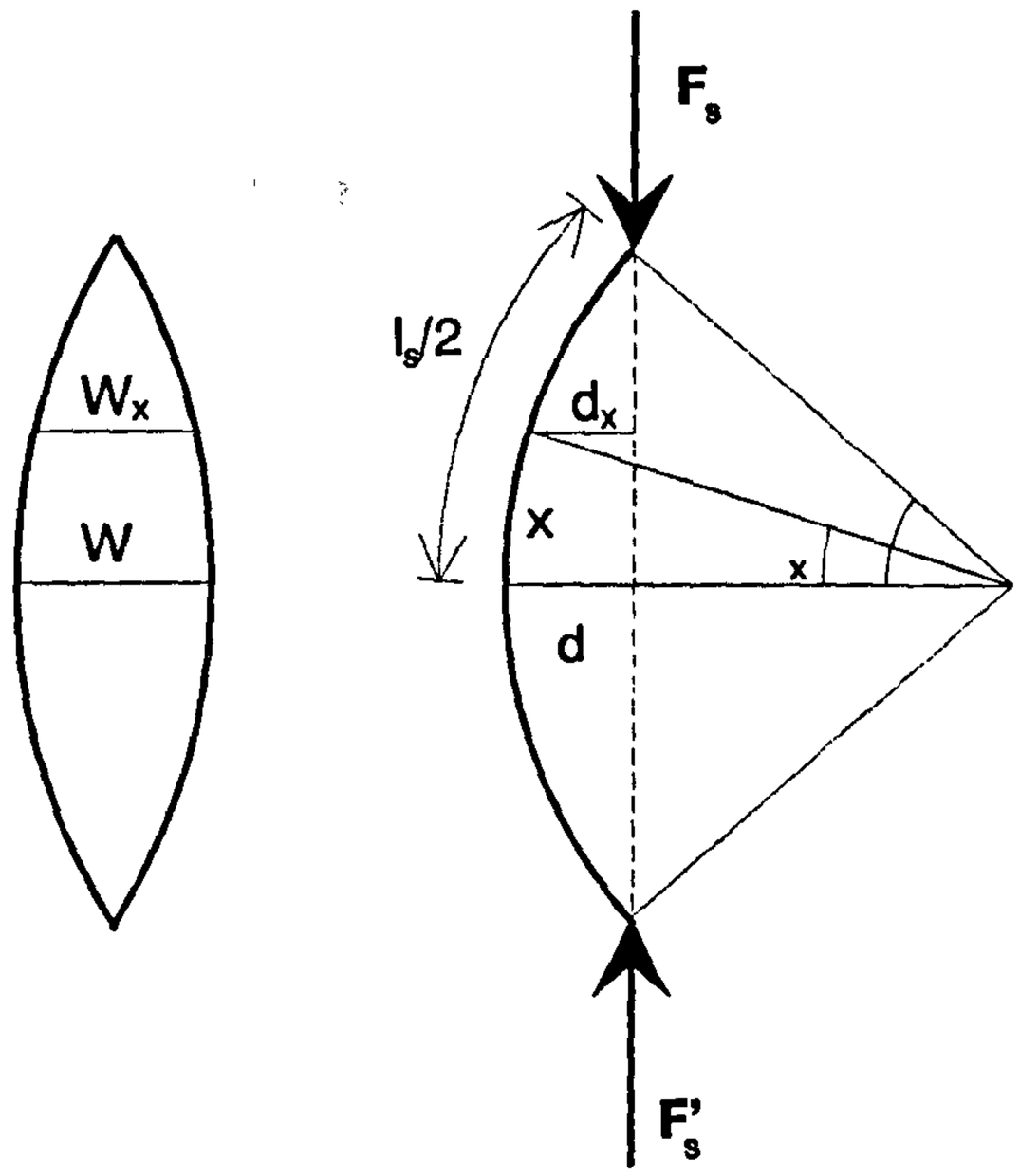

Figure B-4 The buckled spring element

Appendix C

Source Code of the PID Algorithm

The PID control program was written in C++ for the suspension system. The source code of the algorithm is shown as follows.

```
.....(some pre-process for the measured variables x)
  for (i=0;i<2;i++)
  {
  u[i]=0;
    for (j=0;j<6;j++)
    {
    u[i]=u[i]+F[i][j]*x[j];    /* controller */
    }
  u[i]=u[i]*cu[i]+c0[i];
  }
.....(the produced control signals u are sent to D/A port)
```

Because the PID control is for the multi-input and multi-output system, the feedback matrix F is 2-by-6 array. F consists of 3 squire arrays which are the proportional derivative and integral matrix respectively. The physical control values are calculated in the line 6. The digital control values are produced in the line 8, where cu and c0 are the coefficient vectors for the transformation.

Appendix D

Papers Arising from the Work

1) 'Modelling and open-loop performance of a novel active suspension for road vehicles' accepted by the Inter. Conf. on Control'96, IEE, Sept. 1996.

2) 'A transfer function identification method for automotive suspension systems' Proc. of the Inter. Conf. on Identification in Engineering Systems, March 1996.

3) 'An active tuneable vibration absorber for automotive suspension applications' To be published.

4) 'Control strategies for a novel active suspension' To be published.

5) 'Stability and nonlinearity of the zero rate active suspension' To be published.

6) 'Application of fuzzy logic in a novel active suspension system' To be published.